AD600234

ASD-TDR-62-801

INVESTIGATION OF A METHOD FOR THE PREDICTION OF VIBRATORY RESPONSE AND STRESS IN TYPICAL FLIGHT VEHICLE STRUCTURE

TECHNICAL DOCUMENTARY REPORT ASD-TDR-62-801

20080818 043

AUGUST 1963

FLIGHT DYNAMICS LABORATORY
AERONAUTICAL SYSTEMS DIVISION
WRIGHT-PATTERSON AIR FORCE BASE, OHIO

Project No. 1370, Task No. 137009

Prepared under Contract No. AF 33(616)-8219
by Norair Division, Northrop Corporation
1001 E. Broadway, Hawthorne, Calif.
Co-Authors: R. W. White, K. E. Eldred, W. H. Roberts

NOTICES

400 - Sept. 1963 - 5-101 - 162

AD600234

FOREWORD

The research work in this report was performed by the NORAIR Division of Northrop Corporation, Hawthorne, California, for the Flight Dynamics Laboratory*, Directorate of Aeromechanics, Deputy for Technology, Aeronautical Systems Division, Wright-Patterson Air Force Base, under AF contract Nr. AF33(616)-8219. This research is part of a continuing effort to obtain economical methods of vibration prediction, control and measurement for flight vehicles which is part of Air Force Systems Command's Applied Research Program 750 A, The Mechanics of Flight. The Project Nr. is 1370, "Dynamic Problems in Flight Vehicles" and Task Nr. 137009, "Method of Vibration Prediction, Control and Measurement". Channing L. Pao and Lt N. A. Wrobel of the Flight Dynamics Laboratory were the Project Engineers.

The authors express their appreciation for the contributions of Lt Wrobel, Mr. Bingman, Dr. Rogers and other ASD personnel. Contributing personnel of Northrop and Western-Electro Acoustic Laboratory include R. W. White, K. E. Eldred, W. H. Roberts, A. Wang, R. Boyer, R. Barnoski, P. Finwall, N. Kincaid, W. Harger, R. Carlstrand, C. Sexton, U. Sanders and C. Boswell.

***Presently designated Vehicle Dynamics Division of the AF Flight Dynamics Laboratory.**

ABSTRACT

The prediction of the vibratory response of a complex structure such as an aircraft fuselage or missile to a random external forcing function was the primary task of this project. Previous attacks on the problem have shown it is not possible to estimate vibratory response with useable accuracies. Local and remote acceptance, transmission through structure and to substructure, which are all three dimensional phenomena, and randomness are a few of the complexities involved. The timeliness and importance of the study is due to its concern with structural integrity and reliability. The various needs for better handling of new phenomena in structural dynamics are given.

Previous studies have indicated that priority should go to experimental studies, in particular the dynamically similar structural model. The concept is presented along with a demonstration which includes design, construction, and test of such a model. The experimental tool under study will provide a reliability-by-design approach which shortens the design period by providing design inputs early in the development of a new system. The models will be especially useful in space booster projects where different payloads are substituted. Substudies in support of modeling were conducted. Improved model laws and construction techniques were developed. Measured transfer function of complex structure using excitation from noise sources provided new definitions of vibration transmission in complex structure.

PUBLICATION REVIEW

This technical documentary report has been reviewed and is approved.

FOR THE COMMANDER

Walter J. Mykytow

WALTER J. MYKYTOW
Chief, Dynamics Branch
Flight Dynamics Laboratory

TABLE OF CONTENTS

TABLE OF CONTENTS

(Continued)

TABLE OF CONTENTS

(Continued)

LIST OF APPENDICES

LIST OF ILLUSTRATIONS

LIST OF ILLUSTRATIONS

LIST OF ILLUSTRATIONS

(Continued)

LIST OF ILLUSTRATIONS

(Continued)

LIST OF ILLUSTRATIONS
(Continued)

LIST OF ILLUSTRATIONS

(Continued)

LIST OF ILLUSTRATIONS

(Continued)

FIGURE		PAGE

FIGURE		PAGE

FIGURE PAGE

FIGURE PAGE

FIGURE		PAGE

FIGURE PAGE

FIGURE		PAGE

LIST OF ILLUSTRATIONS
(Continued)

LIST OF TABLES

SECTION I

INTRODUCTION

A major experimental program was recently completed by the Northrop Corporation, Norair Division, in the field of vibration response of complex, built-up, structures. Recent studies in structural vibrations, acoustic fatigue and high intensity turbulence show that major difficulties in structural reliability may be expected for many classes of aerospace vehicles experiencing severe environments. The problems of combined loads, combined failure modes, and a host of other complexities indicate that, in general, the avenues of serious attack on the structural reliability problem are few.

The primary objectives of this program were to develop methods for predicting the response of complex structures and to develop an improved understanding of the transmission of vibratory energy through the structure from the location of its acceptance to the areas of potential damage. Emphasis on structure rather than equipment is a feature of the program because of the significant number of structural failures due to acoustic loads and pseudo noise. An unexpected finding of a previous study that substructure is more sensitive than surface structure adds to the complexity and was considered in setting the objectives.

A dynamically similar structural model based on a study of the scaling laws was built to determine its applicability as a response prediction tool. A broad study of the related uses of such a model in environmental and fatigue failure problems was a natural accompaniment to the project. Thermal scaling requirements were established. A definitive statement of experimental technique is given.

A new phenomenon of high intensity turbulence arising from separation, wakes, base pressure fluctuations and oscillating shocks at high dynamic pressures, looms large for vehicles where compromised aerodynamics feature the design. These are large scale excitations more damaging than normal boundary layer turbulence because of their comparable size to characteristic areas of fundamental structural elements.

Choice of scale was made on the basis of not scaling to an impractical size. Model instrumentation, frequency band, and skin gauge provide a lower limit to scaling which it is not desirable to approach. Instrumentation, mass scaling, fuel tank simulation, damping, joint and fabrication were all carefully studied prior to model design and construction. Honeycomb sandwich scaling proved to be a key factor. An improved conceptual model of vibratory transmission has been developed. Modeling ideas to simplify the modeling process were generally outweighed by the necessity to scale with great fidelity.

Manuscript released for Publication October 1962 as an ASD Technical Report.

Considerable study and thought were devoted to the question of using scaled engines to simulate full scale acoustic excitation. Scaled solid propellant rocket engines were shown to be a feasible approach and are ready for application as a link in the overall process of modeling excitation, structural response and failure modes. Off the shelf Jet Assisted Takeoff (JATO) units were chosen and formed a basis for the choice of the scale factor. Throat diameter, thrust, and specific impulse were available all in reasonable agreement with a consistent scale relation to the full scale boosters. Very large solid boosters were used for zero launch capability on the SM-62 strategic intercontinental missile. The full scale units contained 260,000 lb thrust for four seconds and provided a 172 db environment adjacent to key equipment bays, generating a serious reliability problem.

The need for the present approach has been documented in a number of different ways. As a concept which covers most aspects of the problem, it falls in an area where the analytical or empirical approach has been previously shown to be, because of complexity, either marginal or unusable. Certain material sensitivities to random loading have also motivated the complete experimental approach. Combined loads and combined failure modes problems may be an inevitable result of using new structural concepts, new materials and unusual configurations simultaneously on future vehicles.

Section II discusses certain experimental substudies associated with the model design. These substudies include tests of individual and simple built-up model structures to determine the importance of damping, joint transmission, rivet or bonding joint construction including bond thickness, choice of bonding agent, rivet pressures and the number of rivets. An experimental study to determine the vibration characteristics of honeycomb sandwich panels is also presented.

Theoretical discussions are presented in Section III as background material. Structural vibration scaling laws are derived for perfectly elastic materials using the fundamental equations of elasticity. Scaling laws are also discussed in terms of normal mode concepts and are discussed for distorted models and nonlinear dynamic systems. Brief consideration is given to thermal scaling of geometrically similar structures. The theoretical aspects of narrow-band random response characteristics are presented and approximate equations derived for the type of structural transfer functions employed in this report.

Section IV contains a comprehensive discussion of the full scale and model Snark structures and the design and development of the structural model. Also discussed are the accessories in the full scale vehicle which could alter the local structural dynamic characteristics. The deviations and compromises in the construction of the model are presented.

The description of the test facilities, instrumentation, data recording and noise source is presented in Section V, along with the test objectives.

The measured full scale structural responses are discussed in Section VI in terms of vibration transfer functions, defined in that section, which relate the response at one point to random excitation over a given area of the surface at another location. The responses are discussed for different classes of structural components such as bulkheads, longerons and panels. A detailed discussion is given of the comprehensive response survey made on surface and internal structure in a compartment of the full scale structure. The responses obtained in the present test program for localized excitation are compared with the acoustically induced response from booster rocket firings.

Section VII compares the model and full scale responses and interprets certain differences in these responses in terms of compromises made in model construction. Model and full scale comparisons are also made for panel, bulkhead, longeron and floor natural frequencies and associated damping factors.

Section VIII summarizes the various conclusions resulting from the experimental program and from the analysis of the measured response data.

PURPOSE

The purpose of this program has been to provide an experimental tool capable of predicting the vibratory response of typical flight vehicles. The program is based on several straight forward needs. These are to uncover the probable response of substructure located adjacent to surface structure, to provide quantitative understanding of vibration transmission through complex structures, and to relate external acoustic fields to the internal vibration levels. The failure sensitivity of substructure adjacent to surface structure has previously been established. The planned approach to the problem consisted of -

- Design, construction and test of a 1/4 scale dynamically similar structural model, a portion of the SM-62 fuselage
- Procurement of a scaled solid propellant rocket engine
- A series of tests which proved the similarity of the structure
- Excitation from the scaled engine where the response of the model structure and equipment would be compared to previously measured responses of full scale structure and equipment under parallel conditions.

For this program emphasis is placed on the response of structure, and response of equipment is considered of secondary importance.

BACKGROUND

The SM-62 missile (Snark) encountered excessive acoustic environments in 1953 from two solid propellant rocket engines of 260,000 lbs. total thrust. Boosters lying on either side of the fuselage generate thrust of approximately the same amount as that presently available on the Atlas missile to provide zero launch capability. Excessive response of electronic guidance equipment occurred in locations adjacent to nozzles of the side mounted rocket boosters. Extensive testing was done using full scale hardware to determine the nature of the entry of the oscillatory energy from the rockets to the structure. Indications were that an acoustic load path was involved although previously it was generally held to be mechanical transmission of thrust variations.

These 1955 studies therefore were designed to separate mechanical and acoustic paths of transmission by isolating the solid boosters from flight vehicle structure. Nine ground firings backed up by extensive instrumentation generated an unparalleled fund of simultaneous vibration and acoustic data helpful in relating external acoustic excitation to internal vibration response. This extensive data pool was available for substantiating the dynamically similar structural model as an experimental tool of satisfactory accuracy for vibration and acoustics studies during design.

NEED

Since first beginning the study of dynamically similar structural models for the vibration and acoustic area, the possible niche to be filled by this design tool has broadened. At present the designer is fortunate to be given even an approximate idea of the vibration environment which the structure will have to withstand in service. As a result of insufficient information to work with, the designer's task is subverted and appears as redesign and retrofit following the gathering of supplementary test data on prototype vehicles. Several reasons can be suggested to explain why the design attack is not more effective:

- The problem is obviously complex, highly nonlinear, new phenomena such as fatigue damage due to random loading are regularly uncovered.

- Breakdown of the classical analytical approach.

- Experimental work done is inappropriate and inadequate for application to this particular class of problems.

However, the lack of reliability through the design process is not due to these reasons. Rather, the lack results from the fact that no direct use of the design staff is presently accomplished in the vibration and acoustic area in designing reliability into a new vehicle during the design period. Environments are measured on prototype hardware and qualification tests are conducted on completed equipment. This is not reliability by design but reliability by test. It is after-the-fact engineering. Quality control and reliability groups do not function in this problem area during the design period. Reliability by test is a natural consequence of an inadequate state-of-the-art to predict the environment, the responses and the material damage that results. The positive approach of establishing a quantitative amount of reliability for a particular project cannot be handled by the design staff.

The need exists for the initial solutions to the vibration and acoustic problems during the earliest period when the design is being laid down. Configurational research should account for the impact of high energy exhausts on vehicle structure, and should select power plant of least oscillating energy input, and generally tailor the vehicle to avoid this class of problem. When the Snark vehicle was changed from normal aircraft take-off to zero launch capability and the large solid boosters of 50 fold increase in thrust were strapped on to the center of the fuselage (and even larger increases in environment adjacent to the electronics bays took place), the reliability was compromised to the degree that no amount of testing or analysis within the existing state-of-the-art would be able to salvage the vehicle reliability.

REQUIREMENT FOR RELIABILITY APPROACH

The present design criteria approach to structural design depends on a large number of similar designs which precede the current design and from general past experience, a satisfactory feedback of distilled experience is a factor in new designs. A new approach to structural design is predicted for the future which will, in part, incorporate reliability concepts. A melding of the best of two concepts would appear likely and is suggested in Reference 2. Aerospace structures are not compatible with the design criteria model which holds that, given a full scale item of hardware, a test program can be conducted based on loads criteria that qualifies structure for use within its stated mission. The margin of safety is a critical factor based on cut and try from past examples. The whole procedure supposedly results in structure with zero probability of failure. This model has less usefulness in missile and spacecraft areas, where knowledge of the loads, the interaction of the loads, the failure modes and their interaction has been less extensively studied and tested. We are led to the need for the reliability approach by several routes.

- The probabilistic nature of the random loading spectra from acoustics, high intensity turbulence, primary and dynamic loads.
- The probabilistic nature of the failure mechanisms.
- Combined load interaction and combined failure mode interactions.
- Need to define reliability budget allocations for all structure and equipment.
- Poor state-of-the-art in vibration prediction, 6db or 100% error. The error must be assessed and the probability of its occurrence developed.
- Material allowables for new materials will be difficult to establish because of the dispersion of material properties. Reference 3.
- Fabrication variability.

Variability of structural dynamic characteristics is felt not to be a significant factor.

Freudenthal in Reference 2 develops an integrated approach to structural design combining the useful features of the safety factor and the reliability approaches. The problem of statistical confidence arises in attempting to attach numbers to statistical reliability. Lundberg, Reference 4, speculates on predicting the safety levels of the supersonic transport, suggesting it is not possible to guarantee the same fatigue safety level for the supersonic transport as for subsonic aircraft, even at the expense of such high weight penalties as to render it economically unfeasible. The conclusion is mainly based on study of the materials and temperature problem as related to fatigue. Thus, the weight penalties due to the uncertainties were greater than the weight penalties due to temperature. Rather clearly some pitfalls will exist in mathematically measuring structural reliability consistent with statistical theory.

Serious new problems exist in all structural fields--the need for 30,000 hour structure, the need for new materials of unusual performance, high temperature structure and one dimensional structure where one dimensional structure suffices, two dimensional structure where two dimensional structure is all that is required, etc. These unusual needs in the past have usually served only to bring about spectacular and costly failures. Blake, Reference 5, states the uncertainties involved in choice of a test level are too large and numerous to be dealt with by intuition or by making simplifying assumptions on the safe side. His field of interest is vibration qualification testing for which statistical decision theory furnishes a technique for solving the problem of the choice of an optimum test.

Vagueness in engineering is dealt with in each of the above three references. Considerable quantities of new data must be generated to develop the fundamentals in these complex new approaches. New information and new thinking will often be required merely to identify the major sources of lack of reliability.

The tasks which structural models may eventually cover cannot be stated at this time. Problems with size effects, stress gradients and fundamental material behavior intervene in determining their place. However, these impeding variables will fall under intensive study, and if application of new knowledge about these effects is successfully made to the dynamic model, it becomes not only a tool for qualitative and feasibility studies but a quantitative tool as well.

Further need for the proposed tool, however, arises from:

1 Complexity associated with

   nonlinearity of structure and the failure modes such as fatigue failure

   random loads and responses

   three dimensional nature of the excitation, acceptance, transmission and response

   necessity to deal dynamically with all substructure, equipment and dynamically significant items such as heavy masses and liquid fuels

2 Breakdown, perhaps temporary, of the classical analytical approach

   empirical correlation has proven to be the most useful of the analytical approaches and in good hands may be expected to provide a 6 db or 100% error in prediction accuracy.

3 A design tool for design studies to allow the determination of

proper tradeoffs and to establish the significance of various parameters.

4 Combined loads and their interaction and combined failure modes and their interaction

5 New phenomenon of high intensity turbulence is brought about by rather heavily compromised aerodynamics. Separated flow, wakes, base pressure fluctuation and oscillating shock are both a source of direct structural failure and structural vibration leading indirectly to failure.

6 Different vibration transmission characteristics of different vehicles

REQUIREMENT FOR A DYNAMIC MODEL BASED ON LATEST STUDIES IN FATIGUE

The greatest need for the dynamic model may have been established by recent studies in fatigue. An explanation of the very low stress levels associated with acoustic fatigue failures and of the paradox of 2 - 3 second failures of several missile types during launch at the time of transonic or maximum g flights has been obtained. Repeated measurements of acoustic fatigue failures on service vehicles show the stress levels are of the order of 1000-2000 psi rms in aluminum as opposed to 4000 psi given in NASA TN D1 as the endurance limit for panels exposed to jet noise. These rms levels are an order of magnitude below the constant load level endurance limit. Since neither the influence of stress concentrates nor the peak to rms stress ratio nor their combination yields significant calculated damage, an explanation of the service failures is required.

Random loading and response has been studied by Freudenthal (Ref 6) and Valluri (Ref 7) and shows several aspects of fatigue damage due to random loading. Linear cumulative damage in its previous form does not apply as a result of the experimental and theoretical studies, the cumulative damage fraction reaching .2 in aluminum and .1 in steel as opposed to 1.0, accepted as the previous criterion. See Figures 1 and 2. Figure 3 shows the various aspects of fatigue graphically presented. The S-N curve, the loading history, the damage density and the strength remaining are presented. The latter item has also been presented by Valluri and has some substantiation at present as his studies show. Thus other aspects of random damage are reduction in remaining strength, lowering of the endurance limit and damage over a broad stress range which precludes sinusoidal testing. (Ref 11)

Acoustic fatigue service failures are characterized by other loadings on the panels and substructures. Air flow will give pressure loads perpendicular to the panel and other structural loads give in-plane tension and compression. Acoustic fatigue is a combined loads problem, therefore, a fact substantiated by experience in several major weapon systems.

Assessments based on the above inputs were made by Wang in References 8 and 9 and the second major contributing factor, (the first was the several aspects of random damage), was uncovered. Bouton[10] had previously shown the probability of failure behaved rather uniquely as the fatigue damage process continued. Where it would be reasonable to expect that the probability of failure tended to remain at a very low value throughout the fatigue life of any given part and then to rise precipitously just before failure, calculations show, for primary loading spectra derived from Freudenthal's work, that the reverse is true. The probability of failure rises precipitously during the initial phases of the damage process. Wang's contribution consisted of showing that insufficient explanation for acoustic fatigue failures resulted from the acoustic stresses alone even when coupled with Valluri's strength remaining concept but that if random spectra were simultaneously applied, very small acoustic stresses would provide as much as an order of magnitude increase in the probability-of-failure. See Figures 4 and 5.

Further, the acoustic fatigue problem may have been the first combined load problem very damaging on a large scale. But other phenomena of the same type, high intensity turbulent loadings, loom as more intense loadings and should give rise to major structural difficulties in the future. The missile failures possibly associated with combined loads such as primary, separated flow and oscillating shock impinging at one location in structure are occurring in the short 2 - 3 second period of transonic and maximum g flight. This paradox would tend to include all the phenomena discussed above: combined loads, the various aspects of random damage, and random spectra simultaneously applied. These qualitative assessments are not based on demonstrable test data but represent progress in assessing probable causes on which experiments may be based. See Figures 6 and 7.

The nature of the findings is such as to define basic problems which are not correctable in the sense that now that this is known the solution is obvious. Improved material, lessened environment, different mission or a new configuration do not apply. The depth of the problem has been magnified. Improved fatigue resistant structures may barely keep pace with the upward trend of the environment. Thus it is seen that a dynamics tool is definitely a necessity for the future. It is expected to become the primary tool capable of integrating loads, structural characteristics, responses, failure modes and their interactions. The attack on reliability during the early design period is probably best instituted using this experimental tool. The following work will show that the same model usable for dynamics, vibration, and acoustic studies handles thermal problems and transient heat flow as well. Other capabilities and advantages are listed in Table I.

Primary purpose of the model development in this study has been in the field of vibration and acoustics where the difficulties in predicting the response of structure and providing satisfactory hardware presently

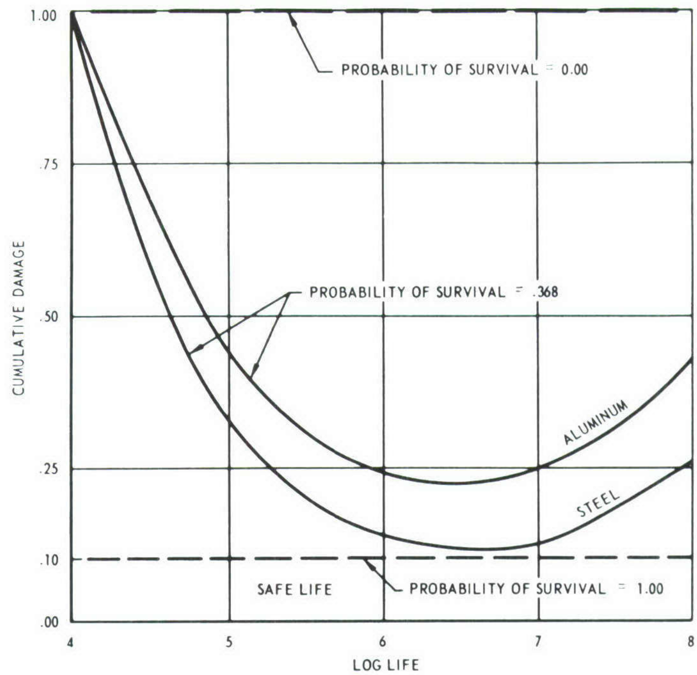

FIGURE 1 FREUDENTHAL'S EXPERIMENTAL DATA

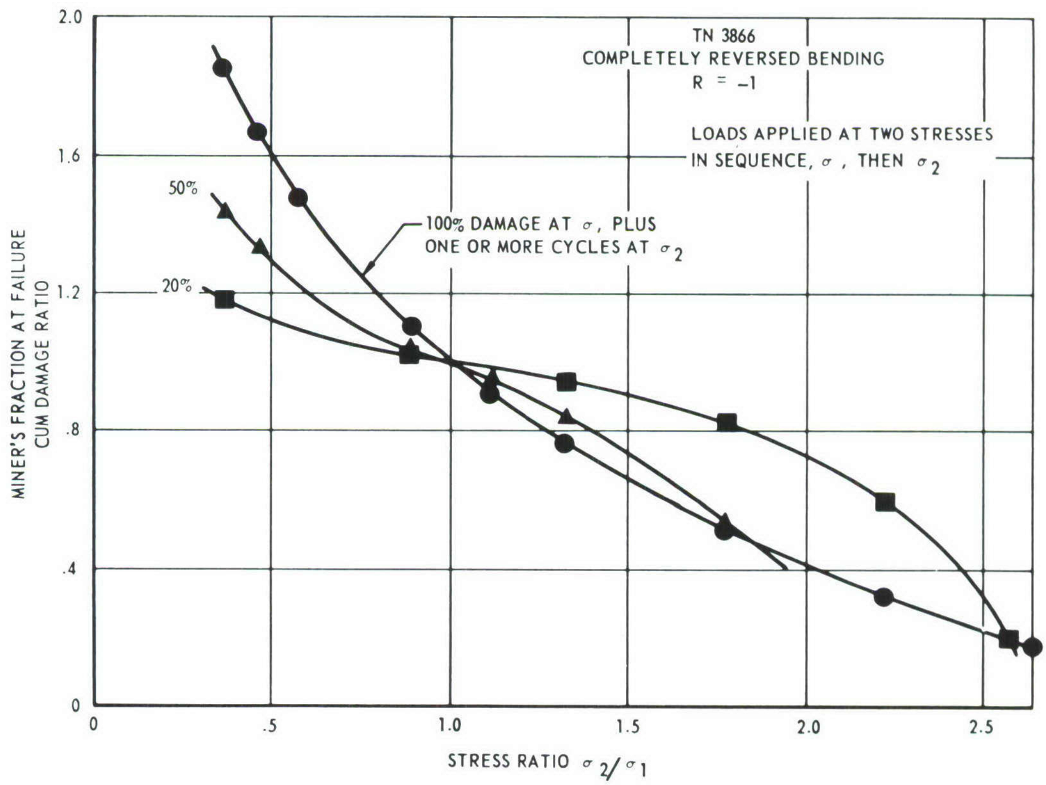

FIGURE 2 VALLURI TWO STEP FATIGUE

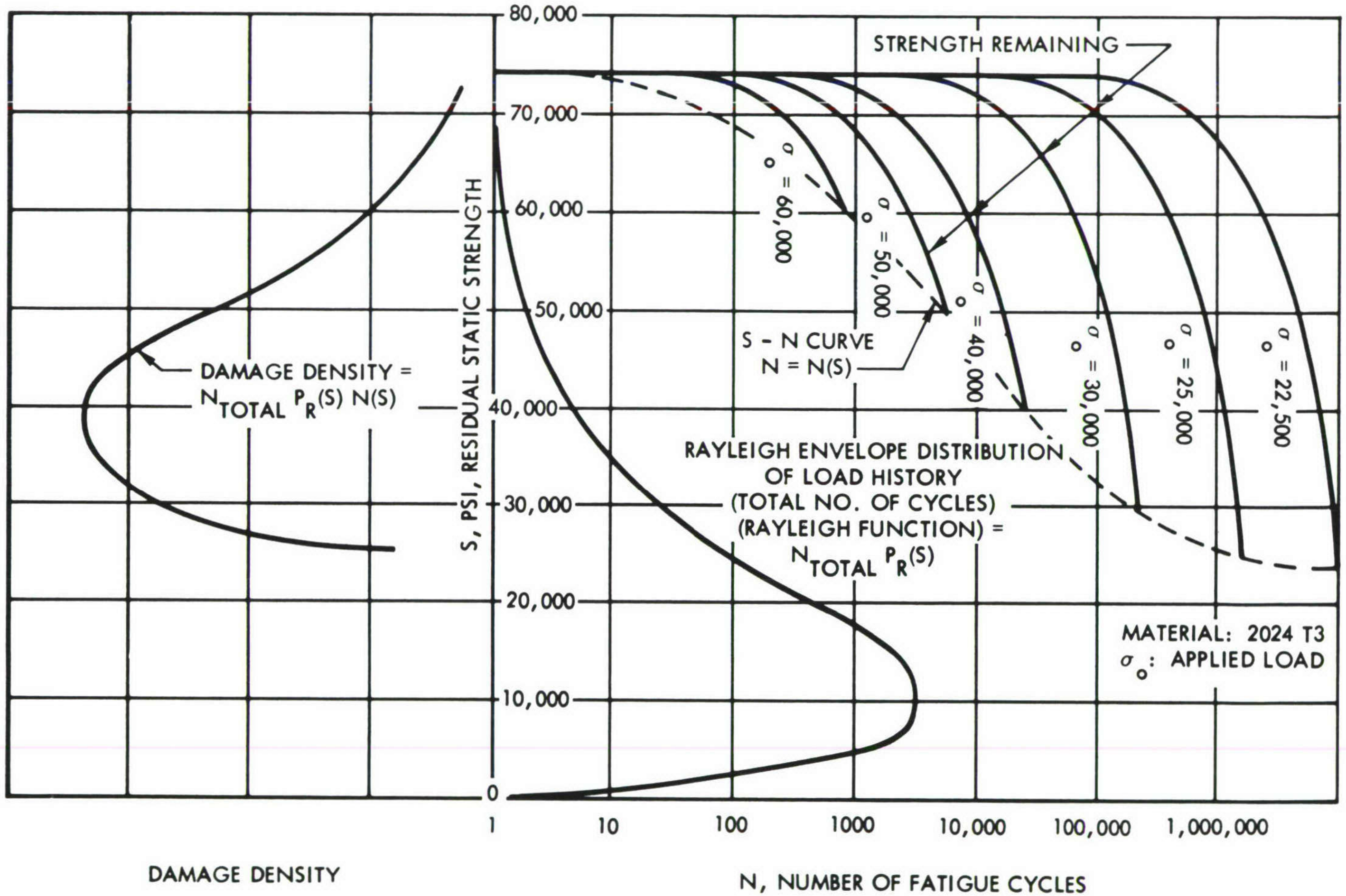

FIGURE 3 THE FOUR SIGNIFICANT ELEMENTS, THE S-N CURVE, THE STRENGTH REMAINING, THE LOAD HISTORY AND THE DAMAGE DENSITY

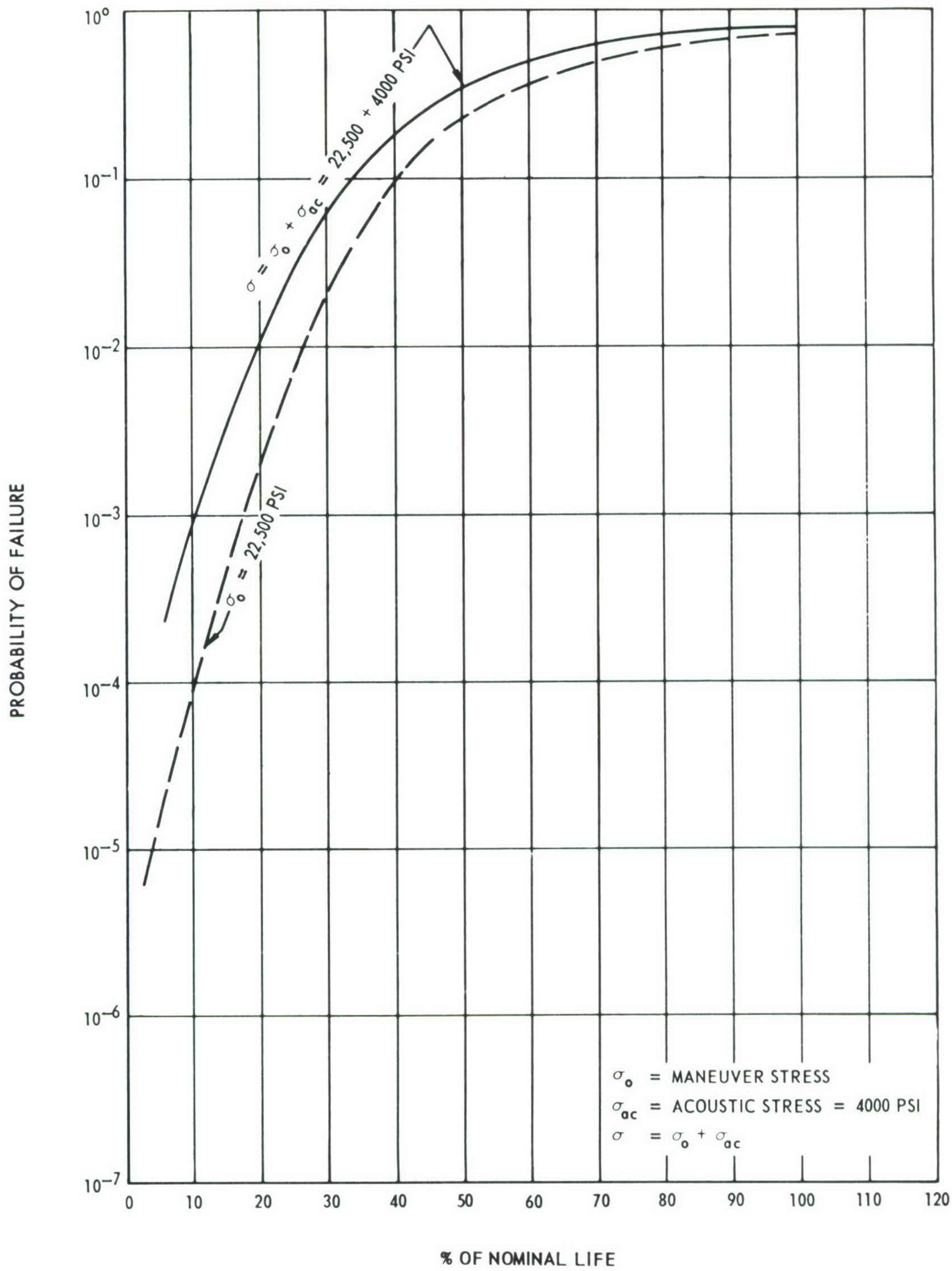

FIGURE 4 PROBABILITY OF FAILURE RATE OF TRANSPORT AIRCRAFT (MIL-A-8866) UNDER MANEUVER AND ACOUSTIC LOADS

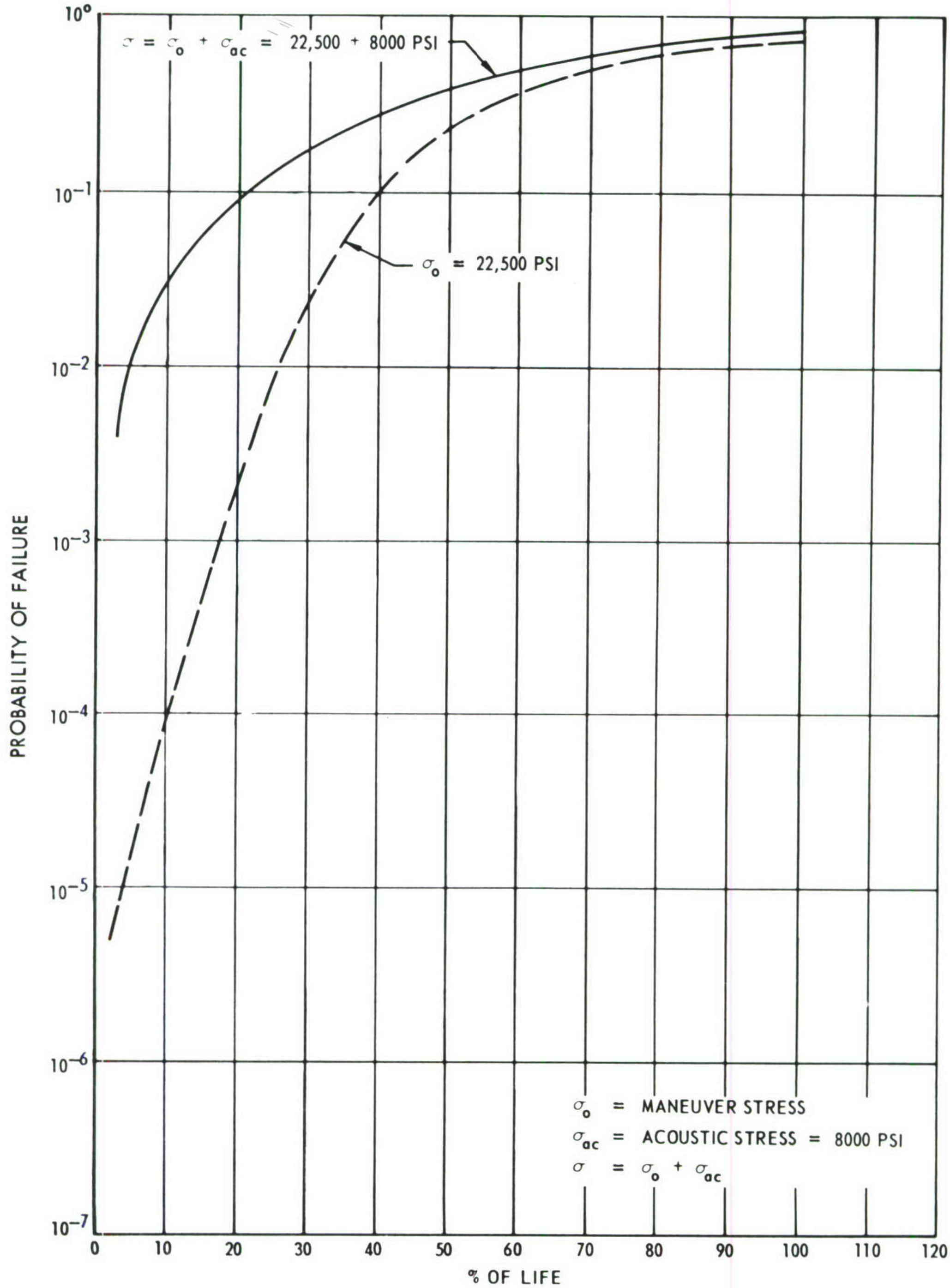

FIGURE 5 PROBABILITY OF FAILURE RATE OF TRANSPORT AIRCRAFT (MIL-A-8866) UNDER MANEUVER AND ACOUSTIC LOADS

ACOUSTIC	AERODYNAMIC	STATIC	DYNAMIC	TEMPERATURE
ENGINE NOISE	BUFFET	MANEUVER	WIND	AEROSPACE HEAT
CAVITY RESONANCE	SEPARATION	INERTIA	WIND SHEAR	ENGINE HEAT
	CONVECTED TURBULENCE	STEADY AIR LOADS	GUST	HOT SPOTS DUE TO TURBULENCE
	BASE PRESSURE FLUCTUATION	GROUND-AIR -GROUND	LAUNCH OR T.O.	
	OSCILLATING SHOCK		GROUND HANDLING	
	WAKES FROM DRAG DEVICES		LANDING GROSS VEHICLE MOTION DURING ENGINE RUNUP	
			MECHANICALLY TRANSMITTED THRUST OSCILLATION	

THE UNDERLINED AERO AND ACOUSTIC LOADS REPRESENT LARGE SCALE TURBULENCE

FIGURE 6 COMBINED LOADS

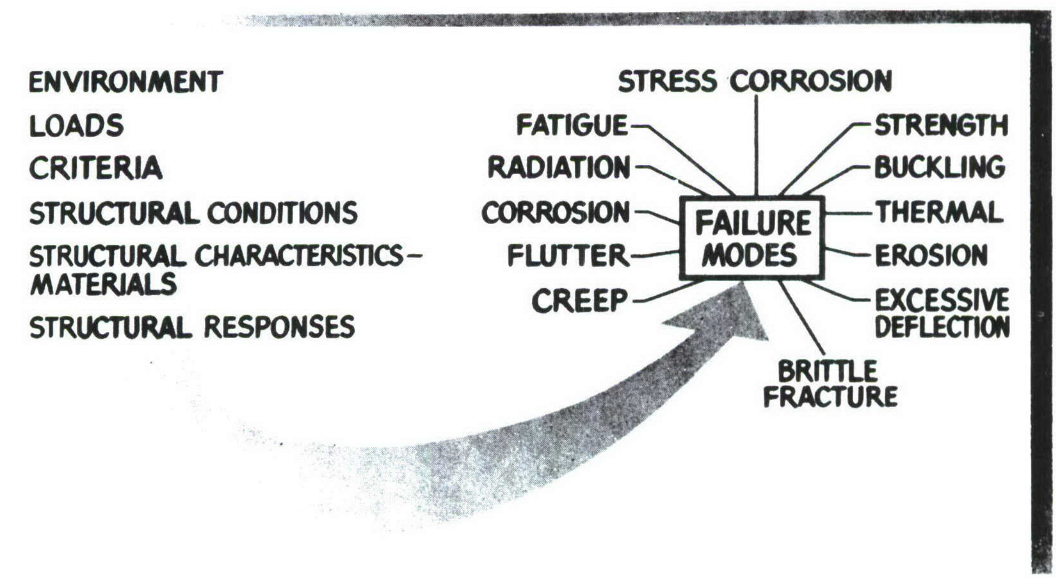

FIGURE 7 COMBINED FAILURE

TABLE I

DYNAMICALLY SIMILAR STRUCTURAL MODEL

The many uses of the dynamically similar models as a design tool include:

1 The design period can be drastically shortened.

2 Structural and equipment reliability can be improved as a result of accurately defining the vibration and acoustic environment.

3 The fundamental modes of the complete vehicle can be measured for dynamics and flutter studies.

4 Structure can be optimized.

5 The separate contributions of mechanically and acoustically transmitted excitations can be measured by firing the engines both attached and detached.

6 More accurate predictions of the fatigue life can be made.

7 Aerodynamic excitations can be measured in the wind tunnel.

8 The effect of variations in configuration or of devices or arrangements to attenuate the excitation reaching the vehicle can be investigated.

In addition to the opportunities the model gives to measure the above quantities, an additional advantage is a large reduction in test time. Test time is shortened for the following reasons:

1 Time scale is shortened proportionately to the scale factor.

2 The scaling laws applicable to fatigue failures, provide early failure in model scale (Reference 12).

3 Further contraction is possible if desired through an arbitrary buildup in the test loads. Time temperature interaction is understood in many areas allowing acceleration of temperature testing. (Reference 13).

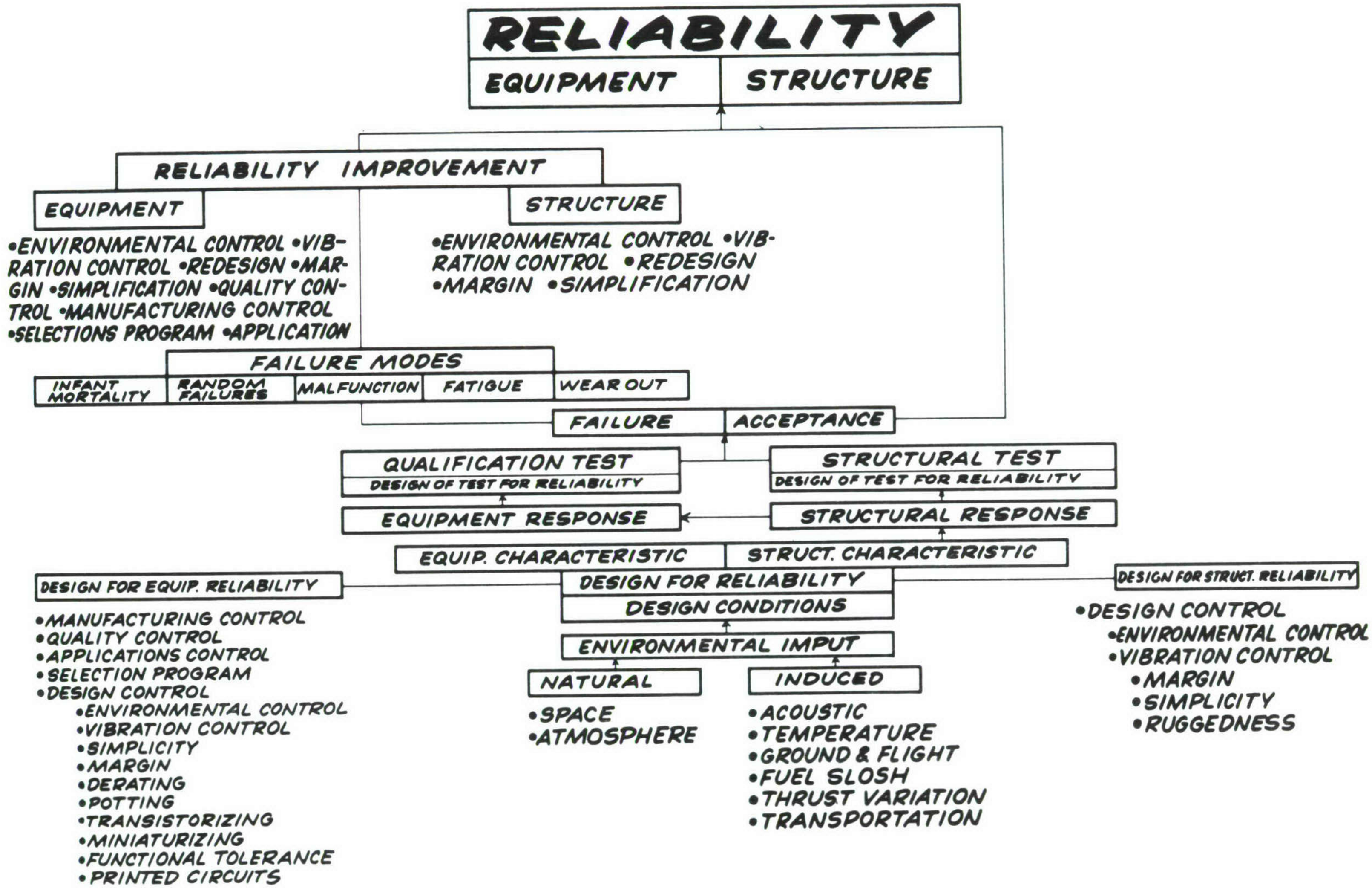

FIGURE 8 KEY DESIGN ELEMENTS OF THE OAL RELIABILITY PROBLEM

require a purely experimental approach. Where the weight of problems in this area may not always be sufficient cause to build a structural model, the other capabilities and needs may do so.

PREVIOUS WORK DONE

The importance of fatigue is that it underlies present difficulties in vibration and structural reliability as shown in Figures 7 and 8. It is a principle failure mode and interacts with most other failure modes. The impact of many of the findings reported above will be understood when the designer understands the restraints imposed by the problem on primary and secondary structure and equipment. A previous ASD-Northrop program was completed in an R & D fatigue study titled "Feasibility of Using Structural Models for Acoustic Fatigue Studies" designed to determine the answer to a basic question: can acoustic fatigue be reduced to model scale? The exploratory program induced acoustic fatigue failure in full scale structural panels with a jet engine and repeated the process in model scale using model jet engines. The model engine was based on a compressed air source, a burner can and a nozzle. Photos of the setup are included in Figures 9 and 10. The feasibility of scaling the entire sonic fatigue process - from jet flow through jet noise, panel dynamic simulation, and strain response to fatigue failure was demonstrated. Theoretical dynamic and jet noise scaling laws were achieved in a controlled manner. Near perfect scaling across the entire frequency band is shown in Figures 11, 12 and 13. Both the excitation recorded by a microphone at the center of the panel and the strain response at the downstream edge for two different panel designs and response characteristics were accurately scaled. The results are noteworthy and indicate that dynamic scaling in the frequency range of acoustic phenomena would follow precisely the same techniques in flutter models. Item-by-item scaling is used in both these cases, and in the relatively low frequency range of the flutter model, equally satisfactory success is achieved as experimental relationship for failure time results from the work and appears in Figure 14.

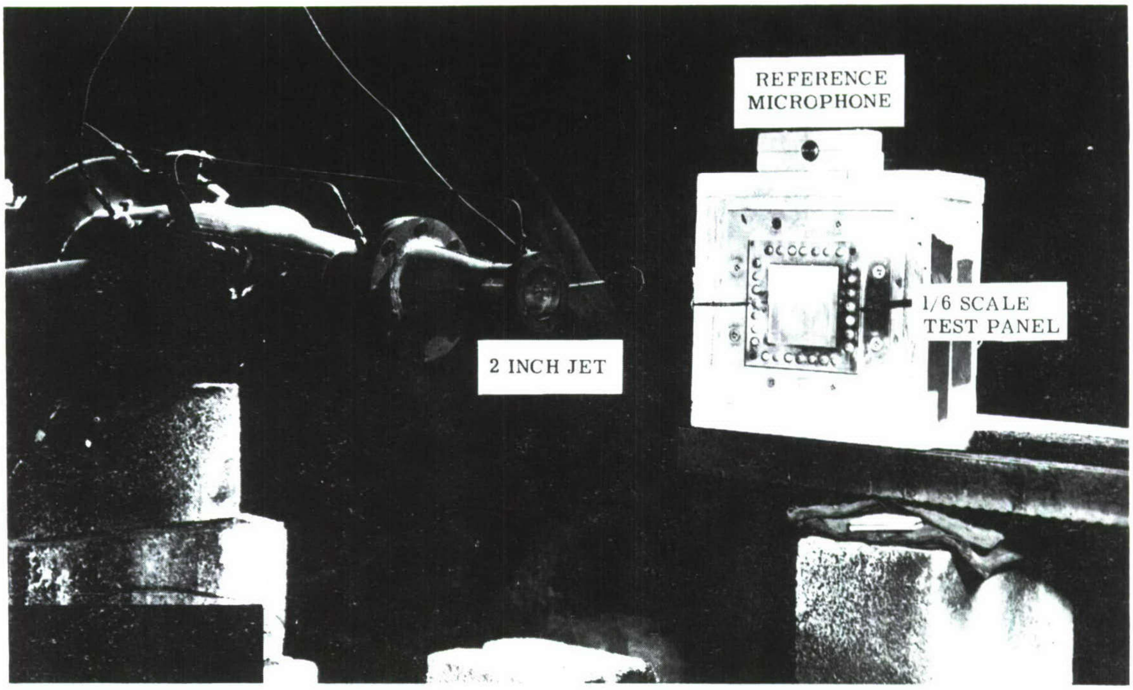

FIGURE 9 MODEL SONIC FATIGUE TEST SET-UP

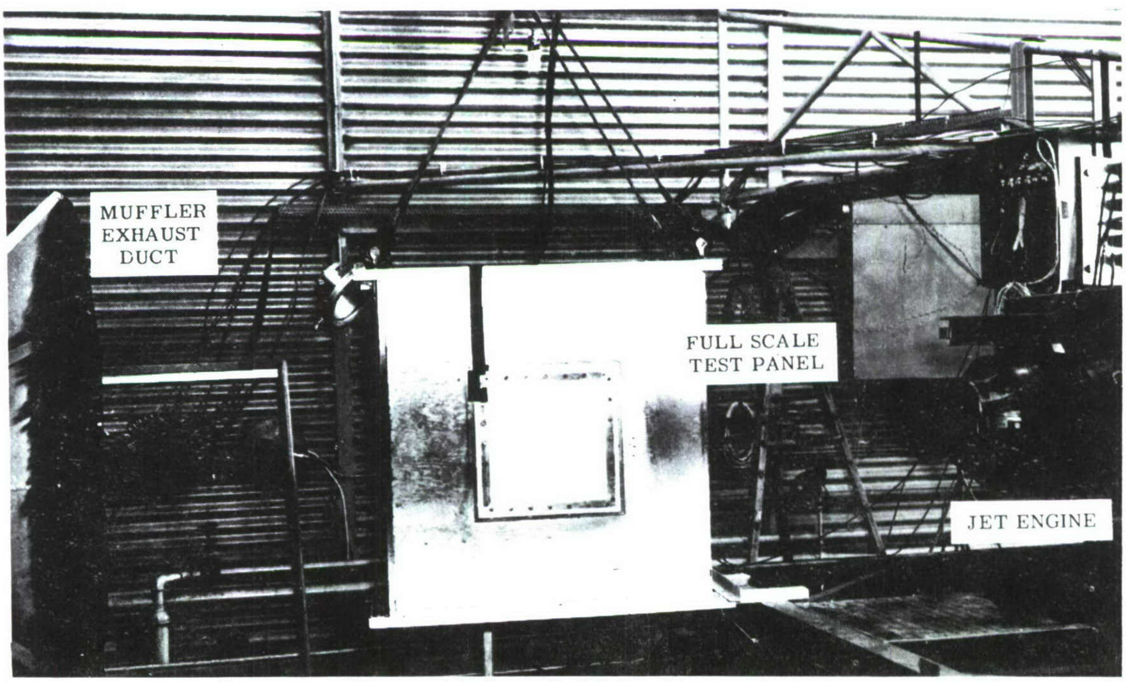

FIGURE 10 FULL SIZE SONIC FATIGUE TEST SET-UP

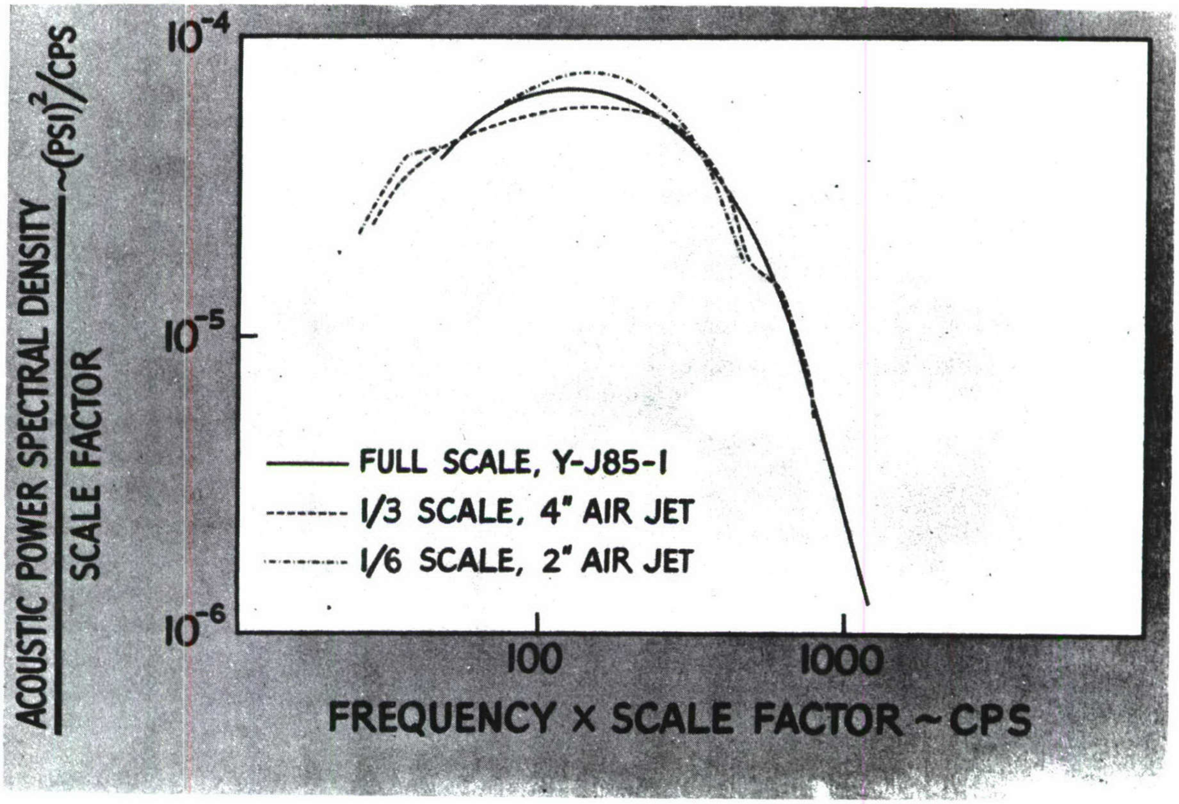

FIGURE 11 EXCITATION AS A FUNCTION OF FREQUENCY

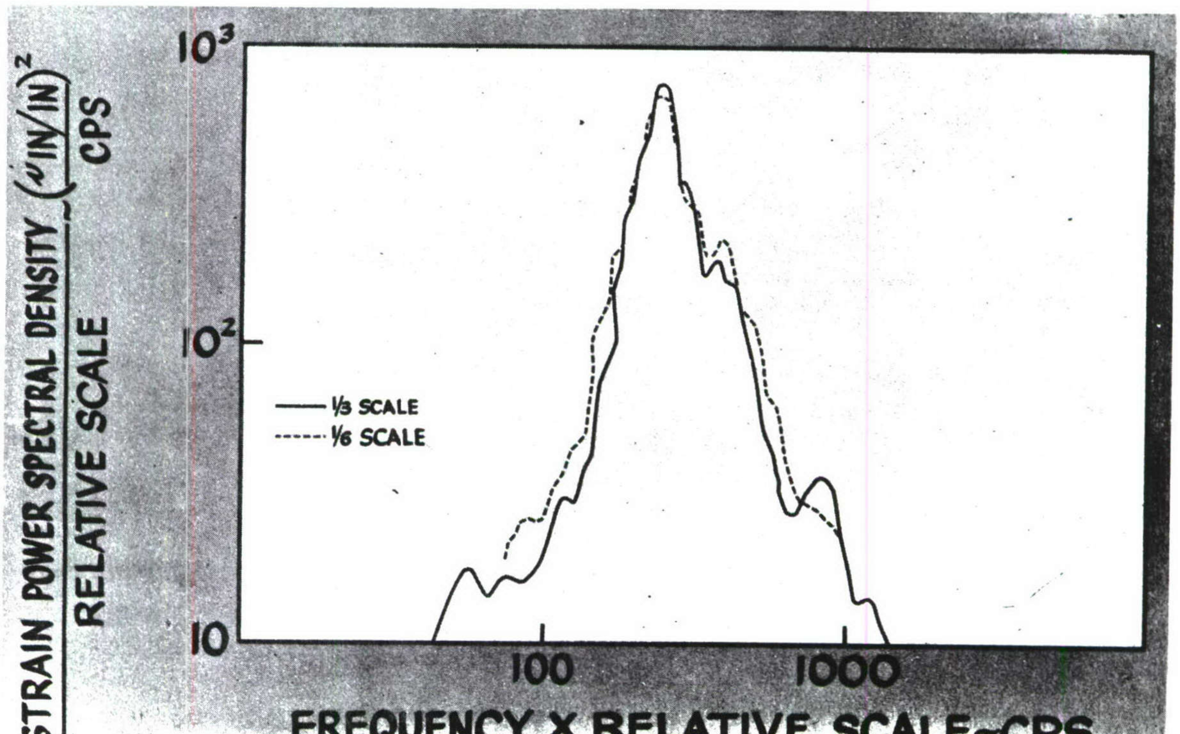

FIGURE 12 STRAIN POWER AS A FUNCTION OF FREQUENCY

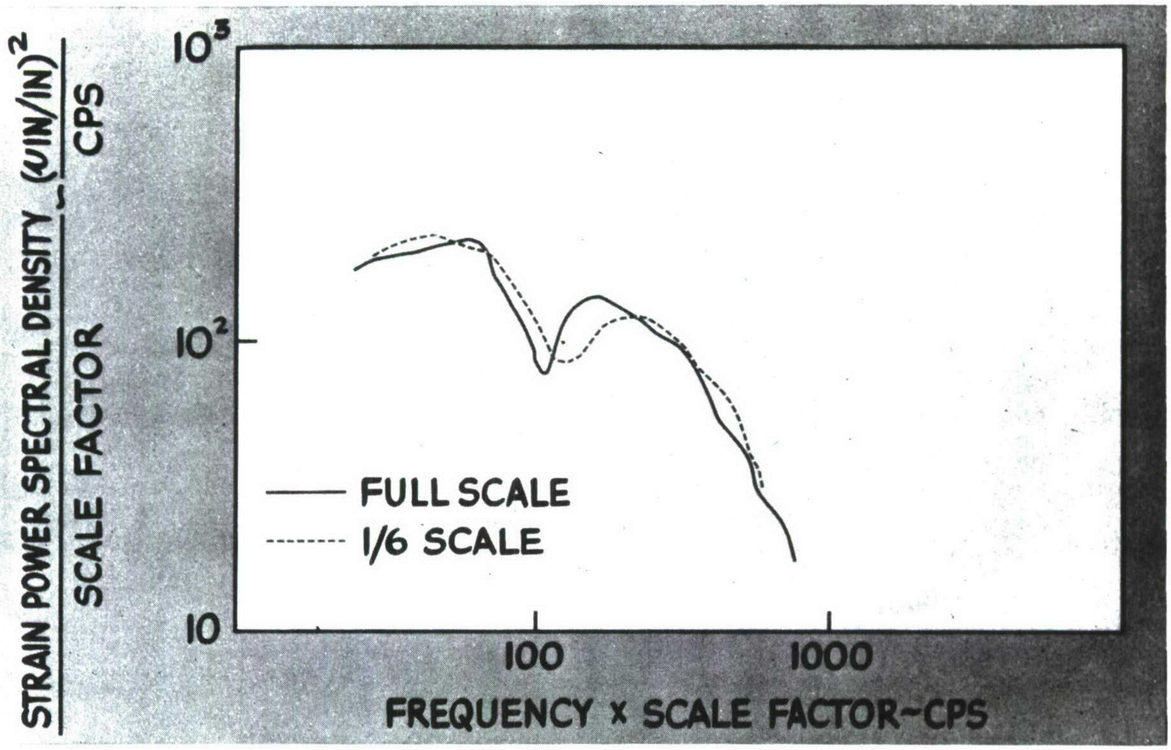

FIGURE 13 STRAIN POWER AS A FUNCTION OF FREQUENCY

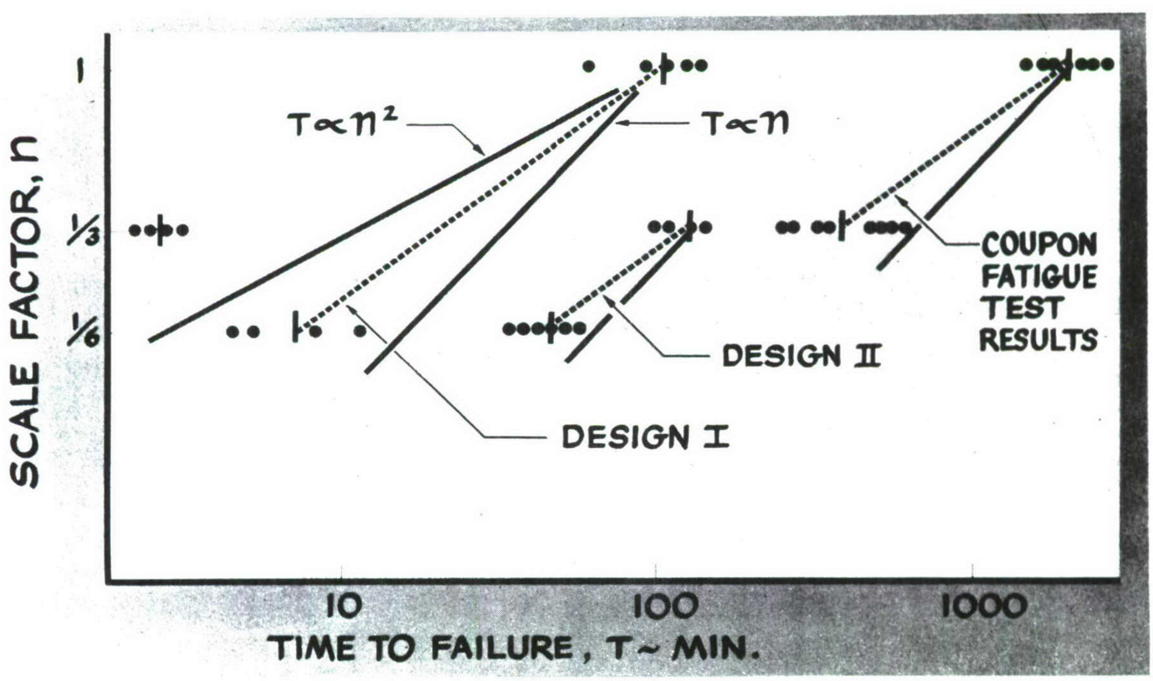

FIGURE 14 FATIGUE FAILURE TIMES-PANELS AND COUPONS

SECTION II

EXPERIMENTAL SUBSTUDIES

SUBSTUDIES IN SUPPORT OF MODEL DESIGN

The major question at the beginning of the program revolved around model design techniques. The degree of simulation was the largest of these questions. A search for simplification was felt to be an important step because of the opportunity to use the concept without high cost arguments intervening each time that it was to be applied. Technical problems concerned joint transmission, damping, and fabrication techniques. Typical full scale structural components in five separate designs were built in all cases followed by model parts tested under scaled conditions. The studies concerned are as follows:

- Damping
- Joint transmission, effect of amplitude
- Rivet versus bonding
- Bond line thickness
- Choice of bonding agent
- Rivet pressure and number of rivets

Drawings, photos, and a report of the damping studies are included in Figures E1 - E6. Five different bonding materials were investigated and most were shown to be unsuitable due to either brittleness or cracking. Hapex 1233 and EC1614 were judged to be satisfactory. The riveting and bonding comparison was somewhat surprising in that the damping associated with the bonded parts was 50 - 200% greater than that in riveted parts. Variations in bond line thickness were investigated from .003 to .030 and it was shown that the thick bond gave an 8% lower natural frequency and a 33% increase in damping in the design shown in Figure E5.

A principle decision to use riveted construction in the model, however, was based on the frequency comparison in design 3 bonded and riveted parts. Design 3 is a T-section where the joint depends on the bracing provided by two simple angles in the juncture point. The bonded joint was consistently stiffer to an unusable degree compared to the riveted joint, which is understandable in retrospect. This particular component was indicative of the way a panel is supported over a stringer or frame and was judged to be sufficiently important to invalidate the use of a bonded structure, in conjunction with the damping result obtained above. The design of these specimens avoided nonlinearity as it occurs in a panel and the resonance technique for measuring damping proved to be usable. No pains were taken in quality control and shop tolerances to determine what variance would occur from normal shop practice. Damping measurements on the other hand were attacked in three different ways. Considerable variability in results does exist and general conclusions regarding the damping were the only ones warranted by the data. Thus, the influence of amplitude in Figures E3 and E4 shows no nonlinearity, and agreement was obtained between model and riveted damping components. Further comparisions are made between the full scale complete vehicle structure with the model complete vehicle structure in Section V.

Figure E1 shows the details of the full scale structural components and the models of these components. Figures A42, A43, and A44 show the models. Figures E2, E3, and E4 show the test setup and the response curves for a hat section specimen with damping. Damping was measured by a decay technique in Figures E3 and E4 and by a resonance technique in Figures E5 and E6.

SECTION III

THEORETICAL BACKGROUND

STRUCTURAL VIBRATION SCALING LAWS

Fundamentally, the concept of modeling is one of comparison of two systems, which obey the same or analogous physical laws, for the purpose of obtaining the characteristics of the one system by operationally determining the corresponding characteristics of the other system. The basis for comparison is the use of scaling or modeling laws which mathematically relate corresponding characteristics of the two systems.

The use of models as experimental and even computational tools has a wide application for system analysis, and the many varieties of models employed are equally broad. Either of the two systems being compared on a model basis may be mechanical, electrical, acoustical, optical, thermal, pneumatic, aerodynamic or mathematical in nature. The role of the mathematical model is well defined for analyzing all types of physical systems, the only limitation being that all the physical phenomena occurring in the system be mathematically definable. The fundamental principle upon which modeling a system by the same or any other physical system is that the nondimensional form of the equations defining the two systems must be identical, or approximately so, for the regimes in which modeling is to occur. Such systems are said to be equivalent or similar. The choice of model for a given system is dictated by the ability of the model system to simulate the degree of detail required for the analysis of the primary system, by the methods available for measuring the input and output of the model system, and by the economics of designing and building the model.

The primary systems of interest in the present discussion are continuous mechanical vibratory systems and, in particular, complex built-up structures of the type employed in flight vehicles. The system characteristics of interest are the detailed structural response characteristics associated with excitation by an external random acoustic field. The only models of these structures to be considered here are equivalent mechanical vibration systems. The structural vibration scaling laws for these models are developed in this section.

Within the class of structural models to be considered it is possible to have models which are (1) geometrically similar and constructed of the same materials, (2) geometrically similar and constructed of different materials having the same elasticity to density ratio and generally the same Poisson's Ratio as the primary structure, (3) distorted models which are dynamically, but not geometrically, similar. The type of structural model desired for a given structural system depends upon the complexity of the primary system, the frequency range of the excitation and the type of excitation forces or pressures applied to the system.

For excitation frequencies at or below the first few structural natural frequencies, the associated structural wave lengths are long relative to structural discontinuities, joints and internal stiffeners so that many of the structural details can be neglected. In this case the structure can often be reduced to an equivalent elementary structure such as a beam, shell or plate, which can be tested experimentally for the desired excitation. Also, the continuous structural parameters can sometimes be lumped and replaced by equivalent simple mass, spring and damper elements forming a mechanical network. When a limited number of these equivalent networks is involved, the system is essentially reducible to direct mathematical or electrical analog analysis. Each of these models is dynamically similar to the primary structure in the above frequency range, although geometrically the two may appear to be quite different. This is often the case with gust and flutter models in which the wing structures are replaced by a single spar for stiffness distribution and a set of concentrated weights to simulate the proper mass distribution.

At higher excitation frequencies, the wave lengths of the propagating elastic waves are equal to the dimensions of many of the individual component elements of the structure. These elements then become resonant and interact with the propagating waves, causing attenuation, reflection, and only partial transmission of the vibratory energy. In general for built-up structures, the geometric and physical details become increasingly important with increasing excitation frequency. The structure no longer acts dynamically as a single unit but becomes a complex multi-branched transmission network at the surface and in the interior of the vehicle. In this frequency region, more refined geometric scaling is required in order to dynamically simulate the local structural vibration response characteristics.

The type of excitation applied to the structure also dictates the type of model required. If the surface pressures acting on the structure are fairly uniform over the surface and are non-propagating, the surface skins may require only geometric scaling in order to maintain a desired shape and area over which the pressures can act. This is often the case for distorted structural models used to determine response to aerodynamic loading. For many vehicles, a major source of excitation is the random noise field which surrounds the vehicle skin. This excitation, which has a broad frequency content, propagates over the skin and causes a coupled acoustic-structure wave phenomenon at the surface of the structure which determines the acceptance of acoustic energy by the structure. It is clear that for this type of excitation, the surface and subsurface mass and stiffness must be scaled as well as the surface geometry. As a third possibility, direct excitation of a flight vehicle structure by an attached engine would require careful modeling at the engine mounts, with the modeling of the remainder of the structure being determined by the oscillatory force direction, frequency content and amplitude.

Further, it is to be noted that for complex structures, dynamic similarity is not guaranteed by geometric similarity alone, since in addition, it is required that the interface pressures at joints and rivet lines be simulated. The major structural damping and the end fixity conditions for the component elements depend markedly upon this simulation.

In many complex built-up flight vehicle structures, nonisotropic materials such as honeycomb sandwich are used. Scaling all structural components constructed of these materials, maintaining the ratios of the elastic constants in each of the various directions insures the most accurate dynamic similarity for the frequency regions and loadings where these structural properties are important.

Structural vibration scaling laws are now derived which relate corresponding response quantities for the primary and model structures, in terms of preassigned scaling factors for size, elasticity, density, excitation frequency and applied pressure amplitude. This is done first for geometrically scaled linear structures consisting of isotropic, perfectly elastic materials which dissipate vibrational energy by mechanisms equivalent to those for linear viscous damping. Brief consideration is then given to the scaling requirements for non-isotropic, perfectly elastic materials. Following this, scaling laws are developed for vibrational energy and power. The normal mode concept is introduced and the scaling of mode shapes, generalized mass, stiffness, damping and force are considered. With this concept developed, the dynamic scaling of distorted models is discussed. Then the scaling requirements for a certain class of structures having nonlinear stiffness properties are considered. Finally, the dynamic scale laws are extended to include thermal scaling.

Scaling of Perfectly Elastic Materials

From elementary elasticity theory, the force in an elastic body due to strain is of the form

$$\mathcal{F}_{\epsilon} = A\sigma = AE\epsilon = AE\frac{\partial U}{\partial X}$$

where

σ = stress in the elastic body

A = area over which the stress acts

ϵ = strain associated with the stress

U = elastic deflection

X = coordinate along which strain occurs.

The strain force per unit volume is then of the form

$$F_\epsilon = \frac{d\,\mathcal{F}_\epsilon}{d\,V} = \frac{1}{A}\,\frac{d\,\mathcal{F}_\epsilon}{d\,x} = E\,\frac{\partial^2 U}{\partial x^2}$$

When this elementary strain force equation is refined to account for the effects of strains in directions orthogonal to the x-axis, the strain force per unit volume becomes (Ref. 1, page 234), for isotropic materials,

$$F_{i_\epsilon} = (\lambda + G)\frac{\partial e}{\partial x_i} + G\,\nabla^2 U_i$$

where

λ = Lame's constant = $\dfrac{E\,\nu}{(1+\nu)(1-2\nu)}$

E = Young's modulus of elasticity

ν = Poisson's ratio

G = modulus of rigidity in shear = $\dfrac{E}{2(1+\nu)}$

e = dilatation = $\dfrac{\partial U_1}{\partial x_1} + \dfrac{\partial U_2}{\partial x_2} + \dfrac{\partial U_3}{\partial x_3}$

$\nabla^2 = \dfrac{\partial^2}{\partial x_1^2} + \dfrac{\partial^2}{\partial x_2^2} + \dfrac{\partial^2}{\partial x_3^2}$

If L denotes some typical structural dimension, then the component strain forces per unit volume may be written in the nondimensional form

$$\overline{F}_{i_\epsilon} = \frac{1}{2(1+\nu)}\left[\overline{\nabla}^2 \overline{U}_i + \frac{1}{1-2\nu}\,\frac{\partial \overline{e}}{\partial \overline{x}_i}\right]$$

where

$F_{i_\epsilon} = \dfrac{E}{L}\,\overline{F}_{i_\epsilon}$

$U_i = L\,\overline{U}_i$

$x_i = L\,\overline{x}_i$

$e = \overline{e}$

$\nabla^2 = \dfrac{1}{L^2}\,\overline{\nabla}^2$ the bars denote dimensionless quantities

In rectangular coordinates, the equations of equilibrium of an elastic body are

$$F_{i_\epsilon} + F_i^* = 0$$

where F_i^* denotes body force components per unit volume. In a mechanical vibratory system, the body forces consist of inertia and damping forces. The inertia force components are

$$F_{i_I} = \rho \frac{\partial^2 U_i}{\partial t^2}$$

ρ = mass density of the material.

This force has the following nondimensional form

$$\overline{F}_{i_I} = \frac{\partial^2 \overline{U}_i}{\partial \overline{t}^2}$$

$$F_{i_I} = \frac{\rho c^2}{L} \overline{F}_{i_I} = \frac{E}{L} \overline{F}_{i_I}$$

$$t = \frac{L}{c} \overline{t}$$

$$c = \sqrt{\frac{E}{\rho}}$$

= velocity of sound in the material

The linear viscous damping force per unit volume has components of the form

$$F_{i_D} = \rho D \frac{\partial U_i}{\partial t}$$

D = linear viscous damping capacity per unit volume of material = ω_0/Q, for harmonic oscillator.

Expressed in nondimensional form, the damping force is

$$\overline{F}_{i_D} = \frac{\partial \overline{U}_i}{\partial \overline{t}}$$

$$F_{i_D} = \rho c D \overline{F}_{i_D}$$

The nondimensional equations of equilibrium are then

$$\overline{F}_{i_I} + \frac{LD}{c}\overline{F}_{i_D} + \overline{F}_{i_\epsilon} = 0$$

or

$$\frac{\partial^2 \overline{U}_i}{\partial \overline{t}^2} + \frac{LD}{c}\frac{\partial \overline{U}_i}{\partial \overline{t}} + \frac{1}{2(1+\nu)}\left[\overline{\nabla}^2 \overline{U}_i + \frac{1}{1-2\nu}\frac{\partial \overline{e}}{\partial \overline{x}_i}\right] = 0 \qquad (1)$$

These equations must be satisfied at every interior point of any perfectly elastic body composed of isotropic materials having linear viscous energy dissipation.

Two geometrically similar structures are dynamically similar throughout if at all corresponding interior points the nondimensional deflections, U_i/L are proportional at each instant, $\frac{c}{L}t$. From the equations of equilibrium, this is possible in general only if Poisson's ratio, ν , and the damping ratio, LD/c, are the same for both structures. These conditions are seen to be necessary, but not sufficient, for dynamic similarity since the equilibrium equations admit an infinity of solutions, where a unique solution depends upon the boundary conditions at the surface of the structure. It is important to note that the nondimensional deflections may be proportional, and not necessarily equal, because of the linearity of the equilibrium equations. It is shown later that for nonlinear structures, equality is required.

The boundary conditions at the surface of an elastic body are given by the equation (Ref. 1, page 234)

$$P_i = \lambda e \gamma_i + G\left[\frac{\partial U_i}{\partial x_j}\gamma_j + \frac{\partial U_j}{\partial x_i}\gamma_j\right]$$

where j is summed over 1,2,3, and where

P_i = applied surface tractions, per unit area

γ_j = direction cosines at the surface

In nondimensional form these boundary conditions are

$$\overline{P}_i = \frac{\nu}{(1+\nu)(1-2\nu)} e\gamma_i + \frac{\gamma_j}{2(1+\nu)}\left[\frac{\partial \overline{U}_i}{\partial \overline{x}_j} + \frac{\partial \overline{U}_j}{\partial \overline{x}_i}\right]$$

$$P_i = E\,\overline{P}_i$$

Thus a third necessary condition for dynamic similarity of geometrically similar structures is that the nondimensional surface tractions, P_i/E, must be proportional at corresponding surface points. Note that the surface tractions include both the applied surface pressures and those tractions associated with structural constraints.

Once the proportionality of the surface tractions is specified, then the proportionality of the deflections is known since the surface deflections uniquely determine the deflections at all interior points of the structure. Let P_o be a constant which denotes the absolute magnitude of the surface tractions at some reference point of the structure. Then the above equations show that for two geometrically and dynamically similar structures, the following quantities are invariants, that is, they are equal for both structures:

$$\frac{U_i}{P_o L}, \quad \frac{P_i}{P_o E}, \quad \frac{L D}{c}, \quad \frac{c t}{L}, \quad \frac{\epsilon}{P_o}, \quad \frac{\sigma}{P_o E}, \quad \nu$$

The first two quantities being compared at corresponding points on the two structures. For linear structures, an equivalent, and more convenient set of invariants is the following

$$\frac{U_i}{L(P_o/E)}, \quad \frac{P_i}{P_o}, \quad \frac{D}{c/L}, \quad \frac{t}{L/c}, \quad \frac{\epsilon}{P_o/E}, \quad \frac{\sigma}{P_o}, \quad \nu$$

The second invariant, P_i/P_o, merely states that the distribution of surface tractions must be the same for both structures.

When the surface tractions, such as acoustic pressures, propagate over the surface of the structure, additional modeling requirements may have to be imposed in order that P_i/P_o be the same at corresponding points and corresponding times for the primary and model structures. This is most easily demonstrated in terms of the following elementary example.

Consider a steady state, plane, acoustic wave of frequency ω, impinging on a flat surface at an angle θ, and let C_o denote the acoustic propagation velocity. The fluctuating acoustic pressure at time t and position x is given by the expression

$$P = P_o \sin \omega \left[t - \frac{1}{C_o} \sin\theta \cdot x \right]$$

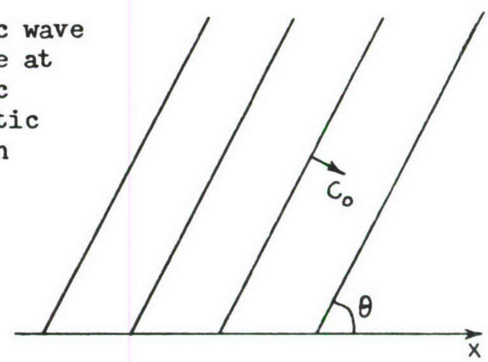

The quantity ωt is nondimensional and must be a model invariant so that $\frac{\omega}{c/L}$ must be a model invariant. Thus, in nondimensional form the pressures are

$$\frac{P}{P_o} = \sin \bar{\omega} \left[\bar{t} - \frac{c}{c_o} \sin\theta \cdot \bar{x} \right]$$

where

$$\omega = \frac{c}{L} \bar{\omega}$$

$$x = L \bar{x}$$

It follows that the quantity $\frac{c}{c_o} \cdot \sin\theta$ must be an invariant. In most cases the speed of sound, c_o, is not a variable so that $c \cdot \sin\theta$ is invariant. The impinging acoustic field used in structural model experiments may be aerodynamically generated in a jet exhaust. For such a field, impinging acoustic waves occur for all angles, θ, in a given angular range; and, because of restrictions on the direction of exhaust flow, these angles may have to remain unchanged. In this case, the material wave velocity, c, or $\sqrt{E/\rho}$, must be a model invariant.

For nonisotropic (aeolotropic, anisotropic) perfectly elastic materials the elastic constants for tension, compression, and shear are different so that the expression for the strain force has the more general form:

$$F_{i_\epsilon} = E_{ijk} \frac{\partial^2 U_j}{\partial x_j \partial x_k}$$

where j and k are summed over 1,2,3. The E_{ijk} are the elastic constants of the material. This equation can be nondimensionalized to give

$$\bar{F}_{i_\epsilon} = \beta_{ijk} \frac{\partial^2 \bar{U}_j}{\partial \bar{x}_j \partial \bar{x}_k}$$

$$F_{i_\epsilon} = \frac{E}{L} \bar{F}_{i_\epsilon}$$

$$\beta_{ijk} = \frac{E_{ijk}}{E}$$

where E is a typical elastic constant belonging to the set E_{ijk}. This nondimensional equation for strain force is the same as that for isotropic materials. Hence structures consisting of nonisotropic materials can be geometrically and dynamically scaled so that the above scaling laws are valid, if the nondimensional ratios of the elastic constants in the structure are maintained.

Normal Mode Concepts

The structural natural frequencies and corresponding mode shapes are obtained by assuming harmonic responses of frequency $\phi(\omega)$, in the nondimensional equations of motion, (1), and by neglecting all applied surface tractions except those associated with boundary constraints. Undamped frequencies and mode shapes are obtained by setting the damping constant, D, equal to zero. Solving the resulting equations gives solutions

$$\bar{U}_i\,(\bar{X}_1, \bar{X}_2, \bar{X}_3\,;\,\bar{\omega})$$

Applying the appropriate boundary conditions gives a characteristic equation for frequency which is satisfied by only certain discrete values of $\bar{\omega}$. These values, $\bar{\omega}_\nu$, $\nu = 1, 2, 3, \ldots$, are the nondimensional natural frequencies of the structure, and, as shown above, these are related to the dimensional natural frequencies by relation

$$\omega_\nu = \frac{c}{L}\,\bar{\omega}_\nu \tag{2}$$

There exists a discrete set of corresponding mode shapes $\bar{U}_i(\bar{X}_j\,;\bar{\omega}_\nu)$ defining the modal deflections of the structure. The functions $\bar{U}_i(\bar{X}_j\,;\bar{\omega}_\nu)$ $i = 1, 2, 3$ constitute a single three dimensional mode shape for a given ν. It is completely general to normalize these three functions by setting the maximum value of the vector $\vec{\bar{U}}(\bar{X}_j\,;\bar{\omega}_\nu)$ equal to unity. The normalized functions are denoted here by the symbol $\psi_{i\nu}$. These normal shapes are nondimensional and hence are the same for the primary and the model structures, that is, they are modeling invariants. For elementary structures having significant response in only one direction, such as beams and plates, three functions $\psi_{i\nu}$ reduce to a single function, ψ_ν, for each natural frequency.

The general response can be expressed as the summation of the response in each normal mode. Thus

$$U_i = \sum_{\nu=1}^{\infty} H_\nu(t)\cdot\,\psi_{i\nu} \tag{3}$$

where $H_\nu(t)$ gives the response amplitude of ν-th mode and is referred to as the ν-th generalized coordinate of the structure. Since $U_i/L(P_o/E)$ is invariant then $H_\nu/L(P_o/E)$ must be model invariants.

The total kinetic energy, T , and the total potential energy, V of the structure are

$$T = \frac{1}{2}\iiint_{volume} \rho\left[\dot{U}_1^2 + \dot{U}_2^2 + \dot{U}_3^2\right] dx_1\, dx_2\, dx_3 \tag{4}$$

$$V = \frac{1}{2}\iiint_{volume} \left[\lambda e^2 + G\, e_{ij}^2\right] dx_1\, dx_2\, dx_3 \tag{5}$$

where the integrals are taken over the volume of the structure and where

$$e_{ij}^2 = e_{ij}\, e_{ij}$$

$$e_{ij} = \frac{1}{2}\left[\frac{\partial U_i}{\partial x_j} + \frac{\partial U_j}{\partial x_i}\right]$$

These energies have the nondimensional forms

$$T = L^3 \rho c^2\, \overline{T} = L^3 E\, \overline{T}$$

$$V = L^3 E\, \overline{V}$$

and hence

$$\frac{T}{L^3 E}\ , \quad \frac{V}{L^3\ E}$$

are modeling invariants for geometric scaling.

It is assumed for simplicity that ρ and E are uniform throughout the structure. If this is not the case, then a reference density and a reference modulus of elasticity can be factored out of the volume integrals in (4) and (5), leaving nondimensional density and elasticity ratios to be integrated.

The energy dissipated by linear viscous damping may be conveniently represented by the function

$$E_D = \frac{1}{2}\iiint_{volume} \rho D\left[\dot{U}_1^2 + \dot{U}_2^2 + \dot{U}_3^2\right] dx_1\, dx_2\, dx_3$$

This expression assumes, for simplicity, that the damping characteristics of the structure are isotropic. For nonisotropic damping, the parameter D must be replaced by the parameters D_1, D_2, D_3 as multipliers of $\dot{U}_1^2$, $\dot{U}_2^2$, $\dot{U}_3^2$, respectively. E_D is nondimensionalized as follows:

$$E_D = L^3 \rho D c^2 \bar{E}_D$$

The form of Lagrange's energy equation which is applicable to dissipative systems with small displacements about the position of equilibrium, is

$$\frac{d}{dt}\left[\frac{\partial T}{\partial \dot{H}_n}\right] + \frac{\partial V}{\partial H_n} + \frac{\partial E_D}{\partial \dot{H}_n} = F_n \qquad (6)$$

where the F_n are the generalized forces acting on the system in the n-th mode. When the modal expansion is substituted into the expressions for T, V and E_D and the resulting expressions substituted into (6), the following modal response equations are obtained:

$$M_n \ddot{H}_n + M_n D_n \dot{H}_n + K_n H_n = F_n \qquad (7)$$

The quantities M_n and K_n are known as the generalized mass and generalized stiffness corresponding to the n-th coupled mode of the structure. The generalized mass is defined as

$$M_n = \iiint_{volume} \rho\left[\psi_{1n}^2 + \psi_{2n}^2 + \psi_{3n}^2\right] dx_1\, dx_2\, dx_3$$

The expression for generalized stiffness comes from the term $\partial V/\partial H_n$. The mathematical complexities involved in arriving at a simple expression for generalized stiffness, using equations (3) and (5), are too cumbersome to present here. An easy way around this difficulty is to note that the modal functions $\psi_{i\nu}$ were effectively determined by imposing the conditions of everywhere-in-phase, free motion satisfying the equation

$$\ddot{H}_\nu + \omega_\nu^2 H_\nu = 0$$

where ω_ν is the undamped natural frequency corresponding to the mode shape defined by the $\psi_{i\nu}$. It follows then that

$$K_\nu = \omega_\nu^2 M_\nu$$

Clearly $M_\nu / L^3 \rho$ is a model invariant, so that

$$M_\nu = L^3 \rho \bar{M}_\nu$$

By using the frequency scaling of (2), the nondimensional modal stiffness satisfies the relations

$$K_\nu = L E \bar{K}_\nu$$

$$\bar{K}_\nu = \bar{\omega}_\nu^2 \bar{M}_\nu$$

and K_ν / LE becomes a model invariant.

The damping parameter D_r replaces the general damping content, D, defined in E_0 above, since in reality the energy dissipation rate varies with the response frequency. In engineering practice, D_r is given as follows:

$$D_\nu = \frac{\omega_\nu}{Q_\nu}$$

where Q_r is the nondimensional single degree of freedom dynamic magnification factor, (DMF), at resonance in the r -th mode. This expression is consistent with the fact that $D/c/L$ and $\omega/c/L$ are modeling invariants, so that

$$\bar{D}_\nu = \frac{\bar{\omega}_\nu}{Q_\nu}$$

Thus the nondimensional DMF, Q_r must be an invariant.

The generalized force F_ν is expressed as

$$F_\nu = \iint\limits_{surface} \left[P_1 \psi_{1\nu} + P_2 \psi_{2\nu} + P_3 \psi_{3\nu} \right] dS$$

S = surface area

P_i = surface tractions on the structure

This expression has the nondimensional form

$$\overline{F}_\nu = \iint\limits_{surface} \left[\overline{P}_1 \psi_{1\nu} + \overline{P}_2 \psi_{2\nu} + \overline{P}_3 \psi_{3\nu} \right] d\overline{S}$$

$$F_\nu = P_o L^2 \overline{F}_\nu$$

$$P_i = P_o \overline{P}_i$$

$$S = L^2 \overline{S}$$

so that $F_\nu / P_o L^2$ is a model invariant.

Equation (7) can now be consistently nondimensionalized giving

$$\overline{\ddot{H}}_\nu + \frac{\overline{\omega}_\nu}{Q_\nu} \overline{\dot{H}}_\nu + \overline{\omega}_\nu^2 \overline{H}_\nu = \frac{\overline{F}_\nu}{\overline{M}_\nu}$$

where

$$\ddot{H}_\nu = \frac{P_o}{E} \frac{c^2}{L} \overline{\ddot{H}}_\nu$$

$$\dot{H}_\nu = \frac{P_o}{E} c \, \overline{\dot{H}}_\nu$$

$$H_\nu = \frac{P_o}{E} L \, \overline{H}_\nu$$

Summary of Geometric and Dynamic Scaling Laws

The following is a summary list of the invariants which must be the same for the two geometrically and dynamically similar perfectly elastic structures having small amplitude vibrations:

$$\frac{E\,L}{P_o\,c^2}\ddot{U}, \quad \frac{E}{P_o\,c}\dot{U}, \quad \frac{E}{P_o\,L}U, \quad \frac{T}{L^3 E}$$

$$\frac{E\,\epsilon}{P_o}, \quad \frac{E\,\sigma}{P_o}, \quad \frac{P}{P_o}, \quad \frac{M}{L^3 \rho}, \quad \frac{K}{E\,L}$$

$$\frac{L\,\omega}{c}, \quad \frac{c\,t}{L}, \quad \frac{F}{P_o L^2}, \quad \nu, \quad Q$$

where T,M,K and F denote energy mass, stiffness and force respectively. It is to be noted that if propagating surface pressure waves constitute the excitation of the structure, and if the angle of incidence remains unchanged, then the quantity c, or E/ρ, must also be invariant.

Now let n_1, n_2, n_3, n_4 be the scale factors of length, elasticity, density and applied pressure respectively, so that

$$L = n_1 \; L^M$$
$$E = n_2 \; E^M$$
$$\rho = n_3 \; \rho^M$$
$$P_o = n_4 \; P_o^M$$

where the superscript (M) denotes the model. Table II presents a summary of scaling relations using these definitions.

TABLE II

SCALING LAWS FOR PERFECTLY ELASTIC GEOMETRICALLY SCALED STRUCTURES

length	$L = n_1 L^M$
elasticity	$E = n_2 E^M$
density	$\rho = \rho^M n_3$
pressure	$P = n_4 P^M$
mass	$M = n_1^3 n_3 M^M$
stiffness	$K = n_1 n_2 K^M$
damping	$Q = Q^M$
material speed of sound	$C = (n_2/n_3)^{1/2} C^M$
time	$t = n_1 (n_3/n_2)^{1/2} t^M$
frequency	$\omega = (n_2/n_3)^{1/2}/n_1 \cdot \omega^M$
acceleration	$\ddot{U} = n_4/n_1 n_3 \cdot \ddot{U}^M$
velocity	$\dot{U} = n_4/(n_2 n_3)^{1/2} \cdot \dot{U}^M$
deflection	$U = n_1 n_4/n_2 \cdot U^M$
strain	$\epsilon = n_2 n_4 \epsilon^M$
stress	$\sigma = n_4 \sigma^M$
force	$F = n_1^2 n_4 F^M$
mode shape	$\psi = \psi^M$
energy	$T = n_1^3 n_2 T^M$

DISTORTED MODELS

The normal mode concept discussed above is a valuable aid in the development of distorted models, that is, models which are not geometrically similar to the primary structure. Such models are generally used to simulate response in a restricted frequency range, primarily at frequencies near the first few fundamental elastic modes. The response mode shapes at these frequencies are relatively smooth functions, even for complex structures, since they represent only broad average response characteristics for the structure taken as a whole; that is, the local discontinuities in mass and stiffness have been averaged out. Thus the response at or near these frequencies varies smoothly throughout the structure, giving the appearance of the response of a more elementary structure.

For higher response frequencies, the mode shapes become increasingly irregular in shape as the local variations in structural mass and stiffness begin to control the distribution of vibratory energy throughout the structure. In general, for higher frequency responses, it is necessary to model the primary structure in rather fine geometric detail in order to arrive at a model with acceptable dynamic similarity.

Above a certain frequency range, complex structures cease to exhibit overall model response. This is due in part to the predominance of the local vibration characteristics of the structure and in part to the cumulative effect of the damping per structural wave length over the large number of such wave lengths existing between structural boundaries. Since it often is impractical to model all of the structural elements which affect this frequency region, practical models will have an upper frequency limit to their range of validity. This upper frequency limit for the models is related in part to the size of the smallest detail which is faithfully reproduced. This implies the normal relationship between transmission velocity, characteristic length and frequency. Transmission velocity varies between 2000'/s for skin waves to 17000'/s for plane waves propagating through the material (magnesium). The smallest characteristic length to be faithfully reproduced for a frequency of 40,000 cps would be determined from $\lambda / L \gg 1$, $\lambda = 2000/40000 = .05$. $L \approx .02$ is suggested. Rivet spacing or rivet size would be significant therefore.

NONLINEAR SCALING

Nonlinear response characteristics have been observed in several types of structures exposed to high pressure oscillatory environments. Examples of these are the thin skin plates and shells of aircraft and missiles excited by jet and rocket exhaust noise. The nature of the nonlinearity is an increase in stiffness with deflection due to stretching of the middle plane of the plate or shell for large lateral deflections. For thin curved shells, large inward deflections may be accompanied by a decrease in stiffness with deflection. The latter condition is probably due to local buckling, or dimpling, of the skin.

Vibratory structural systems for which the stiffness varies with response amplitude are knows as "hard spring" or "soft spring" oscillators. Analysis of the steady state responses of such systems leads to the following type of equation, which was developed for a flat plate, and which relates the deflection response to the excitation frequency:

$$\Omega^2 = 1 + \frac{3}{4}A^2 - \frac{1}{2Q^2} \pm \left[\frac{A_s^2}{A^2} - \frac{1}{Q^2}\left\{1 + \frac{3}{4}A^2\right\} + \frac{1}{4Q^4} \right]^{1/2}$$

where

$\Omega = \omega/\omega_0$

ω = excitation frequency

ω_0 = fundamental natural frequency based on linear theory

$A = c_1 \dfrac{U}{h}$

c_1 = dimensionless constant

U = center plate dynamic deflection

h = plate thickness

$A_s = c_1 \dfrac{U_s}{h}$

U_s = center plate static deflection based on linear theory

For two such structures to be dynamically similar, it is necessary that both satisfy the above nondimensional equation. It is immediately evident that if the two systems are geometrically similar, then the scaling laws in Table II for deflection, frequency and damping remain valid for the hard and soft spring oscillators.

It can be shown for a flat plate with high amplitude oscillatory surface pressures, that the pressure amplitude, P must satisfy relation of the form

$$\frac{U_s}{h} = \eta \frac{P}{\rho} \frac{1}{\omega^2 h^2}$$

where η is a dimensionless plate parameter. Proceeding as before, this expression can be written in terms of nondimensional quantities as follows:

$$U_s = \frac{\eta}{\bar{\omega}^2 \bar{h}^2} \frac{P}{\rho c^2}$$

$$= \frac{\eta}{\bar{\omega}^2 \bar{h}^2} \frac{P}{E}$$

It follows then that the ratio of P/E must be the same for two hard, or soft, spring nonlinear structural systems for dynamic similarity of the two. This requirement is not necessary for linear structural systems.

THERMAL SCALING LAWS

As discussed in Section I, the geometrically scaled structural vibration model has significant advantages for structural component fatigue certification. Metal fatigue is known to depend in detail upon the properties of the structural material. These properties are also known to change with temperature, so that fatigue is actually dependent upon the combined acoustic and temperature environments. It is interesting to note that the geometrically scaled vibration model is automatically scaled for heat flow. A very brief consideration is given below to thermal scaling laws.

Consider the very simple case of a heat source of temperature T_s and a heat receiver of temperature T. The addition of a net quantity of heat, H, to the body causes a temperature rise in the body which is given by the equation

$$H = cM(T - T_o)$$

C = specific heat of material

M = mass of the body

The net rate, $\dot{H}$, at which the body receives heat is the difference between the heat flow rate, $\dot{H}_i$, into the body and the heat flow rate, $\dot{H}_o$, out of the body, that is:

$$\dot{H} = \dot{H}_i - \dot{H}_o = cM\dot{T}$$

Assume that the body receives heat from the source by means of conduction through a thermal resistance R_i . Then by elementary thermodynamics,

$$R_i \dot{H}_i = T_s - T$$

Also assume that heat leaves the body by means of radiation through a thermal resistance R_o . Then with temperature measured in absolute units,

$$R_o \dot{H}_o = \epsilon \sigma T^4$$

ϵ = emissivity of the material

σ = Stefan-Boltzmann constant

Combining the above results gives

$$\frac{1}{R_i}\left(T_s - T\right) - \frac{\epsilon\sigma}{R_o} T^4 = CM\dot{T}$$

or

$$CMR_i\dot{T} + T + \alpha T^4 = T_s$$

$$\alpha = \epsilon\sigma R_i / R_o$$

Thermal modeling of this simple system requires that the above differential equation be satisfied by both the primary and model systems. For fatigue it is desirable to hold the model temperatures and hence the model source temperatures equal to those for the actual full scale environment. Thus each term in the differential equation must have a scale factor of unity.

The thermal resistance R_i is

$$R_i = \frac{1}{KA}$$

K = thermal conductivity of material

A = area through which heat flows

and R_o is

$$R_o = \frac{1}{A'}$$

A' = area over which radiation occurs

Thus R_i / R_o is an invariant if the thermal conductivity remains unchanged, and if further the emissivity remains unchanged, then α is a modeling invariant.

If the model is constructed of the same materials as the full scale structure, then the thermal conductivity, K, emissivity, ϵ, and specific heat, C, remain unchanged in the modeling process. From the above differential equation, it appears then that the quantity MR_i/t, and hence MA/t, must be a scaling invariant. However, for geometric scaling

$$M = n_1^3 M^M$$

$$A = n_1^2 A^M$$

and hence

$$\frac{M^M}{A^M t^M} = \frac{M}{At} = n_1 \frac{M^M}{A^M} \frac{1}{t}$$

so that

$$t = n_1 t^M$$

But this relation between full scale and model time, t, is precisely that shown in Table II since $n_2 = n_3 = 1$ when no changes in material occur. Thus for the simple system considered here, it is seen that even when nonlinear radiant cooling occurs, the geometrically scaled model is thermally scaled. It is not difficult to see how such a result can be generalized to include more complex thermal systems.

THEORETICAL RESPONSE CHARACTERISTICS

The following discussion is concerned with the theoretical aspects of narrow-band-random response characteristics of the type employed in the present study. An expression is derived below for the mean square response to a localized excitation, in a narrow frequency band, over a limited area of the elastic structure. This expression is developed in the form of a correlation, over the limited surface, of the frequency response functions associated with point-force excitation of the structure.

Several simplifying assumptions are introduced in the analysis so that the results will exhibit clearly the fundamental mechanism of response to excitation over an extended area of vehicle. It is assumed first that the excitation is applied only within the specified area on the structure, and, in light of the SPL contours in Figures D1, D2, D3, D4, this is a reasonable approximation of the experimental excitation employed in the closed box tests.

Secondly, it is assumed that the oscillatory pressure amplitudes are equal for each frequency in the narrow band considered. This constitutes an ideal excitation, but it permits the power spectral density (PSD) of the pressure to be constant over the narrow band and further permits the individual pressure magnitudes to be easily separated from the infinite set of pointwise frequency response functions associated with the limited area of excitation.

Finally, it is assumed that the oscillatory surface pressures associated with any given frequency are in-phase and uniform over the excitation surface. This is the case, for example, when plane waves impinge at normal incidence on a plane surface. In the present tests, the excitation was applied to a slightly curved surface and the pressure waves emanating from the horn were naturally of a reverse curvature than the vehicle skin. Thus, in reality, a phase lag occurs in the pressures at the surface, this phase lag being greatest at the upper and lower boundaries of the closed box. Since the excitation in these tests was applied to panels, and since the edges of the panels are very stiff due to longeron, floor, and bulkhead constraint, this phase lag may not be too significant. An implication of the third assumption is that all waves have essentially normal impingement on the vehicle surface. The acoustic lining of the interior walls of the noise cavity minimized the cross propagation of acoustic waves on the vehicle surface.

In order to determine the net structural response to excitation over the entire vehicle surface, such as rocket noise, the 1/3-octave transfer functions determined in these tests might be used, (See section VII for the manner in which the transfer functions were determined from the test data) along with necessary correlation response functions. These correlation functions are thus part of the structural response characteristics of the vehicle. The role of these correlation functions is shown in an expression developed for response to excitation over two limited surface areas of the type defined above.

Define the following quantities:

$\ddot{U}_n$ = steady state acceleration response at an arbitrary fixed point, n, on the structure and in a given direction at that point.

ω = steady state excitation and response frequency

P_m = magnitude of oscillatory pressure applied at the point on the vehicle surface

m = subscript denoting a point within a limited (bounded) surface area

ΔA_m = elemental area of application of

ΔF_m = elemental force at m associated with P_m

$H_{nm}(\omega)$ = frequency response function relating steady state oscillatory force at m to steady state deflection response at n for frequency ω

$\phi_{nm}(\omega)$ = phase angle between force at m and response at n

The steady state oscillatory force ΔF_m at m is:

$$\Delta F_m = P_m \cdot \sin \omega t \cdot \Delta A_m$$

and the resulting acceleration response at n is

$$\ddot{U}_n = \omega^2 \cdot H_{nm}(\omega) \cdot P_m \cdot \sin(\omega t + \phi_{nm}(\omega)) \cdot \Delta A_m$$

The application of several such forces, at frequency ω, to the surface of the structure gives the following response:

$$\begin{aligned}\ddot{U}_n &= \omega^2 \sum_m P_m \cdot H_{nm}(\omega) \cdot \sin(\omega t + \phi_{nm}(\omega)) \cdot \Delta A_m \\ &= \omega^2 P \sum_m H_{nm}(\omega) \cdot \sin(\omega t + \phi_{nm}(\omega)) \cdot \Delta A_m\end{aligned} \tag{1}$$

where the forces are assumed to be in-phase at each point of excitation and the several pressures are taken as equal. Expanding (1) gives:

$$\begin{aligned}\ddot{U}_n &= \omega^2 \cdot P \cdot \sin \omega t \sum_m H_{nm}(\omega) \cdot \cos \phi_{nm}(\omega) \cdot \Delta A_m \\ &+ \omega^2 \cdot P \cdot \cos \omega t \sum H_{nm}(\omega) \cdot \sin \phi_{nm}(\omega) \cdot \Delta A_m\end{aligned} \tag{2}$$

Let A denote the area of localized excitation, and let(2) pass to the limit. This gives

$$\ddot{U}_n = \omega^2 \cdot P \cdot A \cdot \left[a_n \cdot \sin\omega t + b_n \cdot \cos\omega t \right] \tag{3}$$

$$a_n = \int_A H_n(x;\omega) \cdot \cos\phi_n(x;\omega) \cdot \frac{dA}{A}$$

$$b_n = \int_A H_n(x;\omega) \cdot \sin\phi_n(x;\omega) \cdot \frac{dA}{A}$$

Now define $C_n(\omega)$ and $\bar{\phi}_n(\omega)$ as follows:

$$c_n = \sqrt{a_n^2 + b_n^2}$$

$$\cos\bar{\phi}_n(\omega) = \frac{a_n}{c_n}$$

$$\sin\bar{\phi}_n(\omega) = \frac{b_n}{c_n}$$

Then (3) reduces to the simple form

$$\ddot{U}_n = \omega^2 \cdot P \cdot A \cdot c_n(\omega) \cdot \sin\left(\omega t + \bar{\phi}_n(\omega)\right)$$

Consider now that there are forces of the above type for a set of frequencies ω_K . Then the net response is

$$\ddot{U}_n = A \sum_K \omega_K^2 \cdot P_K \cdot c_n(\omega_K) \cdot \sin\left(\omega_K t + \bar{\phi}_n(\omega_K) + \gamma(\omega_K)\right)$$

where

$\gamma(\omega_K)$ = relative phase angle of the K-th frequency component.

The mean square response, $\overline{G_n^2}$, at n is defined as

$$\overline{G_n^2} = \lim_{T\to\infty} \frac{1}{T}\int_0^T \ddot{U}_n^2 \cdot dt$$

so that

$$\overline{G_n^2} = A^2 \sum_{\kappa} \sum_{\nu} \omega_\kappa^2 \cdot \omega_\nu^2 \cdot P_\kappa \cdot P_\nu \cdot C_n(\omega_\kappa) \cdot C_n(\omega_\nu) \cdot B_{n\kappa\nu}$$

where

$$B_{n\kappa\nu} = \lim_{T\to\infty} \frac{1}{T}\int_0^T \sin\left[\omega_\kappa t + \bar{\phi}_n(\omega_\kappa) + \gamma(\omega_\kappa)\right] \cdot \sin\left[\omega_\nu t + \bar{\phi}_n(\omega_\nu) + \gamma(\omega_\nu)\right] \cdot dt$$

Evaluating this integral gives:

$$B_{n\kappa\nu} = 0, \qquad \kappa \neq \nu$$

$$= \frac{1}{2}, \qquad \kappa = \nu$$

Hence the mean square response becomes

$$\overline{G_n^2} = \frac{1}{2} A^2 \sum_{\kappa} \omega_\kappa^4 \cdot P_\kappa^2 \cdot C_n^2(\omega_\kappa) \tag{4}$$

Assuming that the frequencies are infinitely dense, the pressure power spectral density (PSD), S_p, is defined as

$$S_p = \lim_{\Delta\omega \to 0} \frac{P_\kappa^2}{\Delta\omega}$$

Then if S_p is constant over the narrow frequency band, $\delta\omega$, (4) becomes

$$\overline{G_n^2} = \frac{1}{2} \cdot A^2 \cdot S_p \cdot \int_{\delta\omega} \omega^4 \cdot C_n^2(\omega) \cdot d\omega$$

and if the band $\delta\omega$ is sufficiently narrow, this equation is closely approximated by the following equation:

$$\overline{G_n^2} = \frac{1}{2} A^2 \cdot S_p \cdot \omega^4 \int_{\delta\omega} C_n^2(\omega) \cdot d\omega$$

The mean square pressure $\overline{P}^2$ in this frequency band is

$$\overline{P}^2 = S_p \cdot \delta\omega$$

so that

$$\overline{G_n^2} = \frac{1}{2} A^2 \cdot \overline{P}^2 \cdot \omega^4 \int_{\delta\omega} C_n^2(\omega) \frac{d\omega}{\delta\omega} \qquad (5)$$

The integral of (5) can be rewritten in the form of a correlation, over the surface, of pointwise response functions. The quantity C_n^2 is

$$\begin{aligned} C_n^2 &= a_n^2 + b_n^2 \\ &= \frac{1}{A^2}\left[\int_A H_n(x;\omega) \cdot \cos\phi_n(x;\omega) \cdot dA\right] \\ &+ \frac{1}{A^2}\left[\int_A H_n(x;\omega) \cdot \sin\phi_n(x;\omega) \cdot dA\right] \end{aligned}$$

In order to simplify this expression, write the integrals as summations:

$$\begin{aligned} A^2 C_n^2 = &\left[\sum_m H_n(x_m;\omega) \cdot \cos\phi_n(x_m;\omega) \cdot \Delta A_m\right]^2 \\ &+ \left[\sum_m H_n(x_m;\omega) \cdot \sin\phi_n(x_m;\omega) \cdot \Delta A_m\right]^2 \end{aligned}$$

$$= \sum_m H_n^2(x_m;\omega)\cdot(\Delta A)^2$$

$$+ \sum_m \sum_\nu H_n(x_m;\omega)\cdot H_n(x_\nu;\omega)\cdot \cos\phi_n(x_m;\omega)\cdot\cos\phi_n(x_\nu;\omega)\cdot \Delta A_m\cdot\Delta A_\nu$$

$$+ \sum_m \sum_\nu H_n(x_m;\omega)\cdot H_n(x_\nu;\omega)\cdot \sin\phi_n(x_m;\omega)\cdot\sin\phi_n(x_\nu;\omega)\cdot \Delta A_m\cdot\Delta A_\nu$$

In the limit, the first summation goes to zero. Combining the second and third summation gives, in the limit:

$$c_n^2(\omega) = \int_A\int_A H_n(x;\omega)\cdot H_n(y;\omega)\cdot\cos\left[\phi_n(x;\omega)-\phi_n(y;\omega)\right]\frac{dA(x)}{A}\cdot\frac{dA(y)}{A}$$

The mean square response in the narrow band, $\delta\omega$, to an excitation over the area A is then:

$$\boxed{\overline{G_n^2} = \frac{1}{2}A^2\cdot\overline{P}^2\cdot\omega^4\int_{\delta\omega}\int_A\int_A H_n(x;\omega)\cdot H_n(y;\omega)\cdot \cos\left[\phi_n(x;\omega)-\phi_n(y;\omega)\right]\frac{dA(x)}{A}\,\frac{dA(y)}{A}\,\frac{d\omega}{\delta\omega}} \qquad (6)$$

Consider next two distinct areas A and A' over which pressures are applied in the narrow frequency band $\delta\omega$. Then the net response can be written in the form:

$$\ddot{U}_n = A\sum_K \omega_K^2\cdot P_K\cdot C_n(\omega_K)\cdot\sin\left[\omega_K t+\bar{\Phi}_n(\omega_K)+\gamma(\omega_K)\right]$$

$$+ A'\sum \omega_K^2\cdot P_K'\cdot C_n'(\omega_K)\cdot\sin\left[\omega_K t+\bar{\Phi}_n'(\omega_K)+\gamma'(\omega_K)\right]$$

Proceeding as before, the mean square response to this double excitation is then:

$$\overline{G_n^2} = A^2 \sum_{\kappa} \sum_{\nu} \omega_\kappa^2 \cdot \omega_\nu^2 \cdot P_\kappa \cdot P_\nu \cdot C_n(\omega_\kappa) \cdot C_n(\omega_\nu) \cdot B_{n\kappa\nu}$$

$$+ A'^2 \sum_{\kappa} \sum_{\nu} \omega_\kappa^2 \cdot \omega_\nu^2 \cdot P'_\kappa \cdot P'_\nu \cdot C'_n(\omega_\kappa) \cdot C'_n(\omega_\nu) \cdot B'_{n\kappa\nu}$$

$$+ 2AA' \sum_{\kappa} \sum_{\nu} \omega_\kappa^2 \cdot \omega_\nu^2 \cdot P_\kappa \cdot P'_\nu \cdot C_n(\omega_\kappa) \cdot C'_n(\omega_\nu) \cdot B''_{n\kappa\nu}$$

However,

$$B_{n\kappa\nu} = B'_{n\kappa\nu} = B''_{n\kappa\nu} = 0 \quad , \quad \kappa \neq \nu$$

$$B_{n\kappa\nu} = B'_{n\kappa\nu} = \frac{1}{2} \quad , \quad \kappa = \nu$$

$$B''_{n\kappa\nu} = \frac{1}{2} \cos\left[\Phi_n(\omega_\kappa) - \Phi'_n(\omega_\kappa) + \gamma(\omega_\kappa) - \gamma'(\omega_\kappa)\right]$$

Hence

$$\overline{G_n^2} = \frac{1}{2} A^2 \sum_{\kappa} \omega_\kappa^4 \cdot P_\kappa^2 \cdot C_n^2(\omega_\kappa) + \frac{1}{2} A'^2 \sum_{\kappa} \omega_\kappa^4 \cdot P_\kappa'^2 \cdot C_n'^2(\omega_\kappa)$$

$$+ AA' \sum_{\kappa} \omega_\kappa^4 \cdot P_\kappa \cdot P'_\kappa \cdot C_n(\omega_\kappa) \cdot C'_n(\omega_\kappa) \cdot \cos\left[\Phi_n(\omega_\kappa) - \Phi'_n(\omega_\kappa) + \gamma(\omega_\kappa) - \gamma'(\omega_\kappa)\right]$$

Introducing the previous assumptions, this equation reduces to

$$\overline{G_n^2} = \frac{1}{2} A^2 \cdot S_p \cdot \omega^4 \int_{\delta\omega} C_n^2(\omega) \cdot d\omega$$

$$+ \frac{1}{2} A'^2 \cdot S_{p'} \cdot \omega^4 \int_{\delta\omega} C_n'^2(\omega) \cdot d\omega$$

$$+ AA' \cdot S_{pp'} \cdot \omega^4 \int_{\delta\omega} C_n(\omega) \cdot C_n'(\omega) \cdot \cos\left[\bar{\Phi}_n - \bar{\Phi}_n' + \gamma - \gamma'\right] d\omega$$

where

$$S_{p'} = \lim_{\Delta\omega \to 0} \frac{p'^2}{\Delta\omega}$$

$$S_{pp'} = \lim_{\Delta\omega \to 0} \frac{pp'}{\Delta\omega}$$

SECTION IV

DESCRIPTION OF FULL AND MODEL SCALE STRUCTURE

VEHICLE DESCRIPTION

Units of the Snark Missile, U.S. Air Force Model No. SM-62A and Serial No. AF 57-007 which will be referred to in this report as the "missile" were used. Figure A1 shows an N-69E missile which is very similar to the SM-62A missile. The fuselage stations, F.S., of the missile will be used to locate items. The forward main, F.S. 384.0 to 600.0, and the aft main, F.S. 600.0 to 761.15, units of the missile were used for the studies. The two units assembled into one piece of structure will be referred to as the "vehicle." Figures A2 and A3 show the vehicle and the missile fuselage.

The original design requirements for fuel bays, equipment bays and an air intake-engine bay dictated that the vehicle have a bulkhead, floor (deck), longeron and skin structural arrangement. At each bay there is one or more access doors or a cover. The decks, floors and many of the bulkheads are of sandwich construction. The remaining bulkheads are of conventional web and stiffener construction. The forward main unit and the aft main unit are structurally attached at a production break, F.S. 600.0, which consists of four bolts and locating pins. The loading on the four bolts is passed into fittings that transfer the load into the four longerons of the two units. The bulkhead at F.S. 384 contains the required fittings for the release of the ballistic nose of the missile. The wing loading is transferred to the fuselage by the production break fittings on bulkheads F.S. 384.0 and 464.0 and then on down through the major stiffeners of the bulkheads. A structural discontinuity occurs at F.S. 705.9 where the upper longeron tapers out, the lower longeron of the forward main unit inclines up through the aft main unit, and the new lower longeron begins. The lower longeron of the forward main unit is stiffened with doublers and fittings to take the loading of the two rockets. The location of the rockets is shown in Figure A1. These structural details are shown on the structural diagram of Figure 1B and the structural drawings of Figure 2B and 3B.

The complete details of the vehicle structure are shown on the following Northrop Corporation, Norair Division, Hawthorne, California drawings:

5152827 Fuselage Assembly, Sta. 61.962 to Sta. 761.150

5152829 Fuselage Assembly, Forward Main Section

5153200 Structure Assembly, Fuselage Station 384-600

5153134 Fuselage Assembly, Aft Main Section, Complete

5153127 Structure, Fuselage Aft Main Section, Assembly of

There are a number of equipment items and miscellaneous items scattered throughout the vehicle which were impractical to remove prior to testing. Each major item can affect the response frequency of the structural element to which it is attached and to a small degree the response frequency of the adjacent structure. None of these items were simulated on the model and as such the model is a simulation of the clean vehicle. Thus, the test work was performed on the full scale vehicle containing these miscellaneous items and on the model that simulated the clean vehicle.

The "cluttered" vehicle has, in many places, fuel lines running length-wise of the vehicle. These consist of 3/4 inch diameter and 1 1/4 inch diameter stiff tubes that are clipped to structural elements by rubber padded clips. Examples of these fuel lines are shown in Figures A32, A33, and A35.

The attachment of one or more of these tubes to a panel, such as a skin panel, a deck panel, or a floor panel may create a combination that will have different types of vibration modes than that of the clean panel. From Figures 10B-A and 10B-B we see that a rigid attachment of a stiff tube to a panel results in a more complicated fundamental mode (first mode) shape of the panel. This results in a higher fundamental frequency and higher frequencies for the correspondingly higher modes of the panel and tube combination than that of the clean panel.

The cluttered vehicle has, in many places, electrical cables running from one part of the vehicle to another. They range in size from 1/4 inch in diameter (approximately five wires) to 1 1/2 inch in diameter (approximately 50 wires). They are tied to plastic clips which are fastened to various structural elements of the vehicle. These cables are quite flexible, but they have a significant amount of weight per unit length. Examples of these cables may be seen in Figures A32, A33, A34, A36, A37, A39, A40, and A41. The attachment of one of these cables to a stiffener, a frame, or a longeron type of structural element adds mass to the structural element. Thus, these types of cluttered structural elements should have lower response frequencies than the clean type.

The fuel bay of F.S. 384 to 423 of the cluttered vehicle has plastic tape applied to many parts of the fuel bay. The tape is 2 inches wide and of medium weight. The tape is applied to the following parts of the interior of the fuel bay:

a. To all the rivet rows.
b. Heavily applied to all corners.
c. To the whole surface of the backing board at the bottom of the bay.
d. Around the two large bulkhead fuel line fittings.
e. Heavily applied around the access door opening.

The tape introduces damping to the corresponding structural elements and thus reduces the response of these elements to any excitation.

There are many small parts on the cluttered vehicle. A number of examples of these small parts are listed in the following:

a. Plastic electrical cable clips as shown in Figures A30, A32, A37, and A39.
b. Sheet metal clips as shown in Figures A32, A33, A37, and A41.
c. Small fiber blocks attached to the longeron as shown in Figures A36 and A37.
d. Small tubing fittings attached to a frame as shown in Figure A37.
e. Electrical terminal strips as shown in Figure A39.

These small parts probably have only a small effect upon the response of the corresponding structural element to which they are attached. Thus the cluttered vehicle in this case will respond very closely to that of the clean vehicle, which is simulated by the model.

MODEL DESCRIPTION

A dynamically similar structural model of the vehicle, which will be referred to in this report as the "model" was manufactured. That portion of the model that represents the forward main unit of the vehicle, F.S. 384.0 to 600.0 will be referred to as the "forward main of the model." That portion of the model that represents the aft main unit of the vehicle, F.S. 600.0 to 761.15 will be referred to as the "aft main of the model."

Many small detail items were not exactly simulated in accordance with the objective of developing the vibration model as a practical and economic design tool. Therefore, a number of design and/or manufacturing compromises were made in the development of the model.

Within the scope of the present program, it was necessary to focus the major engineering investigation effort on certain key problems, such as bonding versus riveting, rather than conduct a large number of inadequate substudies, of which many would prove unnecessary. The model was designed according to the Scaling Laws for Linear Geometrically Scaled Structure, developed in Section II, which will be referred to as the "scaling laws." For the model of this report the following scaling factors were selected:

a. Linear scaling factor, $n_1 = 4$

b. Young's modulus of elasticity scaling factor, $n_2 = 1$

The use of these scaling factors in equations (1), (2), (3), and (4) of Table II of Section II produces the following scaling expressions for the model:

$$L = n_1 L^m = 4 L^m \tag{1}$$

$$E = n_2 E^m = E^m \tag{2}$$

$$\rho = n_3 \rho^m = \rho^m \tag{3}$$

$$M = n_3 n_1^3 M^m = 64 M^m \tag{4}$$

Expression (1) was satisfied by simply making the majority of the parts of the model to one fourth size of the vehicle. However, in some instances the small detail dimensions of the parts were not scaled exactly, to keep their cost within the scope of the program. Expressions (2), (3), and (4) were satisfied by simply duplicating the material of the vehicle in the model. Thus, the magnesium skins of the vehicle were simulated by magnesium skins on the model, the aluminum skins of the vehicle were simulated by aluminum skins on the model, aluminum structural elements of the vehicle were simulated by aluminum structural elements on the model and similarly for other items of the vehicle.

The following additional features were provided for in the design of the model to allow the performance of additional tests on the model, including comparison of model responses with full scale simulated launch responses:

a. The approximate form and weight of the continuing structure of the fuselage of the missile.

b. The equipment items of the vehicle which were inaccessible after the model was completed.

c. The weight of the wing of the missile.
d. The weight of the engine of the missile.
e. The fuel bladders and fuel of the fuel bays.

Various attach fittings, weights and frames occur on the model to accomplish this and they will be discussed in the following paragraphs.

Figure A5 shows the assembly of the bulkheads and longerons of the forward main unit of the model. Figure A6 shows the assembly of bulkheads, floors, and longerons of the aft main unit of the model to the forward main unit of the model. Figures A8 and A7 show the top of the model where the top skins, top covers and some decks have not been attached. Figures A9 and A10 show the underside of the model, where the skin for the underside of the first three bays has not yet been attached. Here one can see the three underside access doors that just precede the air intake. The plywood frames at each end of the model are for attaching weights to the model to represent continuing structure. The bracket inside of the aft plywood frame as shown in Figure A10 is for attaching a weight to represent the engine of the missile. These plywood frames and weights were not used in the studies of this report. Figure A13 shows the equipment bay of F.S. 600.0 to 647.5, where the cover has not yet been installed. Figure A12 shows the forward two fuel bays of F.S. 384 to 464. Here the deck to cover the bay is yet to be installed. Figure A11 shows the complete model.

The general type of fasteners used on the model followed that of the vehicle. Universal head, 3/32 diameter structural rivets, Air Force-Navy Aeronautical Standard AN 470, were used for most of the rivet fastening. A significant number of universal head, 3/32 diameter blind rivets, RV 850 and RV 800 of Olympic Screw and Rivet Company, were used where the access for riveting would not allow the use of conventional rivets. A universal head, 3/32 diameter soft rivet, Military Standard MS 2420 was used where fastening of sandwich panels or hand bucking was required. The structural bolts of the vehicle were represented with 1/4 diameter Allen Head machine screws. The quick disconnect type of fasteners of the vehicle used to attach large access doors and covers were represented by 3/32 diameter, button head, sheet metal screws. These various fasteners and the fastener patterns used may be seen in Figures A5 through A24.

Metal honeycomb sandwich panels that will be referred to as "sandwich panels" were used in the various bulkheads, floors and decks of the vehicle. These sandwich panels were simulated by laminating a stayfoam core with two aluminum sheets. The stayfoam was 4 lb/cu. ft. density wethane foam and was used in preference to styrofoam because of its immunity to various thinners and availability in thin sheets. Plywood strips replaced the stayfoam at the edges of the panel, at the edges of access holes and at any line of rivets that crossed the panel. The sandwich was bonded with Hapex Corbond, No. 1233, and hardener, No. 1221, and cured at room temperature. This bonding process for styrofoam and aluminum has been used successfully on supersonic flutter models and it was believed that it would work equally well for stayfoam and aluminum bonding. All the panels were 1/4 inch thick, where the aluminum sheets varied in thickness to simulate the corresponding vehicle structure. The sandwich simulation is shown in Figures 4B-A, 4B-B, and 4B-C.

The vehicle has a sandwich panel deck from F.S. 384 to 464, a sandwich panel deck from F.S. 501.5 to 551.5 and a sandwich floor from F.S. 647.5 to 761.15 as shown in Figure 1B. Figures 4B-B and 4B-C show the types of structural ties on the model used in attaching the panels to adjacent structure. These simulated directly the structural ties of the vehicle. Figure A14 shows the deck from F.S. 384 to 464 and its stiffeners, fittings and access holes. Figure A7 shows the floor from F.S. 647.5 to 761.15. These are examples of deck and floor simulation on the model.

The vehicle has full sandwich panel bulkheads at F.S. 423.0, 501.5, and 536.0, and combination sandwich panel and frame bulkheads at F.S. 647.5, 705.9, and 761.15 as shown in Figure 1B. Figure 4B-A shows the types of structural ties of the model used in attaching the panels to adjacent structure. These simulate directly the structural ties of the vehicle. Figures A5, A6, A7, A12, and A19 show some of the typical bulkheads. Figures A23 and A24 show a typical structural tie for a simulated bulkhead.

The vehicle has web and stiffener bulkheads at F.S. 384.0, 464.0, 530.75, 551.5, and 600.0 as shown in Figure 1B. The stiffeners of these bulkheads are of extrusions on the vehicle and they are simulated by sheet metal shapes or machined extrusions on the model. Figure A17 shows the simulation of the bulkhead at F.S. 384, its stiffeners, the ballistic nose pivot point fitting and the wing attach fittings. The ballistic nose release fittings were not simulated. The angle clips at the top corners of the bulkhead were used for attachment of the plywood frame mentioned previously. Figure A18 shows the simulation of the bulkhead at F.S. 600.0 its stiffeners and the production break fittings. The two rubber pads mounted on angle clips are for an equipment simulating weight that was not used in testing.

The longeron parts of the model were machined from bar stock where the corresponding parts of the vehicle were of extrusions, or built up of combinations of extrusions and sheet metal. As a result, the longerons were closely simulated. Examples of machined bar longerons are shown in Figures A5, A8, and A9 and examples of the sheet metal shaped longerons are shown in Figures A6 and A7. The fittings were machined from bar stock and only approximately simulated those of the vehicle. Examples of the fittings for the longerons are shown in A7, A12, A13, A21, and A22. The production break that occurs in the vehicle at F.S. 600.0 is simulated in the model and shown in Figures A21 and A22. Each structural bolt joint of the production break is simulated by a 1/4 inch diameter Allen Head machine screw and two shear pins.

The bottom of each of the fuel bays of the vehicle have a backing board to assure adequate fuel flow and complete drainage from each bay. Each backing board was simulated in the model by a layer of stayfoam bonded to the bottom of the bay. Figure A15 shows an example of a simulated backing board.

The various covers of the vehicle were simulated directly by bending a sheet to the proper contour and adding the appropriate stiffeners. Figure A20 shows the inside of a typical cover. The wing attach fittings of the vehicle at F.S. 384.0 and 464.0 were simulated by machining bar stock. The fittings may be seen in Figures A14 and A17.

The vehicle in its complete form would have the appropriate fuel valves and fuel line fittings in the bottom of each fuel bay. It would also have various electronic equipment units in the equipment bays. These valves, fittings and equipment units are simulated on the model for future tests by steel weights bonded to the corresponding adjacent structural element. The location and representation purpose of the weights are listed in the following

a. Valves and fittings are represented by four weights placed in the backing board on the bottom of the fuel bay, F.S. 423.0 - 464.0.

b. Valves and fittings are represented by four weights placed in the backing board on the bottom of fuel bay F.S. 468.0 - 501.5.

c. Valves and fittings are represented by one weight placed on the bottom side of the deck of fuel bay F.S. 501.5 - 536.0.

d. Some of the equipment units are represented by four weights on the top side of the deck, F.S. 551.5 - 600.0 of the corresponding equipment bay.

e. Some of the equipment units are represented by four weights on the top side of the floor of the equipment bay, F.S. 600.0 - 647.5.

f. Valves and fittings are represented by four weights placed on the bottom side of the floor of the fuel bay F.S. 647.5 - 705.9.

g. Valves and fittings are represented by four weights placed on the bottom side of the floor of the fuel bay F.S. 705.9 - 761.15.

Figure B1 shows the various fuel bays, equipment bays, decks and floors listed above. Figure A16 shows an example of the weights on the model.

The complete details of the model are shown on the following Northrop Corporation, Norair Division, Hawthorne, California model design drawings:

5204954 Sheets 2 through 10 Snark Acoustical Model, 1/4 Scale

ADDITIONAL COMMENTS ON DEGREE OF MODEL SIMULATION

The countersunk rivets of the vehicle were simulated by universal head rivets. The size of rivets used was considerably oversize as compared to the scale size. Their use required larger spacing of the rivets, which resulted in a reduced number of rivets in each row or pattern. The oversize rivets required over scale edge margins, over scale spacing between rows, and over scale distances from rivet to the flange radius. Thus, the model has over scale flanges on stiffeners and longerons. In many instances a double row of rivets of the vehicle was simulated by a single row of rivets.

The skin gages could not be always scaled exactly; however, in most cases a close approximation was obtained with the model skin on the thick side. Figure B9 shows the comparison of the vehicle and the model skin gages. In a small area the skin material and thickness was not directly simulated. This will be discussed in a following paragraph. The out of scale of the skins will affect the various skin panel mode frequencies to a small degree. This type of deviation may be expected on future models.

In the design and manufacture of extended portion of the model where only approximate simulation was intended, three stiffeners were omitted and replaced by an extra thickness of skin in one localized area on each side of the model. This area comprises the area between F.S. 706.9 and F.S. 761.15, and between the floor and the lower longeron. This may be seen in Figures B1 and A11. This type of simulation was instigated as part of an effort to eliminate the small details of the vehicle that would not have a significant effect on the overall results.

The air-intake duct and the structure surrounding, between F.S. 610.0 and 647.5 were not intended to be structurally simulated. See Figures B1, A9, A10, and A11. This part of the vehicle was simulated by a solid balsawood block shaped to the appropriate outside contour.

The bonding of the sandwich panels of the model was not adequate. The sandwich panel deck, F.S. 384.0 to 423.0, was removed from the model and in the process, the aluminum sheets were easily pulled away from the core. In the process of removing the rivets it was found that the bonding of the aluminum sheets to the plywood strips had failed.

Figure A25 shows the disassembled deck panel. The other sandwich panels of the model were checked by a quality control inspector who has a great deal of experience in checking for voids in sandwich panels. The inspector checked the entire area of each side of the panels. The checking was done by tapping on the panel with a large coin and listening for the characteristic sound that occurs when a void is tapped. The inspection showed that a bond did occur throughout the interior of each panel, except for a few small voids in some of the panels. However, the bond at the plywood strips where riveting had been performed had failed in almost all cases. The disassembly of the deck panel indicates that although the bond exists, that it is quite weak.

The backing boards were inadequately simulated. The stayfoam used to simulate the backing boards has a density much lower than that of the actual boards. The stayfoam was bonded to the floor or the skin comprising the bottom of the fuel bay. Due to the bonding the board did not act as a separate element. The bonding of the stayfoam to the adjacent structural element resulted in adding a damping material to it and thus probably reducing its response to excitation.

The outside contour of the vehicle was approximated in a number of places on the model. The forward main of the model was made circular in cross section as compared to the circular section with a flattened top of the vehicle. This may be seen in Figure A5, A14, A18, B5, and B6. The aft main of the model was made of a cross section with a circular top, whereas the vehicle cross section has a flattened top. This may be seen in Figures A6, A19, B7, and B8. The floor edges, the stiffeners and the lower longeron between F.S. 647.5 and 761.15 of the model were fabricated and installed as straight. The vehicle has a contour with a three dimensional curvature in this area and thus requires floor edges, stiffeners and longerons of curvature. The skin on the lower part of the aft main of the model was applied without regard to the three dimensional contour of the vehicle. The result of this is that there exists a number of angular skin joints on the lower part of the aft main of the model. This may be seen in Figure A10. The vehicle has a small airscoop on the right hand side at F.S. 600.0. No attempt was made to simulate this on the model. This may be seen in Figures A4 and A18.

The vehicle has a wing cover, F.S. 384.0 to 464.0, over the deck in the forward part of the vehicle. This is shown in Figures B1 and A3. The vehicle was tested in this condition as shown in Figure A26. No attempt was made to simulate this on the model, as shown in Figures A11, A14, and A29.

The vehicle has a number of small access doors scattered throughout the structure and a sextant window at F.S. 558.8. This may be seen in Figure B1. These doors and window were not simulated at all and only the adjacent structure was simulated if it existed on the vehicle. The effect of this omission is negligible on the response frequency of the corresponding structural element. This results in an adequate simulation that should be continued in future models.

To facilitate future testing, where fuel bladders of the vehicle would be involved, access holes were designed and manufactured into the model. One of these holes is located in the top structural element, deck or skin panel, of each fuel bay. This may be seen in Figures A11, A14, and A25. The cover plates for the holes and the flanges for their attachment were made rather heavy.

The engine bracket that was designed and manufactured for future tests and is shown in Figures A10, A19, A29 was attached to the model during the testing. Nothing similar was on the vehicle during testing as may be seen in Figure A26. The bracket is very rigid and it is fastened to each of the two lower longerons. Any excitation of one longeron or its adjacent skin panels or bulkheads would be transmitted directly across the model tothe structure on the opposite side. This type of energy transfer does not occur on the vehicle.

The various weights placed in the model to represent valves, fittings and equipment were in the model during the test work on the model. The vehicle did not have the corresponding valves, fittings and equipment in it during the test work on the vehicle. The attachment of one of these weights to a simulated structural element will greatly affect the response of the element to any excitation.

The overall weight of the vehicle is 3500 lbs. The overall weight of the model, according to scaling expression (4), should be 55 lbs., whereas the actual overall weight of the model is 94 lbs.

The following items added weight to the model:

a. Engine bracket in aft main of model.

b. Weights throughout the model.

The net effect of these items is an extra overall weight on the model. This extra weight appears, in general, to be spread evenly throughout the model. This extra weight is, in general, concentrated at points and lines of high rigidity, and as a consequence, it has little effect on the frequency response of the individual structural elements.

The experimentally measured model transfer functions defined on Page 112, began as a check of natural frequency, mode shape and damping of eight typical structural elements of the model for comparison to corresponding full scale elements. This portion of the tests was gradually expanded as time permitted to provide better understanding of vibration transmission. Many of the ballast weights necessary for take off gross weight had been permanently fixed in place--some in relatively inaccessible areas--which would not interfere with a test on structural elements. While this was consistent with initial planning, it interferred with the transfer functions associated with near field excitation, except as these are separately used. The comparison had sufficient value to indicate failure to scale in certain areas, as will be indicated by later discussions of the data.

SECTION V

DESCRIPTION OF TESTS

TEST FACILITIES

Both full scale and model tests were conducted in the open air, as far distant from neighboring buildings as was convenient. The full scale test vehicle consisted of an SM-62D fuselage section, between Stations 384 and 761.5. The fuselage was supported at Stations 466 and 706 by belts passing beneath the bulkheads and attached to springs. The springs were suspended from towers by giving a system natural frequency of 1.2 cps. The model SM-62D was suspended in a similar manner but displayed a system natural frequency of 2.73 cps.

A Ling-Altec Model 6786 Electro-Pneumatic Transducer provided the acoustic excitation for tests performed on both full scale and model Snark fuselage sections. This unit, by electrically modulating a powerful air flow, can produce the large sinosoidal or random acoustic energies needed in the test program. The electro-pneumatic transducer was coupled to an exponential horn having a cut-off frequency of approximately 100 cps. A special box lined with fiberglass and contoured to provide close coupling between the sound source and the fuselage section was fabricated for both full scale and model testing, and are shown in Figures A26 and A29.

INSTRUMENTATION

The basic components of the instrumentation system employed in this program are shown in the block diagram presentation of Figure B11. Quantitative measurements of microphone and accelerometer response were recorded in one-third octaves.

Recording

All acoustic measurements were made using Altec 21 BR-180 and Altec 21 BR-150 condenser microphones with the associated cathode follower preamplifiers and microphone power supplies. System sensitivity was -80 db for the 21 BR-180 and -60 db for the 21 BR-150 (re .0002 dynes/cm^2). The frequency response is essentially flat to 2000 cps (4 db max error 2000-8000 cps). One microphone was attached to the enclosure which couples the horn to the fuselage, at a point located on the centerline of the horn at a distance of approximately six inches from the vehicle surface. This transducer was used as a reference for the acoustic input. A second transducer was used as a rover for monitoring and measuring sound pressure levels at various points along the vehicle. Six additional microphones were mounted flush with the vehicle skin at fixed point locations selected to provide a representative scatter over the vehicle. Microphone signals were recorded on a Bruel and Kjaer Type 3311 Audio Frequency Spectrum Recorder and monitored on a dual-beam oscilloscope and a Ballentine Model 320 True RMS voltmeter. Calibration of the microphone system was accomplished by use of an Altec Model 12185 Sound Pressure Calibrator.

Vehicle response was measured using Endevco Type 2213 and 2223 accelerometers, Type 2614 and 2614B amplifiers and Model 111A Kin-Tel Booster amplifiers. One accelerometer was used as a rover to determine the response at any point of interest along the vehicle. Twenty-four additional accelerometers were used as fixed point locations giving a representative definition of vibration throughout the vehicle. Accelerometer signals were recorded on a Bruel and Kjaer spectrum recorder and monitored in the manner previously described. The frequency response of these accelerometers is essentially flat to 2000 cps when calibrated under controlled conditions. A number of tests were made on the response characteristics of the accelerometers using a DTMD Model Z602 Impedance Head, to validate the methods utilized, to cement the accelerometers to the vehicle, and to determine the repeatability. The results demonstrated excellent repeatability and gave a maximum error in acceleration response of ± 2 db over the frequency range up to 5000 cps.

Power Input

The Ling-Altec Electro-Pneumatic Transducer was powered by a General Radio Model 1390-A Random Noise Generator, a clipping and shaping network, an SKL variable band pass filter, and an Altec Model 260A power supply. Effective modulation can be maintained up to 2000 cps where the air noise becomes the predominant factor. By proper shaping and use of air to provide power above 2000 cps an input spectrum was obtained to meet the requirements of the test.

TEST OBJECTIVES

The objectives of the tests performed are fourfold. The first objective was to experimentally determine, for the full scale Snark structure,

a. the acoustical acceptance of several major side panels

b. the vibration energy transfer properties between these panels and numerous points on the vehicle structure

c. the detailed response characteristics and the variations of these characteristics in a localized region of the structure.

These investigations were to be performed using broad band noise from a sound source which was close coupled to the vehicle structure to provide a high level, localized acoustic excitation.

The second test objective was to determine the accuracy with which the geometrically scaled Snark model simulated the vibration response characteristics and transfer properties of the corresponding full scale structure. The measured model response characteristics resulting from scaled, localized, acoustic excitation of the model were to be compared with the corresponding full scale responses to determine the overall and local structural vibration simulation obtainable with the model.

The third test objective was to determine the variation of panel acceptance with angle of incidence of impinging acoustic waves, and to investigate the phenomenon of coincidence. These tests were to be limited to determining the variation in response amplitude and frequency distribution at several points on the structure due to changing the angle of the source relative to the skin.

The fourth objective was to determine the feasibility of using an air modulated siren to simulate the structural response that results from the exhaust noise of the full scale booster rockets. The broad band noise source was to be located in the region where the maximum exhaust noise is generated, and to be directed forward to simulate the propagation of acoustic waves over the surface. Overall comparisons of the resulting responses with previously measured responses to rocket noise would provide at least some indication of the accuracy of rocket simulation obtainable with the siren.

FULL SCALE TESTS

Preparation

The fuselage section was cleared of all accessible electrical conduit, hydraulic lines, and supporting bracketry along the left-hand side of the vehicle. Missing screws and tie-down bolts were replaced and all fuselage access doors were installed.

The accelerometers were mounted to the fuselage using Eastmen 910 cement. Bulkhead installation utilized threaded fasteners. All microphones were flush mounted to the skin surface using a foam block and epoxy cement. The locations of all accelerometer and microphone points are shown.in Figures B12, B16, and B17.

Random Excitation

With the vehicle suspended from springs to eliminate rigid body modes the noise source was close coupled to the fuselage, centered at Sta. 405. The acceptance area of the fuselage was approximately 14 sq. ft. The noise source displayed a continuous spectrum over the frequency range of interest. Measurements of the 24 fixed accelerometers and 6 fixed microphones were made and 60 roving accelerometer points. A survey was made of the sound pressure level along the vehicle. All data was recorded in one-third octaves. The source was then removed 18 inches from the vehicle structure and a selection of four accelerometers and four microphones located over the length of the vehicle were recorded. The purpose of obtaining data with the source removed was to determine the excitation due to the local acoustic field.

The source was then moved to Station 578 and again close coupled to the fuselage section. Again all fixed microphones and accelerometers were recorded. An additional 22 roving accelerometer locations were recorded. A complete survey of the inner compartment (see Figure B17) was made using a roving accelerometer. This compartment survey covered the various classes of structure found in all flight vehicles and provides the necessary information to categorize the response of different types of structure. Photographs of the compartment are shown in Figures A30 through A41. The source was then removed a distance of 18 inches from the surface of the structure and accelerometer and microphone measurements were made at points along the vehicle.

The source was then moved to Station 647 and a similar test was conducted except that only fixed accelerometer and microphone data was obtained. The source was then moved to Station 738 and a similar test was performed. All fixed instrumentation was recorded as well as 60 roving accelerometer points. Further testing was performed at this station at angles of incidence of 30° and 60° with the horn directed at Station 738. A survey of the sound pressure level and vehicle response was made along the length of the fuselage.

A simulated JATO test was conducted by setting the horn directivity along the thrust axis. Microphone and accelerometer measurements were made at selected points along the vehicle length.

Discrete Excitation

Various panels, bulkheads, and major vehicle structure were subjected to discrete excitation for purposes of determining resonances and damping. Generally, it was found that the modes were somewhat complex and difficulty arose in selecting the actual resonant points. A representative sampling of points was obtained using this method. Damping measurements were made, using the method of half power point frequencies, for the sampling of points.

MODEL TESTS

Preparation

The model was instrumented in a manner similar to the full scale vehicle. Positions were duplicated to provide comparative data between the two vehicle structures. A scaled enclosure contoured to fit the fuselage section provided the coupling between noise source and vehicle. The horn used was the same as that for the full scale.

For this reason the input spectrum is not shifted by the scale factor. Locations of all accelerometers and microphones are shown in Figures B13 and B14.

Random Excitation

With the model structure supported from springs to eliminate rigid body modes the noise source was close coupled to the fuselage center at Station 415. For purposes of this discussion, stations referred to will be the equivalent full scale station. The acceptance area of the model was approximately .85 sq. ft. The noise source displayed a continuous spectrum over the frequency range of interest. Measurements of the 24 fixed accelerometers and 6 fixed microphones were made and 34 roving accelerometer points. Sound pressure levels were measured along the vehicle to determine the gradient. All data was recorded in one-third octaves. The source was then removed 4 1/2 inches from the vehicle surface and a selection of four accelerometers and four microphones located over the length of the vehicle were recorded.

The source was then moved, in turn, to Stations 578, 647, and 735, and similar tests were performed utilizing only the fixed accelerometers and microphones. In each case the gradient over the vehicle length was recorded in addition to the above.

Tests at angles of incidence of 30° and 60° with the horn directed at Station 735 were performed in a manner similar to the full scale vehicle.

The horn directivity was also placed along the JATO thrust axis in a manner similar to the full scale tests.

Discrete Excitation

Resonant frequencies and damping of various panels and major structure was obtained using discrete excitation. Again only a representative scattering of points could be obtained due to the complexity of the vehicle modes. In order to eliminate error in panel response, due to accelerometer mass on the light panels, strain gage measurements were made to determine the desired information.

GENERAL

The data from full scale and model investigations has been tabulated and is shown in Appendix C. Values listed for accelerometer response are given in db re 10^{-6} g's. Full scale response data were taken over the frequency range from 160-8000 cps. Source input was maintained between 148 and 150 db for all full scale testing. Model testing was performed at an input level of 148 db and 136 db. The lower input level was used for nearly all testing as it appeared that the higher input was overdriving the model structure.

SECTION VI

FULL SCALE STRUCTURAL RESPONSE

DISCUSSION

An extensive survey of structural vibration response was made on both primary and secondary structure of the full scale Snark missile, for localized, broad band, acoustic excitation over several areas of the vehicle surface. The portion of the vehicle tested is the 31.4 ft. aft section, shown in Figure A3, between fuselage stations (FS) 384 and 761.

The purpose of these tests was basically to determine the overall vibration characteristics of this complex structure and the detailed vibration characteristics of its structural components. These response characteristics are desired, first, to advance the state-of-the-art in understanding and predicting random vibration responses of complex aerospace vehicles, and secondly, to assess the degree of dynamic similarity between the 1/4-scale Snark model and its full scale counterpart.

The vibration response characteristics discussed in this report are defined as the ratio of the steady state response at a given point on the vehicle structure to a steady state random oscillatory force applied over a limited area at another location on the vehicle skin surface. These ratios, referred to as "transfer functions," are expressed as rms averages over third-octave frequency bands.

A complete description of the vibration response characteristics of any structure requires the frequency response characteristics of the type just defined and time correlations, representing phase angles, between the responses at any two points on the structure. Within the time and funds available for the present series of experiments, the structural response characteristics obtained provided the maximum understanding of the response mechanism for the complex Snark structure. Numerous structural points were chosen over the entire vehicle for response measurements, in order to obtain an integrated or overall view of the particular manner in which such a structure vibrates. The frequency response functions obtained were recorded directly in 1/3-octave bands and required a minimum of data reduction. The more complex correlation investigations would have been permissible only at a limited number of structural locations since the associated data reduction must be performed by more costly automatic processes. The understanding of complex structural vibrations provided by the transfer functions will add considerably to an increased efficiency in making correlation measurements in future tests.

The type of acoustic excitation used for the major portion of the response survey was for a normal incidence condition known as the "closed box" input. The "closed box" is so called because the outer edge of the box, shown in Figures A26 and A27, which encloses the horn termination, is in direct contact with the surface of the vehicle, forming a nearly closed acoustic cavity.

Vibration tests were performed with this closed box centered, in turn, at fuselage stations (FS) 407, 578, 647, and 738, as shown in Figure B12. For each of these source locations, the average sound pressure level (SPL) contours along the axis of the vehicle are shown in Figures D1 through D4 for the third-octave frequency bands centered at 50, 100, 200, 500, 1000 and 2000 cps. These graphs show that, except for very low frequencies, a 20 to 30 db attenuation of the SPL was attained across the cavity walls, providing a high concentration of incident acoustic energy over a limited surface area of the vehicle.

It can be reasonably assumed that the relatively low level acoustic field over the structure, outside of the box , produces structural responses which are negligible in comparison to those transmitted through the structure from the concentrated source location. This type of excitation provided the most accurate, and yet practical, manner for experimentally determining the response at a point of the structure to an excitation over an area at another location.

As a precaution against artificial damping and attenuation of the local structural response, at the input location, from the contact pressure between the box and the vehicle skin, a soft rubber molding was attached to the contoured forward edge of the box. Preliminary tests at the forward end of the structure showed no significant response variations due to this contact pressure after application of the rubber molding.

Limited response surveys were also made for other types of acoustic excitation referred to as "open box," "horn only," "angle of incidence" and "simulated JATO."

The open box configuration is the same as the closed box, except that the entire sound system is moved away from the structure so that the forward edge of the box is at 18 inches from the surface of the vehicle. The purpose of such a test is to provide a set of structural response measurements for different, yet similar, SPL contours over the vehicle surface. Comparison of the closed and open box results is then used as a measure of the effect on the structural response characteristics of the SPL contour over the vehicle skin. In particular, it is aimed at investigating the problem of whether or not the acoustically excited vibration response of a complex aerospace vehicle is determined primarily by the local sound pressure field incident on the structure. A limited number of vibration response measurements were made with the open box centered at FS 405, 578, 647, and 738.

The "horn only" configuration is the same as the "open box" configuration except that the box enclosing the horn opening is removed. The induced structural response should be comparable to the "open box" responses. The tests with the horn at 18 inches from the vehicle surface were made near the end of the present series to supplement the limited response data obtained with the "open box".

Angle of incidence tests were performed using the open box described above but oriented at graxing incidence angles of 30° and 60° relative to the skin. The purpose of such tests were to determine the effect on the overall structural response characteristics of the variation of local structural "acceptance" to propagating acoustic waves. These tests were performed with the source center-line beamed at FS 738, as shown in Figure B15, and with the source facing aft, so that only a limited portion of the structural surface was subjected to propagating pressure waves of significant amplitude. Only limited response measurements were made for these tests.

In the full scale simulated JATO test, the mouth of the horn is located at the approximate position of the maximum exhaust noise generation of the booster rockets shown in Figure A1. The orientation of the horn is along the thrust axis of these rockets. This simulated JATO configuration is shown in Figure B15. The structural responses obtained in this test are a valuable check on any method used to predict overall vehicle response from a knowledge of the surface SPL's and the point-to-point structural response characteristics, including the effect of variable angle of incidence. The primary purpose of this test is to determine the feasibility of using an air modulated siren to simulate the booster rocket noise of the full scale Snark.

A total of 133 points were chosen on the full scale Snark structure for investigation of vibration response to the above acoustic excitations. Responses were measured at a select and limited set of these points for each type of input and input location. Forty-nine points are located within the compartment between FS 520 and FS 600, as shown in the compartment schematic of Figure B17, and responses at these points were obtained only for "closed box" excitation at FS 578. The locations of the remaining 84 points are shown in Figure B16. The response measurements made at the latter points are listed in Tables D1, D2 and D3, along with the precise locations, orientations and structural attachments of the accelerometers. The Patrick position accelerometers shown in Figure B16 refers to accelerometer locations used in the 1955 series of tests at Patrick Air Force Base on the full scale snark missile. These accelerometers were not removed after the 1955 test series and were used for measurements in the present tests.

The type structure to which the latter accelerometers are attached and the type of response associated with each, are divided into the following broad classes:

Bulkheads and floors:	radial or lateral in the plane of the bulkhead or floor.
Bulkheads:	vertical, normal to floor surface.
Floors:	longitudinal at bulkhead center.
Longerons:	radial at center of longeron segment between bulkheads.

Side panels: lateral at center

Top, bottom panels: vertical at panel center.

Ribs and ring stiffeners: lateral or radial.

Bulkhead - longeron intersections: longitudinal, lateral, vertical.

The detailed structural response characteristics of the vehicle can be expected to show similarities within each of these classes, while similarities between classes must depend upon the dynamic coupling existing between different types of structural elements. Therefore, in presenting and analyzing the measured structural responses, it is desirable to compare responses of a given class of components, noting what similarities and trends exist, and then to combine these results to obtain, first, a comprehensive understanding of the vibration response of the structure as a whole, and secondly, to distinguish between coupled overall and detailed local response characteristics.

The response survey within the compartment is an order of magnitude more detailed than the above investigation since response measurements were obtained for several locations on each of the major structural elements within the compartment. These responses are discussed in detail later in this section and it is shown that the response characteristics can be classified into similar categories.

The time availability and the economics of the present test program are sufficiently restrictive so that these analyses of the data must be limited to only the more significant correlations and trends in the measured response data. Detailed analyses leading to a more comprehensive understanding of the vibration characteristics of the subject vehicle would require a significantly greater effort.

The form of the transfer functions used to investigate structural response characteristics are developed below.

VIBRATION RESPONSE TRANSFER FUNCTIONS

Assuming linearity of the structure, the relation between structural response and applied acoustic excitation is

$$G_n = C_{nm} F_m \tag{1}$$

G_n = acceleration response, in g's, of the structure at point n

F_m = applied oscillatory force, in lbs., at point m

C_{nm} = linear force to response transfer function, in g's/lb. between points n and m

Define the following quantities:

G_o = reference acceleration response = 10^{-6} g's

P = excitation pressure level, psi

Po = reference excitation pressure = $29 \cdot 10^{-10}$ psi

Am = area over which excitation is applied at m

Ao = reference area = 1 ft^2

$R_n = 20 \ Log_{10} \dfrac{G_n}{G_o}$ = acceleration response in db

$I_m = 20 \ Log_{10} \dfrac{P_m}{P_o} = SPL$ = sound pressure level, (SPL), in db

$AR_m = 20 \ Log_{10} \dfrac{A_m}{A_o}$ = input area ratio in db

$T_{nm} = 20 \ Log_{10} \ C_{nm}$ = acceleration response transfer function in db

With these definitions, (1) can be written as follows

$$\frac{G_n}{G_o} = C_{nm} \frac{F_o}{G_o} \frac{F_m}{F_o}$$

$$= C_{nm} \frac{P_o A_o}{G_o} \frac{A_m}{A_o} \frac{P_m}{P_o}$$

Taking logs of both sides and multiplying by 20 gives:

$$R_n = T_{nm} + AR_m + I_m + 20 \ Log_{10} \frac{P_o A_o}{G_o}$$

Evaluation of the last term in this equation gives:

$$20 \ Log_{10} \frac{P_o A_o}{G_o} = 20 \ Log_{10} \frac{29 \cdot 10^{-10} \frac{lbs}{in^2} \cdot 144 \ in^2}{10^{-6} \ g's}$$

$$= 20 \ Log_{10} (.4175)$$

$$\cong -8$$

Solving for the transfer function Tnm gives:

$$T_{nm} = R_n - I_m - AR_m + 8$$

The area used in all of the full scale transfer functions is 10 ft^2. Thus $A_R = 20$db so that for the full scale structure

$$T_{nm} = R_n - I_m - 12 \quad \sim db.$$

BULKHEAD AND FLOOR RESPONSE

The section of the full scale Snark structure tested has nine bulkheads, some of which are partial bulkheads, located at the fuselage stations:

FS 384, 423, 464, 501, 536
600, 647, 706, 761

The sizes and shapes of these bulkheads are most clearly shown in the model photographs of Figures A5 through A24. Although the various bulkheads vary in size, stiffness and geometry, they are expected to exhibit certain response similarities.

Because of the high stiffness in the plane of a bulkhead, it is expected that the radial responses of opposite edge points on the bulkheads should be equal except at very high frequencies. This is shown to be the case in Figures D5, D6 and D7. In these graphs the lateral (or radial) edge responses of opposite points are shown for the three bulkheads at FS 384, 501 and 600 for two "closed box" excitations of each. It is seen that the responses are not identical, but are very nearly the same for all frequencies and for overall response. The greatest variation occurs for the bulkhead at FS 600. For forward excitation at FS 407, opposite points on the latter bulkhead have essentially the same transfer functions with frequency, but the accumulated differences included in the overall response amounts to 5 db. For direct excitation this overall variation increases to 14 db with some significant differences in the third-octave transfer functions. A possible explanation of these differences is that the opposite accelerometers #33 and #34 were not placed in exactly the same location relative to the very heavy lateral stiffness that extends from side to side across this bulkhead. This stiffener is shown in the isometric drawing of Figure B2. In the near neighborhood of such stiffeners the impedance of the structure is expected to have high space gradients.

Two heavy horizontal structural floors exist in the vehicle section tested. A forward floor is circumscribed by the upper right and left longerons between FS 384 and 461 and by the bulkheads at these stations. The second floor begins at the intersections of the lower longeron and bulkhead at FS 600, and extends diagonally upward, above the air intake duct, to FS 761.

Accelerometers #61 and #62 are located on the left and right upper longerons at approximately FS 445 and the radial response at these points should be significantly influenced by the presence of the forward adjacent floor. Three sets of accelerometers, (73, 74), (43, 44) and (52, 53) are also located at corresponding points on the right and left sides of the aft floor. Each of these pairs of corresponding accelerometers on the two floors show similar, and in some cases, nearly equal response for all frequencies and overall responses to inputs at FS 407 and 738, as seen in Figures D8, D9, and D10.

Since the acoustic excitation was applied to only the left side of the vehicle, the above response similarities indicate that, in an approximate manner, the stiff bulkhead and floor elements provide nearly rigid vibration links across the vehicle structure for the frequency range tested. At much higher frequencies these structural elements will become resonant and will interact with the transmitted vibratory energy causing filtering or attenuation across the structure.

Only a very minor amount of direct excitation is applied to the bulkheads and floors, and hence the lateral responses of these structural elements are determined by the responses of attached structure and the impedence match between these adjacent structures and the bulkheads and floors. In a sense, the bulkhead and floor responses are the dynamically weighted averages of the responses of adjacent structures. Thus if the mass loading of the adjacent structure by the bulkheads and floors were approximately the same in each bay, then the bulkhead and floor lateral responses would be a measure of the relative responses of the various structural bays throughout the vehicle. Assuming this to be true, the approximate axial variations of response along the structure are as shown in Figure D11 for overall responses for the four closed box acoustic excitations. Figures D12, D13 show similar response variations for the 250 cps and 2000 cps third octave bands. The lateral response of the forward bulkhead—forward floor intersection, is included (accelerometer #18). At FS 647 the lateral response shown is measured at the center of the bulkhead.

The axial attenuation of vibration is clearly evident in Figures D11 - D13, especially for excitation at either end of the structure. Excitation at the center of the vehicle shows the least axial attenuation in the aft structural region because of the consistently high response of the next to the last bulkhead at FS 706.

The most consistent attenuation is shown in Figure D13 for forward excitation in the 2000 cps, 1/3-octave band. Here the attenuation in decibels is essentially linear with distance from the source. Such a decay is represented by the relation

$$R_2 - R_1 = 20 \, \mathrm{Log}_{10} \frac{G_2}{G_1} = -\alpha (x_2 - x_1)$$

R_2 = response at x_2 in decibels

R_1 = response at x_1 in decibels

G_2 = response at x_2 in g's

G_1 = response at x_1 in g's

α = attenuation constant

or its equivalent

$$\frac{G_2}{G_1} = 10^{-\alpha(x_2 - x_1)} = e^{-2.3\alpha(x_2 - x_1)}$$

For this case the constant $\alpha \approx$ .09 decibels/in or approximately 1.1 decibels/ft. The best estimates of α for excitation at FS 738 is 1.2 decibels/ft.

For 250 cps excitation at the forward and aft ends, α is grossly estimated to be .84 db/ft and .48 db/ft respectively. The low frequency attenuation is expected to be somewhat lower than for high frequencies. These values compare with .6 at 250 cps and 1.2 at 1000 cps found several years ago, ref. 9 and 10, on a section of fuselage extending from Station 300 to 600. These old data represent radial excitation with a shaker at Station 600 and responses measured radially at various bulkheads.

The above axial attenuations to localized excitation have been briefly considered for lateral responses of a particular type of structure. It is interesting to note that this general axial attenuation also occurs for a wide variety of structural components and principle response directions. Figure D14 shows the response transfer functions for 14 different locations on the structure which include longitudinal, lateral, and vertical response directions. The responses are presented for excitation at FS 407 and 738. Note that the general structural response levels at the center of the vehicle are approximately equal for excitation at either end.

The response transfer functions T_{nm} are summarized in Figures D15 through D28 for lateral responses at the edges of floors and bulkheads. On reviewing these data as a group, the following summary general trends are to be noted:

1. In the lower 1/3-octave bands, the responses of various bulkheads to excitation over a given area, and the responses at a point due to excitation at several locations are of the same order of magnitude, and in some cases appear to have similar variations with frequency.

2. The frequency regime from 100 cps to 500 cps appears to be predominantly resonant with a large number of resonance peaks occurring in the 250 cps and 400 cps 1/3-octave bands.

3. The responses tend to be minimum in the 500 cps to 1000 cps frequency range.

4. At or near 1000 cps the responses increase with increasing frequency, in some cases very abruptly, to response maximums at or above 2000 cps.

5. For direct excitation certain responses exhibit an average increase with frequency of 5 - 6 db/octave indicating an approximate constant velocity response.

6. For excitation at a considerable distance from the local excitation, several of the responses decrease with increasing frequency at a rate of approximately 6 db per octave showing the axial attenuation of the vehicle.

It is interesting to note that for a single degree of freedom system, a constant velocity response with frequency corresponds to a predominance of damping in the system. The structural components of the vehicle which exhibit such response have high local damping. It is also possible that these structures are merely transmitting the major portion of incoming vibratory energy so that a sort of structural radiation impedance is producing an effect equivalent to damping. This point is discussed more fully later in this section in connection with the compartment survey.

The vertical response transfer functions for typical heavy structure are shown in Figures D29 - D33 for the four "closed box" excitation locations. The response characteristics are similar to those found above for lateral excitations of equivalent heavy structure. The 250 cps resonance is apparent in several of the responses but the resonance at 400 cps is much less pronounced. The accelerometer #13 at FS. 600 is located at the upper longeron-bulkhead intersection. As is shown below in the compartment survey, the frequency response at this point is typical of the responses obtained within this compartment, and hence represents a local structural vibration characteristic.

The longitudinal responses of heavy structure are shown in Figures D34 through D38 for the excitation at the various closed box input locations. The most striking feature of these responses is the very high resonant peak for accelerometer #4 at FS. 600. This high response occurs consistently for excitation at all locations. Comparison of this response with the longitudinal response at other points, indicates that this condition is primarily local since only minor resonances occur in this band at the other points.

A rather large attenuation of longitudinal response occurs between the bulkheads at FS 600 and 647 for excitation at FS 407 and 578. This is evident from a comparison of Figures D37 and D38.

A rather detailed survey was made of the responses of the forward bulkhead at FS 384 to a local lateral excitation at FS 407. The responses shown in Figure D39 are lateral, vertical, and radial. A predominant resonance occurs at 400 cps and this resonance is evident in all response directions and locations on the bulkhead. The resonance for accelerometer #7 is much more broad than the other resonances. This is probably caused by the horizontal slotted opening in the face of the bulkhead which partially separates the upper cap of the bulkhead from the lower portion of the bulkhead. Further, it is to be noted that the rate at which the response increases at the higher frequencies is approximately the same for all variations and locations of the pickups.

LONGERON RESPONSE

The fuselage section tested contains four main longerons between FS 384 and 600. These longerons are shown in the isometric drawings of Figure B2, and can also be seen in the partially assembled model shown in Figure A5. The longerons are relatively stiff structural members which form the primary longitudinal ties between the various bulkheads.

Since these structural components are continuous along the axis of the above portion of the fuselage, the radial responses, at various axial locations, of any one longeron are expected to exhibit a certain similarity. This is shown to be the case in Figure D40 for accelerometers #68 and #71 located on the upper left longeron at FS 487 and 576 respectively; the excitation is at FS 405. Similarly for the lower left longeron at the same fuselage stations, the responses measured by accelerometer #66 and #72 to excitation at FS 407 are seen to be quite similar. In Figures D42 and D43, the above similarities are observed in the frequency distributions of the responses; however, the effect of axial attenuation is apparent.

As shown in Figure D40, the response of the upper left longeron, accelerometer #61, forward of the double bulkhead at FS 465 has a somewhat different frequency distribution. This can be attributed either to the presence of the adjacent upper floor or to the massive double bulkhead at FS 465. The latter possibility appears more plausible in the light of Figures D41 and D44. Accelerometers #63 on the lower left longeron, forward of the double bulkhead has a significantly different response than #66 on the same longeron but aft of the double bulkhead. In Figure D44, accelerometers #60 and #64 forward of this bulkhead and on the lower right longeron have resonant responses at a single frequency which differs from the single frequency resonances of accelerometers #65 and #69 aft of this bulkhead. Probably the double bulkhead and the floor constitute significant structural discontinuities in the longerons, at least at the lower frequencies. At high frequencies the above responses exhibit a lesser influence by these structural components.

A partial correlation of response attenuation provided by the double bulkhead, for all four longerons and for local excitation at FS. 407 is shown in Figure D45. At selected 1/3-octave frequency bands of 160, 250, 400, 1000 and 1250 cps, the response differences (db) across this bulkhead are essentially the same for the two lower right and left longerons, with a one db variation at 250 cps. Greater differences in attenuation are noted for the upper longerons, except at 250 cps where once again there is only a one db difference variation. At all other frequencies the attenuations for corresponding right and left side longerons have no apparent correlation. Further, for excitation at FS. 738 there appears to be no such correlation at any frequency, other than accidental attenuation equalities. It is to be noted that the selected frequencies correspond generally to resonances and antiresonances in both the longerons and bulkhead measured responses. A resonance response occurs at 250 cps for a large number of these response functions.

It was shown previously that the responses of bulkheads in the plane of their edges were nearly equal at opposite edge points for vehicle lateral response. Since the longerons are attached to the bulkheads and because the corresponding right and left side main structural components are identical, then the corresponding right and left longeron segments between bulkheads should have similar responses. This is shown to be the case in Figures D46, D47, and D48 for three locations on the upper and lower longerons for excitation FS. 407 and 738. The greatest variation occurs in the lower longeron, forward of the double bulkhead, to excitation at FS. 738.

Comparing Figures D44 and D49 shows the general difference in response level of the upper and lower right longerons to excitation at FS. 407. The lower longeron has a higher response, probably due to its large surface area which is directly exposed to the excitation. It is interesting to note that the upper and lower left longeron segments in the central bay (FS. 550 to 600) however show approximately the same response to excitation for the nearly equidistant source locations at FS. 407 and 738, Figure D50.

Figures D51 and D52 show the characteristic attenuation through the structure for excitation at a distance source, FS. 738, the attenuation increasing with frequency. This characteristic also occurs for the heavy bulkhead and floor components.

Finally, the variation of longeron response with location of the excitation is given in Figures D53 through D56 for four different accelerometers. The primary feature to notice here is that, on the average, a 15 to 20 db difference in response occurs between local excitation and excitation at a large distance.

PANEL RESPONSES

The stiff floors and bulkheads of the full scale Snark fuselage were shown above to be primary, low attenuation, vibratory energy paths which rigidly link both the right and left side structures. As a result, corresponding longeron segments on the two sides of the vehicle were shown to exhibit similar response characteristics, even for single side acoustic loading. Since the side panels forward of FS. 600 are mounted on these bulkheads and longerons, it is expected that opposite panels might exhibit similar response characteristics. Comparisons of opposite side panels are shown in Figures D57 and D58 for excitation at FS. 407 and 738. These comparisons are made for opposite panels forward of the double bulkhead and for opposite panels aft of this bulkhead. Corresponding panels directly aft of the double bulkhead, Figure D58, show nearly equal responses while those forward of the bulkhead are similar in frequency distribution but show significant amplitude differences. This excitation however is precisely that which was observed for the longerons attached to these four panels. The main difference in response of the panels aft of the double bulkhead is that the resonant peaks of the right panels are sharply defined while those of the left panels are quite broad.

Accelerometers #45 and #46 show, in Figure D59, that the pair of aft panels at FS 684 have almost identical responses to excitation at FS 405. Greater response level differences occur for local excitation at FS 738. This indicates that as the vibratory energy is transmitted axially through the various bulkheads, floors, longerons and panels, the energy over a given cross-section of the fuselage approaches a uniform distribution, the level of the response depending primarily upon the local mass and stiffness of the structure.

For excitation at FS. 407, Figures D60 and D61 show that a major panel resonance occurs in the 250 cps, 1/3-octave band for both right and left side panels forward of FS. 600. This resonance is apparent also in the second and fourth bulkheads at FS. 420 and 501 respectively, as shown by Figures D20 and D21. It is interesting to note that the forward bulkhead at FS. 384 and the bulkheads at FS. 536 and 600 show only minor resonant tendencies at 250 cps; see Figures D22, D23, and D24. The longerons adjacent to the above panels show significant resonances at 250 cps as seen in Figures D46 through D50, and these include longeron segments as far aft as FS. 600. Indications are then that bending waves are propagated down the panel region, between the upper and lower longerons, forward of FS. 600, with the bulkhead edges acting approximately as node lines.

It is interesting to note that a large amount of energy in the 250 cps band is being transferred to longitudinal response at the longeron-bulkhead intersection at FS 600. See Figure D37.

Figures D5, D6, and D7 and Figures D41 through D48 show generally that the bulkheads and longerons exhibit certain resonant responses in the 315 cps and 400 cps, 1/3-octave bands. These resonances are considered to be those associated with the broad resonant responses of the left side panels as seen in Figure D60. The right side panels in Figure D61 do not show such broad resonances.

A general summary of panel responses to the various closed box acoustic excitations is given in Figures D62-D70. These show that the relationship between panel response level and distance to the input location is about the same as for the bulkheads and longerons.

In order to see more clearly the interactions of the main structural component of the Snark fuselage, responses are presented in Figures D71 and D72 for the left upper and lower longerons, bulkhead, panel and ring stiffener in the bay between FS. 536 and 600. These responses are shown for inputs at FS. 407 and 578.

For closed box excitation at FS. 407, the response of this panel is primarily due to vibratory energy transmitted through the structure since the incident sound energy on the panel is relatively low. In Figure D71 the response of the bulkhead at FS. 600 is seen to be far below the panel response except at frequencies below 160 cps and above 1600 cps. The bulkhead acts as a rigid foundation in this intermediate frequency regime. At 200 cps the lower longeron response is high and this accounts for the correspondingly high panel response. In the 250 cps, 1/3-octave band, both the upper and lower longerons are in resonance as in the ring stiffener at FS. 536, and these contribute to the high panel response in this band. In the 315 cps band the longerons continue to have a relatively high response as does the panel. At 400 cps the upper and lower longeron responses drop considerably below the panel response, but the ring stiffener enters another resonance. It was concluded above that this frequency probably corresponds to bending wave propagation along the left side panels, between the upper and lower longerons; and this appears to be consistent with the presence of the ring stiffener resonance. The broad resonant panel response is thus due to several major component resonances. Above 600 cps the responses of the panel and adjacent structural elements are nearly equal, except the bulkhead. It is interesting to note the abrupt rise in the response of all components at 1000 cps.

Responses to the direct excitation of the panel are shown in Figure D72 . Here the panel response is higher than the adjacent structural components as expected, since for direct panel excitation, the panel "drives" all structure attached to it. The resonance at 100 cps is associated with a basic vehicle resonance. The other resonances which appeared for excitation at FS. 407 are not so dominant for direct excitation indicating that the response is much more a forced response than a resonant response.

A summary of full scale response transfer functions are presented in Figures D73 through D81 for intersection points of longerons and bulkheads and for aft sub-skin stiffeners. These are not analyzed in the present discussion.

ANGLE OF INCIDENCE TESTS

Response of four accelerometers, #58, 71, 73, and 84 to acoustic excitation centered at FS. 738, but directed at 30°, 60°, and 90° grazing incidence angles are presented in Figures D82, D83, D84, and D85.

In general the 30° and 60° grazing inputs produced similar frequency response functions, while the responses corresponding to normal incidence are seen to be somewhat different in shape but not significantly differnt in magnitude. The greatest differences in magnitude are of the order of 10 db.

For accelerometers #58, 71 and 73 the grazing incidence excitations produce resonant responses at several frequencies which are apparently resonant to normally incident excitation. Although the tests were limited, as well as the response data measured, these results might indicate limitations to normal incidence tests for simulation of propagating acoustic waves over the surface of a vehicle.

For accelerometers #58, 71 and 73, the responses to local excitation using the closed box at FS. 738 are shown in figures D82, D83 and D84. It is interesting to note that in each case, the greatest variation in the "closed box" response and the "angle of incidence" responses occurs at 200 cps and 1250 to 1600 cps; and for these frequencies the angle of incidence tests produced higher response. The latter appear to cause a resonant excitation at 1250 cps whereas the closed box tests produced an antiresonant type of response.

COMPARTMENT STUDY

A detailed study was made of the vibration response of structure located in the compartment between Stations 536 and 600. Measurements were taken at 49 positions, illustrated in Figure B17, with the compartment excited from the noise box located adjacent to the left side panel. The objectives of this study were to gain insight into the transmission of vibration into complex structure with local acoustic excitation, and to determine the variability of responses on different types of structural elements. The resulting transfer functions are summarized in Figures D86 through D94.

Figure D86 gives the transfer function on the main part left side panel which is directly excited, and Figure D87 gives the transfer function at two positions on the left side panel located in the small stiff portion forward of the rib. The majority of the data, with the exception of 27 which is located in the stiff lower forward corner, exhibit a major resonance at 250 cps. However, the most striking feature in Figure D86 is the average upward slope of approximately 6 db/octave above the resonant frequency range.

To determine the possible significance of the slope of the transfer function with frequency it is useful to note the slopes expected for stiffness, mass and resistance controlled responses. In the stiffness controlled response region, displacement is directly proportional to force. The transfer function is proportional to 20 times the logarithm of the ratio of rms acceleration to rms force. Therefore, when displacement ÷ force is constant, acceleration ÷ force is proportional to the square of frequency and the transfer function should increase at 12 db per octave. On the other hand, in the mass controlled region, acceleration is directly proportional to force and hence, the transfer function should be constant, independent of frequency. In the resistance controlled region, assuming linear viscous damping, the velocity is proportional to force, hence acceleration ÷ force varies directly with the frequency, and the transfer function increases at 6 db/octave.

Therefore, the positive slope of 6 db/octave seen in Figures D86 and D87 above the response of the input panel is controlled primarily by resistance. On reflection, this result is not surprising, for it merely states that the panel is acting as a source of mechanical power to the remainder of the vehicle. Since the panel representing the first element in the mechanical system is the receiver of the acoustic forces, it certainly has to transmit any power which flows into the vehicle. Therefore, when resonant responses in the receiving panel, in the local vicinity of the panel, or in a vehicle coupled mode, do not control the receiving panel's response, its response must be controlled by the effective resistance at its boundaries, when the panel looks into the total vehicle as does a mechanical driver.

The response on the stiff honeycomb forward raised floor again exhibits the characteristic 6 db/octave mean upward slope; however at a level approximately 12 db lower than on the directly excited forward left side panel. The small resonant responses at 200-250 and 400-500 cps are associated with the honeycomb forward bulkhead as seen in Figure D89. Here, two large resonant response regions are evident. However, the very stiff lower left corner has very low response at both resonances, and the upper outboard pickups, 11 and 12, which are located near the upper longerons respond at a lower level in the low frequency resonance region and appear unaffected at the higher frequency resonance. Comparison of Figures D88 and D89 shows that the values of the transfer function are identical at the 400-500 cps resonance indicating a possible coupled mode of these two structures. Further, the responses at all positions on the bulkhead become almost identical above the second resonance and have the same level as those previously seen in the forward upper floor, Figure D88.

The characteristics of the transfer functions in Figure D90 on the light-weight built-up main floor section are entirely different from those previously encountered on the driving panel and the stiff forward structures. Here the transfer function is characterized by a high resonance region between 160 and 250 cps, followed by a relatively constant value of approximately -25 db. Note that in the frequency region of constant transfer function is associated with mass controlled response, and that below 1000 cps the floor vibration is significantly higher than that of surrounding stiff structure, thus, it is probable that the floor vibration is controlled primarily by its own mass-stiffness-damping characteristic rather than by the impedance at its boundary. Hence, it acts primarily as a receiver of power, rather than as a transmitter.

The transfer functions for the aft bulkhead are given in Figure D91. At the highest frequencies, 1600 and 2000 cps the values of the transfer functions have increased to the level seen on the forward bulkhead and floor. The responses at 17, 33, and 31, which are located along the top and bottom of the bulkhead, are similar in level to the responses on the forward floor, except for an increase in the transfer function at a resonance between 160 and 200 cps. The response in the center of the panel at position 32 is generally high throughout the frequency range. However, the vertical response on the substructure at position 49 is considerably lower than elsewhere, and of the same order as the normal response at the stiff lower corner 13 of the forward bulkhead.

Figures D92 and D93 summarize the transfer function's measured on the light-weight built-up bay cover. Although there are immeasurable details which can be seen with careful study of this mass of data, only major trends are noted. In general, the responses on the side near the excitation are higher than the responses at similar locations on the far side. Secondly, the general trend of each of the responses show strong local and coupled resonances below 600 cps, followed by constant, or rising, transfer function values as frequency is increased. Thus, the responses of the light bay cover, although more complex, are primarily locally controlled in a manner similar to those on the light-weight main floor.

The transfer functions of the right side panel are given in Figure D94. The responses are similar at all locations, with the exception of pickup 48, which is located in the lower forward corner. This transfer function has approximately the same relationship to the other responses as does its mirror image 27 on the left side, see Figure D86. The response of 48 is 12 db lower than that at 27 at frequencies above 315 cps, but exhibits a 12 db resonance in the 200-250 cps region which does not occur at 27. The value of the transfer function at this resonance equals the value of the same resonance found on the forward upper floor which connects these two points.

For the majority of the positions on the right side the transfer function at 200-250 cps resonance is approximately 6 db below that on the directly excited panel, whereas the transfer function in the higher frequencies above 500 cps is approximately 12 to 14 db below that on the left side panel. Again, the high frequency transfer functions illustrate the 6 db rise, characteristic of resistance termination. The presence of lower attenuation at the 200-250 cps resonance might be anticipated because of the major resonances in these frequency ranges on the stiff bulkheads. It is probable that several of the resonances in this range are coupled modes involving several structural elements.

On the other hand, the difference at the high frequencies between the levels on the driving panel and other stiff panels in the compartment is almost constant. This effect would suggest the presence of a reverberant field within the compartment, where the energy density is essentially uniform.

These results, together with the attenuation in response as a function of axial distance shown previously, suggest the basic form of a model for transmission of vibration through a complex vehicle. There appear to be three primary frequency ranges which must be considered in this model:

a. Low frequency, characterized by basic vehicle modes where the entire vehicle participates in model response.

b. Medium frequency, characterized by fundamental panel-bulkhead-floor modes.

c. High frequency, characterized by local area or compartment reverberation and attenuated wave transmission along vehicle.

The low frequency region is generally below 100 cps and was not investigated in detail on the present vehicle. However, inspection of many of the transfer functions illustrates that the vibration amplitudes are similar on both ends of the vehicle as expected for a free body bending.

The medium frequency region appears to be generally between 100 and 600 cps from the data obtained here. In this region the responses of major panels, bulkheads, and floors are determined primarily by their own individual resonance characteristics, and are primarily in their fundamental and second harmonic modes. In many cases clear evidence exists of resonance associated with the coupling of two or more connected parts. Although these individual resonances dominate any local response functions they do not appear to play a dominant role in the transmission of vibration power through the vehicle beyond the region of local influence of the part. Rather the preponderant portion of the power in this frequency region appears transmitted by the stiff structure, for example in plane transmission through floors and bulkheads, and transmission through longerons and heavy framing. Since the responses in this medium frequency region appear controlled by individual mass-stiffness and damping parameters the response of light-weight flexible structure is considerably greater than that of heavy structure, for example, the bay cover and light main floor of the compartment as compared to the stiffer forward upper floor and bulkhead.

The high frequency region in these data, variously above 600-1000 cps, is above the basic modes of panels-bulkheads-floors main frames and longerons. The motion of these items near to the source of vibratory power tends to have constant velocity. Thus, these elements near the source act as though their motion is resistance controlled. This resistance control implies that these elements are acting as links in a transmission line which transmits vibratory power to adjacent portions of the vehicle. Furthermore, the evidence suggests that local compartment areas of the structure can be considered reverberant, as seen from the uniform energy density throughout the stiffer structure in the compartment study.

For the present vehicle the primary damping occurs at the joints. Therefore, within each reverberant area power is absorbed at each joint in the bay. However, the major power absorption mechanism is believed to be transmission of power longitudinally through the vehicle, rather than local absorption. This result is apparent when it is recognized that the axial attenuations of the order of one db per foot found for the vehicle reduce the level of energy reflected from distant portions of the vehicle so that it does not contribute significantly to the local reverberant energy density. Thus, definition of the local area of the vehicle in which reverberation is significant depends upon the structural configuration which, in turn, defines major reflecting boundaries, the number of joints, extent of continuous stiff structure, dissimilarity of adjacent structure, and attenuation factor.

COMPARISON OF LOCALIZED ACOUSTIC EXCITATION WITH ROCKET FIRINGS

It is interesting to compare the results of the transfer function studies of localized acoustic excitation with results obtained from rocket firings on the full scale vehicle. In Reference 9 a comparison is given between vibration on main stiff structural intersections and the acoustic level from rocket firings. These data were obtained during the 1955 tests at Patrick when the complete vehicle was tested in launch configuration except that the rocket boosters were mechanically detached from the fuselage.

The comparisons given in Reference 9 demonstrated that the vibration in the aft portions of the vehicle which were exposed to the highest noise levels were generally related to the external SPL. However, the vibration in the forward portion of the fuselage was not related to the comparatively low level noise external to the measurement location except at the highest frequencies. Rather the vibration in the forward sections primarily resulted from vibratory power transmitted from the highly excited aft fuselage.

In order to compare these results with the present transfer functions, it is necessary to determine the force input to the vehicle resulting from rocket noise excitation over the entire vehicle. However, as previously discussed in reference to the definition of the transfer functions, the response at any point in the vehicle is dependent on both the transfer function from each localized area and the phase relation between the various transfer forcing functions.

Recognizing this limitation, it is still interesting to estimate the transfer functions between external pressures and the adjacent internal vibration. This estimate is most worthwhile for the aft section of the vehicle where the internal response is probably most directly related to the adjacent external SPL. To obtain this estimate, it is necessary to estimate the effective area external to the location to determine the approximate force. A first estimate of this area was to assume that the effective area extended 1/4 around the circumference of the vehicle (approximately 6 ft. diameter) and covered one - two typical bays, approximately 6 ft. The transfer functions were computed utilizing the data of Reference 9, Figure 100b which gives the internal acceleration in octave bands for an octave band external SPL of 150 db.

The results are summarized in Figure D95 and compared with data from the present study. The eleven transfer functions for the localized excitation were obtained from responses at bulkhead and floor intersections with the surface resulting from adjacent local excitation. The estimate for the rocket data appears to be close to the median of the new data. Although the estimate of the rocket transfer function was somewhat oversimplified, the agreement is significant for the gross prediction of structural response. Further, the result suggests that the response of lightweight internal structure to rocket noise could be estimated from their transfer functions as long as the structure is located in regions of maximum excitation so that the assumption of the relationship between internal vibration and adjacent external noise holds. In addition, noting that the original comparison in Figure 100a, Reference 9 showed that the average B-52 and B-58 responses were similar to those obtained in Snark, the general levels of the transfer functions obtained in this Snark study may be typical for other vehicles.

SECTION VII

MODEL RESPONSE

The vibration experiments on the 1/4-scale Snark model were similar to those for the full scale vehicle. The major response data were obtained for "closed box" acoustic excitation at the four fuselage stations, FS. 415, 578, 647, and 738. Responses were measured at a total of 59 locations as opposed to the 133 for the full scale vehicle.

Key structural elements were chosen on the model for response measurements. Because the side panels on the model were quite light and because of the mass loading of these panels with the accelerometer, no panel response measurements were possible. Thus, the measurements were limited to stiff structural components such as bulkhead and floor edges and longerons. The number and location of the chosen response points are not sufficient to describe in detail the response characteristics of the model structure. Instead, it was decided that if the full scale and model responses at the points chosen showed that the model was truly scaled for vibration response, then the purpose of this portion of the program would be satisfied. If on the other hand, these responses showed variances in scaling, then additional measurements would be of value only for investigating the reason for the model inaccuracies. The measurements made give sufficient clues to model inaccuracies.

The model and full scale structural transfer functions can be compared by adjusting the frequencies and amplitudes of the model transfer functions to the comparable full scale values. This is done by using the scaling laws applicable for perfect geometrical and physical scaling of the model. From Table I it is seen that the model frequencies are four times higher than the full scale frequencies, so that for example, a model response at 1000 cps is shown as 250 cps in the graphical presentations of the transfer functions. The full scale and model transfer functions are

$$T^{FS} = R^{FS} - I^{FS} - AR^{FS} + 8$$

$$T^{M} = R^{M} - I^{M} - AR^{M} + 8$$

where

R = response in decibels, re 10^{-6} g's

I = sound pressure level in decibels, re 29×10^{-10} psi

AR = area ratio in decibels, re 1 ft^2

T = transfer function in decibels

The area over which the excitation is applied on the 1/4-scale model is 1/16 that for the full scale, so that

$$\mathcal{R}^{FS} = \mathcal{R}^{M} + 24 = 20$$

According to the scaling laws for acceleration in Table II, the magnitudes of model accelerations should be four times the comparable full scale accelerations so that

$$R^{M} = R^{FS} + 12$$

Thus for the same SPL on the vehicle surface, the full scale and model transfer functions differ by 36 db, that is,

$$T^{M} = T^{FS} + 36$$

if the model is perfectly scaled for vibration response. In order to compare model and full scale responses, it is necessary to account for the 36 db. Now the model transfer function is

$$T^{M} = R^{M} - I^{M} + 12$$

so that the adjusted model transfer function becomes

$$\begin{aligned} T^{M}_{adjusted} &= T^{M} - 36 \\ &= R^{M} - I^{M} - 24 \end{aligned}$$

The latter form of the equation for model transfer function is used throughout the remainder of this section.

COMPARISON OF FULL SCALE AND MODEL RESPONSES

The first comparisons of full scale and model response are for longitudinal vibrations as measured by accelerometer #4 at the intersection of the upper left longeron and bulkhead at FS. 600. The corresponding transfer functions are shown in Figures D96 and D97 for inputs at FS. 407 (415) and 578 respectively. The third octave amplitude variations with frequency of the full scale and model responses are seen to be essentially the same, however, there exists a small frequency and amplitude variance in the model responses. It is interesting to note that the error in overall response, in both cases, is within one db of the response error that exists between the resonant peaks.

Considering the fact that a frequency shift of 4-times has been made in the model, and an amplitude shift of 36 db in the model, the responses to forward excitation compare reasonably well. The variation is much greater however for direct excitation, as shown in Figure D97.

The lower left longeron responses are compared in Figure D98 for excitation at FS. 407 (415). Both the model and full scale show resonant tendencies at 250 cps and 400 cps. The radial model responses are seen to be higher than the corresponding full scale responses. The lower right longeron responses are compared in Figure D99. Here also the model responses are higher than the corresponding full scale responses.

A rather large variation in response level is shown for the upper left and right longerons as shown in Figures D100 and D101. It is seen that the model responses are considerably higher than they should be. It was seen in Section V that the lateral response of the upper forward floor and possibly the adjacent double bulkhead dominated the radial response of the attached upper longerons. There is a good indication that the scaled stiffnesses of this floor and other structure in this region are quite low causing a large local response. This is based partly upon the fact that the scaled structural masses in this section of the vehicle should be at least those of the full scale structure, and possibly higher, and upon the knowledge that the floors and bulkheads in this region were constructed with cores of stayfoam and plywood rather than steel honeycomb. Also, the stiffness of the bulkhead flanges to which the longerons are attached may not be properly scaled, and any reduced stiffness in these flanges would greatly increase the responses of the longerons.

It should be noted however that the construction used was sufficiently stiff to transmit vibration loads with little attenuation between the two sides of the vehicle. This is shown in Figure D102 for opposite accelerometers at FS 445. In this regard the full scale and model vehicles have similar characteristics.

Accelerometer #11, measuring vertical response, is located on this floor very near to the upper left longeron and bulkhead intersection. The full scale and model transfer functions at this point are shown in Figure D103. The responses compare reasonably well below 250 cps but diverge above this frequency. Because of the high structural impedance gradients that exist near joints, it is not known whether these transfer functions represent the vertical response of the floor or the response of the bulkhead and joint. At the higher frequencies the response is probably more typical of floor response. Note that at high frequencies the model response drops sharply while the full scale response increases. This indicates that the model is providing too high damping at high frequencies and this may be the effect of the stayfoam in floors and bulkheads.

Another example which indicates the possibility of the reduced stiffness of the model bulkheads is given by accelerometer #28 in Figure D104. This accelerometer measures the lateral response of the edge of the bulkhead at FS. 501. As seen, the model bulkhead scaled response is 15 to 30 db higher than the corresponding full scale response.

Full scale and model responses for the upper longeron segment, between FS. 536 and 600, are compared in Figure D105. Here the model response levels appear to be of the right order of magnitude, but show significantly different amplitude distributions with frequency. These frequency variations may be due partially to the fact that the brackets shown in Figures A34 and A36 which attach the longeron to the skin were not included in the model.

COMPARISON OF FULL SCALE AND MODEL RESONANT FREQUENCIES AND DAMPING FACTORS

Resonant frequencies of certain full scale and 1/4-scale model structural components were obtained by applying sinusoidal acoustic excitation at normal incidence, with the horn only, to localized regions of the two structures. These data are listed in Table III and Table IV.

Numerous resonant frequencies were present at each structural location, and those presented in these tables had the most dominant peaks. While running the tests it was possible in some cases to observe visually what structural elements had the highest responses and which resonances appeared to be fundamental resonances, and these are included in the tables under "remarks."

Table II shows that the resonant frequencies of the 1/4-scale Snark model, and any of its component elements, should be four times higher than the corresponding resonant frequencies of the full scale vehicle. From Table III and IV it appears that the following elements have fundamental natural frequencies which are nearly exactly scaled:

lower left longeron at FS. 405

left panel at FS. 440

and the elements which are scaled to within 40% are:

upper left longeron at FS. 405: 27%

upper forward floor at FS. 405: 40%

upper longeron at FS. 578: 30%

The apparent fundamental frequencies of the remaining structural components are either not scaled or the visual inspection of the structural response was inaccurate in determining which resonant frequency represented the fundamental mode of mode of response.

With one exception in these tests it was not possible to determine which resonances corresponded to higher natural frequencies of these structural elements. For such studies it would be necessary to use two or more pickups simultaneously and to determine the instantaneous phase relations between the measured responses.

It should be noted in the data of Tables III and IV that a large number of significant resonance peaks were measured at floors and bulkheads, including the upper longeron at FS. 405. These stiff structural members act primarily as transmitters of internal vibratory forces, and less as elastic resonators, so that their measured responses exhibit resonances of all adjacent, attached structural components. For such structures as panels, it is expected that the responses would be dominated by panel natural frequencies, and this was generally observed in the measurements.

The damping factors measured at certain full scale and model resonances are presented in Tables V and VI. The natural frequencies and bandwidths were determined using a frequency counter over 10 second intervals to give an accuracy of 0.1 cps. The quantity Q is defined as in the case of linear viscous damping in the single degree of freedom system:

$$Q = \frac{f_n}{\Delta f}$$

f_n = resonant frequency

$\Delta f = f_2 - f_1$

f_1 = lower frequency where response is .707 of the response at resonant frequency

f_2 = upper frequency where response is .707 of the response at resonant frequency

These data show, with a few exceptions, that the "quality factor," decreases with increasing frequency and hence the damping increases with frequency; and, this is true for both the full scale and model. The range of the damping factors for the two vehicles generally overlap and it is not possible to conclude with any certainty which vehicle has the greater overall damping. Considering the one panel measurement mode at FS. 578, the model panels may have considerably less damping. Comparing the bulkhead at FS. 384, it is seen that the full scale structure has the greater damping.

TABLE III

RESONANT FREQUENCIES OF FULL SCALE SNARK STRUCTURES

Fuselage Station	Structural Component	Resonant Frequencies	Remarks
405	Lower Left Longeron	151 cps 174 380, 473	Strong resonance Fundamental
405	Upper Left Longeron	189, 242, 346 370 391, 405 433 530	 Fundamental Floor resonance
405	Upper Right Longeron	233 373 430 540	Panel resonance Fundamental Floor resonance
405	Upper Forward Floor	111 162 178 214 247 288 347, 352, 373 430 530	 Broad resonance Weak resonance Strong resonance Strong fundamental Strong resonance
440	Center of Left panel	238 255 310 528	Strong fundamental Broad resonance
384	Forward Bulkhead; Fore and Aft Excitation	123, 175 197 283 344 404 671	 Fundamental Panel resonance Stringer resonance All stringers resonance
578	Upper Longeron	263 283 313 348, 463, 838	Lower longeron res. Fundamental Upper bay cover
735	Center of left panel	106 147, 175 254 274 331 369, 400	All panels locally Panel and stringers Second panel Second mode First panel

TABLE IV

RESONANT FREQUENCIES OF 1/4-SCALE SNARK MODEL

Fuselage Station	Structural Component	Resonant Frequencies	Remarks
405	Lower Left Longeron	284, 581, 1203 318, 401 664 795 926	Accelerometer #2 Fundamental Upper fwd. floor Fwd. bulkhead
405	Upper Left Longeron	462, 580 853 935 1168	Accelerometer #2 Fwd. bulkhead Fundamental
405	Upper Right Longeron	570, 680 652, 787, 810, 887 943 973, 1008, 1080 1268, 1467, 1568	Accelerometer #2 Fwd. bulkhead Strong resonances
405 ❷	Upper Forward Floor	227, 400 314, 454, 582, 680, 907 1099, 1213 797	Accelerometer #2 Fundamental
440	Center of Left panel	462 926 795 1207, 1475	Accelerometer #2 Fundamental Lower longeron
384 ❸	Forward bulkhead; Fore and Aft Excitation	77 116 228 341, 503, 526 560, 585, 710 774, 979	Accelerometer #3 Accelerometer #2 Fundamental Strong resonance
578 ❶	Upper Longeron	397 705 746 774 867	Accelerometer #2 Bulkhead Panel Fundamental
578 ❶	Lower Left Longeron	679 835 1173	Panel Fundamental

TABLE IV

(Continued)

Fuselage Station	Structural Component	Resonant Frequencies	Remarks
738	Left side Panel	255 418, 653	Aft floor
738 ❶	Left side Panel	305, 316 398, 670 808	Fundamental
460	Bulkhead Edge	244, 410, 475 586, 656, 693 836, 925, 1027 295 320 778	Fundamental Strong resonance Accelerometer #2

❶ Determined by use of a bending beam

❷ Excitation from left side of vehicle

❸ Fore and aft (longitudinal) excitation at forward bulkhead.

TABLE V

FULL SCALE MEASURED DAMPING FACTORS

	Location	af CPS	af CPS	Q
	384 Bulkhead	196.1	3.7	53.0
	384 Bulkhead	305.9	9.2	33.3
(1)	405 Floor	190.6	7.2	26.4
	405 Floor	247.5	3.4	72.8
	405 Floor	330.7	7.8	42.5
	405 Floor	248.3	4.3	57.8
(2)	405 Floor	288.7	10.7	27.0
	405 Floor	346.7	6.3	55.0
	578 Panel,Ctr.	194	5.5	35.3
	578 Upper Longeron	280.9	8.1	34.7
	647 Bulkhead	110.1	2.2	50.2

(1) Driven from forward end
(2) Driven from side of vehicle

TABLE VI

1/4-SCALE MODEL MEASURED DAMPING FACTORS

Location	fn CPS	af CPS	Q
384 Bulkhead	205.8	6.8	30.3
384 Bulkhead	502.6	20.7	24.2
384 Bulkhead	582.6	41.9	13.9
405 Floor	231.8	6.4	36.2
405 Floor	480.6	20.3	23.6
405 Floor	524.3	26.3	19.9
405 Floor	693.2	27.1	25.6
405 Floor	774.8	14.9	52.0
578 Upper Longeron	368.7	6.6	56.0
578 Upper Longeron	540.9	6.7	80.9
578 Upper Longeron	885.1	36.2	24.4
578 Panel	779.6	8.7	89.6

SECTION VIII

CONCLUDING REMARKS

The need of the dynamicist for the experimental dynamics tool resulting from the development of the total dynamically similar structural model concept was established at the beginning of the program. The importance of the experimental technique presented is that it shortens the design period by providing solutions, within the design stage, to the problem of response prediction and fatigue life. These predictions are needed for structural reliability. A positive approach to structural reliability is thereby accomplished. Therefore, reliability tradeoffs between the value of reliability and the cost per unit of reliability for upgrading individual items can begin with knowledge of the structure and equipment responses.

This work was directed towards several specific steps within the overall reliability problem. The results lead to the following conclusions:

1. **An excellent concept for applying dynamically similar structural models to vibration and acoustic studies in a high frequency range has been presented. It is based on scaling law development, scaled engines and feasibility studies in complex structures, and (in a previous study) acoustic fatigue failures of panels.**

2. **The concept is based on item-by-item scaling of all significant structure, mass items, including fluids, equipment or fittings, stiffness, damping, and the excitation forces. Thermal scaling can be accomplished within this same concept including transient temperature variations based on the use of scaled heat sources.**

3. The concept has been successful in flutter models in scaling the gross structural motions in the primary vehicle modes of wings, empennages, and fuselages. Scaling has been demonstrated at the smallest component level in panels. Demonstration was attempted in complex structure in this study.

4. In skilled hands, the concept may be applied in attempting larger projects, including complete vehicle complex structure. A parallel development of substudies to upgrade further the statement of technique would be required. The scale of the substudy development would need only to be in scale with the project attempted. The substudy effort in this case was of the order of 15% of the total.

5. Dynamic similarity studies made under this program: damping, joint, and fabrication, support the conclusion that no limitation was encountered or indicated. The degree of accuracy to be expected for the vehicle as a whole cannot be defined because the demonstration contained a major impedance.

6. It was shown that the structural sandwich scaling was easily accomplished when the idea of simplification and material substitution was dropped in favor of direct honeycomb scaling.

7. Original impressions of riveting costs and honeycomb simulation costs were shown to be incorrect and direct simulation of these details were successful and would not add to the cost of the model. The main conclusions of this work however has been that the degree of fidelity required in the modeling must be free of compromise and free of unsupported or untested model structural design techniques.

8. Three basic frequency regions can be defined for vibration response of and transmission by major structural units. These definitions, which should assist in the orientation of both empirical and analytical prediction techniques, are:

   Low frequency, characterized by basic vehicle modes when the entire vehicle participates in model response.

   Median frequency, characterized by fundamental panel - bulkhead - floor coupled and uncoupled mode.

   High frequency - characterized by local area or compartment reverberation and attenuated wave transmission through the vehicle.

9. Stiff members, such as bulkheads and floors in plane, act as reasonably rigid links across the vehicle, such that the vibration response tends to be identical on both sides within the frequency regime under study, which is below the first longitudinal wave resonance.

10. A definitive statement of the modeling technique is given in Table VII.

TABLE VII

DEFINITIVE STATEMENT OF TECHNIQUE

1. Item-by-item scaling of all structure is accomplished by a linear reduction of all dimensions. Mass and equipment items are also scaled to the degree of obtaining at least weight, center of gravity, inertia and attachment simulation. Special consideration must be given to fluid scaling. The special objective of each particular project will determine the nature of the mass simulation.

2. Structural stiffness, mass and damping are each of equal importance in simulating the full scale dynamics.

3. Stiffness simulation of each structural element requires the area moments of inertia about the three principle axes to be simulated at all points of the elements.

4. Mass simulation requires the mass moments of inertia about the three principle axes to be simulated.

5. Damping is nonlinear with frequency and amplitude. Because the frequency scale is increased, the model damping may tend to increase over the full scale value. Slip damping is the mechanism which generates damping in complex structure, and this depends on surface contact pressures. Fabrication and joining should consider a reasonable duplication of these pressures.

6. The degree of fidelity required in the modeling is very high. Compromises unsupported by test should not be used. The means of attachment and assembly should be followed carefully. Sheet metal angles will not ordinarily be a satisfactory substitute for extrusions, etc.

7. Scaled instrumentation, such as accelerometers and strain gauges, is required for accurate comparison between model and full scale response.

8. A reduction in scale should be governed by choice and practical availability of the scaled excitation. If a scaled engine is used the engine size should be considered in setting the scale factor.

9. Scaling limitations result from practical problems associated with skin gauges, instrumentation, frequency capability of the instrumentation and tolerances.

10. Thermal scaling is obtained by the use of scaled heat sources. The heat input crossing the external envelope of the vehicle is required and its distribution must be simulated. Heat losses and their distribution may also be required.

11. Use of the model may be made in a wind tunnel to determine the aerodynamic excitations. Limitations exist due to failure to scale Reynold's number, Mach number, and dynamic pressure simultaneously along with other demensionless flow variables. The approximate interaction between response and excitation may be obtained. Thermal data or thermal scaling is generally considered unsatisfactory in a wind tunnel.

12. The models may be used for environment or combined load determinations, structural characteristics, structural response or failure mode determination. Development in this project was mainly for response determination. For many failure modes, the scaling relationship may not be known. For the fatigue failure mode, for example, the scaling laws based on scaled crack propagation do not apply and experimental relationships must be used. Substudies are indicated on failure modes of importance to particular projects.

13. Substudy support to the modeling design should be in balance with the project attempted. This substudy support may be a small percent of the total cost but should not be omitted.

14. The usable frequency band is related in part to the size of the smallest detail which is faithfully reproduced. This implies the normal relationship between transmission velocity, wave length, and frequency.

15. Full scale responses are obtained from model scale response via the relation

$$\delta_{f.s.} = \frac{\delta_{model}}{n}$$

Vibration velocities are equal in both scales.

16. Structural sandwich scaling must be faithfully reproduced including edge attachment and edgemembers. Core density in pounds per square foot remains the same.

APPENDIX A

FULL SCALE AND MODEL PHOTOGRAPHS

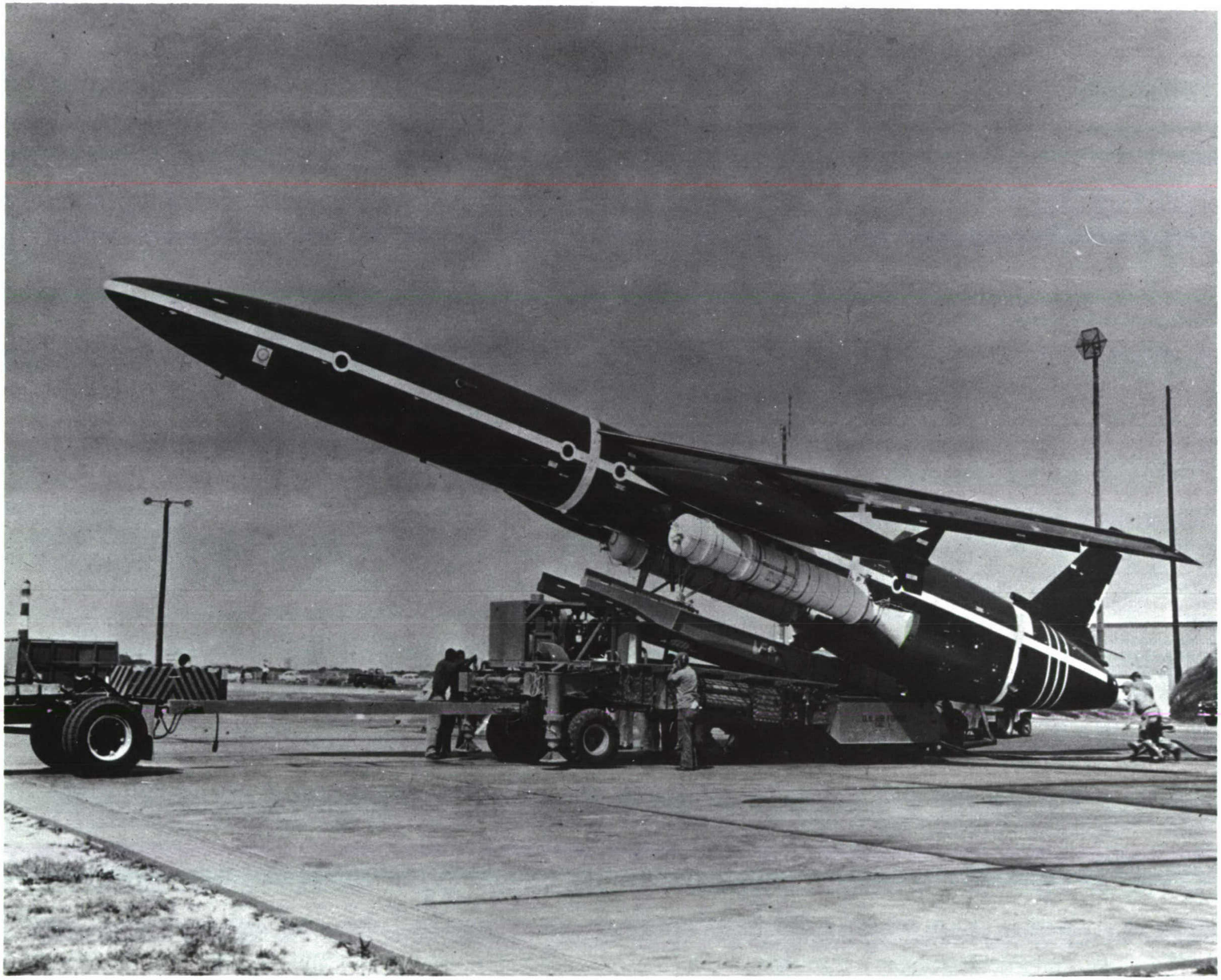

FIGURE A1 SNARK MISSILE

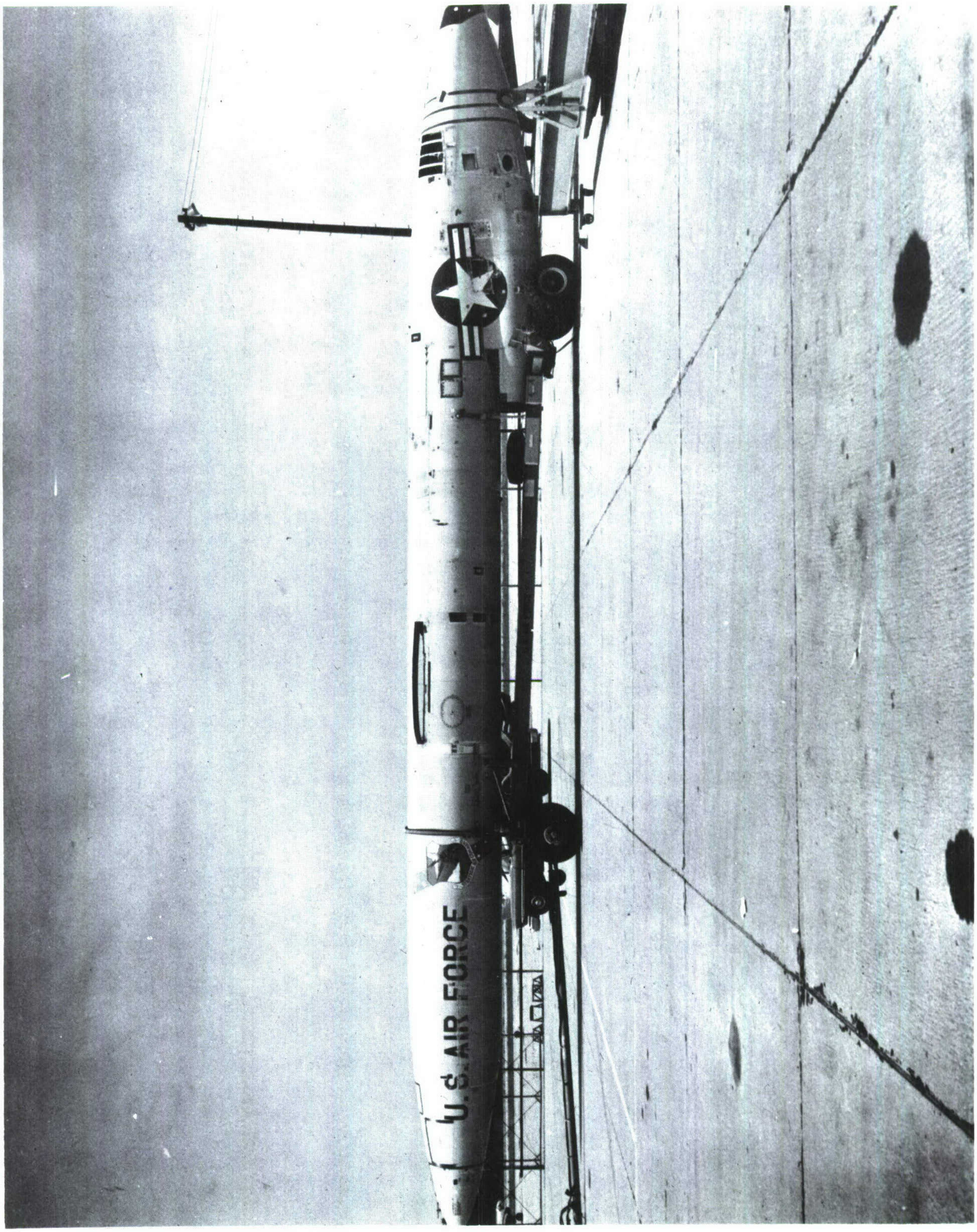

FIGURE A2 MISSILE FUSELAGE, SM-62A

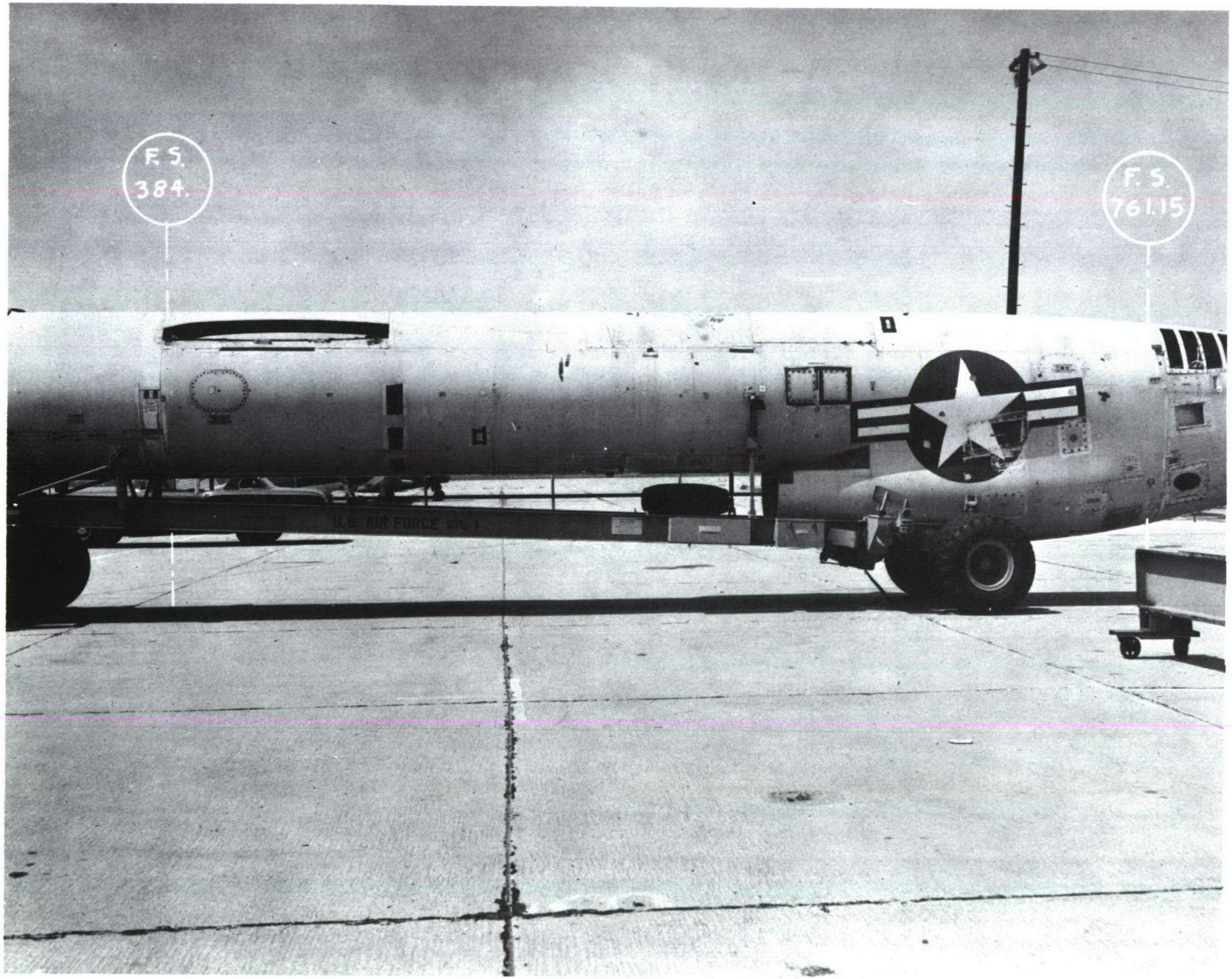

FIGURE A3 VEHICLE, SM-62A

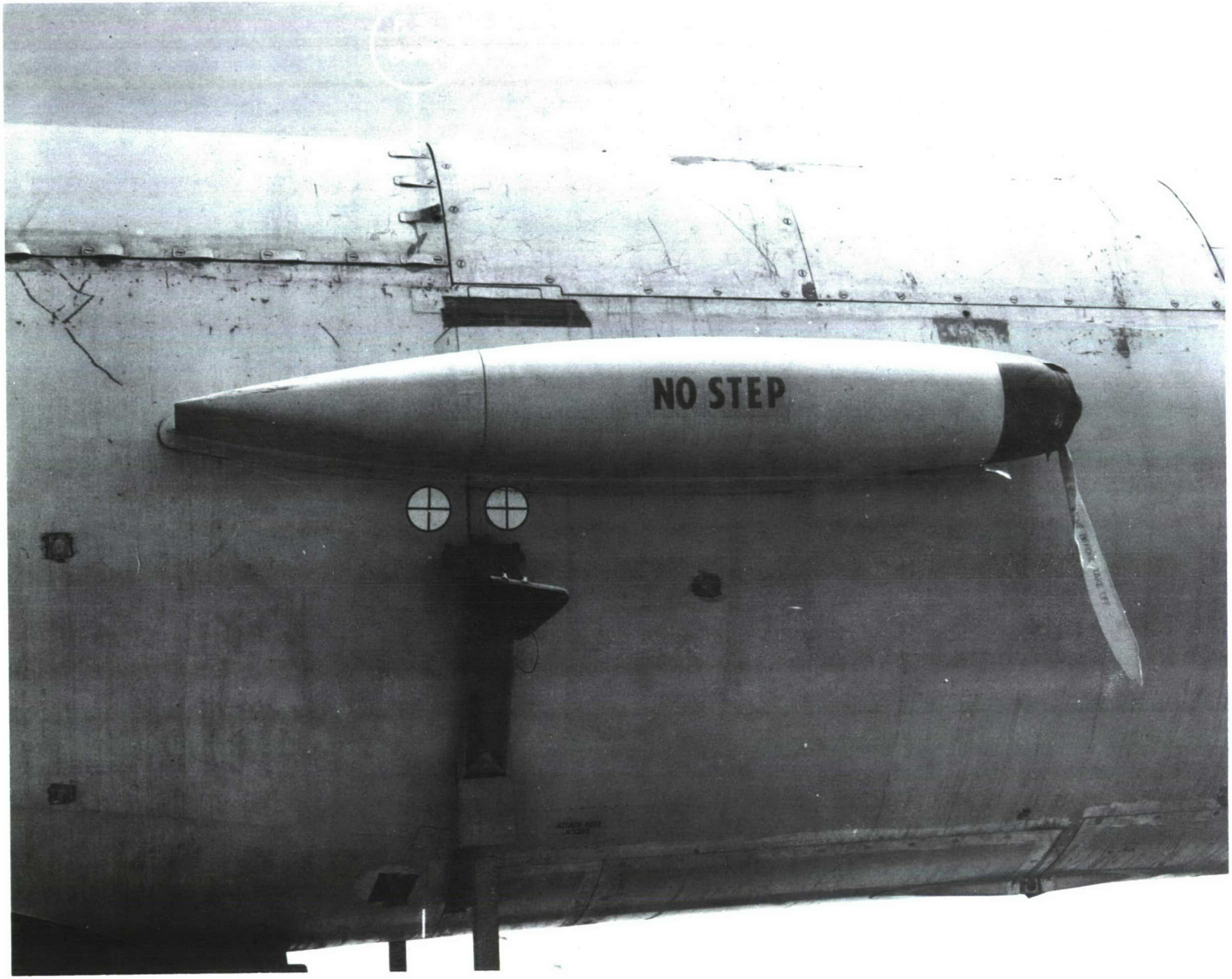

FIGURE A4   AIR SCOOP ON R.H. SIDE OF VEHICLE

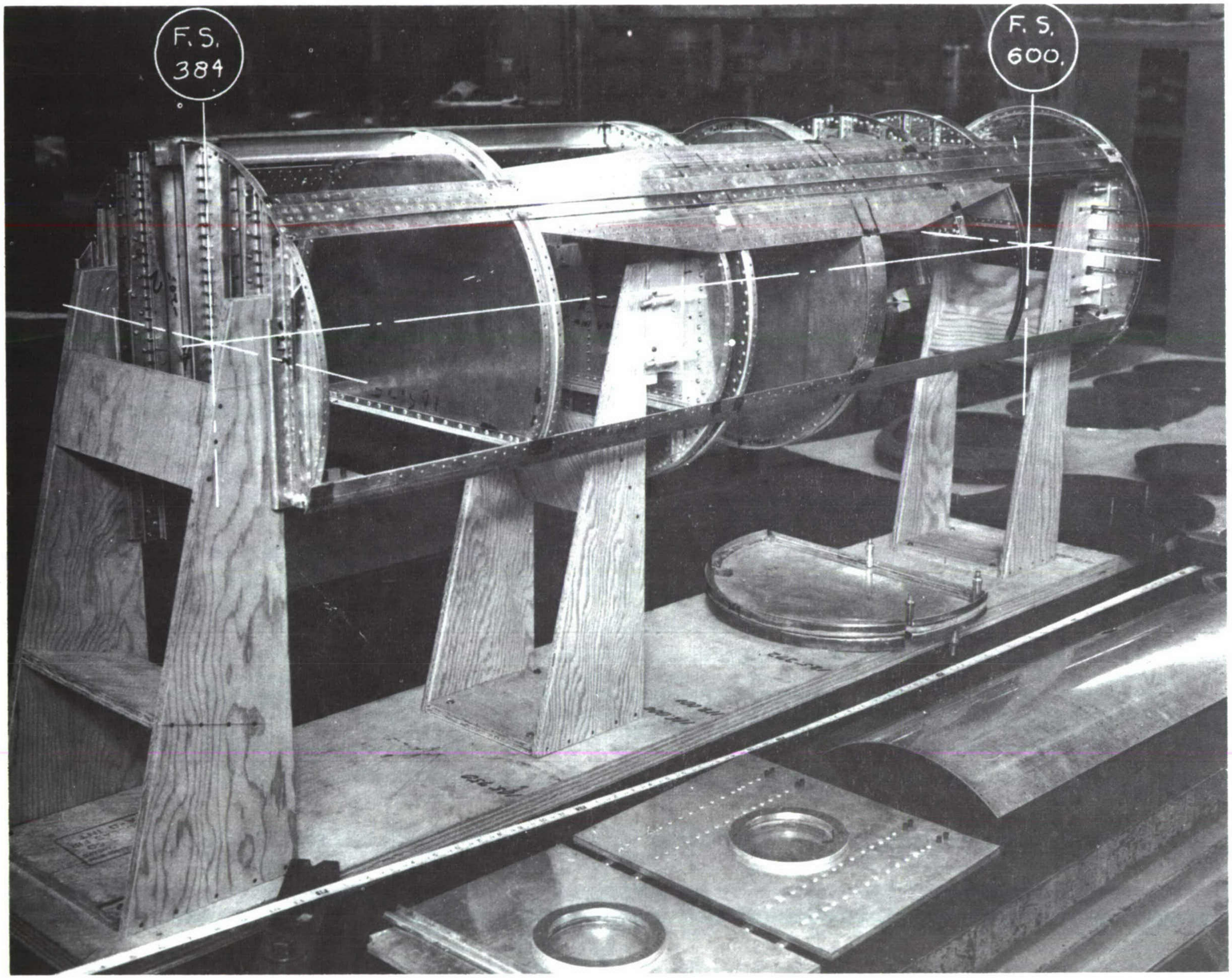

FIGURE A5 FORWARD MAIN OF MODEL ASSEMBLY SHOWN IN UPSIDE DOWN POSITION

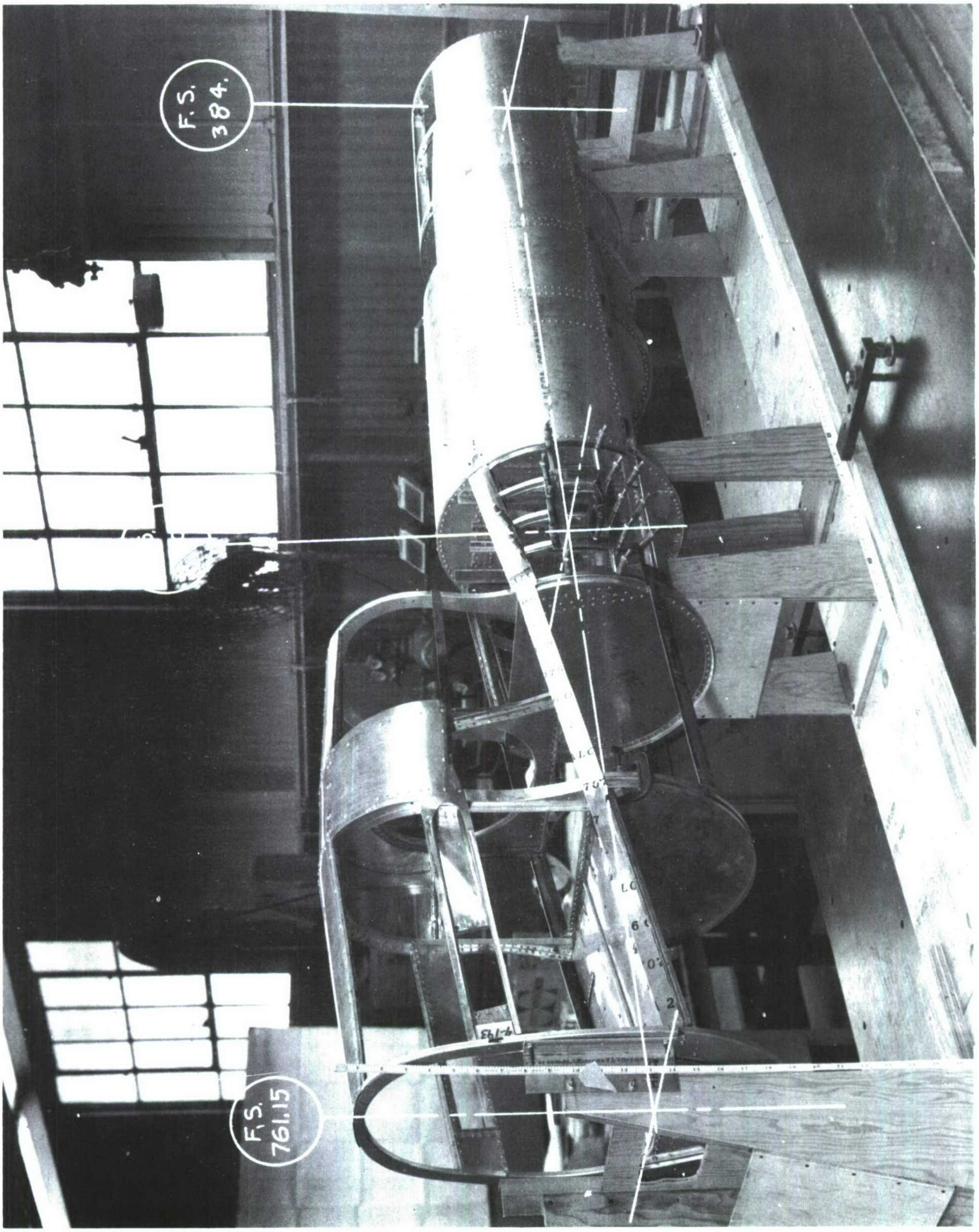

FIGURE A6 AFT MAIN OF MODEL ASSEMBLED

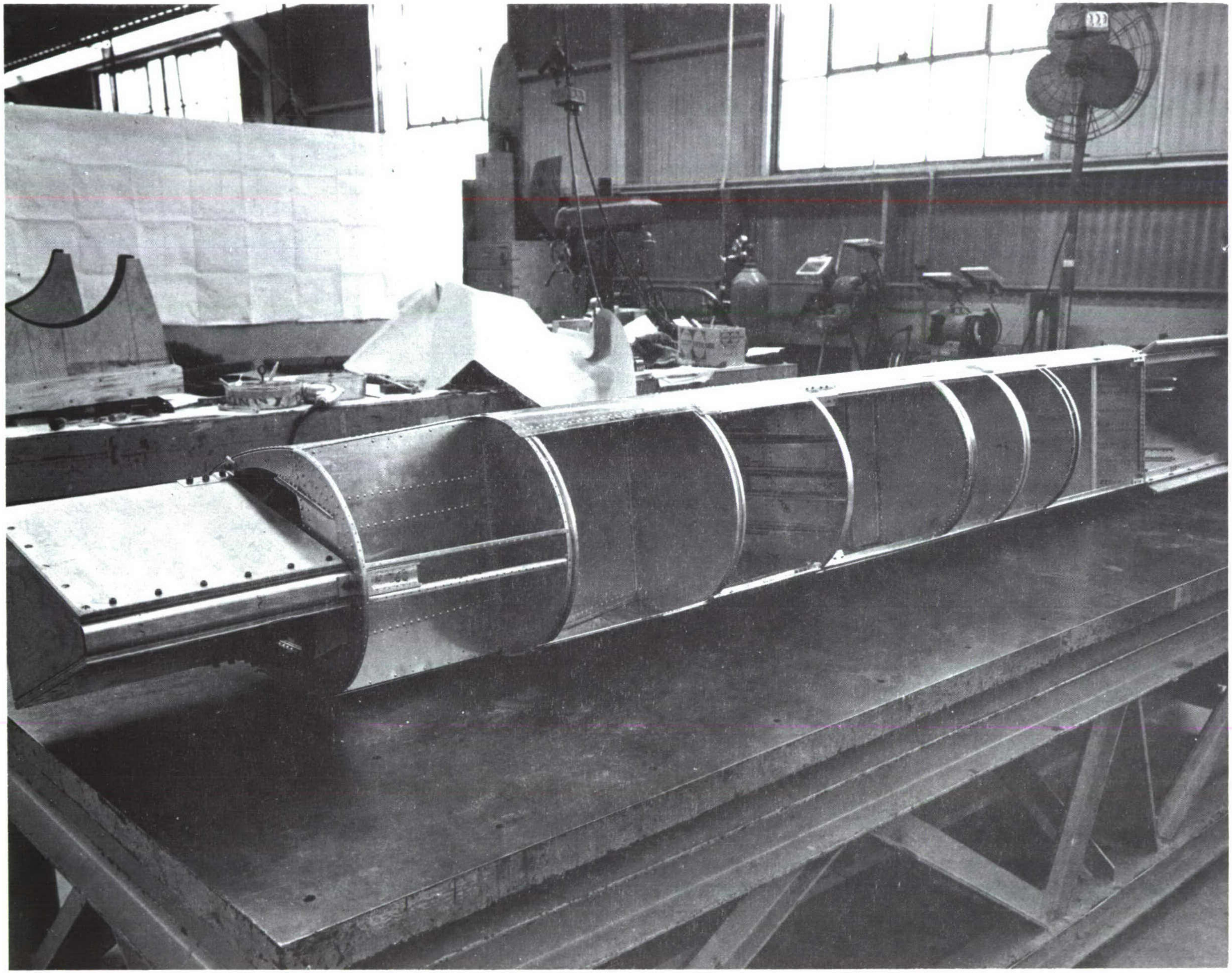

FIGURE A7   TOP VIEW OF MODEL

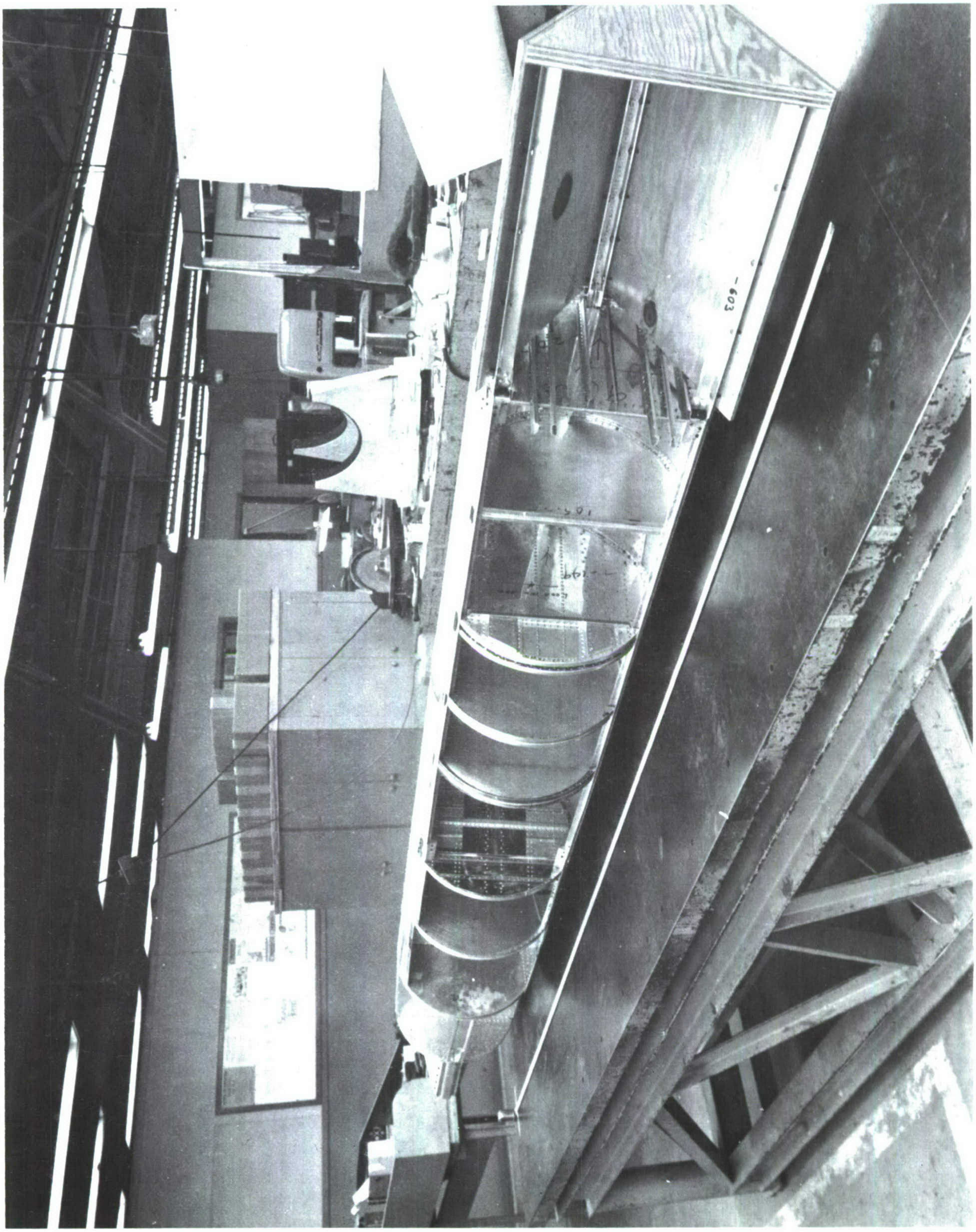

FIGURE A8 TOP VIEW OF MODEL

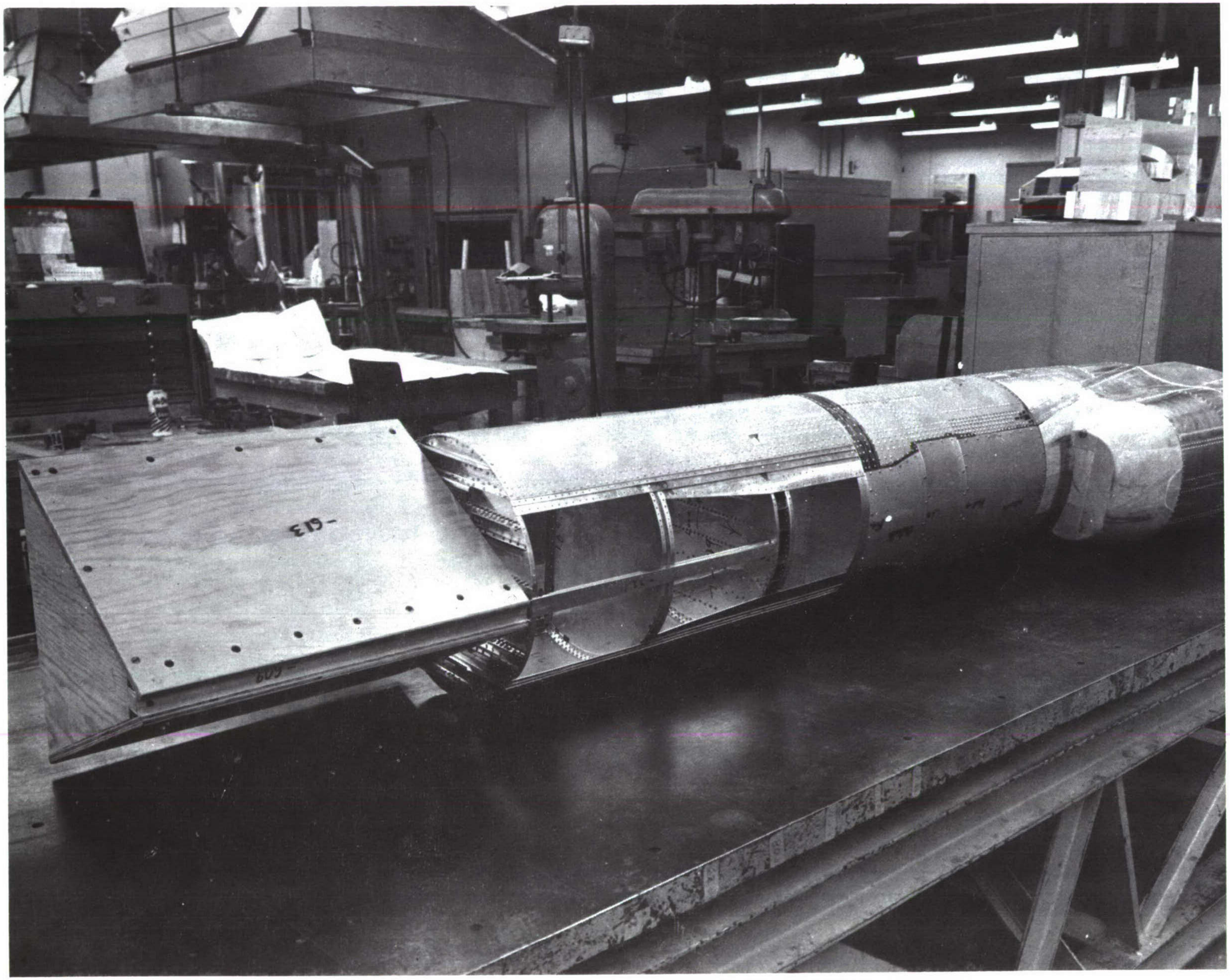

FIGURE A9 BOTTOM VIEW OF MODEL

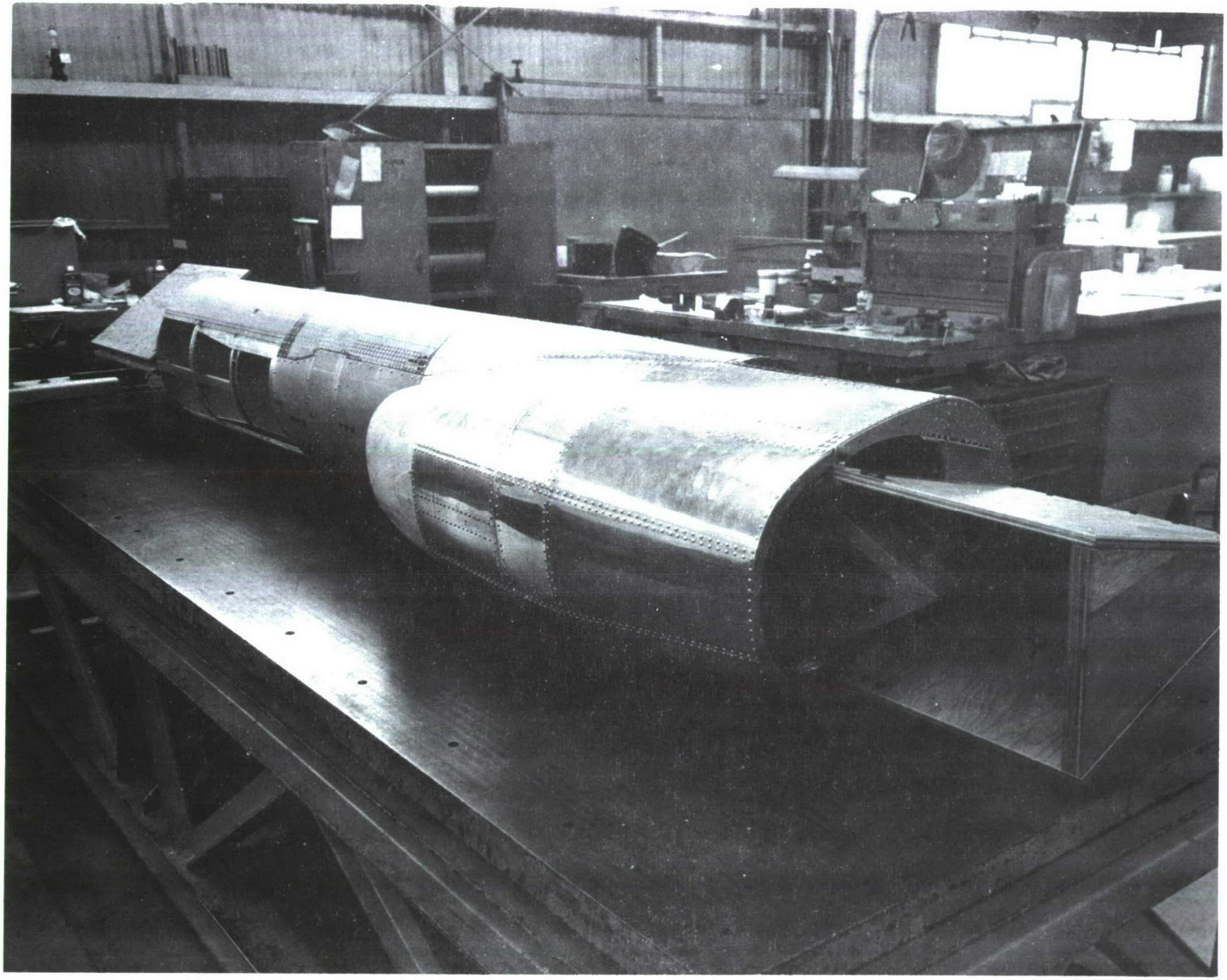

FIGURE A10 BOTTOM VIEW OF MODEL

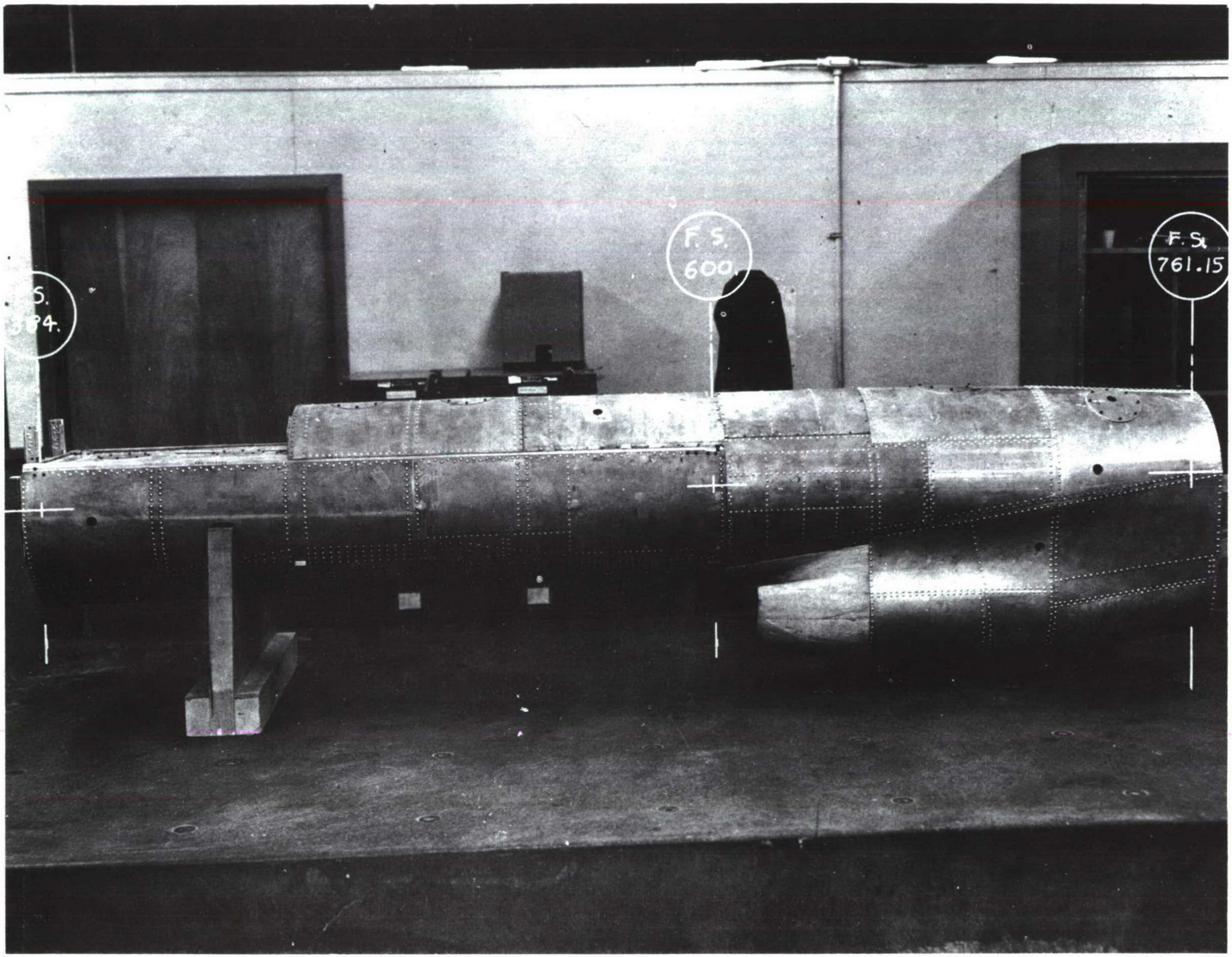

FIGURE A11 L.H. SIDE VIEW OF MODEL

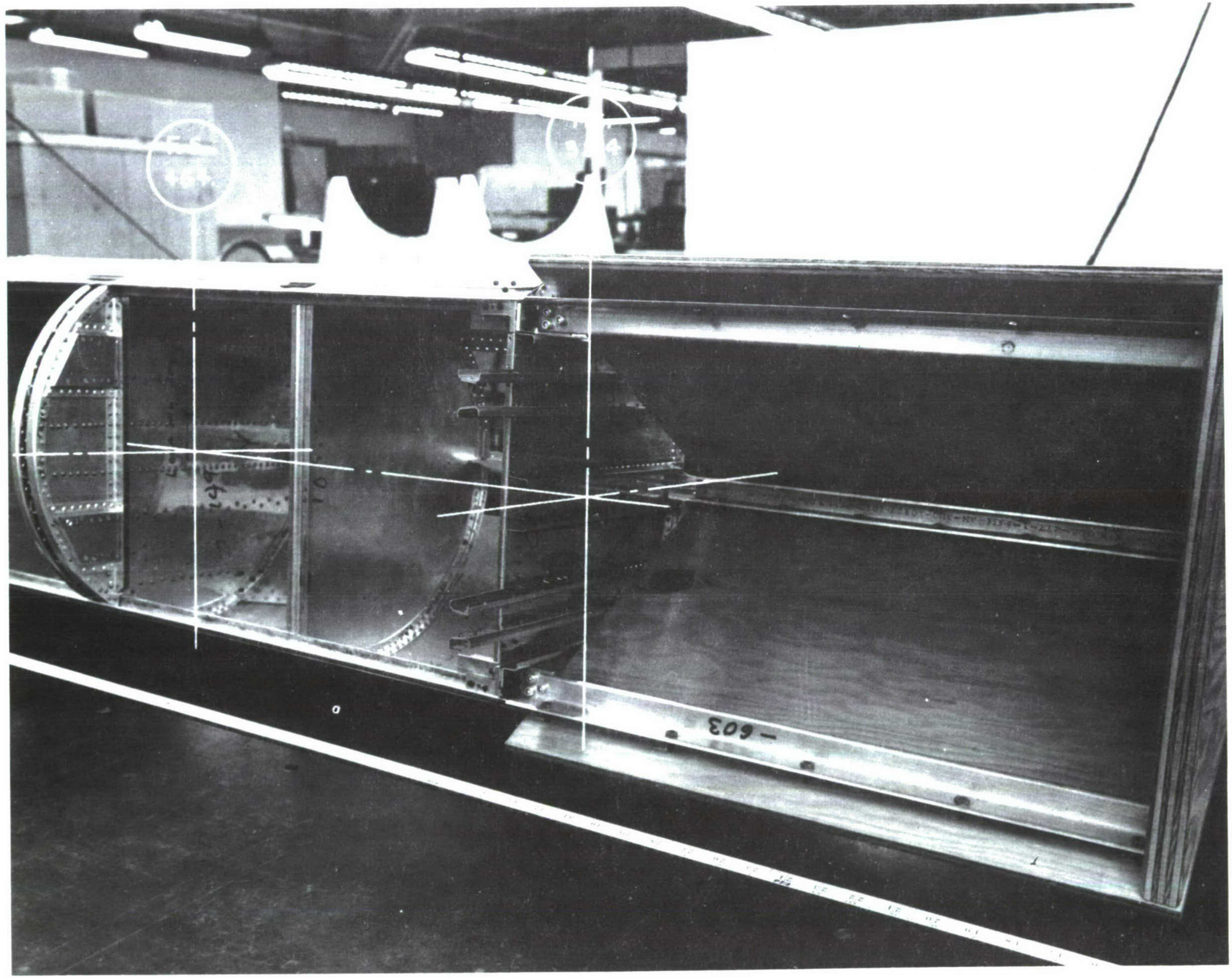

FIGURE A12 TOP VIEW OF FORWARD FUEL BAYS OF MODEL

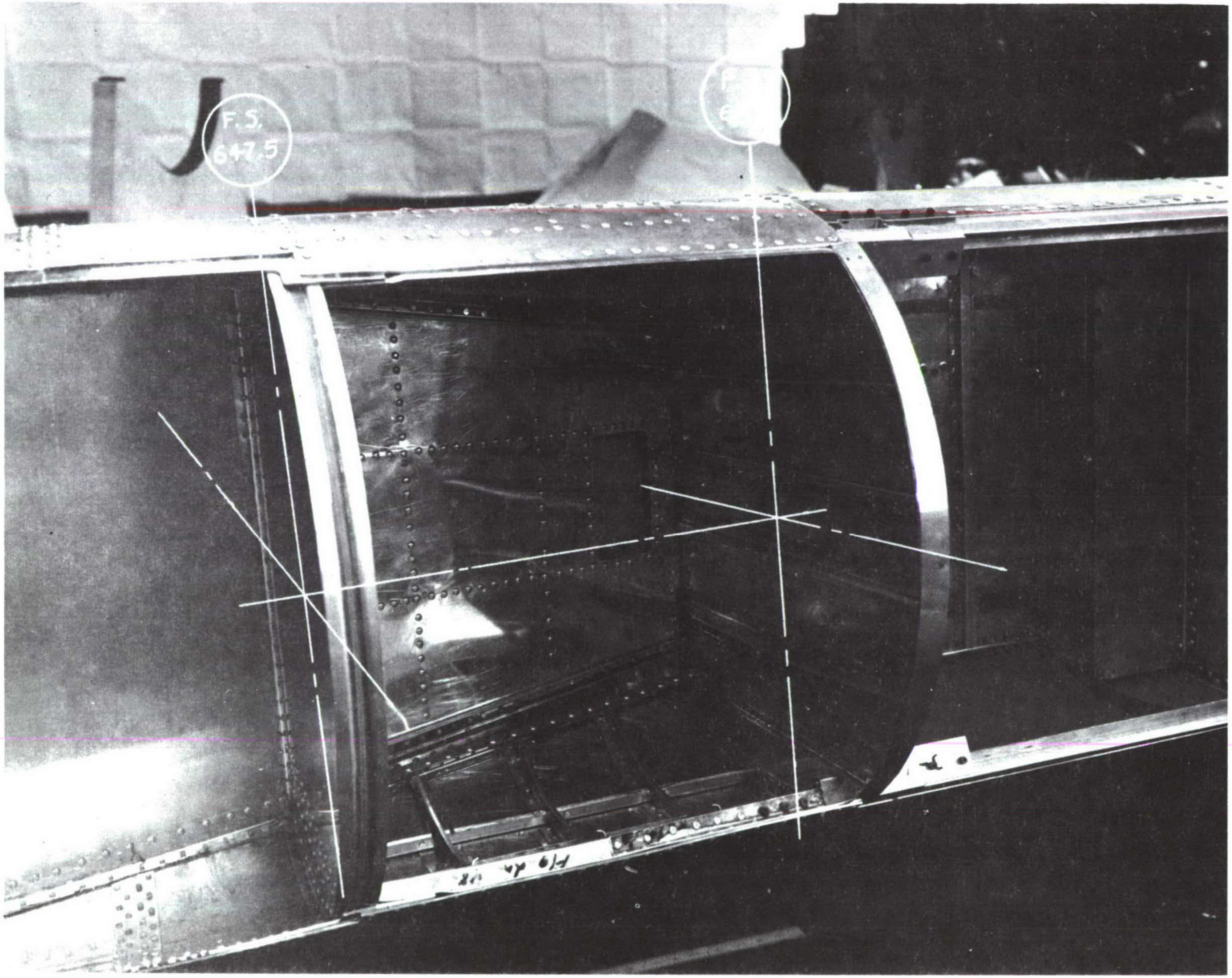

FIGURE A13   TOP VIEW OF EQUIPMENT BAY OF MODEL

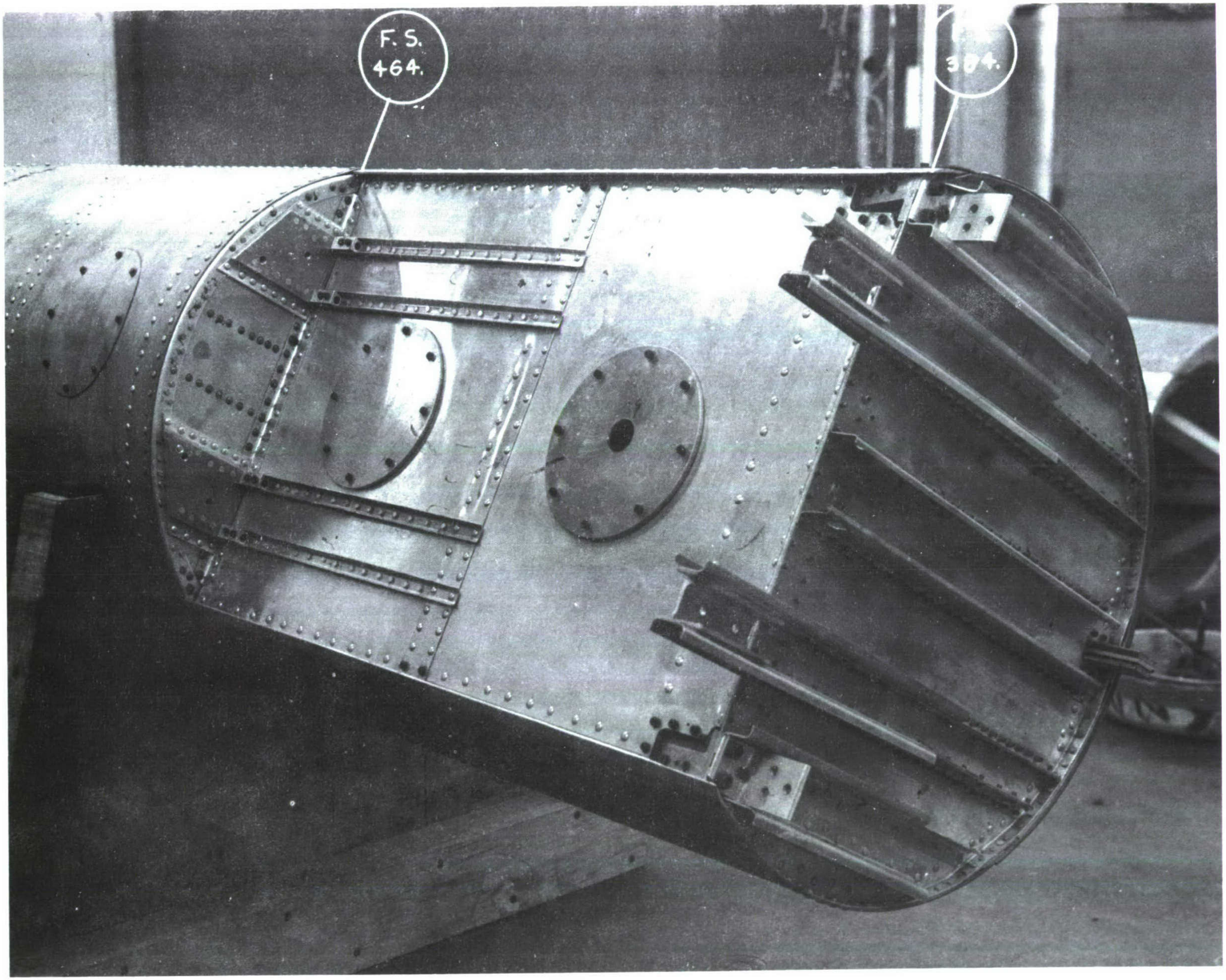

FIGURE A14 TOP VIEW OF DECK OF MODEL F.S. 384.0-464.0

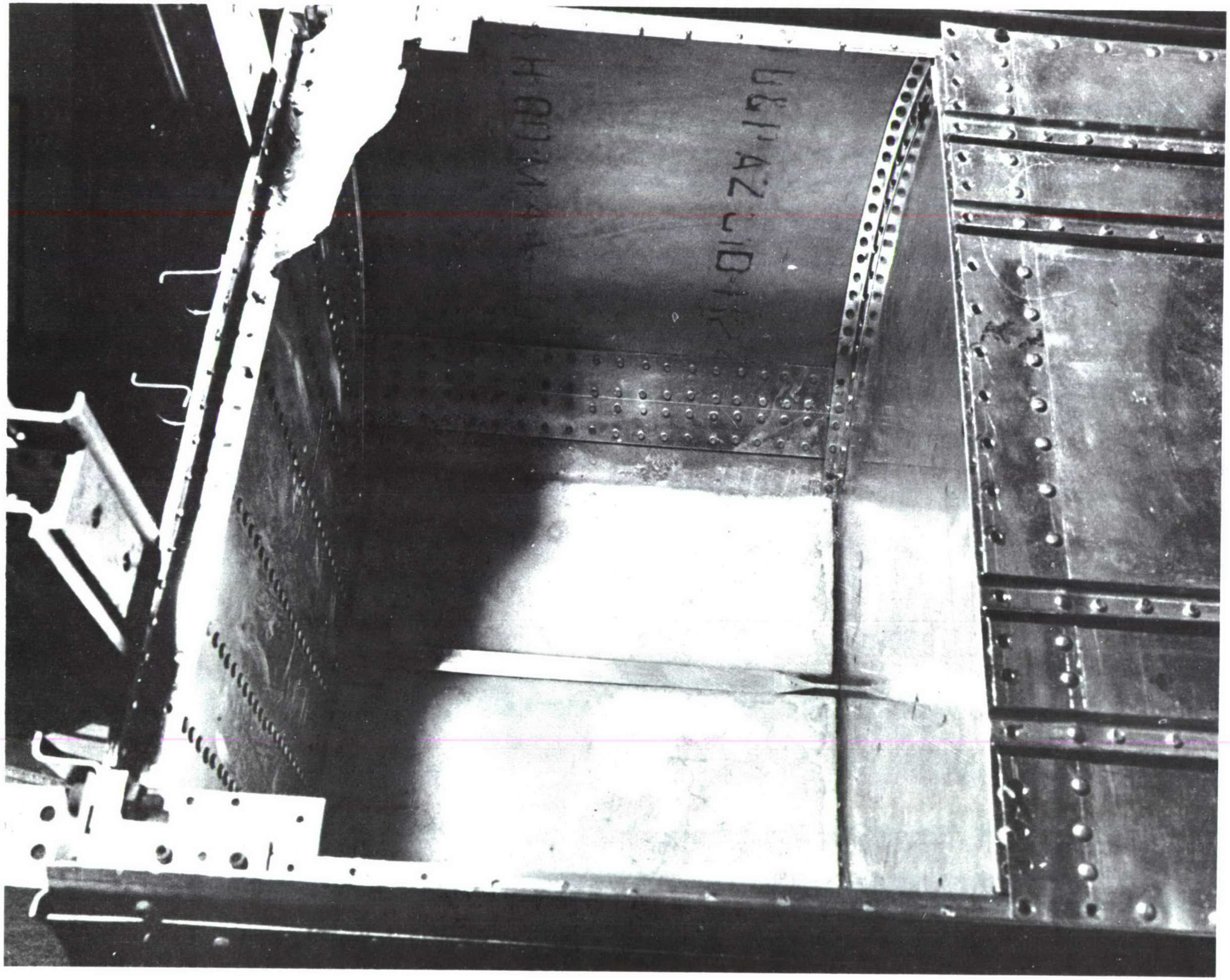

FIGURE A15 VIEW OF BACKING BOARD ON MODEL F.S. 384.0-423.0

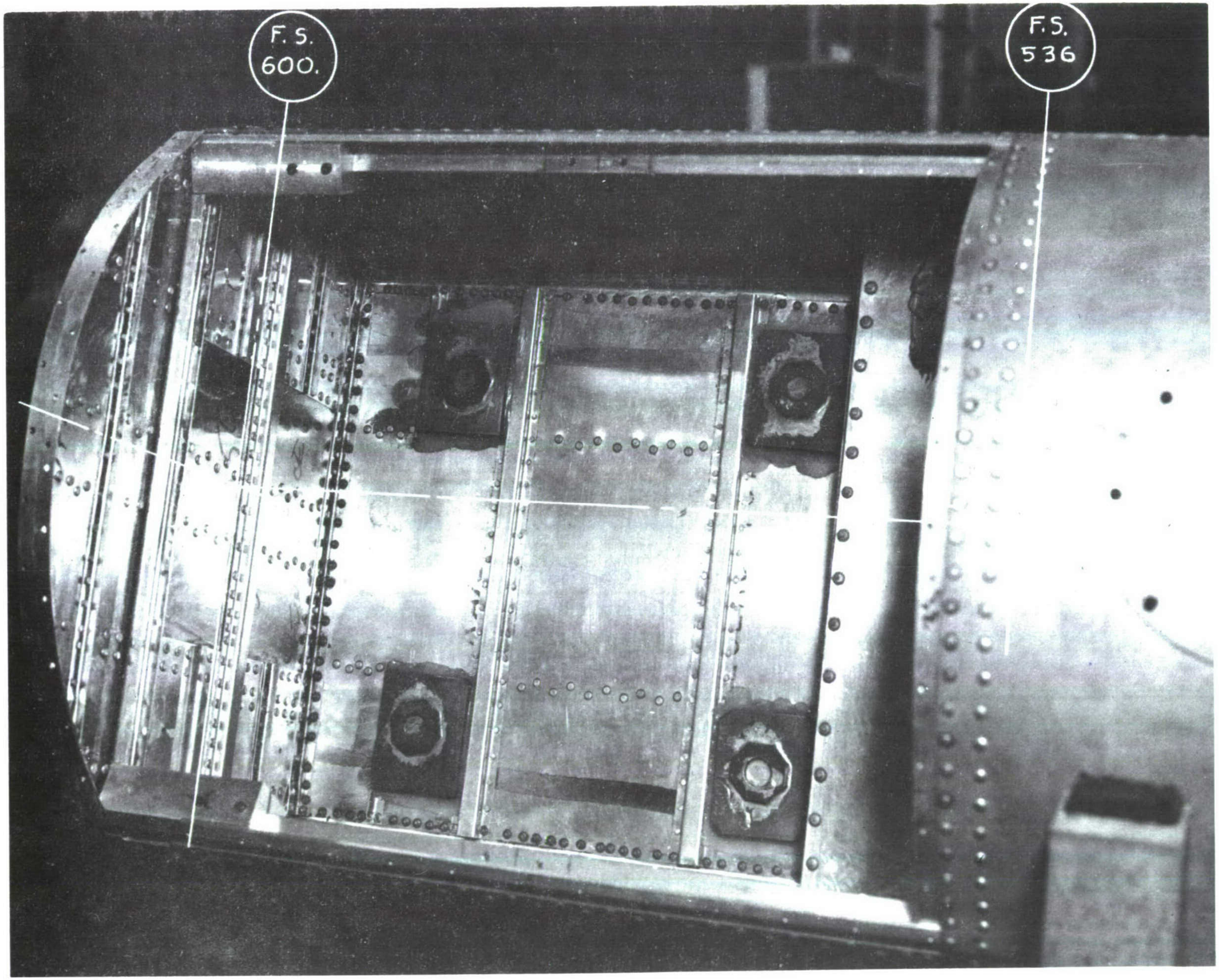

FIGURE A16 VIEW OF DECK OF MODEL

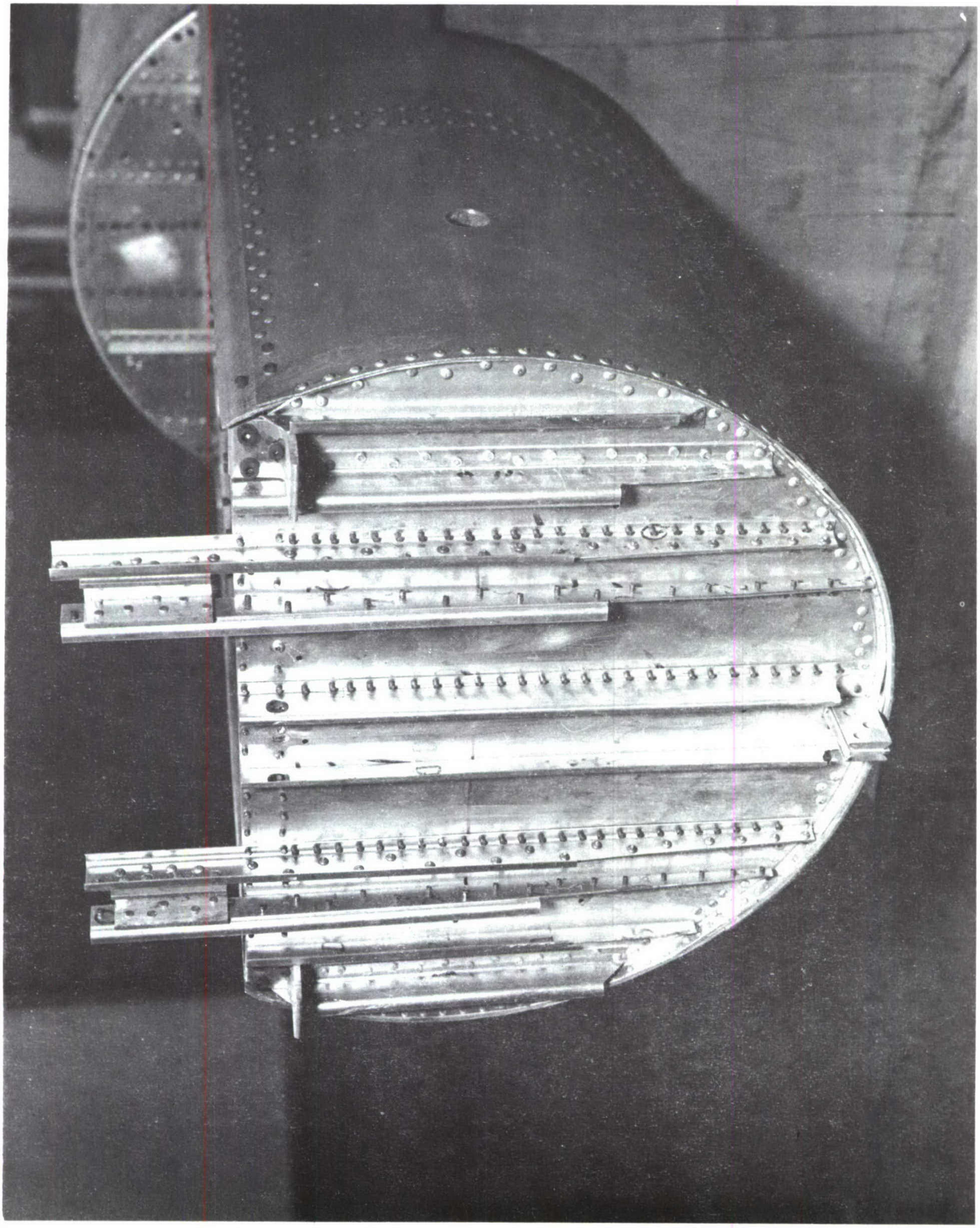

FIGURE A17 FRONT VIEW OF BULKHEAD OF MODEL AT F.S. 384

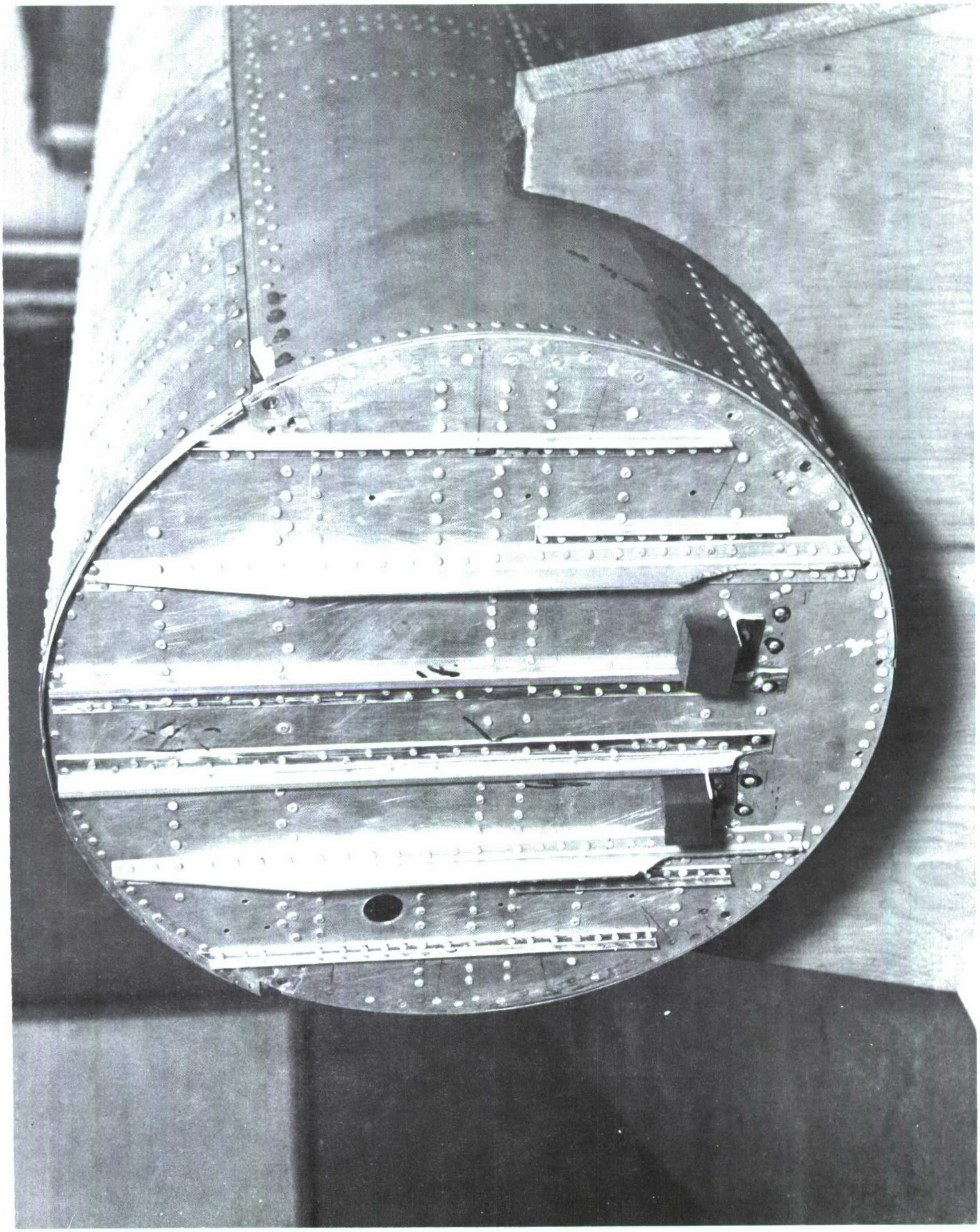

FIGURE A18 AFT VIEW OF BULKHEAD OF MODEL AT F.S. 600.0

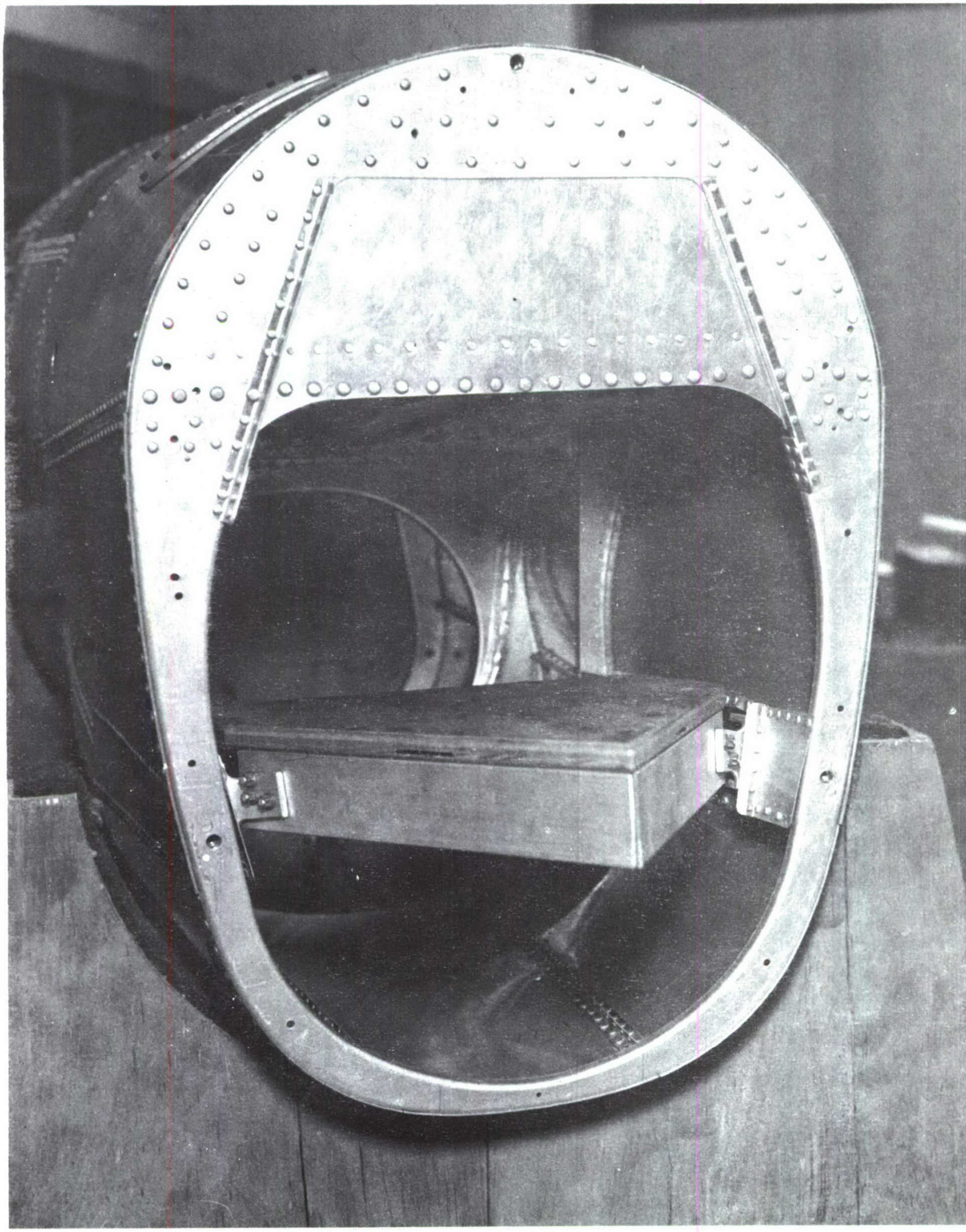

FIGURE A 19 AFT VIEW OF BULKHEAD OF MODEL AT F.S. 761.15

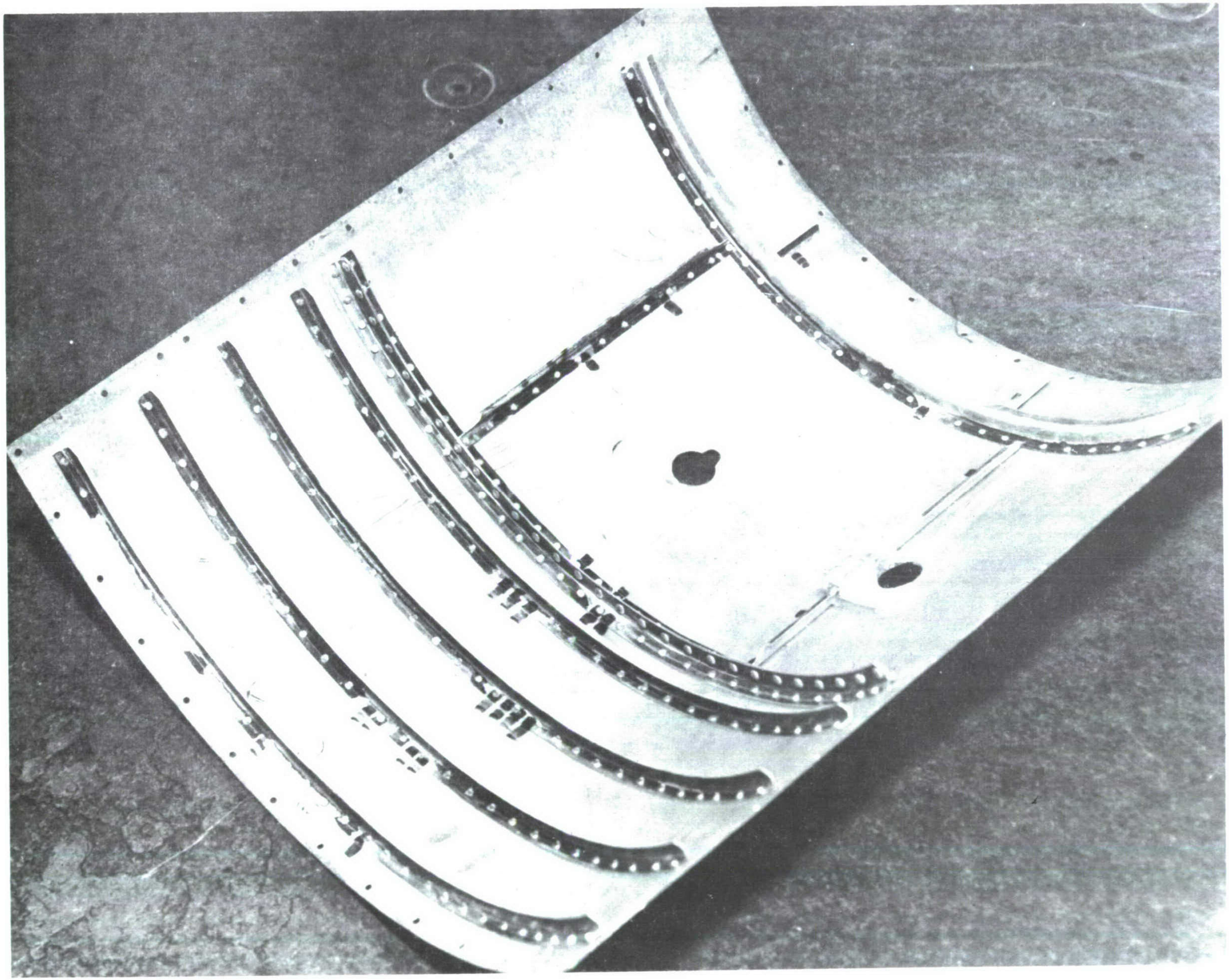

FIGURE A20   VIEW OF UNDERSIDE OF COVER FOR MODEL F.S. 536.0-600.0

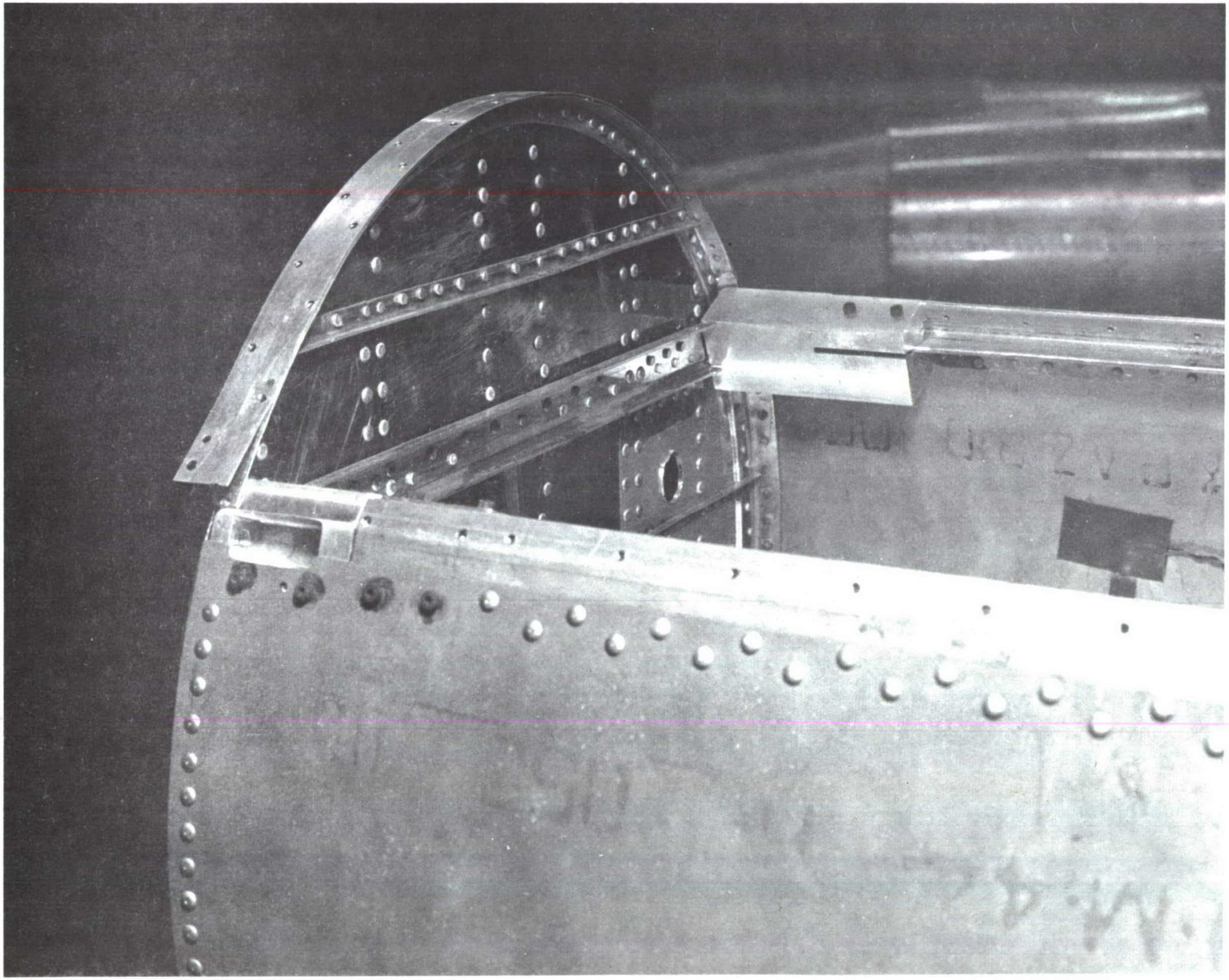

FIGURE A21 UPPER LONGERON FORWARD FITTINGS OF MODEL- PRODUCTION BREAK AT F.S. 600.0

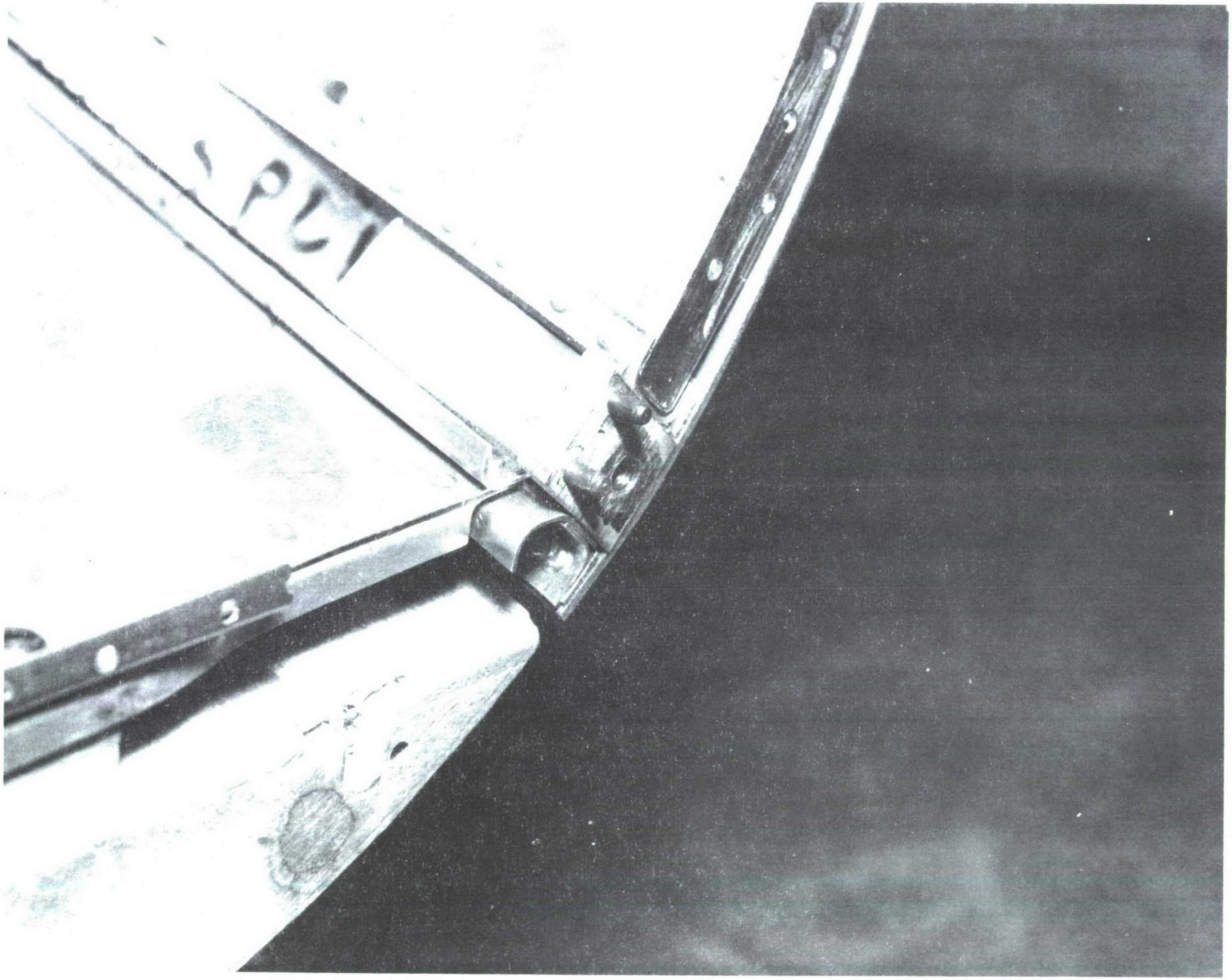

FIGURE A22 LOWER LONGERON AFT FITTING OF MODEL-PRODUCTION BREAK AT F.S. 600.0

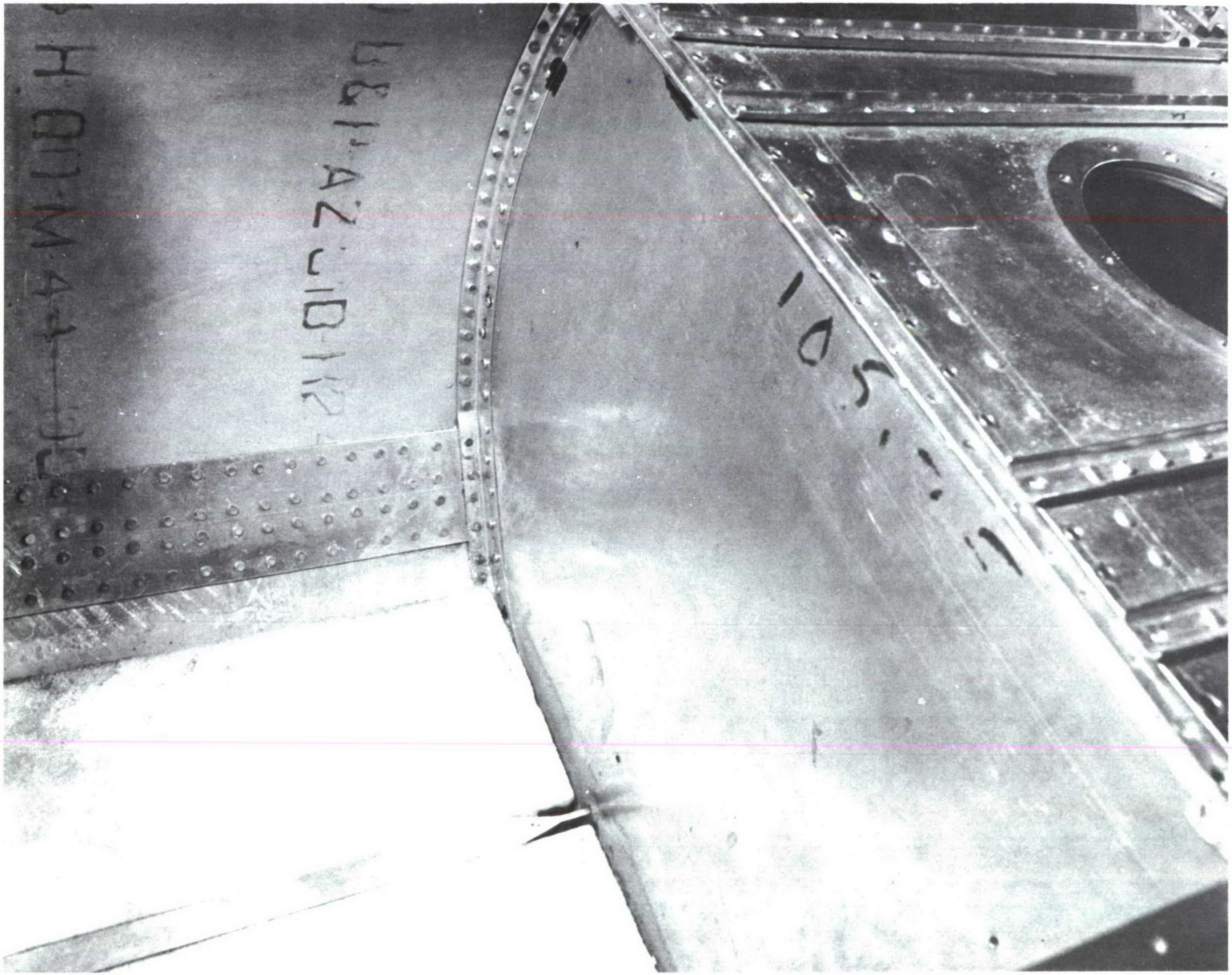

FIGURE A23 VIEW OF FORWARD BULKHEAD STRUCTURAL TIE AT F.S. 423 OF MODEL

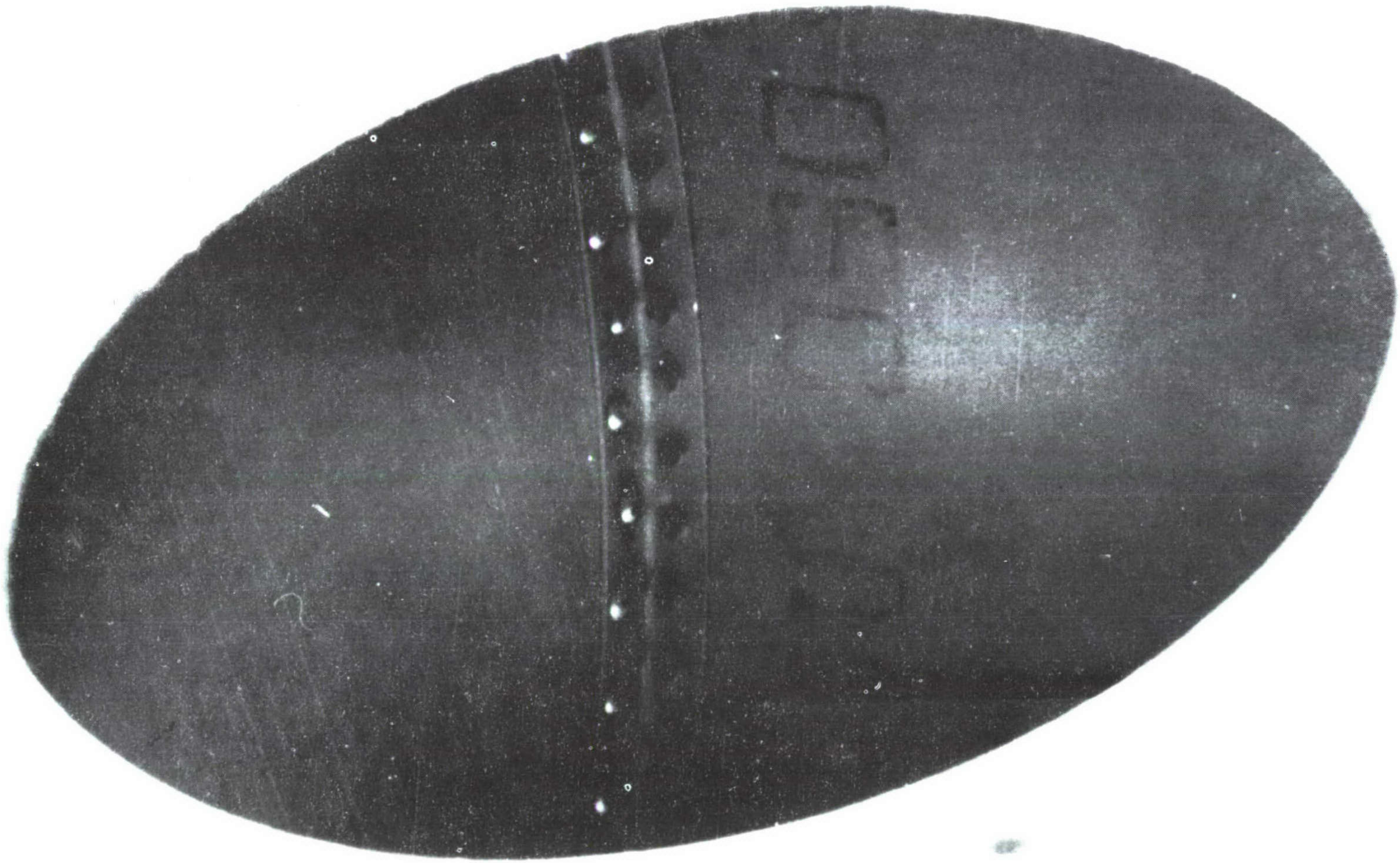

FIGURE A24 VIEW OF AFT BULKHEAD STRUCTURAL TIE AT F.S. 423 OF MODEL

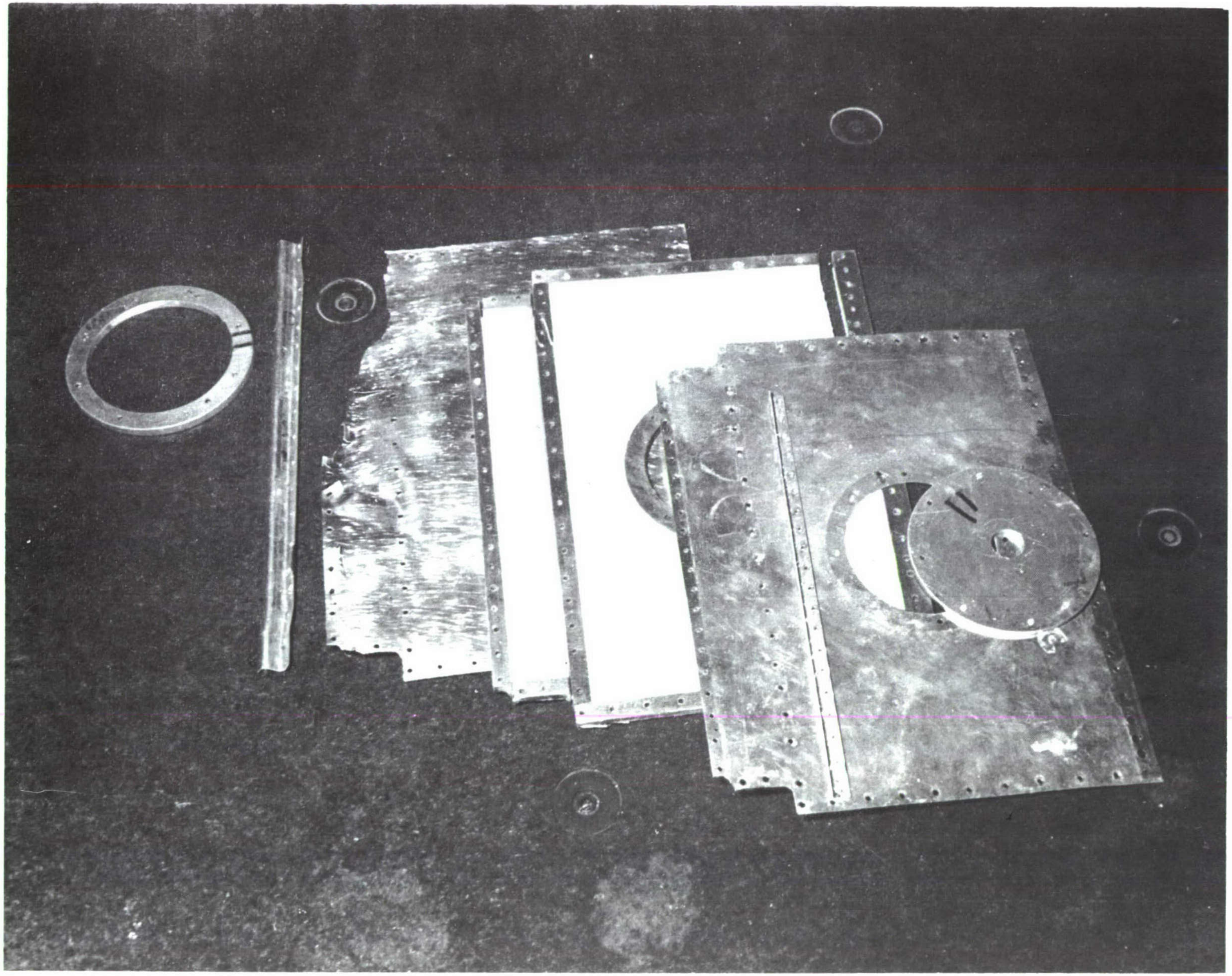

FIGURE A25 DISASSEMBLED MODEL DECK-F.S. 384.0-423.0

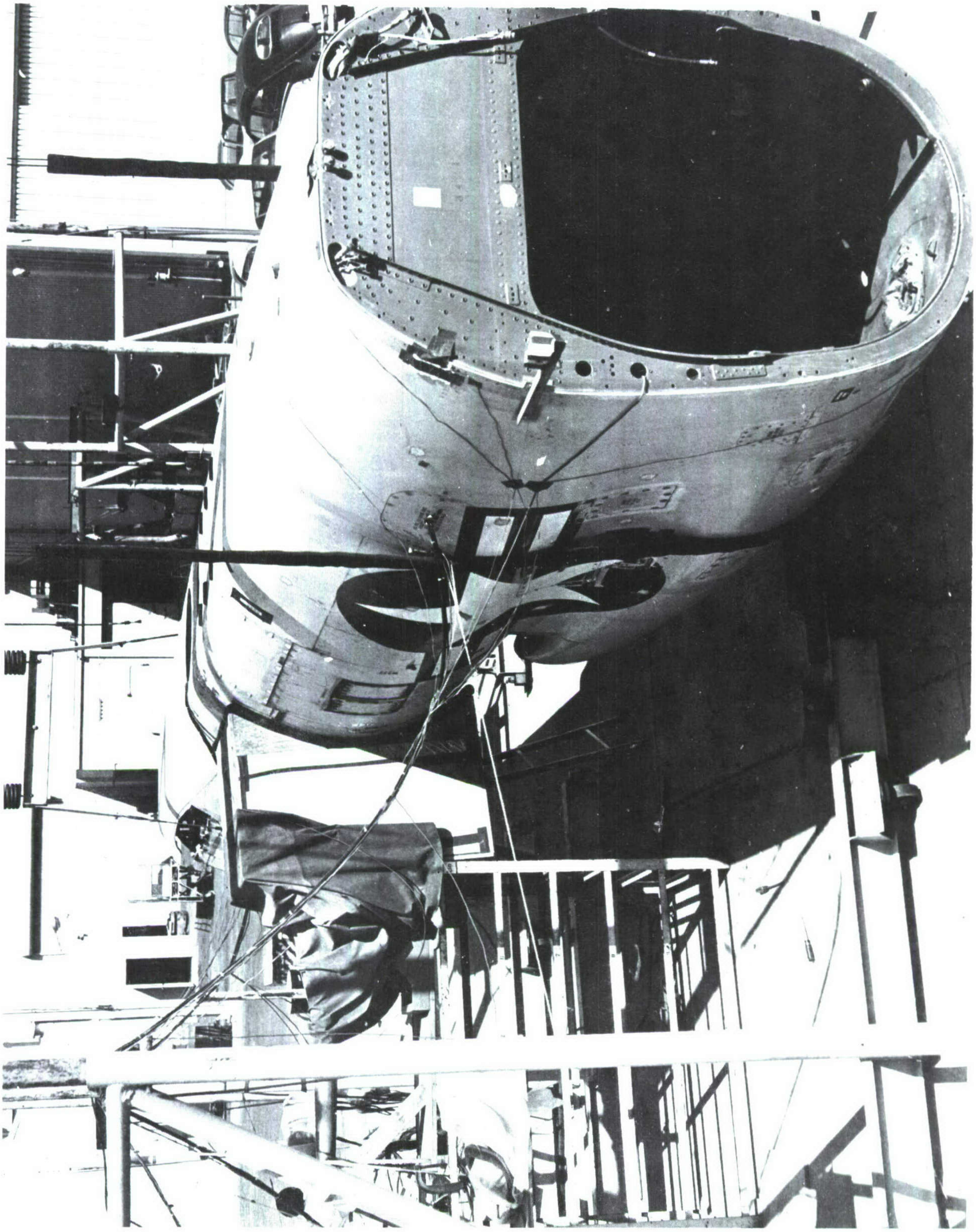

FIGURE A26 VEHICLE AND HORN IN TEST INSTALLATION

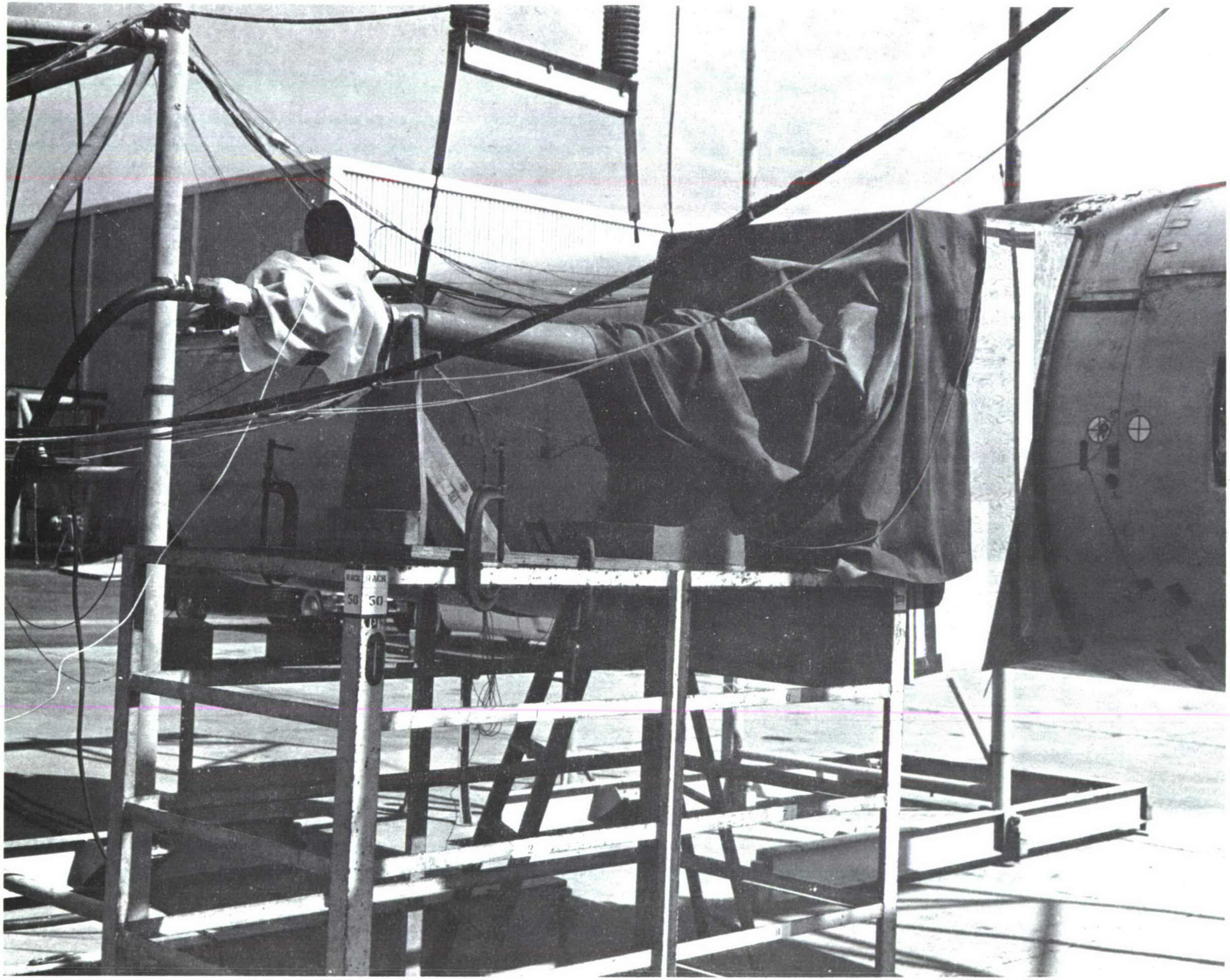

FIGURE A27 VEHICLE AND HORN IN TEST INSTALLATION

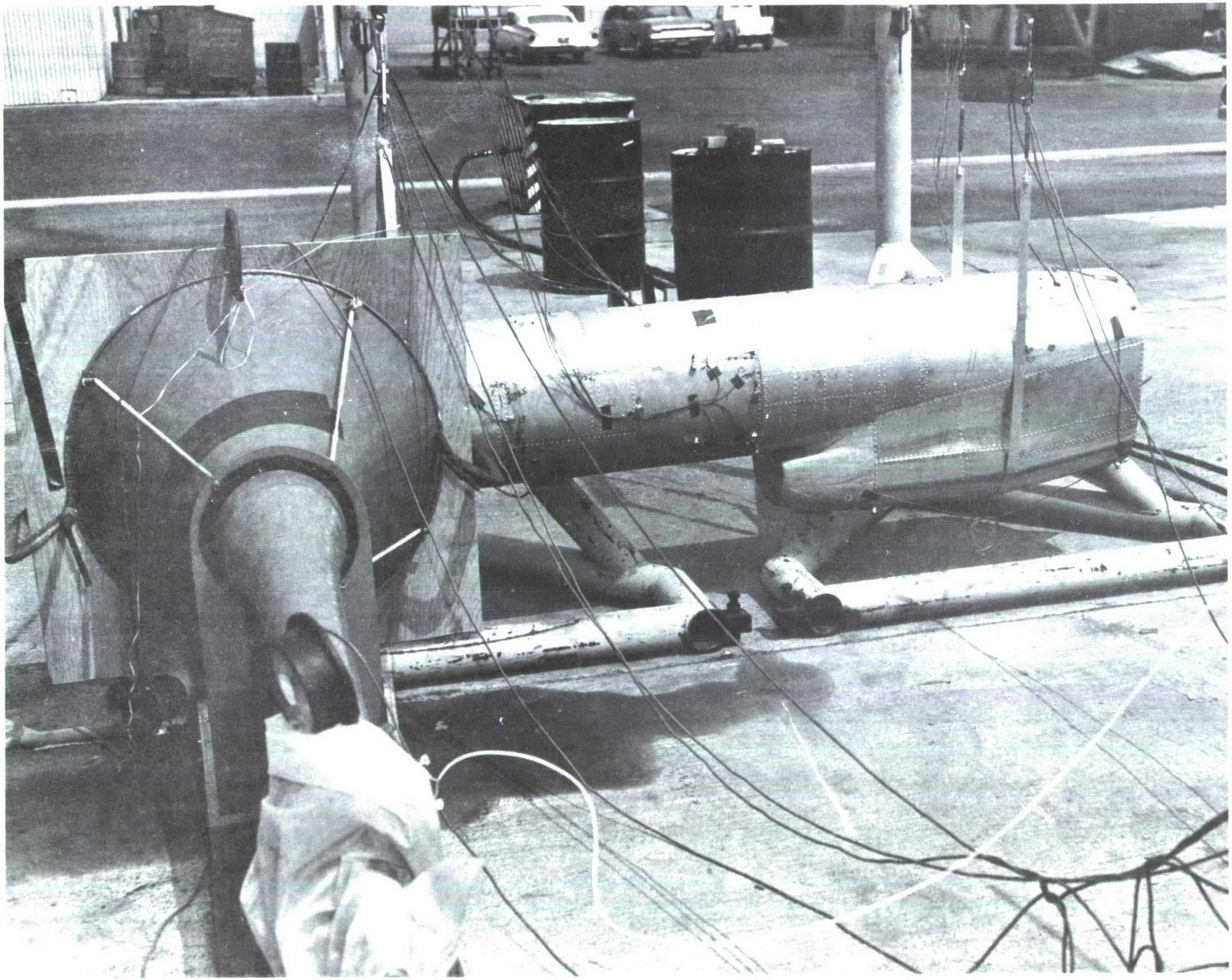

FIGURE A28 MODEL AND HORN IN TEST INSTALLATION

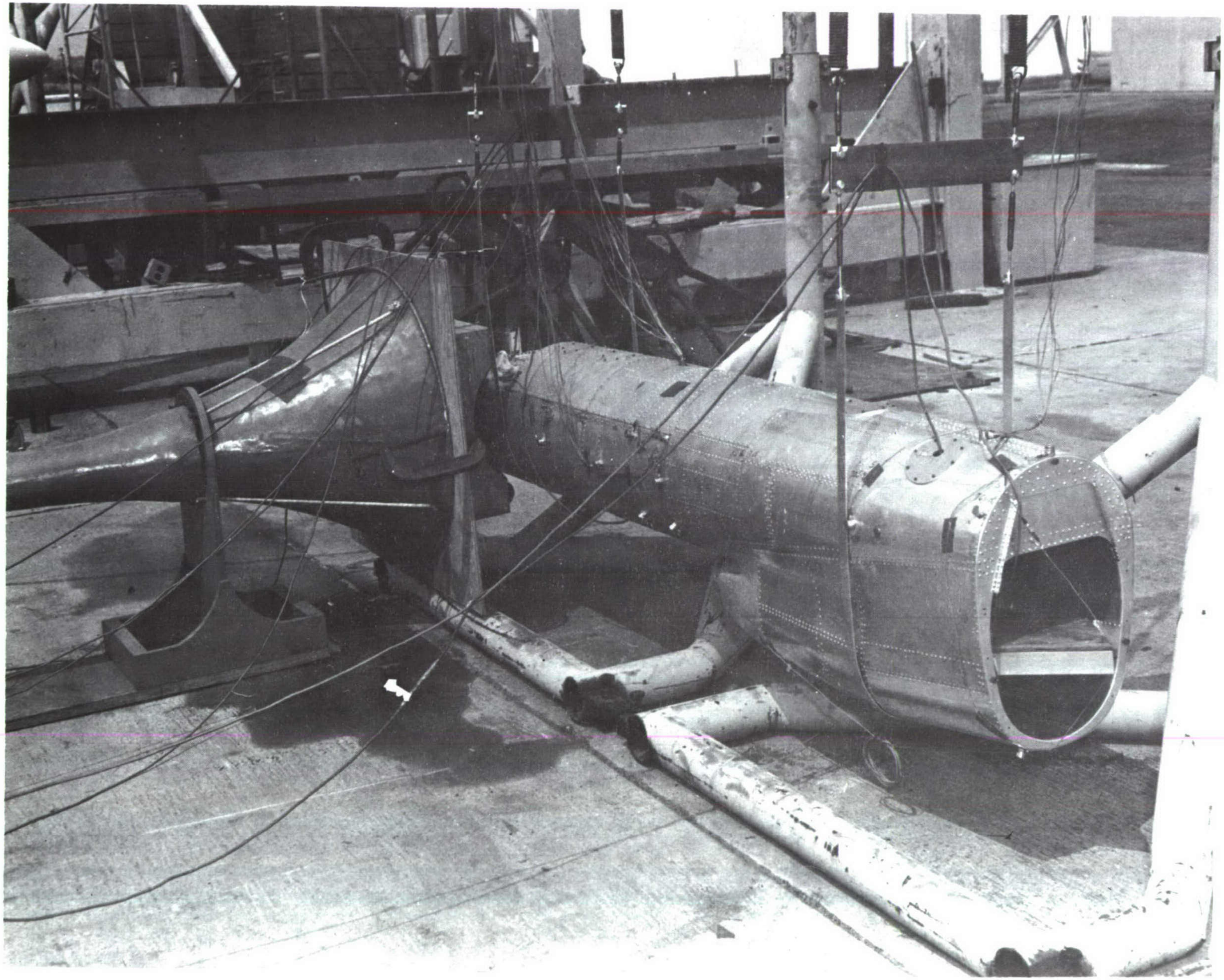

FIGURE A29   MODEL AND HORN IN TEST INSTALLATION

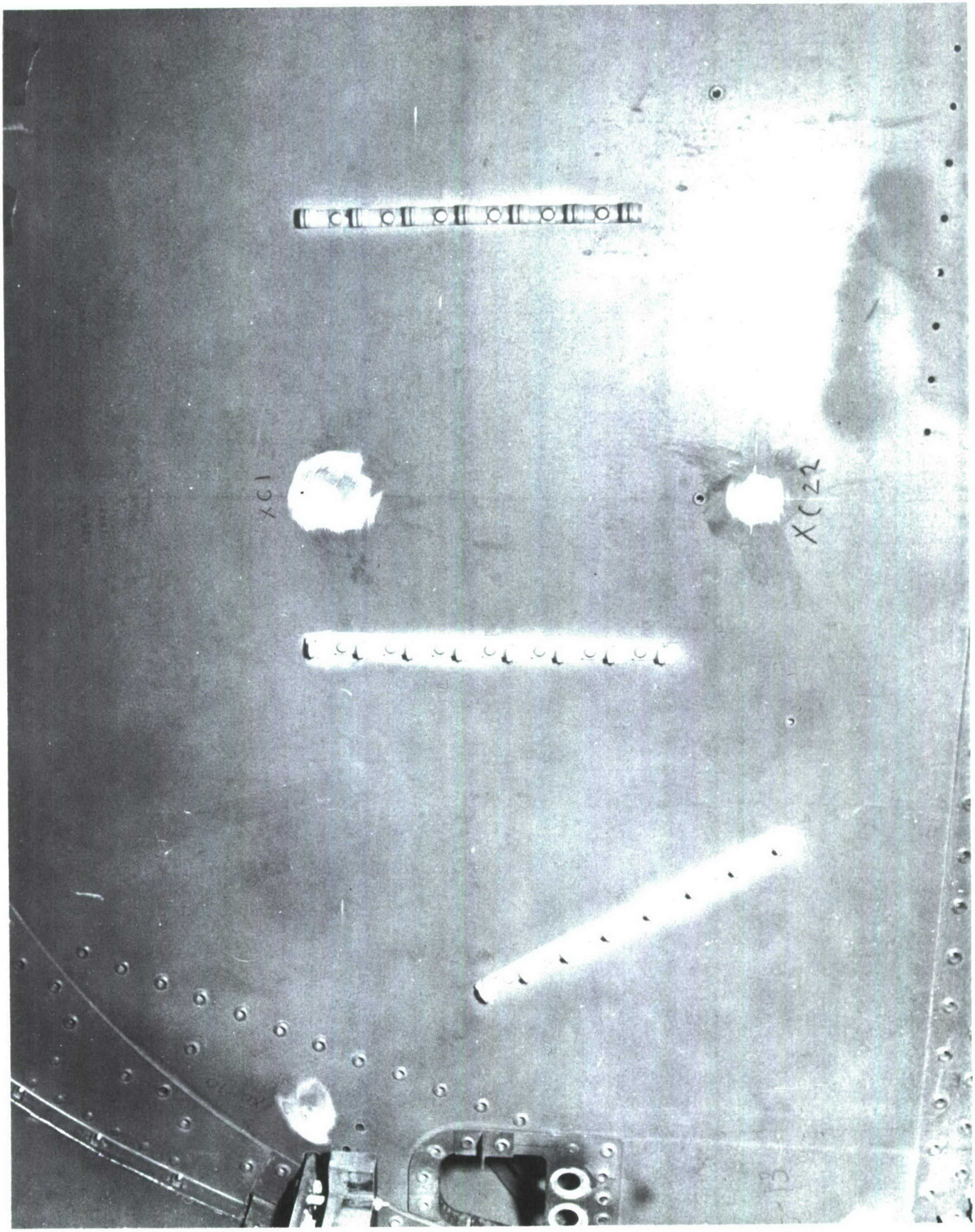

FIGURE A30 AFT VIEW OF VEHICLE BULKHEAD AT F.S. 536.0

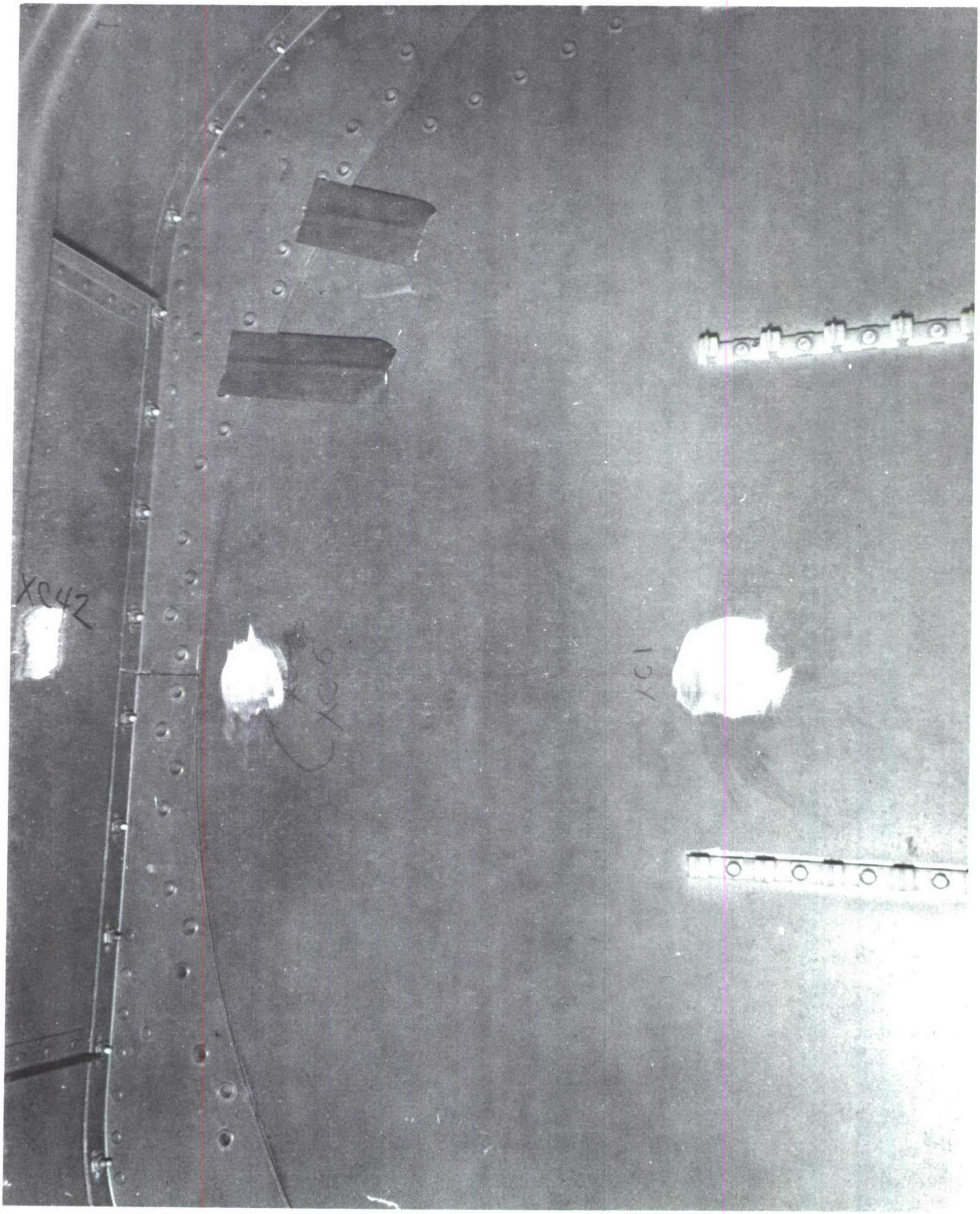

FIGURE A31 AFT VIEW OF VEHICLE BULKHEAD AT F.S. 536.0

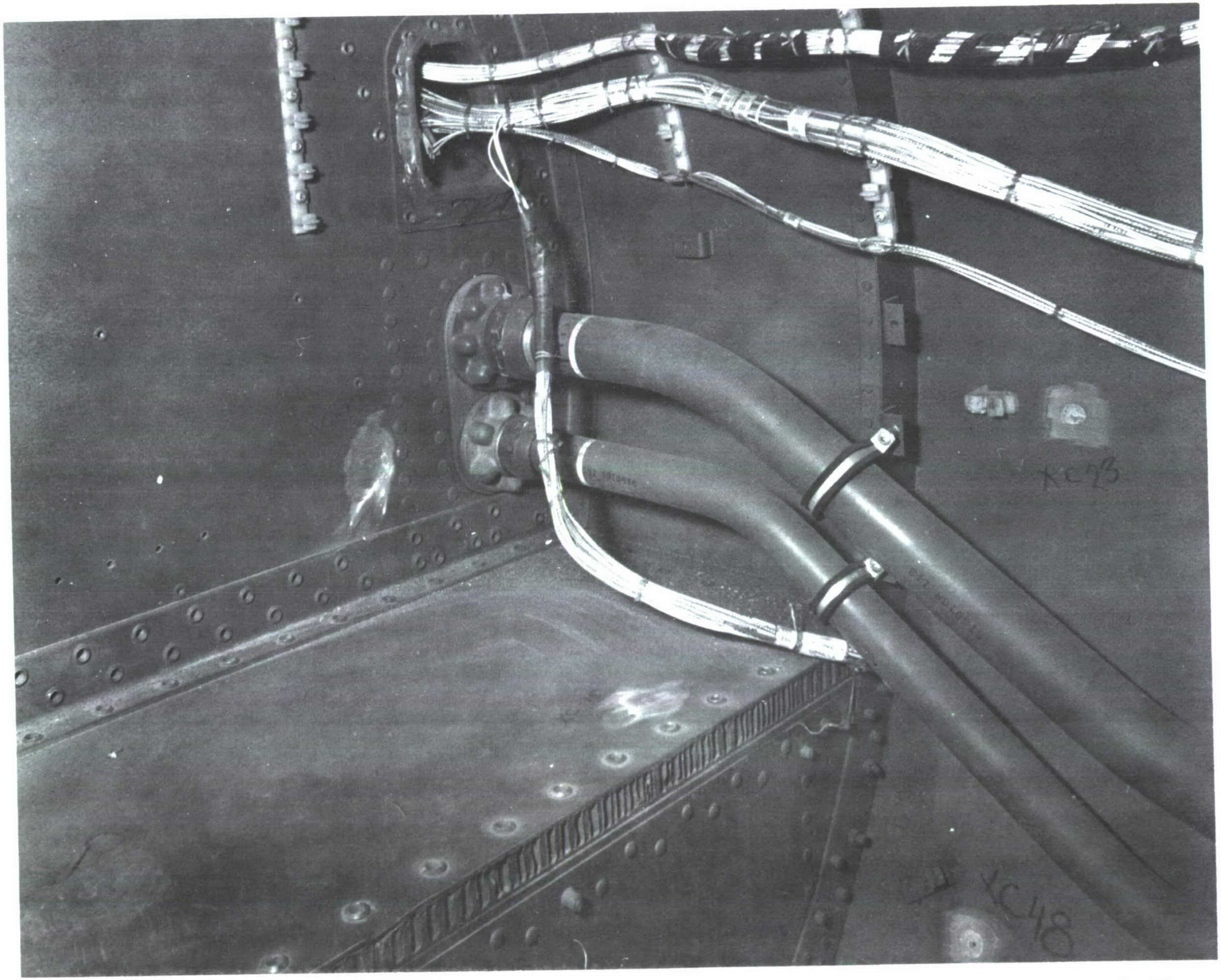

FIGURE A32 INSIDE VIEW OF FORWARD R.H. CORNER OF VEHICLE EQUIPMENT BAY, F.S. 536.0-600.0

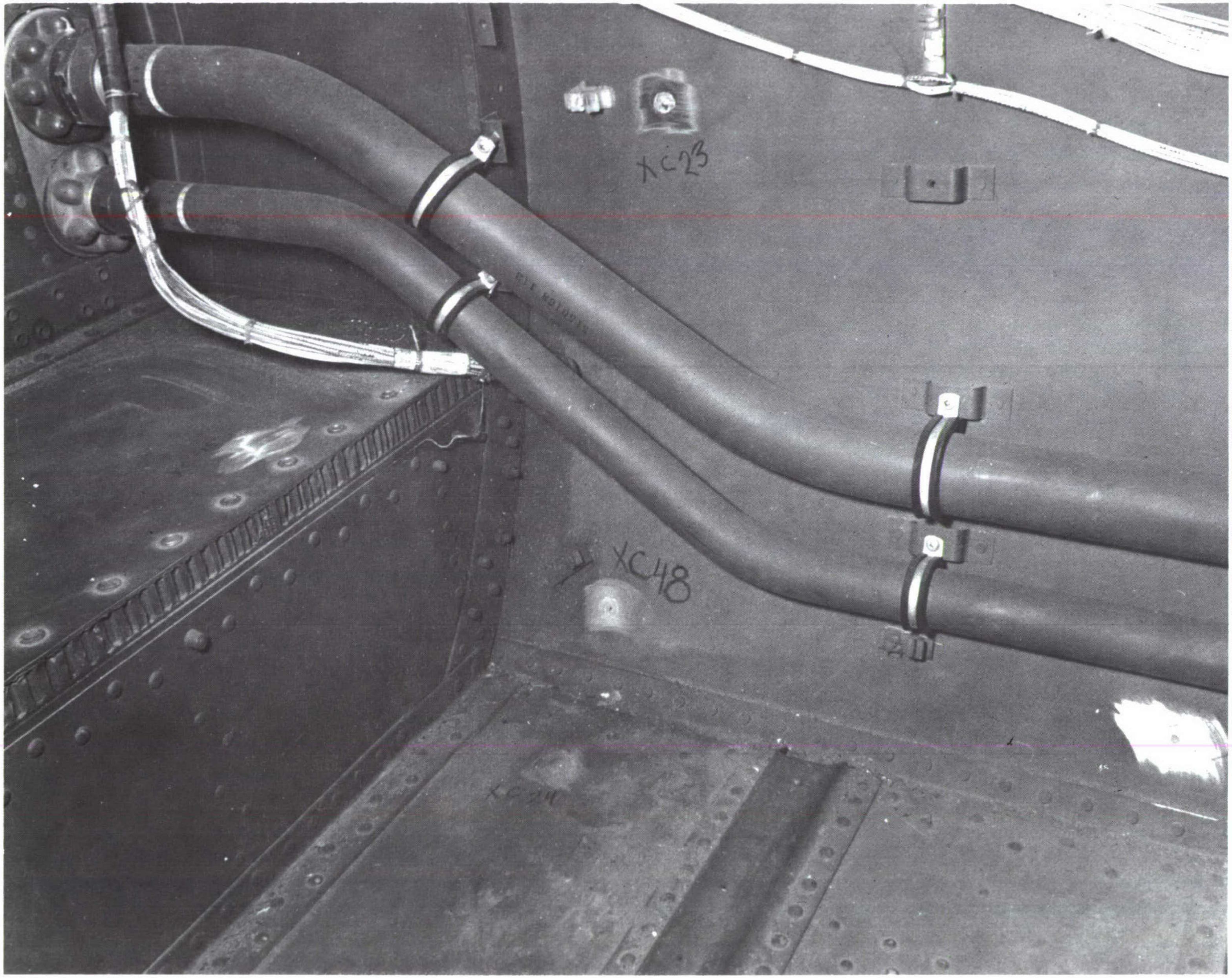

FIGURE A33 INSIDE VIEW OF R.H. SIDE OF VEHICLE EQUIPMENT BAY, F.S. 536.0-600.0

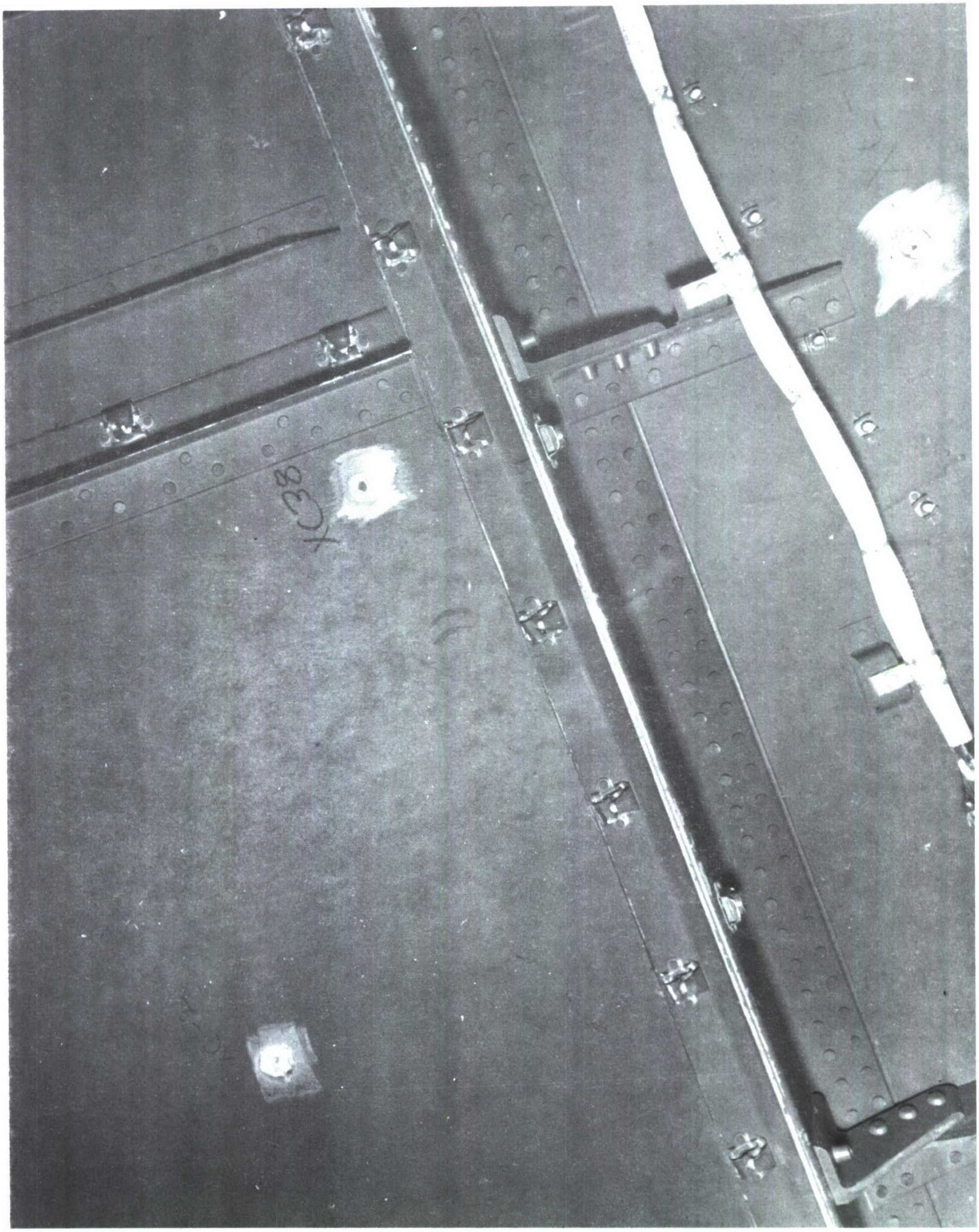

FIGURE A34 INSIDE VIEW OF R.H. SIDE OF VEHICLE EQUIPMENT BAY, F.S. 536.0-600.0

FIGURE A35 INSIDE VIEW OF R.H. SIDE OF VEHICLE EQUIPMENT BAY, F.S. 536.0-600.0

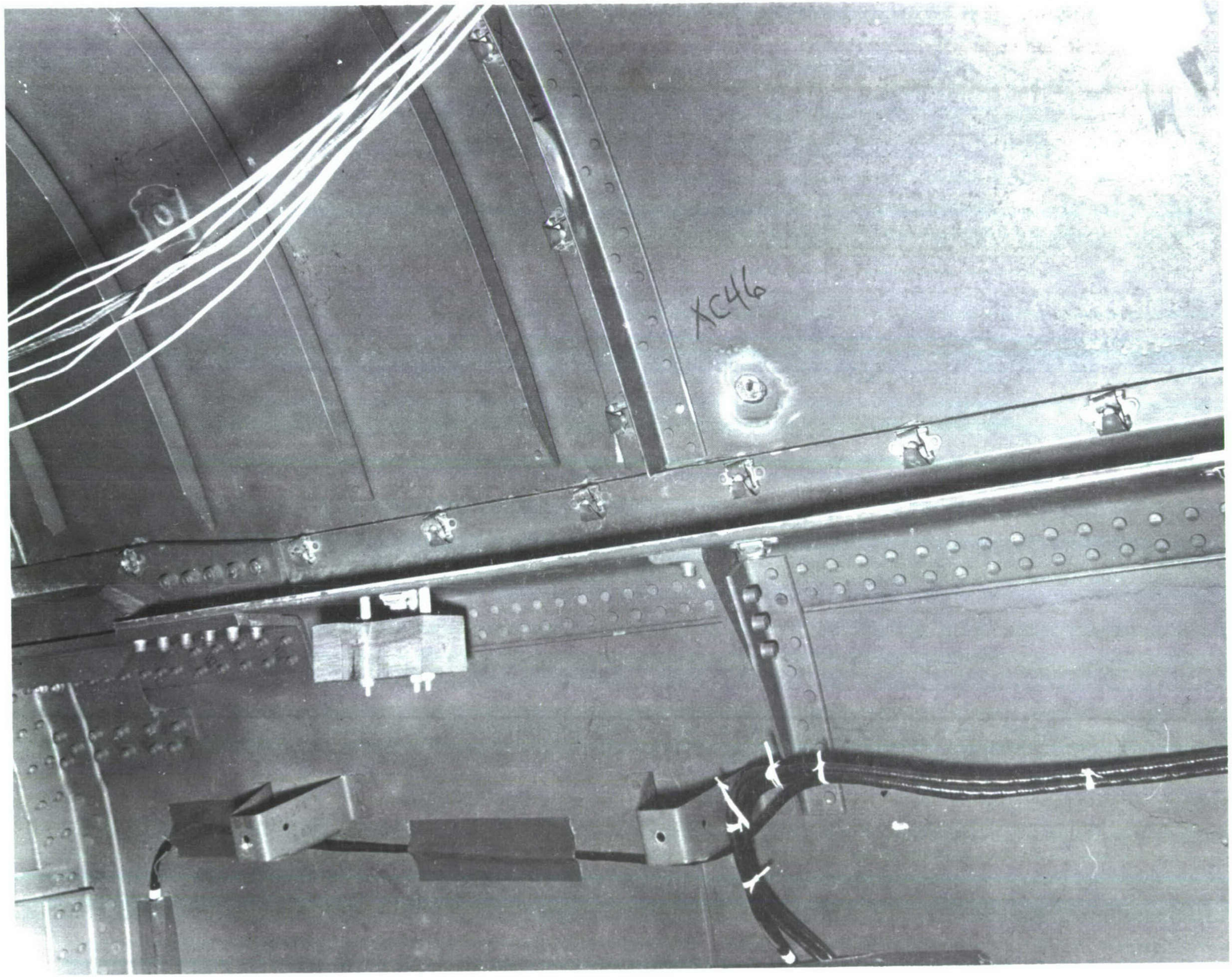

FIGURE A36 INSIDE VIEW OF L.H. SIDE OF VEHICLE EQUIPMENT BAY, F.S. 536.0-600.0

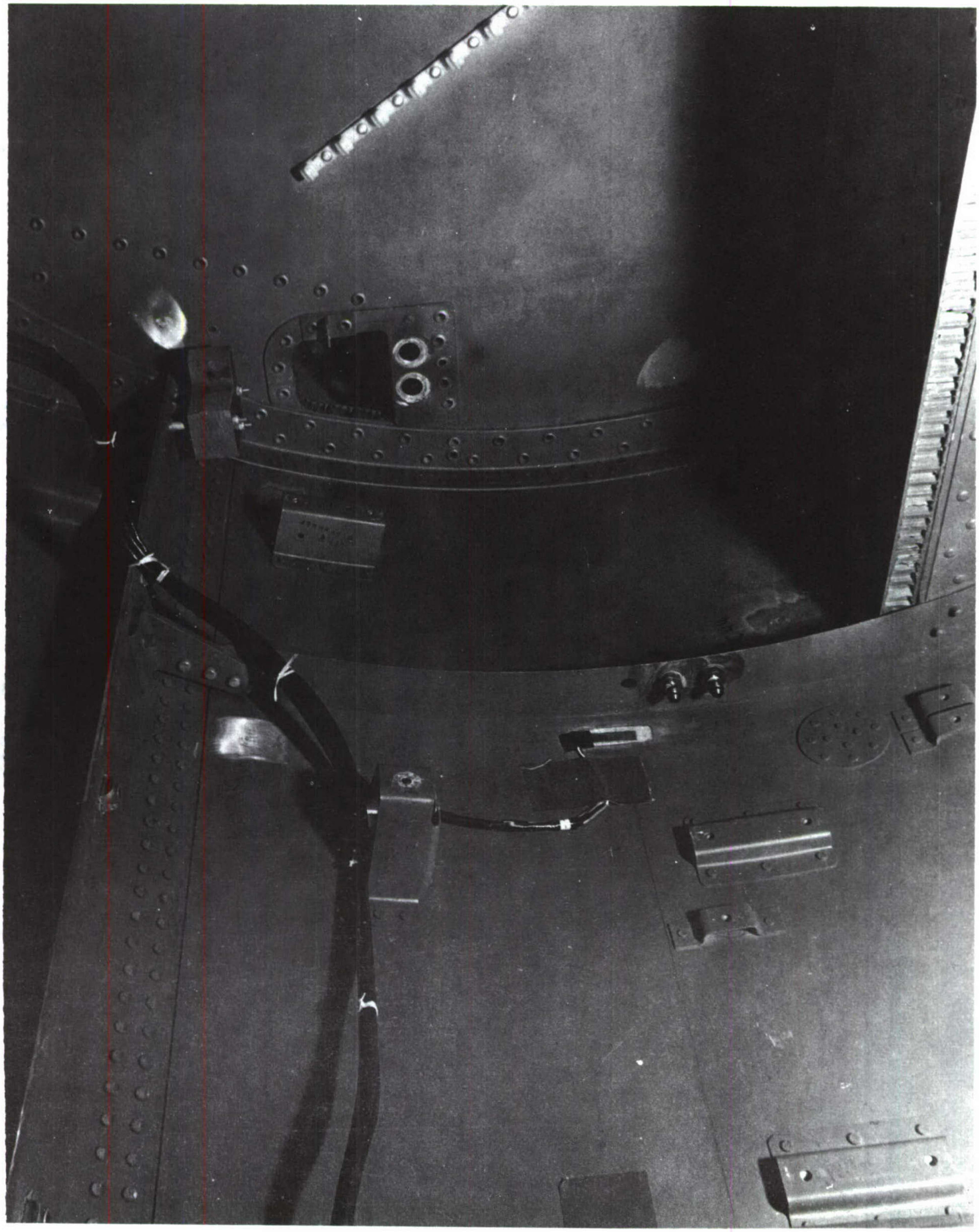

FIGURE A37 INSIDE VIEW OF L.H. SIDE OF VEHICLE EQUIPMENT BAY, F.S. 536.0-600.0

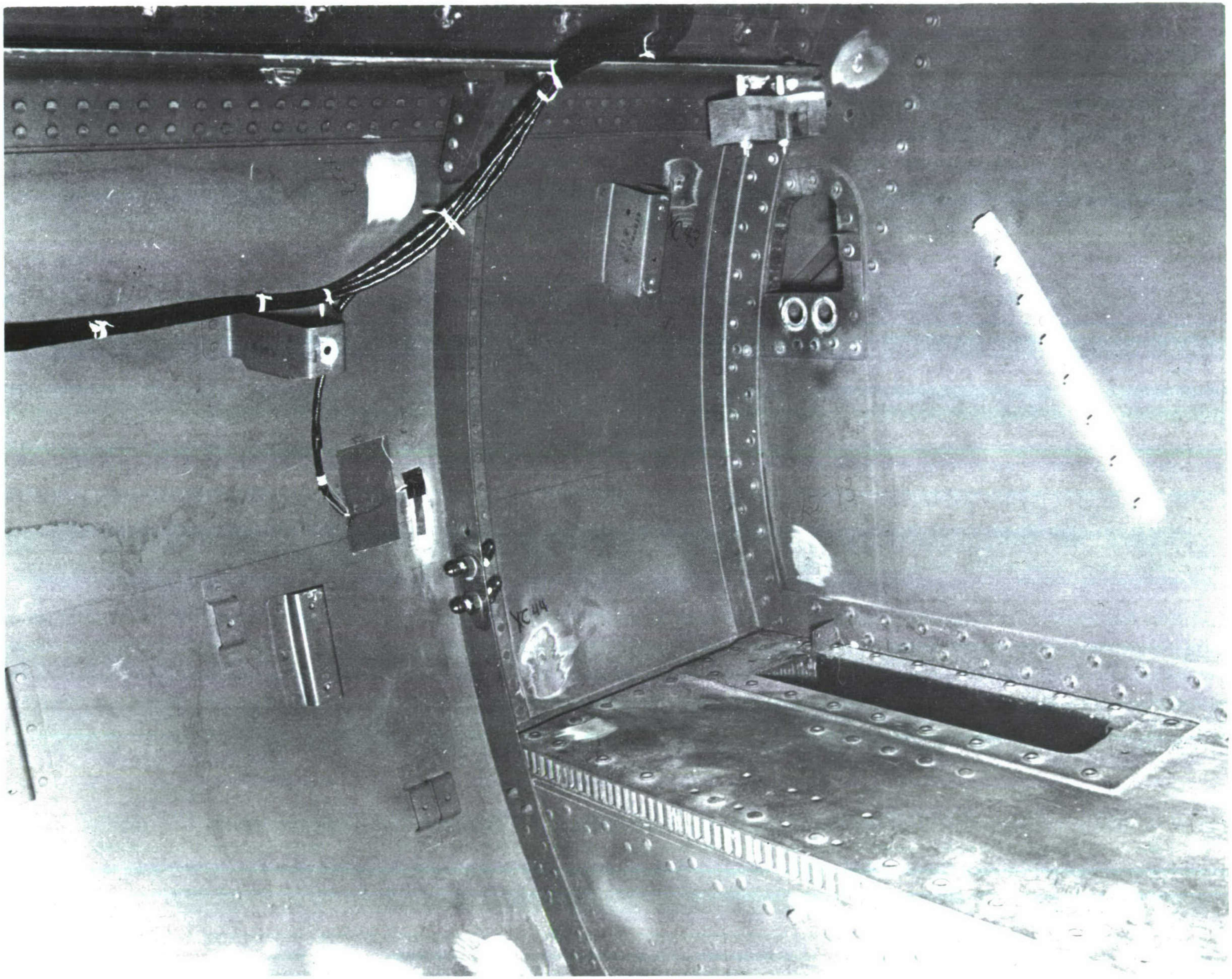

FIGURE A38 INSIDE VIEW OF L.H. SIDE OF VEHICLE EQUIPMENT BAY, F.S. 536.0-600.0

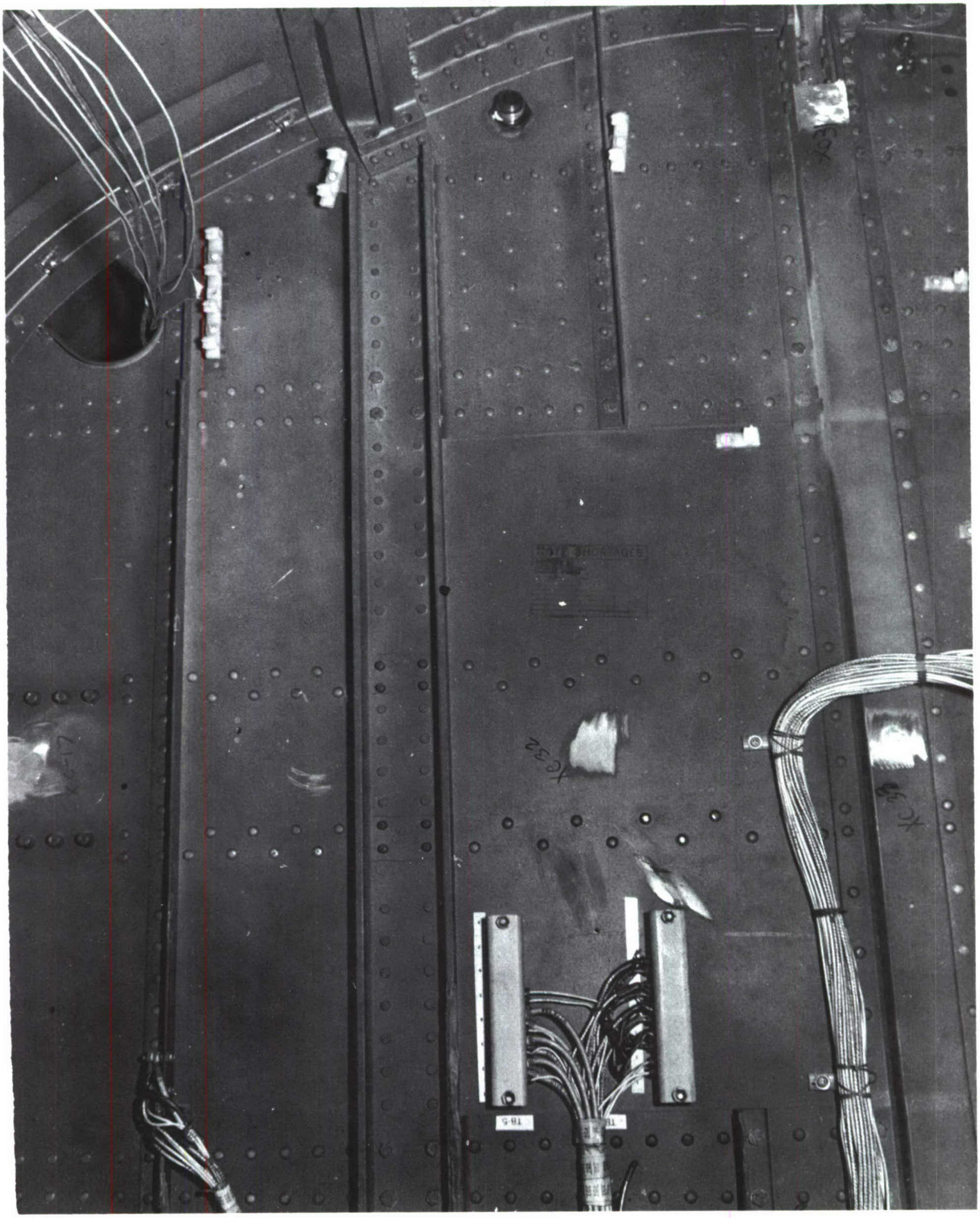

FIGURE A39 FORWARD VIEW OF VEHICLE BULKHEAD AT F.S. 600.0

FIGURE A40 BOTTOM VIEW OF VEHICLE COVER F.S. 536.0-600.0

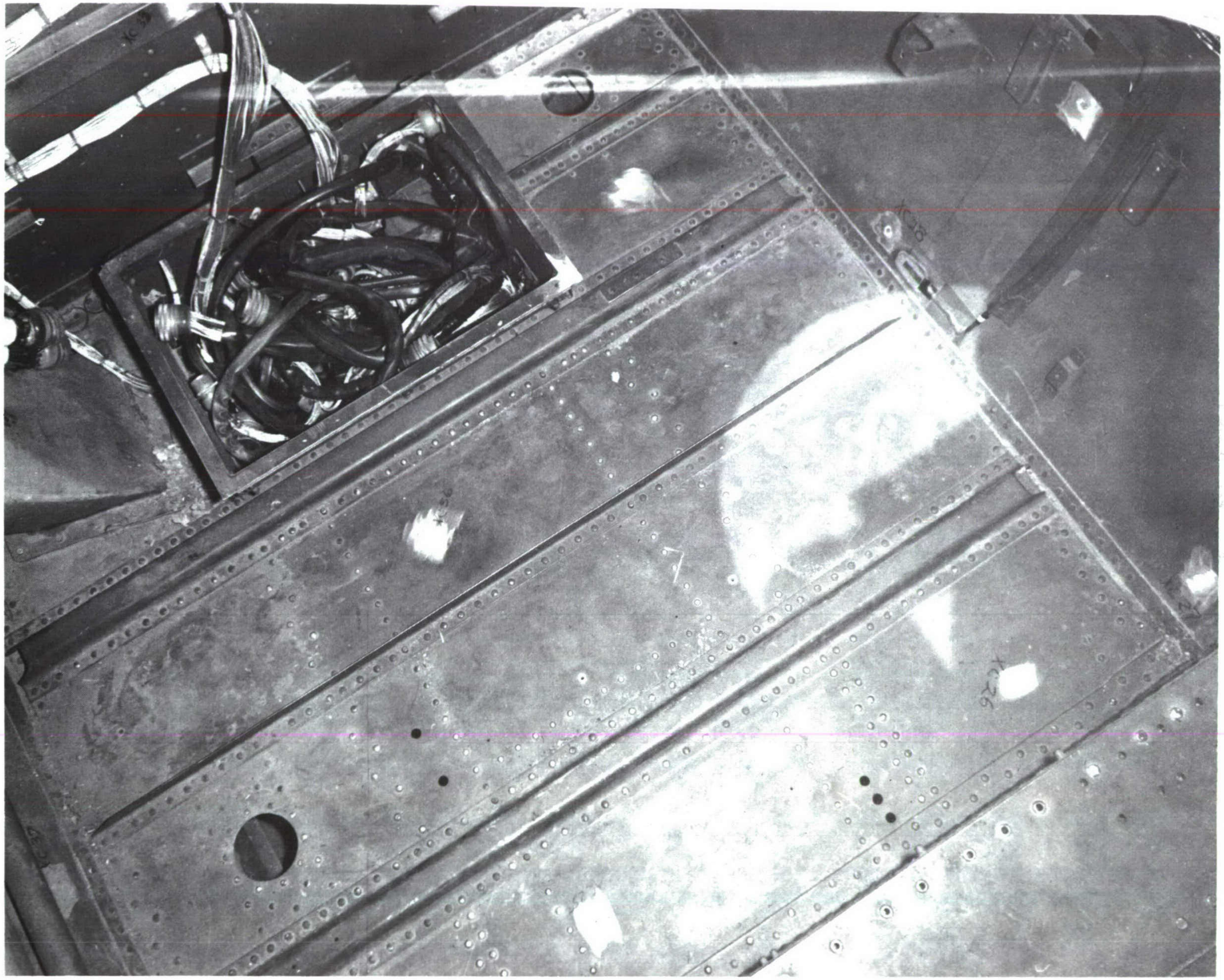

FIGURE A41 TOP VIEW OF VEHICLE DECK F.S. 551.5-600.0

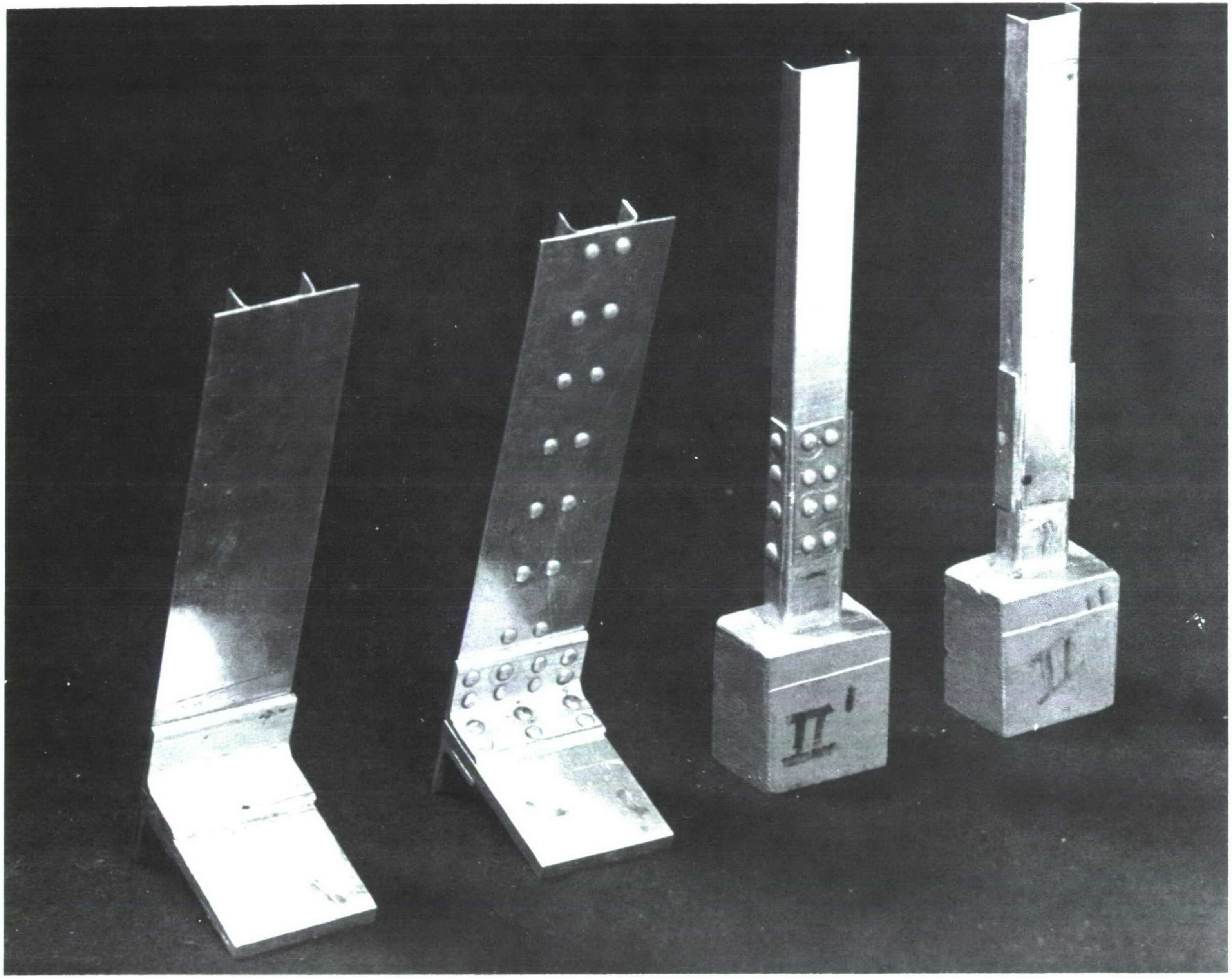

FIGURE A42 SUBSTUDY TEST SPECIMENS

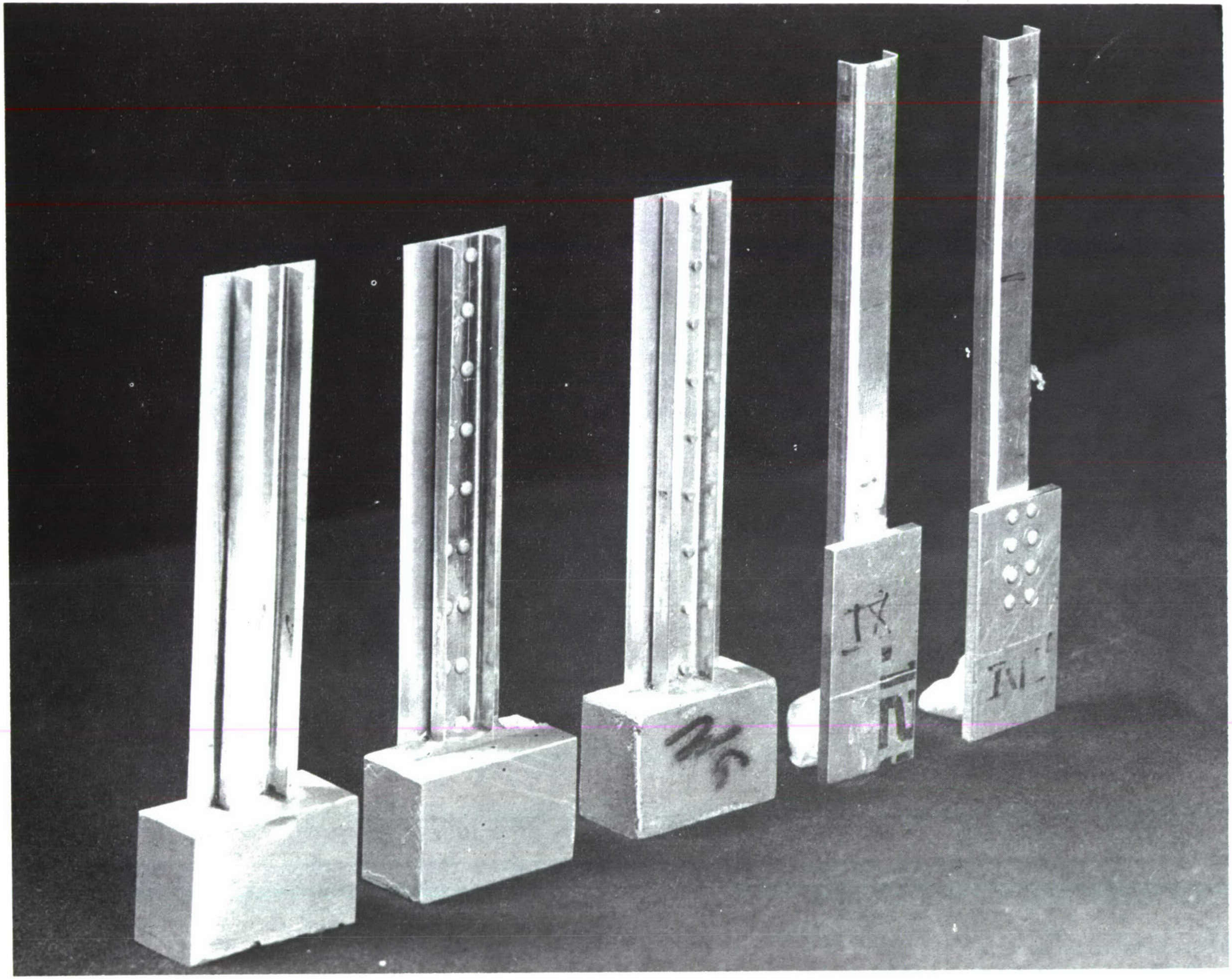

FIGURE A43 SUBSTUDY TEST SPECIMENS

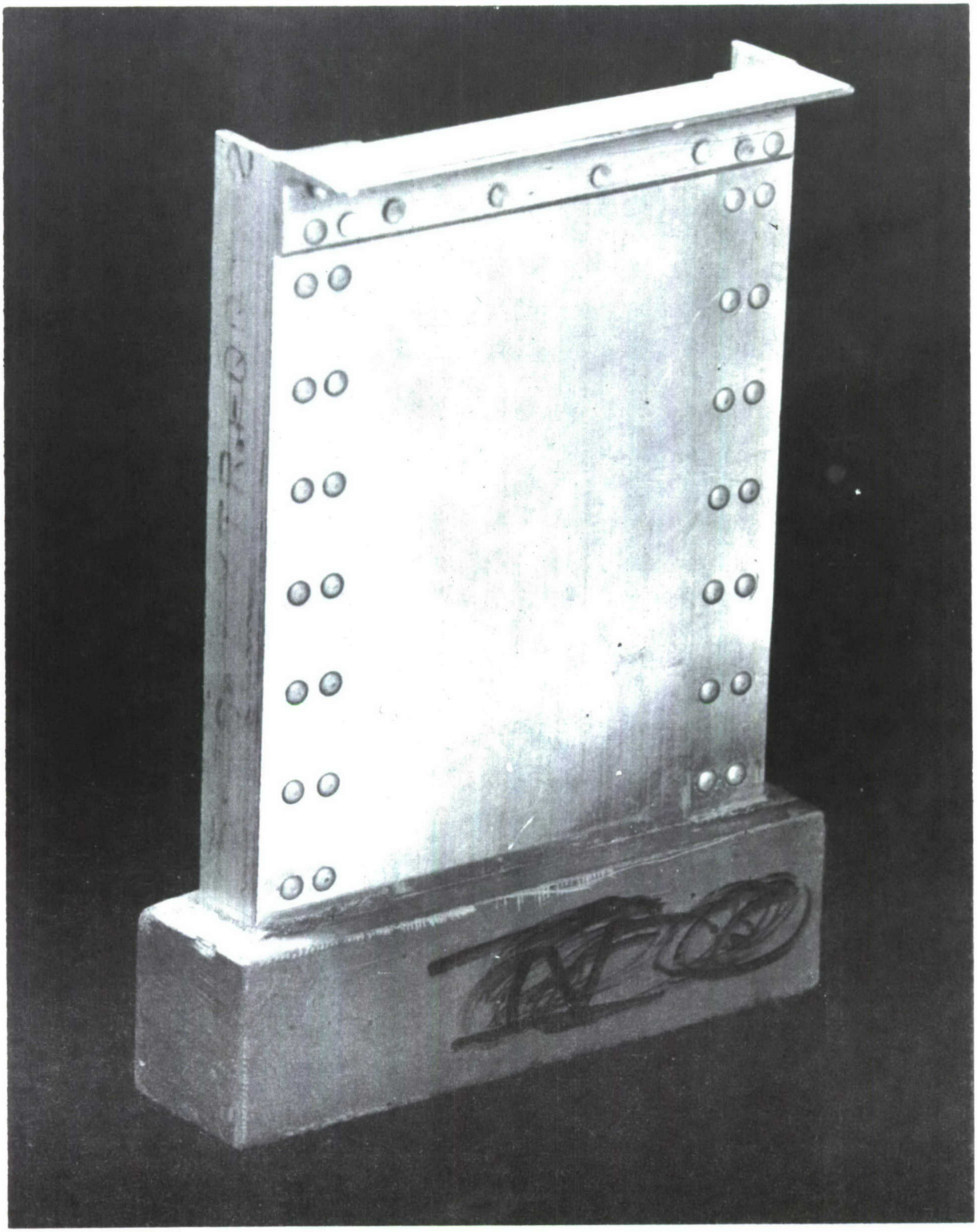

FIGURE A44 SUBSTUDY TEST SPECIMENS

APPENDIX B

STRUCTURAL AND INSTRUMENTATION LOCATION DIAGRAMS

VIEW LOOKING INBD. AT R.H. SIDE

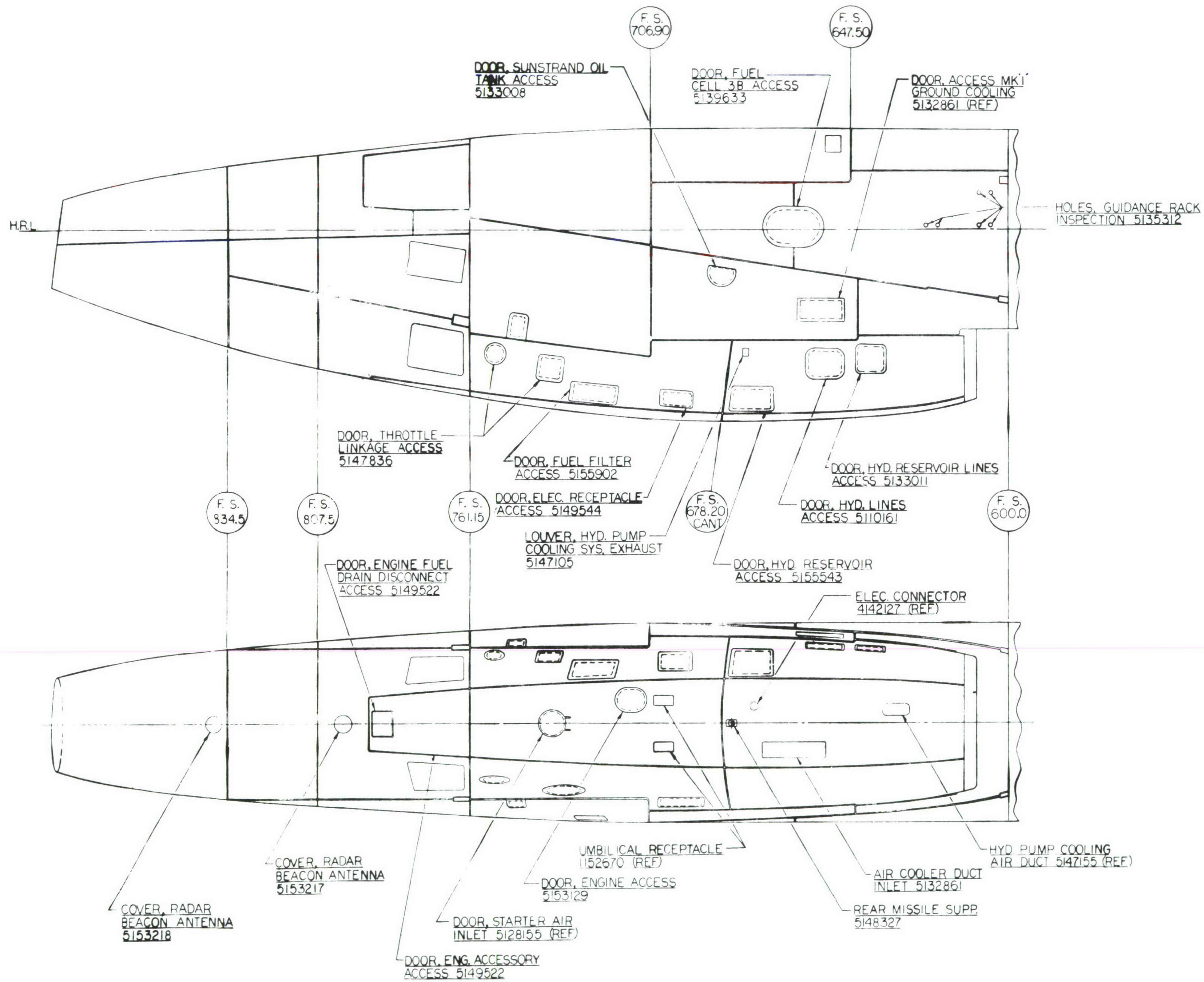

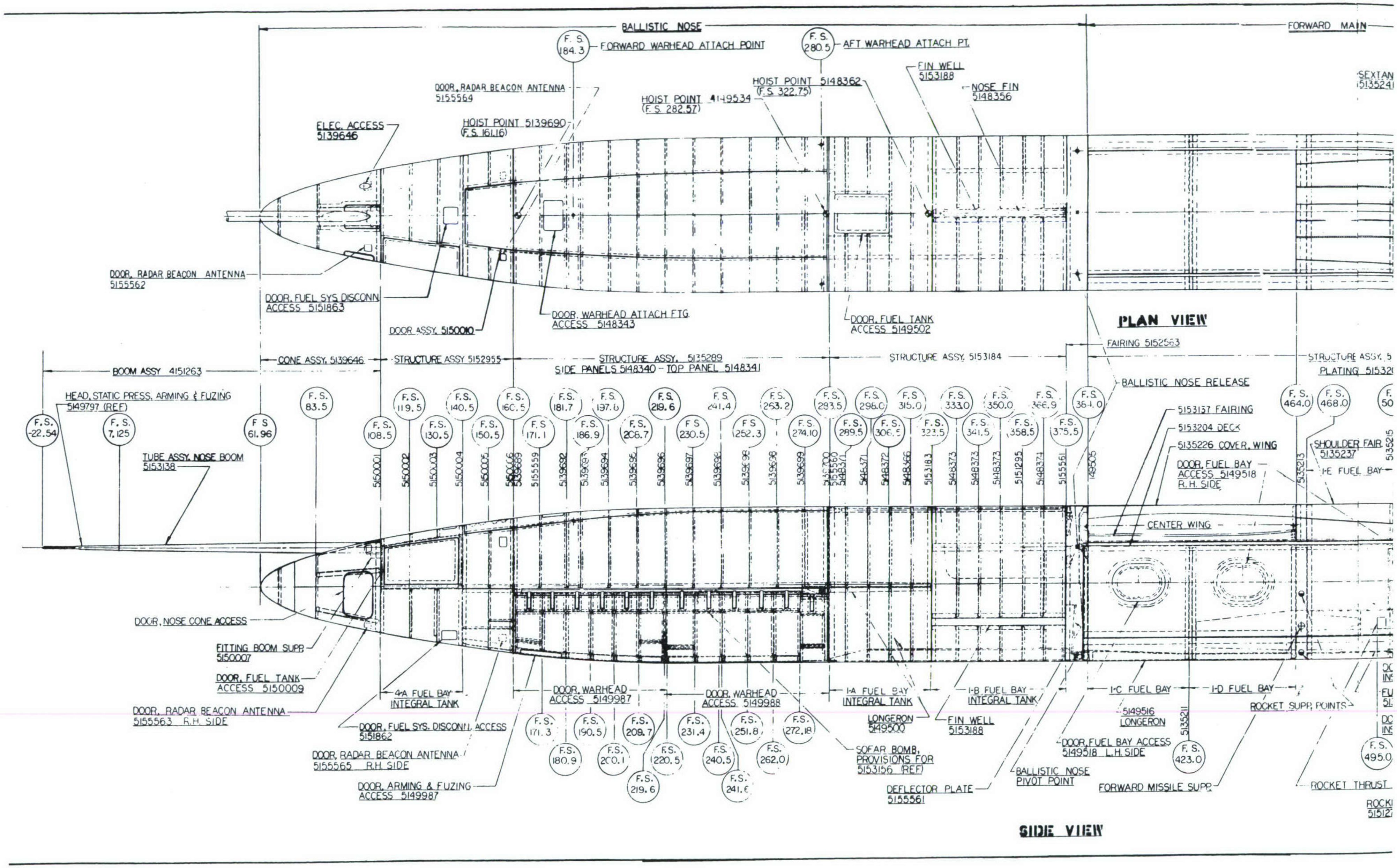
BALLISTIC NOSE
FORWARD MAIN
F.S. 184.3 FORWARD WARHEAD ATTACH POINT
F.S. 280.5 AFT WARHEAD ATTACH PT.
DOOR, RADAR BEACON ANTENNA 5155564
HOIST POINT 4149534 (F.S. 282.57)
HOIST POINT 5148362 (F.S. 322.75)
FIN WELL 5153188
NOSE FIN 5148356
ELEC. ACCESS 5139646
HOIST POINT 5139690 (F.S. 161.16)
DOOR, RADAR BEACON ANTENNA 5155562
DOOR, FUEL SYS DISCONN ACCESS 5151863
DOOR ASSY. 5150010
DOOR, WARHEAD ATTACH FTG. ACCESS 5148343
DOOR, FUEL TANK ACCESS 5149502
PLAN VIEW
FAIRING 5152563
BOOM ASSY 4151263
CONE ASSY. 5139646
STRUCTURE ASSY 5152955
STRUCTURE ASSY. 5135289
SIDE PANELS 5148340 - TOP PANEL 5148341
STRUCTURE ASSY. 5153184
BALLISTIC NOSE RELEASE
HEAD, STATIC PRESS, ARMING & FUZING 5149797 (REF)
TUBE ASSY. NOSE BOOM 5153138
5153137 FAIRING
5153204 DECK
5135226 COVER, WING
SHOULDER FAIR 5135237
DOOR, FUEL BAY ACCESS 5149518 R.H. SIDE
CENTER WING
DOOR, NOSE CONE ACCESS
FITTING BOOM SUPP. 5150007
DOOR, FUEL TANK ACCESS 5150009
DOOR, RADAR BEACON ANTENNA 5155563 R.H. SIDE
4-A FUEL BAY INTEGRAL TANK
DOOR, FUEL SYS. DISCONN. ACCESS 5151862
DOOR, RADAR BEACON ANTENNA 5155565 R.H. SIDE
DOOR, ARMING & FUZING ACCESS 5149987
DOOR, WARHEAD ACCESS 5149987
DOOR, WARHEAD ACCESS 5149988
1-A FUEL BAY INTEGRAL TANK
LONGERON 5149500
1-B FUEL BAY INTEGRAL TANK
FIN WELL 5153188
SOFAR BOMB, PROVISIONS FOR 5153156 (REF)
DEFLECTOR PLATE 5155561
BALLISTIC NOSE PIVOT POINT
1-C FUEL BAY
5149516 LONGERON
DOOR, FUEL BAY ACCESS 5149518 L.H. SIDE
1-D FUEL BAY
F.S. 423.0
FORWARD MISSILE SUPP.
ROCKET SUPP. POINTS
ROCKET THRUST
SIDE VIEW
F.S. -22.54
F.S. 7.125
F.S. 61.96
F.S. 83.5
F.S. 108.5
F.S. 119.5
F.S. 130.5
F.S. 140.5
F.S. 150.5
F.S. 160.5
F.S. 171.1
F.S. 181.7
F.S. 186.9
F.S. 197.6
F.S. 206.7
F.S. 219.6
F.S. 230.5
F.S. 241.4
F.S. 252.3
F.S. 253.2
F.S. 274.10
F.S. 283.5
F.S. 289.5
F.S. 296.0
F.S. 315.0
F.S. 323.5
F.S. 333.0
F.S. 341.5
F.S. 350.0
F.S. 358.5
F.S. 366.9
F.S. 375.5
F.S. 364.0
F.S. 464.0
F.S. 468.0
F.S. 171.3
F.S. 180.9
F.S. 190.5
F.S. 200.1
F.S. 208.7
F.S. 219.6
F.S. 220.5
F.S. 231.4
F.S. 240.5
F.S. 251.8
F.S. 262.0
F.S. 272.18
F.S. 495.0

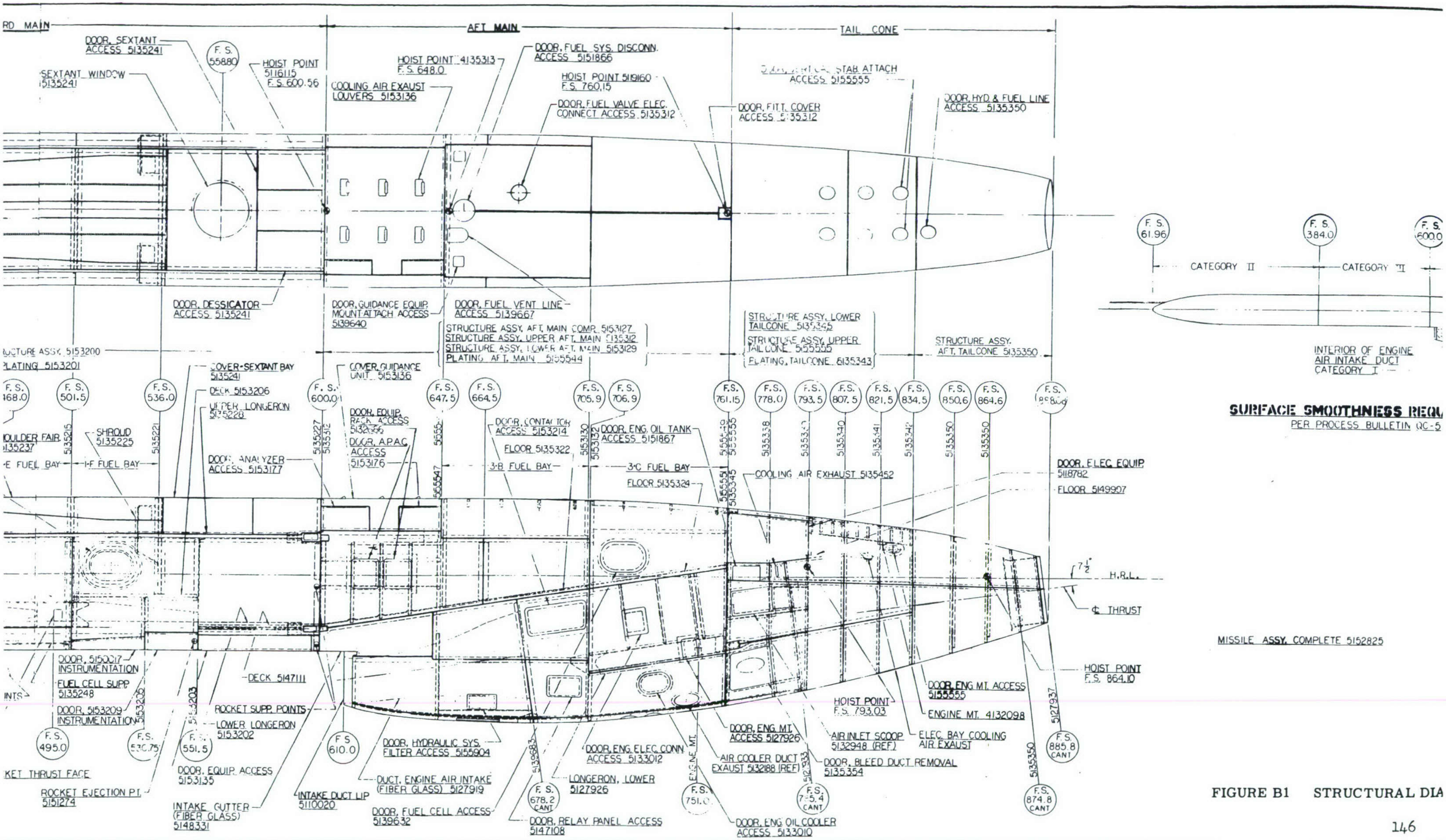

FIGURE B1 STRUCTURAL DIA

2

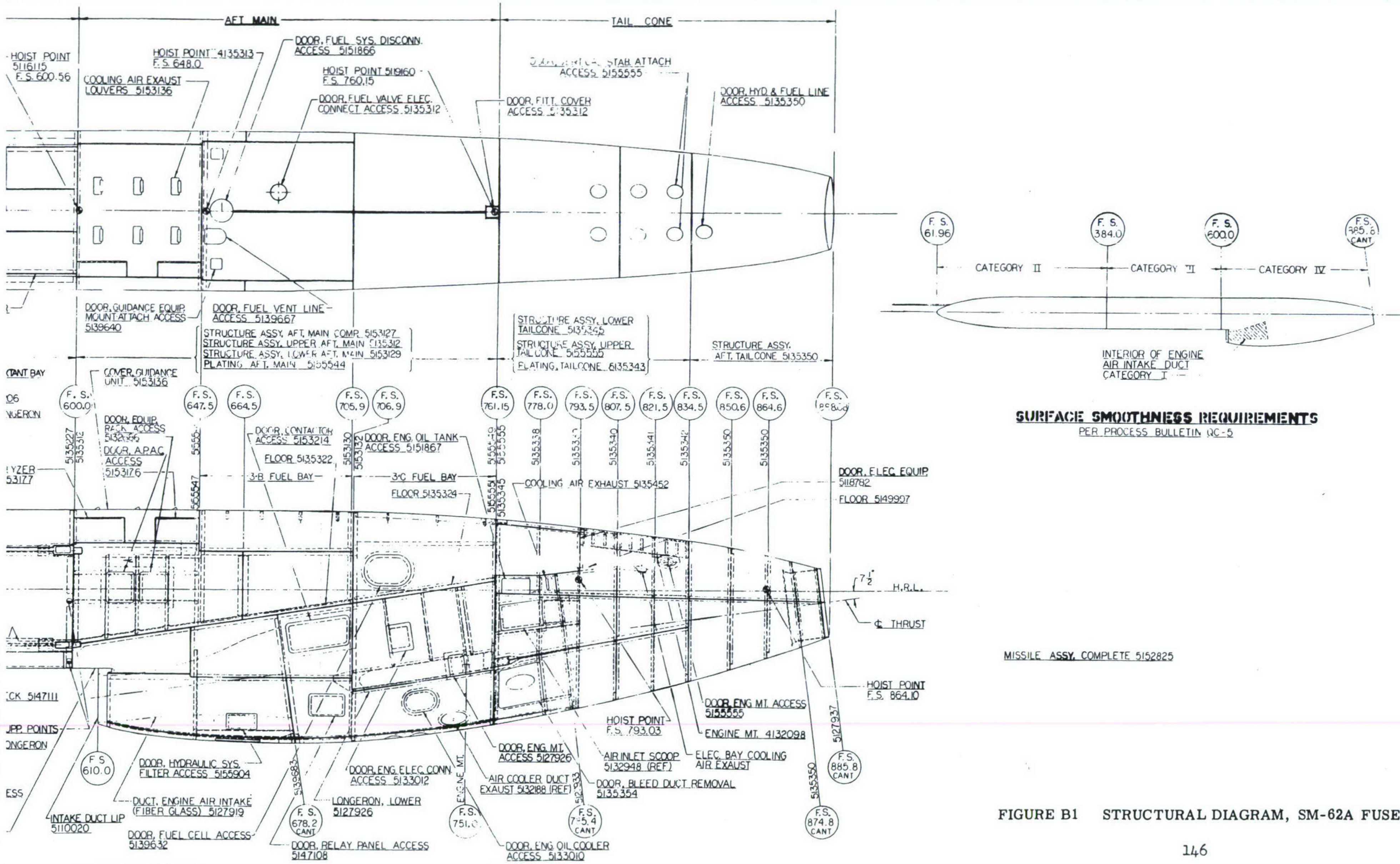

FIGURE B1 STRUCTURAL DIAGRAM, SM-62A FUSELAGE

3

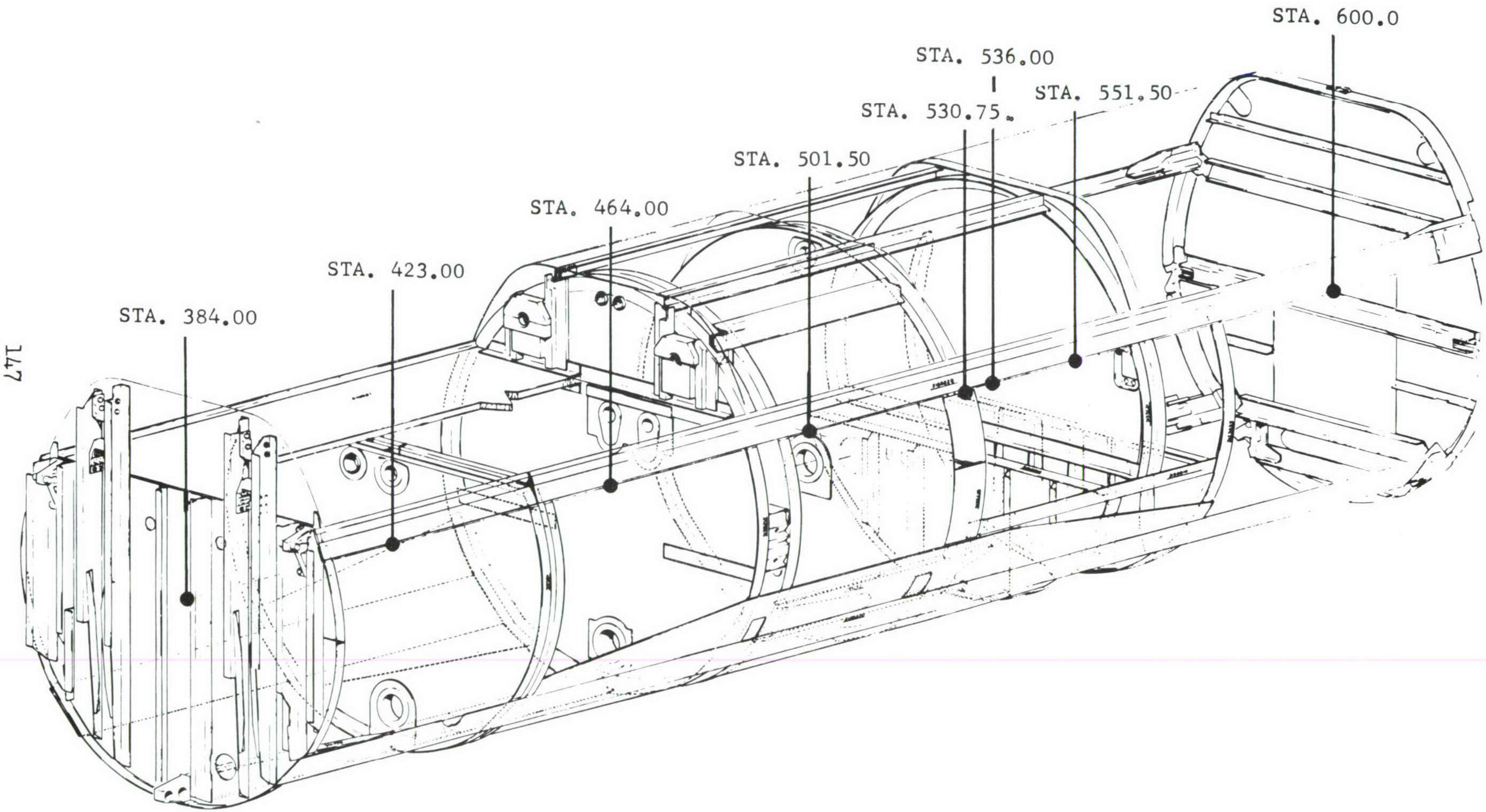

FIGURE B2 STRUCTURAL DRAWING-SM-62A FORWARD MAIN UNIT F.S. 384-600

5135309 STRUCTURE ASSEMBLY-FUS. AFT MAIN SECTION
5135312 STRUCTURE ASSEMBLY-FUS. AFT MAIN SECTION UPPER
5135326 STRUCTURE ASSEMBLY-FUS. AFT MAIN SECTION LOWER

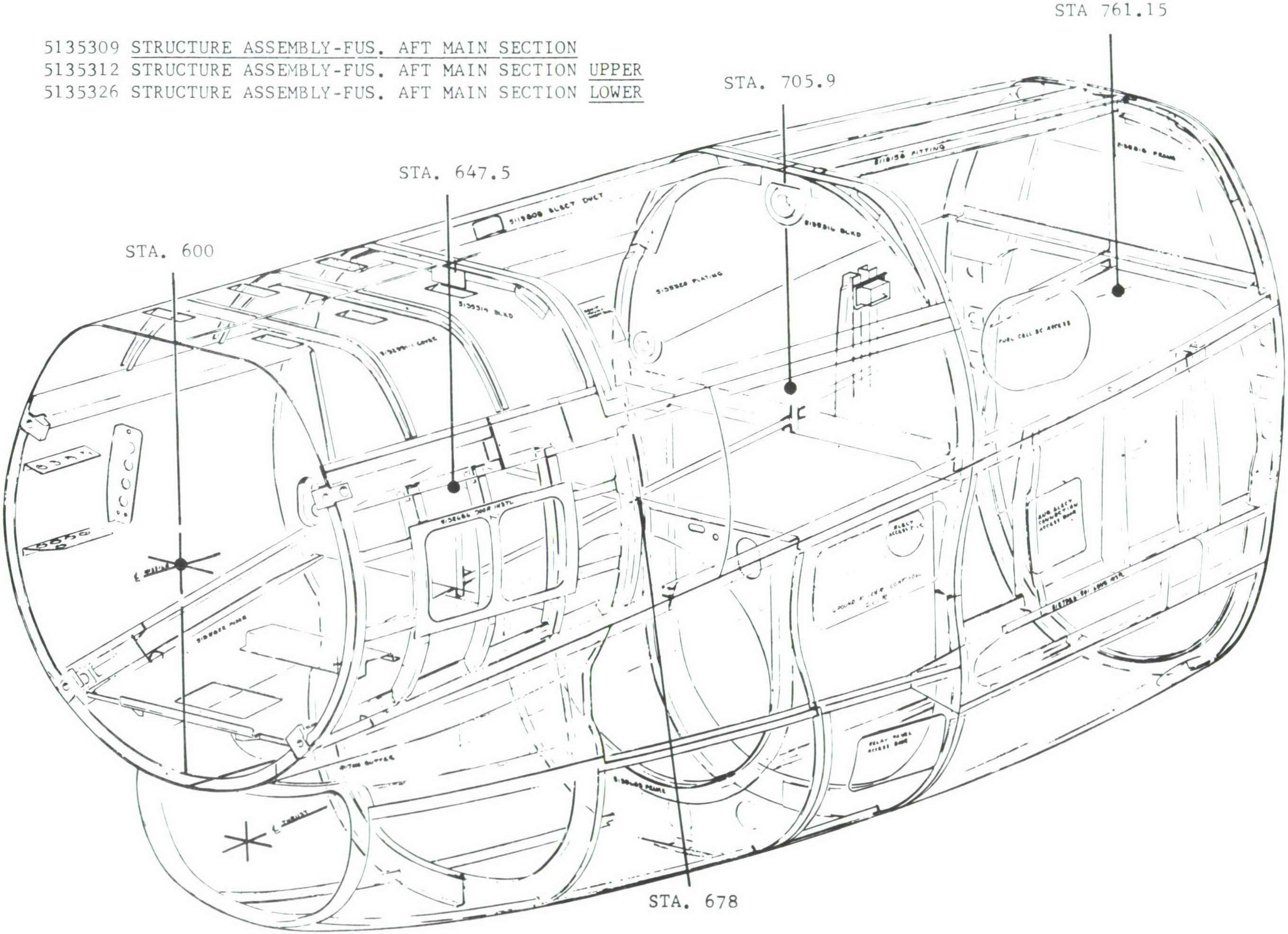

FIGURE B3 STRUCTURAL DRAWING-SM62A AFT MAIN UNIT F.S. 600-761

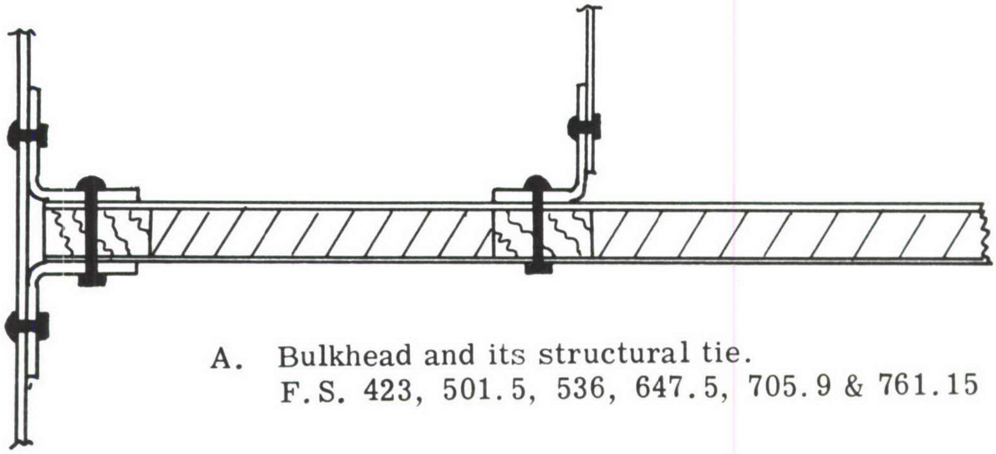

A. Bulkhead and its structural tie.
F.S. 423, 501.5, 536, 647.5, 705.9 & 761.15

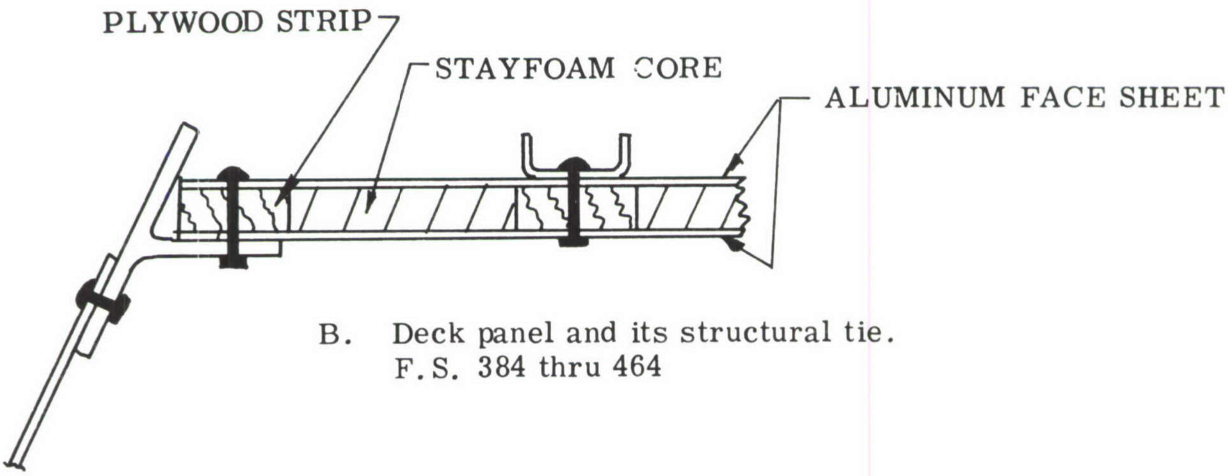

B. Deck panel and its structural tie.
F.S. 384 thru 464

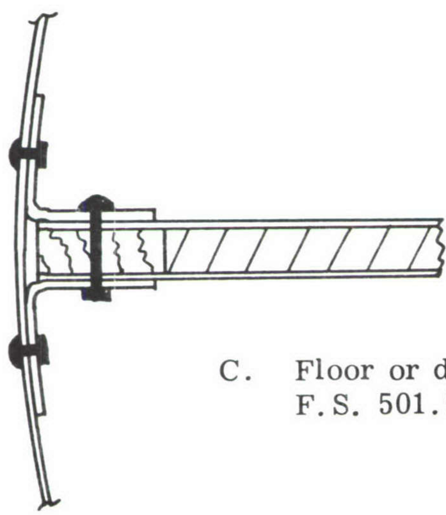

C. Floor or deck panel and its structural tie.
F.S. 501.5 thru 600 & 647.5 thru 761.15

FIGURE B4 TYPICAL SANDWICH SIMULATION AND STRUCTURAL TIES

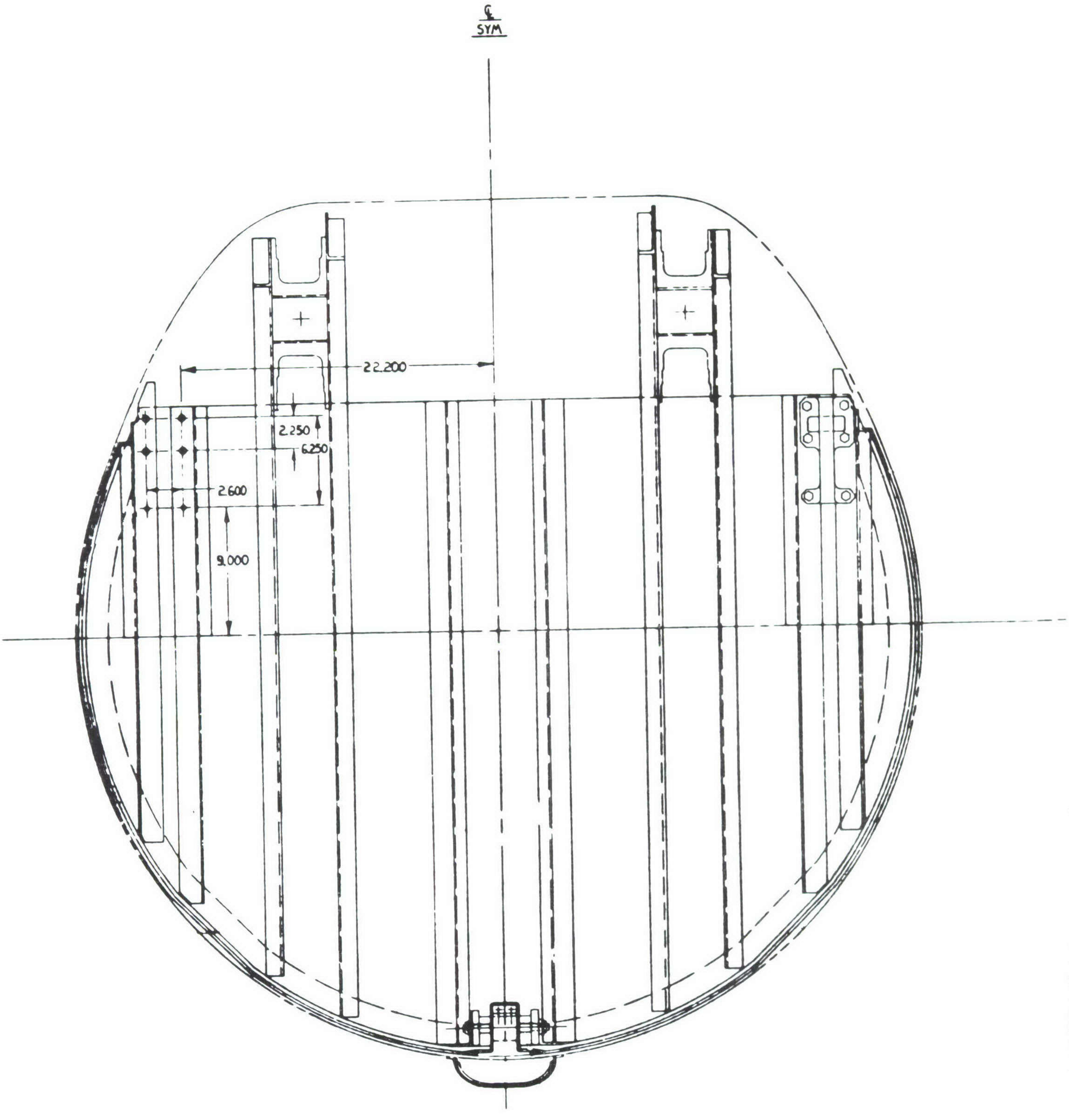

FIGURE B5 VIEW OF VEHICLE LOOKING AFT AT F.S. 384.0

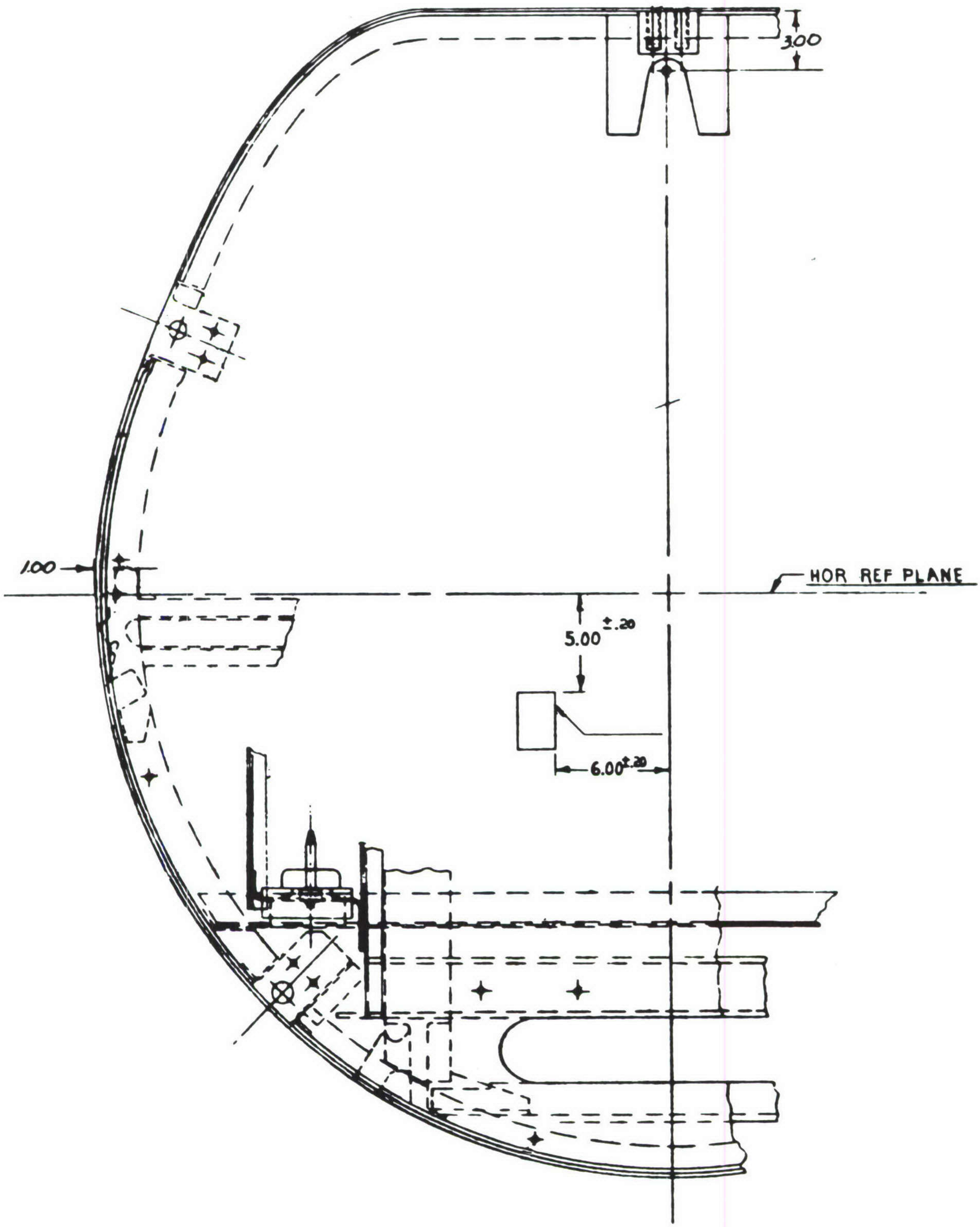

FIGURE B6 VIEW OF VEHICLE LOOKING FORWARD AT F.S. 600.0

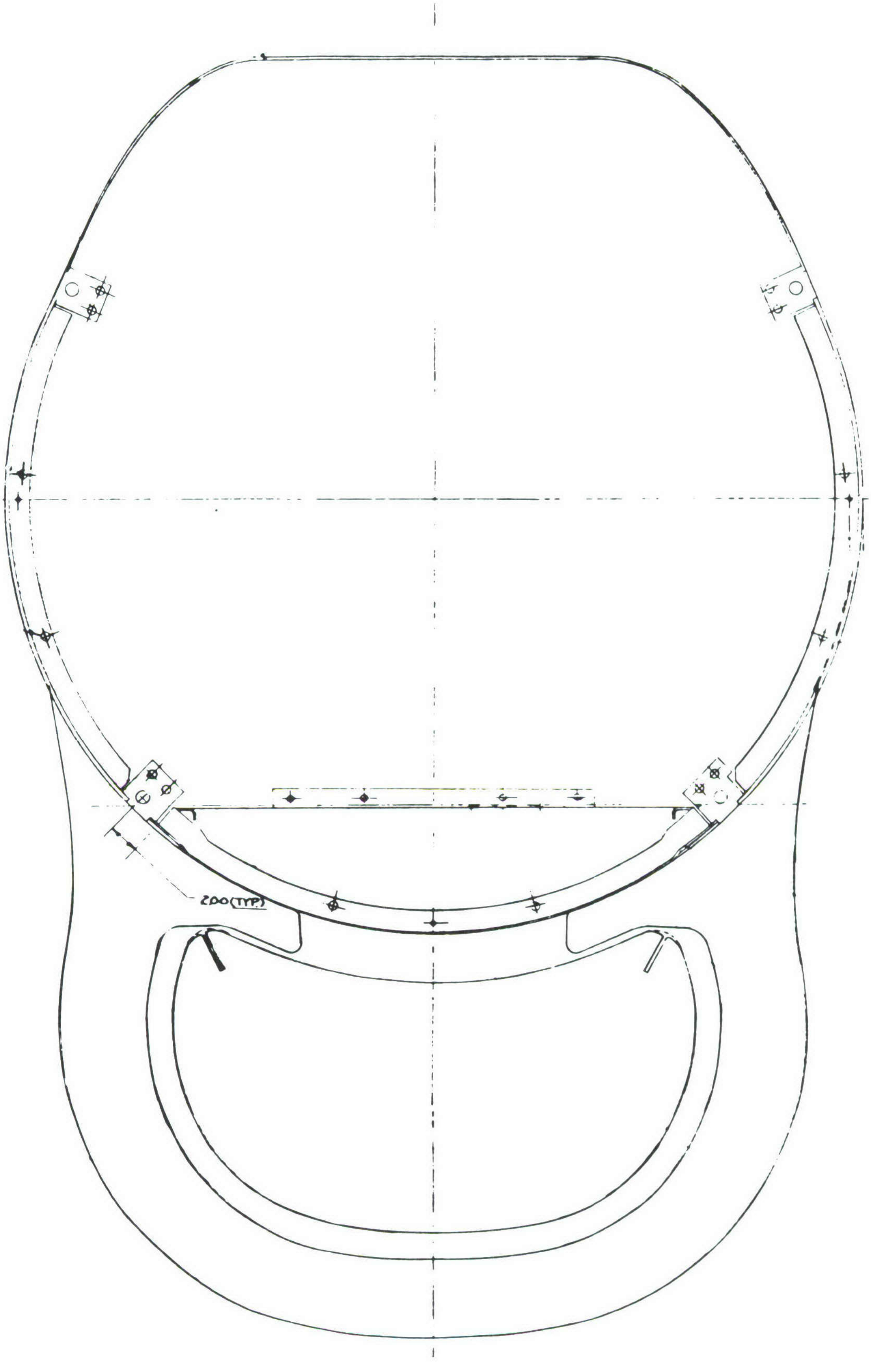

FIGURE B7 VIEW OF VEHICLE LOOKING AFT AT F.S. 600.0

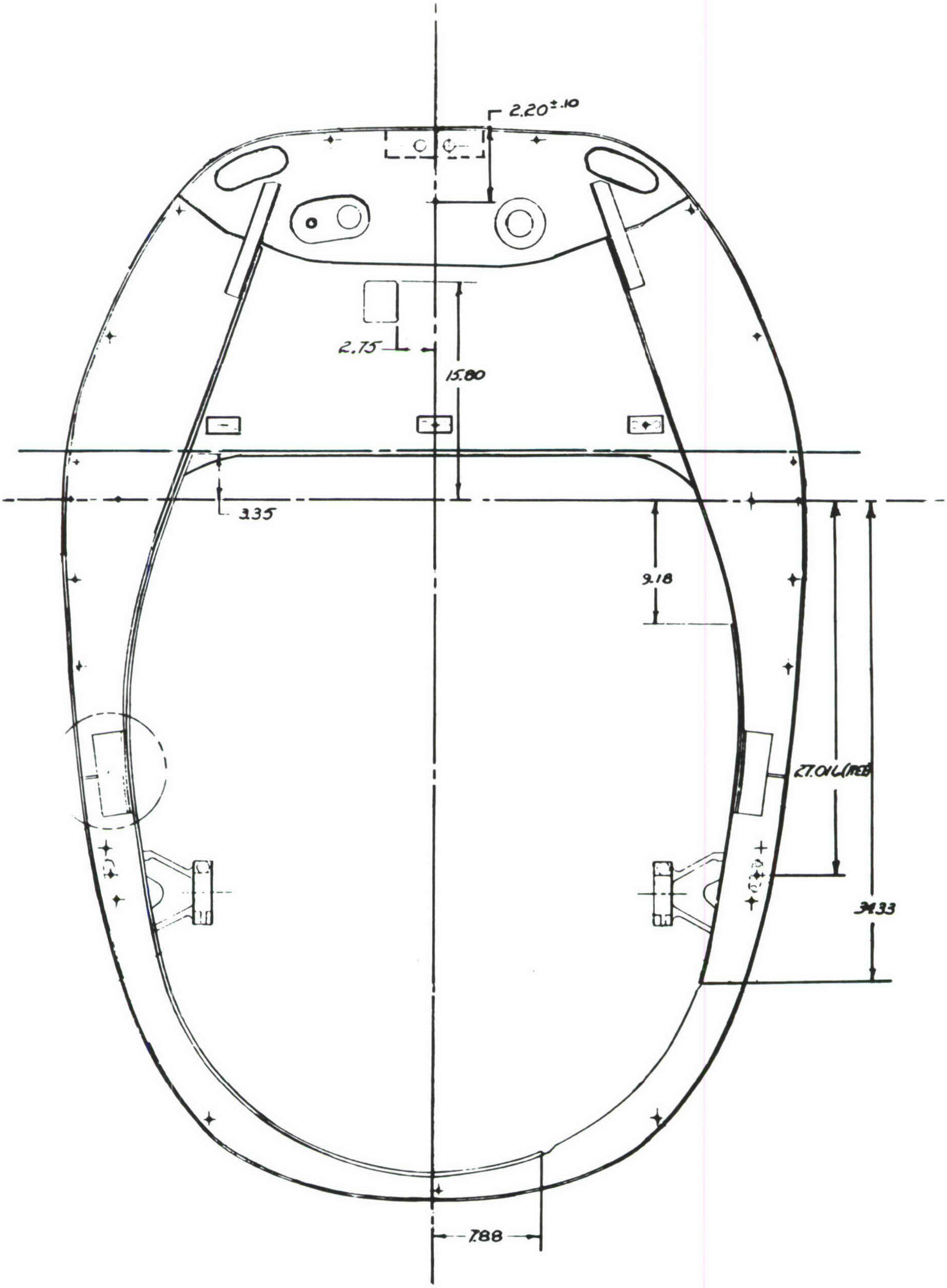

FIGURE B8 VIEW OF VEHICLE LOOKING FORWARD AT F.S. 761.15

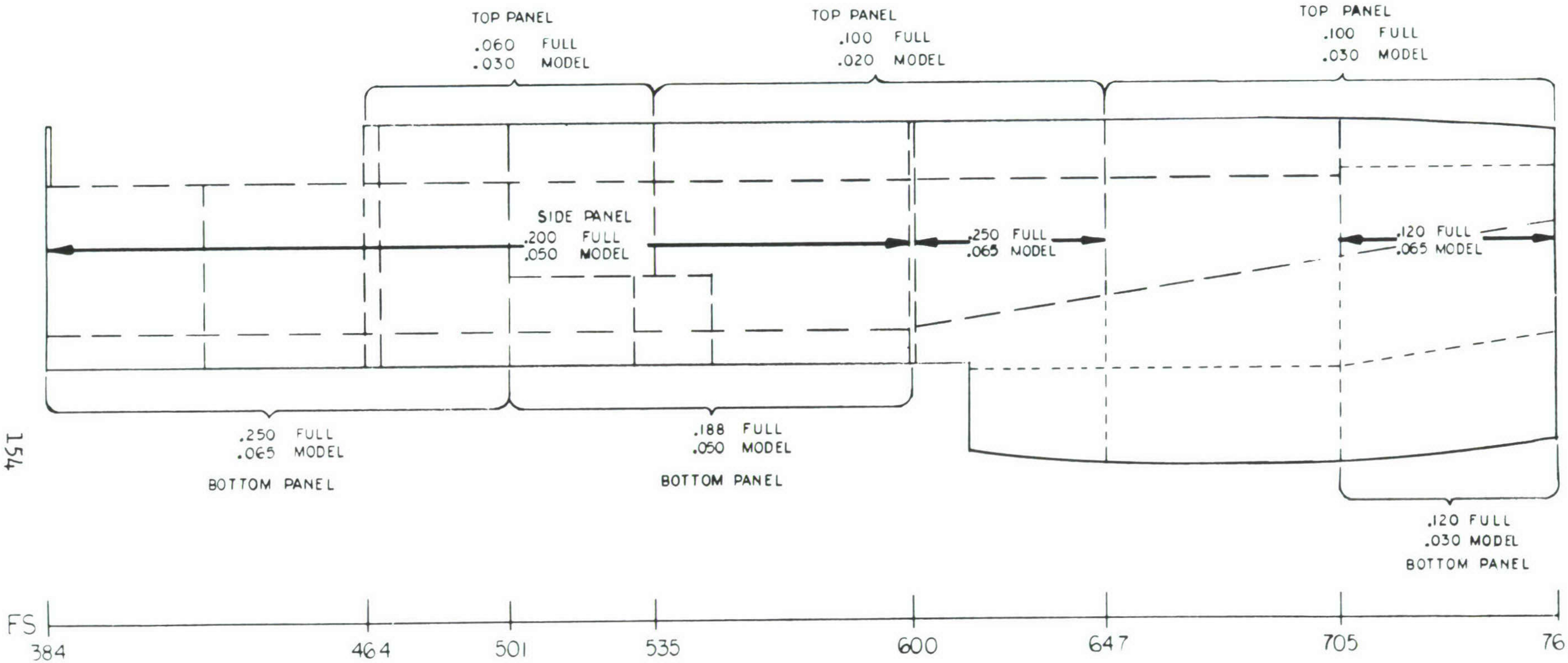

FIGURE B9 MODEL TO FULL SCALE GAGE COMPARISON

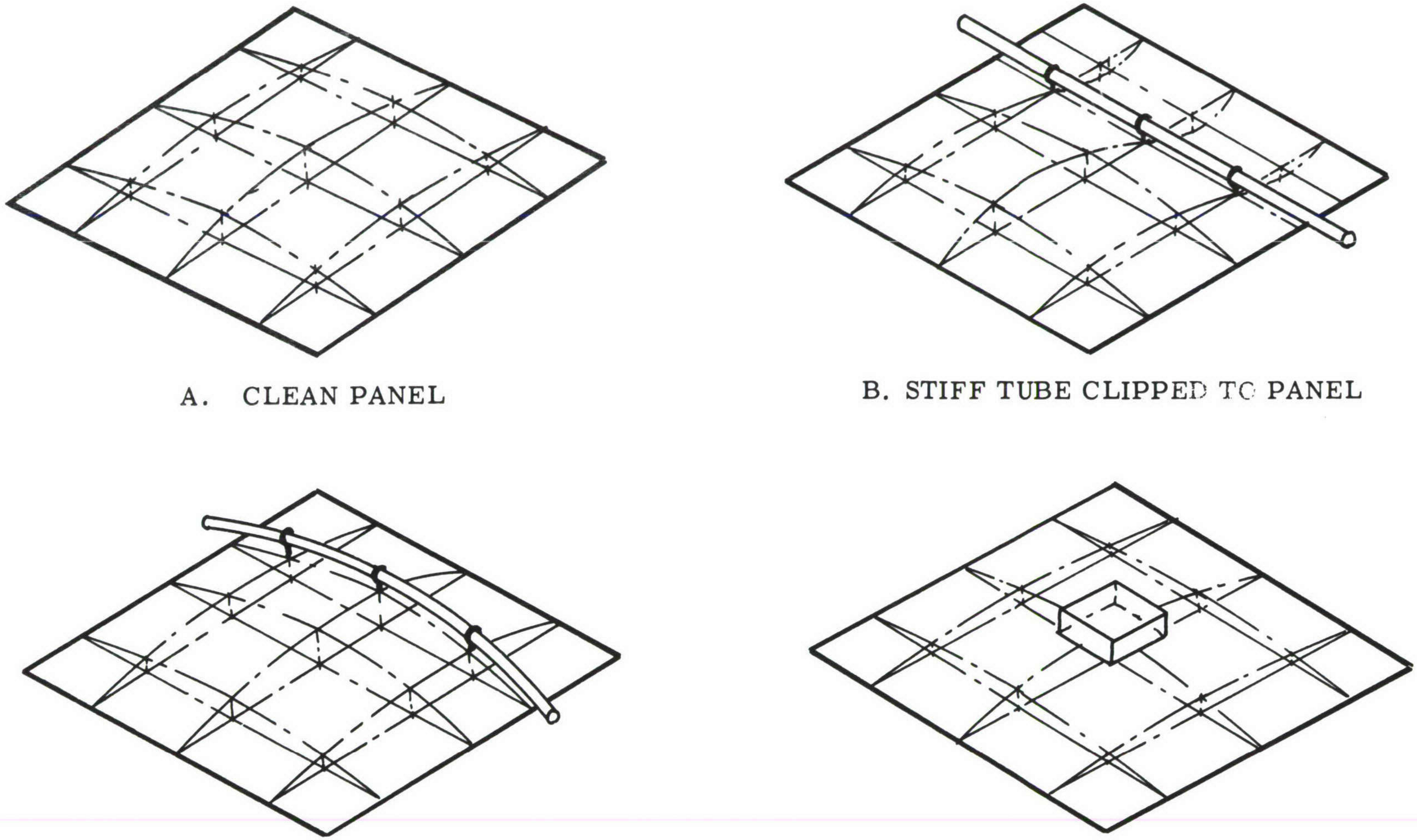

A. CLEAN PANEL

B. STIFF TUBE CLIPPED TO PANEL

C. ELECTRICAL CABLE CLIPPED TO PANEL

D. LARGE WEIGHT ATTACHED TO PANEL

FIGURE B10 EXAMPLE FUNDAMENTAL (FIRST MODE) VIBRATION MODES OF VARIOUS SQUARE PANEL COMBINATIONS

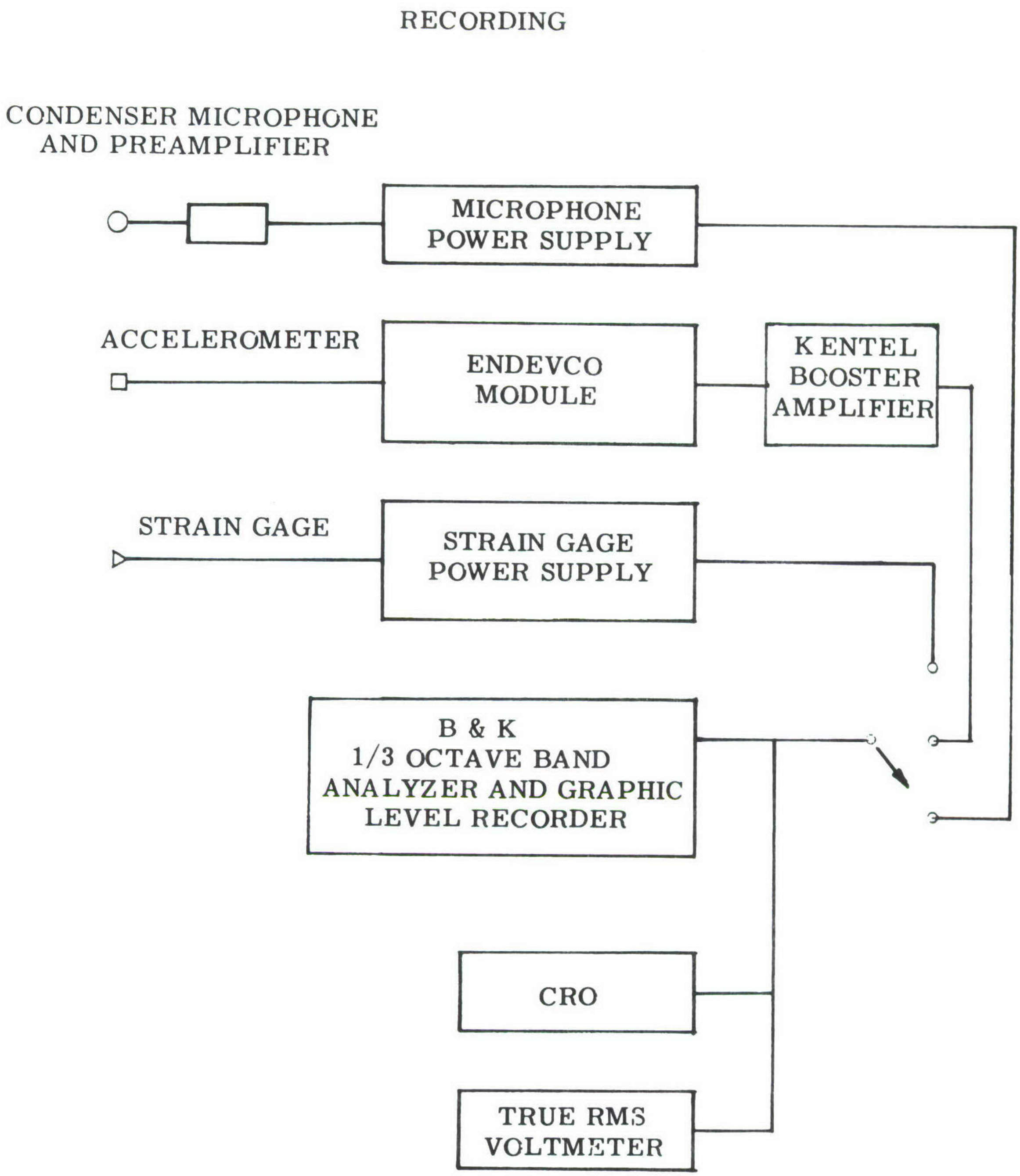

FIGURE B11 INSTRUMENTATION BLOCK DIAGRAM

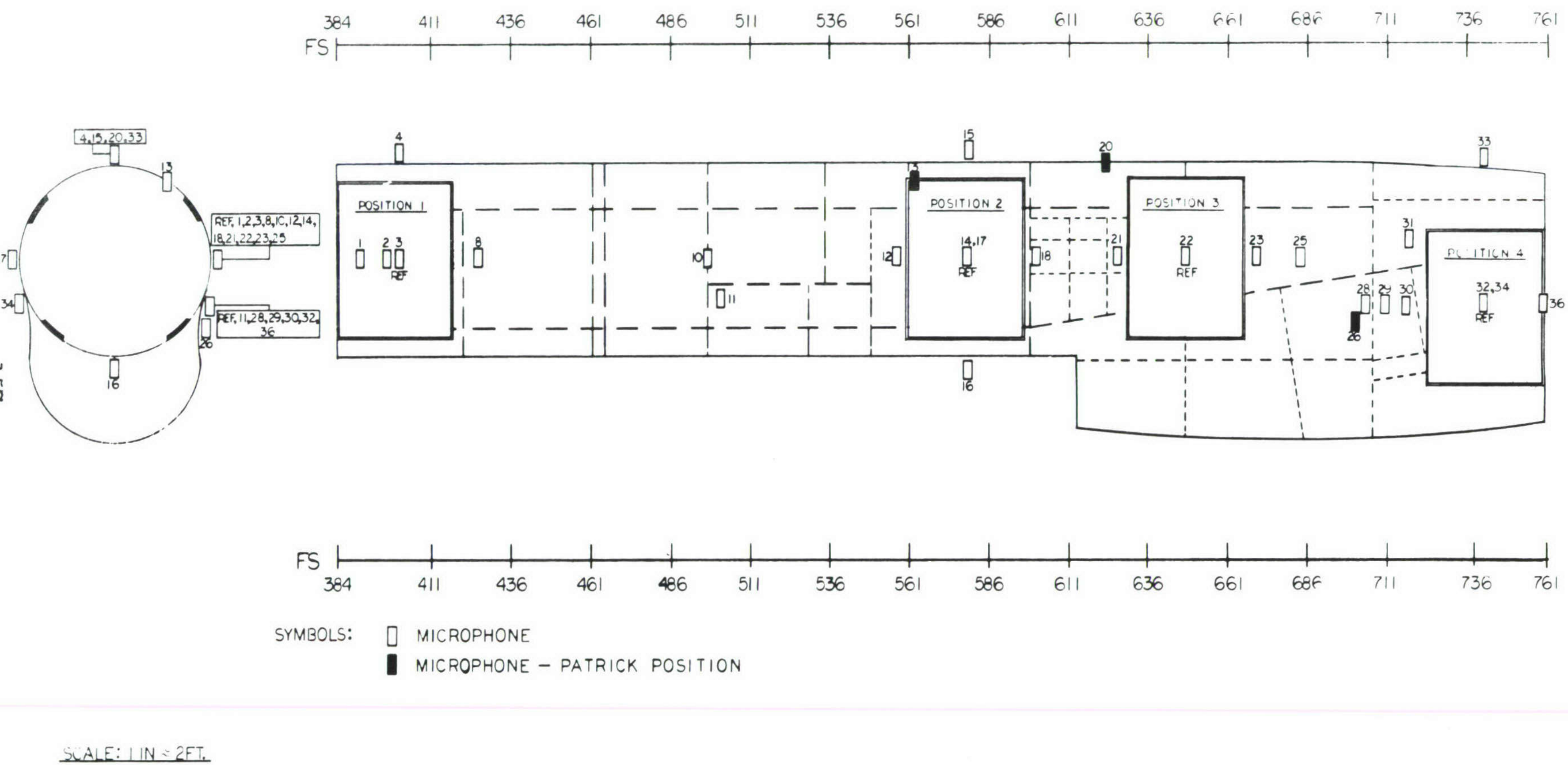

FIGURE B12 FULL SCALE SOURCE POSITION AND MICROPHONE LOCATIONS

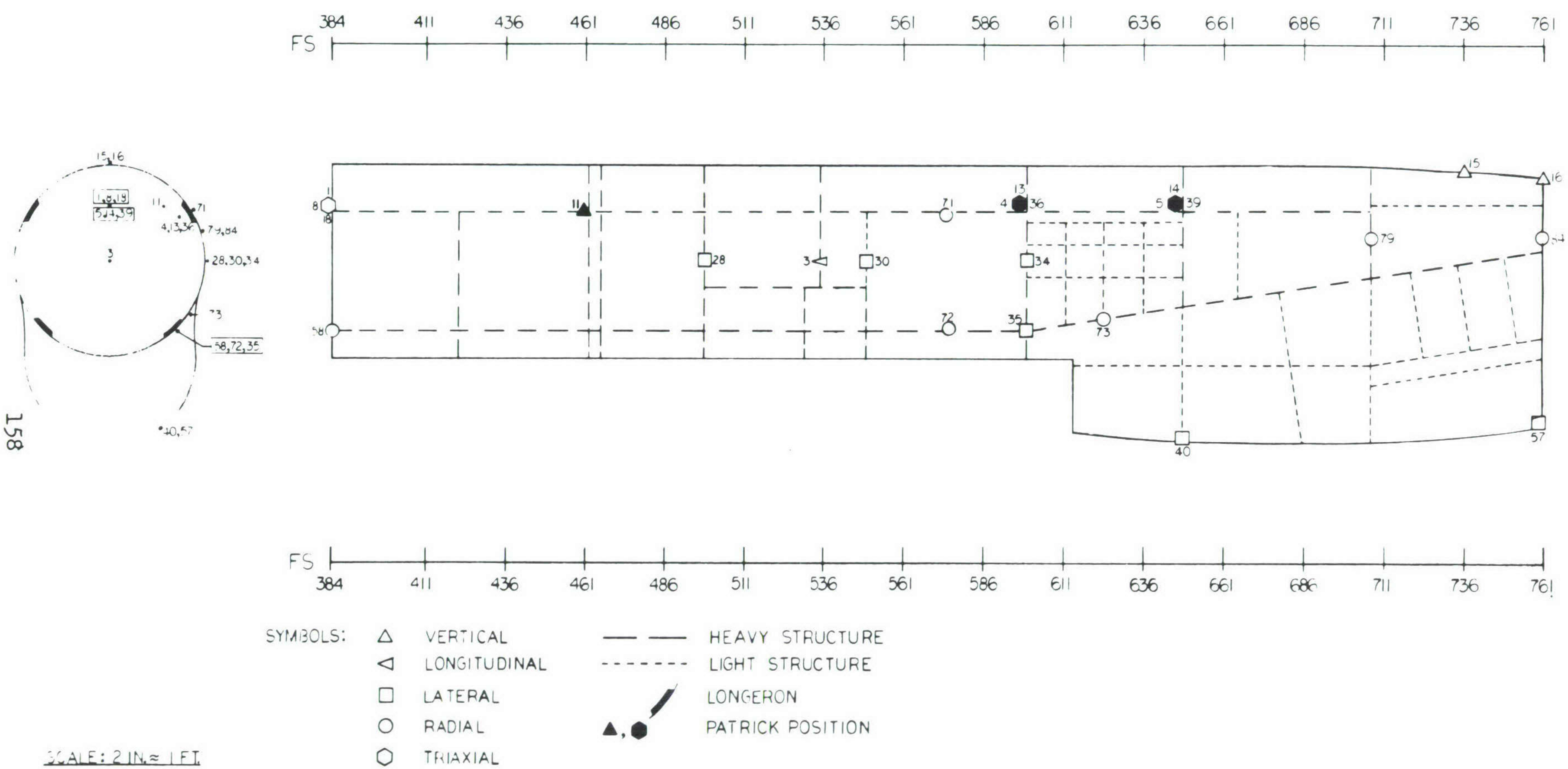

FIGURE B13 SCALE MODEL ACCELEROMETER LOCATIONS

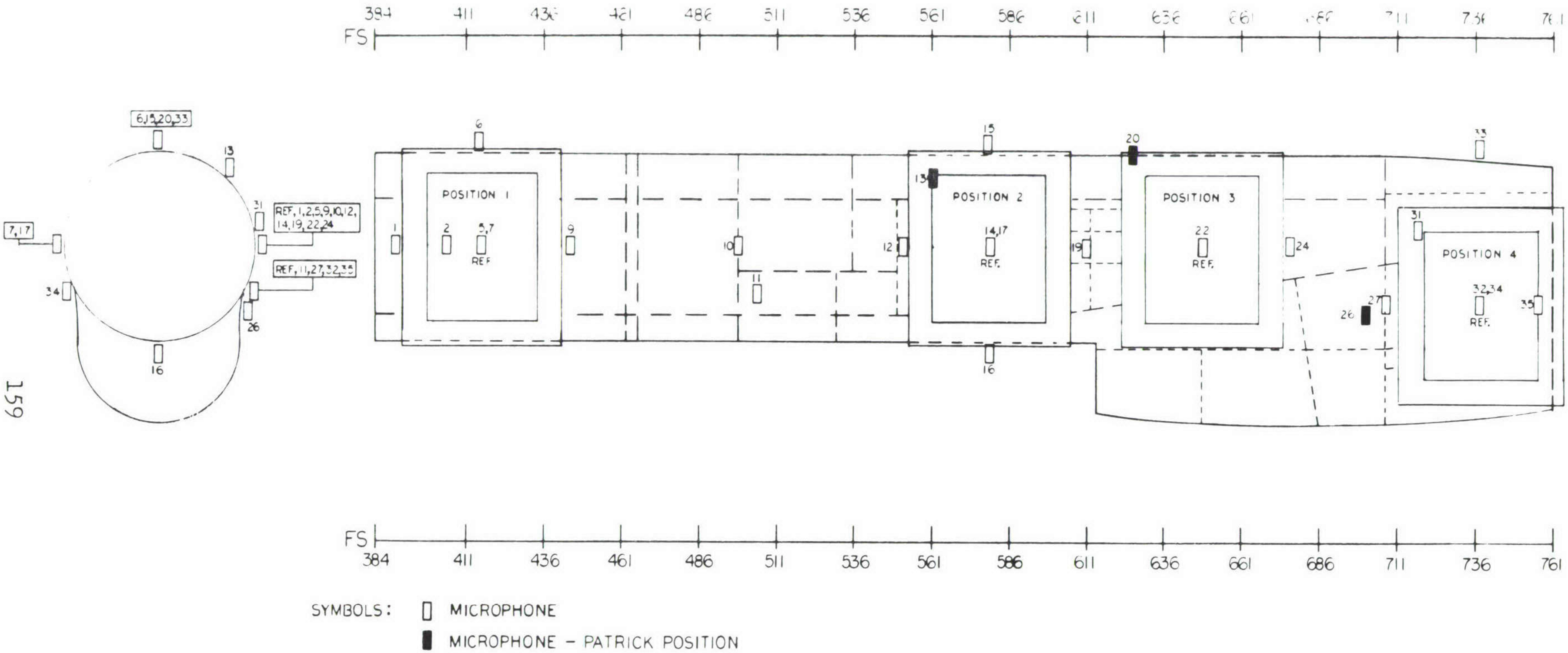

SCALE: 2 IN ≈ 1 FT

FIGURE B14 SCALE MODEL SOURCE POSITION AND MICROPHONE LOCATIONS

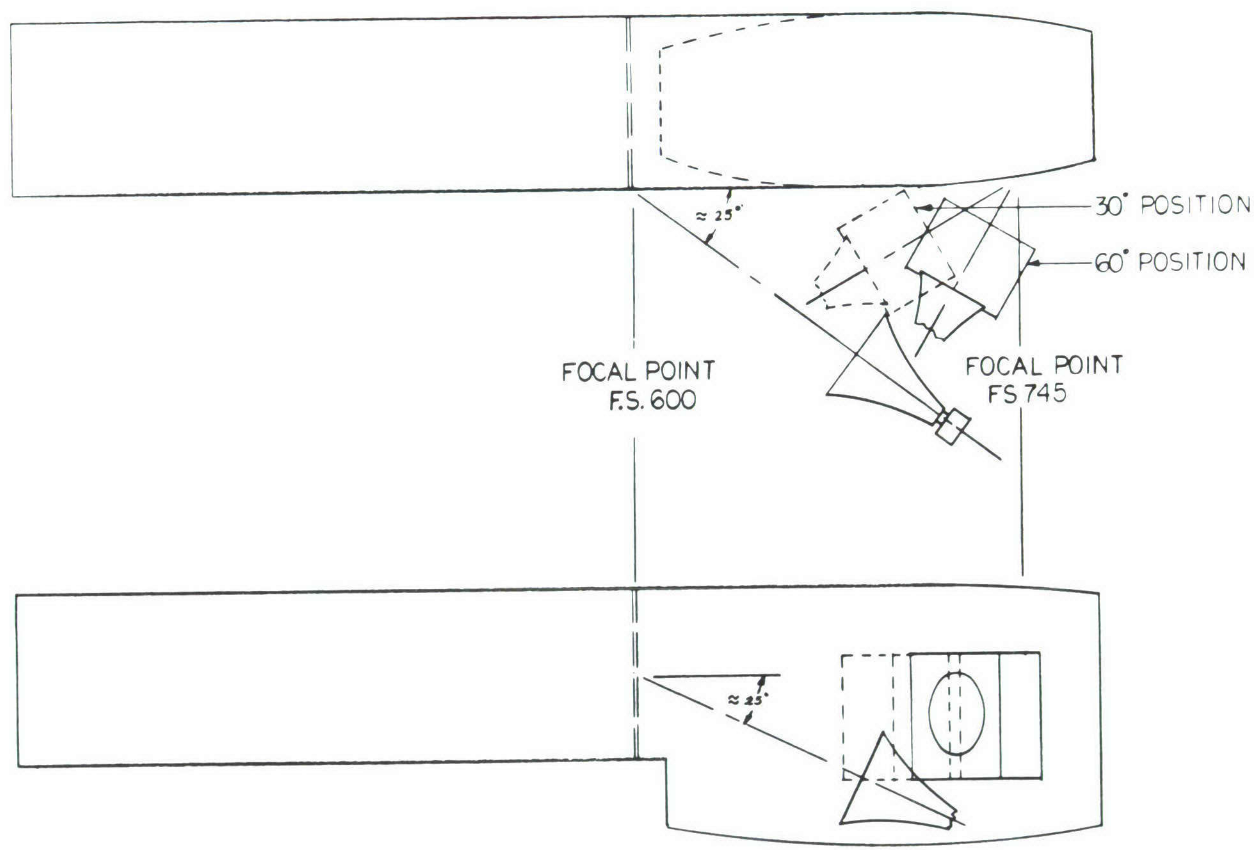

SCALE : 1 IN.= 40 IN.

FIGURE B15 ANGLE OF INCIDENCE AND SIMULATED JATO SOURCE POSITION

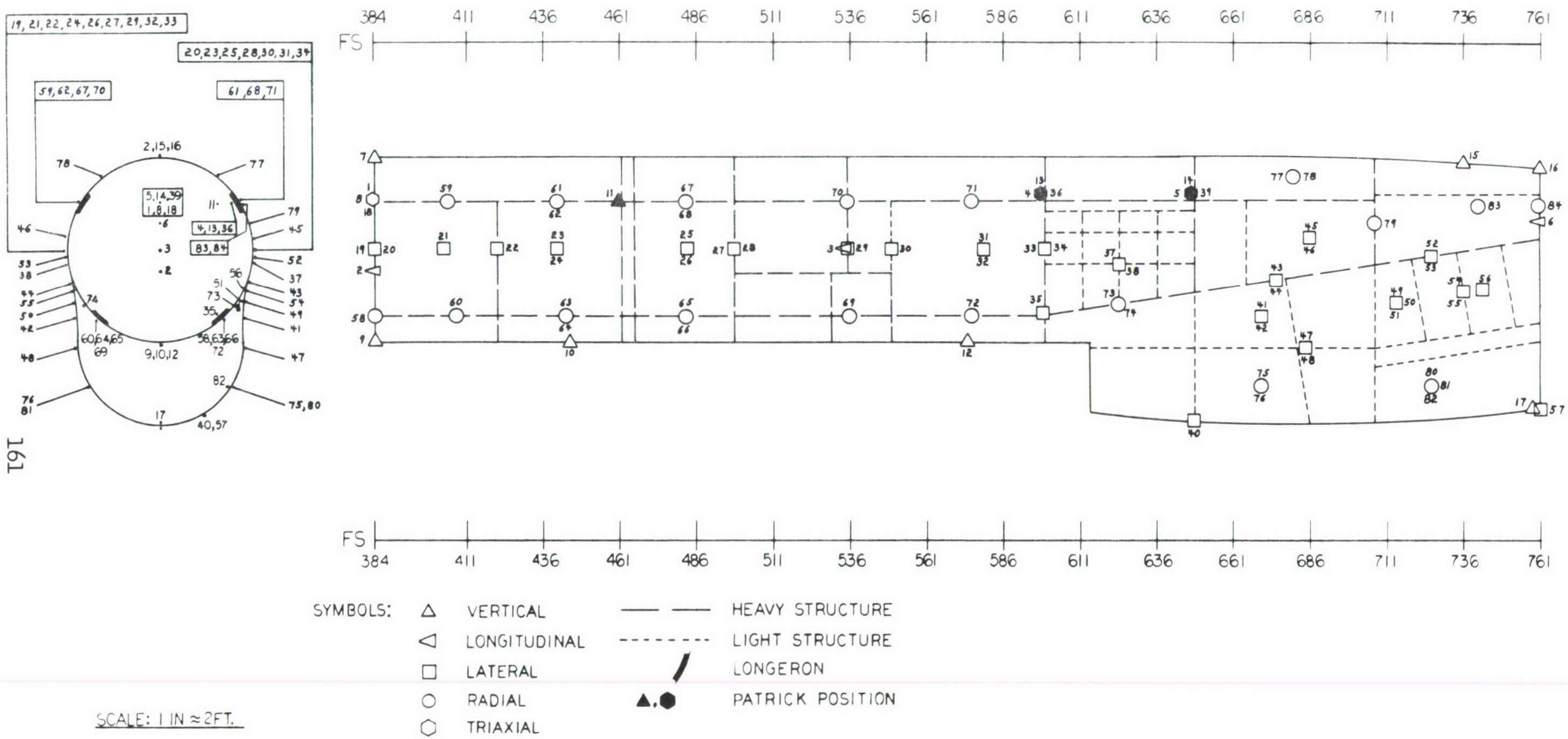

FIGURE B16 FULL SCALE ACCELEROMETER LOCATIONS

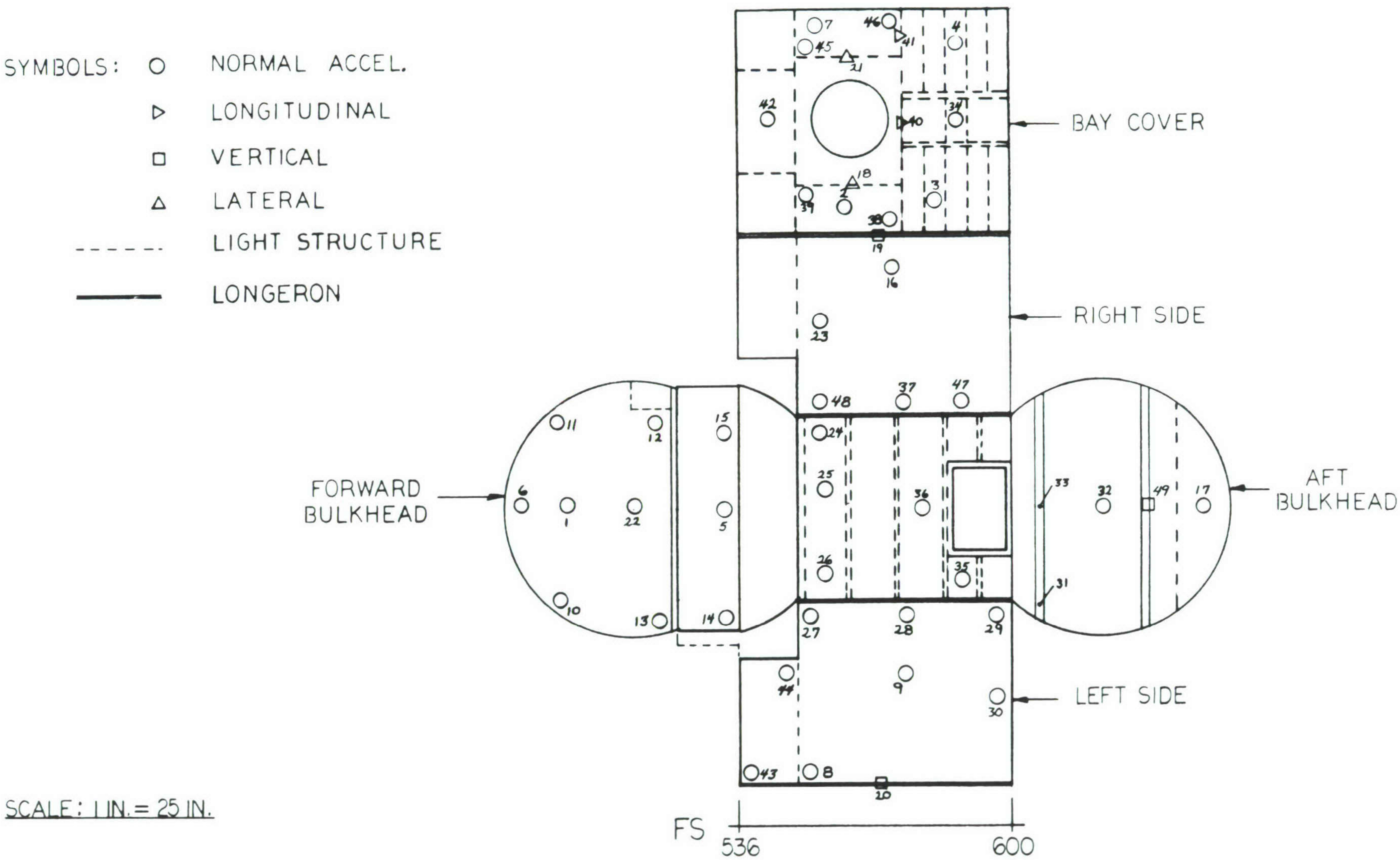

FIGURE B17 ACCELEROMETER LOCATIONS FOR COMPARTMENT BETWEEN STATION 536 and STATION 600

APPENDIX C

SOUND PRESSURE LEVEL AND ACCELERATION RESPONSE DATA SUMMARIES

CPS	40	50	62	80	100	125	160	200	250	320	400	500	625	800	1000	1250	1600	2000	OVERALL
M3			110	110	124	120	127	131	128	132	132	139	140	139	137	124	125	124	149
1				82		84			87	84	93	86	91	106	109	106	105	113	121
2					97	97	98	107	109	109	117	116	113	116	111	108	107	108	125
3				83	83	86	106	112	99	89	109	112	112	112	107	103	101	97	122
4					83	81	95	103	112	100	107	103	108	102	98	101	101	97	118
5				68	76	84	93	88	89	92	93	82	85	81	80	80	89	92	106
6				83	90				87	94	94	93	92				81	80	104
7					95		101	105	110	113	114	120	119	108	108	109	113	109	126
8			78		81	83	88	92	90	85	99	98	99	99	106	103	106	104	116
9									95	101	105	107	111	107	103	103	103	102	118
10							105	111	106	107	107	105	105	108	103	94	92	90	118
11					91	91	105	109	106	109	108	118	117	114	114	109	109	109	127
12							105	105	105	93	102	99	98	94	94	91	90	88	109
13	73	86	97	80	80	90	83	88	93	82	91	96	104	100	96	98	98	99	111
14									84		69	80	84	79	78	76	78	74	94
15				76	95	92	88	86	85	84	103	105	97	95	81	82	84	81	111
16					83	84	81	82	85	78	89	88	90	100	88	75	74	78	104
17		94	101	98	116	109	103	105	109	113	110	105	112	110	104	105	105	100	126
18				88	91	87	92	102	101	90	105	102	101	98	95	94	101	107	117
19					92	89	98	103	103	109	115	112	115	119	118	118	118	115	128
20					93		104	111	107	112	114	114	117	117	117	114	112	116	129
21					96		108	112	122	120	120	123	121	123	120	119	117	113	133
22							100	104	113	100	105	104	107	108	106	106	104	106	121
23							114	121	122	121	120	126	125	126	123	117	116	114	135
24							107	110	109	117	122	119	121	119	114	115	113	114	130
25					96		99	112	113	117	116	112	115	114	112	110	109	107	126
26					98		99	103	119	115	114	115	114	116	112	109	108	107	125
27					90		88		90	93	95	95	96	96	93	95	98	101	110
28		75		75	88	83	85	89	89	84	94	96	96	96	93	93	100	100	111
29					98		97	99	95	91	102	99	92	91	87	92	92	95	110
30	80	87		80	93	93	92	100	104	97	107	109	105	104	102	102	99	99	117
31				80	95		87	107	105	110	109	109	108	107	104	101	100	94	120
32					92		98	102	106	106	105	105	109	108	100	97	96	95	116
33					86		87		89	89	87	86	91	90	90	89	89	88	102
34	71	78		75	92		86	90	91	93	83	89	89	88	87	88	92	96	107
35		75	81		86		87	89	89	93	74	99	103	103	101	101	101	98	112
36	69	77	86	70	86	77	82	84	87	78	90	94	101	98	94	94	90	87	107
37					94		95	104	106	99	95	98	102	93	88	91	92	85	111
38					92		94	94	101	106	99	105	99	98	98	95	95	92	112
39	73			76	84				85	74	87	88	93	90	86	83	83	80	102

FIGURE C1 FULL SCALE SNARK RESPONSE IN DB, INPUT AT STA. 407, CLOSED BOX

CPS	40	50	62	80	100	125	160	200	250	320	400	500	625	800	1000	1250	1600	2000	OVERALL
40					85		85	90	93	84	96	100	95	94	95	100	101	97	109
41				81	101	98	96	96	94	94	94	98	100	96	94	94	93	87	109
42					104	96	86	88	96	99	96	97	94	93	92	89	89	86	108
43									87	89	91	90	84	83	80	91	83	82	102
44					87		85	89	85	87	90	88	84	85	82	85	85	84	100
45					94		91	98	103	103	100	100	100	98	98	96	93	89	112
46					92	88	91	96	100	99	100	100	101	95	92	92	91	87	110
47										87	86	89	88	87	83	85	86	83	100
49				83	87		88		91	95	92	89	86	84	90	97	95	80	109
50							89	92	92	98	101	101	98	91	90	85	83	83	106
52					94				87	85	87	85	83	80	81	80	82	82	100
54	80			93	112	110	107	102	101	106	107	104	99	93	87	97	95	94	119
55				84	104	99	98	98	99	102	101	98	98	94		84	83	81	113
57				75	94	89	85	87	88	86	91	94	95	92	87	89	89	90	105
58				89	96	91	99	100	100	93	107	112	117	114	116	119	114	113	128
59					87		92	96	106	102	110	116	116	116	111	109	109	109	125
60					93	97	122	115	119	119	119	122	119	116	114	113	112	111	131
61							94	99	101	105	110	108	109	111	110	106	104	104	120
62					90		91	95	93	102	105	105	106	110	107	104	100	105	117
63					93		114	117	114	115	119	114	116	118	111	106	103	105	128
64					89	92	120	118	110	114	113	114	116	108	108	107	106	104	126
65					89		101	101	114	103	105	107	102	106	99	96	96	94	119
66					92		98	110	117	106	108	109	104	106	101	99	98	93	120
67					96		91	99	106	106	107	104	104	104	102	102	98	94	116
68					88		88	96	109	112	108	104	105	101	96	101	99	95	118
69					93		98	101	116	115	106	103	104	102	94	91	94	91	119
70					89		88	90	93	93	102	99	98	94	94	91	90	88	109
71	80			90	109	102	96	99	109	107	97	102	106	104	104	105	105	101	119
72		84		81	98	96	104	106	109	108	96	108	106	104	102	101	101	100	119
73	80			81	99		93	95	102	103	102	101	101	96	92	94	93	89	112
74					93		92	92	96	100	101	100	96	90	86	92	92	90	109
75					92		89	99	108	96	96	102	99	99	96	98	95	90	112
77					85		92	95	102	103	103	102	100	94	92	91	88	84	112
78					87		100	101	101	99	104	105	104	98	91	91	91	86	112
79									85	82	97	97	95	95	91	95	95	86	106
80							88	91	98	101	99	99	98	98	88	87	86	82	110
81					88	81	80	82	86	91	92	96	92	91	88	87	84	80	104
83					91		95	95	98	101	101	102	93	91	87	84	83	77	109
84					90	84	87	89	88	79	88	88	93	87	83	80	79	78	102

FIGURE C2 FULL SCALE SNARK RESPONSE IN DB,
INPUT AT STA. 407, CLOSED BOX (CONT.)

CPS	40	50	62	80	100	125	160	200	250	320	400	500	625	800	1000	1250	1600	2000	OVERALL
M14	106	114	117	122	123	131	135	135	135	140	139	142	144	143	139	132	124	130	150
1					80				89	90	98	98	91	91	88	90	92	95	106
2					89	95	100	116	115	109	110	111	105	104	94	93	93	85	120
3	70			89	99	99	116	121	112	122	122	121	115	123	116	113	111	113	129
4	82	89	97	99	109	109	117	126	140	134	128	125	130	126	118	119	116	112	142
5				74	84	96	100	98	98	104	102	102	106	104	103	99	100	99	114
8	68	81	90	75	80	86	87	89	91	92	93	91	85	85	85	85	89	89	102
10							94	99	102	99	95	94	92	94	87	87	86		109
11				82	96	96	102	104	104	109	110	105	102	102	99	96	95	93	117
13	69	82	91	78	87	86	96	97	101	104	108	116	125	123	120	116	113	108	129
14				75	82	82	92	92	92	92	95	96	102	99	97	95	94	92	108
15	94	107	116	104	114	111	116	116	119	120	117	117	117	116	118	120	115	112	130
16	74	86	94	88	96	94	97	100	103	104	108	109	110	117	113	102	102	106	123
17					86		91	90	93	97	100	104	104	103	97	93	90	87	112
18	67			81	93	89	85	89	96	93	93	92	87	84	77	79	83	95	104
19								91	95	99	100	99	96	99	98	100	100	96	111
20					88		89	94	95	99	97	94	91	90	91	92	92	90	108
22									94	96	97	100	87	87	87	88	89	87	107
23					96		101	117	130	115	112	119	120	116	117	115	113	108	133
25					90		93	109	117	118	122	117	116	113	113	110	107	105	128
26					89		89	103	116	114	111	114	120	111	109	102	100	97	126
28	73			85	96	90	90	98	108	105	107	106	102	104	103	102	104	105	120
29		89			90		103	108	108	106	108	106	104	100	100	104	102	105	121
30	86	94	93	99	112	111	121	127	132	131	129	134	132	137	132	126	122	122	143
33					88		98	99	99	98	102	101	108	108	107	105	102	101	118
34	89	81		80	93	92	104	106	103	105	109	106	109	111	109	108	113	122	132
35				88	100	98	102	102	105	115	120	123	127	129	125	126	124	125	136
36	74	83	91	83	95	93	105	104	105	103	108	116	124	121	120	115	113	110	129
37				88	109	104	110	111	115	111	114	117	121	117	114	113	110	108	128
39				76	83	83	94	90	89	92	95	94	95	99	97	90	93	92	106
40	85	95	104	93	105	113	99	99	103	97	99	93	96	96	96	96	96	97	118
43							98	94	92	91	98	97	98	100	98	95	99	99	111
45					99	93	107	110	112	110	116	115	117	113	112	109	107	103	125
46					92		103	103	109	106	110	111	114	108	105	103	102	99	120
49							95	91	94	103	103	100	105	109	99	96	95	90	116
53							89		91	91	94	94	93	95	95	97	93	88	106
54				90	106	102	112	108	108	107	108	104	104	103	97	95	93	90	120
57	78	87	93	93	102	103	113	111	107	111	115	116	116	113	108	105	107	104	124
58					92	89	94	93	98	98	95	94	95	93	96	97	92	89	108
63							92	101	103	100	103	100	102	98	93	95	93	89	113
64							90	100	101	99	102	100	98	92	92	89	89	83	112

FIGURE C3 FULL SCALE SNARK RESPONSE IN DB. INPUT AT STA. 578. CLOSED BOX

CPS	40	50	62	80	100	125	160	200	250	320	400	500	625	800	1000	1250	1600	2000	CVERALL
71	91	98	106	116	128	121	125	127	125	129	132	128	130	130	127	130	129	131	142
72	81	86		94	104	108	122	124	123	131	127	126	125	125	127	119	121	120	138
75							95	101	114	107	111	115	115	118	114	111	107	102	125
79			95	92	99	104	102	101	104	111	113	113	112	116	111	113	113	108	123
83					93	95	106	109	108	111	111	111	104	104	100	96	94	90	120
84			91	84	88	92	89	86	86	83	83	82	80	82	79	79	70	80	106

FIGURE C4 FULL SCALE SNARK RESPONSE IN DB, INPUT AT STA. 578, CLOSED BOX (CONT.)

CPS	40	50	62	80	100	125	160	200	250	320	400	500	625	800	1000	1250	1600	2000	OVERALL
M22		107	108	109	121	107	127	128	130	138	133	131	135	133	124	125	127	127	146
1					78	83	79	83	87	93	92	93	86	87	82	85	85	87	102
3					88	87	95	102	104	105	109	113	104	103	100	98	98	96	119
4							103	118	132	125	121	121	120	112	108	113	107	102	140
5					91	99	101	101	109	126	118	113	118	116	116	116	111	111	130
8	64	70	80	64	78	84	85	84	87	91	88	88	79	79	79	78	80	83	99
11					90	94	94	96	99	103	97	100	95	92	88	86	85	83	110
13			86			84	88	92	98	102	104	112	116	110	1111	112	103	98	121
14			81			79	81	83	88	96	104	108	108	105	105	104	103	101	118
15					98	97	103	102	104	113	118	126	120	116	109	108	109	106	130
16					82	84	96	90	96	106	103	108	109	116	110	100	98	108	121
18						83	85	85	88	92	88	89	84	82	82	72	76	85	100
28					85	82	82	85	94	100	96	96	92	92	91	91	91	92	110
30				84	90	92	100	107	111	114	115	111	113	113	111	109	106	106	124
34				78	93	92	94	94	99	106	105	103	100	94	96	111	115	107	118
35					87	89	87	96	103	110	107	113	112	112	113	111	110	107	123
36			86		87	85	95	92	99	106	106	109	116	111	110	111	106	99	121
39			80		82	84	96	95	93	103	101	102	100	104	105	102	100	101	116
40					89	89	95	98	104	113	111	116	120	117	117	121	120	118	129
54				83	95	93	95	95	101	111	108	109	111	113	109	106	109	107	121
55					88	84	90	88	92	94	90	94	90	91	89	93	88	86	104
71				93	107	103	105	108	119	125	115	115	108	112	112	116	114	111	130
72					91	99	109	111	115	125	115	117	113	110	108	106	106	105	127
79					88	88	102	104	105	115	116	116	114	117	115	116	117	114	127
84				80	90	90	99	102	99	106	102	100	102	106	103	103	105	104	117

FIGURE C5 FULL SCALE SNARK RESPONSE IN DB, INPUT AT STA. 647, CLOSED BOX

CPS	40	50	62	80	100	125	160	200	250	320	400	500	625	800	1000	1250	1600	2000	OVERALL
M32			108	109	121	117	129	132	129	133	136	137	135	128	131	134	132	127	147
1							80	85	89	89	89	92	87	77	75	78	78	81	100
2					79		84	81	88	98	105	103	96	91	86	85	81	76	110
3					86	88	102	108	103	104	104	105	104	97	96	94	90	91	115
4					89	86	90	104	113	118	117	109	108	98	92	95	91	85	124
5					83	84	84	86	91	115	111	111	112	101	103	105	102	101	121
7				78	90	86	87	91	98	103	104	101	91	85	80	78	75		111
8				70	78	81	78		82	86	86	86	80	69	73	74	77	78	96
9					77	84	84	87	87	91	95	94	93	81	75	78	75	73	102
10					80	82	94	95	92	88	92	88	83	82	78	77	77	76	102
11				77	85	85	96	93	89	99	101	100	92	88	86	84	80	82	108
12					92	97	103	101	105	103	110	110	107	106	106	103	97	95	118
13		78	87	72	80	75	81	85	92	93	97	99	104	97	97	97	87	84	109
14		74			80	79	81	85	91	98	99	103	101	95	93	92	91	90	111
15					105	103	104	105	115	124	125	129	123	114	110	111	112	111	134
16					88	94	95	100	107	110	114	116	113	116	113	100	103	114	127
18	69		76	79	96	89	86	86	85	87	90	88	84	74	67	69	70	80	101
19					93	87	82	83	84	90	95	94	88	89	92	94	94	94	105
20					94	90	84	85	90	91	89	92	88	85	86	85	85	89	104
21				85	99	97	99	111	116	116	113	114	108	105	105	104	99	98	123
22				80	95	90	87	90	95	96	97	96	86	80	83	84	83	82	106
23					94	91	92	104	113	107	103	110	105	101	102	100	96	93	118
24				76	89	86	93	93	92	96	101	96	96	94	91	91	87	84	108
25				83	98	93	92	103	115	111	111	107	104	102	102	98	97	93	118
26				85	99	95	86	95	103	112	109	109	104	97	92	95	90	87	118
27				76	90	86	85	86	92	97	98	97	90	84	83	84	85	92	106
28				80	97	88	83	82	89	98	94	97	91	88	89	89	89	93	108
29	83			87	90	97	92	95	93	90	95	95	90	85	85	84	83	83	108
30	81	85		82	92		95	98	102	104	108	106	102	104	104	101	96	96	116
32				87	97	93	95	102	104	107	114	110	109	104	102	99	94	89	120
33				80	92	88	90	90	90	95	91	94	90	88	91	88	87	84	105
34	74			83	95	94	88	88	93	93	96	98	92	86	86	86	90	95	108
36		78	86	79	91	89	86	85	91	96	97	98	103	95	95	94	90	86	109
37	86			84	99	93	105	111	110	109	107	104	103	102	99	98	95	94	119
38				83	103	100	102	106	109	113	113	111	109	106	104	101	101	99	121
39				75	86	86	79	79	95	103	100	98	96	92	88	90	92	93	110
40				86	98	97	95	98	107	114	113	113	110	105	107	107	109	108	122

FIGURE C6 FULL SCALE SNARK RESPONSE IN DB, INPUT AT STA. 738, CLOSED BOX

CPS	40	50	62	80	100	125	160	200	250	320	400	500	625	800	1000	1250	1600	2000	OVERALL
41					97	94	96	98	104	112	113	112	112	109	112	107	106	103	122
42					97	100	104	110	118	124	121	122	114	112	112	109	107	103	130
43				86	97	94	96	93	97	105	102	102	102	103	103	104	105	102	117
44	84			82	95	91	90	93	99	106	105	99	101	101	100	99	100	99	114
45					104	100	105	112	118	126	127	124	125	117	114	1 110	112	108	134
46					108	104	107	107	114	118	118	121	119	112	114	109	108	104	128
47				82	98	95	97	99	106	107	107	106	105	105	106	104	106	100	120
48					100	100	101	107	106	116	117	110	108	107	106	106	105	102	123
50				93	111	105	107	107	110	124	125	123	119	117	115	112	110	107	131
51					108		106	110	119	126	135	137	138	136	132	125	124	121	145
53				90	110	107	104	105	108	111	114	117	111	105	109	110	108	104	124
55				97	116	116	115	107	116	118	116	121	116	116	116	114	119	120	130
56		99	101	105	120	119	120	118	119	125	122	122	129	126	121	122	122	120	137
57					109	105	106	109	116	127	126	129	128	123	122	121	123	126	138
58					992	85	85	85	84	90	92	92	89	85	86	87	84	82	102
59					86	86	81	85	85	90	97	95	93	87	84	81	81	79	104
60					91	85	84	99	99	103	99	99	95	91	87	88	83	79	110
61					76	80	75	81	84	87	91	92	90	82	80	80	77	74	100
62					82	80	81	85	88	92	93	91	88	86	86	81	80	79	102
63				82	98	91	90	93	105	97	100	98	96	90	95	94	90	86	108
64					82	82	92	97	93	93	97	94	93	85	84	81	78	75	105
65					92	90	91	96	102	98	100	101	92	89	86	81	78	74	110
66					94	87	90	95	99	97	98	96	89	92	86	92	88	86	107
67				84	100	92	89	91	92	104	99	95	90	85	83	82	79	74	110
68					94	85	83	88	96	101	100	96	86	86	82	82	80	76	108
69					87	84	89	97	105	109	103	103	99	92	88	84	82	80	114
70	81			86	91	87	88	90	93	93	97	97	93	90	87	83	78	78	106
71	84			93	111	102	97	100	107	110	111	108	100	103	105	103	102	99	120
72	78			84	95	97	98	100	105	108	107	110	104	101	100	98	95	94	117
73				79	98	92	101	98	107	111	108	108	104	99	99	99	98	95	118
74				85	100	96	100	105	106	110	116	106	105	97	97	98	98	96	120

FIGURE C7 FULL SCALE SNARK RESPONSE IN DB,
INPUT AT STA. 738, CLOSED BOX (CONT.)

CPS	40	50	62	80	100	125	160	200	250	320	400	500	625	800	1000	1250	1600	2000	OVERALL
STA. 738-30° ANGLE OF INCIDENCE																			
58		65	74	78	90	87	86	87	86	87	93	92	93	91	91	93	89	87	104
71			87	91	111	102	103	101	105	106	113	108	108	105	106	106	103	102	121
73			82	87	100	94	106	104	108	113	113	112	110	106	104	102	103	99	121
84			89	101	103	105	101	108	108	109	112	111	111	105	106	106	109	108	124
M1			75	81	90	90	94	94	94	97	101	105	102	95	92	88	86	86	111
M14		86	86	91	95	93	106	110	111	106	120	118	113	102	100	96	96	95	125
M22			90	91	104	105	111	115	114	116	122	120	118	111	105	102	99	98	128
M28				105	119	118	120	122	123	121	132	130	126	121	118	114	108	101	139
M29				111	127	122	125	130	129	127	138	139	139	135	128	123	124	120	147
M32				112	126	120	120	124	122	130	133	136	135	137	132	127	127	125	147
M35				106	120	118	124	126	128	131	132	132	132	133	126	127	127	119	144
STA. 738-60° ANGLE OF INCIDENCE																			
58			72	79	88	88	88	87	83	82	89	93	94	93	93	93	87	83	103
71			83	84	99	95	101	98	100	100	108	103	105	103	102	104	101	98	117
73			82	86	100	96	106	104	105	110	112	113	112	108	101	104	102	99	121
84				90	102	99	100	106	102	108	111	109	109	105	105	108	109	109	127
M1			79	82	90	88	94	94	99	112	111	113	109	100	101	95	92	89	117
M14				85	93	92	100	102	103	108	117	11[illegible]	111	93	99	95	94	90	123
M22				92	109	106	112	112	106	120	128	126	120	110	102	105	100	98	132
M28				108	120	120	121	125	121	127	134	135	131	124	119	115	108	102	140
M29				111	124	122	124	128	128	125	138	139	139	134	127	125	124	123	140
M32				111	123	121	120	126	122	131	134	135	137	137	131	127	125	125	147
M35					117	114	120	126	126	128	131	131	131	131	131	130	122	119	143
STA. 738-18 IN GAP																			
58		66	72	75	84	85	85	88	82	87	93	94	93	93	92	97	90	90	105
71			88	93	113	102	102	105	106	107	111	106	110	110	110	113	106	108	122
73		74	82	88	87	92	110	109	108	113	113	113	112	105	104	107	105	104	122
84			88	99	105	103	98	104	109	108	108	108	109	107	106	108	109	110	122
M1			80	86	100	97	97	98	99	101	107	111	107	100	96	97	96	93	117
M14			86	90	102	95	102	109	111	109	117	117	113	106	112	111	109	108	125
M22				93	106	105	114	119	113	113	123	124	118	112	110	108	105	103	130
M32				111	123	121	124	127	129	133	136	135	134	133	134	132	128	117	147

FIGURE C8 FULL SCALE SNARK RESPONSE IN DB, INPUT NOTED

CPS	40	50	62	80	100	125	160	200	250	320	400	500	625	800	1000	1250	1600	2000	OVERALL
HORN ONLY-STA. 407																			
58					98	97	100	99	103	106	102	117	118	125	119	119	118	117	131
71				95	110	102	101	107	115	109	107	111	112	115	113	114	115	110	127
73				85	100	94	98	98	99	108	100	110	108	105	105	103	104	103	120
84		78	86	82	84	86	89	91	93	97	87	96	90	95	91	89	91	88	107
M3				120	127	125	130	134	140	144	137	146	146	142	139	120	123	126	155
M14				93	101	97	108	113	117	117	111	117	112	112	108	108	108	107	128
M22				91	104	97	99	86	106	108	108	118	112	108	108	101	101	98	126
M35				88	101	101	97	101	107	113	103	113	108	106	102	102	101	98	121
HORN ONLY-STA. 578																			
58				80	88	85	92	93	98	104	102	96	98	106	113	104	101	100	115
71				114	128	119	121	125	132	134	139	136	137	136	133	136	135	134	148
73				97	111	104	111	112	120	123	122	118	123	115	115	119	117	113	132
84		79	85	82	91	91	95	94	97	99	102	101	97	100	99	95	97	94	112
M1				87	99	94	105	110	111	109	115	113	111	111	105	99	99	98	123
M14	118	119	118	118	126	125	130	133	137	140	143	144	142	141	138	135	128	120	153
M22				102	110	110	116	115	121	125	125	125	125	120	114	114	113	111	134
M35					97	96	105	109	116	117	113	115	111	113	106	103	103	102	125
HORN ONLY-STA. 647																			
58				71	88	86	90	88	89	90	92	94	97	99	96	96	93	91	108
71				100	119	108	105	107	122	123	121	119	116	121	118	119	119	117	132
73					99	104	111	110	119	120	119	121	125	122	118	118	116	114	133
84			82	77	85	91	97	99	98	104	103	104	104	104	100	99	99	100	116
M1				83	99	93	95	105	109	110	106	109	107	108	101	96	95	94	119
M14				92	109	108	111	112	117	118	120	118	114	119	111	107	106	104	128
M22				115	123	121	126	130	135	139	139	142	141	137	131	129	124	127	150
M35				88	102	102	111	114	116	115	115	116	114	113	107	106	104	102	126
SIMULATED JATO																			
7				98	101	103	101	109	120	118	122	120	125	126	125	125	122	125	137
23					92	92	93	102	109	109	118	119	119	119	125	122	116	115	131
31					102	99	109	117	119	122	123	129	130	130	133	126	121	120	139
58					80	84	89	88	91	94	97	102	106	110	107	108	105	102	116
73					99	99	109	111	121	120	123	123	127	125	126	126	125	122	136
84		82	89	86	99	95	98	100	101	108	109	104	103	101	102	100	103	103	118
M1					106	101	103	104	110	115	124	123	120	117	113	112	109	106	137
M14					107	106	110	115	124	128	130	130	131	126	116	120	117	107	139
M22					115	111	118	121	126	126	132	130	126	120	125	125	125	116	140
M35				93	109	104	110	116	124	122	121	119	117	115	111	106	103	100	130

FIGURE C9 FULL SCALE SNARK RESPONSE IN DB, HORN ONLY AND SIMULATED JATO

CPS	40	50	62	80	100	125	160	200	250	320	400	500	625	800	1000	1250	1600	2000	OVERALL
STA 407																			
M3		109	109	111	129	119	129	131	127	126	132	139	140	139	135	128	125	123	148
M4					92	91	100	99	100	101	103	102	99	95	95	96	92	87	114
M8		86	89		107	100	110	111	111	104	114	113	111	110	104	99	99	97	124
M10					98	94	98	104	106	99	106	103	104	105	96	93	94	90	118
M11				80	91	95	101	106	106	98	97	107	103	100	93	92	92	90	116
M12					86		89	103	104	95	103	104	102	99	93	90	90	86	114
M13	97	103	106	104	104	106	106	113	121	109	101	111	111	107	100	94	94	90	124
M15					84	83	88	94	93	88	96	96	89	87	83	81	81	76	105
M16					89	93	97	102	101	97	104	105	104	99	91	91	92	88	114
M17								93	95	87	99	98	99	89	83	85	81	79	107
M26			76		92			92	95	95	94	104	97	92	88	86	83	85	112
M31					85	86	80	78	93	90	87	95	89	89	81	80	78	77	105
M36								85	90	86	93	96	93	87	82	83	82	80	104
STA 578																			
M1		74	79	76	89	81	93	104	105	105	102	106	103	93	92	89	87	87	114
M2		77		84	93	89	98	104	107	105	102	104	100	94	93	92	90	85	114
M10		79	82	82	97	98	104	105	107	106	108	113	107	101	96	94	93	91	119
M11			86		98	99	106	108	105	107	110	107	107	106	102	98	95	92	117
M12		89	93	93	110	104	110	114	111	108	116	117	114	113	106	102	104	99	126
M13	103	105	106	106	112	114	123	125	123	120	119	123	117	115	112	110	108	108	132
M14	106	114	117	122	133	131	135	135	135	140	139	142	144	143	139	132	129	130	150
M15			80	83	92	92	104	106	108	113	110	110	110	109	106	105	105	104	122
M16	85	86	85	85	103	98	105	105	112	116	116	105	107	110	108	109	105	105	125
M17		77	77	78	76	85	85	96	99	109	106	108	107	104	102	98	96	96	117
M20			83		89	95	105	102	99	99	99	102	102	98	92	88	89	92	112
M25						107					115			113	109		103	101	124
M26		88			93	91	103	107	111	104	109	107	102	102	97	92	92	91	117
M31	87	90	89	88	90	91	101	102	103	102	102	102	96	93	90	88	84	82	112
M36					85	83	99	101	101	99	104	108	99	96	92	92	84	83	113
STA 647																			
M1						85	92	98	102	99	99	99	95	92	88	88	85	81	109
M2					91	84	95	102	106	91	104	103	100	93	92	93	89	86	112
M10				81		83	102	102	99	98	101	101	100	95	91	92	89	86	111
M11							95	104	105	90	104	103	103	98	93	89	88	86	113
M12					86	89	99	100	100	100	101	99	100	95	92	88	86	82	111
M13	103	104	104	105	106	107	109	113	119	115	117	116	116	111	107	103	101	100	126

FIGURE C10 FULL SCALE SNARK-MICROPHONE RESPONSE IN DB, CLOSED BOX

CPS	40	50	62	80	100	125	160	200	250	320	400	500	625	800	1000	1250	1600	2000	OVERALL
STA 738																			
M1				73			87	91	93	98	97	99	95	90	88	85	83	80	107
M2					88	83	88	96	96	100	103	101	100	91	89	86	86	84	110
M10				77	90		86	94	97	102	105	101	97	96	92	88	88	84	112
M11				80	88	84	88	94	94	100	104	102	97	95	91	88	87	85	111
M12				75			88	100	101	104	104	102	98	96	92	88	87	84	113
M13	88	90		91	95	90	96	107	108	106	104	104	106	97	94	95	88	86	117
M15				73			88	95	96	99	98	95	92	91	86	84	80	80	106
M16				76	90		92	94	95	97	100	104	98	93	91	90	85	84	109
M18				79	88		95	105	103	107	104	104	104	99	94	90	89	87	115
M20					88	83	94	93	91	99	97	97	92	90	85	83	81	76	106
M26	92	93		94	105	101	113	114	115	119	124	121	116	114	109	110	112	113	130
M30					103	102	108	113	110	113	121	120	116	110	105	104	101	98	128
M31	96	100	101	101	102	103	108	110	112	113	114	117	115	111	111	110	105	103	125
M32			108	109	121	117	129	132	129	133	136	137	135	128	131	134	132	127	147
M33							97	99	101	107	105	104	97	95	93	89	89	84	114
M34			74	77	95		95	97	99	99	98	98	93	90	86	87	84	80	109

FIGURE C11 FULL SCALE SNARK-MICROPHONE RESPONSE IN DB. CLOSED BOX (CONT.)

CPS	40	50	62	80	100	125	160	200	250	320	400	500	625	800	1000	1250	1600	2000	OVERALL
STA 407																			
M3		107	110	112	123	123	127	131	129	122	131	131	135	130	127	130	129	125	145
M4			90	93	104	99	103	106	109	110	113	114	108	104	105	105	103	98	124
M8		101	105	107	119	115	119	123	125	116	132	132	132	128	120	121	119	115	140
M10				88	102	100	102	108	106	99	106	103	104	105	96	93	94	90	118
M12				85	95	91	102	108	107	98	108	111	109	108	101	98	97	94	121
M15					91	89	90	92	94	90	99	101	99	94	89	89	86	82	109
M16				86	95	97	97	102	102	97	91	112	111	107	104	101	97	96	120
M17					94	91	86	96	99	94	107	104	106	99	91	92	90	89	114
M36								88	92	87	100	103	97	93	92	91	86	84	110
STA 578																			
18					81	85	87	89	93	96	94	98	91	84	80	81	84	81	105
35					102		99	103	105	114	121	125	129	129	127	126	124	123	137
M14		107	112	111	129	124	128	133	133	137	134	133	137	131	124	128	131	128	146
STA 647																			
18					92	87	84	85	89	92	89	92	87	82	74	75	77	86	102
35				88	85	85	86	96	103	108	106	116	117	112	114	114	113	109	124
M1					84	87	93	101	102	100	105	103	103	97	94	94	91	89	114
M10					93	89	103	107	106	106	109	111	108	102	99	98	95	93	119
M12					99	97	106	111	104	104	111	112	111	106	105	100	98	97	121
M15					93	92	101	103	102	104	106	111	105	100	99	96	91	90	117
M16					94	90	100	106	102	110	108	113	106	101	101	97	97	93	119
M17					91	86	94	98	94	102	99	104	102	98	92	90	87	83	111
M22		107	114	109	127	131	127	130	132	137	133	133	136	129	124	129	130	122	146
M36					98	95	103	109	103	104	113	112	110	102	101	101	98	95	121
M15					90	84	96	100	99	99	101	101	99	94	92	91	88	84	110
M16					89	86	93	101	100	98	99	105	101	96	94	93	90	85	111
M17						81	94	98	92	92	94	97	95	92	86	84	80	77	106
M20		85	86		89	90	107	99	108	107	109	114	109	104	100	101	95	92	123
M21	82	86	89	92	108	103	111	110	104	109	112	111	111	108	104	99	98	94	122
M22		107	108	109	121	107	127	128	130	138	133	131	135	133	124	125	127	127	146
M23	89	91	96	99	104	105	116	116	117	118	119	119	113	110	113	111	108	106	129
M26		83		86	97	97	107	108	108	99	113	115	108	106	100	98	96	92	122
M31	90	92	89	88	97	92	99	101	102	98	107	109	102	99	99	95	93	90	117
M36					92	91	102	106	102	102	104	114	103	100	93	92	90	86	116

FIGURE C12 FULL SCALE SNARK RESPONSE IN DB, OPEN BOX INPUT NOTED

CPS	40	50	62	80	100	125	160	200	250	320	400	500	625	800	1000	1250	1600	2000	OVERALL
M15					122	118	125	127	129	139	137	137	140	138	134	130	124	121	150
C1					99	33	110	118	113	109	114	114	110	116	113	108	109	109	126
2					99		117	122	128	129	123	126	126	121	118	111	110	110	135
3					99		112	117	118	122	132	130	119	118	119	117	112	111	136
4			112	117	112	12	117	125	122	138	145	146	142	132	126	130	128	128	150
5							98	105	109	113	118	116	116	118	115	113	114	112	128
6					87		104	107	108	110	112	115	111	115	111	112	111	112	125
7						117	131	138	143	145	144	149	144	140	139	134	130	128	154
8					113	105	109	113	123	125	126	131	132	132	135	133	132	131	143
9							116	124	129	139	138	136	132	136	137	132	130	129	148
10					96	90	101	106	108	107	108	109	114	114	110	110	112	115	126
11					87		108	109	109	107	107	108	112	114	110	111	116	115	124
12				86	91	87	93	100	99	108	112	115	106	110	111	113	112	109	124
13					90		89	89	97	98	103	105	107	110	111	112	114	117	128
14							103	107	109	111	115	116	121	121	115	115	114	115	130
15					91		94	103	108	111	116	113	115	123	118	114	114	113	129
16				96	100	93	104	107	119	121	115	121	121	128	124	117	118	117	133
17						91	103	110	118	117	117	118	118	122	125	122	113	115	131
18					104		115	124	125	130	124	129	130	131	126	122	121	115	140
19				92	99	95	105	109	116	121	115	124	120	120	115	115	116	113	131
20					119	108	124	125	127	132	129	128	129	130	128	126	128	129	144
21					105	103	119	124	129	126	130	131	135	132	129	129	126	121	142
22					92		110	114	108	106	116	118	115	118	115	113	112	113	128
23				96	100		105	113	114	119	123	122	126	128	121	116	116	118	134
24							119	126	133	130	131	130	126	122	117	114	113	109	140
25							126	123	127	132	130	125	129	126	122	112	109	109	140
26						100	116	118	120	130	128	129	129	124	123	101	116	116	138
27							109	111	114	123	122	124	129	135	110	137	131	126	145
28					113		109	117	124	129	131	129	138	138	137	135	134	132	146
29							108	122	126	121	126	128	133	137	136	135	132	129	144
30							111	116	125	131	131	139	139	139	137	129	127	126	147
31					90		102	108	112	112	113	116	119	119	117	112	112	109	128
32							99	108	117	117	129	131	128	125	115	107	105	104	137
33			97	97	107	97	110	115	118	115	111	114	116	115	112	108	111	111	127
34					112	117	134	138	138	141	132	138	133	133	129	129	125	124	149
35					105	107	131	132	132	134	128	129	124	128	123	123	118	116	142
36						102	119	121	126	122	120	123	123	123	114	114	111	110	134
37							103	113	120	114	118	122	124	126	120	118	118	114	134
38						103	124	126	131	135	130	134	130	125	121	120	119	115	142

FIGURE C13 FULL SCALE SNARK RESPONSE IN DB, INPUT AT STA. 578, COMPARTMENT DATA

CPS	40	50	62	80	100	125	160	200	250	320	400	500	625	800	1000	1250	1600	2000	OVERALL
39					104	97	106	112	114	116	120	123	127	130	125	122	118	112	135
40		110	117	114	121	117	130	133	133	138	128	132	133	136	132	122	117	119	145
41		108	111	110	126	118	119	127	131	126	125	131	141	141	132	129	124	121	146
42					117	120	132	137	147	141	129	131	135	131	132	126	120	120	150
43					108			107	112	118	122	132	132	135	134	128	126	125	142
44					99		109	114	115	119	120	125	126	130	131	127	125	122	138
45							119	123	124	128	133	137	141	139	135	131	126	120	146
46					122	116	129	135	141	147	149	151	141	139	137	134	129	127	156
47							98	113	119	120	120	121	122	124	123	118	116	114	132
48					94		102	109	113	110	110	120	120	126	126	119	114	114	132
49			84	85	95	91	95	99	104	104	107	109	111	109	106	106	106	112	122

FIGURE C14 FULL SCALE SNARK RESPONSE IN DB, INPUT AT STA. 578, COMPARTMENT DATA (CONT.)

STA.	LOC. CPS	160	200	250	320	400	500	625	800	1000	1250	1600	2000	2500	3200	4000	5000	6250	8000	OVERALL
	M5	109	116	116	125	128	117	121	125	117	119	116	111	113	119	117	116	121	120	136
645	LLL	110	108	104	110	110	101	108	118	118	115	114	113	106	102	99	96	96	94	125
625	LLL	102	100	104	106	106	98	113	129	120	113	116	110	104	100	90	88			130
600	LLL	98	103	102	103	114	105	114	116	114	118	121	107	101	90					126
575	LLL	99	105	102	104	114	107	117	129	124	116	117	111	106	102	94				133
540	LLL		104	97	102	106	99	111	132	136	119	124	113	107	107	106	102	104	103	138
505	LLL	88	97	94	103	103	98	106	109	113	114	124	120	107	105	103	99	100	97	127
480	LLL		97	98	104	111	104	117	128	124	116	119	117	116	115	113	112	114	112	132
445	LLL			100	103	120	112	128	134	133	132	130	127	125	123	119	113	116	115	141
445	LUL	95	99	103	104	105	98	107	124	123	117	122	127	131	128	120	117	118	119	136
480	LUL		97	100	103	108	109	129	129	126	122	127	118	117	111	112	106	111	111	136
505	LUL		96	96	101	105	100	113	133	131	120	115	117	114	105	106	103	104	107	137
540	LUL		104	96	100	102	98	113	134	128	121	119	108	107	106	101	101	104	102	136
575	LUL	99	110	115	111	117	106	110	118	113	114	119	114	106	104	97	94	96	94	128
600	LUL	106	108	108	108	112	107	119	117	116	106	109	105	107	108	107	99	97	93	127
625	LUL	97	102	102	105	117	114	125	119	118	115	115	109	105	99	93	92	94	93	128
645	LUL	99	103	99	103	110	106	112	116	116	117	114	109	109	102	100	95	96	95	125
645	RUL	106	108	105	105	114	106	105	112	113	115	116	111	107	105	101	97	93	89	125
625	RUL	101	108	102	102	114	112	123	120	117	112	116	108	103	98	93		90		129
600	RUL	92	105	102	102	110	106	119	124	122	110	110	104	96						130
575	RUL	93	104	104	106	111	100	112	120	120	110	114	111	106	106	101	94	98	96	126
540	RUL	100/94	106	102	104	108	93	102	116	114	114	119	116	106	98	96	94	97	96	126
505	RUL	91	97	96	101	106	101	109	121	117	115	122	123	113	109	103	99	102	99	129
480	RUL		96	99	104	109	103	118	131	124	114	117	115	116	113	108	105	110	108	134
445	RUL	98	106	105	106	110	101	107	122	122	121	124	125	121	119	113	110	110	108	133
415	RUL	100	108	104	108	113	105	116	130	128	134	124	121	123	119	118	114	113	112	138
415	RLL	98	108	108	109	119	123	119	129	134	134	125	118	117	116	110	109	114	114	139
445	RLL		101	102	102	105	123	114	124	133	130	125	120	118	116	114	110	113	113	138
505	RLL	93	102	97	104	107	103	106	119	121	120	120	114	107	107	107	102	99	97	128
545	RLL	97	104	98	103	108	102	114	128	128	121	116	109	108	101	96	96	99	99	133
575	RLL	96	103	98	99	107	101	107	113	117	113	117	112	109	108	97	95	95	94	125
600	RLL	98	108	102	102	112	103	108	120	116	117	125	112	103	98	92	88	91	91	129
615	RLL	99	101	100	102	103	98	112	124	122	113	112	112	107	102	93	88	88	87	128
645	RLL	102	103	101	106	107	99	104	117	116	112	115	114	110	102	99	95	93	90	126
480	RLL		101	101	108	116	100	122	134	124	118	119	117	116	115	110	106	109	110	135

FIGURE C15 1/4 SCALE SNARK RESPONSE IN DB. INPUT AT STA. 415, CLOSED BOX

CPS	160	200	250	320	400	500	625	800	1000	1250	1600	2000	2500	3200	4000	5000	6250	8000	OVERALL
M5	110	118	122	127	129	120	120	122	113	114	111	110	114	117	116	114	120	120	136
1				90	98	95	104	113	108	115	108	98	97	96	98	100	103	100	120
3				91	86	84	92	87	81	77	79	74	77	77	70	66	70	70	99
4		79	82	98	101	98	102	97	98	107	103	96	88	83	83	87	91	90	111
5			84	84	94	89	87	91	79	74	73	74	71	71	71	74	78	71	99
8		79	87	102	103	100	96	101	95	94	94	98	101	112	99	101	105	102	114
11		88	93	110	103	106	118	112	103	106	108	112	115	114	102	95	95	99	124
13	70	75	80	98	101	98	102	97	98	94	95	85	83	82	83	88	93	91	110
14		74	77	90	97	98	88	95	84	76	80	80	84	84	82	85	85	80	105
15		81	92	111	107	100	101	105	102	93	94	90	84	79					117
16	76	77	83	92	99	99	110	110	107	95	86	77					77		116
18	88	97	98	98	108	101	106	112	106	110	103	94	96	99	98	98	111	107	121
28			87	97	103	93	97	111	111	107	102	108	100	95	89	87	91	91	118
30	92	99	97	100	104	98	110	116	107	104	107	103	98	91	92	90	92	92	120
34	87	96	93	95	102	93	99	104	108	104	99	104	104	93	88	86	88	86	115
35	86	96	92	94	102	94	101	111	109	94	98	104	96	87	84	82	86	84	116
36	84	97	92	97	107	99	92	98	94	91	94	90	84	84	85	89	94	91	112
39	84	88	89	97	105	99	95	89	86	83	84	84	85	80	84	84	92	84	110
40		96	93	97	96	98	102	111	109	102	96	91	81	84	77		86	81	116
54	83	89	91	108	104	98	106	105	102	96	100	93	89	87	81	80	81	79	115
55		94	95	99	108	100	111	115	117	121	124	109	116	120	112	105	110	110	130
71	91	100	101	107	109	99	113	115	107	97	104	105	97	93	87	87	91	91	121
72	93	98	95	87	101	100	111	111	109	101	104	98	94	87	84	87	87	86	118
79	87	93	87	84	94	90	99	105	97	93	99	91	83	77			76	74	112
84	82	97	89	95	101	95	106	103	104	97	91	83	77	74			79	78	112

FIGURE C16 1/4 SCALE SNARK RESPONSE IN DB, INPUT AT STA. 415, CLOSED BOX (CONT.)

CPS	160	200	250	320	400	500	625	800	1000	1250	1600	2000	2500	3200	4000	5000	6250	8000	OVERALL
M14	112	121	124	128	129	120	121	123	117	117	116	110	97	121	120	120	123	122	136
1				83	95	93	108	110	107	107	101	94	85	85	80	84	89	84	116
3			96	91	87	91	101	101	96	84	86	81	79	79	77	73	79	81	107
4		86	89	103	103	104	109	111	110	115	115	105	101	98	97	101	107	106	122
5		82	84	88	92	90	94	97	88	84	86	85	87	84	87	84	87	86	104
8	73	81	88	97	101	96	97	99	94	89	88	89	87	88	82	85	90	86	108
11		88	89	94	93	106	120	116	104	100	98	99	96	94	91	82			128
13		97	92	94	95	104	114	124	116	108	108	96	99	98	99	105	108	108	118
14	88	97	89	90	91	96	109	114	107	94	95	97	97	98	96	97	95	92	110
18	89	97	97	99	106	99	108	111	103	103	94	87	82	82	80	83	95	90	116
28		99	98	104	108	98	105	121	124	117	107	116	109	99	94	93	99	99	128
30		104	101	103	106	114	130	137	130	126	125	118	115	112	112	108	110	112	140
34	92	98	93	89	98	100	114	119	123	119	116	116	116	113	104	102	109	110	128
35		97	91	93	103	104	119	122	121	112	109	111	107	106	102	106	105	104	129
36	87	97	93	96	100	101	102	107	105	106	106	98	99	96	98	101	111	107	118
39	82	90	93	94	99	101	103	97	94	87	90	94	95	94	95	96	102	96	112
40		97	92	94	95	104	114	121	116	110	106	99	94	94	85		89		124
54	89	101	96	97	98	102	118	116	113	105	108	101	99	97	90	88	87	86	124
55	88	97	94	100	104	96	103	108	114	106	107	101	100	100	93	85	89	86	119
71		105	105	112	112	111	134	133	124	116	122	121	115	112	108	107	112	112	138
72	97	102	97	101	98	116	127	129	124	117	119	112	109	105	103	104	109	109	133
79	88	97	89	90	91	96	109	114	107	107	112	99	93	87	81	81	83	84	119
84	89	101	96	97	98	102	118	116	113	106	98	93	88	85					122

FIGURE C17 1/4 SCALE SNARK RESPONSE IN DB. INPUT AT STA. 578, CLOSED BOX

CPS	160	200	250	320	400	500	625	800	1000	1250	1600	2000	2500	3200	4000	5000	6250	8000	OVERALL
M22	113	123	126	130	126	114	120	121	120	115	118	118	113	118	118	118	121	121	136
1			83	92	99	94	114	116	107	103	99	91	81				80		119
3				92	84	77	91	93	91	76	78	76	73	71					102
4			76	102	100	98	103	111	109	111	112	102	98	97	98	98	103	100	119
5		72	80	86	95	90	102	107	96	88	89	89	87	90	93	94	94	92	110
8	75	86	93	105	108	97	102	103	91	84	84	86	80	80	77	80	83	78	113
11		90	95	105	100	105	120	115	102	100	99	94	86	86	85				122
13		79	84	93	95	95	101	107	105	105	105	92	92	96	96	99	104	102	115
14		82	85	95	102	99	104	105	101	93	97	99	99	103	106	106	113	112	116
15			91	111	106	99	110	117	113	104	101	100	91	93	89	83	83	83	123
16				97	100	100	117	120	125	108	100	90							127
18	87	93	89	101	101	93	112	113	103	102	95	88	82		79	79	88	82	117
28	88	105	97	105	106	97	107	116	114	109	103	109	100	90	87	85	86	85	123
30		93	93	96	96	97	124	129	122	111	102	108	102	98	96	94	96	96	130
34	82	84		85	85	91	103	114	117	113	107	110	112	106	100	97	100	99	122
35					85	90	113	120	122	102	105	119	111	104	99	96	98	94	126
36	85	86	88	96	97	98	101	107	104	104	106	98	99	99	99	99	108	101	115
39	79	78	85	97	101	96	103	98	96	92	93	97	97	96	101	102	107	101	113
40		100	100	105	109	110	119	125	126	121	119	108	103	103	97	92	93	92	131
54		88	91	105	112	96	113	120	115	114	111	109	104	100	98	89	90	89	124
55	93	91	94	108	104	98	107	112	107	109	108	99	97	95	86	82	84	79	119
71		92	97	106	103	99	121	123	118	107	110	110	106	102	100	97	103	97	127
72	86	87	87	94	91	102	118	116	111	101	103	94	89	86	82		83	82	122
79	85	86	86	94	97	94	113	120	112	110	118	106	100	93	88	88	94	94	124
84		88		98	100	99	124	122	116	113	103	99	93	92			89	88	127

FIGURE C18 1/4 SCALE SNARK RESPONSE IN DB, INPUT AT STA. 647, CLOSED BOX

CPS	160	200	250	320	400	500	625	800	1000	1250	1600	2000	2500	3200	4000	5000	6250	8000	OVERALL
M32	111	123	124	130	126	116	116	115	114	110	116	116	113	116	115	117	120	120	136
1				83	103	92	106	112	99	99	94	86					78		116
3			99	109	102	89	102	94	83	75	77								113
4		82	95	111	118	101	106	112	99	105	105	95	87	84	84	85	92	88	121
5		74	85	98	101	94	99	106	90	86	84	82	81	82	81	81	85	86	109
8		81	99	116	116	100	101	102	88	83	81	82					84		119
11		86	92	109	104	104	119	112	93	92	93	91							122
13	79	82	88	105	112	100	103	109	98	103	100	83	82	85	85	88	92	90	117
14		78	87	107	106	103	98	105	93	92	92	90	92	94	92	91	95	95	115
15			103	122	117	112	123	126	117	113	115	110	108	100	99	95	96	96	132
16		91	99	114	116	109	120	124	123	114	109	100	93	90	90		92	94	130
18	91	94	90	100	99	93	105	106	94	96	88	81	74			74	82	76	114
28			94	108	108	93	100	115	109	102	100	102	91	83	81		82	83	119
30	93	102	98	108	112	99	117	124	113	107	104	97	90						127
34	87	98	92	94	99	96	108	114	111	105	99	102	100	90	86	81	86	83	118
35	90	95	91	97	101	96	109	115	112	99	100	105	94	87	84				119
36	88	93	91	102	106	100	100	106	95	97	96	87	84	83	82	84	92	88	113
39	86	84	93	110	112	99	103	101	92	93	95	92	94	92	90	95	101	88	118
40		92	93	107	112	106	120	124	121	115	111	104	96	93	89		91	90	128
54		96	104	121	126	113	129	125	116	116	121	114	111	106	101	98	98	97	136
55	91	96	95	106	105	93	103	108	100	103	103	93	89	87	83	77	81		115
71	93	100	102	115	116	104	123	123	108	101	104	102	96	90					128
72	94	99	99	105	104	107	122	121	112	102	101	94	87						126
79		101	101	112	118	108	125	137	119	115	123	109	109	105	101	105	101	107	138
84		99		112	117	110	132	127	120	111	114	108	105	104			97	100	135

FIGURE C19 1/4 SCALE SNARK RESPONSE IN DB. INPUT AT STA. 738. CLOSED BOX

CPS	160	200	250	320	400	500	625	800	1000	1250	1600	2000	2500	3200	4000	5000	6250	8000	OVERALL	
STA 738 - 30° ANGLE OF INCIDENCE																				
58	89	92	98	109	108	108	107	113	109	109	107	94	93	92	84				120	1
71		97	98	104	107	102	121	121	111	107	106	96	90						126	2
73		114	113	121	123	121	138	146	132	122	125	122	115	109					148	24
84		104	100	108	116	120	130	132	131	118	110	105	101	99	99	100	100	100	137	7
M1	88	90	91	96	102	98	98	101	92	85	82	81	74	73	71	71	74	74	110	
M14	95	94	94	102	106	106	108	108	98	93	90	85	84	77			81	81	117	
M22	102	109	113	117	122	115	115	115	109	101	97	92	89	87			87	88	127	
M25	108	116	119	123	124	122	123	123	124	113	109	98		97			100	104	135	
M32	105	111	114	122	125	125	125	127	124	118	120	116	109	100		101	108	113	136	
M36	99	103	107	115	119	119	121	123	121	116	117	116	112	108	102	98	105	108	133	
STA 738 - 60° ANGLE OF INCIDENCE																				
58	90	100	100	104	108	102	106	113	106	107	107	92	92	90	82				120	1
71	87	99	97	106	110	102	123	120	109	98	99	94	89						125	1.8
73	105	111	110	119	120	117	139	142	129	118	123	118	110	107					145	18
84	103	101	108	115	117	130	131	126	115	113	104	98	98	97					136	6
M1	87	93	93	93	97	92	93	95	93	91	82	81							105	
M14	92	94	96	94	92	96	105	104	95	91	88	84	83	81					112	
M22	100	108	111	114	118	110	114	109	101	99	98	93	88	86	86		89	91	124	
M25	106	115	117	122	122	121	126	125	117	115	108	97	98	97		97	107	104	134	
M32	96	114	118	124	124	123	124	127	123	117	118	113	102	102	106	108	109	110	136	
M36	100	106	110	115	118	118	118	123	120	114	114	110	102	99	96	93	100	108	130	
SIMULATED JATO, AIMED AT STA 600																				
58	95	100	100	103	119	116	117	122	120	122	118	113	112	110	105	106	99	96	131	3.7
71	92	100	102	110	114	110	124	126	117	111	115	112	111	109	104	101	97	98	130	3
73				126	127	132	148	153	149	135	138	140	131	128	123	123	120	117	156	65
84	98	104	105	114	121	117	131	129	129	119	110	107	100						138	8
M1	92	99	98	99	115	112	117	115	112	108	110	103	99	91	90	90	89	87	126	
M14	103	112	115	114	125	124	124	125	123	118	117	116	110	107	113	109	105	109	136	
M22	116	126	119	115	128	127	126	127	122	117	111	107	106	104	100	99	102	104	138	
M36	96	109	113	109	117	113	111	115	112	102	98	94	91	89					126	

FIGURE C20 1/4 SCALE SNARK RESPONSE IN DB, INPUT NOTED

CPS	160	200	250	320	400	500	625	800	1000	1250	1600	2000	2500	3200	4000	5000	6250	8000	OVERALL	
STA 415																				
55		94	95	103	102	108	117	117	125	123	129	130	114	116	110	106	108	107	134	4.8
71	83	90	93	101	98	97	113	113	105	94	98	87	83	80		82	82	82	118	.8
73	104	105	107	112	103	110	123	131	119	123	118	114	105	105	98				134	5
84	83	95	93	99	104	102	114	112	113	101	99	86					83		120	1
M1	106	116	118	122	126	122	126	128	126	120	120	116	109	102	106	105	108	101	136	
M14	88	94	96	99	102	98	102	106	94	92	88	90	89	84	80	82	87	87	112	
M22	86	93	95	93	98	95	101	104	96	86	92	88	86	83	78	78	84	83	110	
M32	81	90	91	91	93	94	95	96	93	88	87	85	83	82					105	
STA 578																				
55	95	97	96	104	108	106	112	109	115	111	111	102	99	99	95	90	92	88	122	1.3
71	92	97	98	102	104	109	129	126	117	109	113	107	101	101	95	96	99	99	131	3.5
73	116	115	113	113	115	125	142	141	122	124	129	127	120	116	111	109	108	107	145	17
84	93	104	100	105	106	112	125	120	121	111	102	93							129	2.8
M1	90	95	97	100	101	98	103	108	102	95	96	90	89	86	81	81	86	90	113	
M14	107	115	117	123	126	123	126	128	125	120	118	115	107	103	103	101	111	113	136	
M22	99	106	107	110	113	107	115	117	109	104	103	101	97	93	91	90	95	96	123	
M32	89	93	95	98	104	100	106	108	99	93	93	90	87	85	82	82	89	90	114	
STA 647																				
55	102	102	101	106	103	102	106	111	111	110	111	100	97	95	92	85	87	86	119	.9
71	86	91	95	106	103	104	123	122	112	101	104	105	93	91	88	86	87	88	126	2
73	111			118	118	125	140	146	134	125	129	130	121	123	111	110	112	110	149	27
84		97	96	109	110	110	130	126	126	115	105	99	95						133	4.5
M1	90	94	98	97	102	94	102	107	103	92	94	93	88	83	82	81	77	90	112	
M14	98	103	107	108	110	102	113	116	108	103	101	98	96	90	89	91	96	96	122	
M22	107	115	117	123	126	122	124	128	125	120	118	116	109	104	106	103	112	114	136	
M32	92	98	99	104	105	98	108	112	105	98	97	95	93	91	87	88	94	95	117	
STA 738																				
55	92	99	99	110	110	105	111	114	108	109	110	95	84	93	85	82	83	82	120	1
71	75	86	86	95	99	96	112	108	100	87	89	85	78						124	1.5
73	79	83	80	91	92	90	112	111	100	90	95	88	80	79					145	16
84		101	98	110	112	115	130	130	127	117	114	104	98	95					135	5.5
M1	85	91	95	97	101	95	98	98	96	89	86	84	82	89	84	84	86	82	108	
M14	92	100	101	102	106	101	107	108	101	97	91	90	90	83	81	82	84	92	115	
M22	97	102	105	108	113	102	111	111	106	100	98	96	93	87	85	85	88	96	120	
M32	107	114	116	123	124	122	126	128	126	119	1117	113	103	102	102	103	108	114	136	

FIGURE C21 1/4 SCALE SNARK RESPONSE IN DB, INPUT NOTED OPEN BOX

CPS	160	200	250	320	400	500	625	800	1000	1250	1600	2000	2500	3200	4000	5000	6250	8000	OVERALL
1				102	113	107	114	124	116	122	111	99	96	94	96	99	102	98	130
3		94	108	120	112	109	117	111	103	101	100	93	90	90					124
4		93	97	113	119	109	108	110	107	109	108	99	90			89	93	91	123
5	93	99	99	99	106	117	112	103	97	93	91	87	86	83			84	86	120
8		89	97	113	121	110	105	111	106	104	100	99	99	99	97	101	104	102	124
11		98	104	121	113	114	124	115	109	113	113	114	113	111	101	94	93	93	131
13		95	96	108	119	109	101	104	105	105	101	87	84	84	84	89	93	92	121
14	75	89	89	100	108	108	100	103	93	88	86	86	86	84	84	86	84	81	114
15		94	103	125	117	112	107	109	110	104	101	94							127
16	87	88	94	100	105	107	111	117	115	103	93								122
18	98	112	112	113	119	113	116	122	114	119	107	99	93	96	96	99	111	106	129
28	96	101	101	114	118	108	106	124	123	117	107	113	102	93					129
30	106	114	110	111	116	109	121	124	118	114	117	106	98	91	89	89	91	91	129
34	95	108	104	109	115	105	109	110	117	117	111	104	100	92					126
35	99	112	111	114	123	119	114	114	118	105	101	93							128
36	98	110	106	113	121	111	103	105	104	103	100	94	87	86	85	90	96	91	124
39	73	75	88	99	107	97	95	100	88	84	76	76	72	70	70	74	76	71	110
40	88	106	106	110	108	109	117	113	118	109	99	93							125
57	90	100	105	122	117	108	111	110	110	105	103	96	87	86					126
58	94	105	107	112	120	111	118	121	123	124	123	122	114	118	110	105	109	108	133
71	104	116	114	121	125	109	122	119	115	109	108	107	98	95					131
72	103	109	108	112	116	113	113	114	114	112	109	100	94						129
79	98	108	100	100	108	104	108	120	109	104	106	97	86						124
84	92	110	102	106	110	104	114	112	107	105	103	89					83		121
M5	124	136	136	143	143	135	131	133	125	123	119	118	115	121	119	117	120	121	149
M6	83	87	90	101	107	102	102	108	104	99	99	92	83	82	79	81	86	80	115
M9	93	102	104	110	112	104	109	108	106	104	98	100	90	89	88	91	95	94	120
M10	92	99	100	101	107	106	105	110	104	98	96	93	93	90	86	88	93	90	116
M11	92	101	101	98	101	104	105	101	100	94	93	88	91	87	83	83	88	91	114
M12	89	95	94	93	100	103	101	99	94	93	93	91	86	85	85	85	86	84	111
M13	84	86	92	103	103	101	101	99	98	90	89	87	81	80	77	79	81	82	111
M15	82	90	91	96	96	97	97	96	92	86	82	83	79	75	73	75	76	74	107
M16	90	101	105	104	105	98	102	101	99	93	92	92	91	91	84	87	91	88	114
M19	85	94	96	92	95	96	99	94	92	86	92	84	83	81	79	82	86	82	107
M20	80	85	90	90	100	95	94	94	88	83	79	77	72	69	67	68	70	70	105
M26	87	99	100	100	102	99	98	97	92	91	89	89	83	83	78	80	84	80	110
M31	91	100	100	104	106	88	100	102	96	89	89	88	84	81	78	80	80	84	113
M35	80	93	95	90	98	91	93	90	89	87	82	83	81	76	72	76	80	78	104
M36	83	94	95	92	96	92	97	95	90	85	88	87	81	79	77	78	82	78	106

FIGURE C22 1/4 SCALE SNARK RESPONSE IN DB, INPUT AT STA. 415, CLOSED BOX, HIGH LEVEL

CPS	160	200	250	320	400	500	625	800	1000	1250	1600	2000	2500	3200	4000	5000	6250	8000	OVERALL
1			82	97	107	104	112	117	116	113	107	96	86	83		83	85	82	122
3		97	115	124	117	114	121	125	119	108	107	100	97	94				93	132
4		94	101	117	115	114	117	119	119	120	121	109	94	96	97	102	107	105	128
5		83	95	106	108	104	105	110	100	92	90	88	88	85	85	85	85	84	115
8	83	91	104	115	118	109	106	109	106	97	96	93	88	89	83	86	89	86	121
11		99	101	107	108	116	129	125	113	104	105	104	99	94					131
13		88	94	105	112	112	111	113	113	114	114	100	100	96	96	103	109	108	123
14		86	89	101	110	113	113	109	103	97	99	97	100	98	99	99	99	95	119
15		89	101	123	113	111	115	118	115	112	108	99	93	87					127
16			95	106	105	112	123	124	127	112	105								131
18	97	109	107	112	118	110	115	116	114	111	102	91	86				92	88	125
28	96	111	108	114	122	110	111	128	132	124	113	117	111	97			98	98	135
30		114	111	115	116	120	137	146	139	132	129	123	117	112	111			110	148
34	98	111	106	107	113	114	122	128	134	129	121	118	114	111	104	102	105	106	138
35	98	111	106	104	119	122	131	134	131	121	117	110	104	104	99	98	102	105	138
36	93	106	106	109	109	112	109	112	114	112	111	102	99	97	98	100	109	104	124
39	95	102	106	110	113	112	116	110	105	100	100	98	99	96	95	99	105	97	121
40		108	106	108	105	112	123	128	126	119	113	104	98						132
57	92	99	107	123	118	111	123	124	121	113	115	104	100	96	91				131
58	95	108	106	114	116	109	109	115	120	112	112	108	105	101	91		89		126
71		115	117	123	126	131	140	139	131	124	127	124	119	112	105	105	110	110	145
72	103	114	110	115	113	121	135	139	135	127	124	118	115	108	103	105	108	111	141
79	102	113	104	105	109	109	118	125	118	116	121	106	99	91					130
84	94	112	105	110	110	111	129	126	117	115	111	96							132
M1	88	97	94	93	98	100	100	101	95	96	91	86	86	86	82	82	87	86	110
M2	92	104	104	108	106	104	105	107	98	98	95	88	84	87	82	82	82	86	116
M10	93	103	103	103	113	105	105	106	105	99	99	95	95	91	88	91	93	92	118
M11	96	107	105	107	112	105	104	102	108	102	99	92	91	88	86	83	91	89	119
M12	99	107	108	115	118	104	114	110	110	108	104	102	100	100	94	96	103	100	124
M14	122	135	136	141	142	140	131	132	126	126	120	118	118	122	119	118	120	120	148
M15	93	104	106	112	114	105	107	111	104	98	99	99	94	91	89	90	94	91	121
M16	97	108	107	111	113	111	114	114	113	111	114	110	104	99	98	100	105	96	126
M17	91	100	99	103	98	99	109	111	101	102	97	97	94	89	86	86	92	92	116
M19	99	112	112	119	119	115	114	110	111	108	105	101	97	97	95	99	99	98	125
M20	87	99	102	105	107	98	100	106	97	91	90	86	86	86	78	80	85	84	115
M22	91	102	102	107	113	104	105	108	106	98	95	89	94	91	86	89	93	88	119
M26	94	97	99	101	103	106	103	107	100	96	96	95	91	90	86	87	93	91	115
M31	92	94	97	100	102	104	103	102	102	93	90	87	86	82	80	79	84	86	113
M36	86	92	93	96	99	99	99	103	97	91	92	89	86	86	83	83	89	85	110

FIGURE C23 1/4 SCALE SNARK RESPONSE IN DB, INPUT AT STA. 578, CLOSED BOX, HIGH LEVEL

CPS	160	200	250	320	400	500	625	800	1000	1250	1600	2000	2500	3200	4000	5000	6250	8000	OVERALL
1		87	92	106	112	105	122	124	112	111	104	93							128
3		92	107	122	107	99	109	109	104	90	89	84							122
4		88	103	117	114	113	117	120	118	116	117	105	102	98	97	98	100	98	128
5			94	102	109	110	110	116	104	98	92	92	88	88	91	92	92	92	120
8	88	101	108	123	120	108	113	112	102	94	90	91							126
11		95	104	118	109	112	126	121	108	104	101	98	90						128
13	83	95	101	111	110	113	113	118	114	111	110	97	97	98	97	99	103	100	124
14		97	99	115	117	117	112	117	110	103	102	102	101	102	105	106	104	103	125
15		99	116	135	125	117	126	130	126	118	112	107	105						140
16			100	116	116	117	130	131	133	116	107								137
18	99	100	101	114	113	105	121	120	110	107	99	91							126
28	97	105	109	115	114	106	108	125	125	116	107	114	102						130
30	104	110	113	117	117	113	133	140	134	121	121	112	106						142
34	98	103	103	107	108	108	117	121	126	126	117	113	113	107	99	97	97	95	131
35	97	102	104	102	113	118	126	130	132	115	107	100	97						136
36	95	103	104	114	111	114	114	117	113	111	112	102	102	100	100	101	107	101	124
39	91	90	97	111	115	109	112	109	104	100	96	98	99	96	98	101	105	100	122
40		105	107	120	121	118	140	137	127	124	119	107							142
57		100	115	128	130	116	131	129	126	124	121	116	109	103	99				138
58	95	100	103	120	113	107	111	117	113	108	111	105	99	97	90				125
71	101	111	118	129	123	113	133	135	127	117	118	113	108	103	99		100		139
72	101	104	107	116	109	122	134	132	127	115	115	107	101						138
79	98	103	105	115	114	110	122	135	121	118	123	110	103						137
M1	86	97	98	99	99	94	104	103	97	94	92	84	77	77	77	77	78	75	110
M2	90	97	102	111	105	97	106	106	100	94	94	88	80	80	83	86	86	88	116
M10	88	98	99	101	104	100	103	102	96	96	89	85	79	81	78	79	79	75	112
M11	93	100	104	110	104	100	108	108	99	100	96	86	80						116
M12	92	99	103	108	108	102	103	106	104	97	95	91	82	84	83	81	80	78	117
M13	93	104	107	117	112	102	103	106	101	98	96	93	92	86	84	84	86	86	121
M15	92	105	107	113	109	100	108	106	104	98	95	93	89	84	80	80	85	82	119
M16	94	101	106	107	108	103	114	115	105	105	102	94	89	85	82	83	84	83	120
M19	99	109	113	120	117	103	116	114	114	112	105	93	94	93	88	88	88	88	127
M20	96	106	110	114	109	101	114	111	101	97	95	91	87	86	85	84	88	91	121
M22	122	135	137	142	139	129	128	128	127	121	120	119	117	116	121	117	119	119	147
M24	103	116	117	121	117	107	120	123	116	111	104	100	99	98	93	93	94	93	130
M26	101	113	115	120	121	108	112	124	120	112	110	104	98	98	94	92	93	94	130
M31	102	107	116	122	117	109	116	111	110	110	105	103	102	102	96	89	88	90	127
M35	90	103	103	108	106	102	109	110	103	99	92	91	89	85	80	81	83	81	117

FIGURE C24 1/4 SCALE SNARK RESPONSE IN DB, INPUT AT STA. 647, CLOSED BOX, HIGH LEVEL

CPS	160	200	250	320	400	500	625	800	1000	1250	1600	2000	2500	3200	4000	5000	6250	8000	OVERALL
STA 415																			
M2	114	121	125	130	132	124	126	128	119	120	120	116	117	111	106	103	107	112	140
M6	85	97	100	100	105	99	101	107	102	95	97	94	94	95	93	94	98	97	116
M7		86	87	87	90	85	98	100	92	87	89	97	93	89	87	85	87		107
M9	87	96	98	100	104	91	103	99	98	98	94	97	93	92	86	91	96	96	113
M10	81	87	87	90	100	93	91	98	94	86	86	90	91	88	84	85	91	91	107
M11	83	88	89	89	91	95	94	93	91	91	90	86	91	88	84	85	91	91	106
M12	79	81	81	78	89	92	92	92	88	87	86	87	82	84	84		84		102
M13	74	76	83	91	91	88	91	91	88	81	81	84	81	82	77	78	84	84	101
M15	76	79	79	80	91	87	88	90	85	80	81	83	80	79					99
M16	83	92	94	88	87	87	91	92	90	82	85	90	88	83	83				104
M19		82	83	80	85	84	90	88	85	78	82	83	79	81		78	83		99
M20	76	78	81	82	90	87	89	90	84	82	80	82	80	80	75	75	77	74	99
M22		80	82	78	84	84	89	87	82	75	81	79	79	76			81		97
M26	81	89	89	91	97	92	94	92	90	87	90	88	87	88	85	86	91	87	104
STA 578																			
M1		81	79	79	79	79	85	85	83	86	85	84		85			85	85	97
M2			88	95	92	90	95	97	94	89	93	92	85	91	86	82	86	83	105
M10	77	88	87	90	95	87	88	93	92	89	91	90	91	86	87	84	91	92	105
M11		87	92	93	94	87	91	90	95	95	90	90	91	89	85	84	89	89	106
M12	86	93	97	99	101	89	102	101	101	99	97	95	97	95	94	93	91	97	113
M14	110	121	123	127	127	119	119	122	114	116	113	108	115	120	119	119	121	121	136
M15	78	89	90	93	95	89	93	102	95	87	91	93	89	89	82	81	89	91	109
M16	87	95	94	93	96	95	104	104	103	100	103	104	96	95	92	93	101	97	115
M17	77	88	87	87	80	81	96	98	88	90	91	90	86	84	81		82	85	104
M19	85	97	96	98	101	91	99	98	96	95	96	92	90	89	86	90	94	94	111
M20		89	91	94	94	89	94	103	92	89	87	89	87	88		86	90	88	107
M22	80	89	88	89	98	94	93	95	93	87	87	83	88	87	81	85	87	85	105
M26	81	84	85	85	88	90	92	97	94	92	93	92		91	90	90	94	93	106
M31	80	85	87	95	97	95	96	94	96		86	86		84	83	83	85	87	105
M35	83	90	90	91	95	95	97	98	94	90	92	90	88	88	86	88	94	94	108

FIGURE C25 1/4 SCALE SNARK MICROPHONE RESPONSE IN DB. CLOSED BOX

CPS	160	200	250	320	400	500	625	800	1000	1250	1600	2000	2500	3200	4000	5000	6250	8000	OVERALL
STA 647																			
M1	76	81	81	84	83	81	89	94	86	83	83								99
M2			88	96	93	86	94	99	93	89	88	83	83	84	82	78	81	81	105
M10	78	88	86	88	86	85	93	92	88	89	85							79	102
M11		83	83	88	84	82	93	98	88	92	90	83	81	83	79	79	82	79	103
M12	86	92	94	98	99	92	97	101	98	96	94	89	84	84	83	82	83	84	109
M13		88	89	96	94	83	88	93	89	85	86	87	85	87	82	82	86	87	105
M15	81	94	96	99	98	89	99	99	97	81	89	87	84	83	77	76	81	82	109
M16	88	93	106	106	106	91	104	109	101	98	97	88	87	87	83	81	89	87	113
M19	87	97	99	103	101	91	105	106	106	103	96	90	94	93	88	92	93	93	114
M20		96	92	96	92	81	103	104	92	90	92	90	92	92	92	90	94	93	110
M22	114	126	127	131	128	117	120	121	119	115	118	118	114	118	119	119	121	120	138
M24	89	102	102	105	104	97	109	116	108	101	95	97	97	93	91	91	96	97	119
M26		98		104	106	95	103	116	112	105	105	106	101	100	95	95	97	96	120
M31	86	96	97	102	101	91	97	101	99	100	93	93	91	85	85	83	91	91	111
M35	76	85	85	89	89	85	95	98	90	89	88	90	86	83				86	104
STA 738																			
M1		84	83	87	88	82	89	85	79										97
M2			89	96	96	86	95	96	84	86	83	83	79	79	79	79	79	80	105
M10	77	84	86	88	86	86	96	93	84	83	81								101
M11		88	88	95	93	87	95	93	84	83	80	80	77	81	77	75	79	78	103
M12	79	87	88	87	86	87	94	92	84	80	80	77							101
M13		85	89	101	101	90	94	95	85	83	83	79	79	83	81	79	83	82	108
M15			81	92	92	85	89	89	79	77	79								100
M16	82	87	90	94	90	88	89	92	87	81	87	82	82						103
M20			89	99	95	87	91	92	84	83	84	81	79	80	76	74	78	76	105
M26	94	100	104	111	98	102	110	115	105	98	103	102	99	106	100	100	106	103	122
M28	91	99	103	111	105	95	109	111	102	97	94	97	94	90	89	89	96	96	119
M31	110	116	121	128	125	115	125	128	116	113	109	115	115	112	107	106	107	111	137
M32	111	124	124	130	127	126	127	126	114	111	116	116	112	117	117	118	121	120	136
M33	86	97	99	104	102	96	107	106	97	90	91	95	96	94	91	90	93	95	115
M34	83	93	93	96	97	89	98	96	89	89	89	84	83						107

FIGURE C26 1/4 SCALE SNARK MICROPHONE RESPONSE IN DB CLOSED BOX (CONT.)

APPENDIX D

GRAPHICAL SUMMARY OF VIBRATION RESPONSE TRANSFER FUNCTIONS

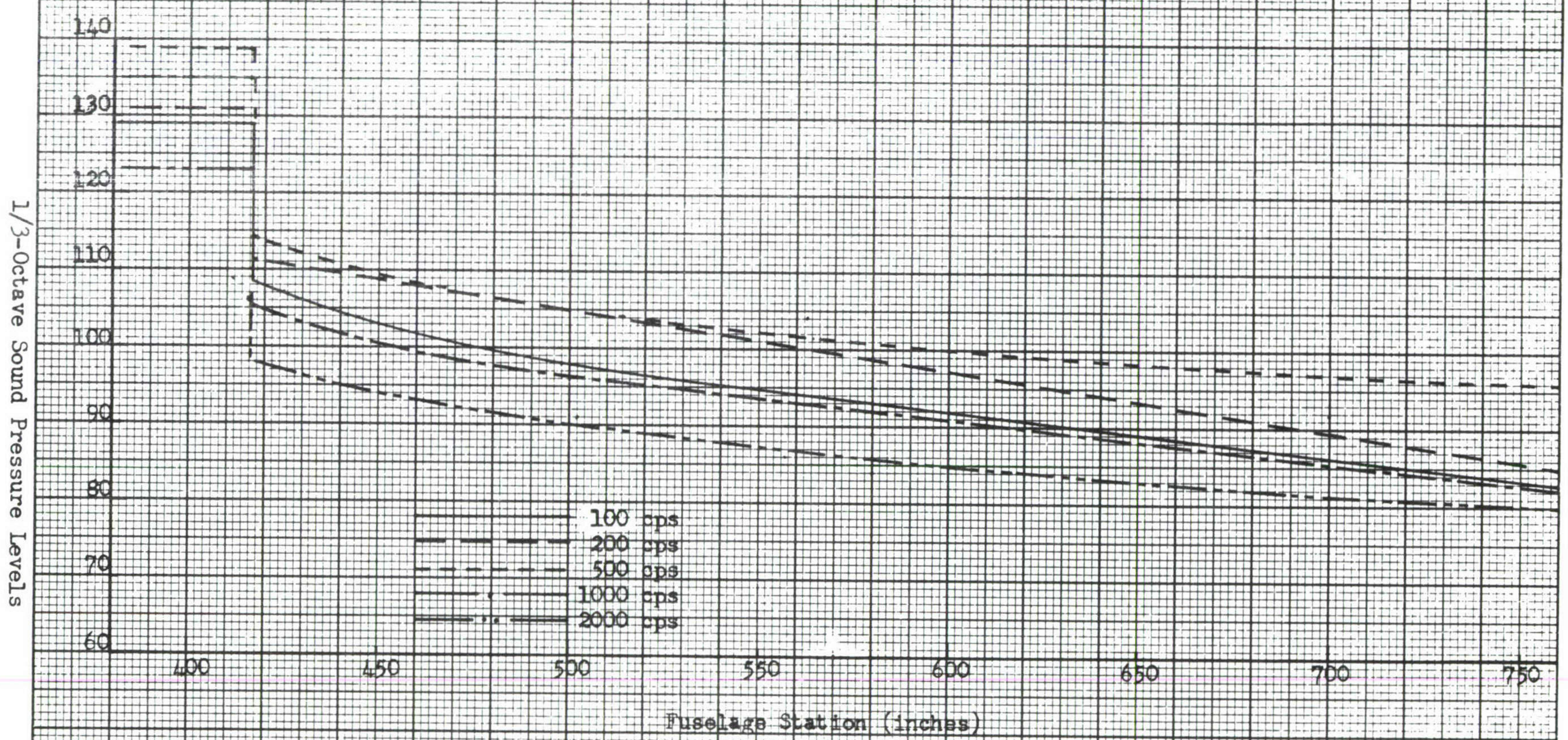

FIGURE D1 1/3 OCTAVE SOUND PRESSURE LEVEL CONTOURS FOR "CLOSED BOX" ACOUSTIC EXCITATION AT F.S. 407, REFERENCE MICROPHONE #3

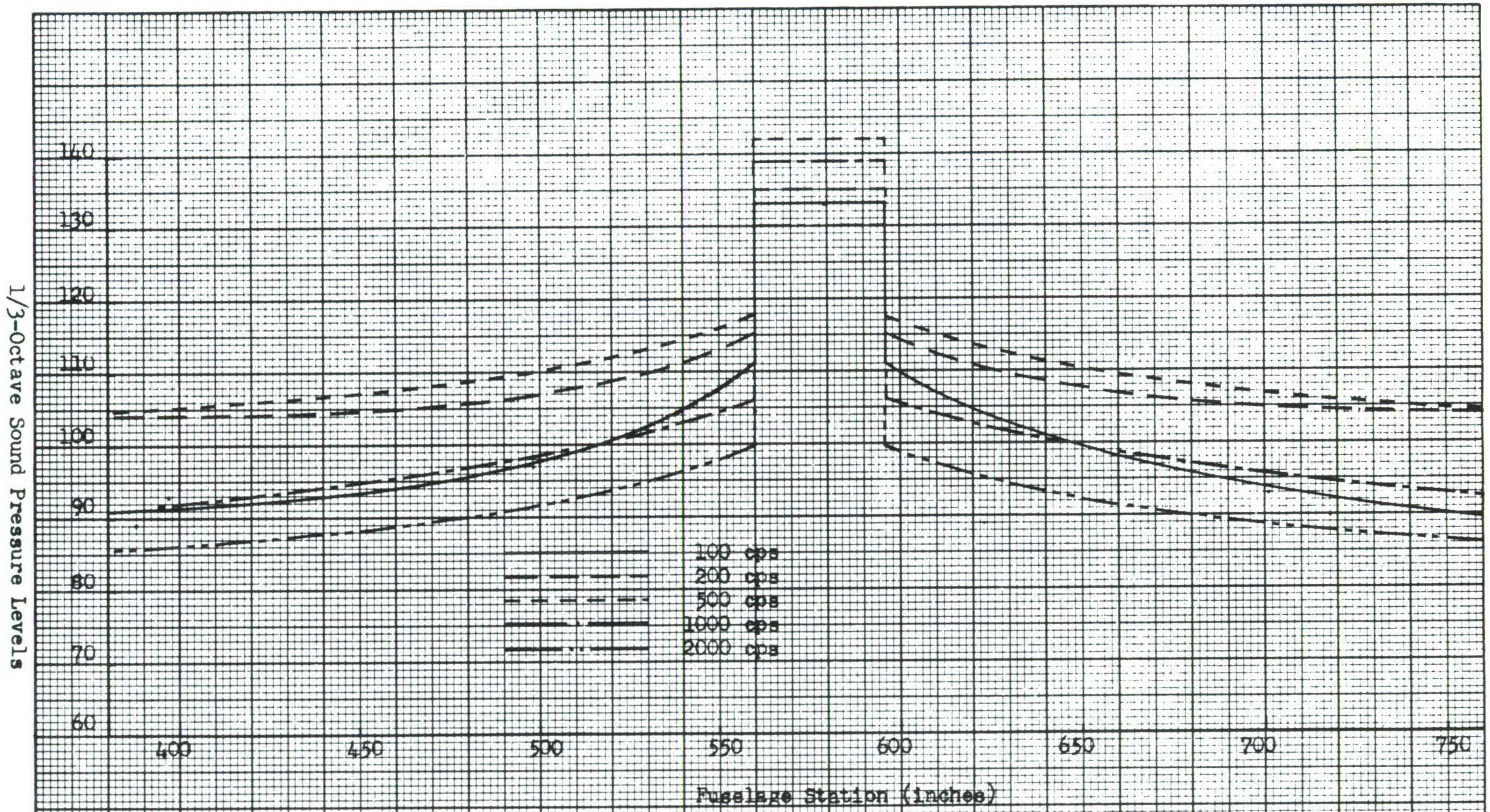

FIGURE D2 1/3 OCTAVE SOUND PRESSURE LEVEL CONTOURS FOR "CLOSED BOX" ACOUSTIC EXCITATION AT F.S. 578, REFERENCE MICROPHONE #14

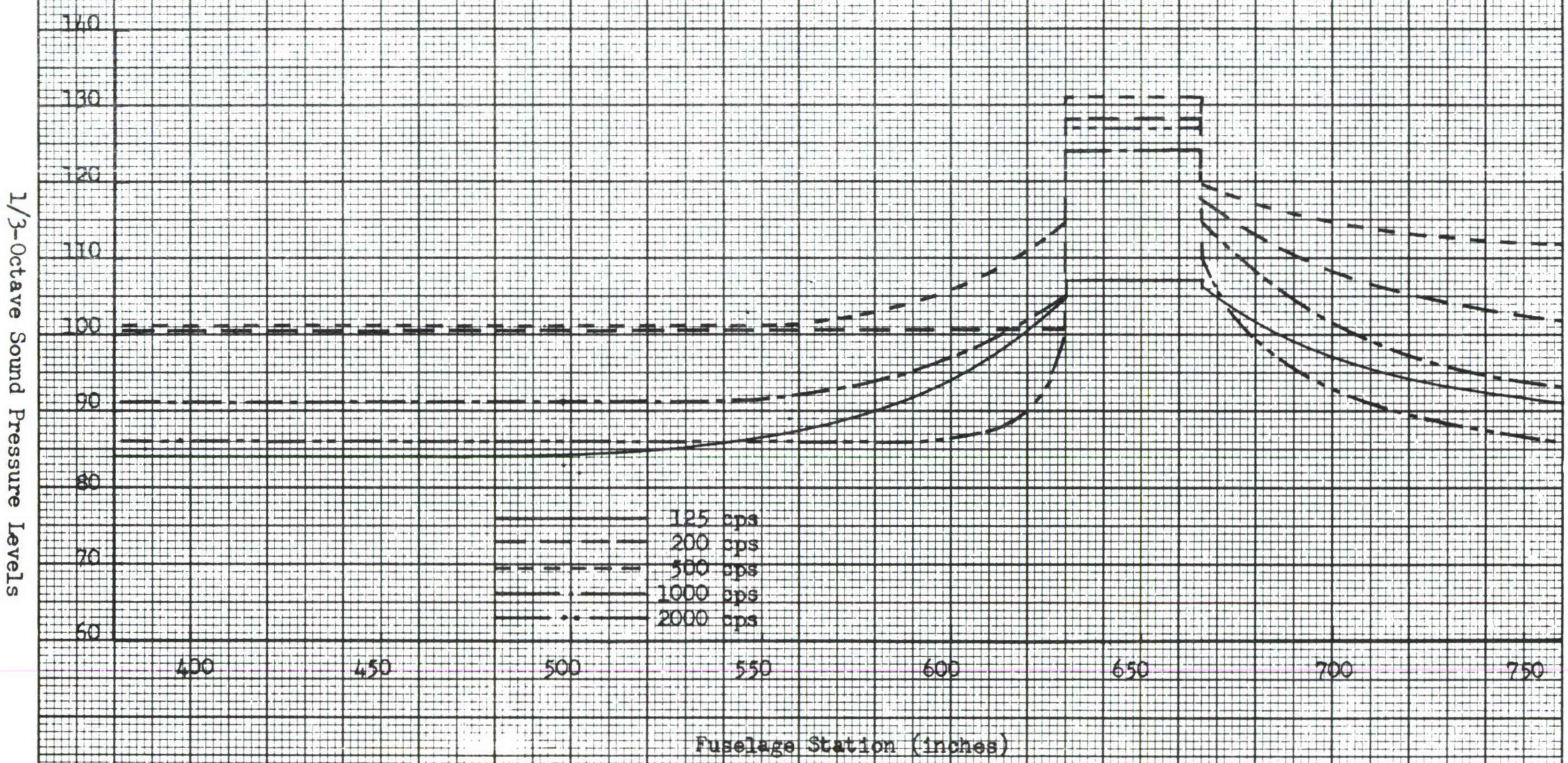

FIGURE D3 1/3 OCTAVE SOUND PRESSURE LEVEL CONTOURS FOR "CLOSED BOX" ACOUSTIC EXCITATION AT F.S. 647, REFERENCE MICROPHONE #22

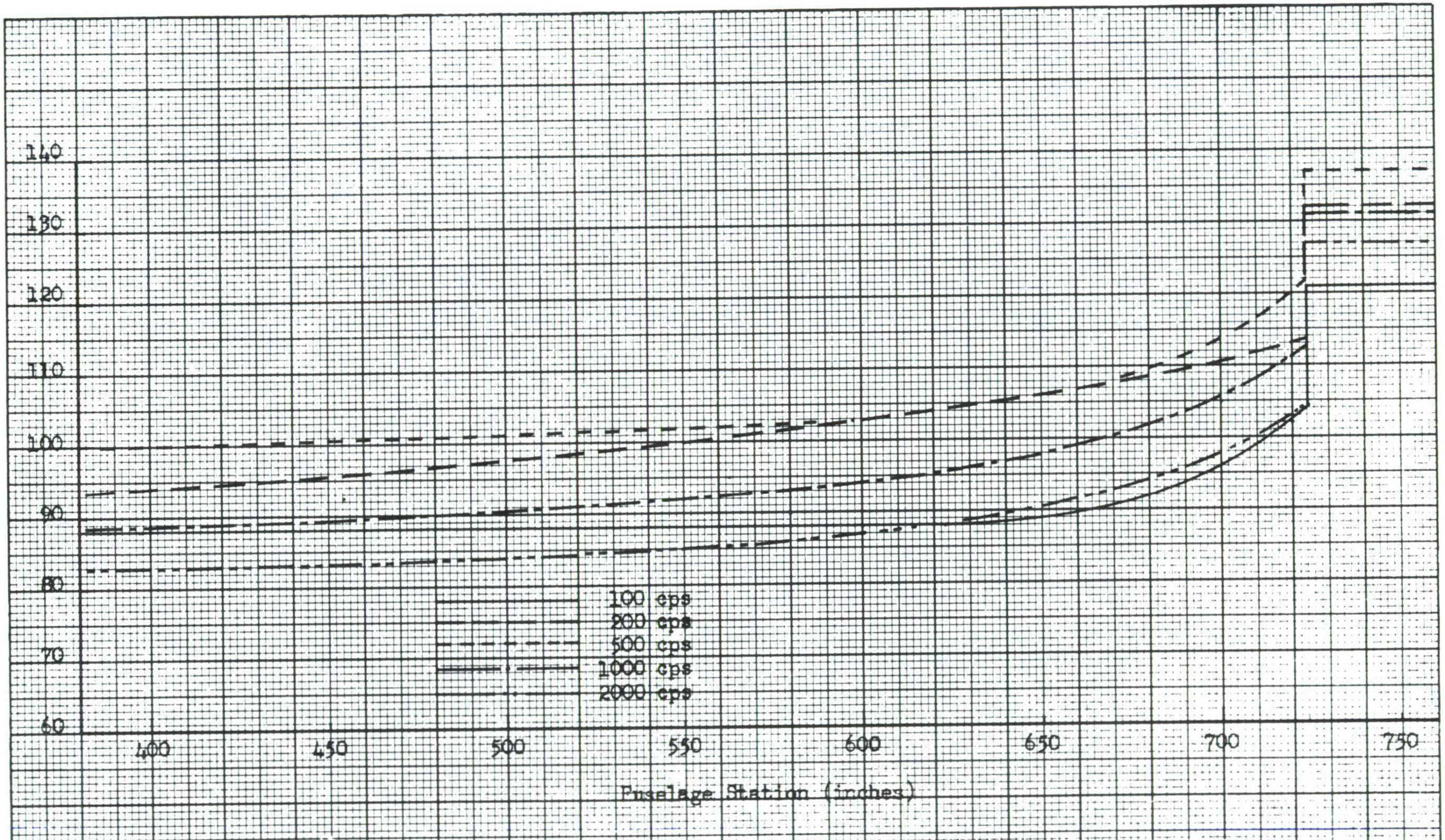

FIGURE D4 1/3 OCTAVE SOUND PRESSURE LEVEL CONTOURS FOR "CLOSED BOX" ACOUSTIC EXCITATION AT F.S. 738, REFERENCE MICROPHONE #32

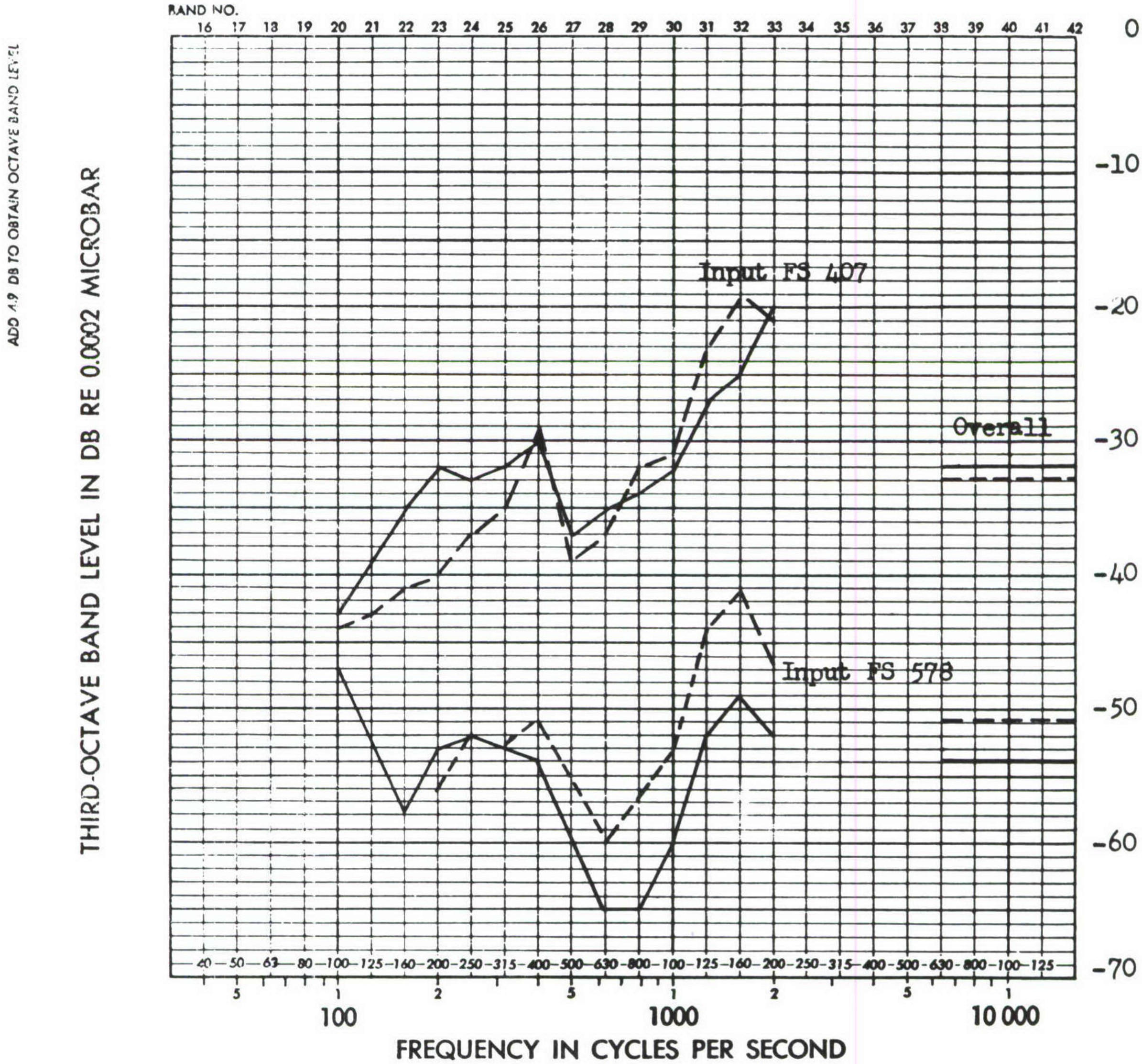

- - - - - - - Accelerometer 19
———————— Accelerometer 20

FIGURE D5 COMPARISON OF FULL SCALE RESPONSE TRANSFER FUNCTIONS (DB) FOR LATERAL RESPONSES OF OPPOSITE EDGE POINTS ON THE FORWARD BULKHEAD AT F.S. 384, EXCITATION AT F.S. 407 AND 578

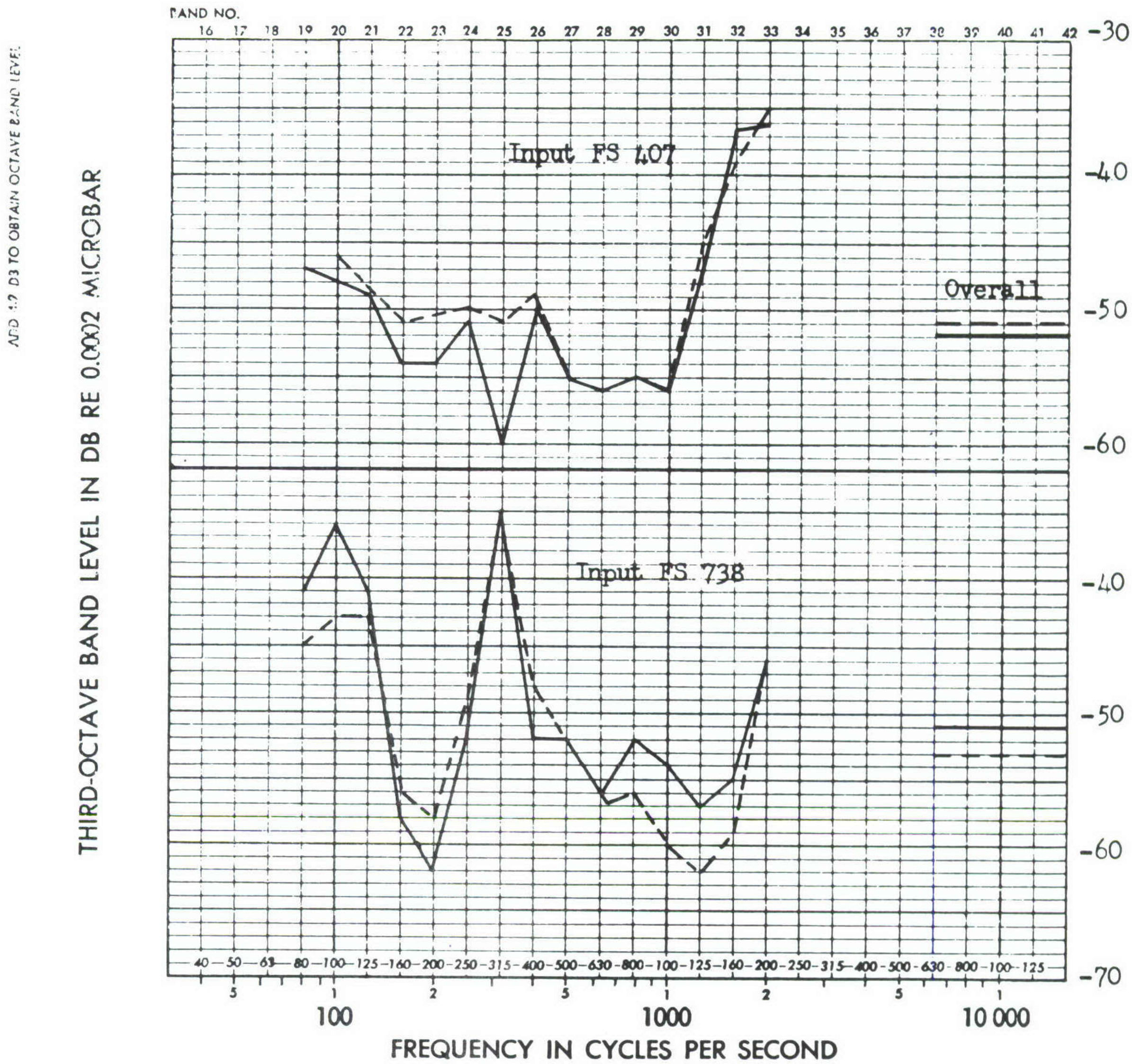

– – – – – – – Accelerometer 27
——————— Accelerometer 28

FIGURE D6 COMPARISON OF FULL SCALE RESPONSE TRANSFER FUNCTIONS (DB) FOR LATERAL RESPONSES OF OPPOSITE EDGE POINTS ON THE BULKHEAD AT F.S. 501, EXCITATION AT F.S. 407 AND 738

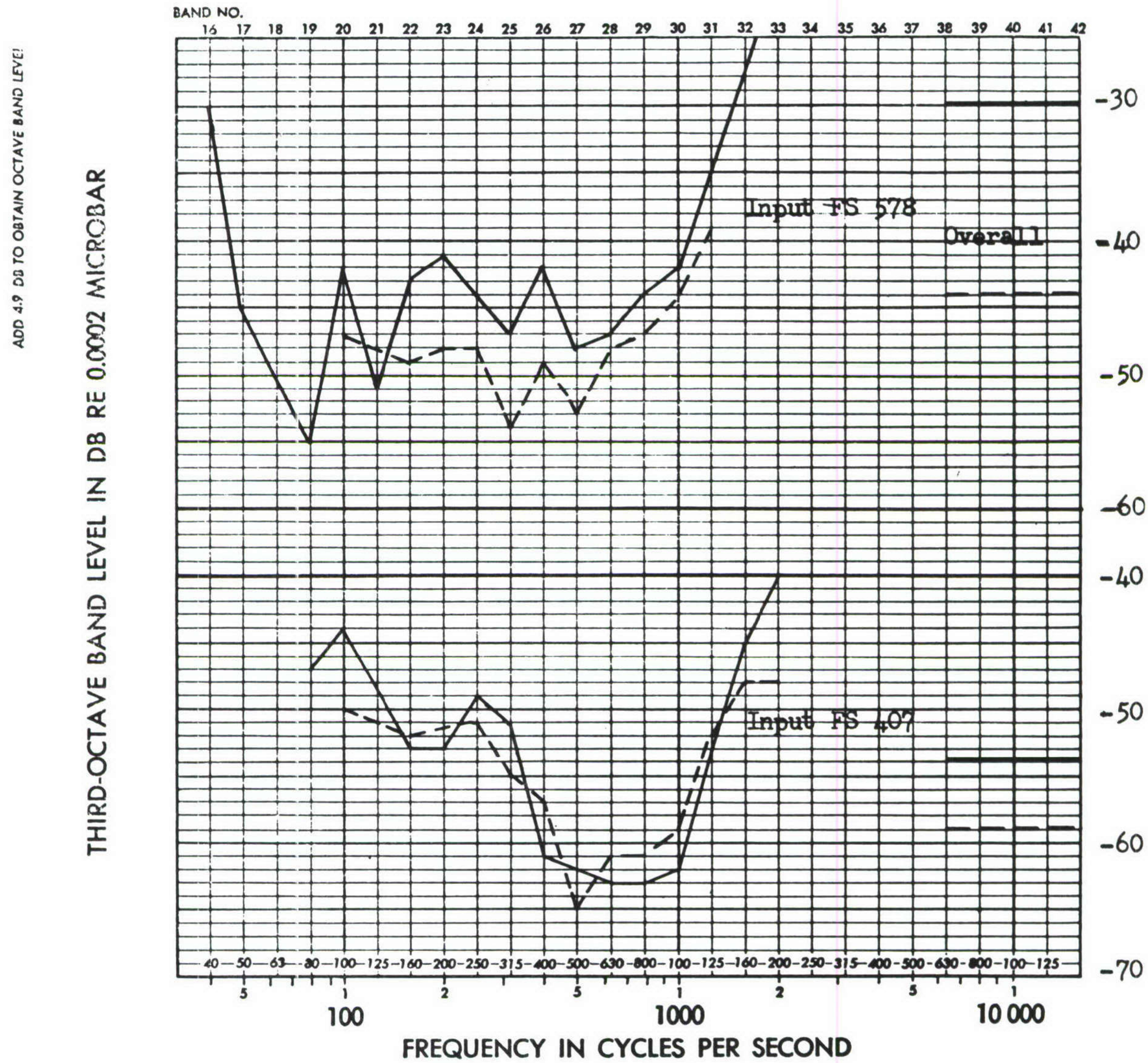

------ Accelerometer 33
——— Accelerometer 34

FIGURE D7 COMPARISON OF FULL SCALE RESPONSE TRANSFER FUNCTIONS (DB) FOR LATERAL RESPONSES OF OPPOSITE EDGE POINTS ON THE BULKHEAD AT F.S. 600, EXCITATION AT F.S. 407 AND 578

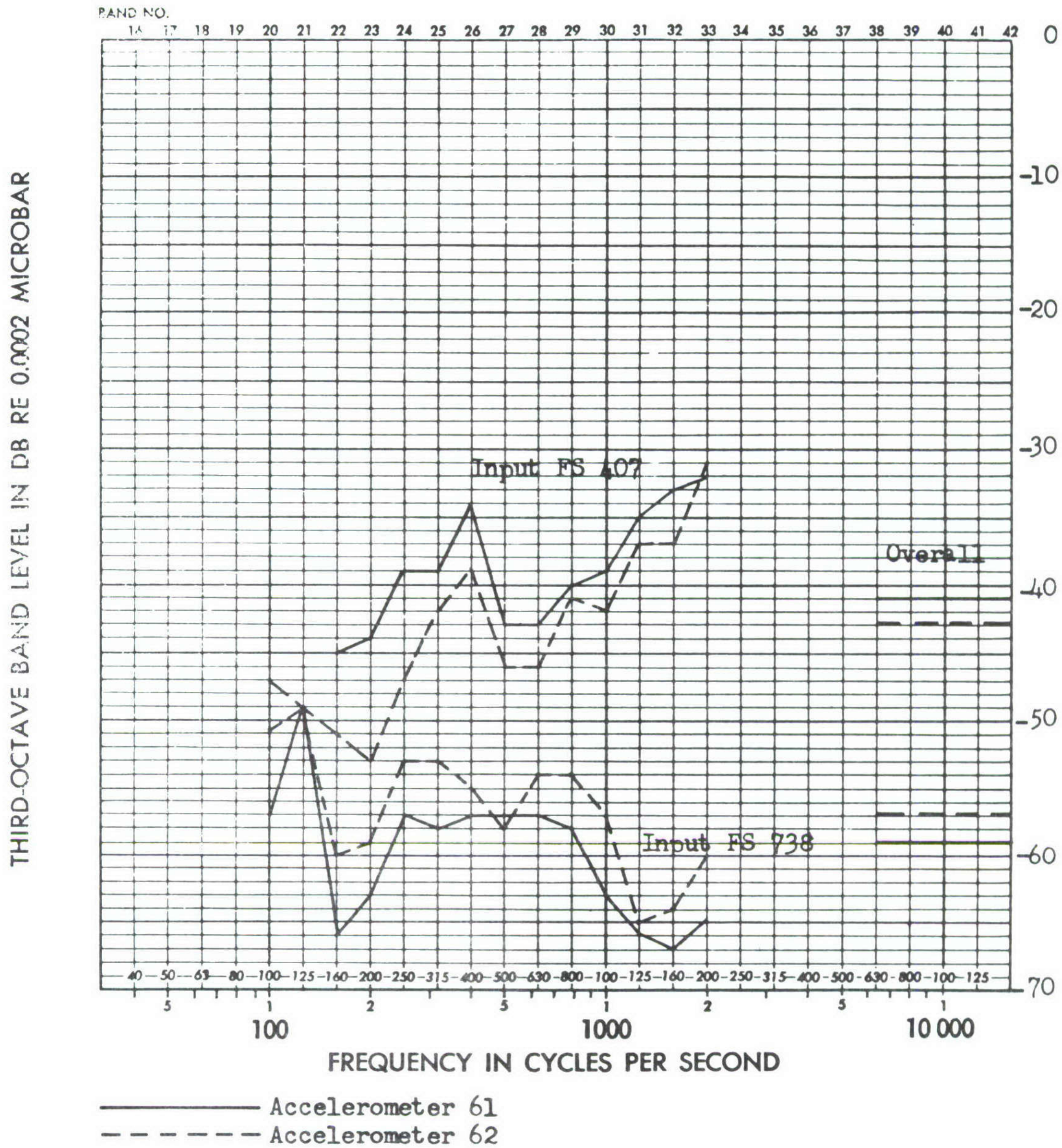

FIGURE D8 COMPARISON OF FULL SCALE RESPONSE TRANSFER FUNCTIONS (DB) FOR LATERAL RESPONSES OF OPPOSITE EDGE POINTS ON THE FORWARD FLOOR AT F.S. 445, EXCITATION AT F.S. 407 AND 738

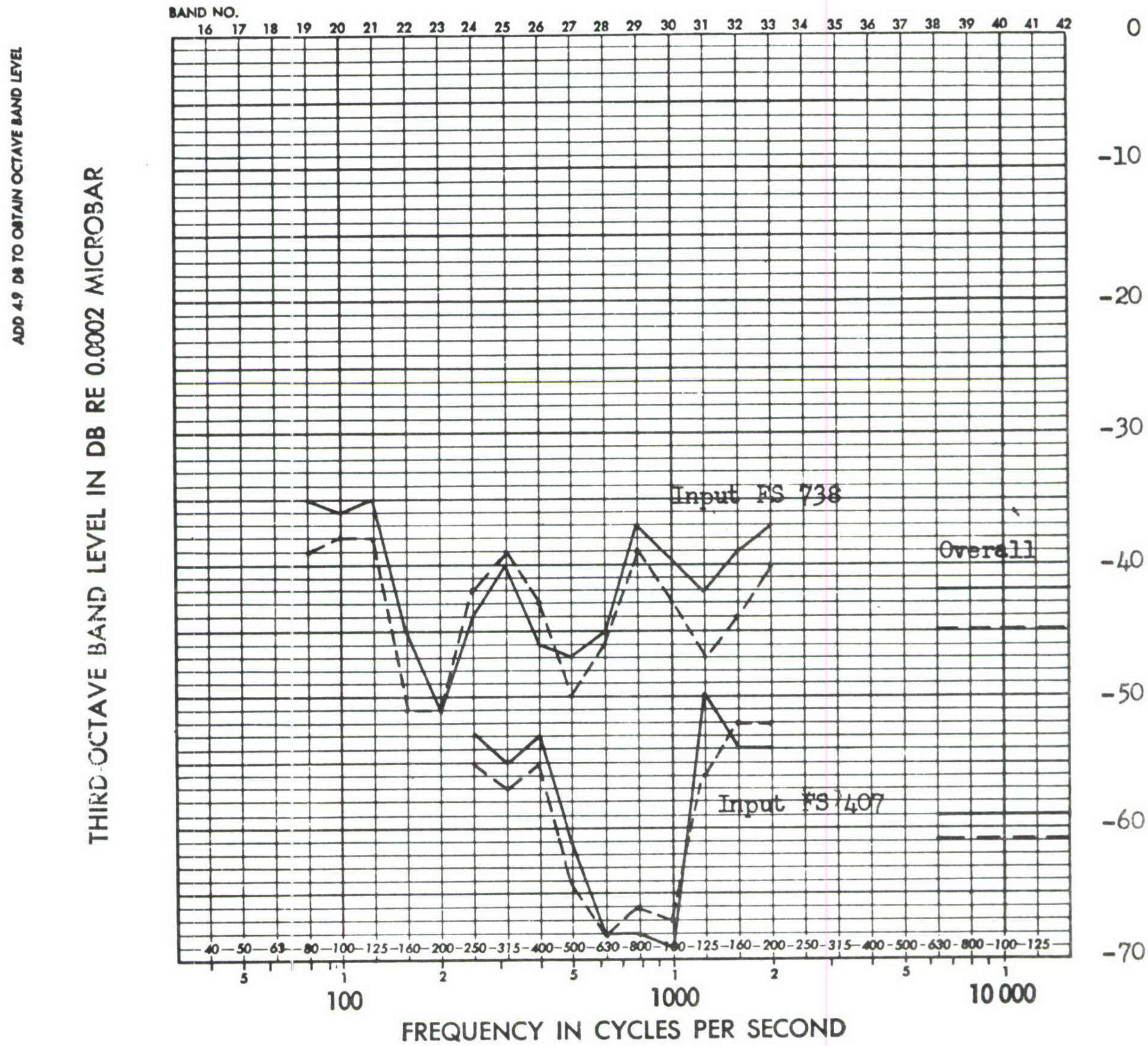

Accelerometer 43

Accelerometer 44

FIGURE D9 COMPARISON OF FULL SCALE RESPONSE TRANSFER FUNCTIONS (DB) FOR LATERAL RESPONSES OF OPPOSITE EDGE POINTS ON THE AFT FLOOR AT F.S. 675, EXCITATION AT F.S. 407 AND 738

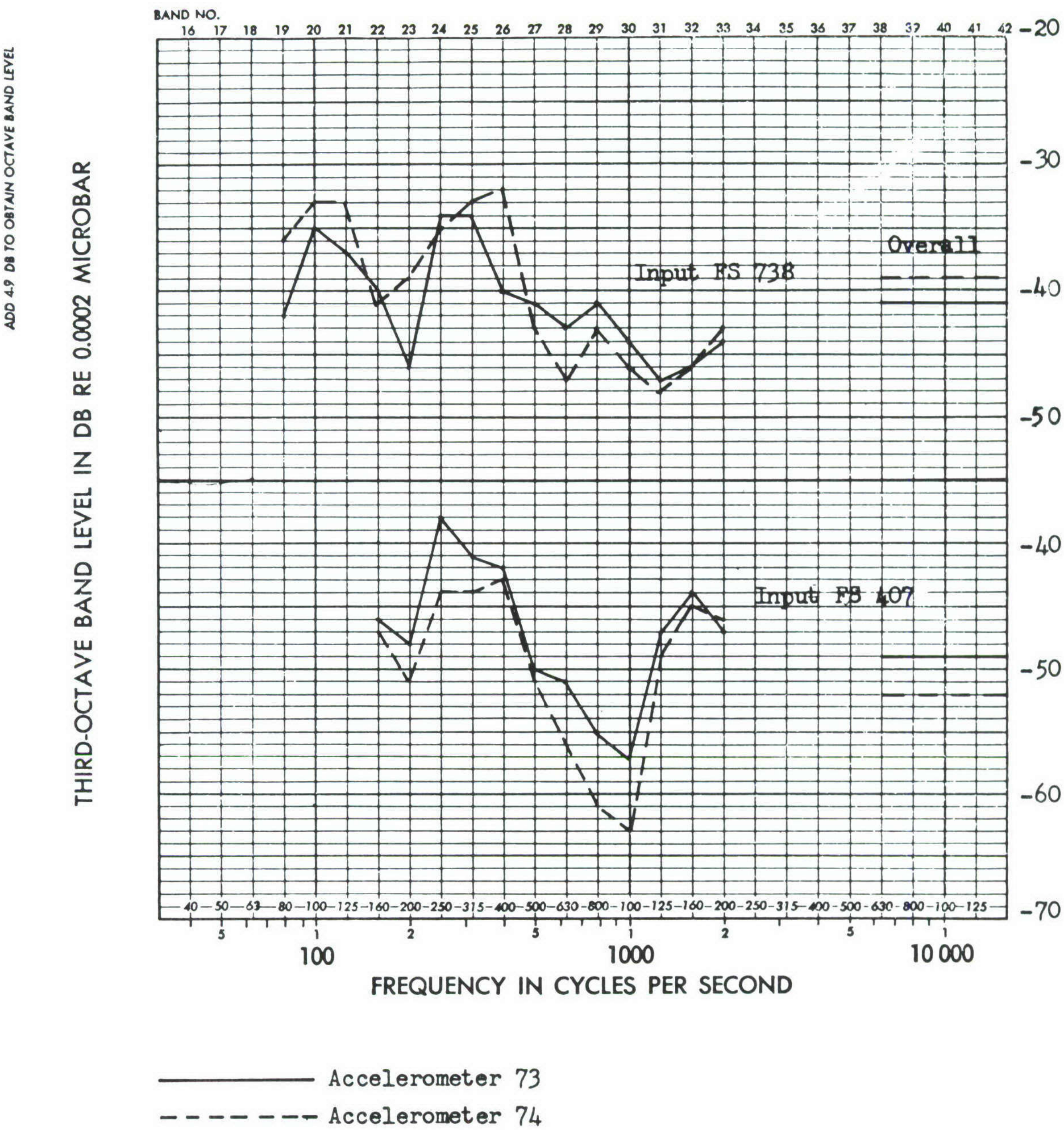

FIGURE D10 COMPARISON OF FULL SCALE RESPONSE TRANSFER FUNCTIONS (DB) FOR LATERAL RESPONSES OF OPPOSITE EDGE POINTS ON THE AFT FLOOR AT F.S. 625, EXCITATION AT F.S. 407 AND 738

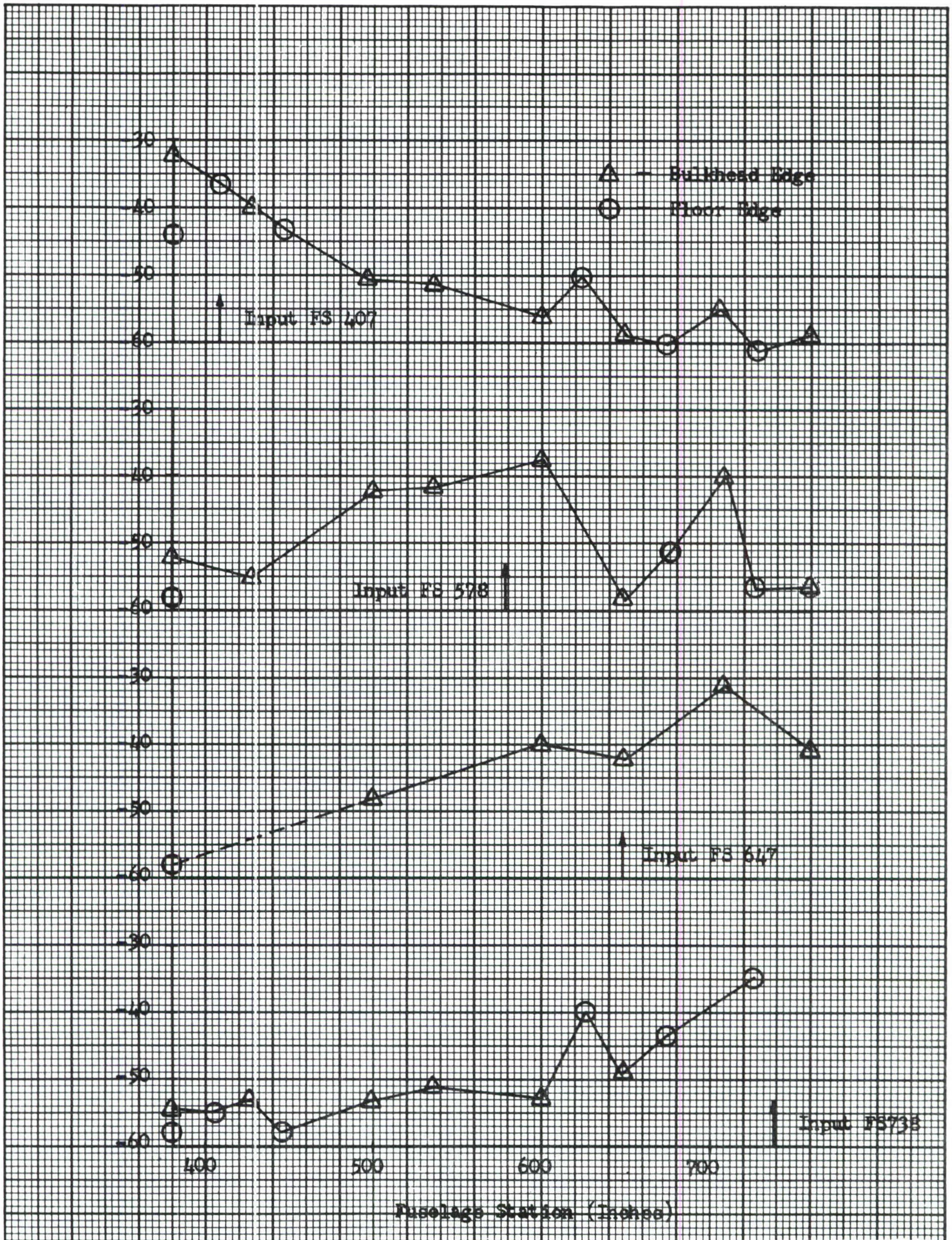

FIGURE D11 FULL SCALE RESPONSE TRANSFER FUNCTIONS (DB) FOR BULKHEAD AND FLOOR EDGES, OVER-ALL LATERAL RESPONSE, EXCITATION AT F.S. 407, 578, 647, AND 738

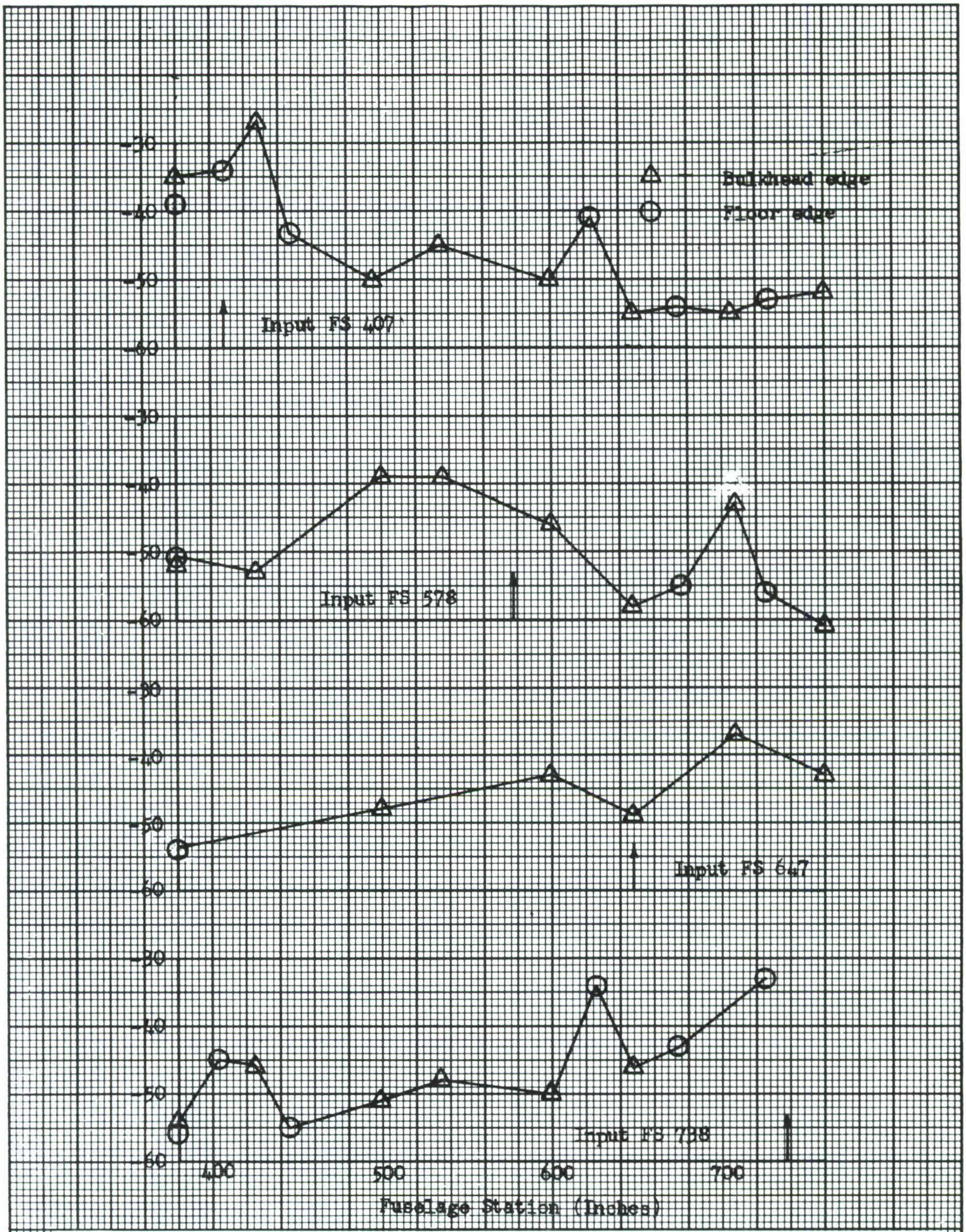

FIGURE D12 FULL SCALE RESPONSE TRANSFER FUNCTIONS (DB) FOR BULKHEAD AND FLOOR EDGES, LATERAL RESPONSE IN 250 CPS, 1/3 OCTAVE BAND, EXCITATION AT F.S. 407, 578, 647 & 738

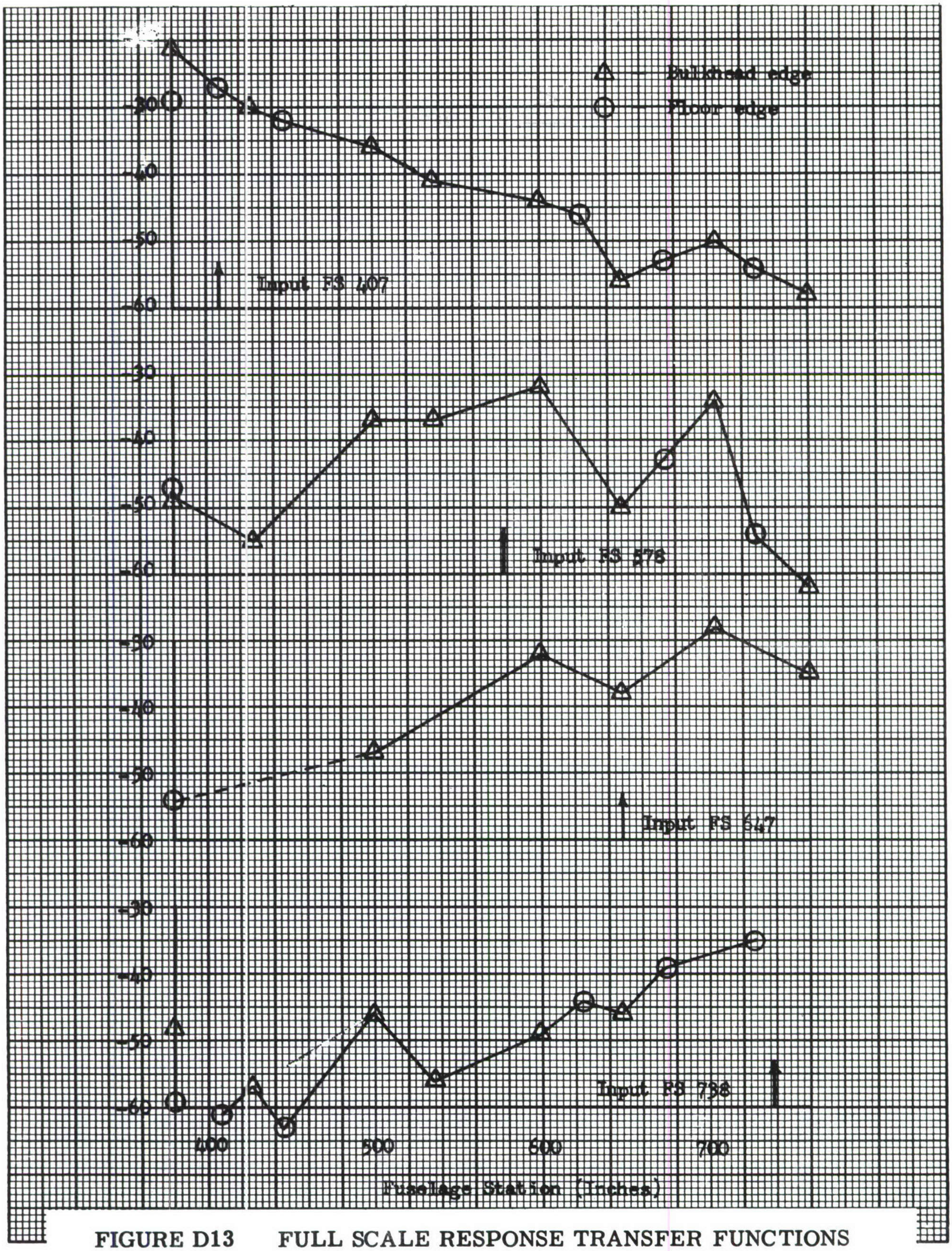

FIGURE D13 FULL SCALE RESPONSE TRANSFER FUNCTIONS (DB) FOR BULKHEAD AND FLOOR EDGES, LATERAL RESPONSE IN 2000 CPS, 1/3 OCTAVE BAND, EXCITATION AT F.S. 407, 578, 647, & 738

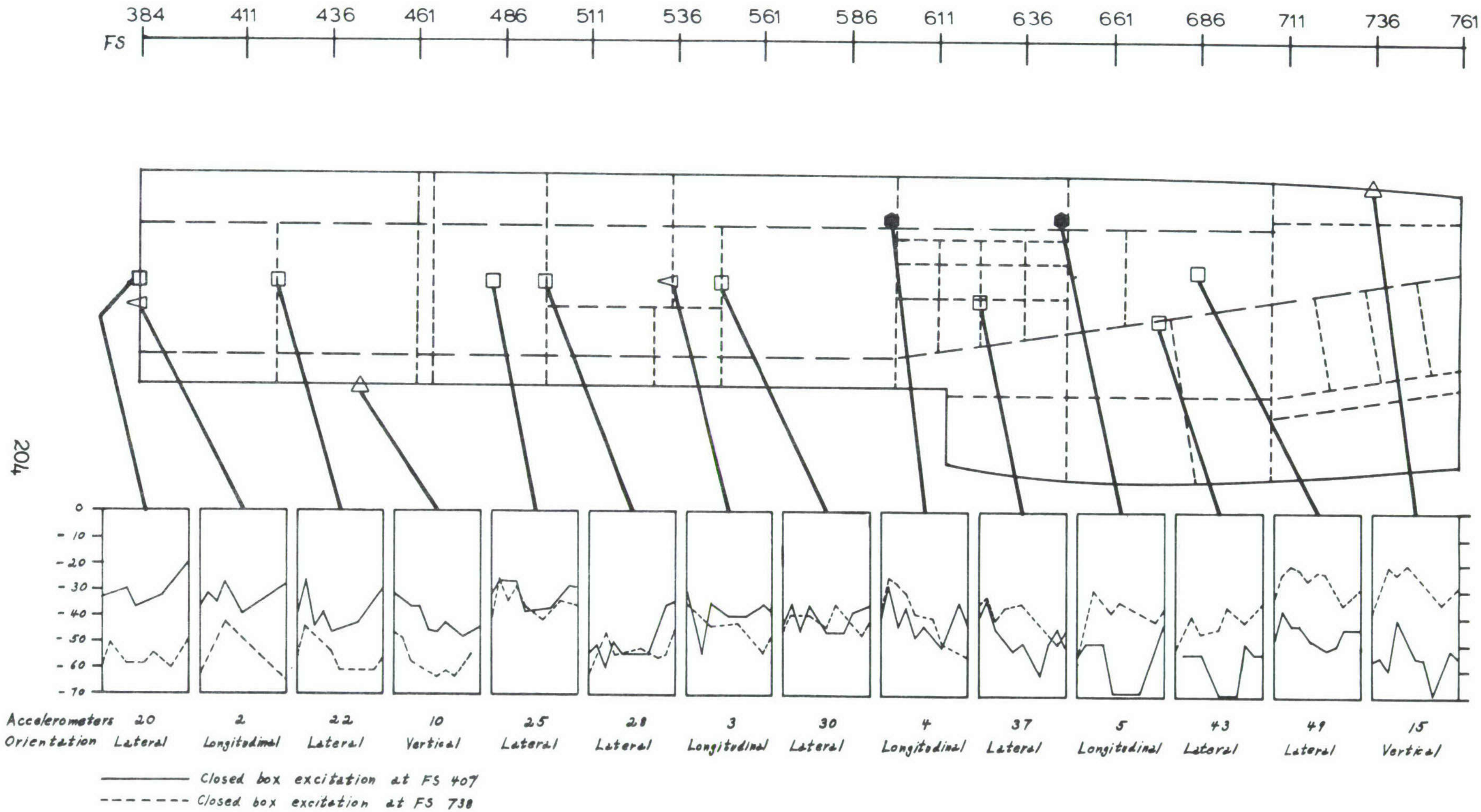

FIGURE D14 COMPARISON OF VARIOUS FULL SCALE STRUCTURAL RESPONSES FOR LATERAL EXCITATION AT F.S. 407 AND 738, SHOWING THE GENERAL AXIAL ATTENUATION OF RESPONSE

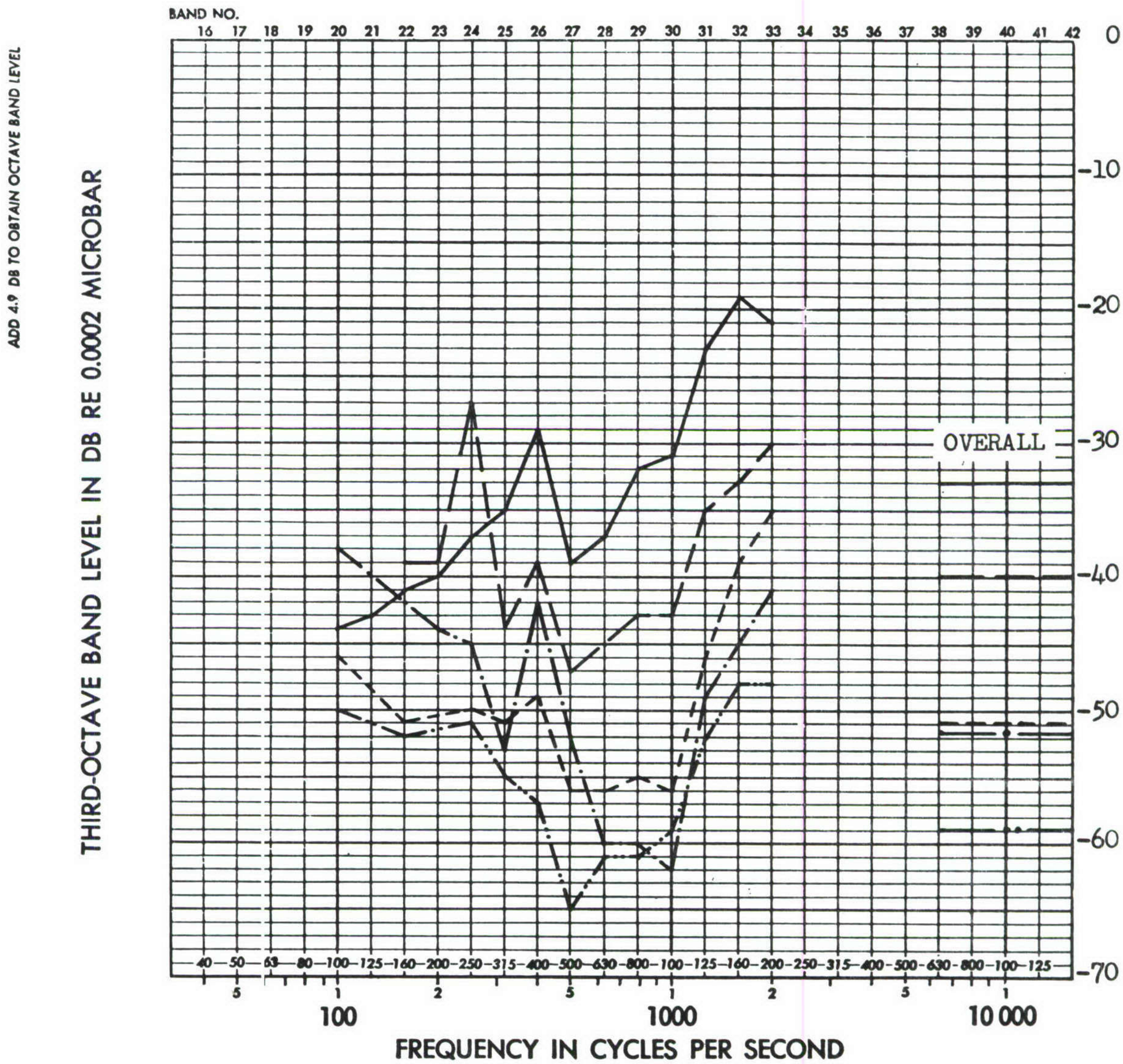

———————	Accelerometer 19 FS. 384	Input at FS. 407
— — — —	Accelerometer 22 FS. 426	Lateral Response
- - - -·- - -	Accelerometer 27 FS. 501	Bulkheads, right side
———·———	Accelerometer 29 FS. 536	
———··———	Accelerometer 33 FS. 600	

FIGURE D15 FULL SCALE RESPONSE TRANSFER FUNCTIONS (DB) FOR BULKHEADS FORWARD OF F.S. 600 (RIGHT SIDE)

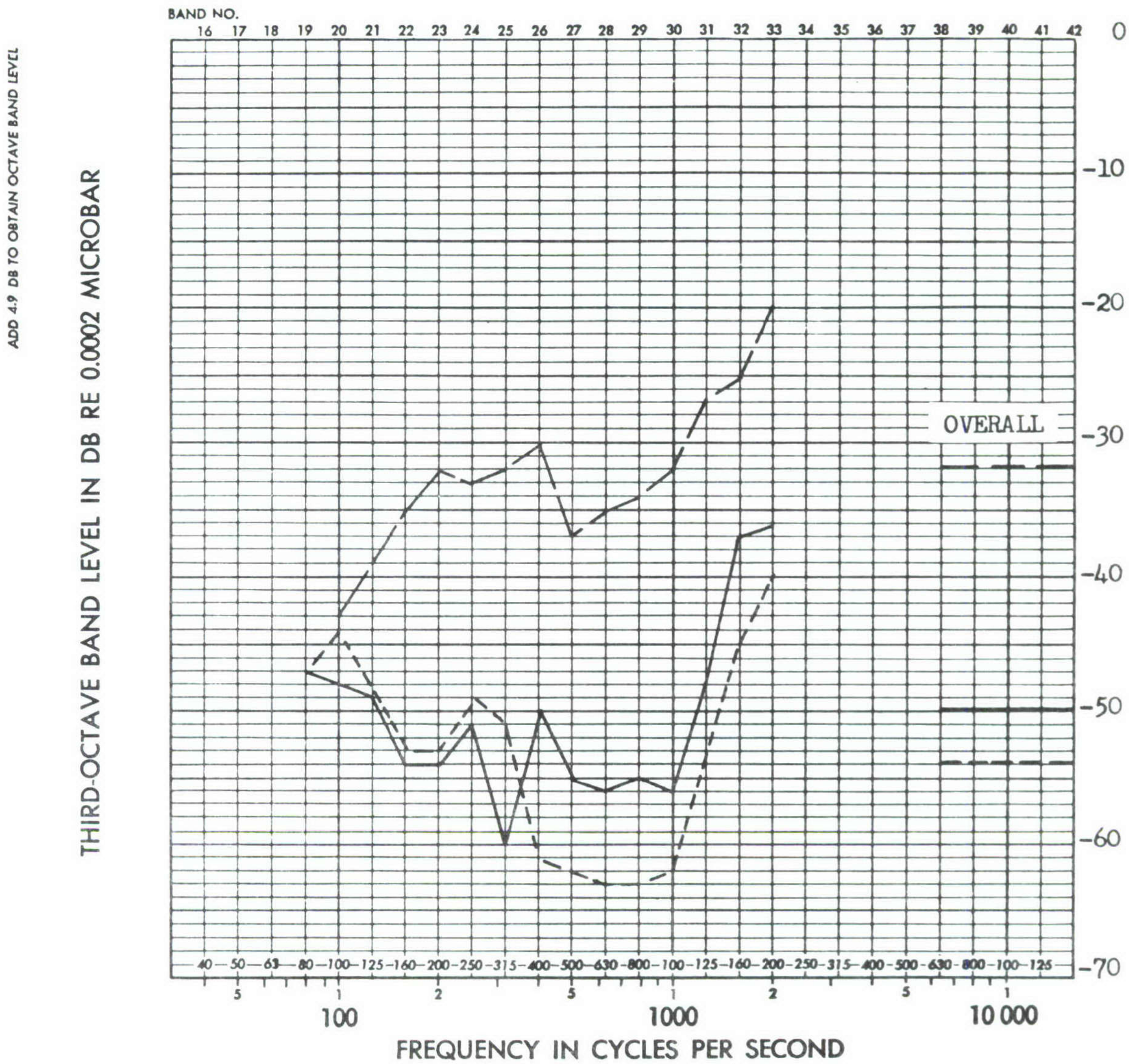

— — —	Accelerometer 20	FS. 384	Input at FS. 407
———	Accelerometer 28	FS 502	Lateral response
- - - - - -	Accelerometer 34	FS: 600	Bulkheads, left side

FIGURE D16 FULL SCALE RESPONSE TRANSFER FUNCTIONS (DB) FOR BULKHEADS FORWARD OF F.S. 600 (LEFT SIDE)

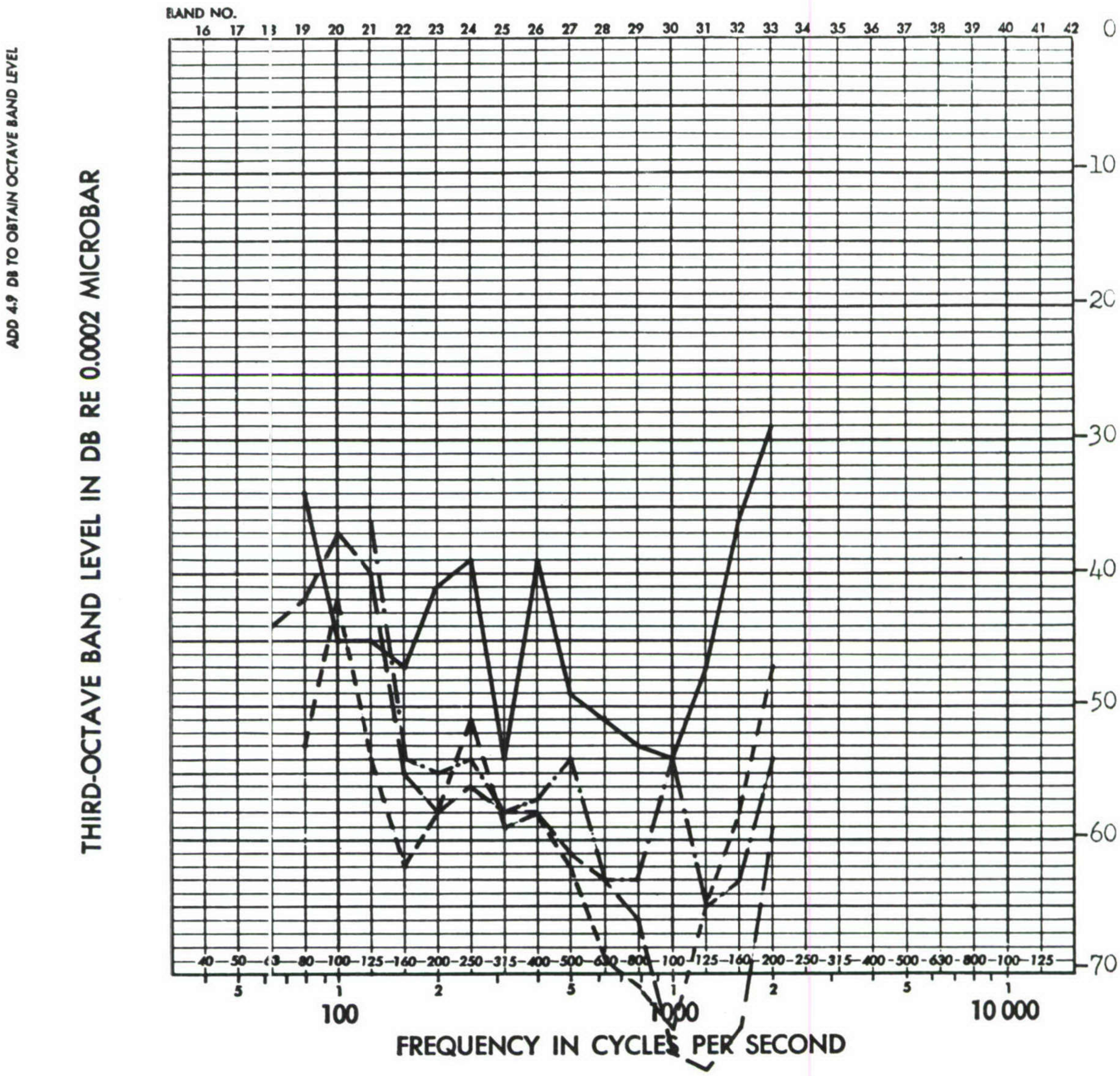

————————	Input at FS. 407
------·----	Input at FS. 568
———·———	Input at FS. 647
—— —·——	Input at FS. 738

Accelerometer 18
Lateral response
FS. 384

FIGURE D17 FULL SCALE RESPONSE TRANSFER FUNCTION (DB) FOR INTERSECTION OF FORWARD BULKHEAD AND UPPER FLOOR

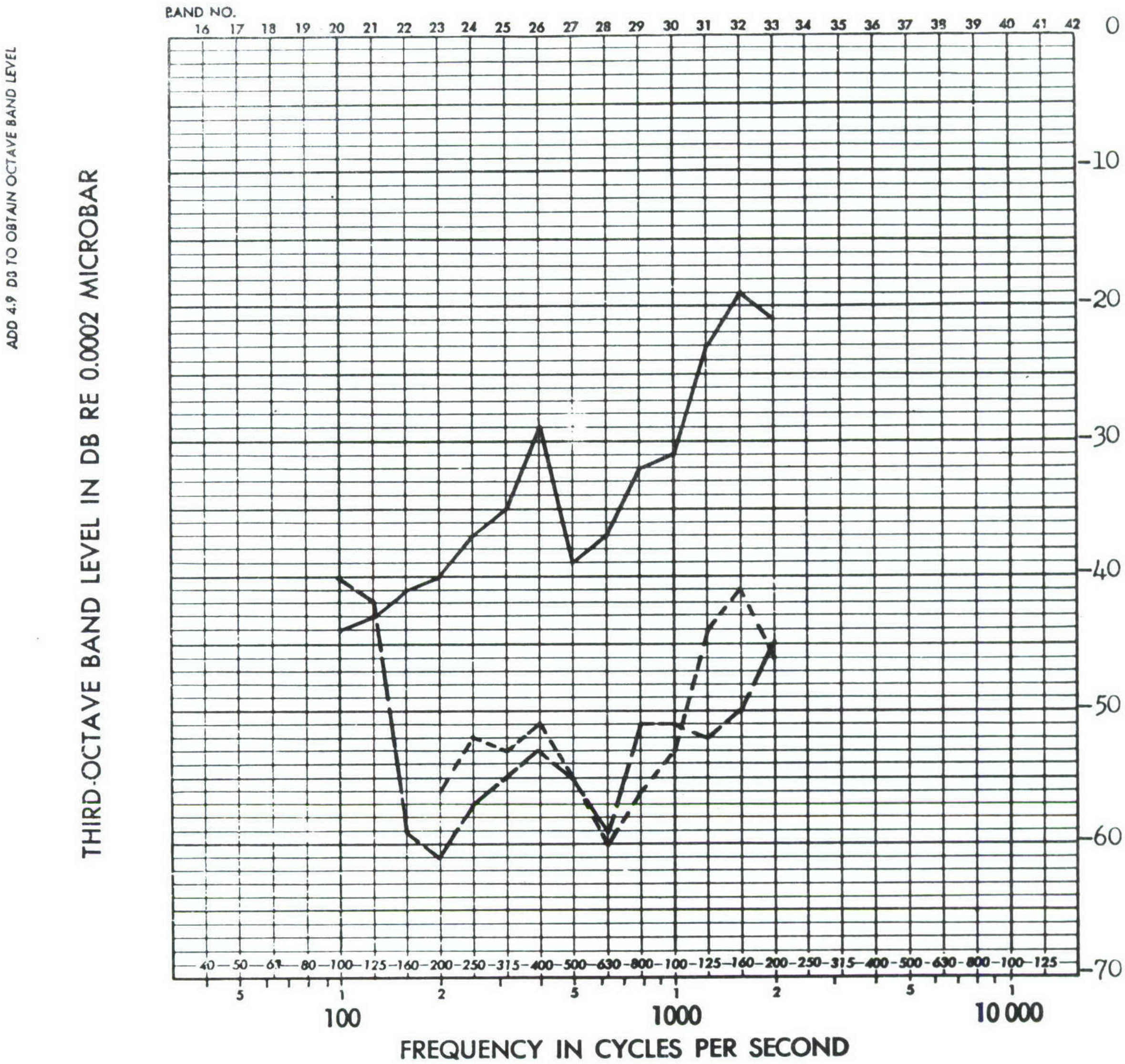

————————	Input at FS. 407	Accelerometer 19
- - - - - - - -	Input at FS. 578	Lateral response
—— —— ——	Input at FS. 738	FS. 384

FIGURE D18 FULL SCALE RESPONSE TRANSFER FUNCTION (DB) FOR RIGHT EDGE OF FORWARD BULKHEAD

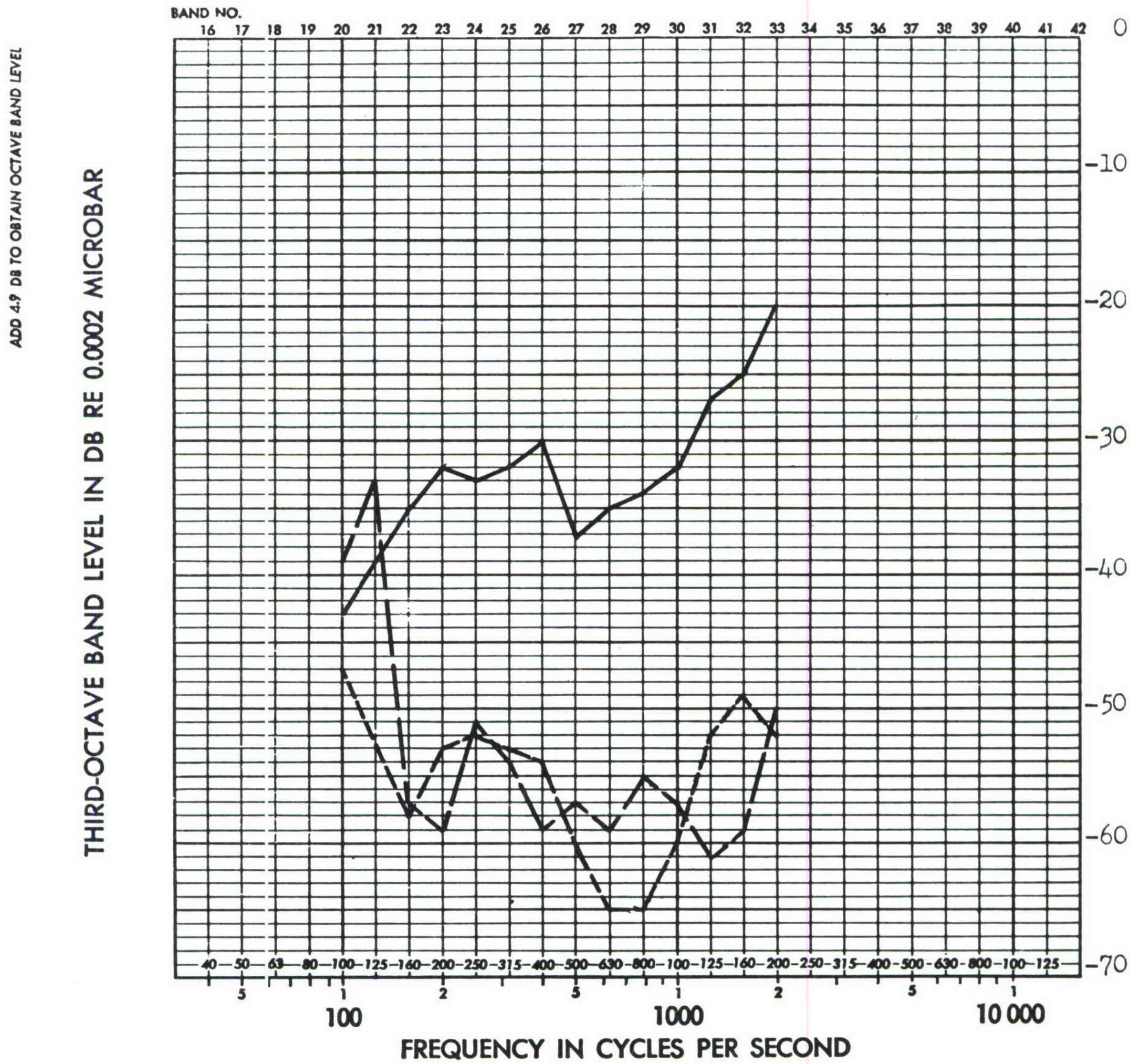

————	Input at FS. 407	Accelerometer 20
– – – – – –	Input at FS. 578	Lateral response
— — — —	Input at FS. 738	FS. 384

FIGURE D19 FULL SCALE RESPONSE TRANSFER FUNCTION (DB) FOR LEFT EDGE OF FORWARD BULKHEAD

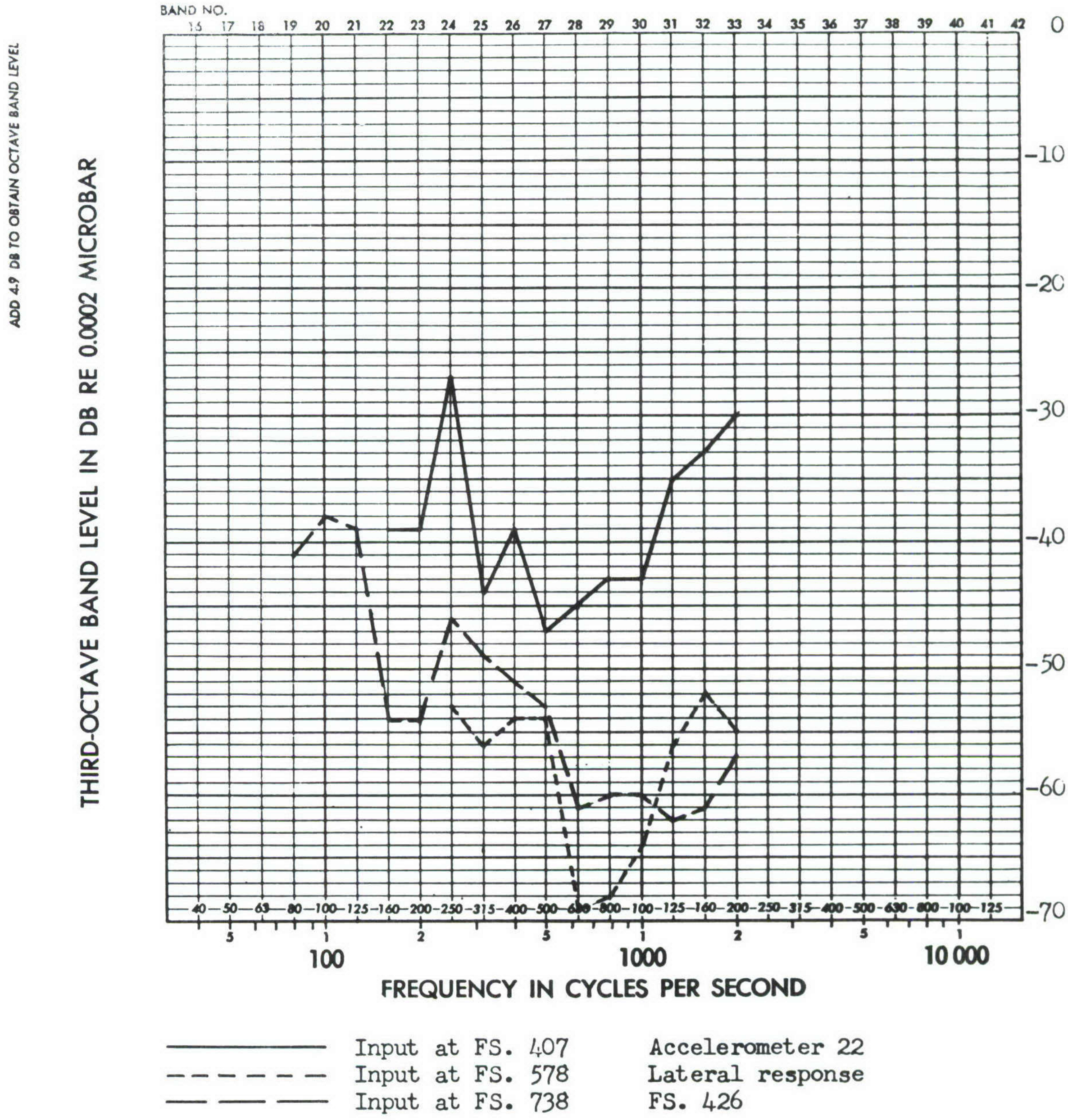

FIGURE D20 FULL SCALE RESPONSE TRANSFER FUNCTION (DB) RIGHT SIDE OF BULKHEAD, FORWARD SECTION

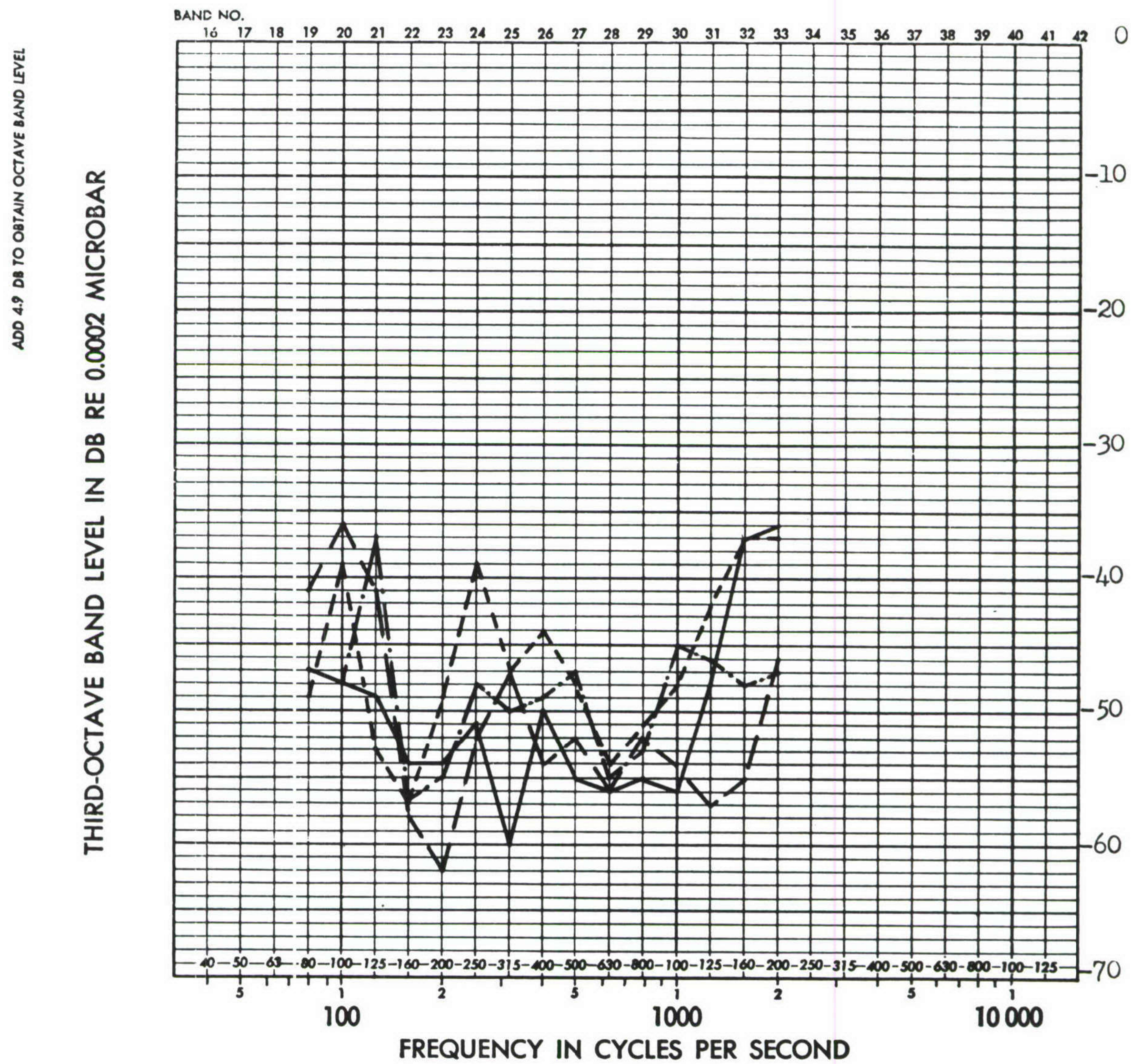

————	Input at FS. 407	Accelerometer 28
— — —·—	Input at FS. 578	Lateral response
—·—·—	Input at FS. 647	FS. 502
— — — —	Input at FS. 738	

FIGURE D21 FULL SCALE RESPONSE TRANSFER FUNCTION (DB) FOR LEFT EDGE OF BULKHEAD

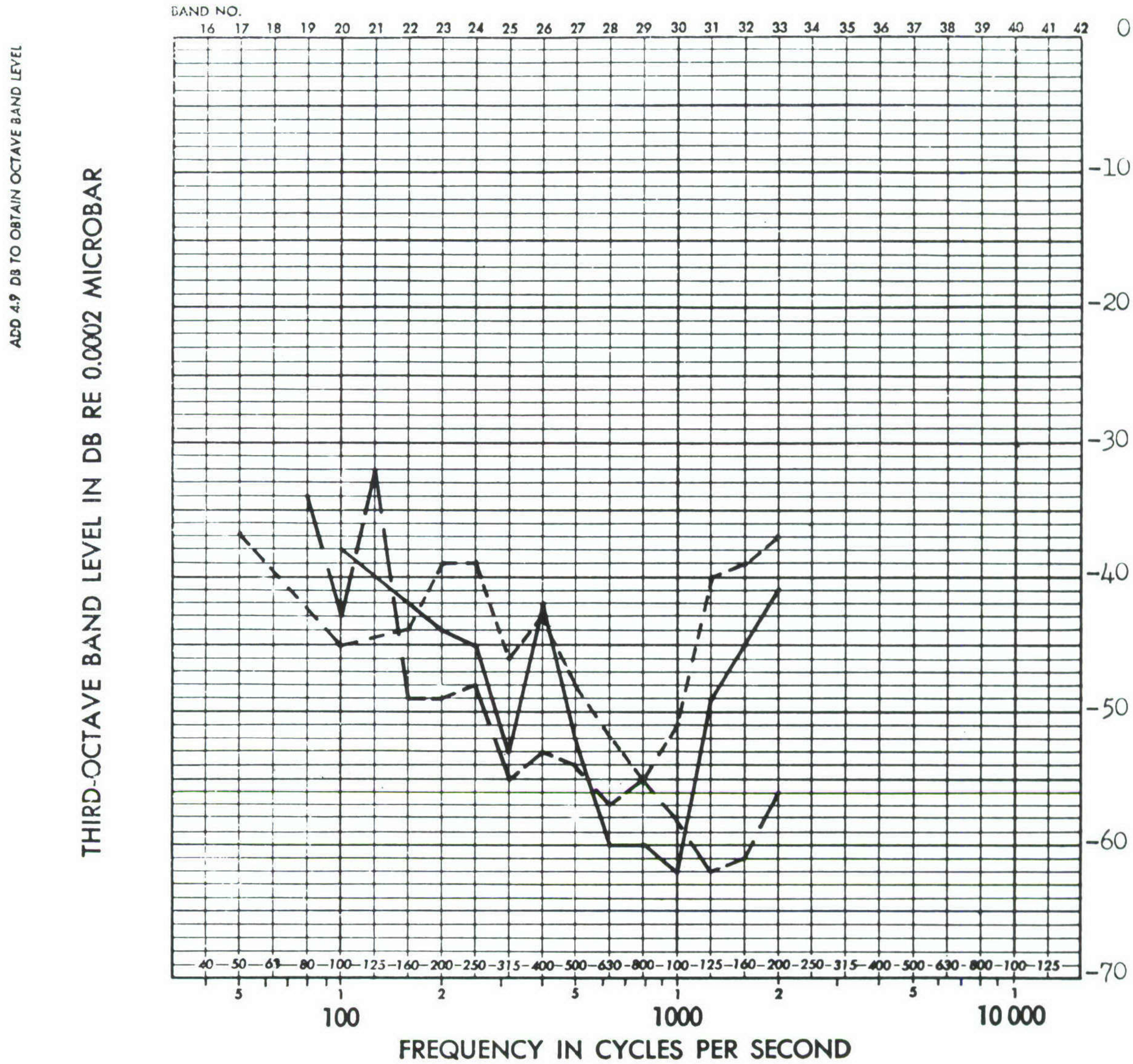

Input at FS. 407 Accelerometer 29
Input at FS. 578 Lateral response
Input at FS. 738 FS. 536
Full scale response transfer function (db) for

FIGURE D22 FULL SCALE RESPONSE TRANSFER FUNCTION (DB) FOR RIGHT EDGE OF BULKHEAD

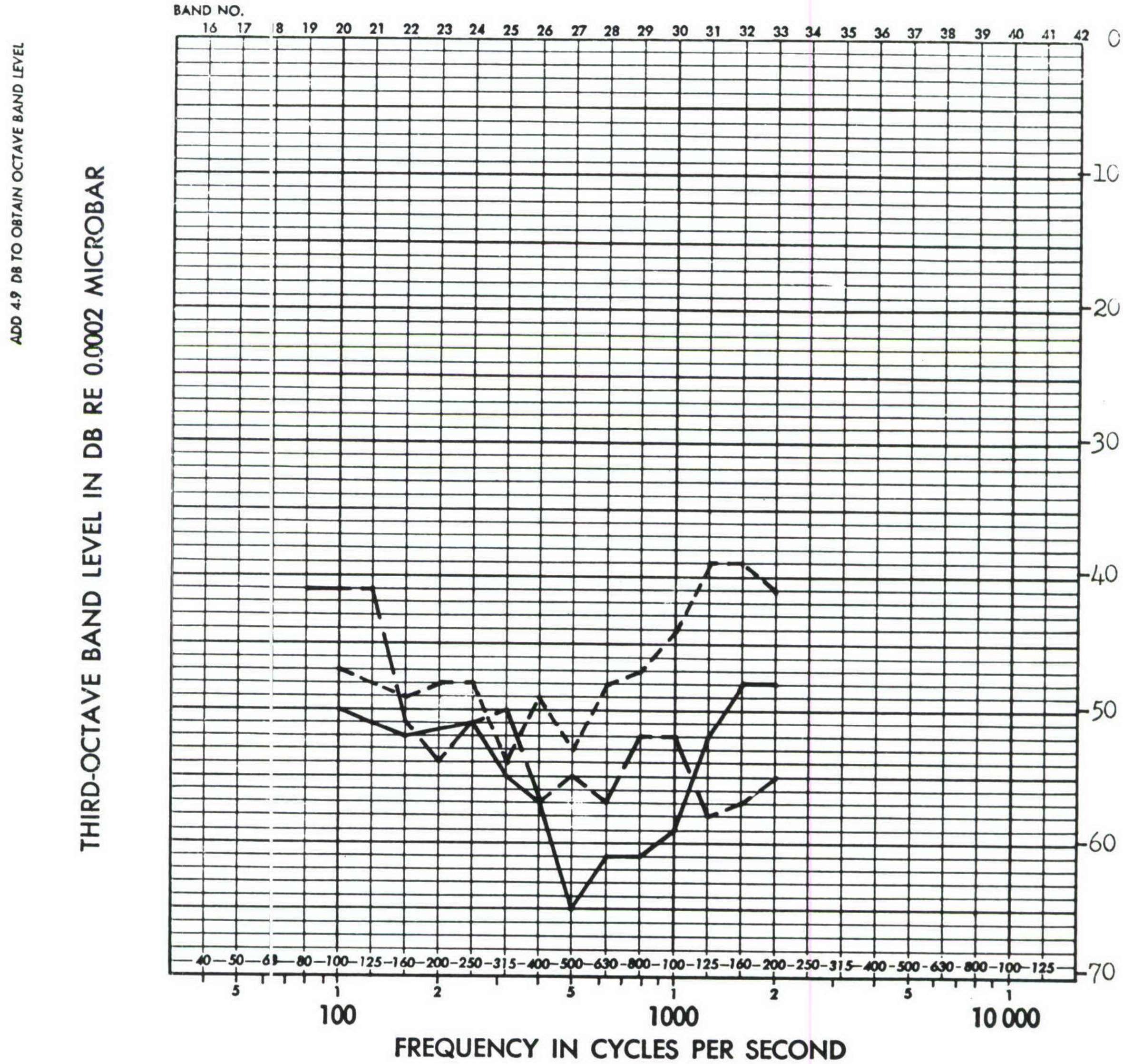

Input at FS. 407 — Accelerometer 33
Input at FS. 578 — Lateral response
Input at FS. 738 — FS. 600

FIGURE D23 FULL SCALE RESPONSE TRANSFER FUNCTION (DB) FOR RIGHT EDGE OF BULKHEAD, FORWARD SECTION

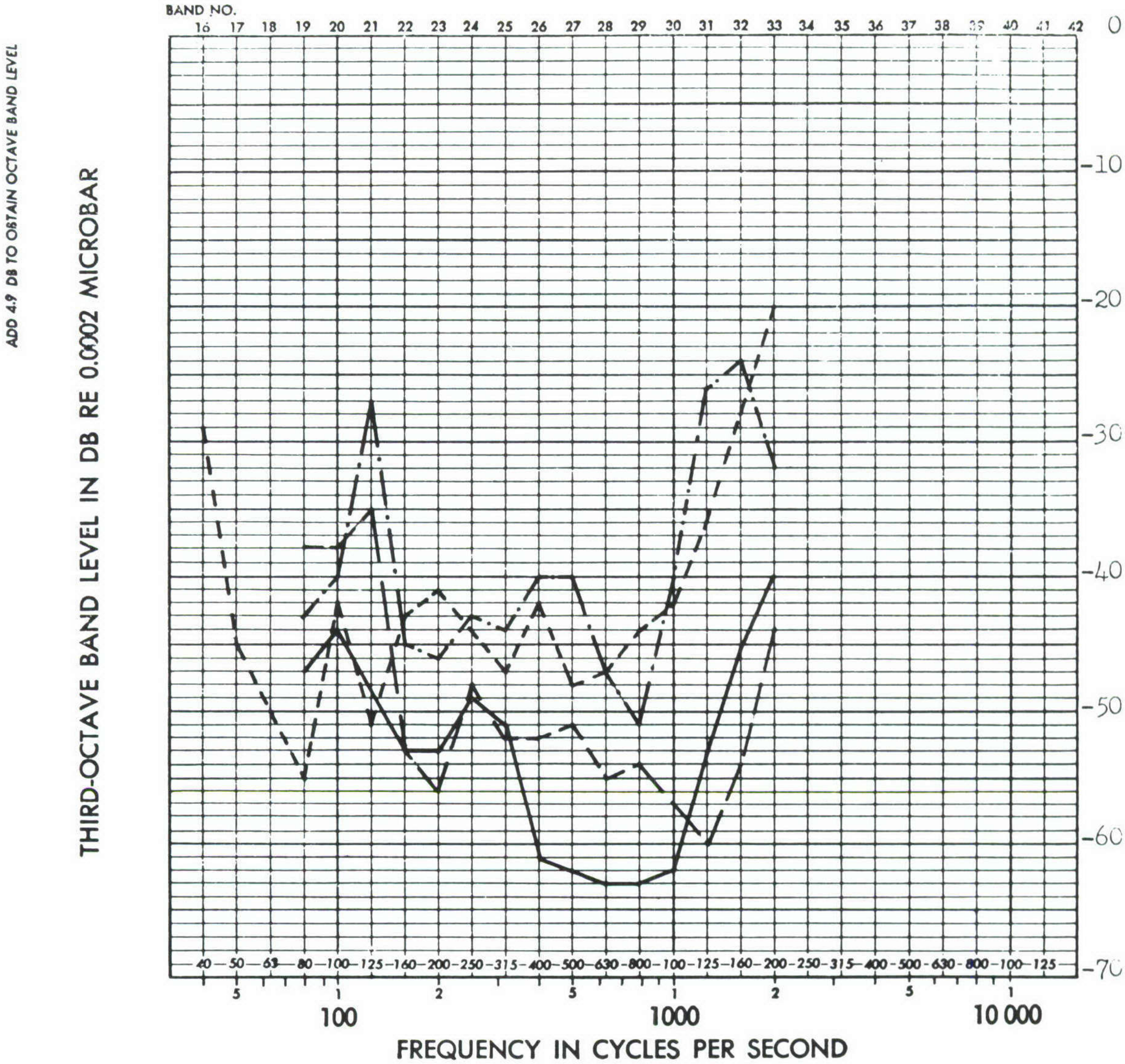

Input at FS. 407
Input at FS. 578
Input at FS. 647
Input at FS. 738

Accelerometer 34
Lateral response
FS. 600

FIGURE D24 FULL SCALE RESPONSE TRANSFER FUNCTION (DB) FOR LEFT EDGE OF BULKHEAD

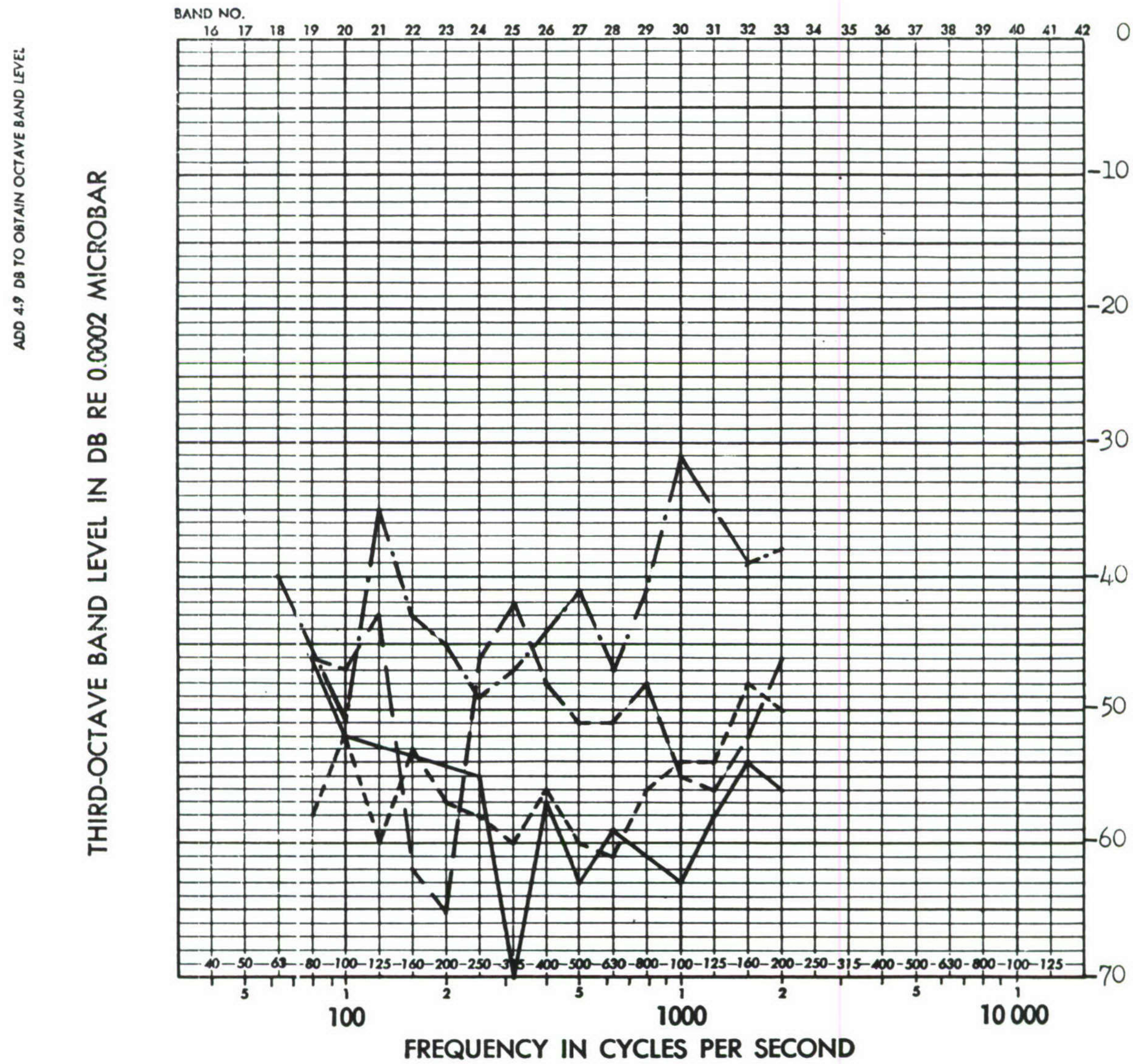

————————	Input at FS. 407	Accelerometer 39
- - - - - - - -	Input at FS. 568	Lateral response
——·——·——	Input at FS. 647	FS. 647
—— —— ——	Input at FS. 738	PATRICK ACCELEROMETER

FIGURE D25 FULL SCALE RESPONSE TRANSFER FUNCTION (DB) FOR INTERSECTION OF UPPER LEFT LONGERON AND BULKHEAD

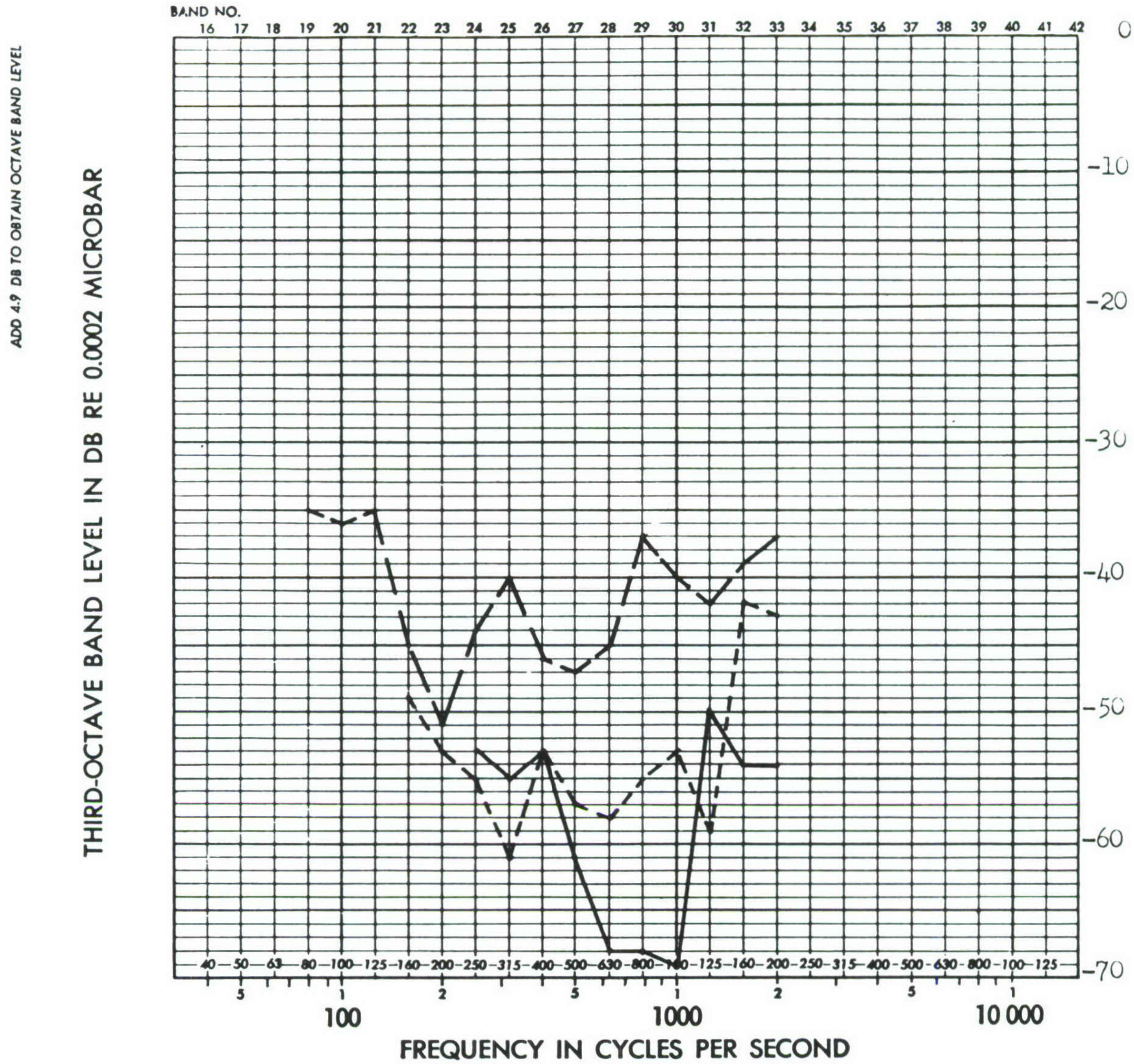

Input at FS. 407 — Accelerometer 43

Input at FS. 578 — Lateral response

Input at FS. 738 — FS. 675

FIGURE D26 FULL SCALE RESPONSE TRANSFER FUNCTION (DB) FOR LEFT EDGE OF AFT FLOOR

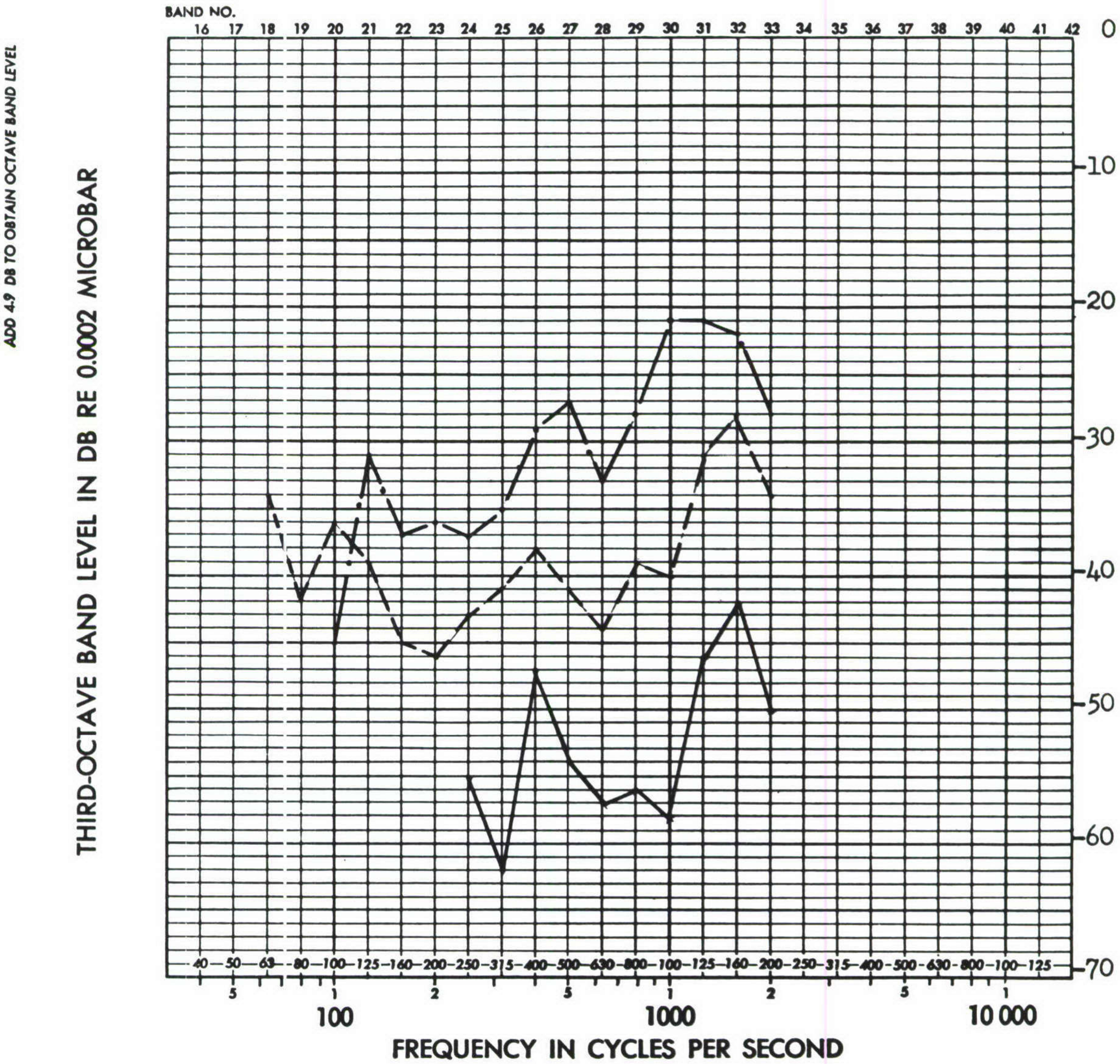

Input at FS. 407 — Accelerometer 79
Input at FS. 578 — Radial response
Input at FS. 647 — FS. 706

FIGURE D27 FULL SCALE RESPONSE TRANSFER FUNCTION (DB) FOR UPPER LEFT EDGE OF BULKHEAD

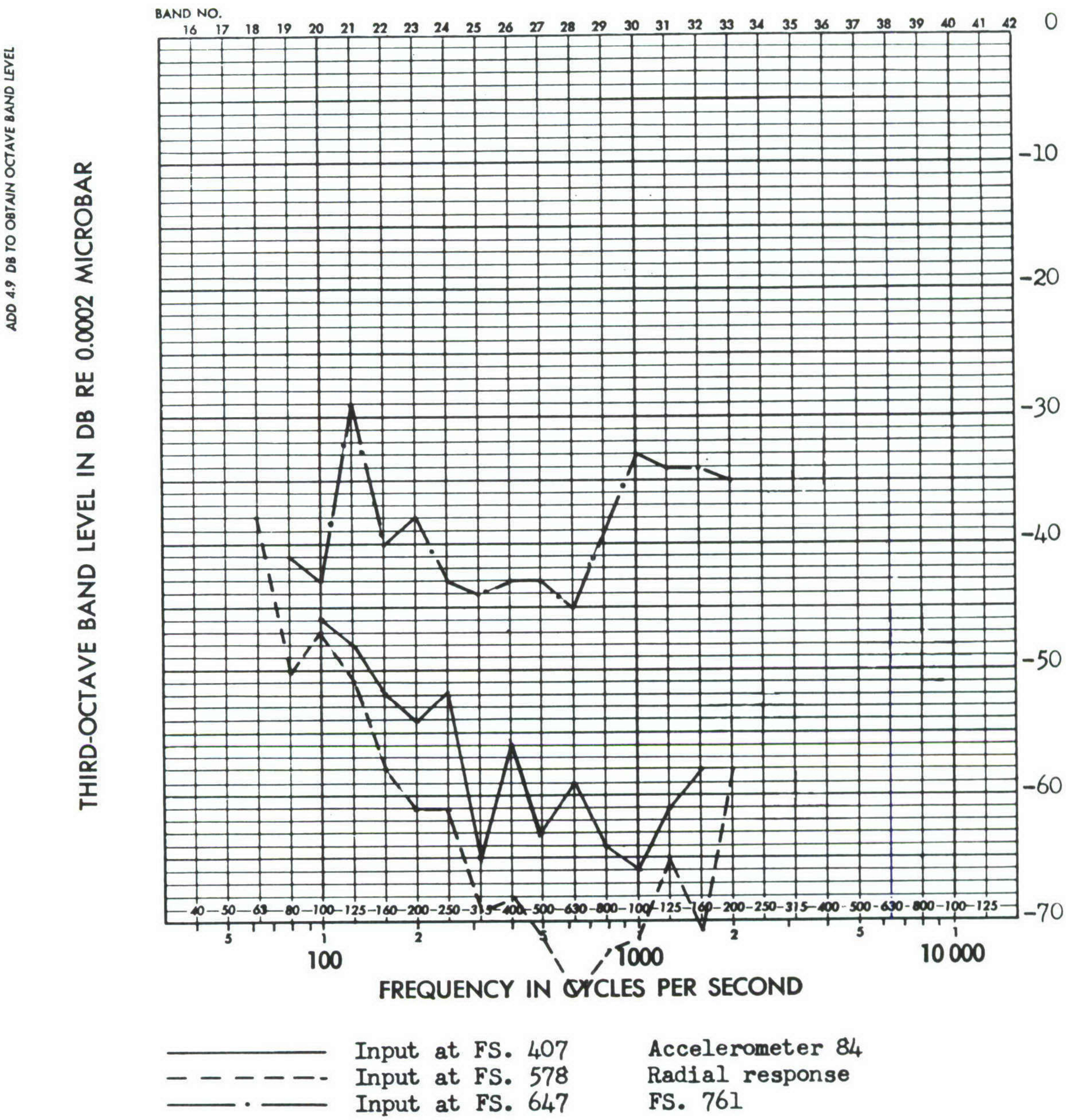

FIGURE D28 FULL SCALE RESPONSE TRANSFER FUNCTION (DB) UPPER LEFT EDGE OF AFT BULKHEAD

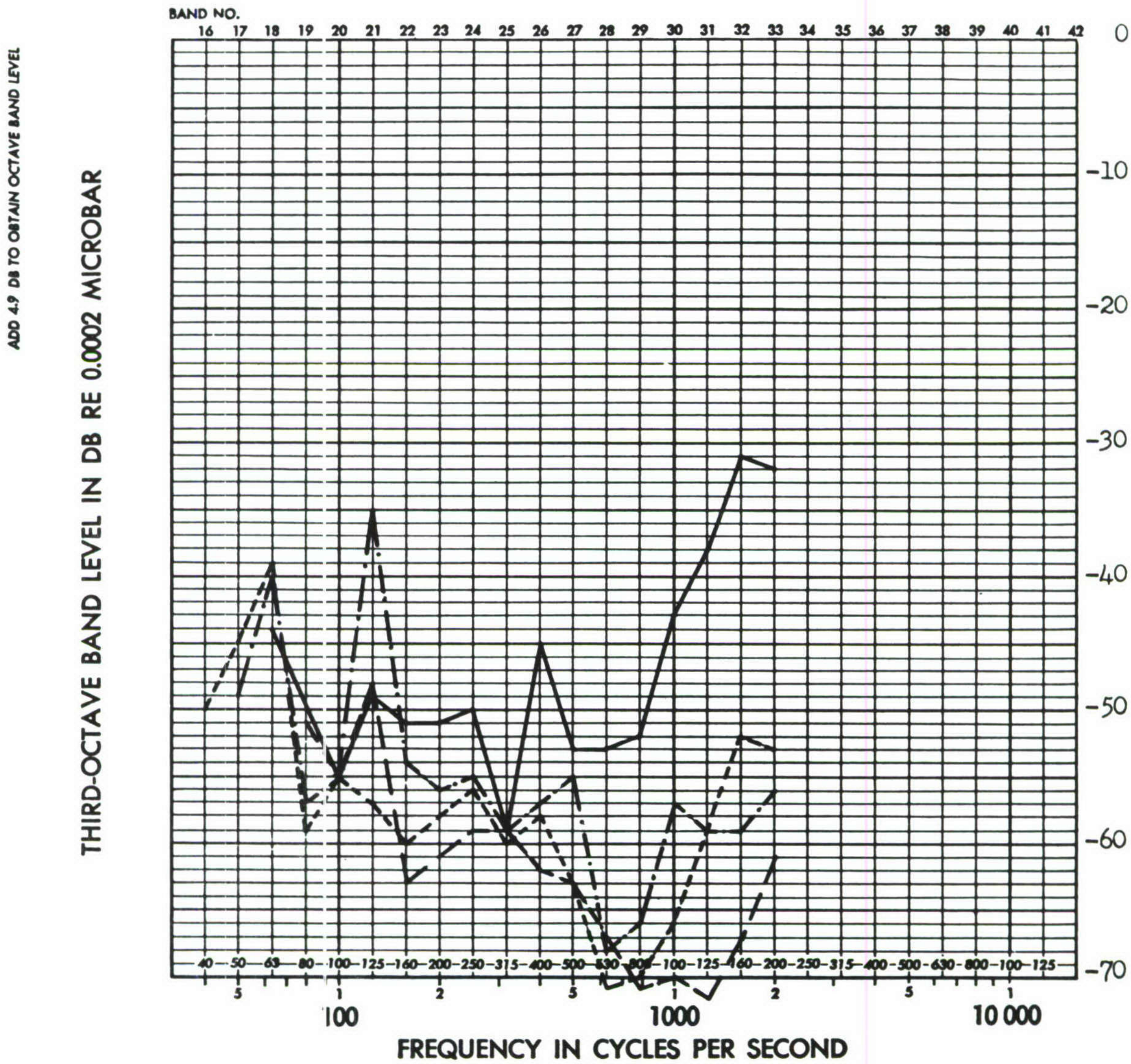

Input at FS. 407
Input at FS. 578
Input at FS. 647
Input at FS. 738

Accelerometer 8
Vertical response
FS. 384

FIGURE D29 FULL SCALE RESPONSE TRANSFER FUNCTION (DB) FOR INTERSECTION OF FORWARD BULKHEAD AND UPPER FLOOR

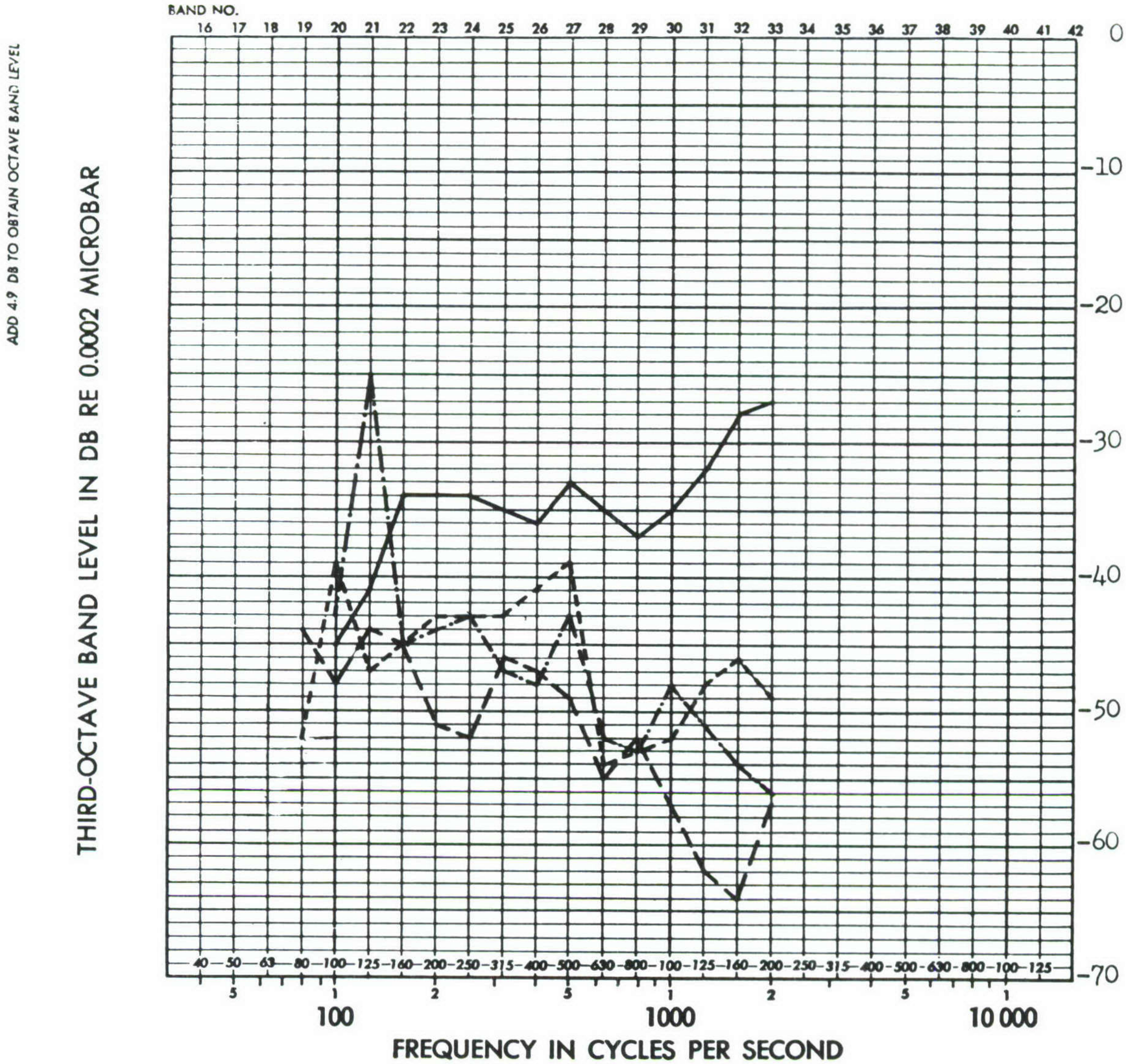

Input at FS. 407 Accelerometer 11
Input at FS. 578 Vertical response
Input at FS. 647 FS. 463
Input at FS. 738 Patrick Accelerometer

FIGURE D30 FULL SCALE RESPONSE TRANSFER FUNCTION (DB) FOR FORWARD FLOOR NEAR INTERSECTION OF FLOOR, UPPER LEFT LONGERON AND DOUBLE BULKHEAD

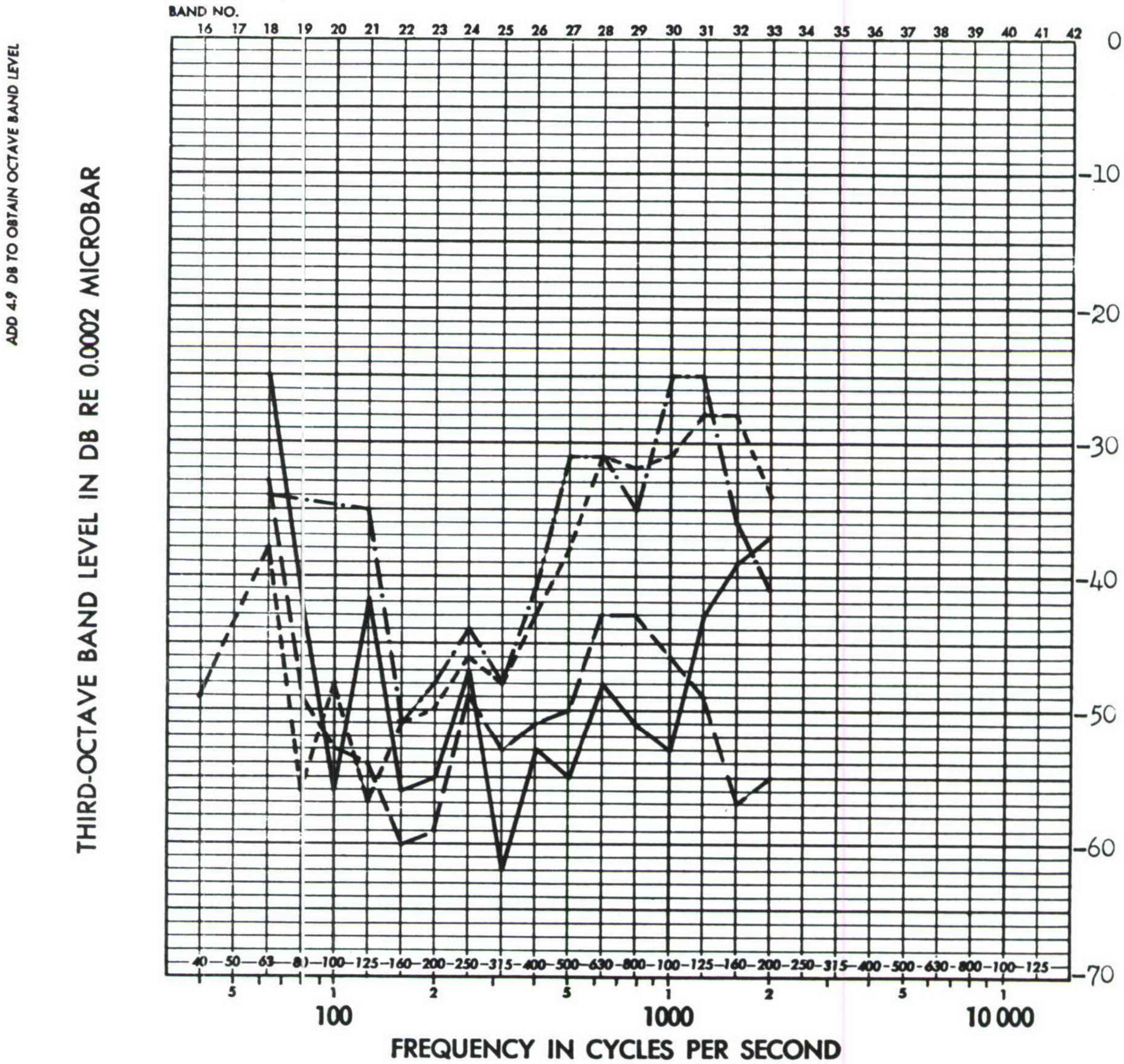

———————— Input at FS. 407	Accelerometer 13
- - - - - - - - Input at FS. 578	Vertical Response
——·——·— Input at FS. 647	FS. 600
—— —— —— Input at FS. 738	Patrick Accelerometer

FIGURE D31 FULL SCALE RESPONSE TRANSFER FUNCTIONS (DB) FOR UPPER LEFT LONGERON, BULKHEAD INTERSECTION

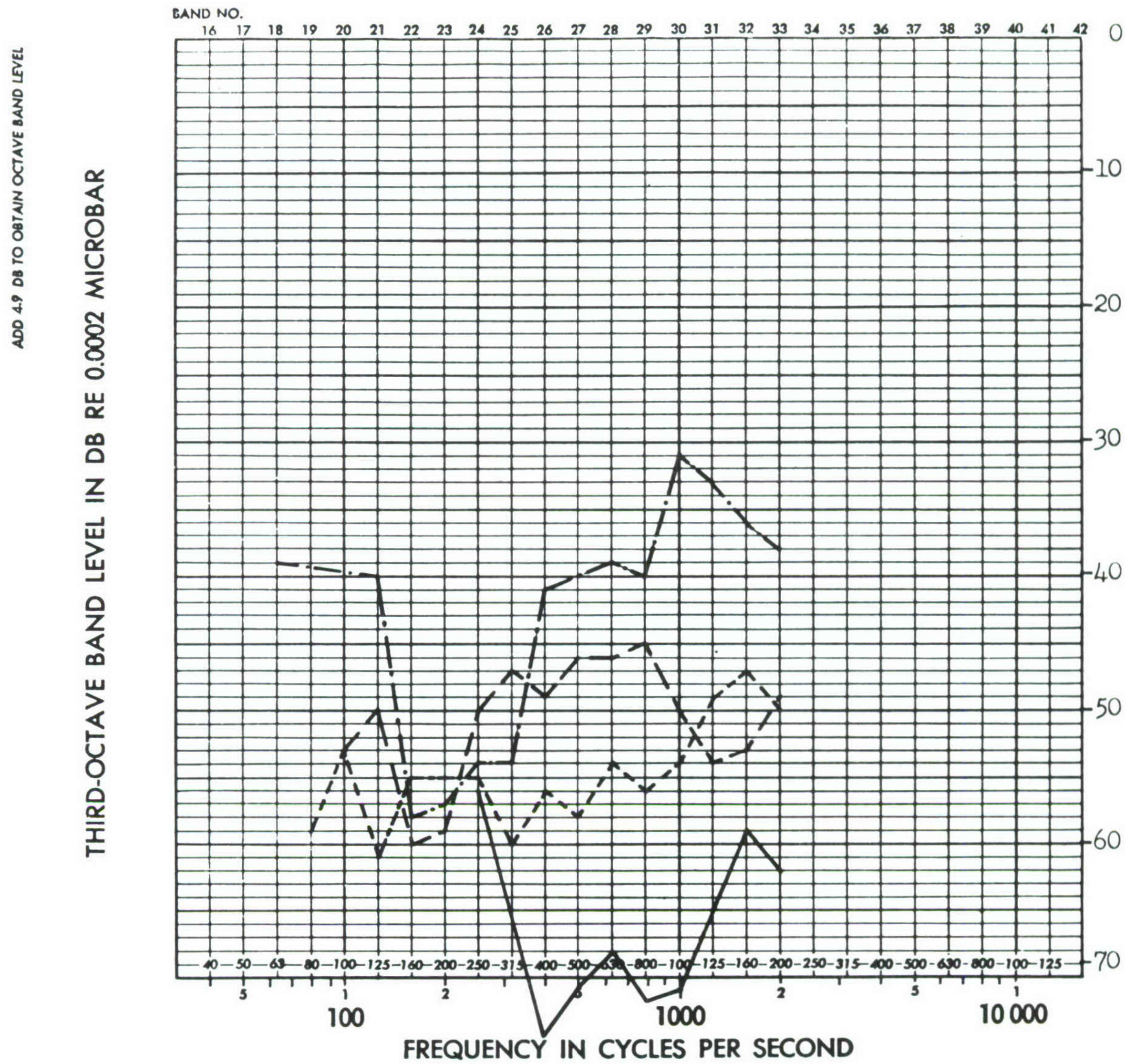

————————	Input at FS. 407	Accelerometer 14
- - - - - - - -	Input at FS. 578	Vertical response
— · — · —	Input at FS. 647	FS. 647
—— —— ——	Input at FS. 738	Patrick Accelerometer

FIGURE D32 FULL SCALE RESPONSE TRANSFER FUNCTION (DB) FOR INTERSECTION OF LEFT (UPPER) LONGERON AND BULKHEAD

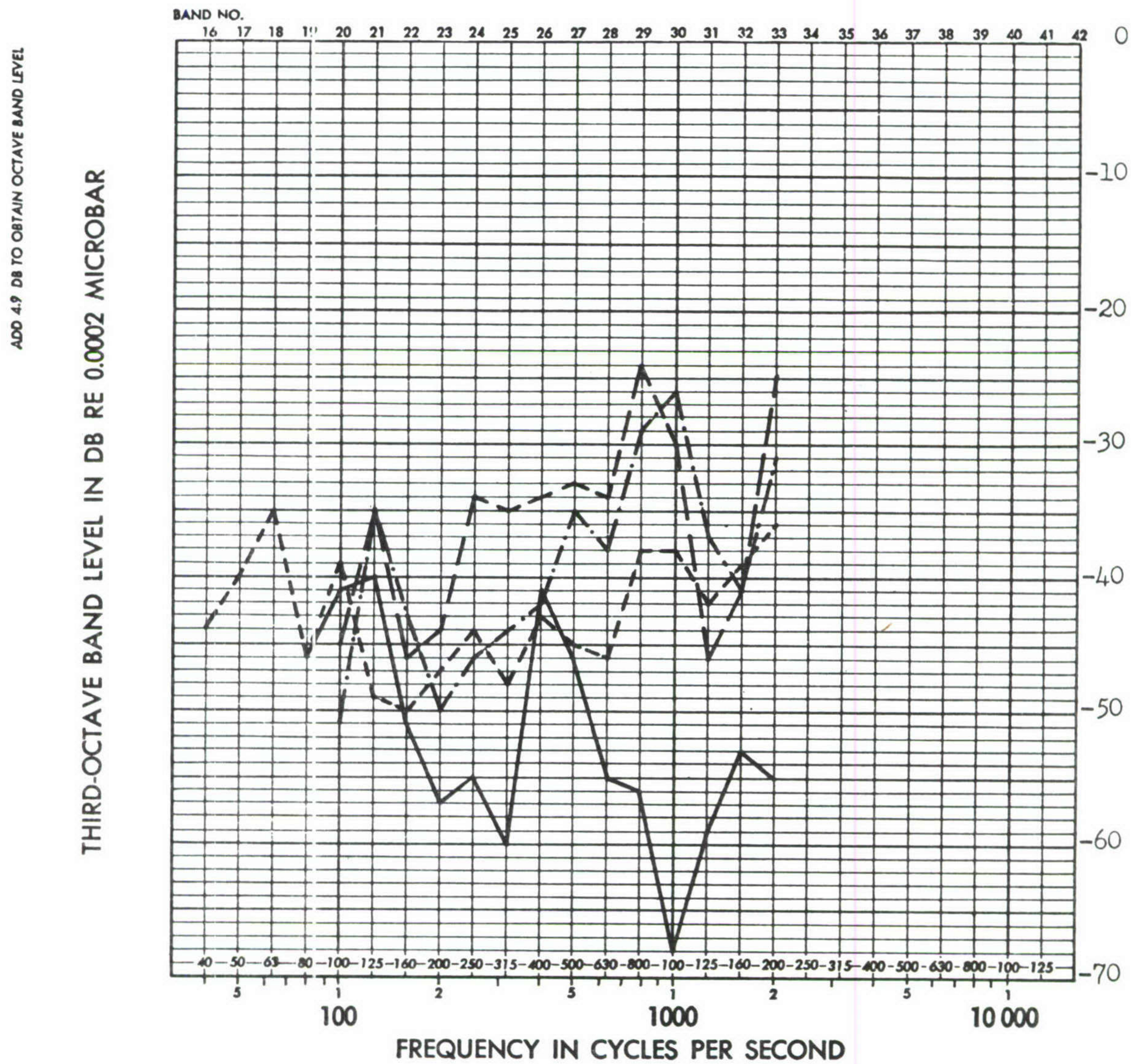

————————	Input at FS. 407	Accelerometer 16
— — — — — —	Input at FS. 578	Vertical response
——— · ———	Input at FS. 647	FS. 761
——— ——— ·—	Input at FS. 738	

FIGURE D33 FULL SCALE RESPONSE TRANSFER FUNCTION (DB) FOR TOP CENTER OF MOST AFT BULKHEAD

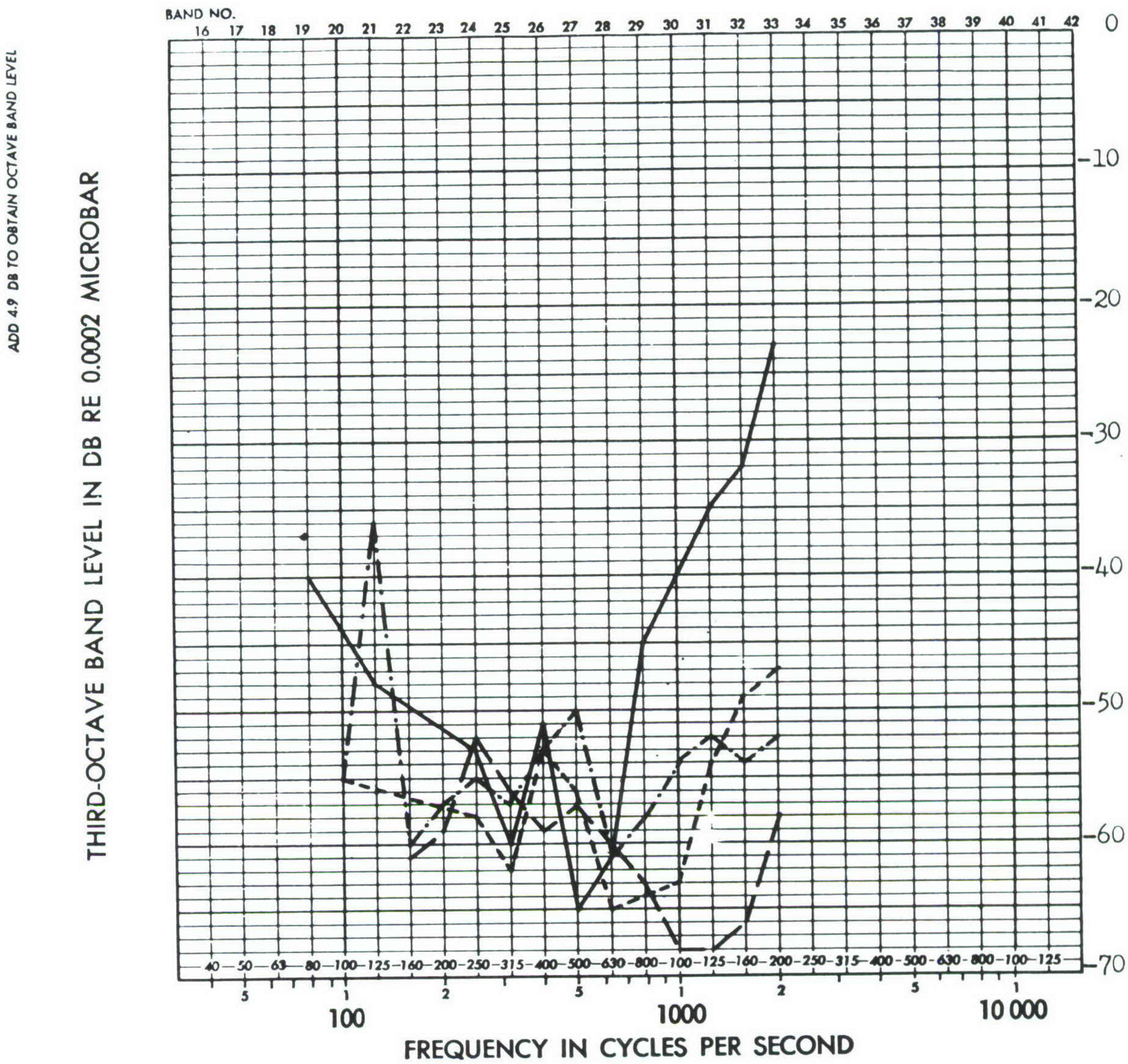

Input at FS. 407
Input at FS. 578
Input at FS. 642
Input at FS. 738

Accelerometer 1
Longitudinal Response
FS. 384

FIGURE D34 FULL SCALE RESPONSE TRANSFER FUNCTIONS (DB) FOR INTERSECTION OF FORWARD BULKHEAD AND UPPER FLOOR

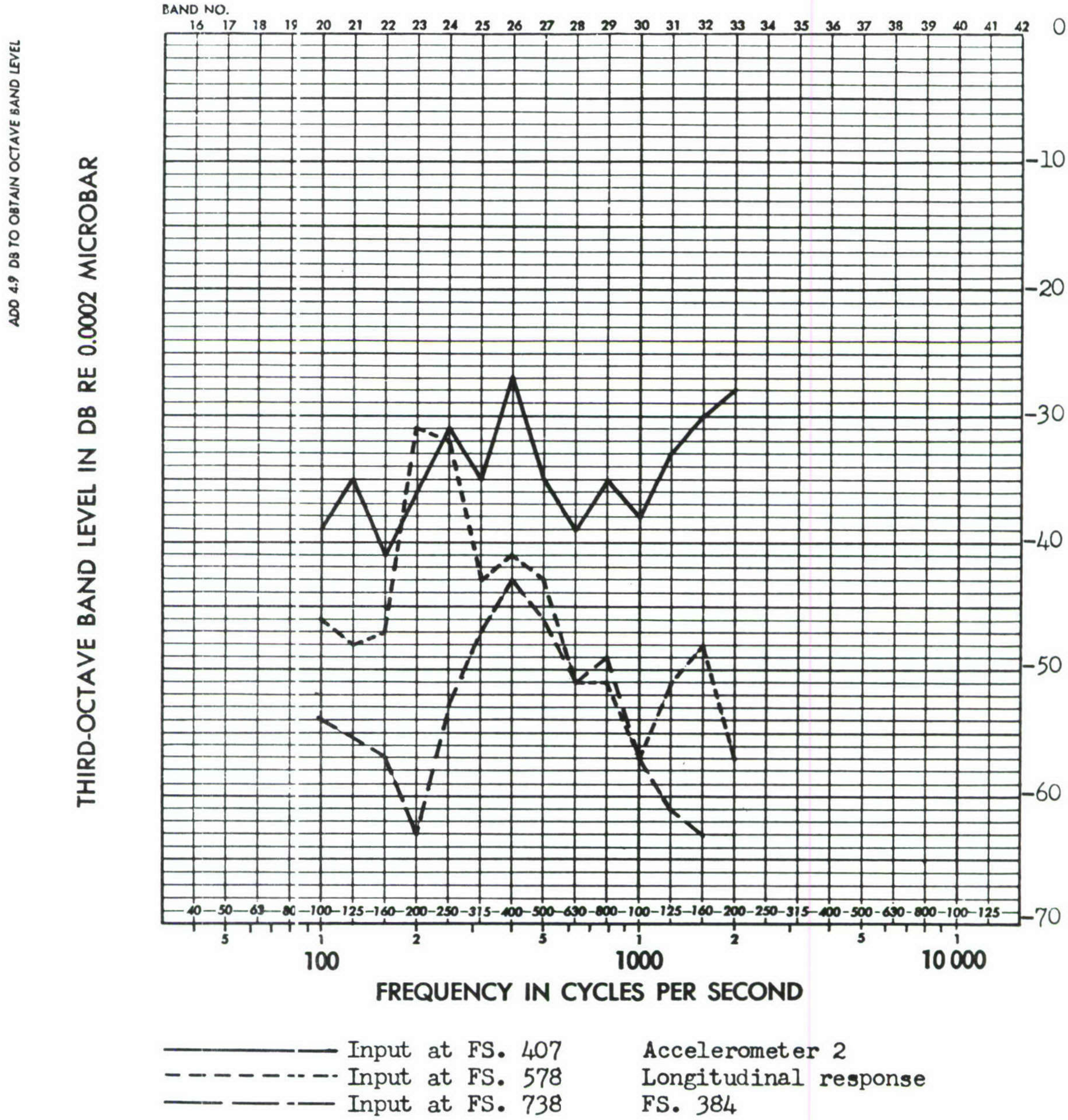

FIGURE D35 FULL SCALE RESPONSE TRANSFER FUNCTION (DB) FOR CENTER OF FORWARD BULKHEAD, LIGHT SKIN BETWEEN STIFFENERS

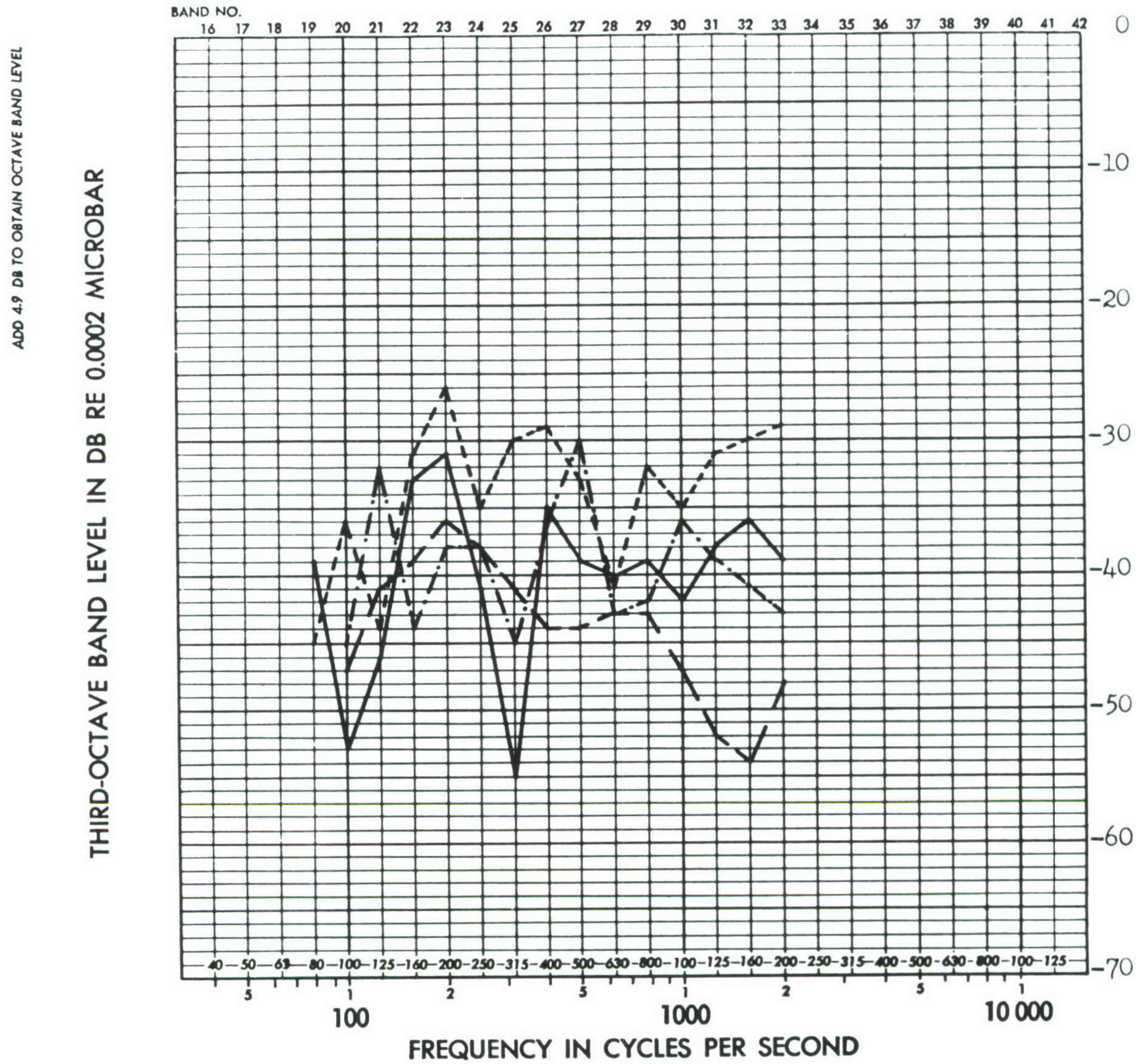

——————— Input at FS. 407	Accelerometer 3
– – – – – – – Input at FS. 568	Longitudinal response
———— · ———— Input at FS. 647	FS. 536
——— ——— ——— Input at FS. 738	

FIGURE D36 FULL SCALE RESPONSE TRANSFER FUNCTION (DB) FOR CENTER OF BULKHEAD

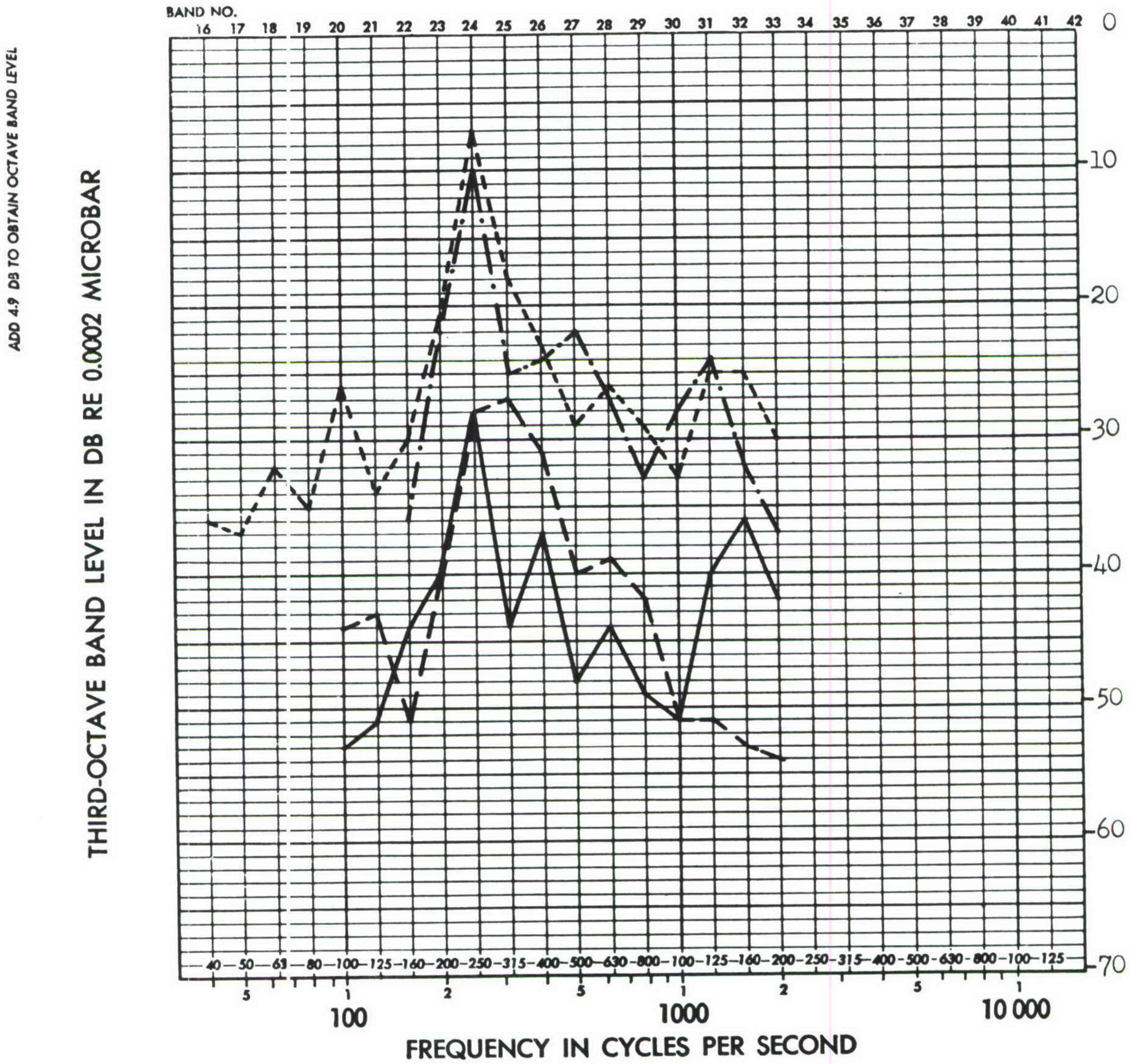

———————	Input at FS. 407	Accelerometer 4
– – – – - – – –	Input at FS. 578	Longitudinal response
—— · ——— · ——	Input at FS. 647	FS. 600
—— —— ——	Input at FS. 738	Patrick accelerometer

FIGURE D37 FULL SCALE RESPONSE TRANSFER FUNCTION (DB) FOR INTERSECTION OF UPPER LEFT LONGERON AND BULKHEAD

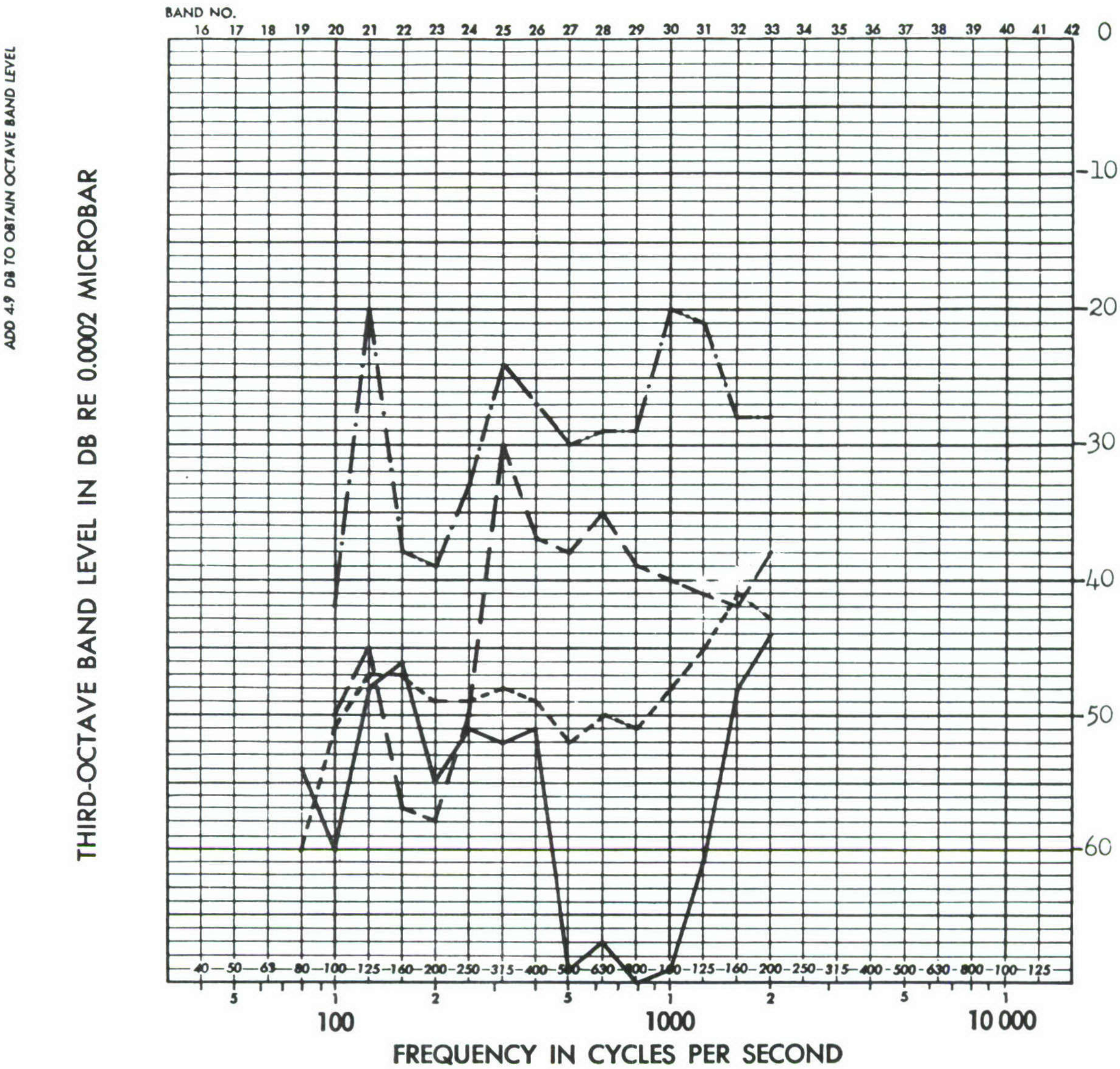

————————	Input at FS. 407	Accelerometer 5
- - - - - - - -	Input at FS. 568	Longitudinal
——·——·—	Input at FS. 647	FS. 647
—— —— ——	Input at FS. 738	Patrick Accelerometer

FIGURE D38 FULL SCALE RESPONSE TRANSFER FUNCTION (DB) FOR INTERSECTION OF UPPER LEFT LONGERON AND BULKHEAD

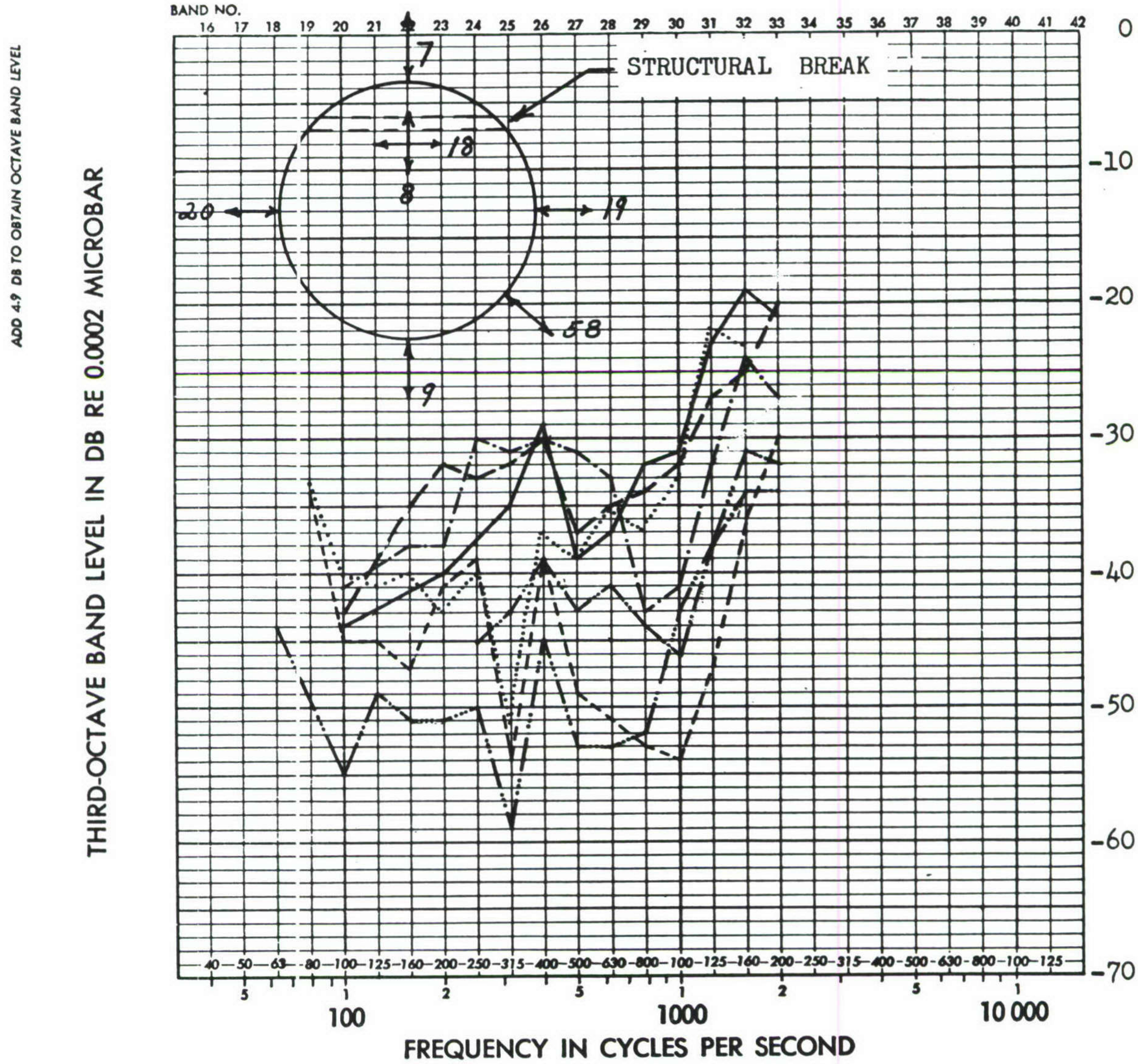

Accelerometer 7
Accelerometer 8
Accelerometer 9
Accelerometer 18
Accelerometer 19
Accelerometer 20
Accelerometer 58

Input FS 407

FIGURE D39 FULL SCALE RESPONSE TRANSFER FUNCTIONS (DB) FOR THE FORWARD BULKHEAD AT F.S. 384, EXCITATION AT F.S. 407

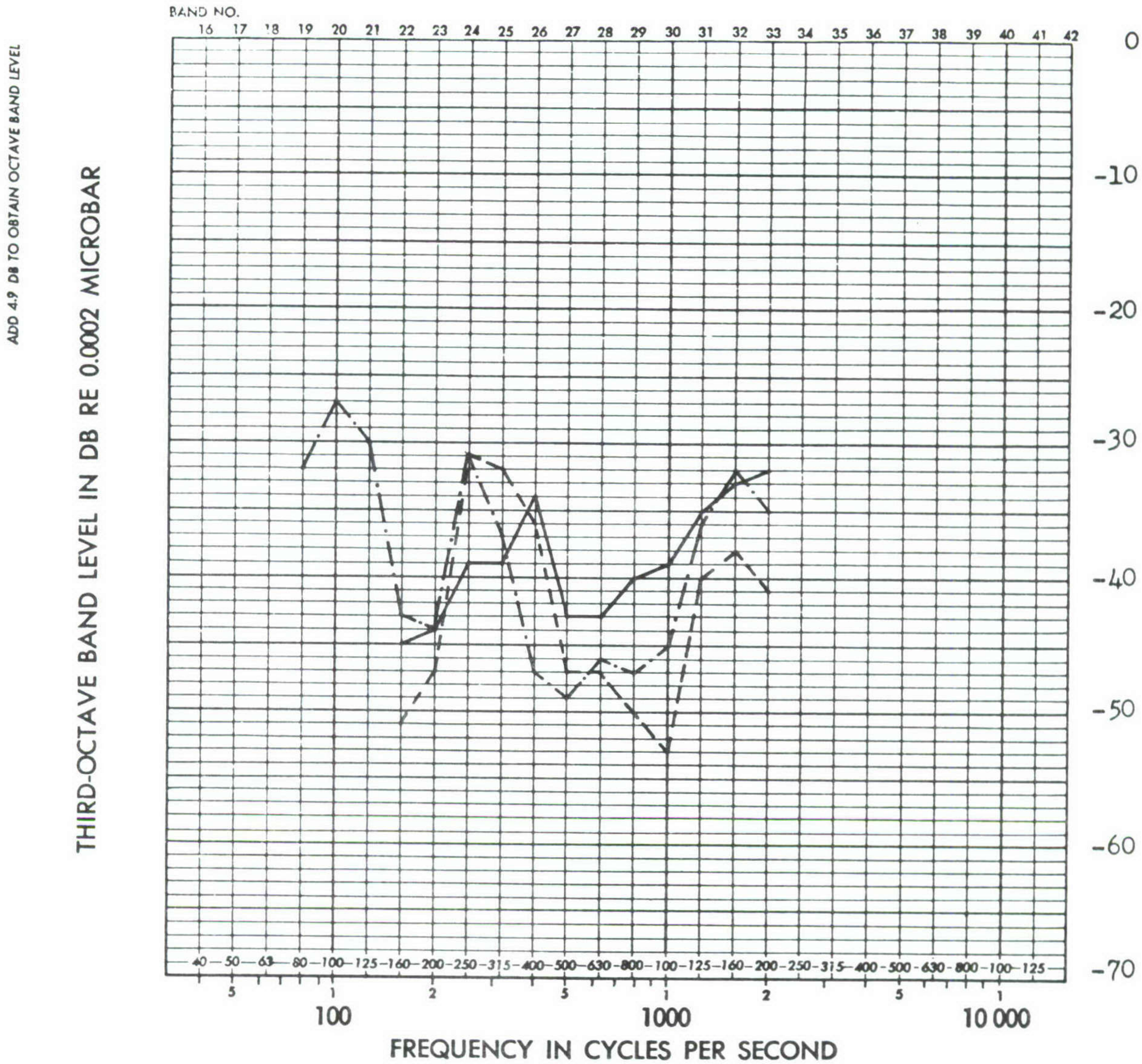

————	Accelerometer 61	Input FS 407
— — — —	Accelerometer 68	Upper left longeron
——·——	Accelerometer 71	Radial response

FIGURE D40 FULL SCALE RESPONSE TRANSFER FUNCTIONS (DB) FOR UPPER LEFT LONGERON, RADIAL RESPONSE MEASURED BETWEEN ADJACENT BULKHEADS

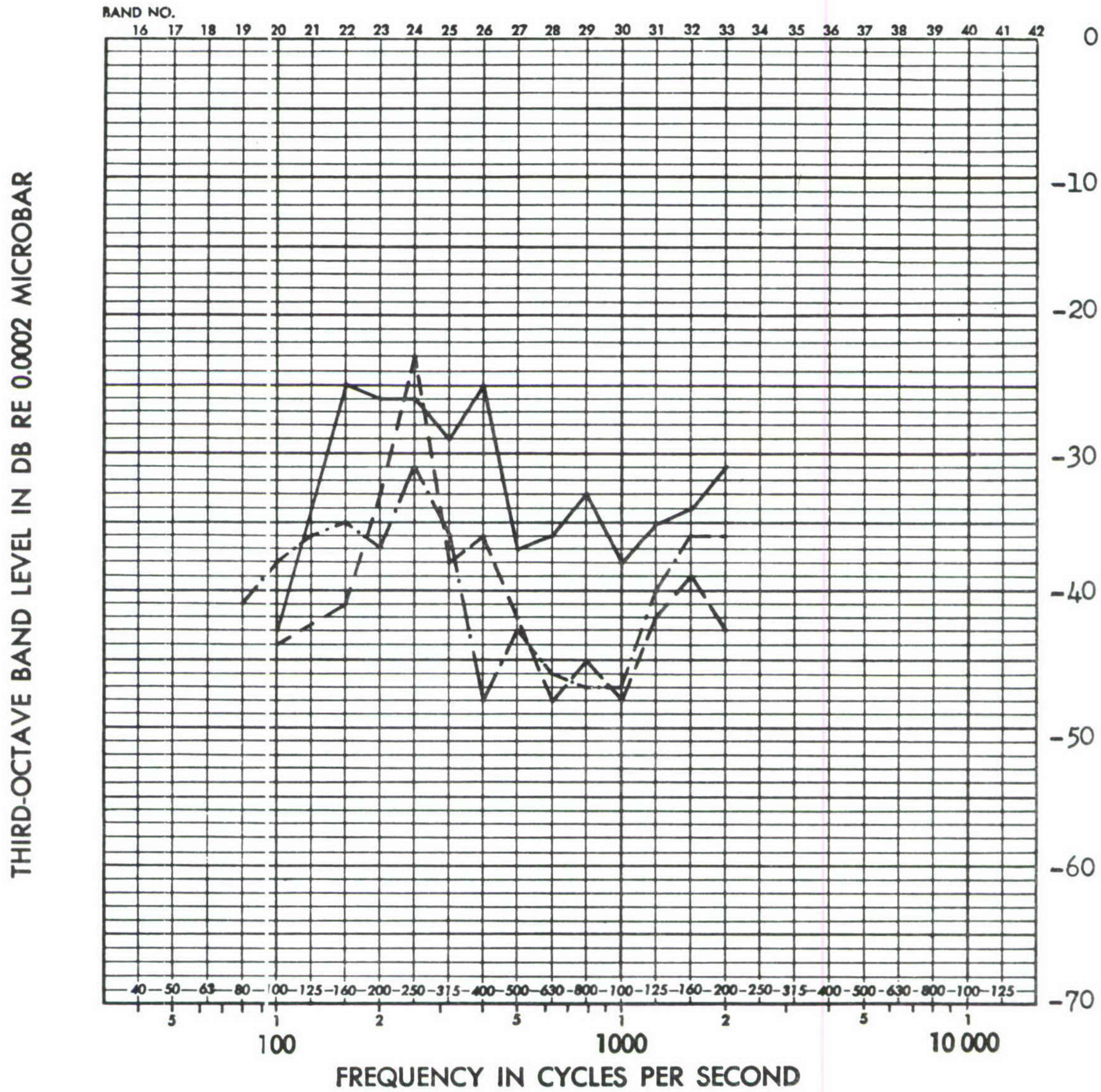

———	Accelerometer 63	Input FS 407
— — —	Accelerometer 66	Lower left longeron
—·—	Accelerometer 72	Radial response

FIGURE D41 FULL SCALE RESPONSE TRANSFER FUNCTIONS (DB) FOR LOWER LEFT LONGERON, MEASURED BETWEEN ADJACENT BULKHEADS

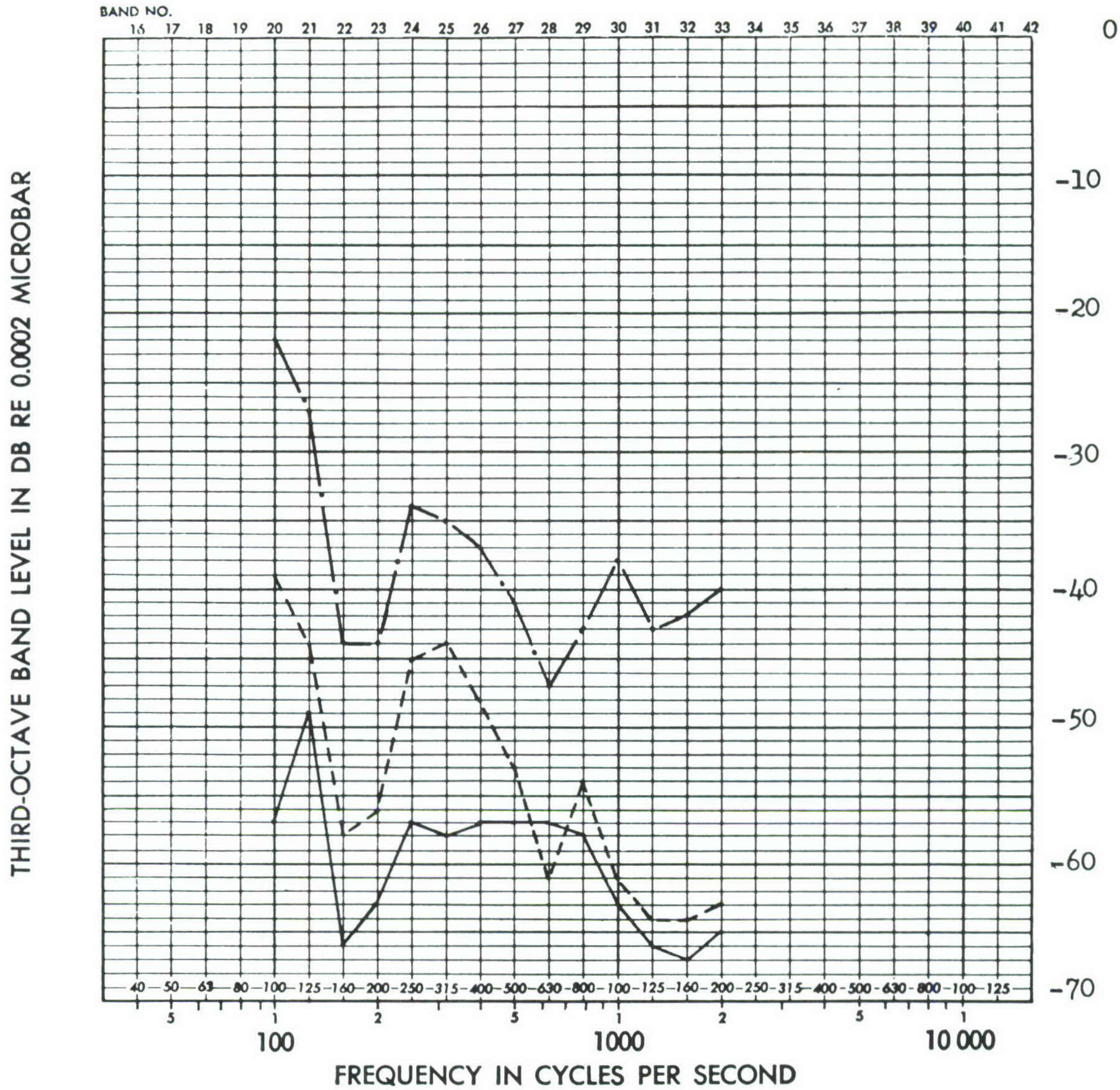

————	Accelerometer 61	Input FS 738
– – – –	Accelerometer 68	Upper left longeron
—·—	Accelerometer 71	Radial response

FIGURE D42 FULL SCALE RESPONSE TRANSFER FUNCTIONS (DB) FOR UPPER LEFT LONGERON, RADIAL RESPONSE MEASURED BETWEEN ADJACENT BULKHEADS

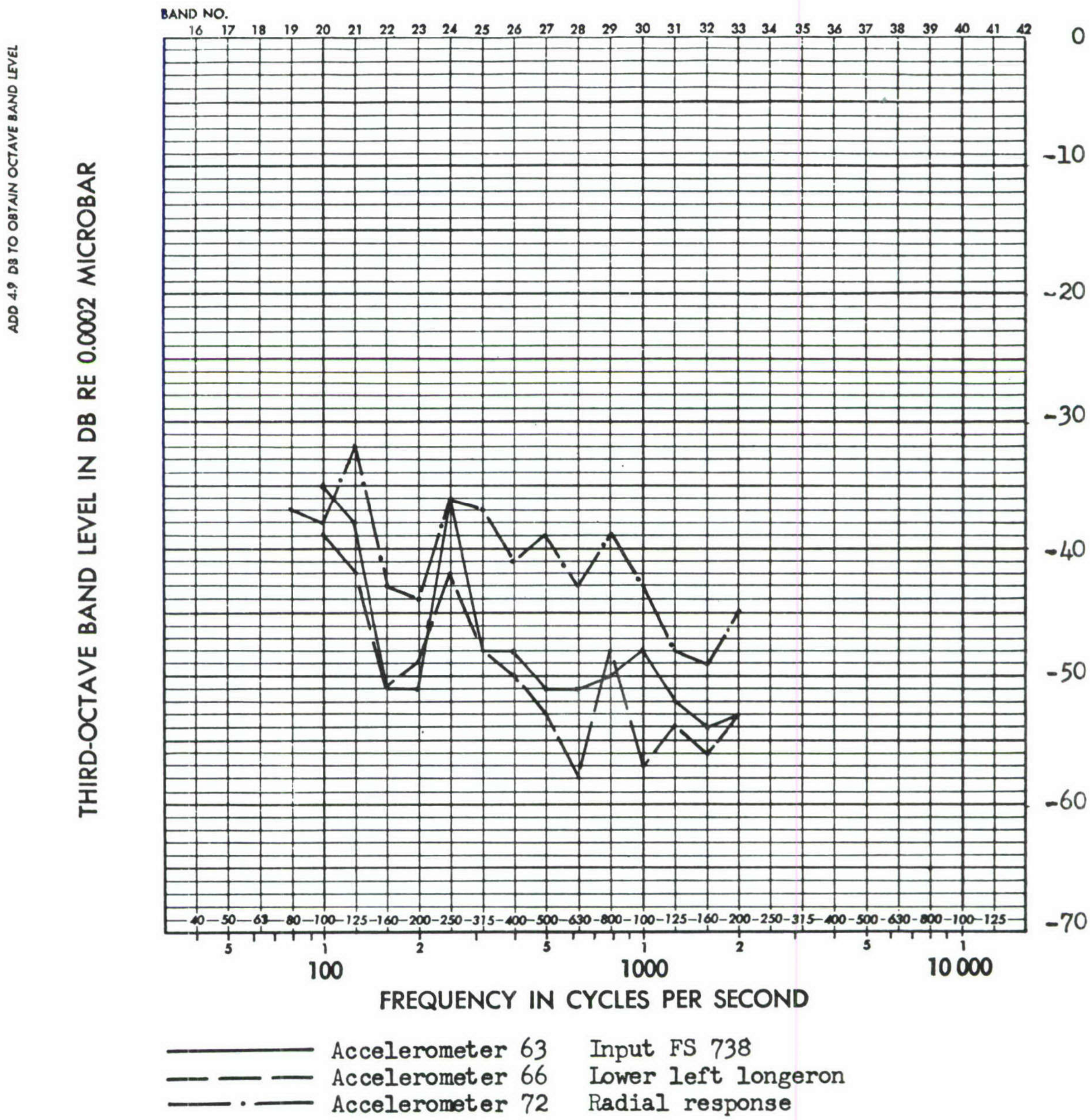

FIGURE D43 FULL SCALE RESPONSE TRANSFER FUNCTIONS (DB) FOR LOWER LEFT LONGERON, MEASURED BETWEEN ADJACENT BULKHEADS

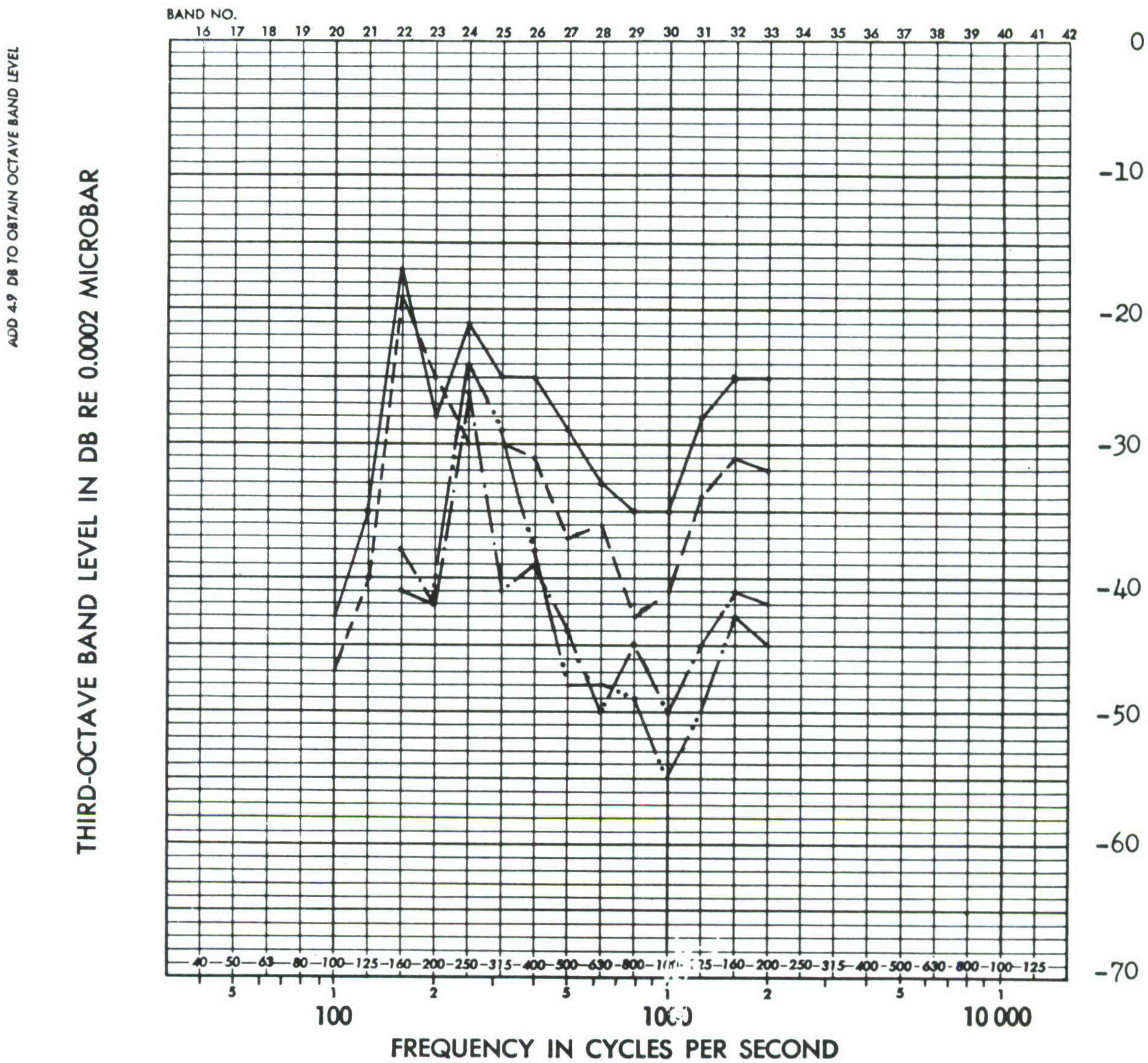

———————	Accelerometer 60	Input FS 407
– – – – – –	Accelerometer 64	Lower right longeron
——·——	Accelerometer 65	Radial response
——··——	Accelerometer 69	

FIGURE D44 FULL SCALE RESPONSE TRANSFER FUNCTIONS (DB) FOR LOWER RIGHT LONGERON, MEASURED BETWEEN ADJACENT BULKHEADS

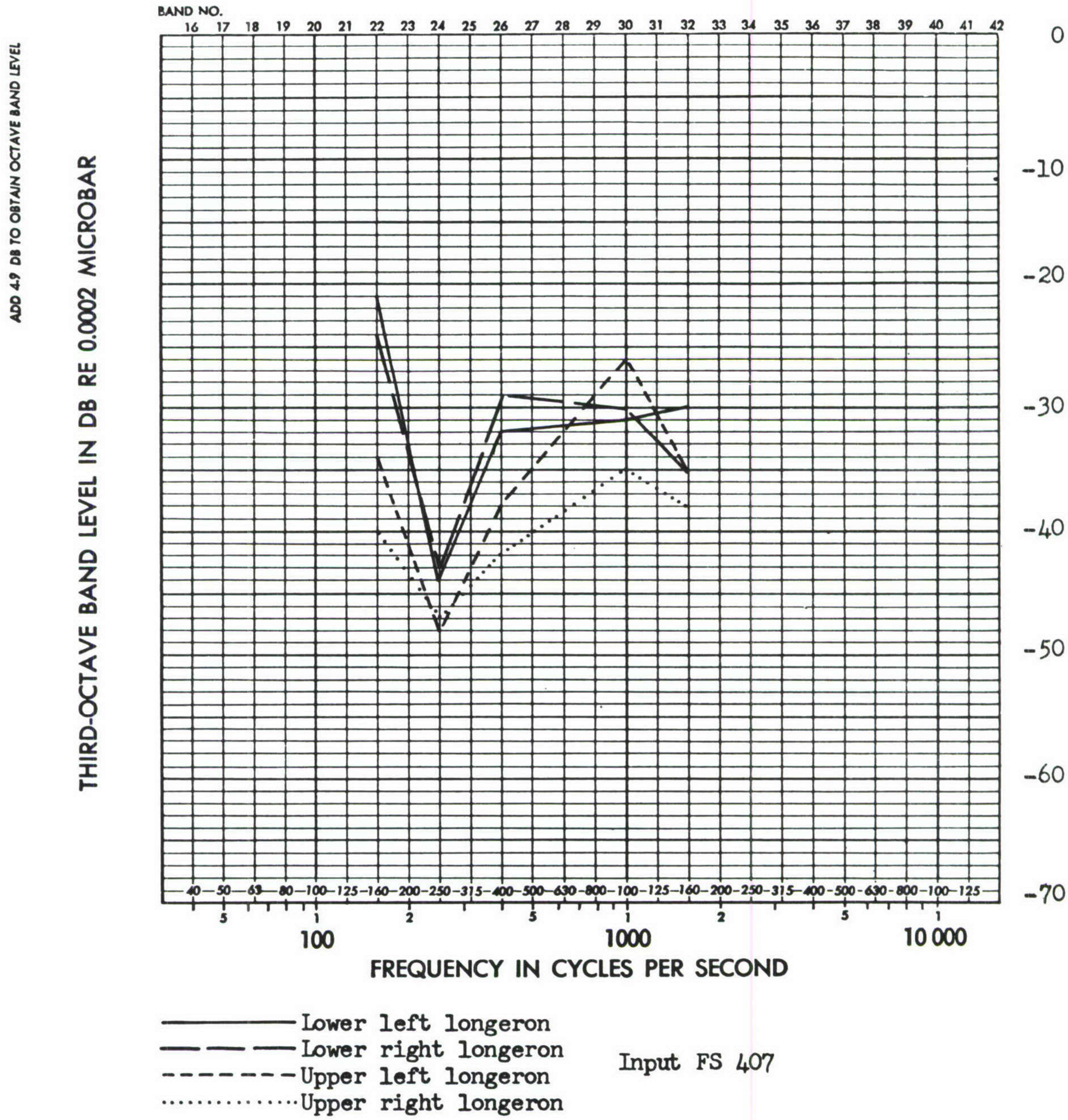

FIGURE D45 DIFFERENCE OF LONGERON RESPONSE (DB) ACROSS THE DOUBLE BULKHEAD AT F.S. 464, FOR SELECTED FREQUENCIES OF 160, 250, 400, 1000 & 1600 CPS

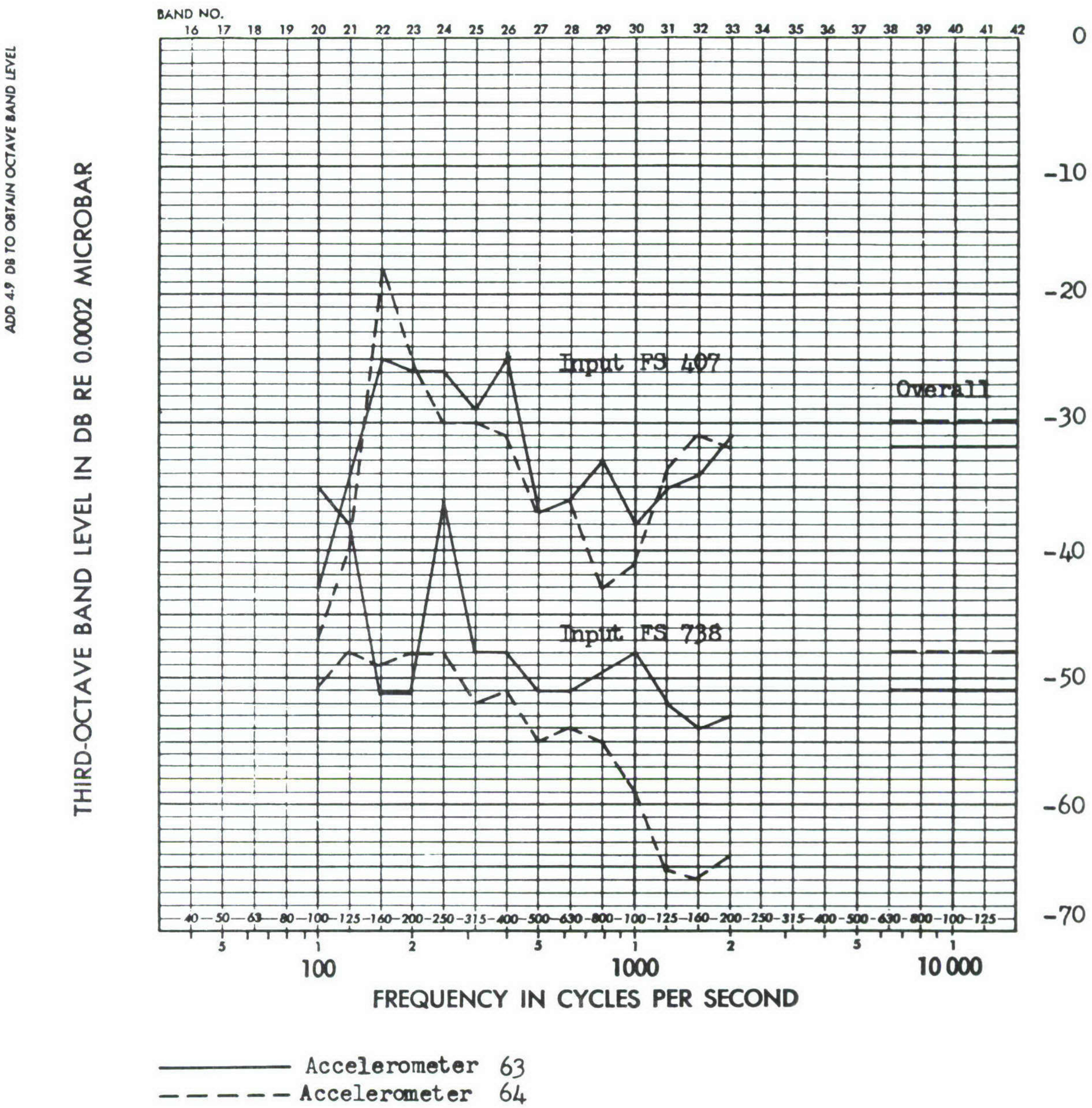

FIGURE D46 FULL SCALE RESPONSE TRANSFER FUNCTIONS (DB) FOR LOWER RIGHT AND LEFT LONGERONS AT F.S. 447, RADIAL RESPONSE MEASURED BETWEEN BULKHEADS, EXCITATION AT F.S. 407 & 738

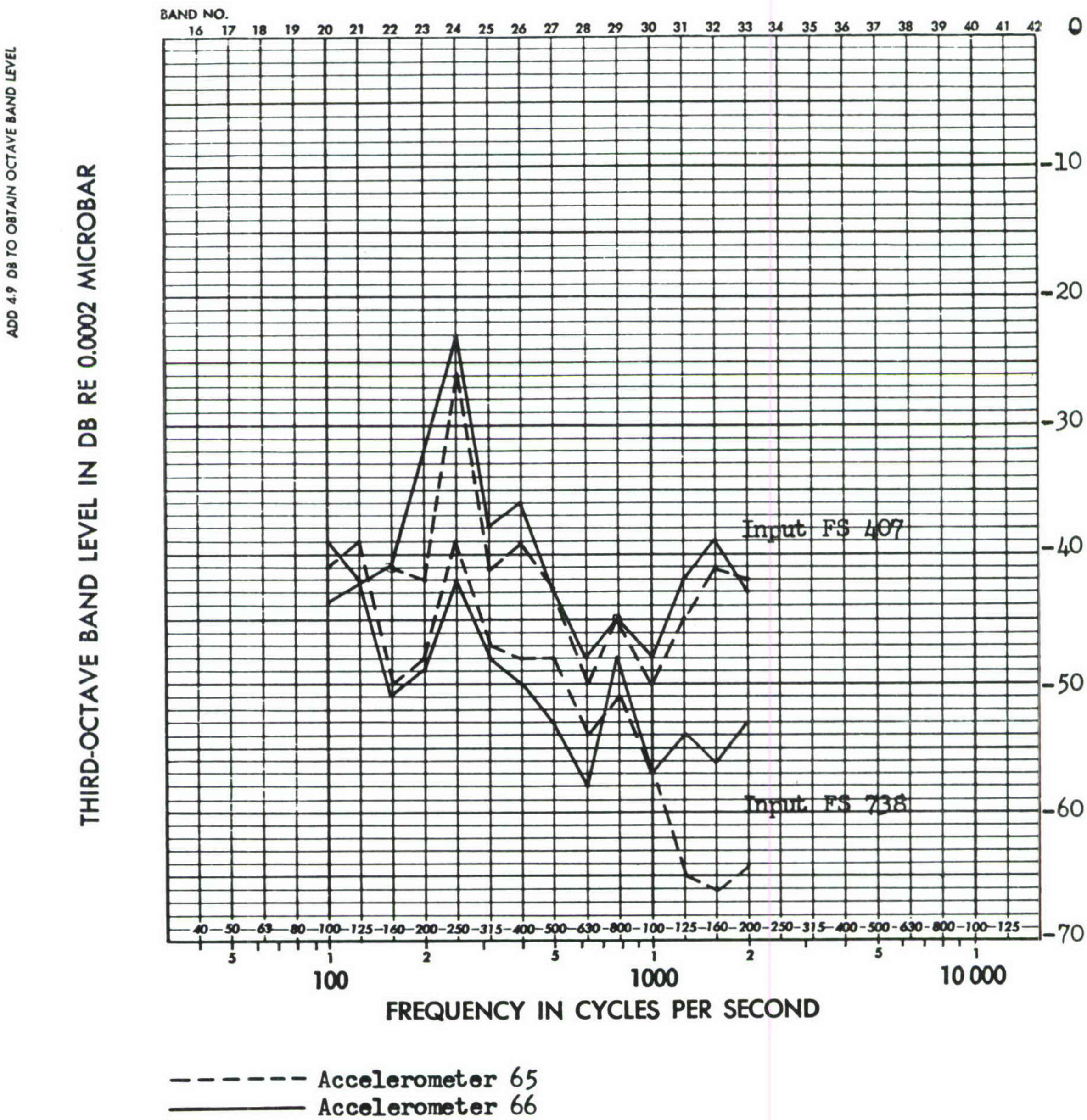

FIGURE D47 FULL SCALE RESPONSE TRANSFER FUNCTIONS (DB) FOR OPPOSITE LOWER LONGERONS AT F.S. 486, RADIAL RESPONSE MEASURED BETWEEN BULKHEADS, EXCITATION AT F.S. 407 & 738

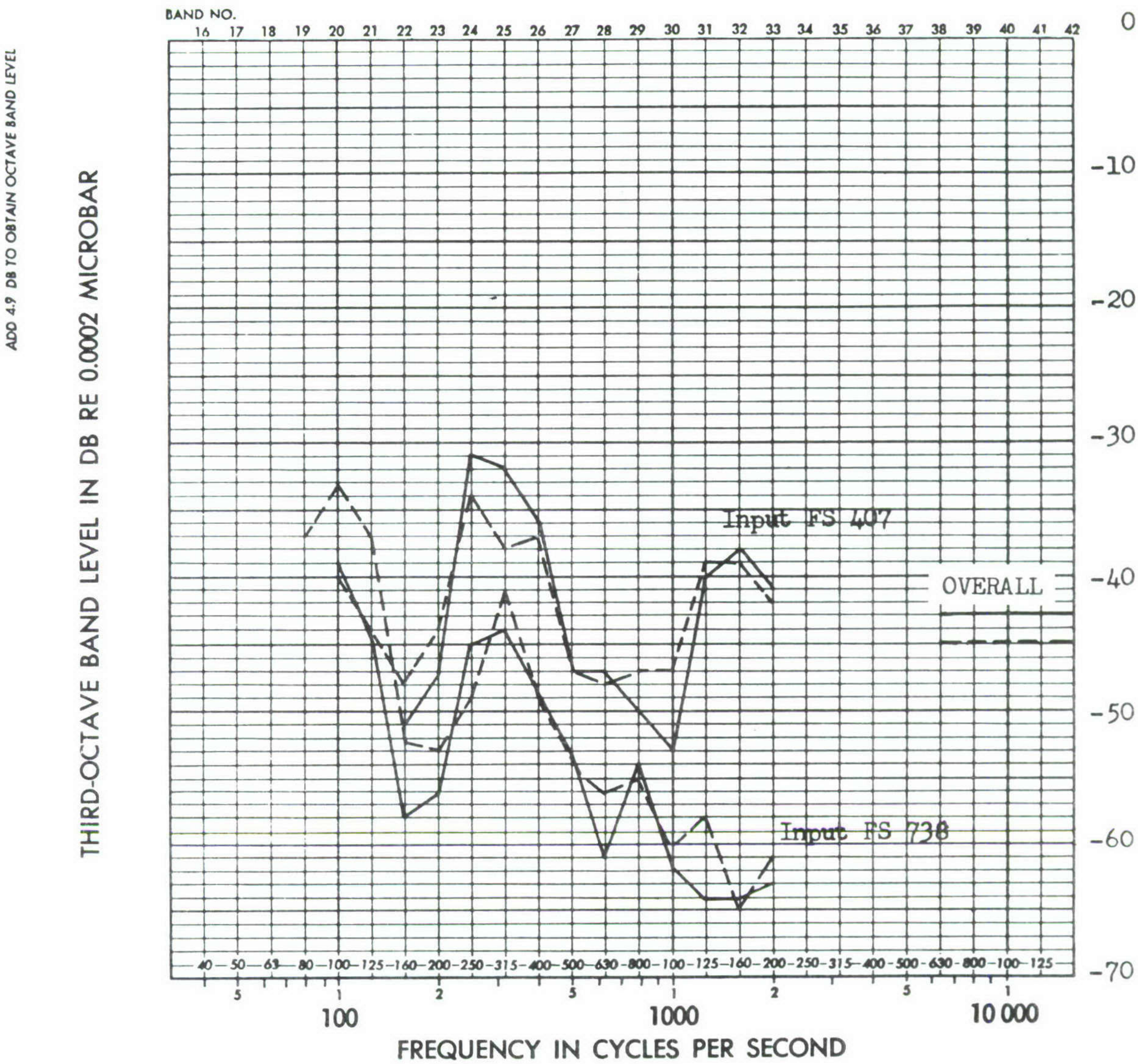

-------- Accelerometer 67

———— Accelerometer 68

FIGURE D48 FULL SCALE RESPONSE TRANSFER FUNCTIONS (DB) FOR RIGHT AND LEFT UPPER LONGERONS AT F.S. 486, RADIAL RESPONSE MEASURED BETWEEN ADJACENT BULKHEADS, EXCITATION AT F.S. 407 & 738

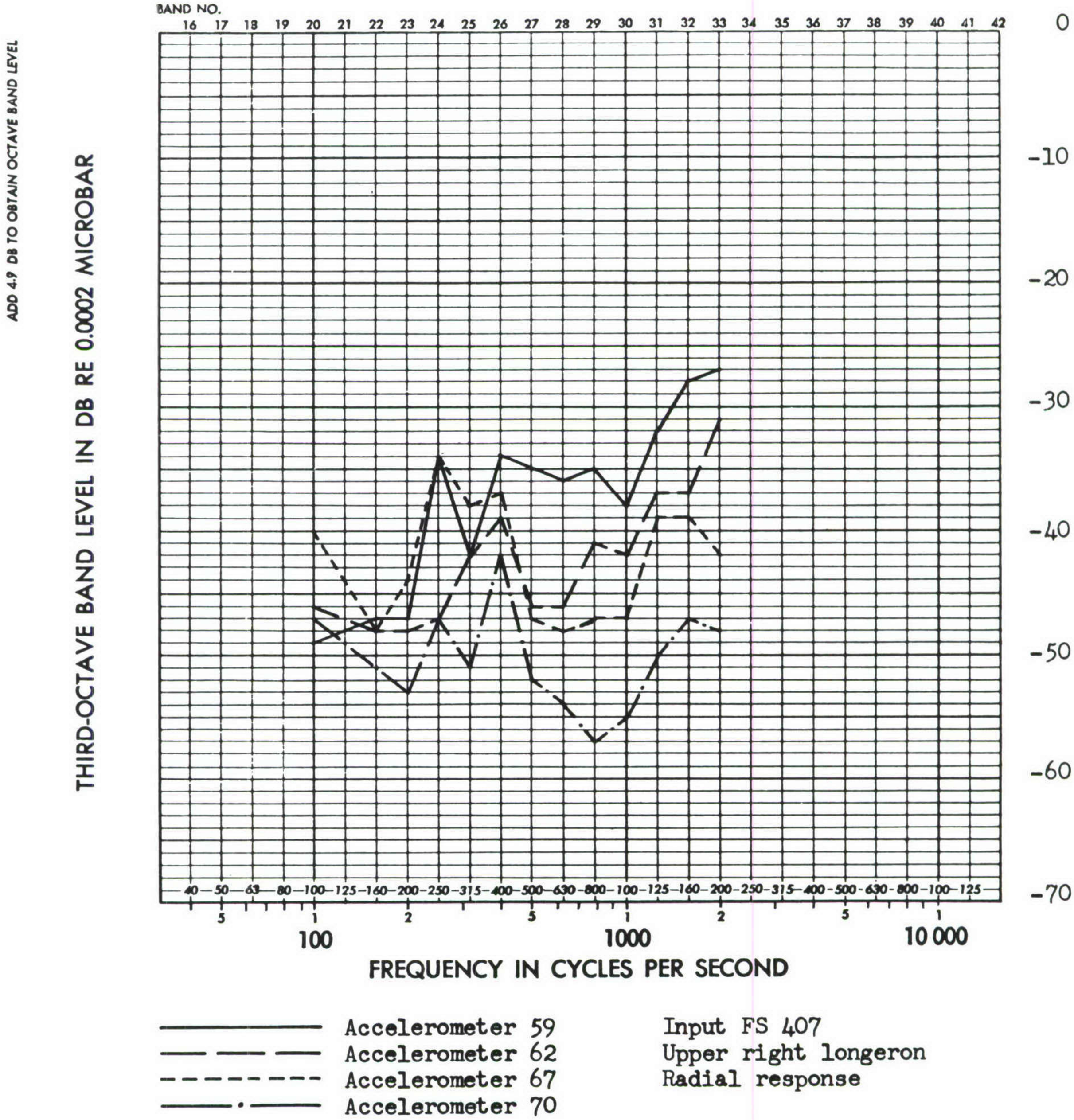

FIGURE D49 FULL SCALE RESPONSE TRANSFER FUNCTIONS (DB) FOR UPPER RIGHT LONGERON, RADIAL RESPONSE MEASURED BETWEEN ADJACENT BULKHEADS

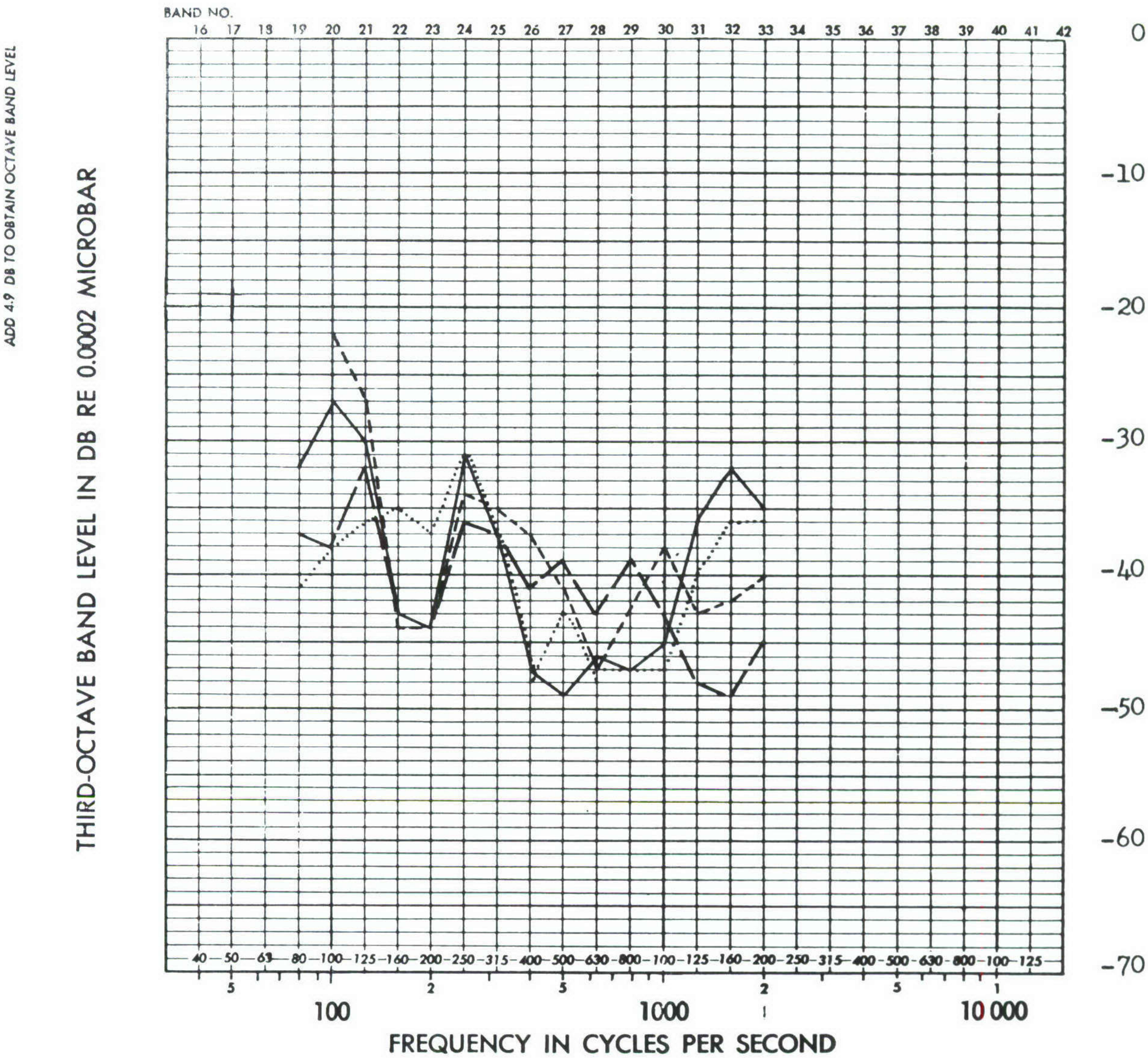

————	Accelerometer 71	Input at FS 407
···········	Accelerometer 72	Input at FS 407
- - - - - -	Accelerometer 71	Input at FS 738
— — —	Accelerometer 72	Input at FS 738

FIGURE D50 FULL SCALE RESPONSE TRANSFER FUNCTIONS (DB) FOR UPPER AND LOWER LEFT LONGERONS AT F.S. 576, RADIAL RESPONSE MEASURED BETWEEN ADJACENT BULKHEADS

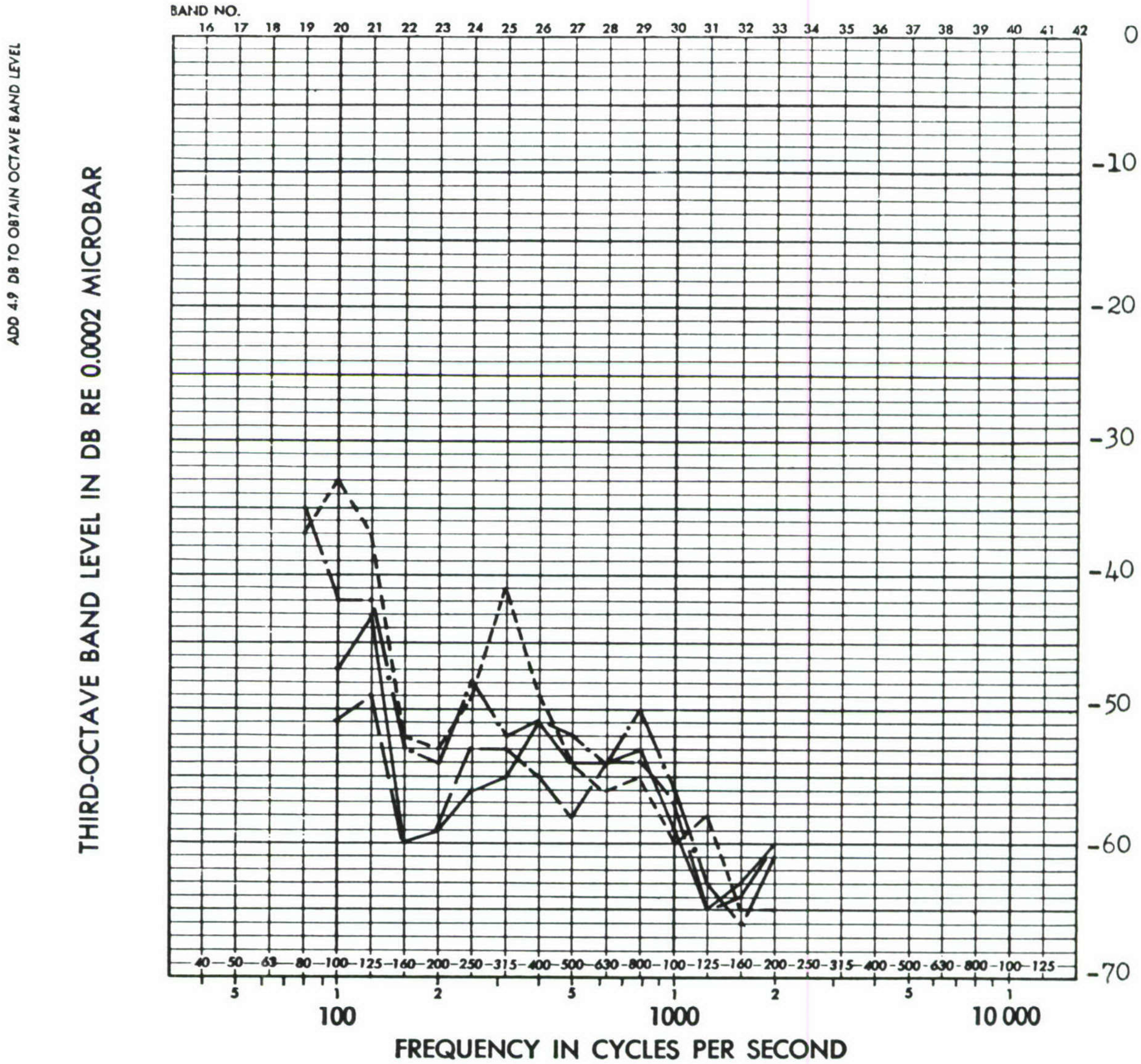

——————Accelerometer 59 Input FS 738
— — — Accelerometer 62 Upper right longeron
– – – – – – Accelerometer 67 Radial response
———·———Accelerometer 70

FIGURE D51 FULL SCALE RESPONSE TRANSFER FUNCTIONS (DB) FOR UPPER RIGHT LONGERON, RADIAL RESPONSE MEASURED ADJACENT BULKHEADS

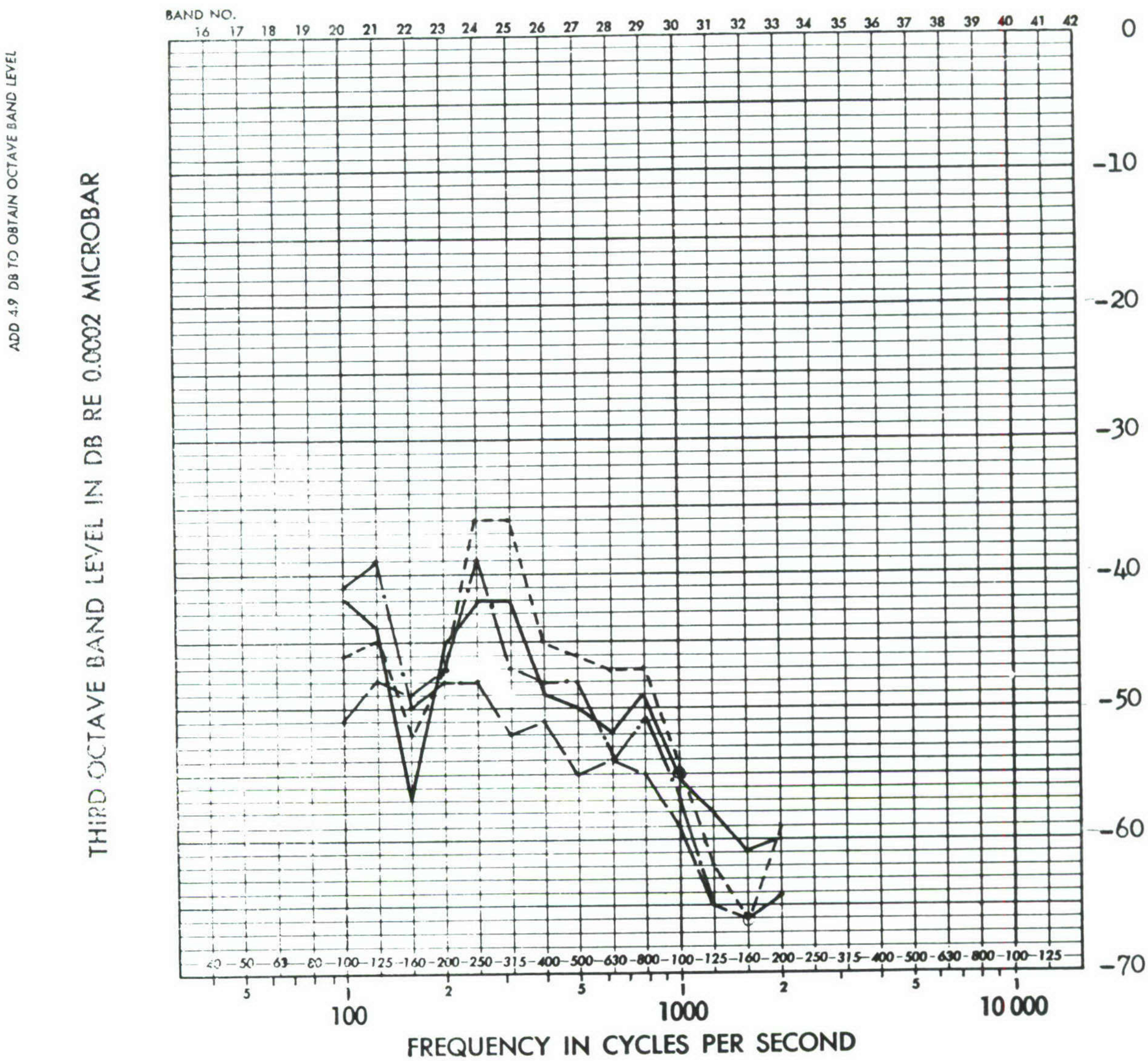

Accelerometer 60
Accelerometer 64
Accelerometer 65
Accelerometer 69

Input FS 738
Lower right longeron
Radial response

FIGURE D52 FULL SCALE RESPONSE TRANSFER FUNCTIONS (DB) FOR LOWER RIGHT LONGERON, MEASURED BETWEEN ADJACENT BULKHEADS

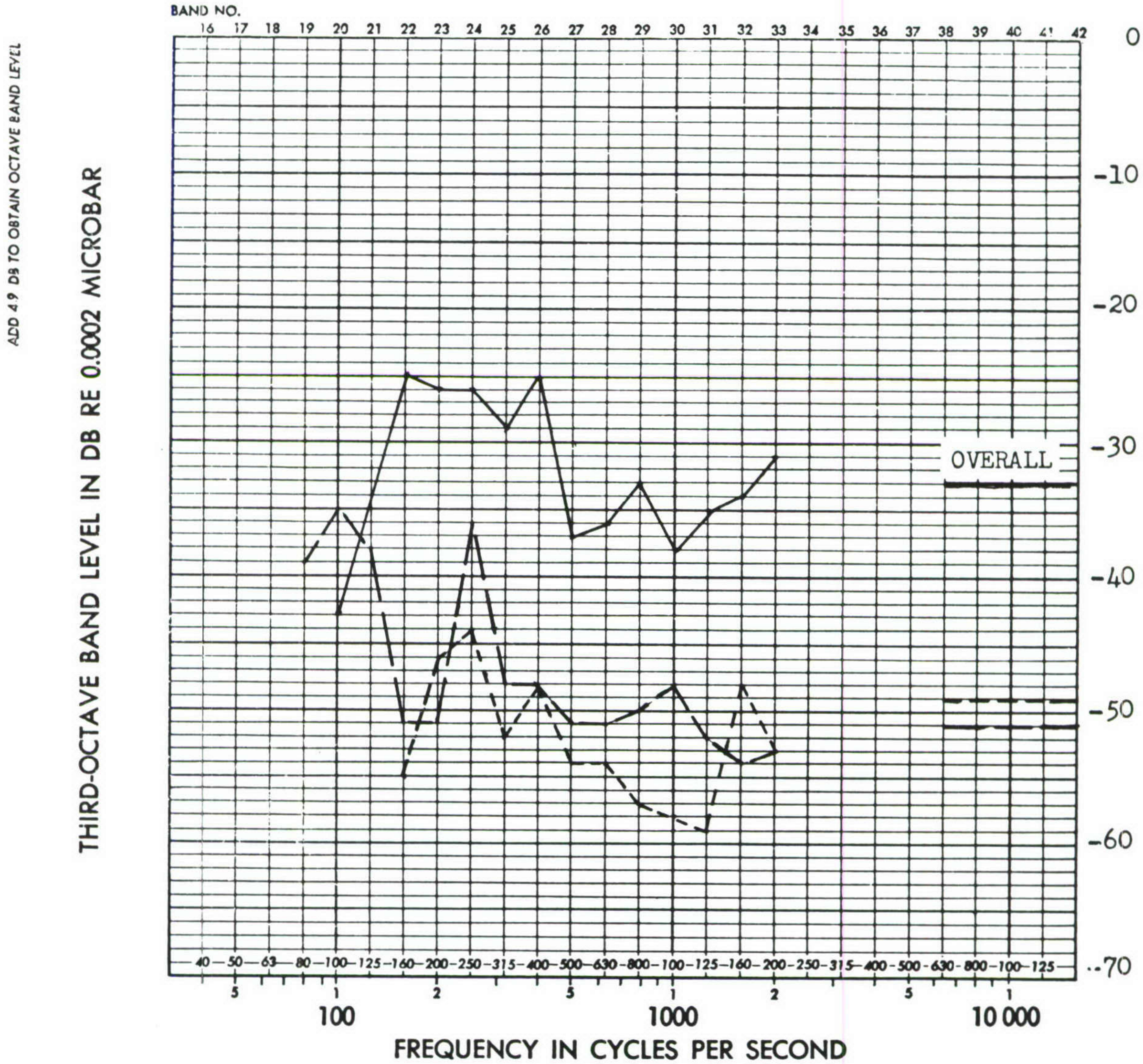

Input at FS 407
Input at FS 578
Input at FS 738

Accelerometer 63
Radial response
FS 447
Patrick accelerometer

FIGURE D53 FULL SCALE RESPONSE TRANSFER FUNCTIONS (DB) FOR LOWER LONGERON, MEASURED BETWEEN ADJACENT BULKHEADS, EXCITATION AT F.S. 407, 578 & 738

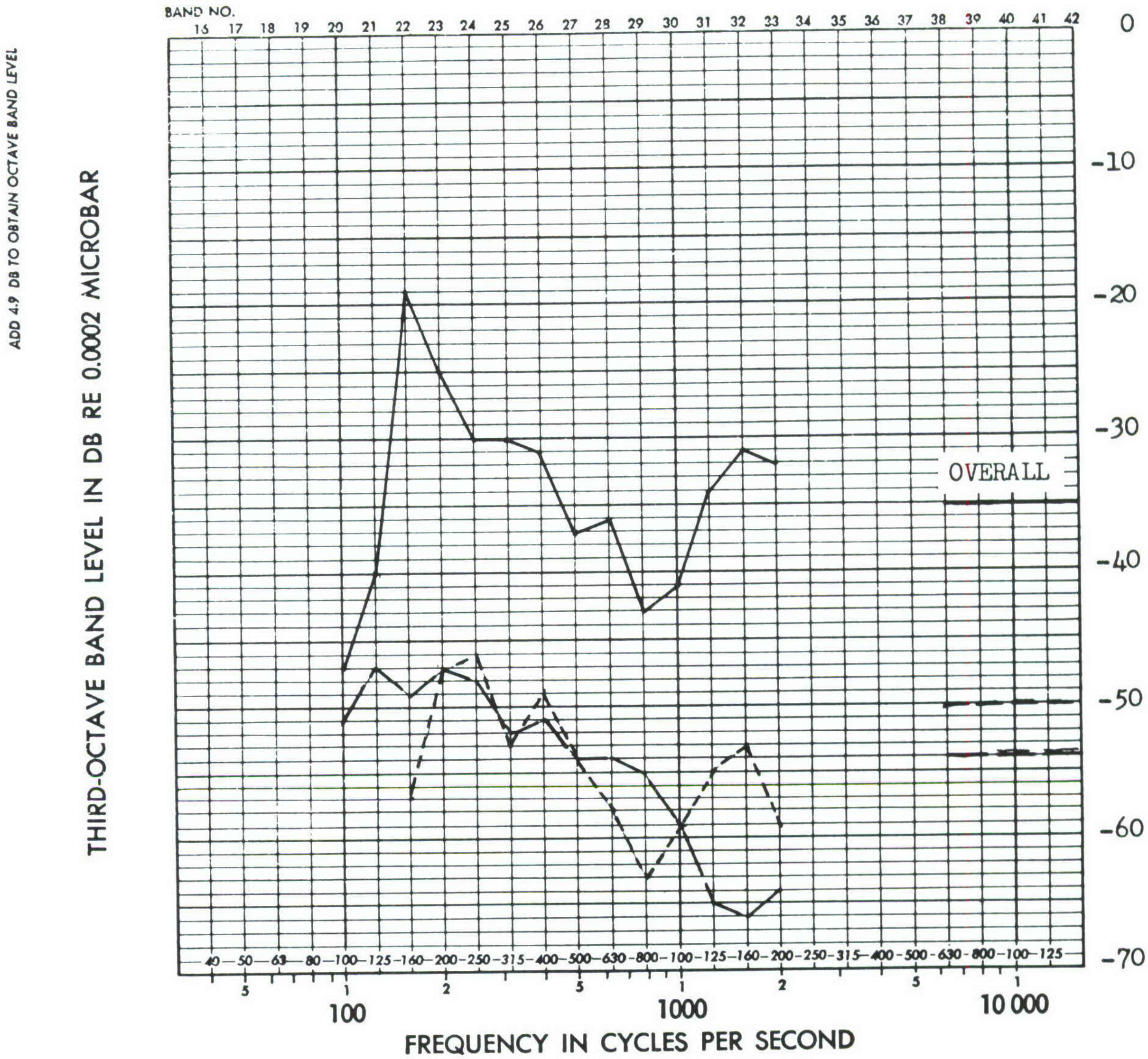

——— Input at FS 405
- - - - - Input at FS 578
— — — Input at FS 738

Accelerometer 64
Lower right longeron
Radial response

FIGURE D54 FULL SCALE RESPONSE TRANSFER FUNCTIONS (DB) FOR LOWER RIGHT LONGERON, RESPONSE MEASURED BETWEEN ADJACENT BULKHEADS

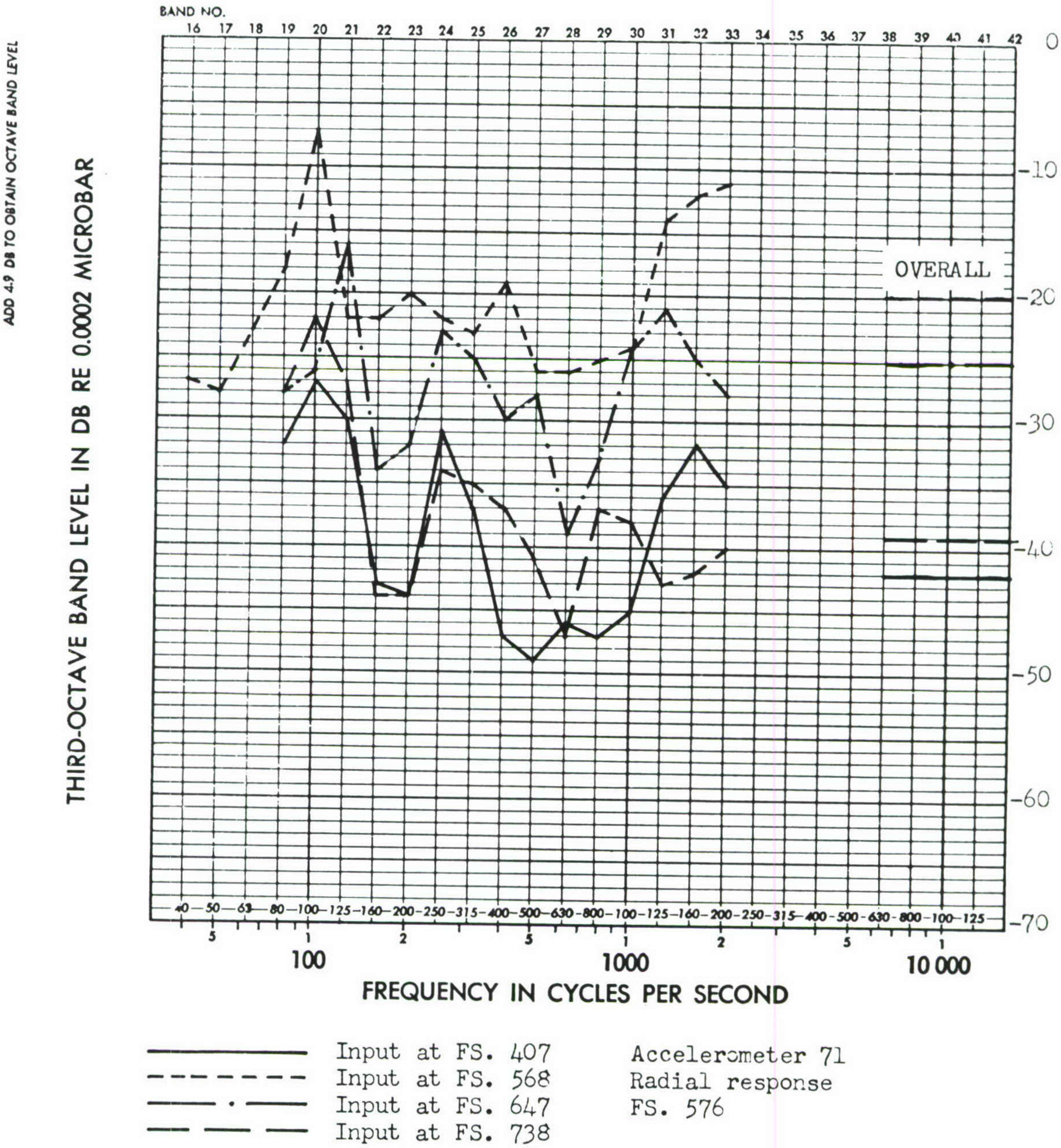

FIGURE D55 FULL SCALE RESPONSE TRANSFER FUNCTIONS (DB) FOR UPPER LEFT LONGERON CENTERED BETWEEN BULKHEADS

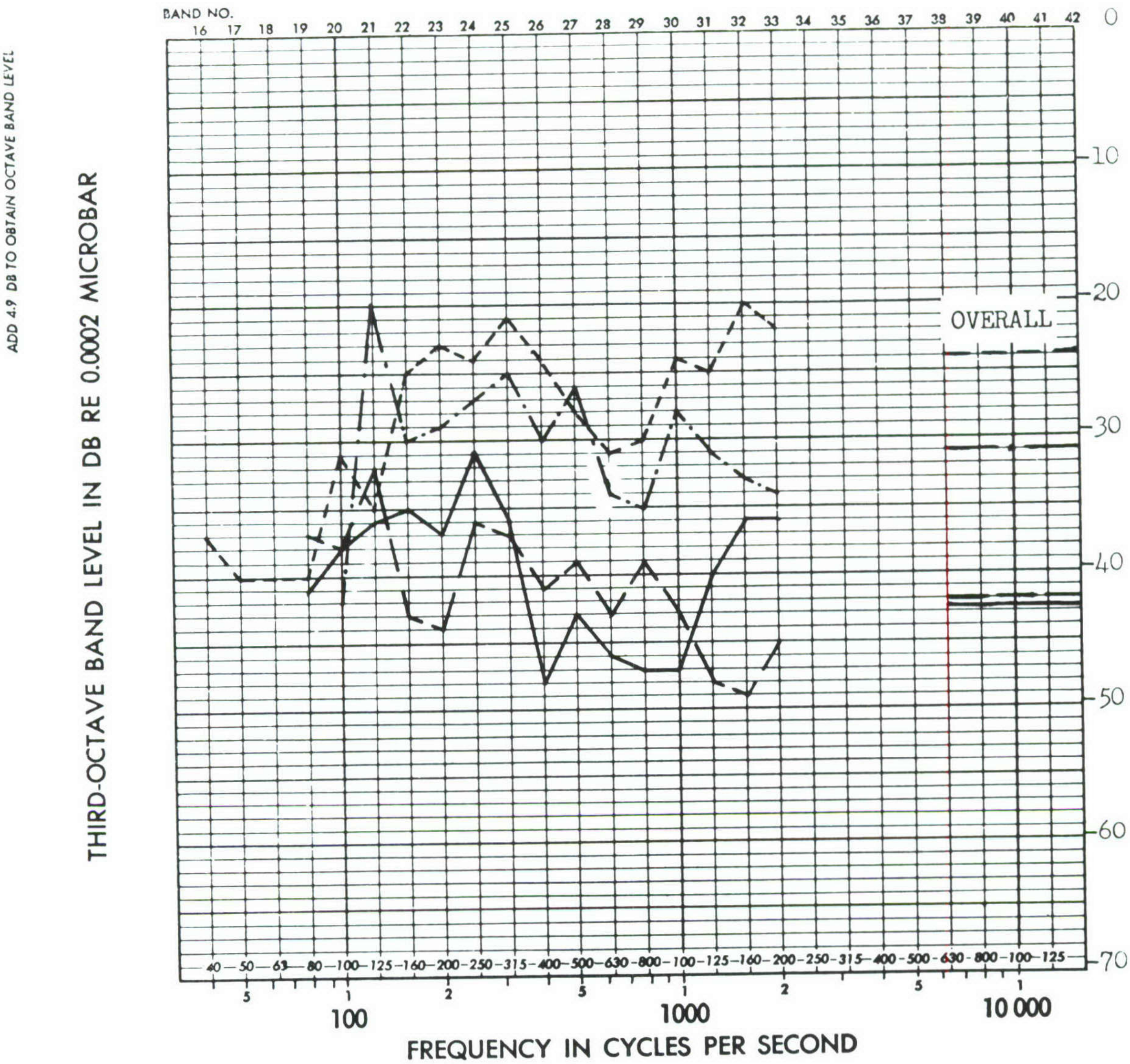

———————	Input at FS. 407	Accelerometer 72
– – – – – –	Input at FS. 568	Radial response
——— · ———	Input at FS. 647	FS. 576
—— —— ——	Input at FS. 738	

FIGURE D56 FULL SCALE RESPONSE TRANSFER FUNCTIONS (DB) FOR LOWER LEFT LONGERON CENTERED BETWEEN BULKHEADS

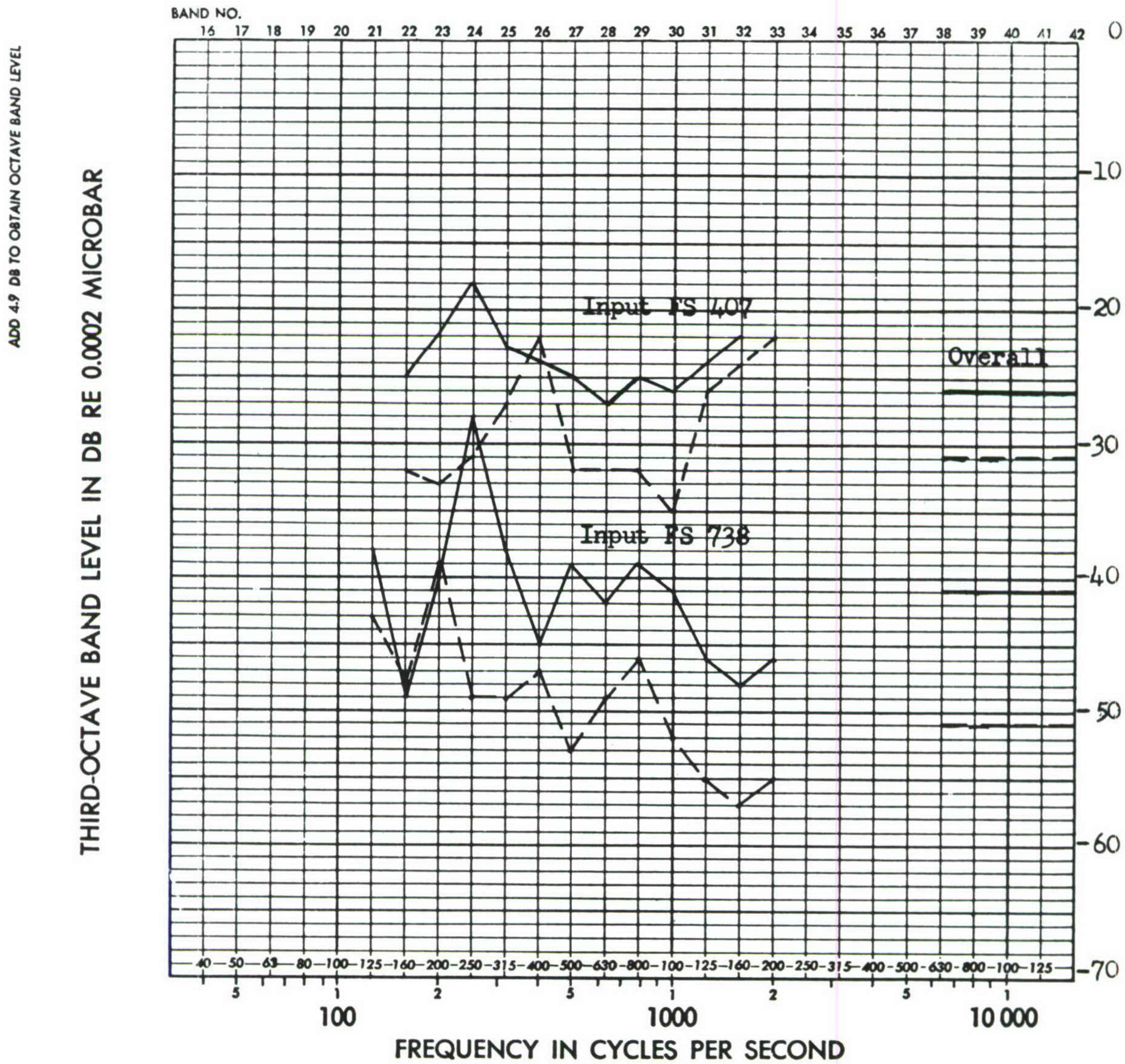

——————— Accelerometer 23
– – – – – – Accelerometer 24

FIGURE D57 FULL SCALE RESPONSE TRANSFER FUNCTIONS (DB) FOR THE CENTER OF OPPOSITE SIDE PANELS AT F.S. 445

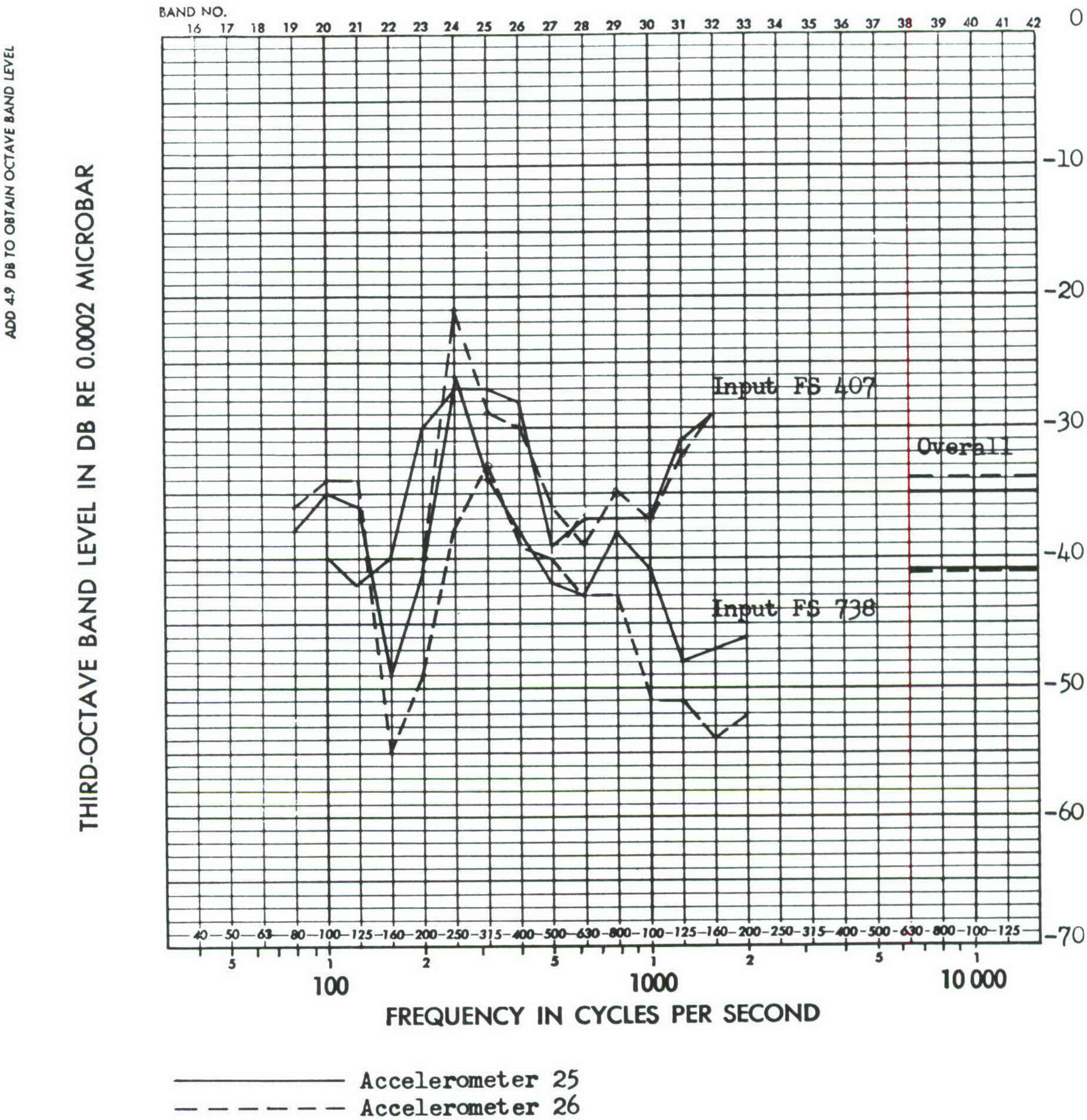

FIGURE D58 FULL SCALE RESPONSE TRANSFER FUNCTIONS (DB) FOR THE CENTER OF OPPOSITE SIDE PANELS AT F.S. 485

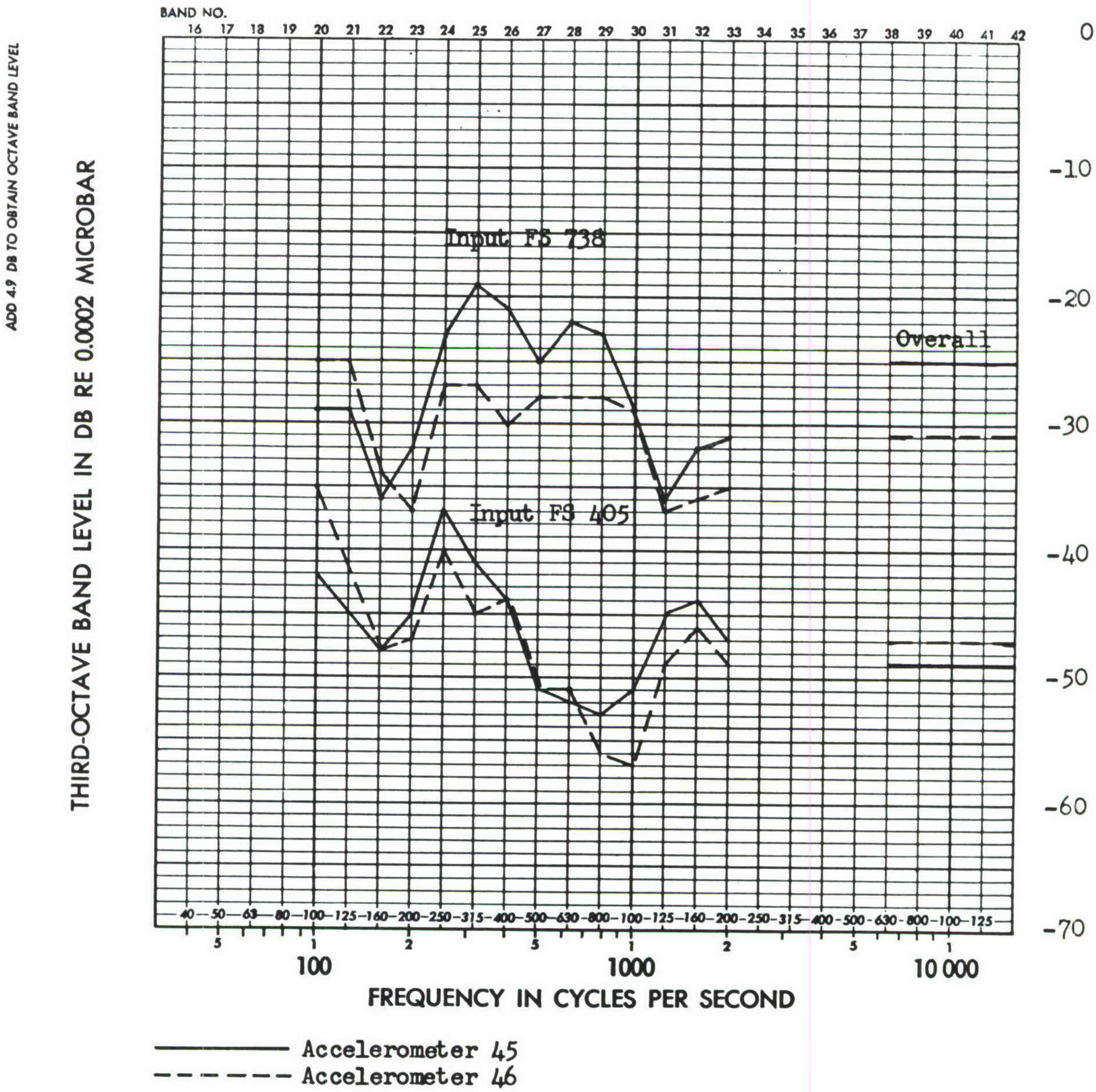

FIGURE D59 FULL SCALE RESPONSE TRANSFER FUNCTIONS (DB) FOR RIGHT AND LEFT SIDE (OPPOSITE) AFT PANELS AT F.S. 684, EXCITATION AT F.S. 405 & 738

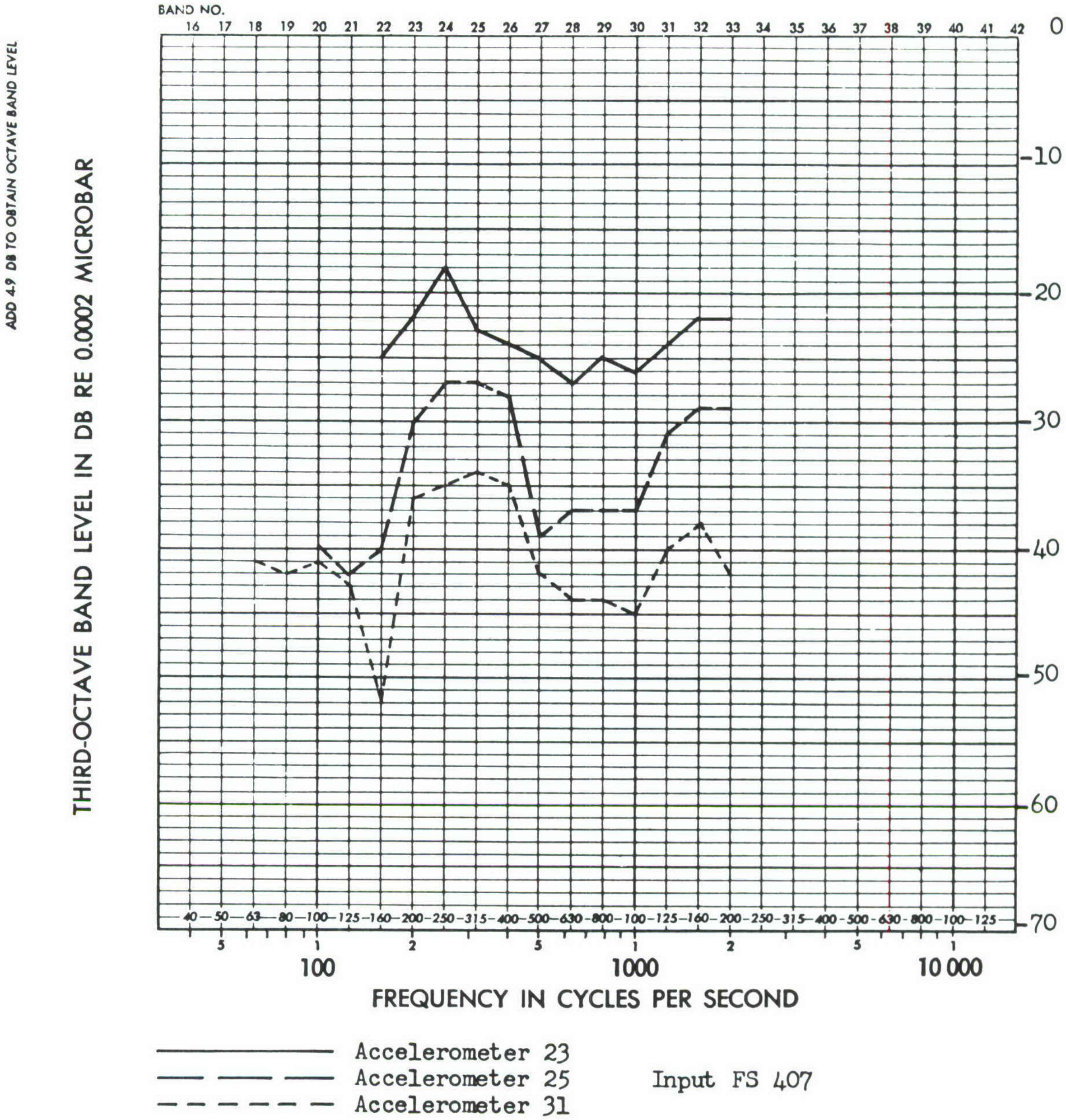

FIGURE D60 FULL SCALE RESPONSE TRANSFER FUNCTIONS (DB) FOR LEFT SIDE PANELS AT F.S. 443, 485 AND 580, EXCITATION AT F.S. 407

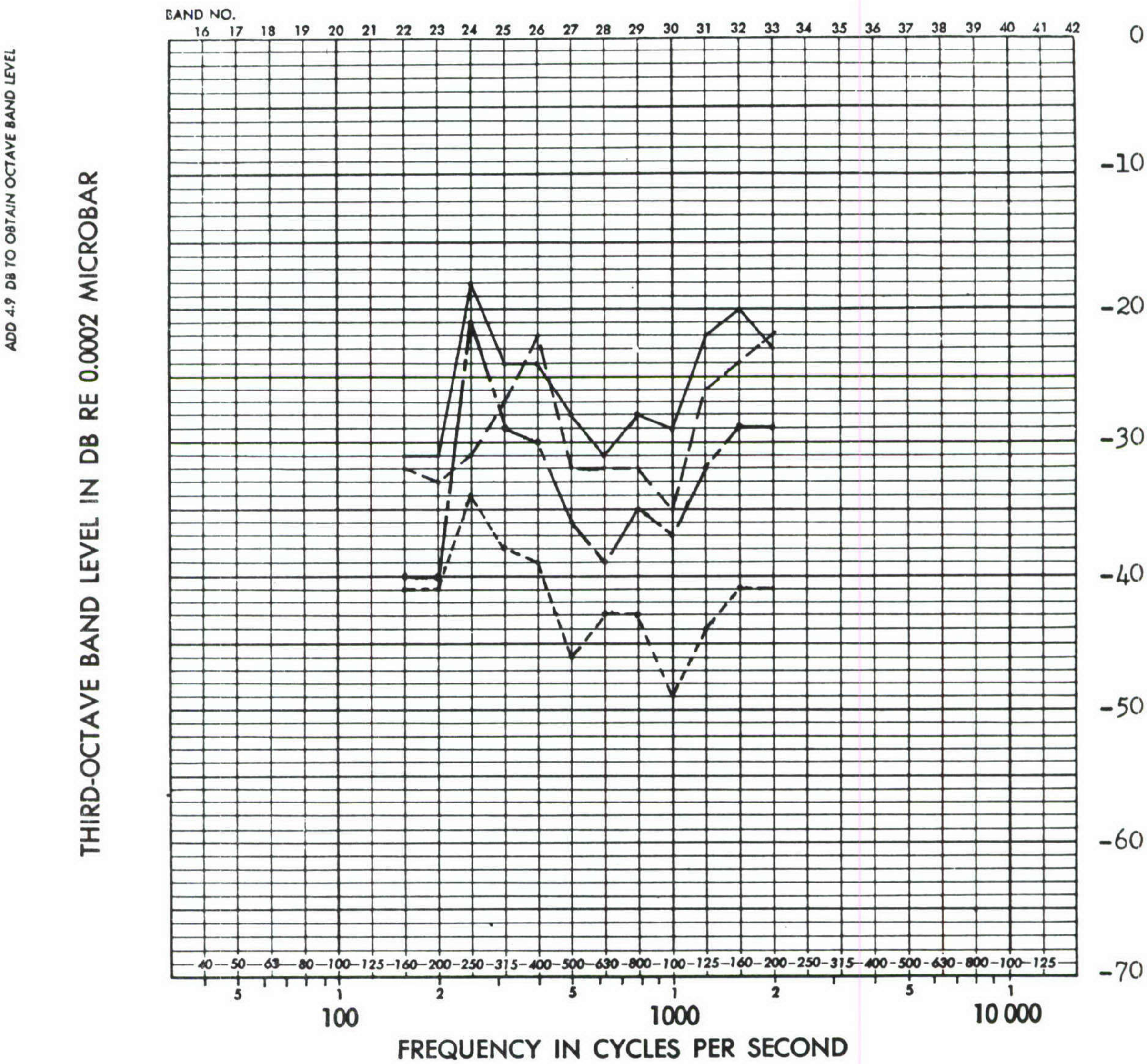

Accelerometer 21 Input FS 407

Accelerometer 24

Accelerometer 26

Accelerometer 32

FIGURE D61 FULL SCALE RESPONSE TRANSFER FUNCTIONS (DB) FOR RIGHT SIDE PANELS AT F.S. 407, 447, 486 AND 582, EXCITATION AT F.S. 407

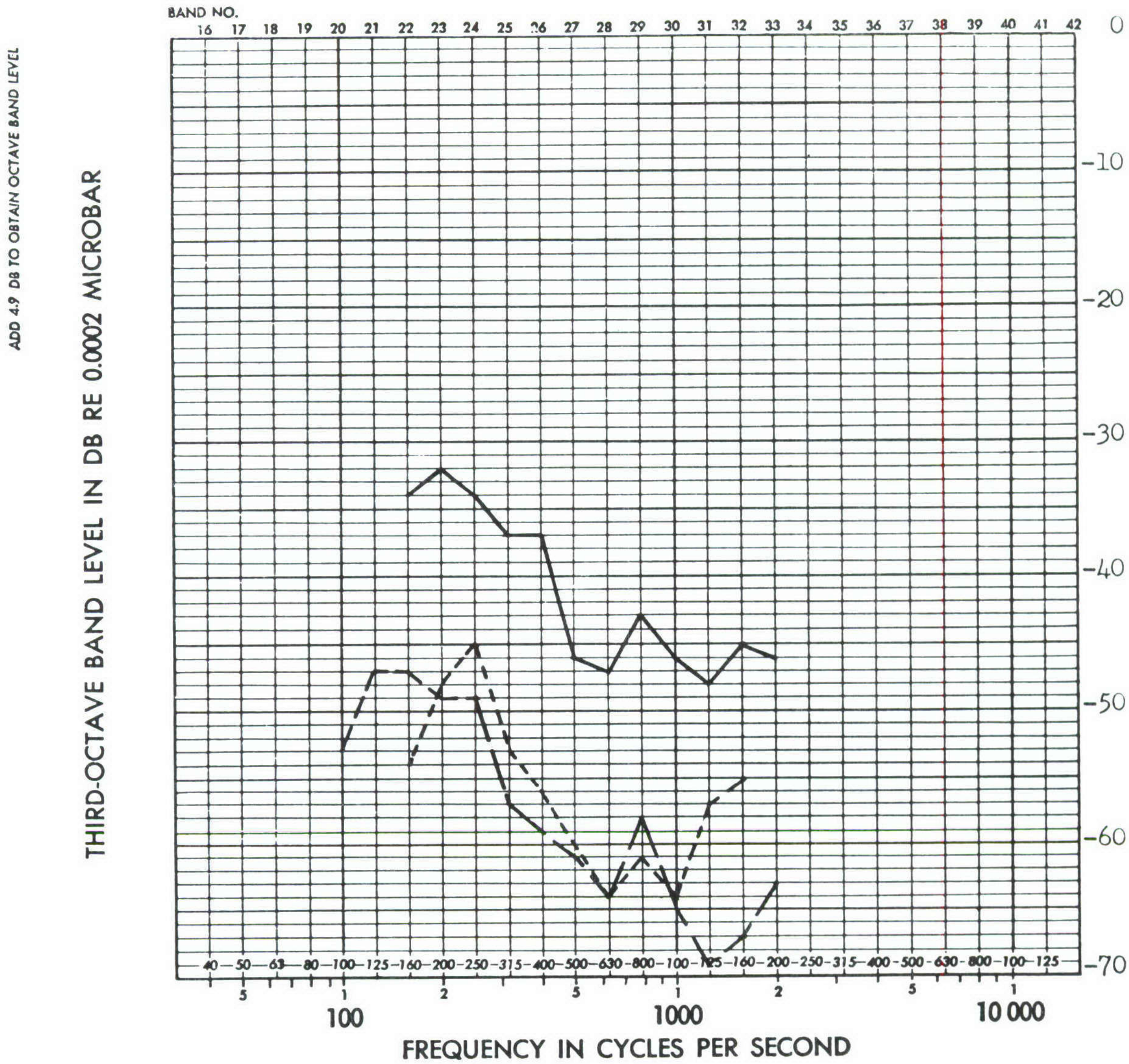

————————	Input at FS. 407	Accelerometer 10
— — — — — —	Input at FS. 578	Vertical response
—— —— ——	Input at FS. 738	FS. 447

FIGURE D62 FULL SCALE RESPONSE TRANSFER FUNCTIONS (DB) FOR CENTER OF BOTTOM CURVED PANEL, FORWARD SECTION

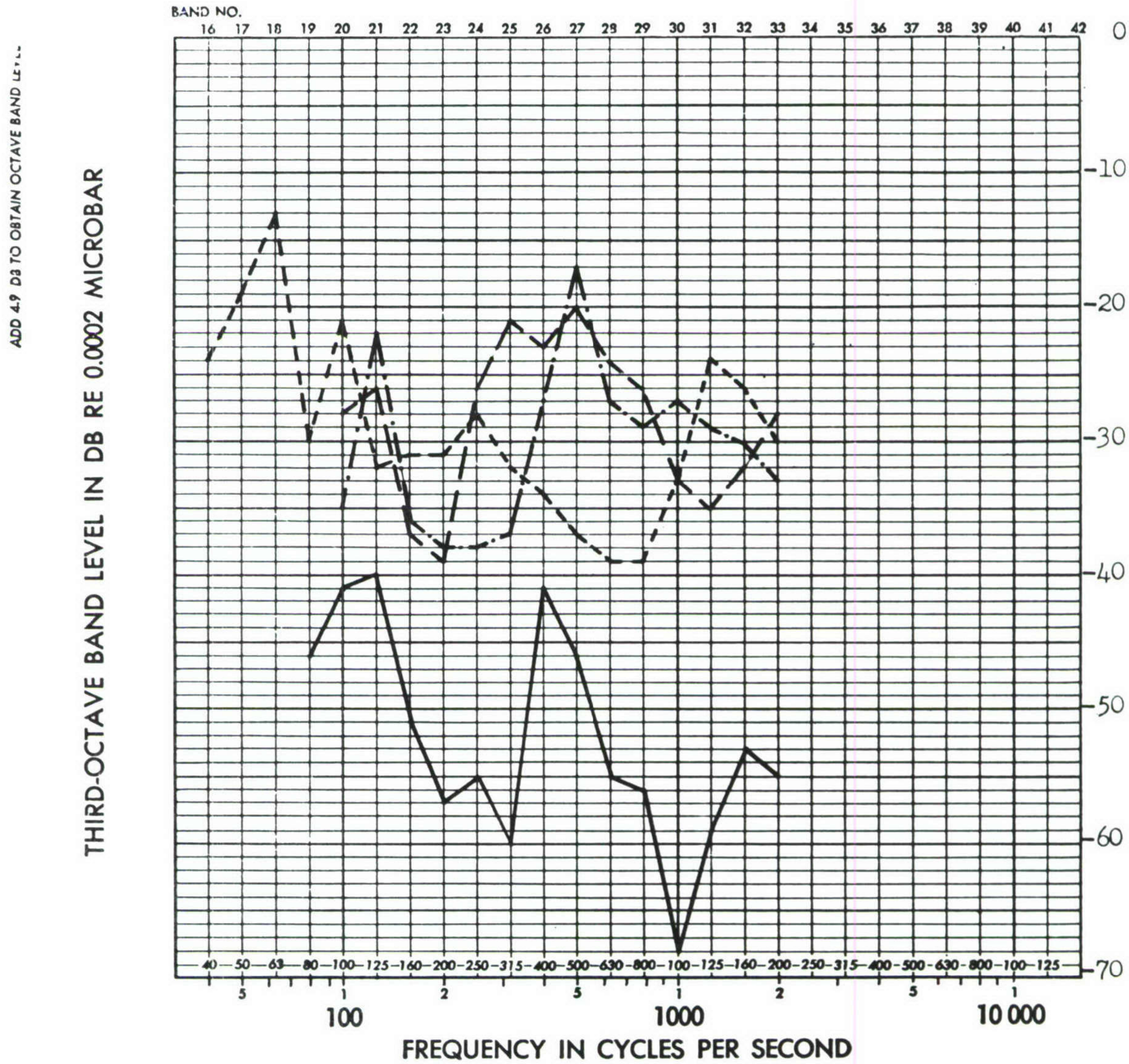

Input at FS. 407
Input at FS. 568
Input at FS. 647
Input at FS. 738

Accelerometer 15
Vertical response
FS. 735

FIGURE D63 FULL SCALE RESPONSE TRANSFER FUNCTIONS (DB) FOR TOP CENTER OF AFT SKIN COVER

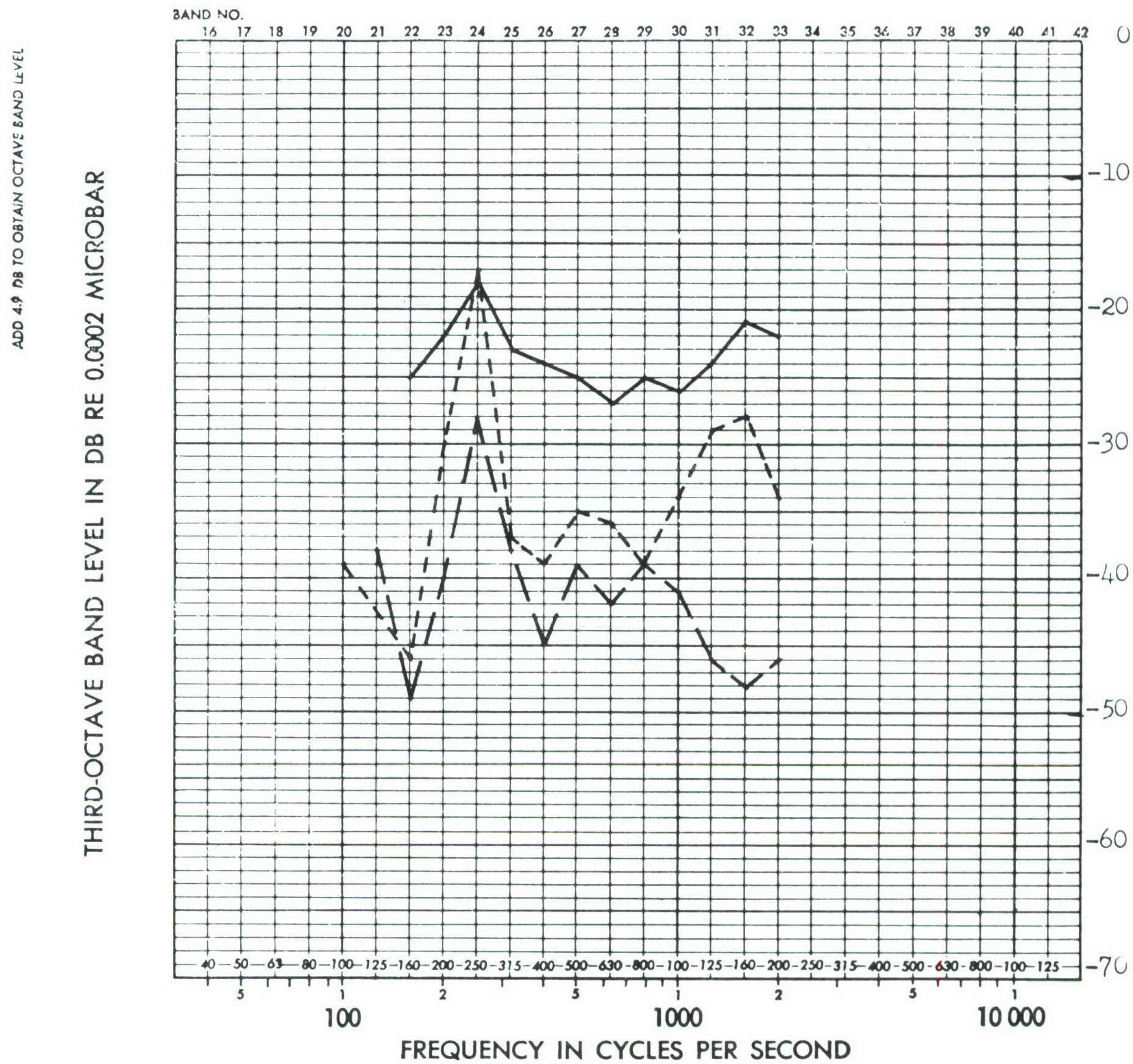

———————	Input at FS. 407	Accelerometer 23
— — — — — —	Input at FS. 578	Lateral response
——— ——— ———	Input at FS. 738	FS. 443

FIGURE D64 FULL SCALE RESPONSE TRANSFER FUNCTIONS (DB) FOR CENTER OF SIDE PANEL, LEFT SIDE, FORWARD SECTION

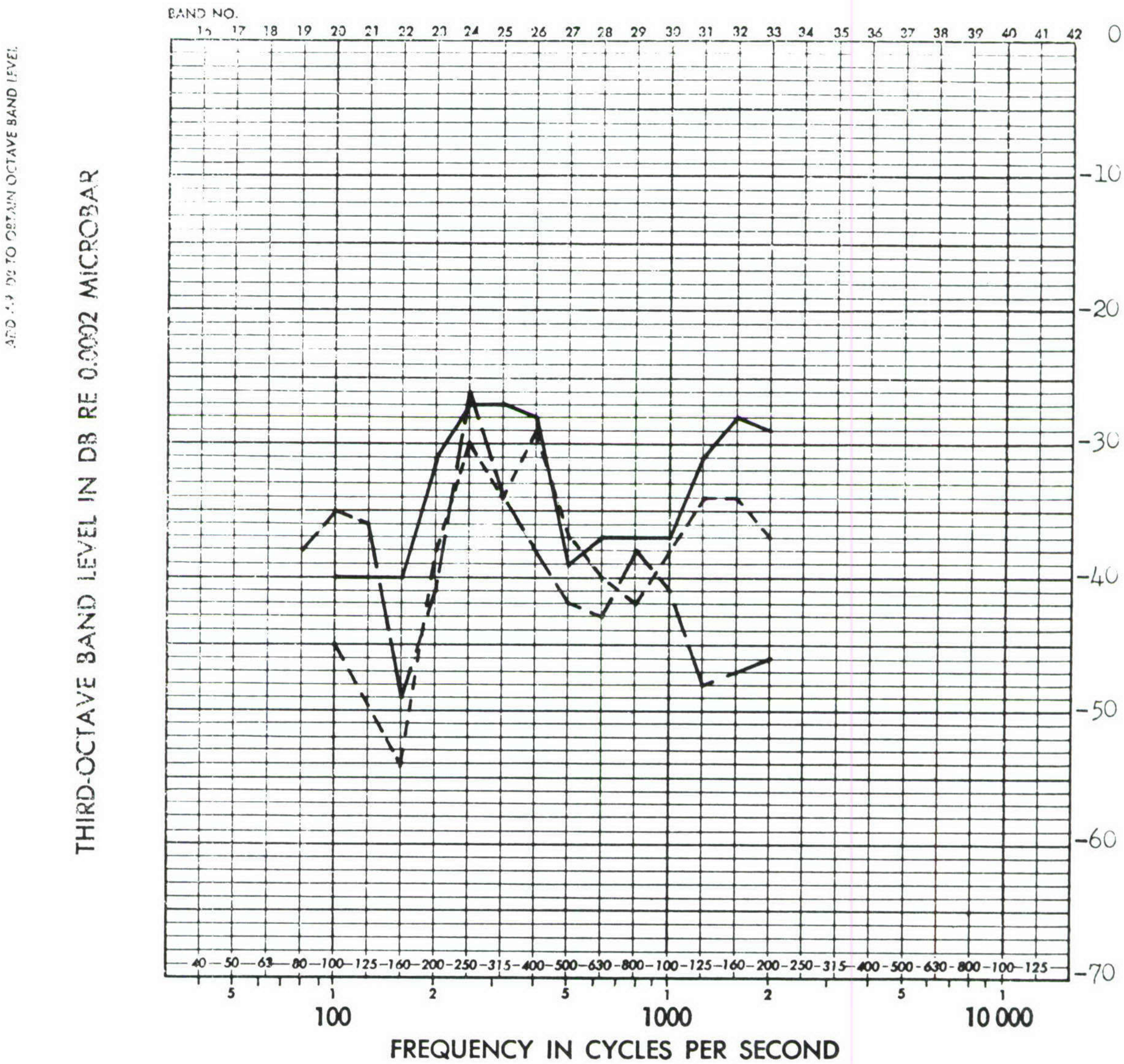

————————	Input at FS. 407	Accelerometer 25
– – – – – –	Input at FS. 578	Lateral response
—— —— ——	Input at FS. 738	FS. 485

FIGURE D65 FULL SCALE RESPONSE TRANSFER FUNCTIONS (DB) FOR CENTER OF SIDE PANEL, LEFT SIDE, FORWARD SECTION

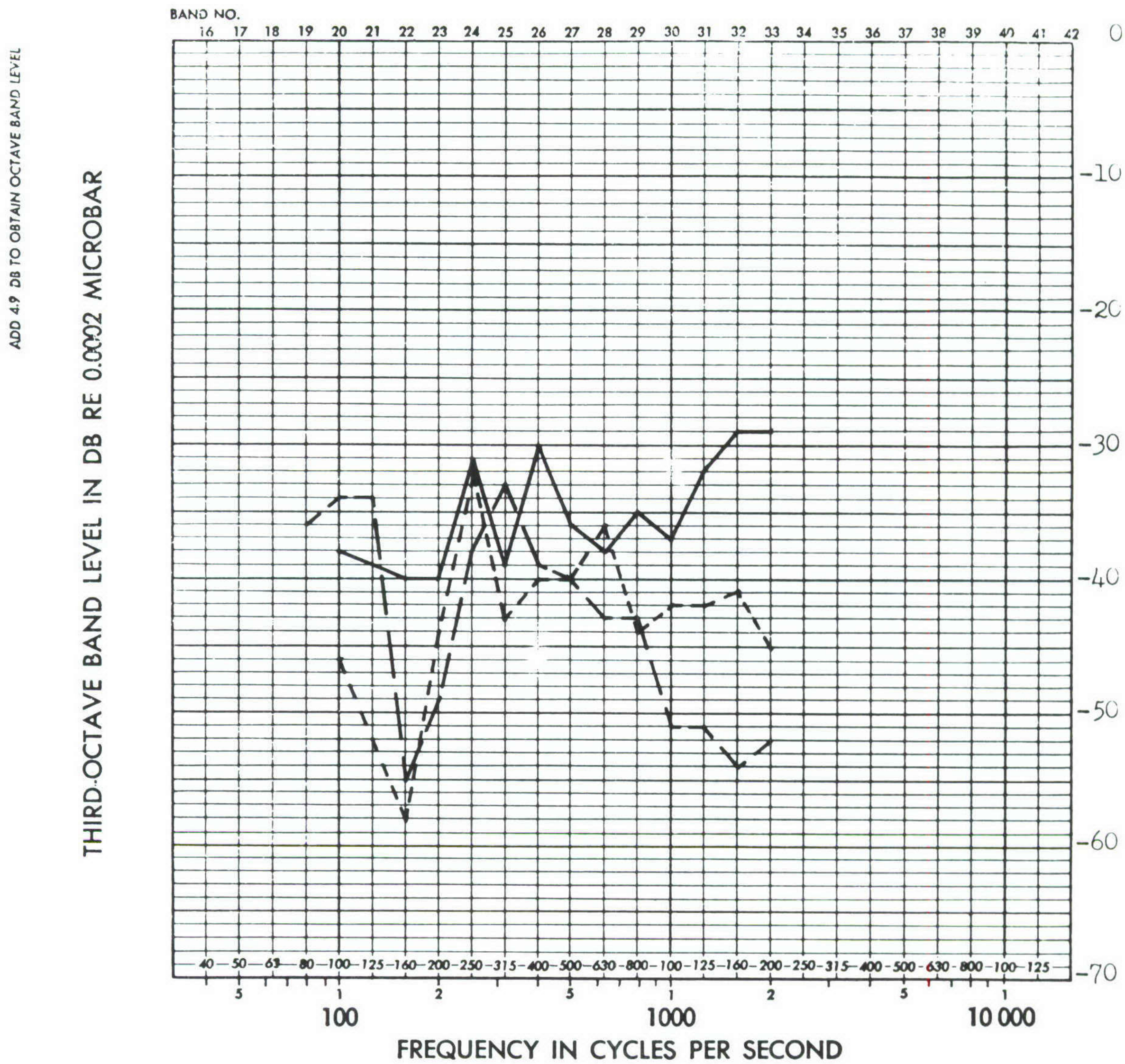

————————	Input at FS. 407	Accelerometer 26
— — — — — —	Input at FS. 578	Lateral response
——— ——— ———	Input at FS. 738	FS. 485

FIGURE D66 FULL SCALE RESPONSE TRANSFER FUNCTIONS (DB) FOR CENTER OF SIDE PANEL, RIGHT SIDE, FORWARD SECTION

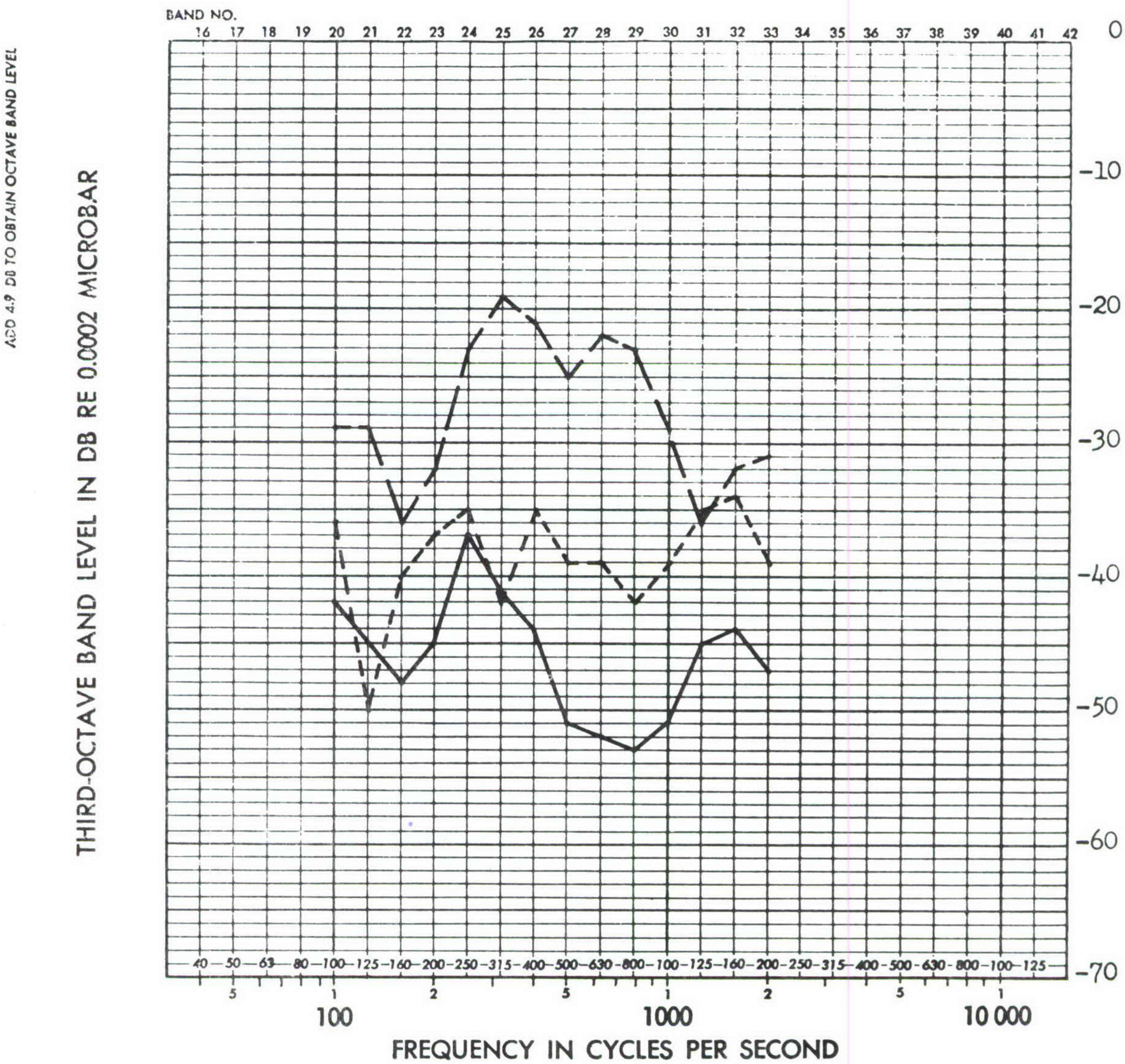

Input at FS. 407 — Accelerometer 45
Input at FS. 578 — Lateral response
Input at FS. 738 — FS. 684

FIGURE D67 FULL SCALE RESPONSE TRANSFER FUNCTIONS (DB) FOR CENTER AND UPPER PANEL, LEFT SIDE, AFT SECTION

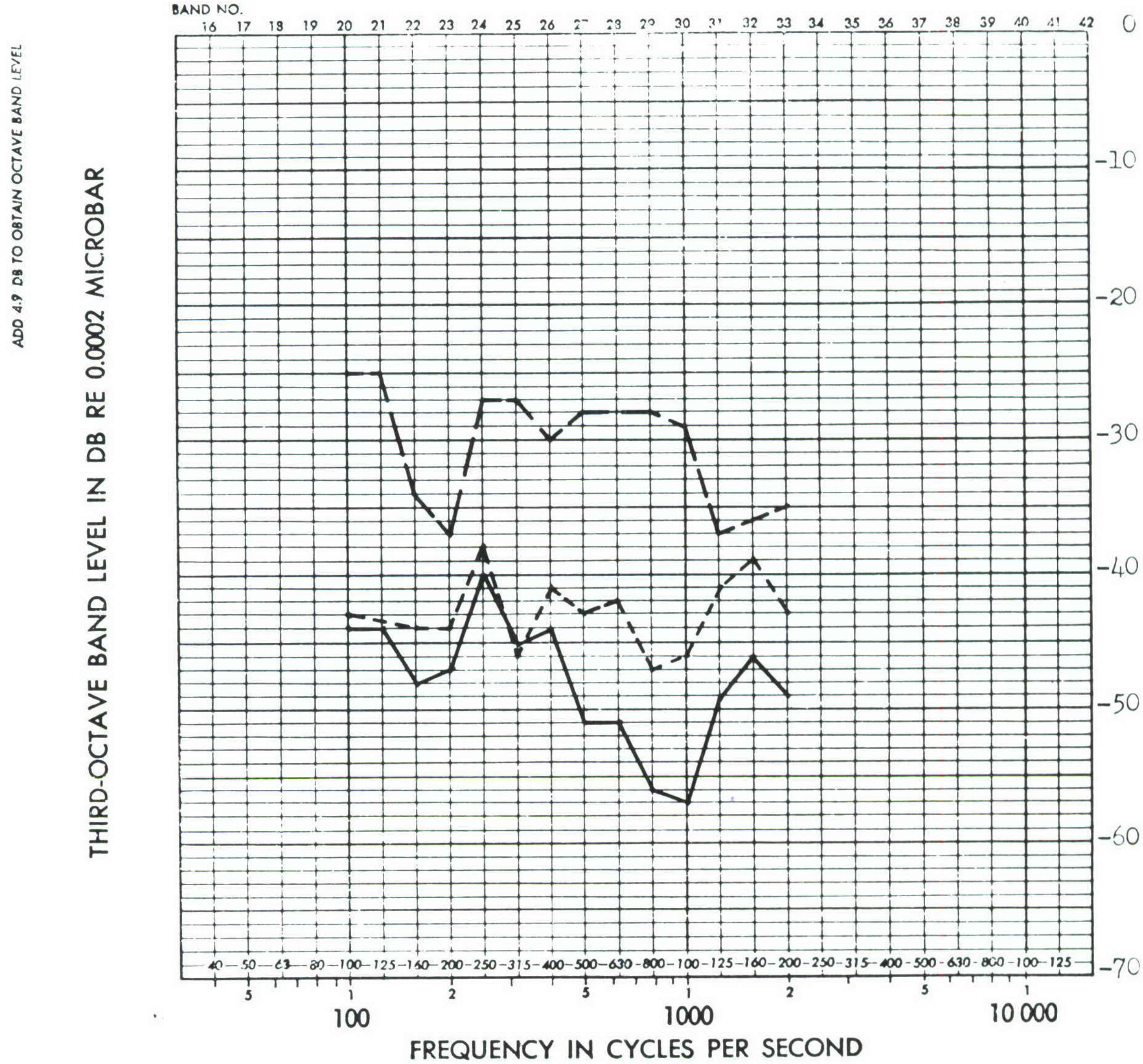

———————— Input at FS. 407 Accelerometer 46
— — — — — — Input at FS. 578 Lateral response
—— —— —— Input at FS. 738 FS. 684

FIGURE D68 FULL SCALE RESPONSE TRANSFER FUNCTIONS (DB) FOR CENTER OF UPPER PANEL, RIGHT SIDE, AFT SECTION

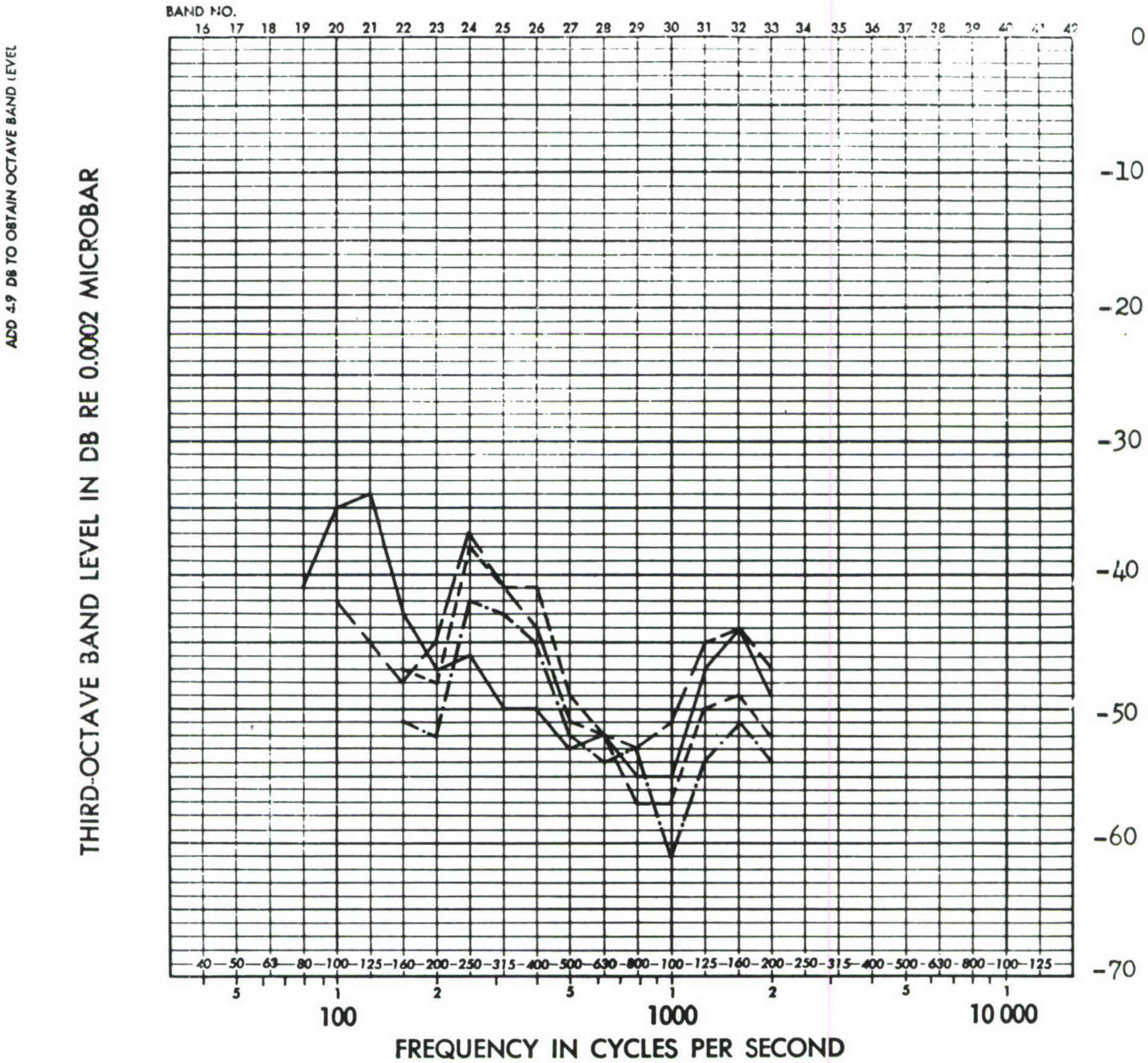

Accelerometer 41
Accelerometer 45
Accelerometer 77
Accelerometer 80

Input FS 407

FIGURE D69 FULL SCALE RESPONSE TRANSFER FUNCTIONS (DB) FOR RIGHT SIDE AFT PANELS AT FS. 670, 684, 680, 725; EXCITATION AT FS. 407

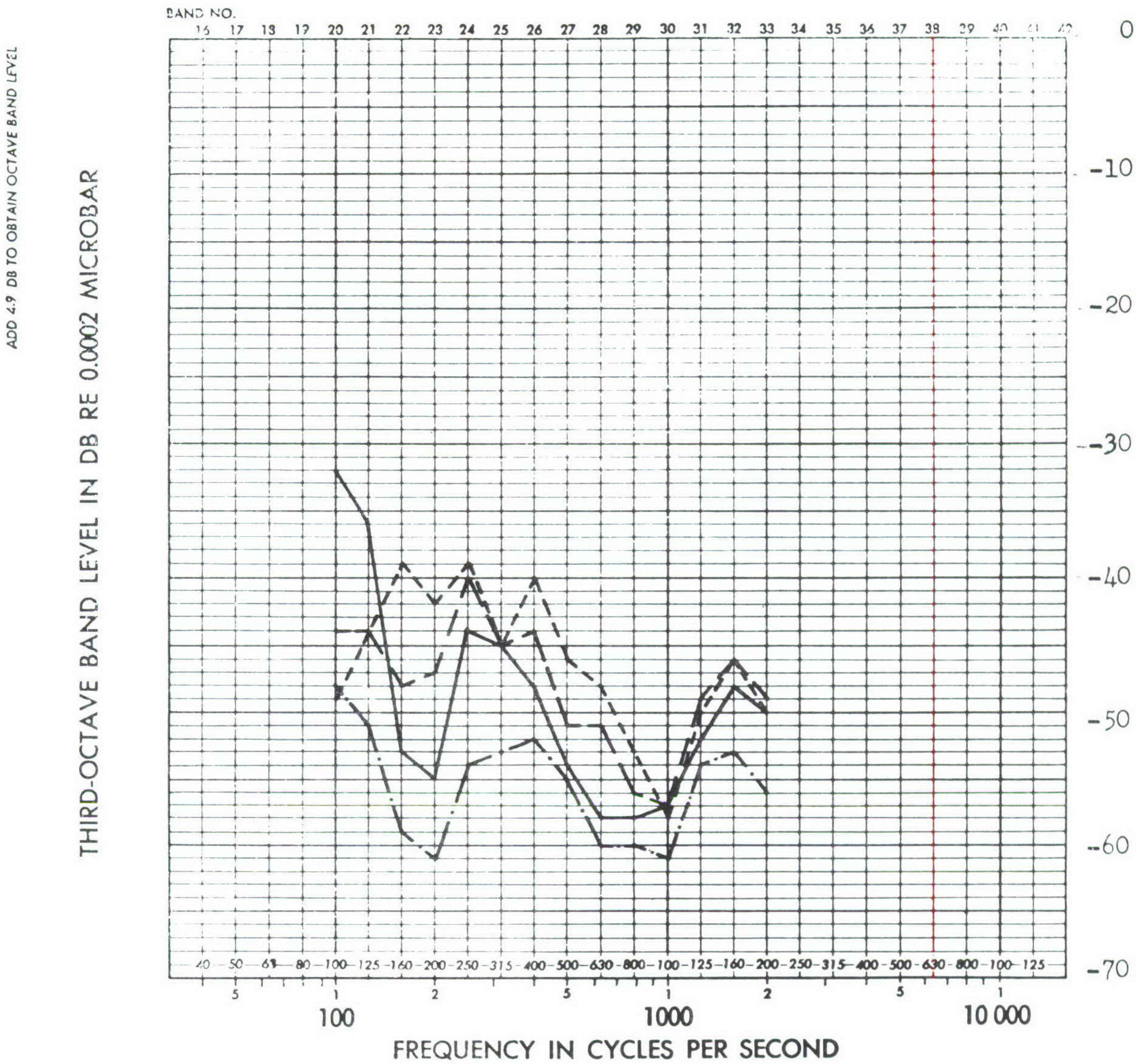

Accelerometer 42
Accelerometer 46
Accelerometer 78
Accelerometer 81

Input FS 407

FIGURE D70 FULL SCALE RESPONSE TRANSFER FUNCTIONS (DB) FOR RIGHT SIDE AFT PANELS AT FS. 670, 684, 680, 725; EXCITATION AT FS. 407

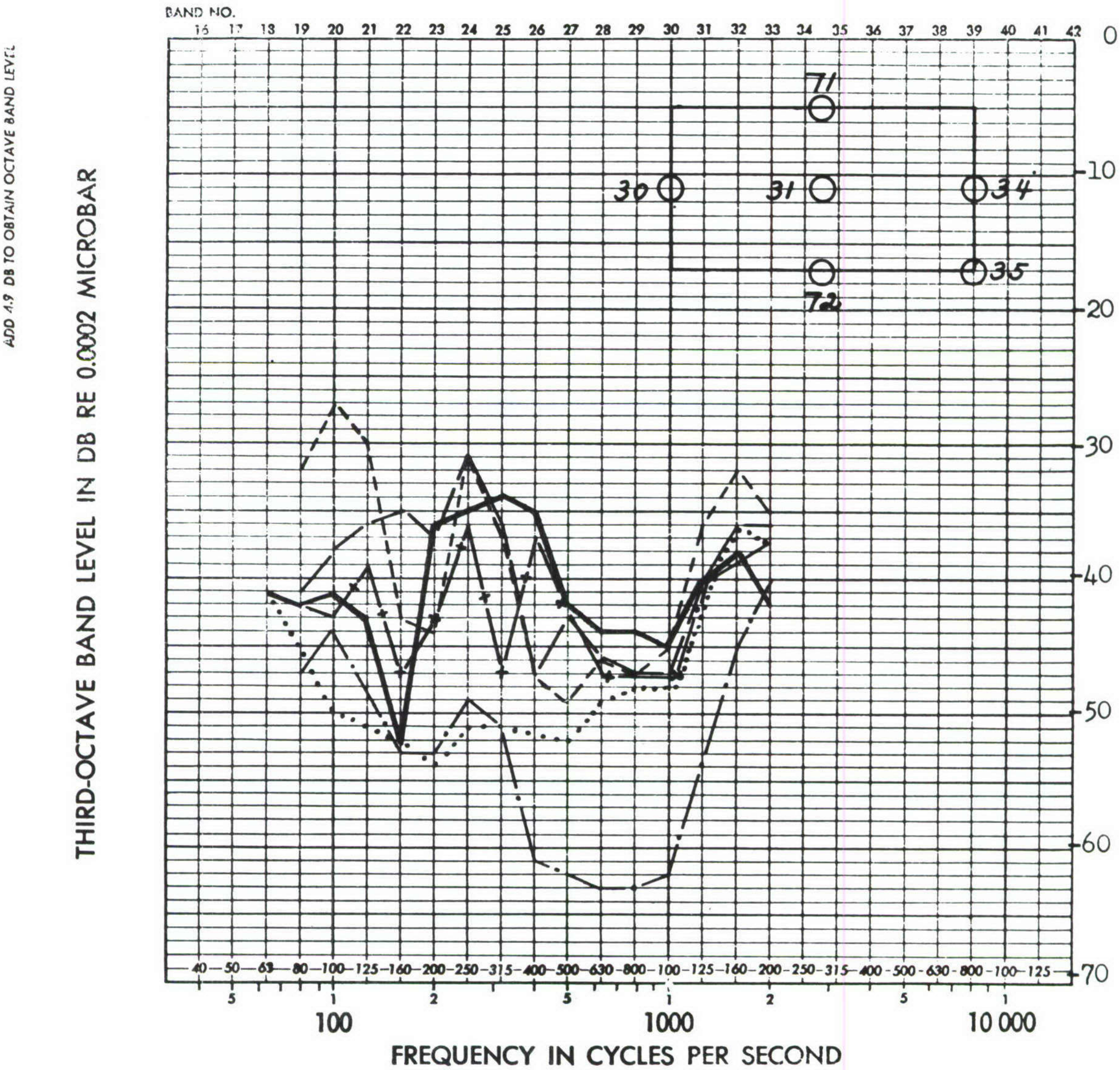

——+—— Accelerometer 30
——— Accelerometer 31
——·—— Accelerometer 34
··········· Accelerometer 35
— — — — Accelerometer 71
—— — — Accelerometer 72

Input FS. 407

FIGURE D71 COMPARISON OF FULL SCALE RESPONSE TRANSFER FUNCTIONS FOR UPPER AND LOWER LEFT LONGERONS, BULKHEAD EDGE, RING STIFFENER, AND INCLUDED PANEL FOR LEFT SIDE STRUCTURE BETWEEN FS. 536 AND 600; EXCITATION AT FS. 407

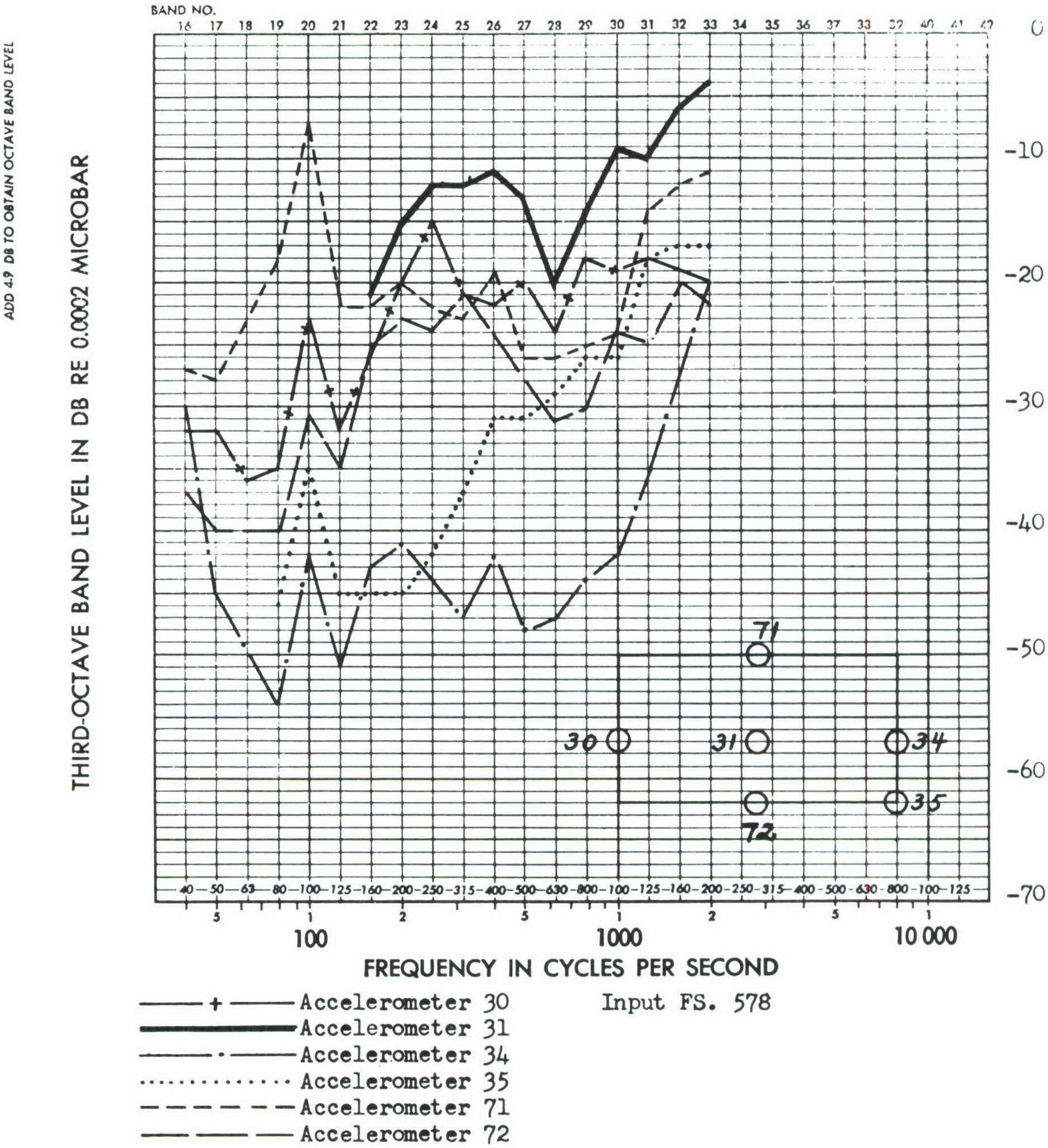

FIGURE D72 COMPARISON OF FULL SCALE RESPONSE TRANSFER FUNCTIONS FOR UPPER AND LOWER LEFT LONGERONS, BULKHEAD EDGE, RING STIFFENER, AND INCLUDED PANEL FOR LEFT SIDE STRUCTURE BETWEEN FS. 536 AND 600; EXCITATION AT FS. 578

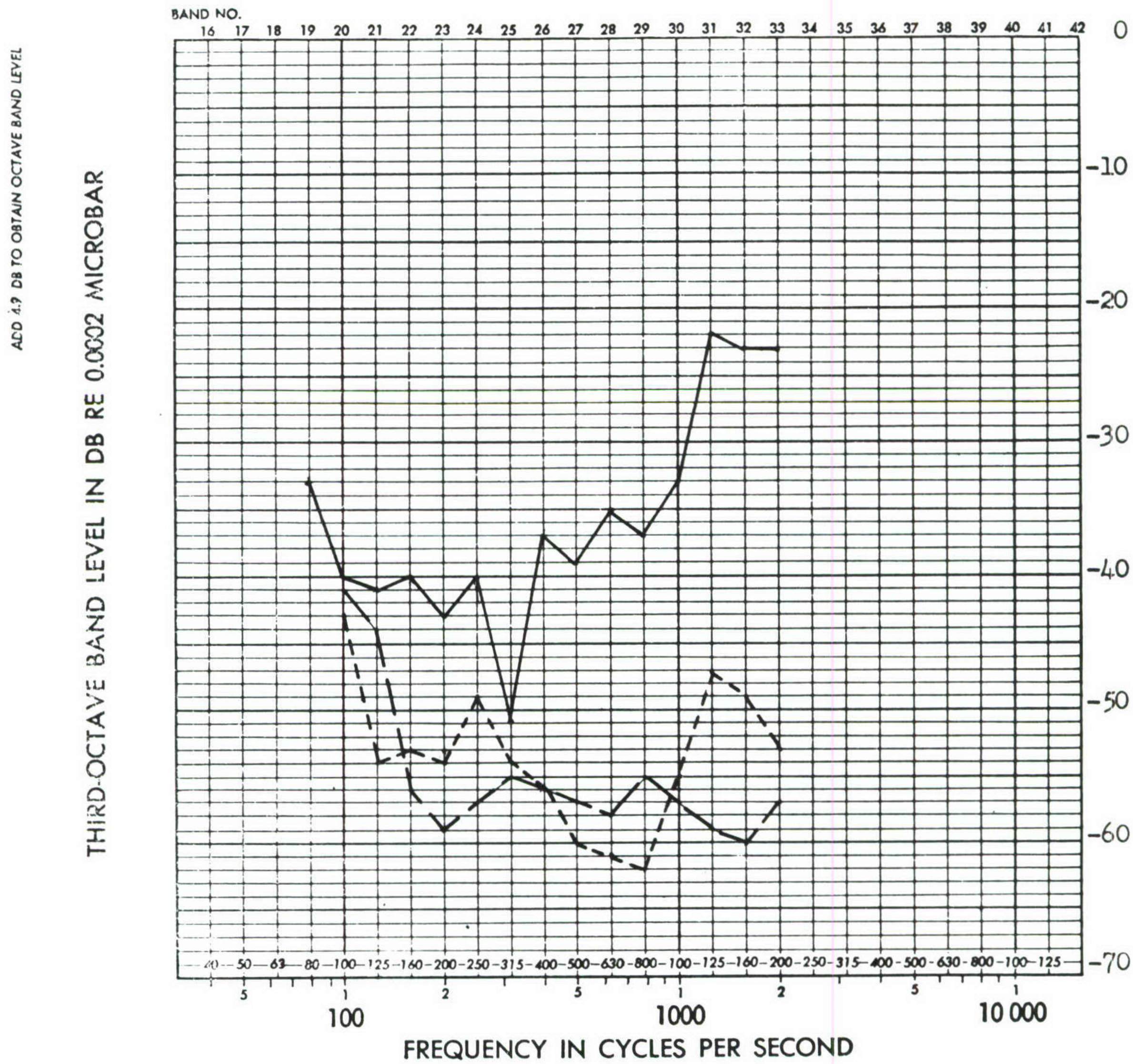

——————— Input at FS. 407 Accelerometer 58

– – – – – – – Input at FS. 578 Radial response

——— ——— —— Input at FS. 738 FS. 384

FIGURE D73 FULL SCALE RESPONSE TRANSFER FUNCTIONS (DB) FOR INTERSECTION OF LOWER LEFT LONGERON AND FORWARD BULKHEAD

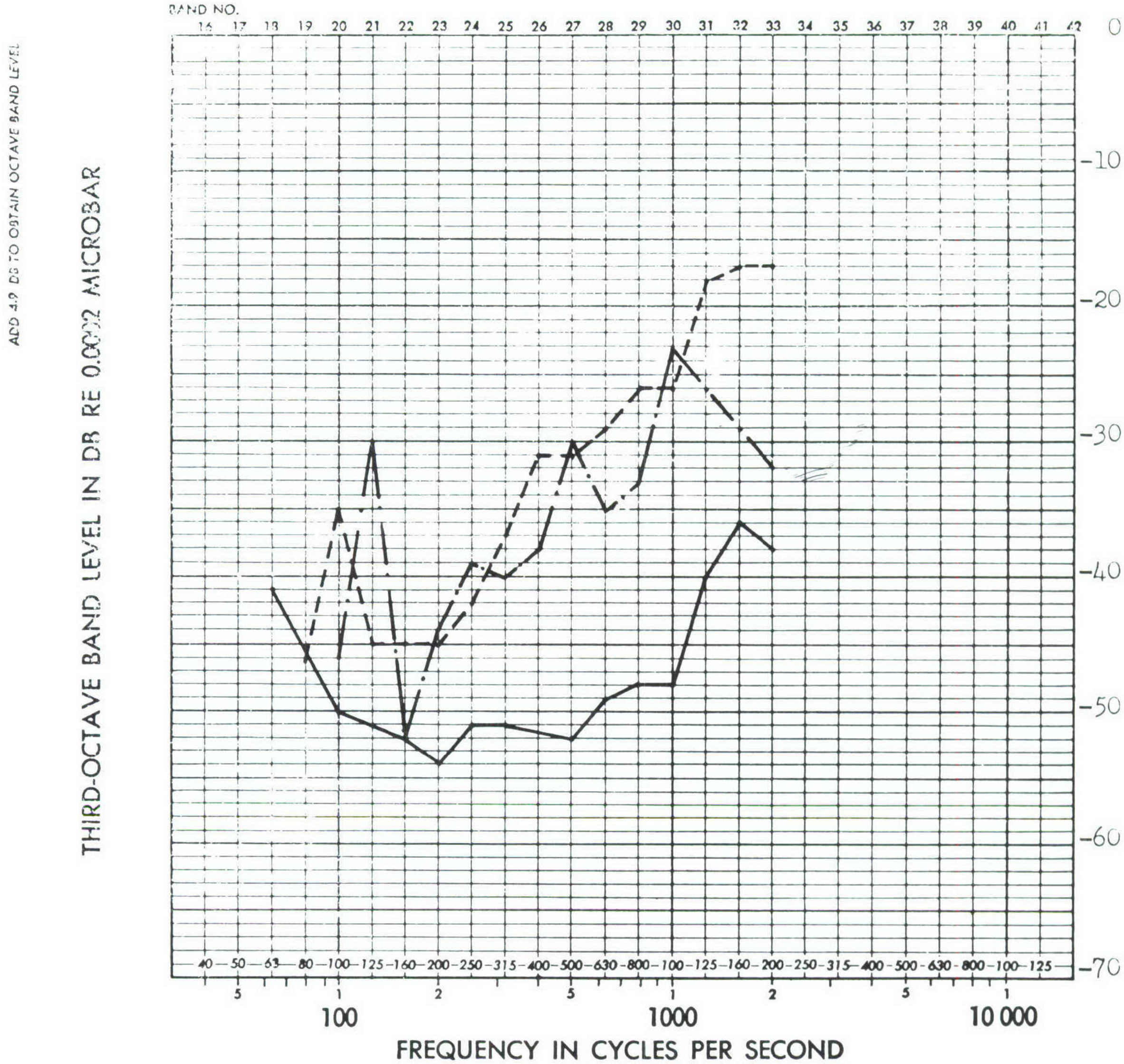

————	Input at FS. 407	Accelerometer 35
— — — —	Input at FS. 578	Lateral response
—— · ——	Input at FS. 647	FS. 600

FIGURE D 74 FULL SCALE RESPONSE TRANSFER FUNCTIONS (DB) FOR INTERSECTION OF LOWER LEFT LONGERON AND BULKHEAD

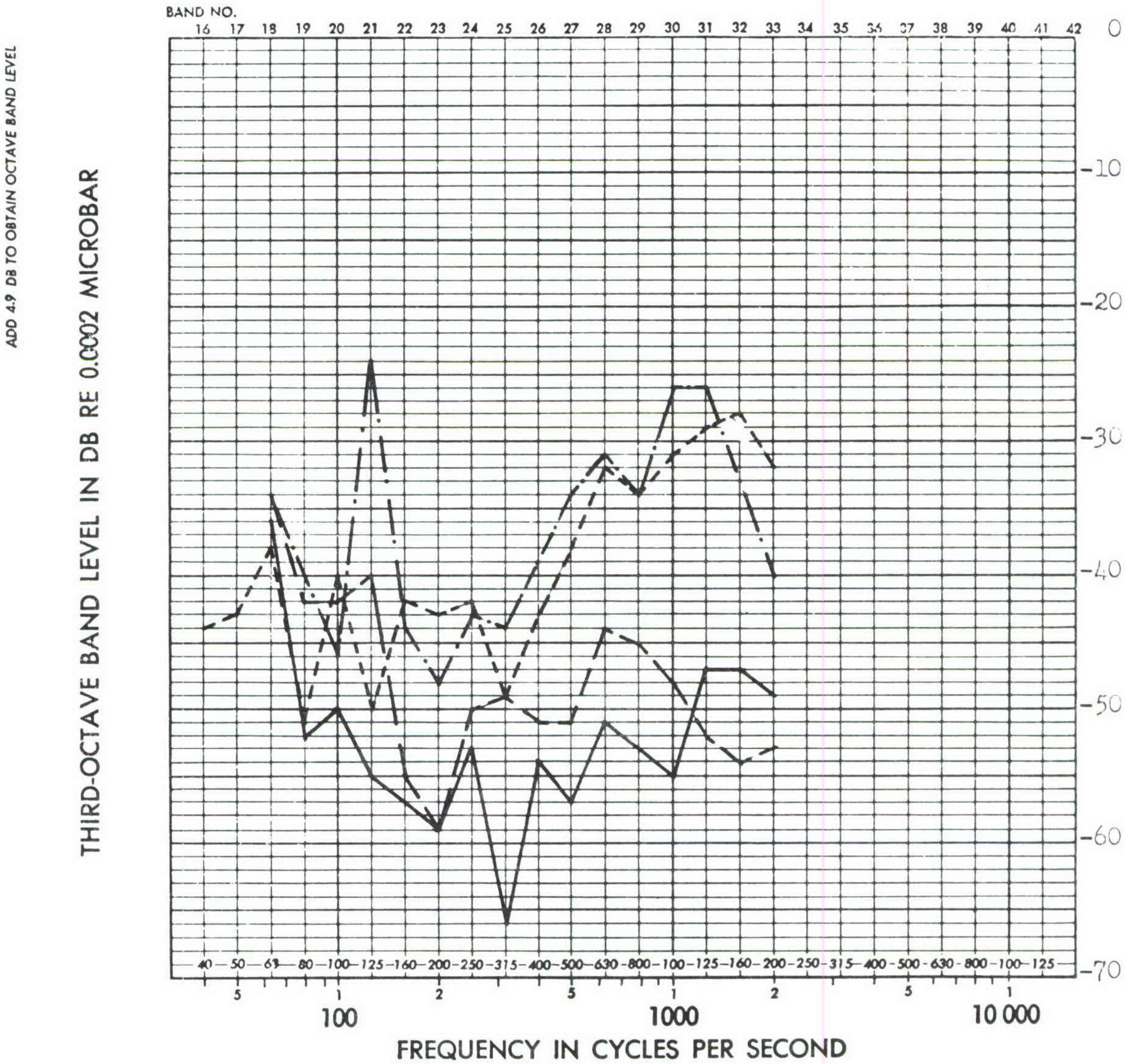

————————	Input at FS. 407	Accelerometer 36
- - - - - - - -	Input at FS. 568	Lateral response
—— · —— · ——	Input at FS. 647	FS. 600
—— —— ——	Input at FS. 738	Patrick accelerometer

FIGURE D75 FULL SCALE RESPONSE TRANSFER FUNCTIONS (DB) FOR INTERSECTION OF UPPER LEFT LONGERON AND BULKHEAD

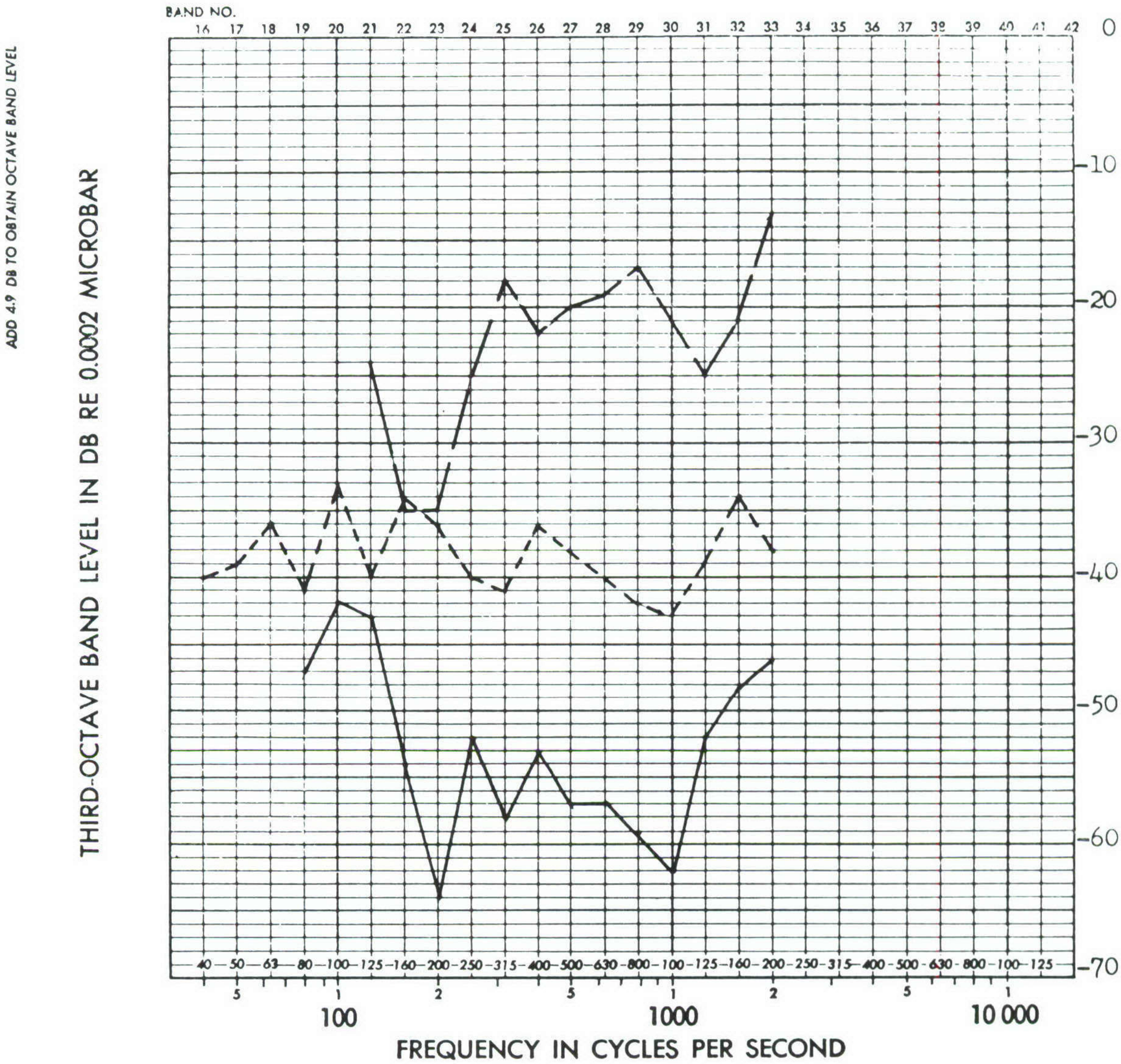

————————	Input at FS. 407	Accelerometer 57
– – – – – – –	Input at FS. 578	Radial response
—— —— ——	Input at FS. 738	FS. 761

FIGURE D76 FULL SCALE RESPONSE TRANSFER FUNCTIONS (DB) FOR LOWER LEFT EDGE OF AFT BULKHEAD

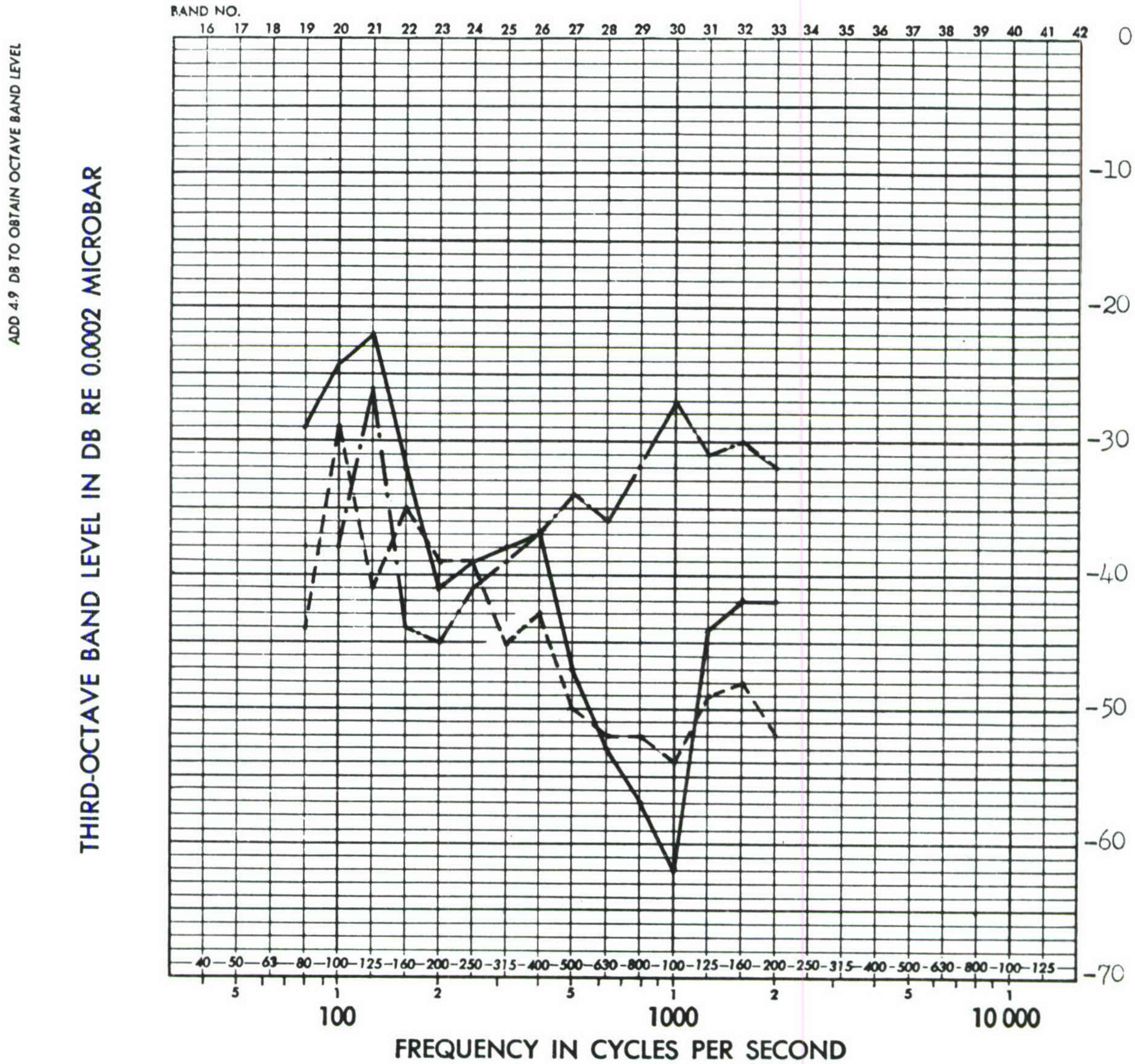

————	Input at FS. 407	Accelerometer 54
— — — —	Input at FS. 578	Lateral response
—— —— ——	Input at FS. 647	FS. 735

FIGURE D77 FULL SCALE RESPONSE TRANSFER FUNCTIONS (DB) FOR CENTER OF SKIN STIFFENERS, LEFT SIDE, AFT SECTION

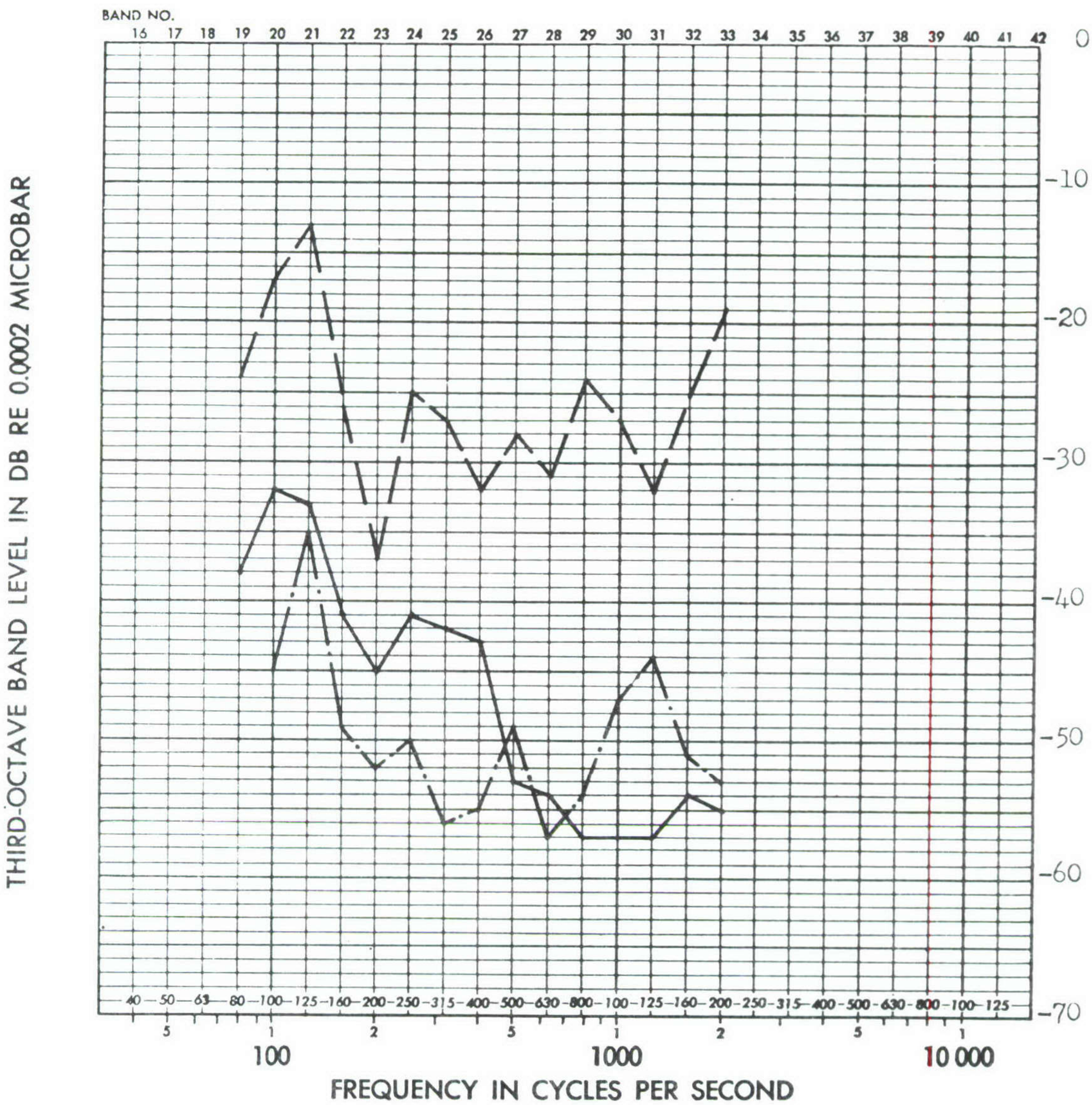

————————	Input at FS. 407	Accelerometer 55
——— • ———	Input at FS. 647	Lateral response
—— —— ——	Input at FS. 738	FS. 735

FIGURE D78 FULL SCALE RESPONSE TRANSFER FUNCTIONS (DB) FOR CENTER OF SKIN STIFFENERS, RIGHT SIDE, AFT SECTION

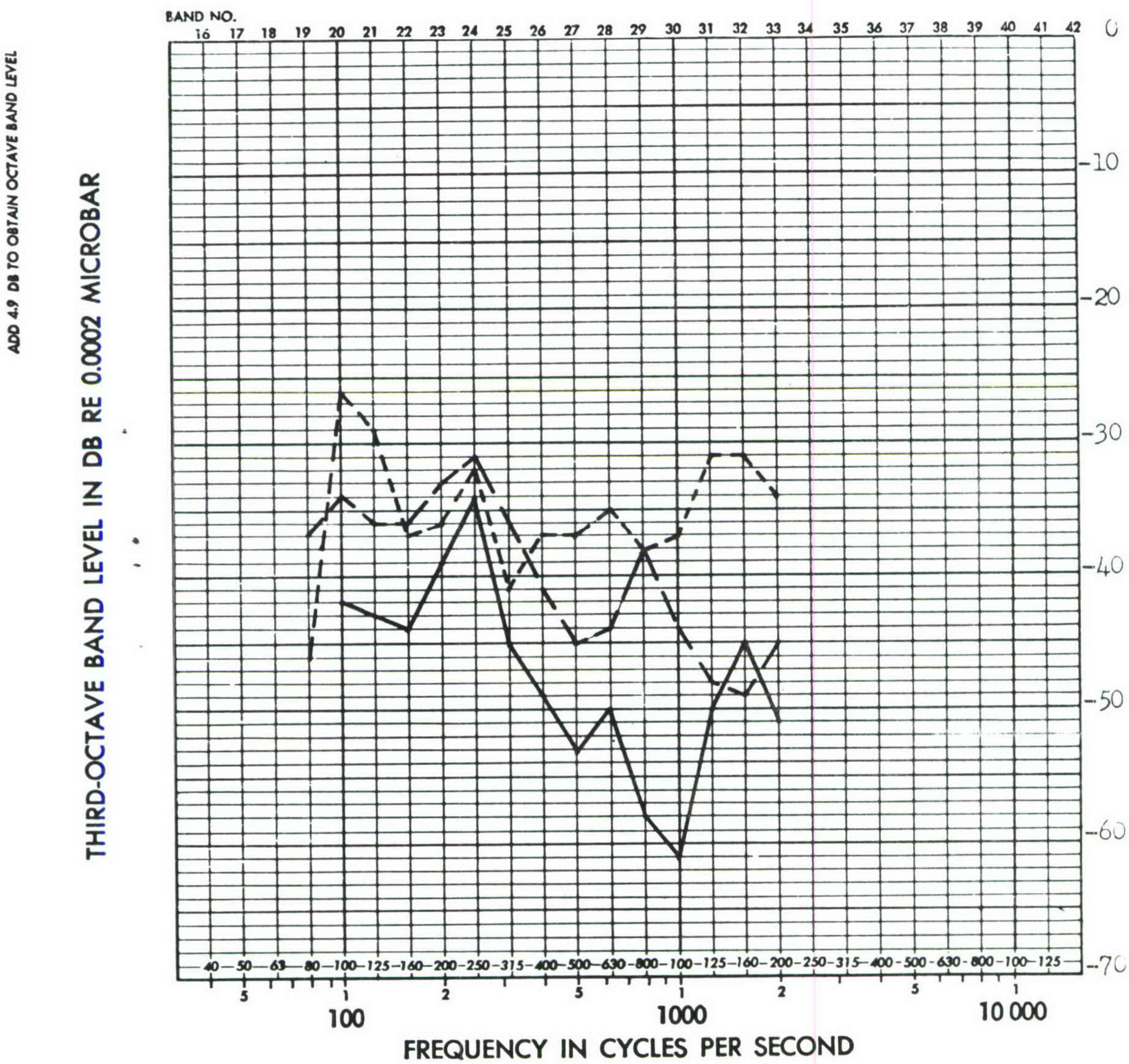

———————— Input at FS. 407 Accelerometer 37

– – – – – – Input at FS. 578 Lateral responsel

—— —— —— Input at FS. 738 FS. 624

FIGURE D79 FULL SCALE RESPONSE TRANSFER FUNCTIONS (DB) FOR INTERSECTION OF HORIZONTAL AND VERTICAL SKIN STIFFENERS, LEFT SIDE, AFT SECTION

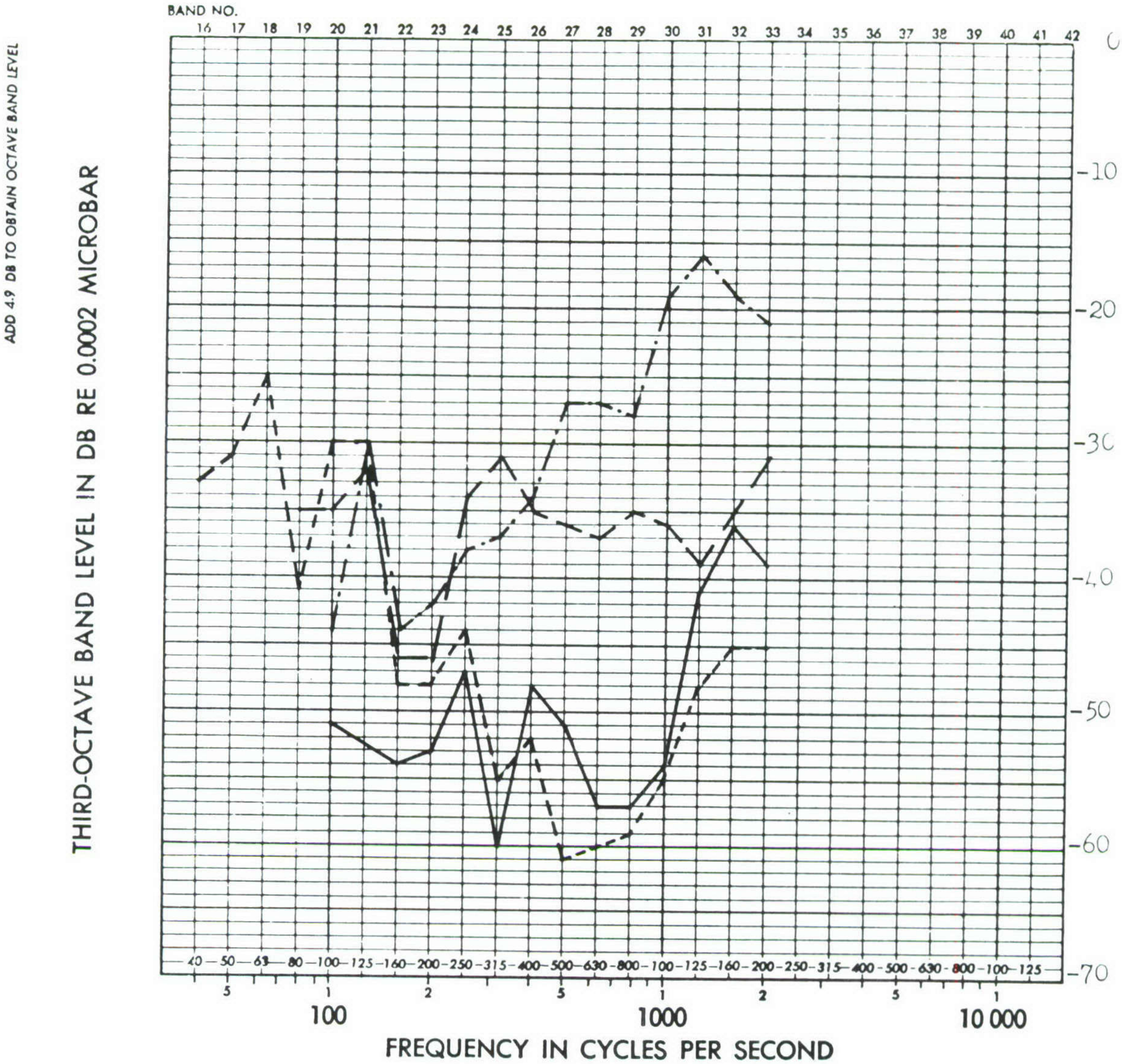

————————	Input at FS. 407	Accelerometer 40
— — — — — —	Input at FS. 568	Lateral response
———·———	Input at FS. 647	FS. 647
—— —— ——	Input at FS. 738	

FIGURE D80 FULL SCALE RESPONSE TRANSFER FUNCTIONS (DB) FOR LOWER LEFT INLET DUCT RIB

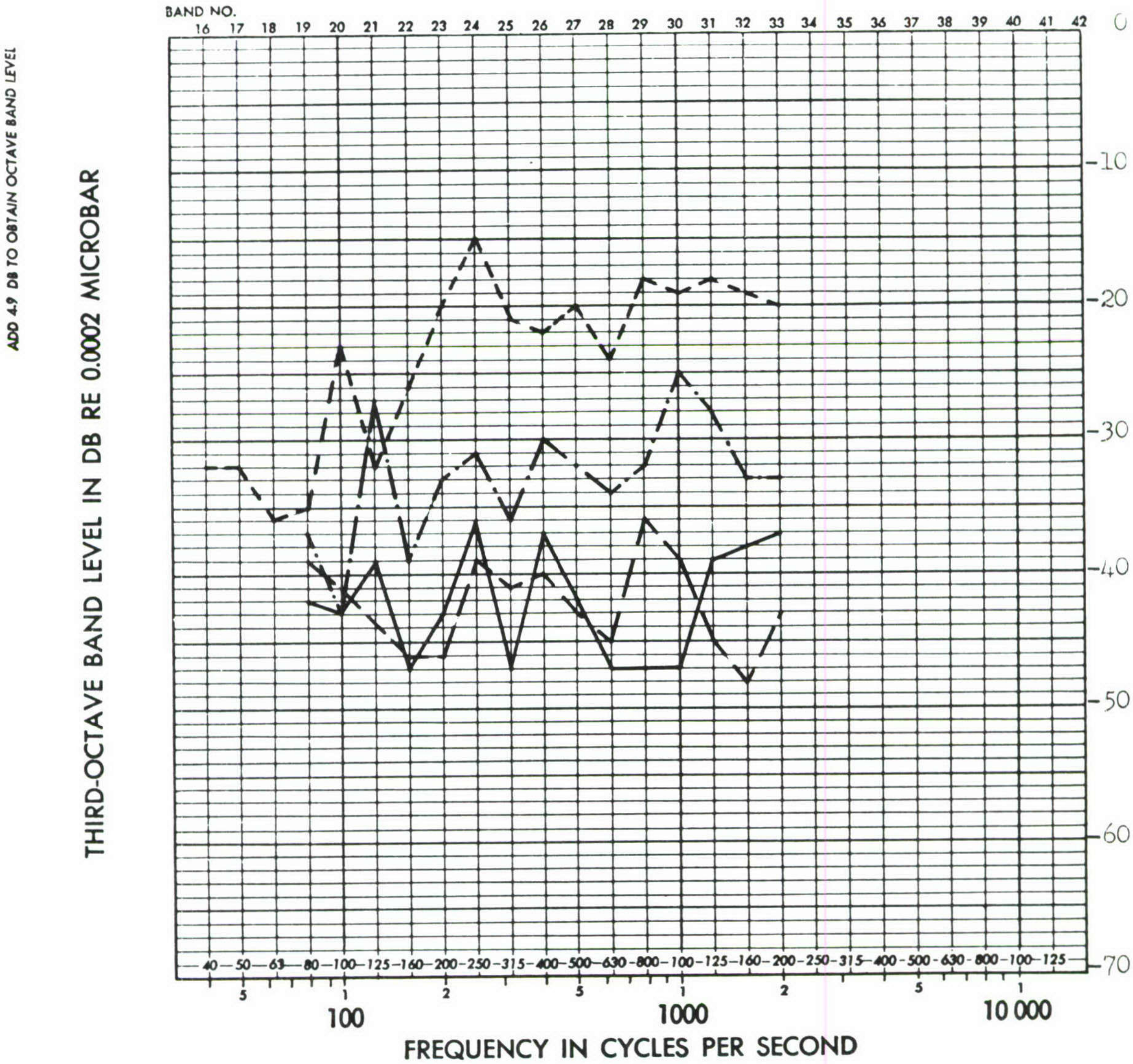

———— Input at FS. 407
– – – – Input at FS. 568
——•—— Input at FS. 647
—— —— Input at FS. 738

Accelerometer 30
Lateral response
FS. 552

FIGURE D81 FULL SCALE RESPONSE TRANSFER FUNCTIONS (DB) FOR RIB STIFFENER ATTACHED TO SKIN

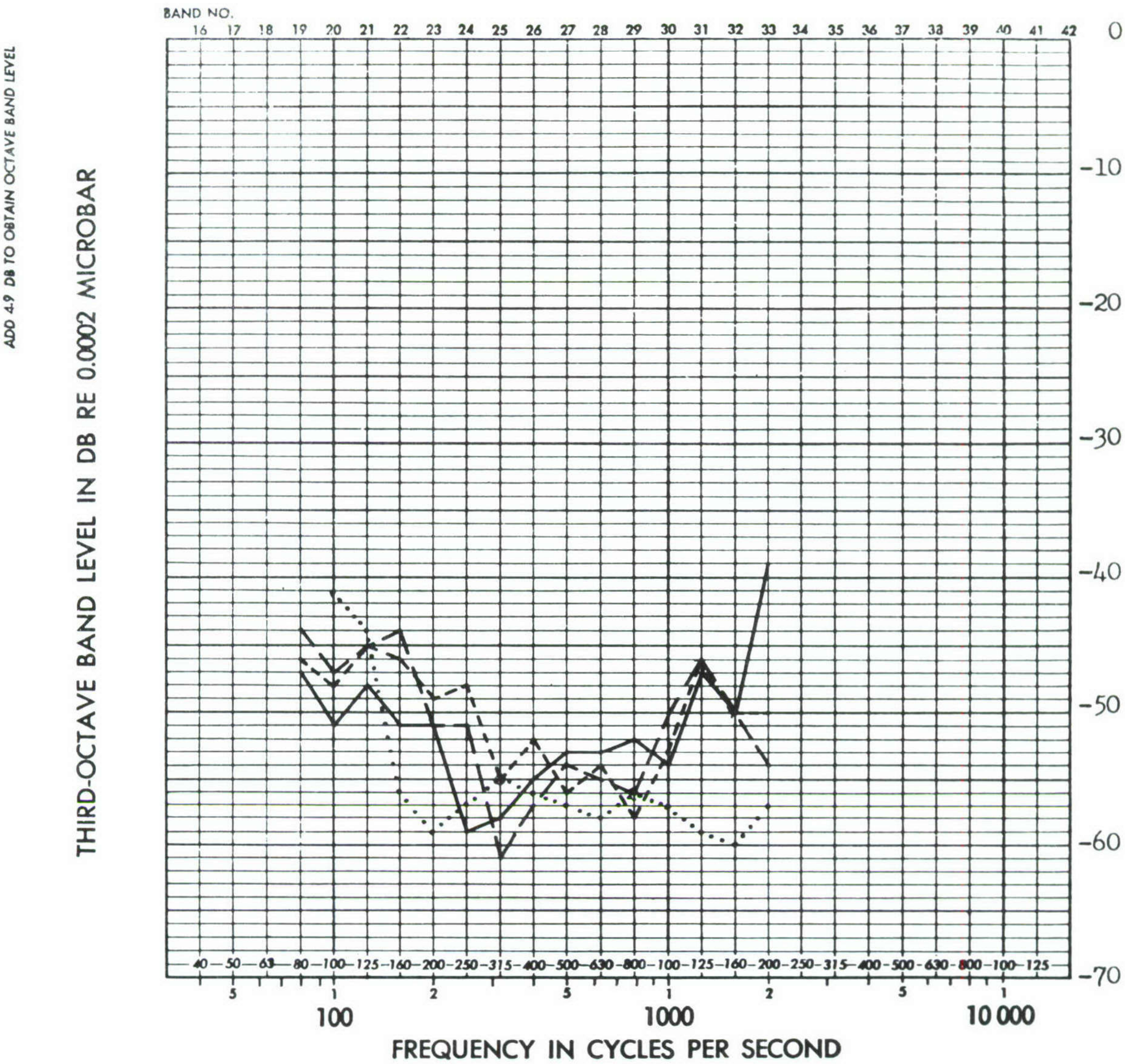

Open box, normal to skin — Input FS. 738

Open box, 60° grazing incidence

Open box, 30° grazing incidence — Accelerometer 58

Radial response

Closed box

FIGURE D82 FULL SCALE RADIAL RESPONSE TRANSFER FUNCTIONS (DB) AT LOWER LEFT LONGERON, BULKHEAD INTERSECTION, FS. 384, FOR VARIOUS ANGLE OF INCIDENCE INPUTS AT FS. 738

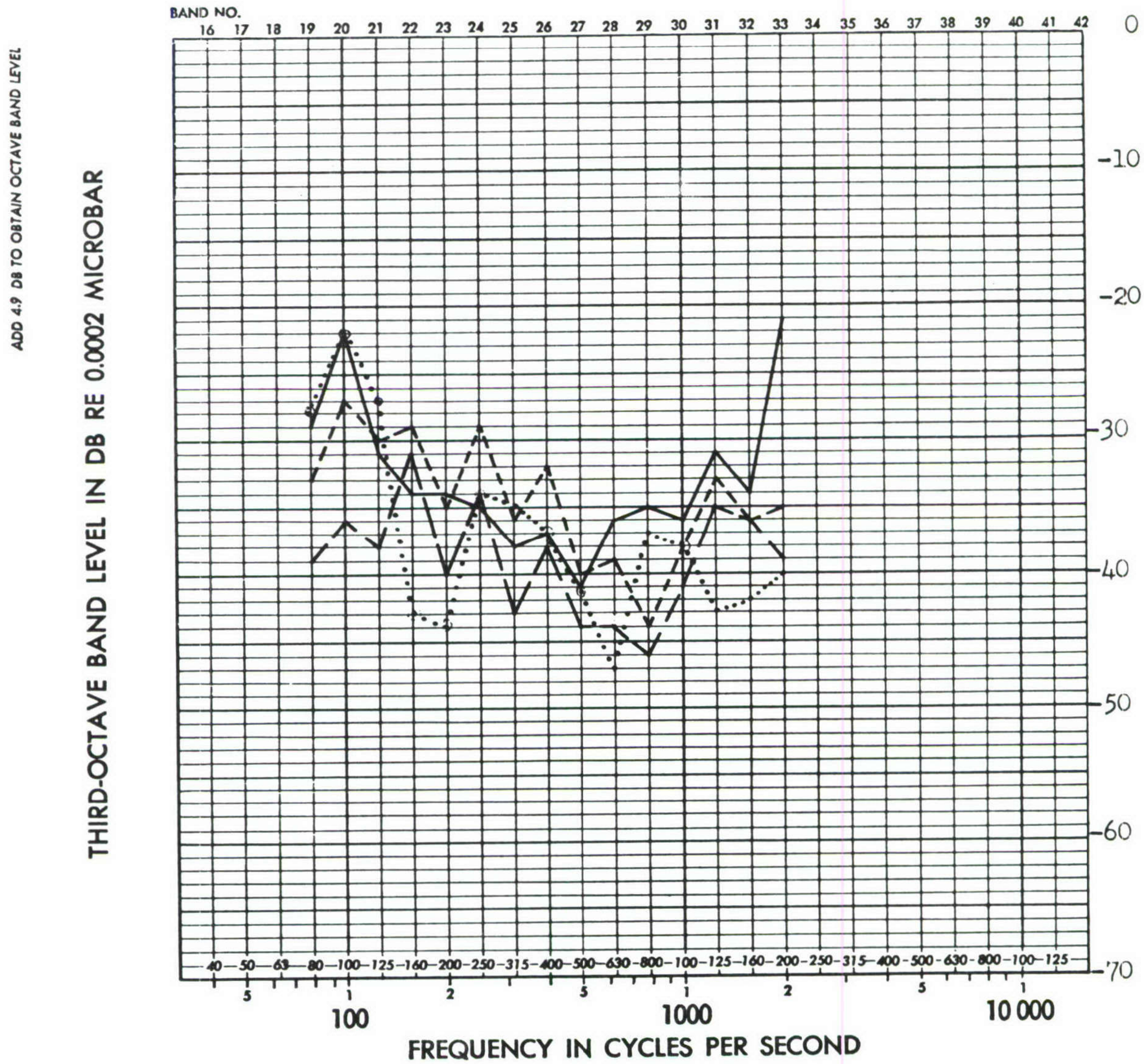

Open box, normal to skin
Open box, 60° grazing incidence
Open box, 30° grazing incidence
CLOSED BOX

Input FS. 738
Accelerometer 71
Radial response

FIGURE D83 FULL SCALE RADIAL RESPONSE TRANSFER FUNCTIONS (DB) AT UPPER LEFT LONGERON FS. 576, FOR VARIOUS ANGLE OF INCIDENCE INPUTS AT FS. 738

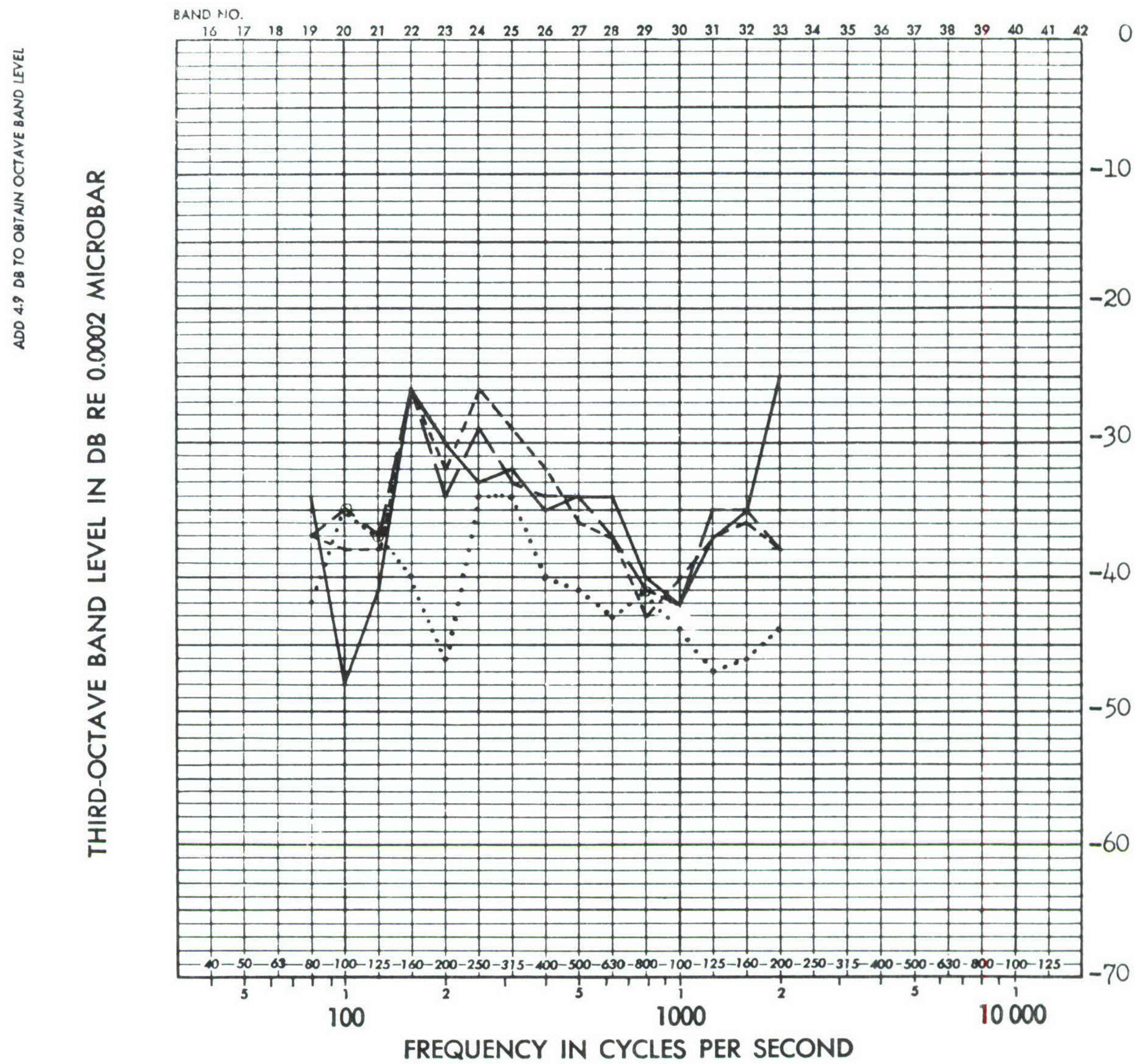

———————— Open box, normal to skin
— — — — Open box, 60° grazing incidence
- - - - - - Open box, 30° grazing incidence
·············· Closed box

Input FS. 738
Accelerometer 73
Lateral response.

FIGURE D84 FULL SCALE LATERAL RESPONSE TRANSFER FUNCTIONS (DB) LEFT SIDE EDGE OF AFT FLOOR, FS. 624, FOR VARIOUS ANGLE OF INCIDENCE INPUTS AT FS. 738

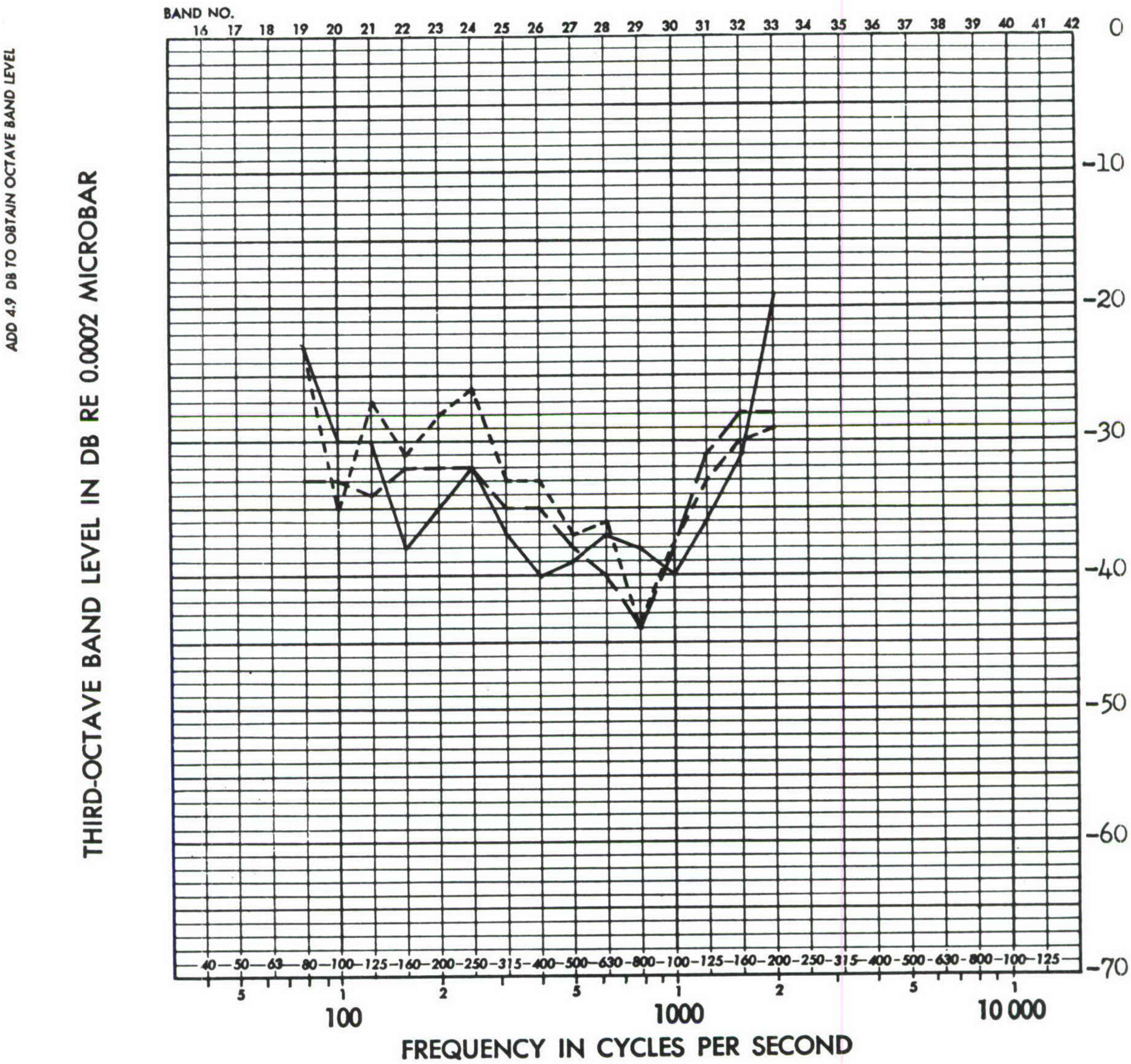

————————	Open box, normal to skin	Input FS. 738
——— ——— ———	Open box, 60° grazing incidence	Accelerometer 84
- - - - - -	Open box, 30° grazing incidence	Radial response

FIGURE D85 FULL SCALE RADIAL RESPONSE TRANSFER FUNCTIONS (DB) AT AFT BULKHEAD EDGE, FS. 761, FOR VARIOUS ANGLE OF INCIDENCE INPUTS AT FS. 738

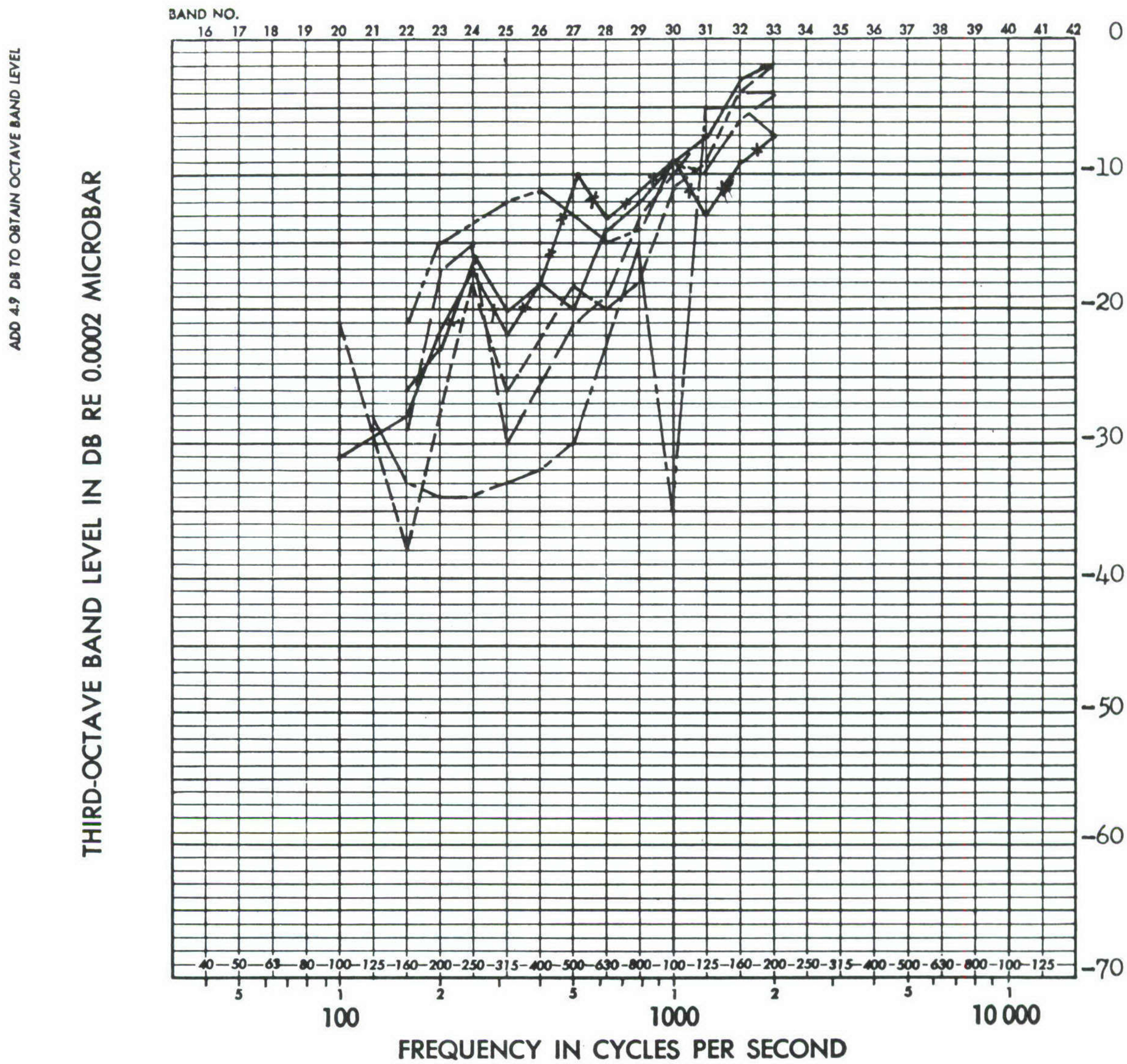

- - - - - - - - Accelerometer C8
———- - -——— Accelerometer C9
———- - ——— Accelerometer C27
———————— Accelerometer C28
——— ——— —— Accelerometer C29
———*——— Accelerometer C30

Input FS. 578
Left side panel of
compartment
Radial response

FIGURE D86 FULL SCALE RADIAL RESPONSE TRANSFER FUNCTIONS (DB) FOR LEFT SIDE PANEL OF COMPARTMENT BETWEEN FS. 536 AND 600; EXCITATION, LEFT SIDE, AT FS. 578

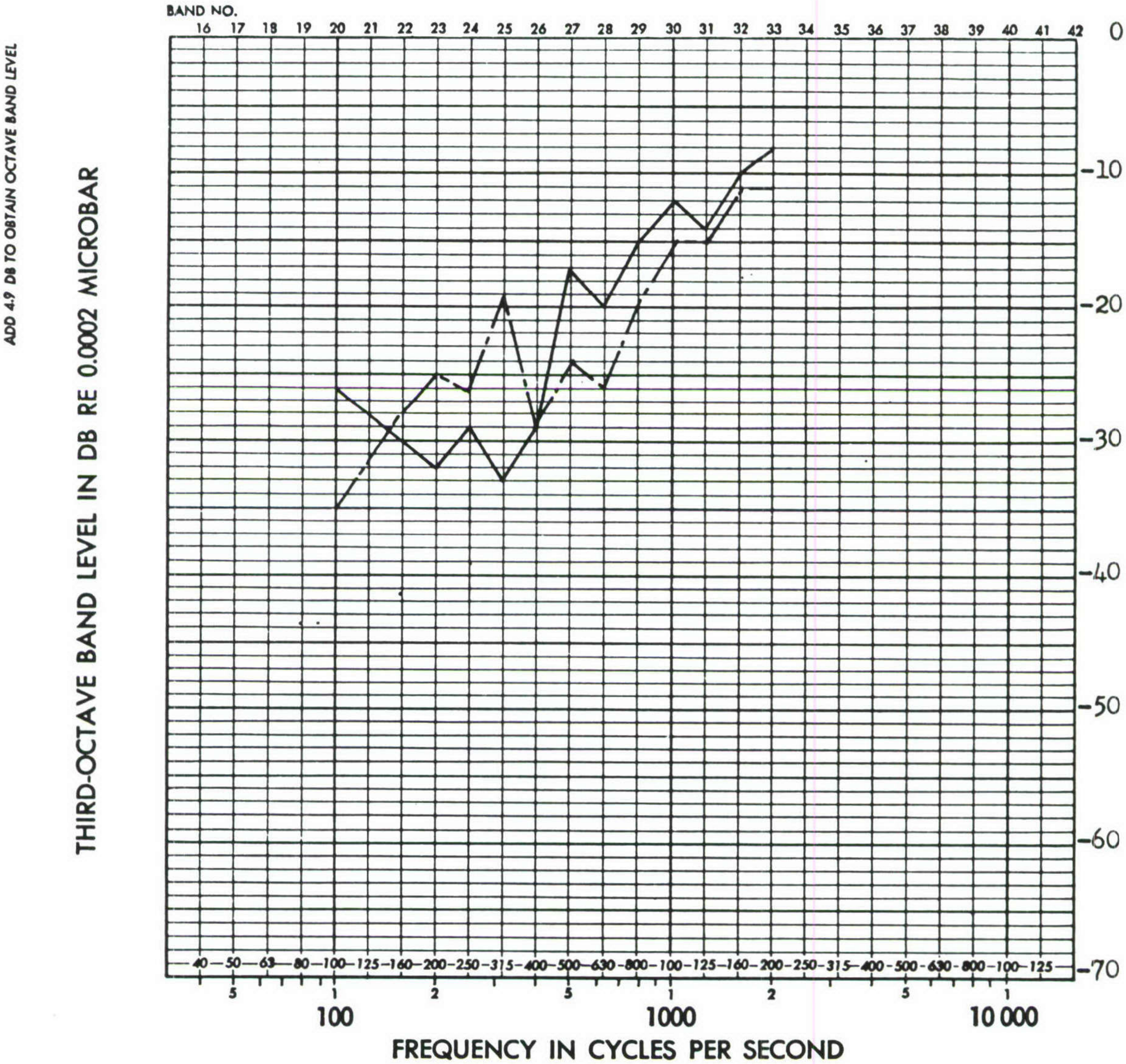

——————— Accelerometer C43   Input FS. 578

——— – ——— Accelerometer C44   Left side forward panel of compartment

Radial response

FIGURE D87   FULL SCALE RADIAL RESPONSE TRANSFER FUNCTIONS (DB) FOR FORWARD LEFT SIDE PANEL OF COMPARTMENT BETWEEN FS. 536 AND 600; EXCITATION, LEFT SIDE, AT FS. 578

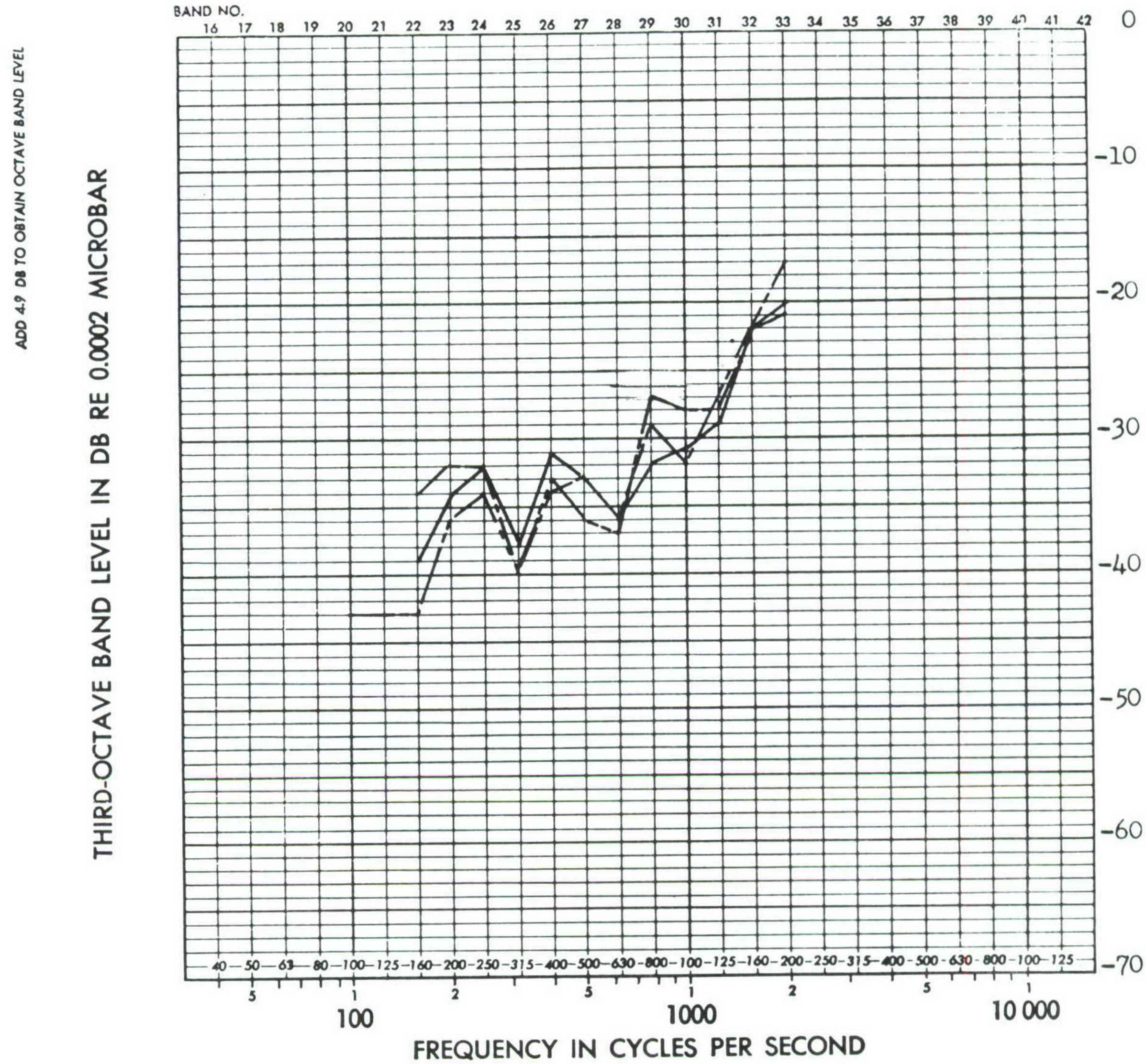

Accelerometer C5
Accelerometer C14
Accelerometer C15

Input FS. 578
Forward upper floor of
compartment
Vertical response

FIGURE D88 FULL SCALE VERTICAL RESPONSE TRANSFER FUNCTIONS (DB) FOR FORWARD UPPER FLOOR OF COMPARTMENT BETWEEN FS. 536 AND 600; EXCITATION, LEFT SIDE, AT FS. 578

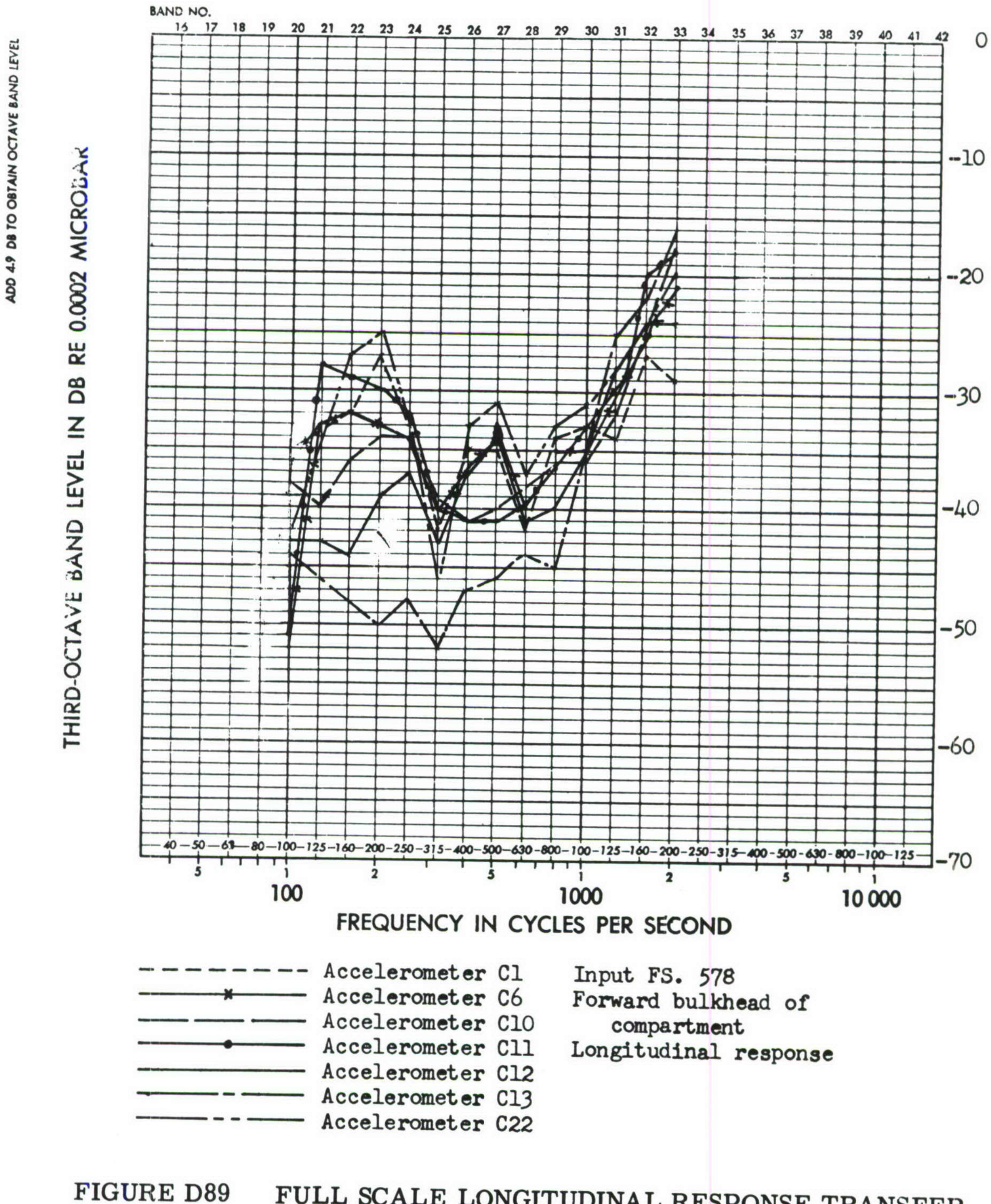

FIGURE D89 FULL SCALE LONGITUDINAL RESPONSE TRANSFER FUNCTIONS (DB) FOR FORWARD BULKHEAD OF COMPARTMENT BETWEEN FS. 536 AND 600; EXCITATION, LEFT SIDE, AND FS. 578

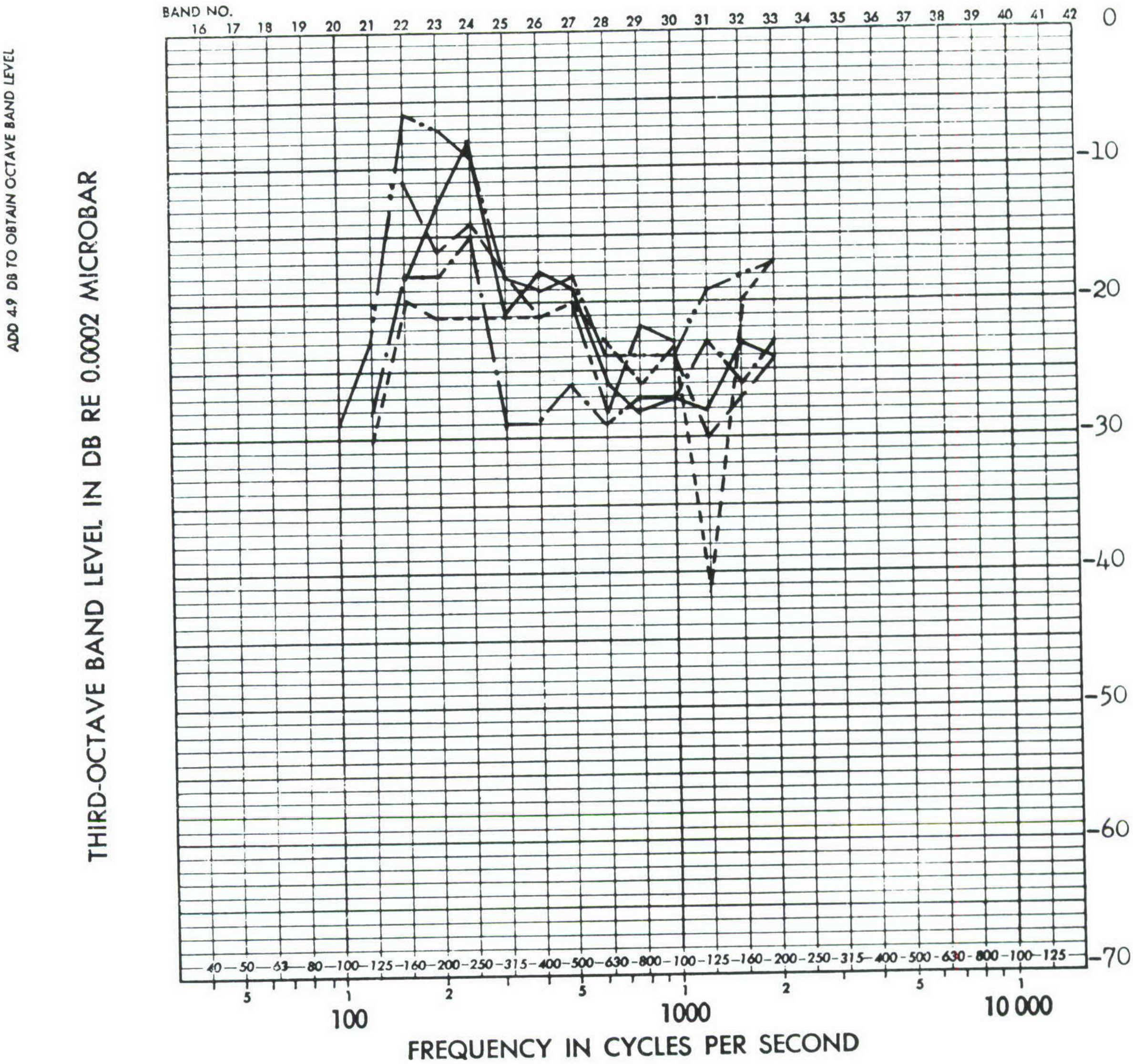

———————	Accelerometer C24	Input FS. 578
—— —— ——	Accelerometer C25	Compartment floor
– – – – – – –	Accelerometer C26	Vertical Response
——— · · ———	Accelerometer C35	
——— · ———	Accelerometer C36	

FIGURE D90 FULL SCALE VERTICAL RESPONSE TRANSFER FUNCTIONS (DB) FOR FLOOR OF COMPARTMENT BETWEEN FS. 536 AND 600; EXCITATION, LEFT SIDE, AT FS. 578

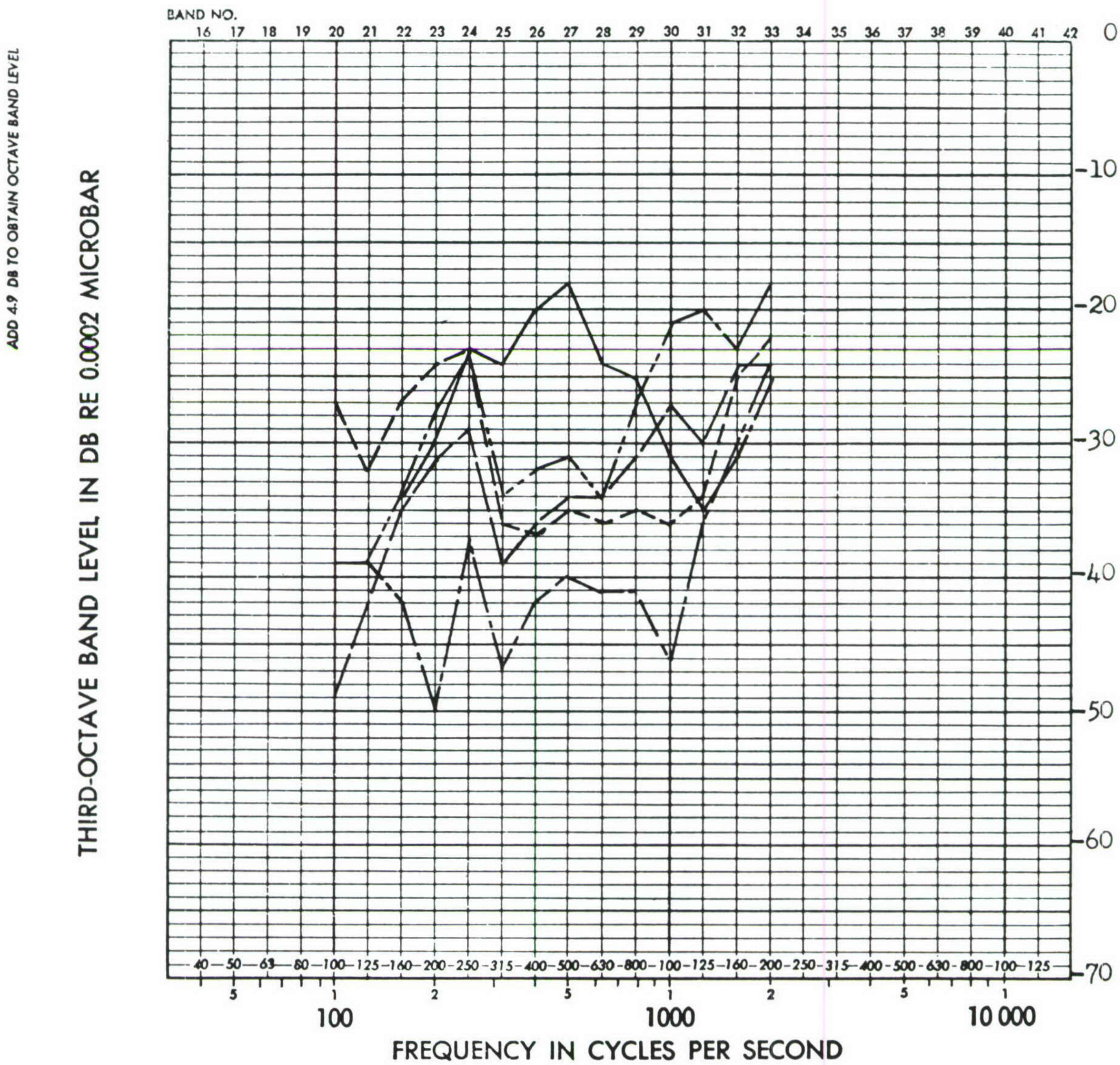

Accelerometer C17   Input FS. 578

Accelerometer C31   Aft bulkhead of compartment

Accelerometer C32

Accelerometer C33

Accelerometer C49

FIGURE D91   FULL SCALE RESPONSE TRANSFER FUNCTIONS (DB) FOR AFT BULKHEAD OF COMPARTMENT BETWEEN FS. 536 AND 600; EXCITATION, LEFT SIDE, AT FS. 578

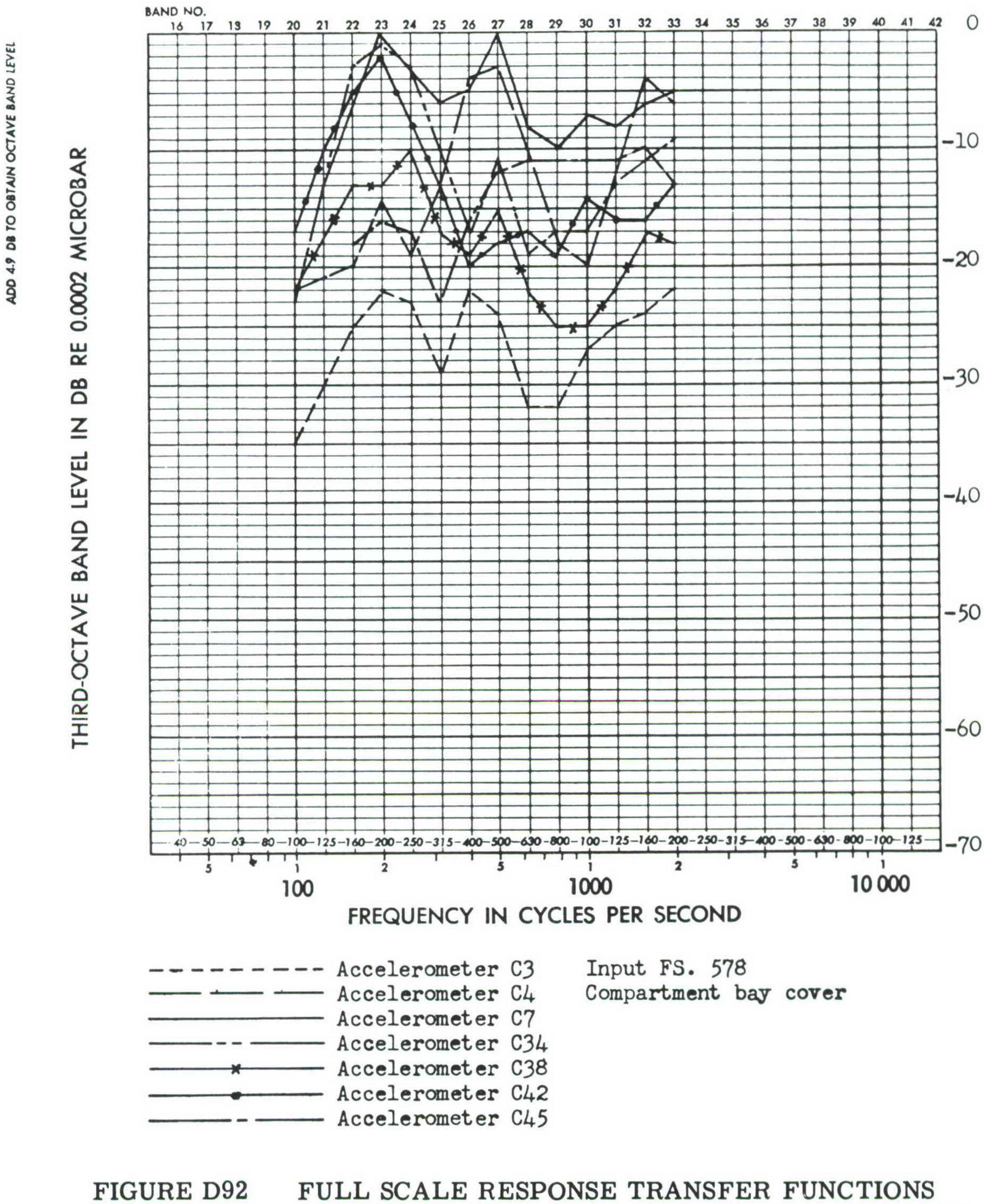

FIGURE D92 FULL SCALE RESPONSE TRANSFER FUNCTIONS (DB) FOR COMPARTMENT BAY COVER, BETWEEN FS. 536 AND 600; EXCITATION, LEFT SIDE, FS. 578

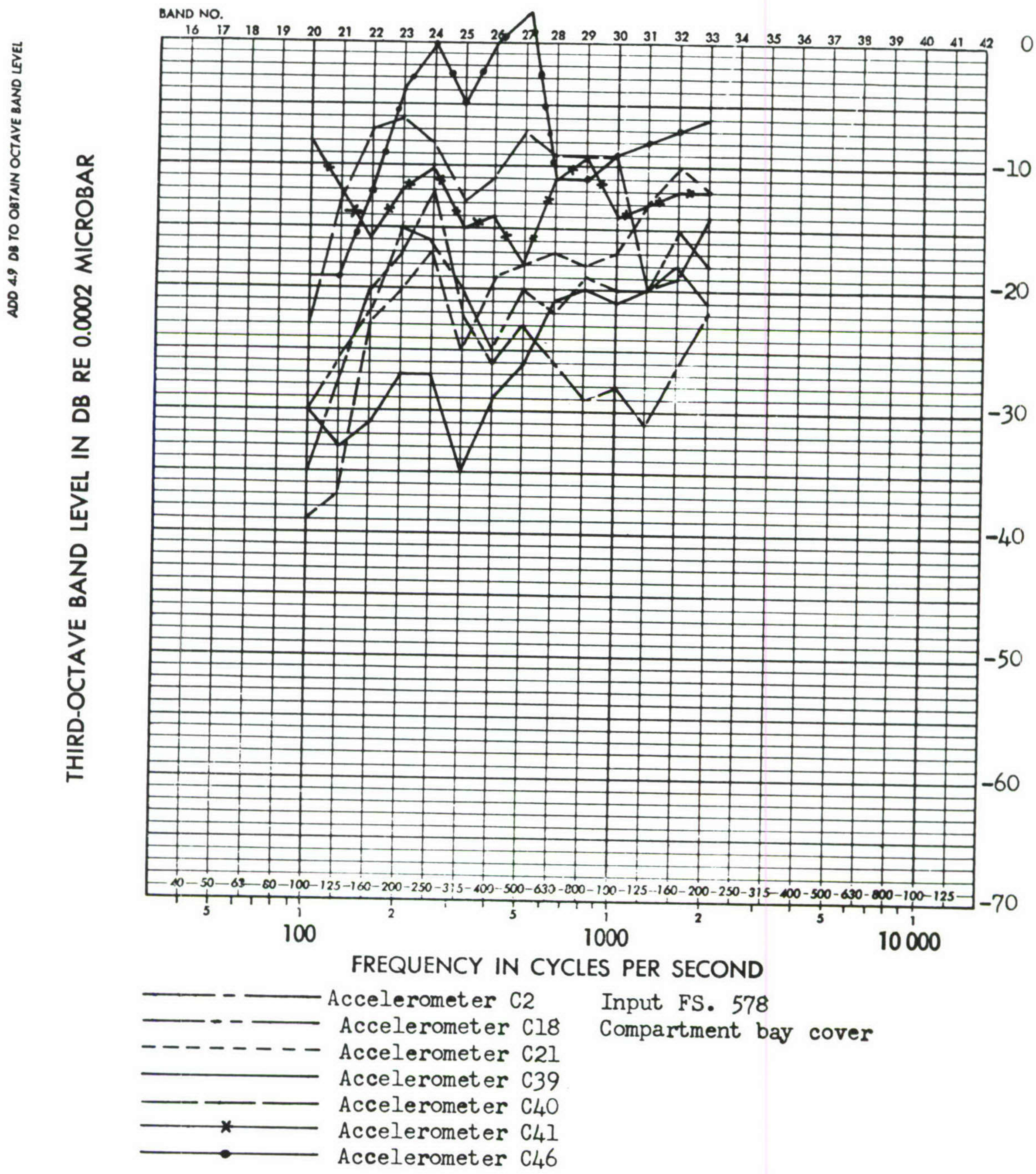

FIGURE D93 FULL SCALE RESPONSE TRANSFER FUNCTIONS (DB) FOR COMPARTMENT BAY COVER BETWEEN FS. 536 AND 600; EXCITATION, LEFT SIDE, AT FS. 578

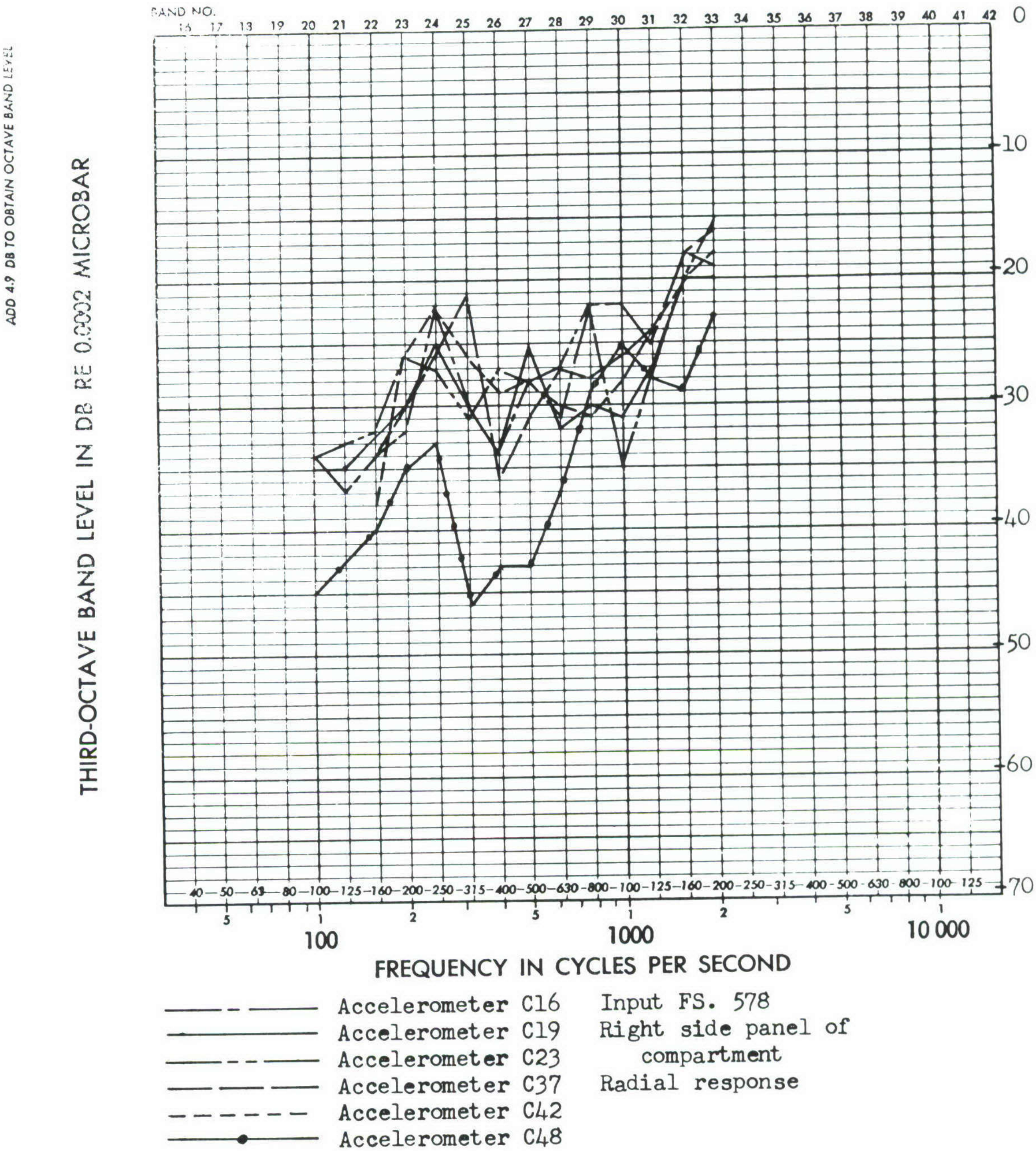

FIGURE D94 FULL SCALE RESPONSE TRANSFER FUNCTIONS (DB) FOR RIGHT SIDE PANEL OF COMPARTMENT BETWEEN FS. 536 AND 600; EXCITATION, LEFT SIDE, AT FS. 576

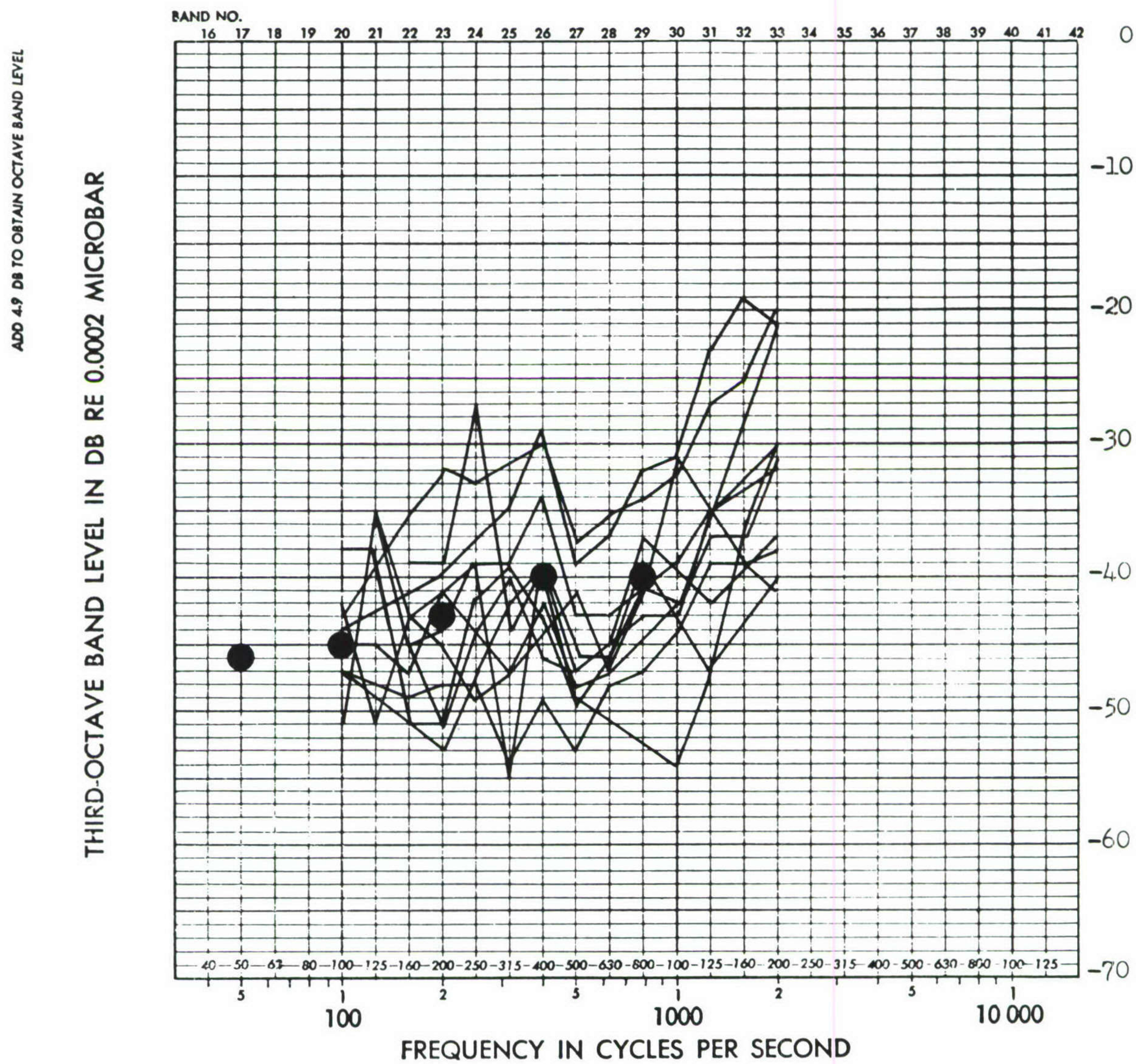

Accelerometers 18, 19, 20, 22, 33, 34, 39, 43, 44, 61, 62;

Closed byx localized acoustic excitation
Accelerations induced by rocket noise

FIGURE D95 COMPARISON OF ACCELERATION RESPONSE TRANSFER FUNCTIONS LOCALIZED, CLOSED BOX, ACOUSTIC EXCITATION AND FOR ACTUAL ROCKET FIRINGS

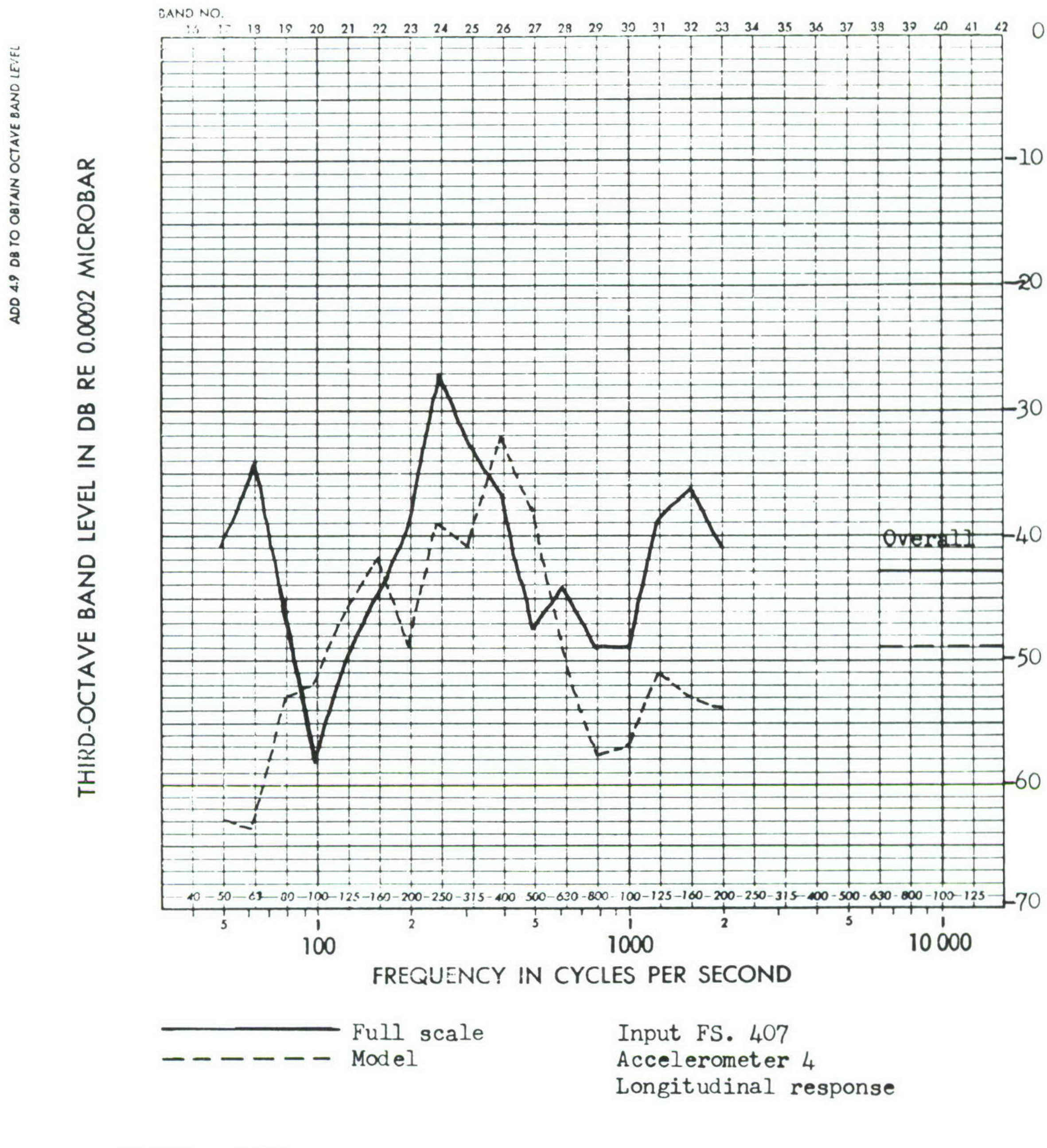

FIGURE D96 COMPARISON OF FULL SCALE AND MODEL LONGITUDINAL RESPONSE TRANSFER FUNCTIONS (DB) FOR UPPER LEFT LONGERON AND BULKHEAD INTERSECTION AT FS. 600; EXCITATION AT FS. 407

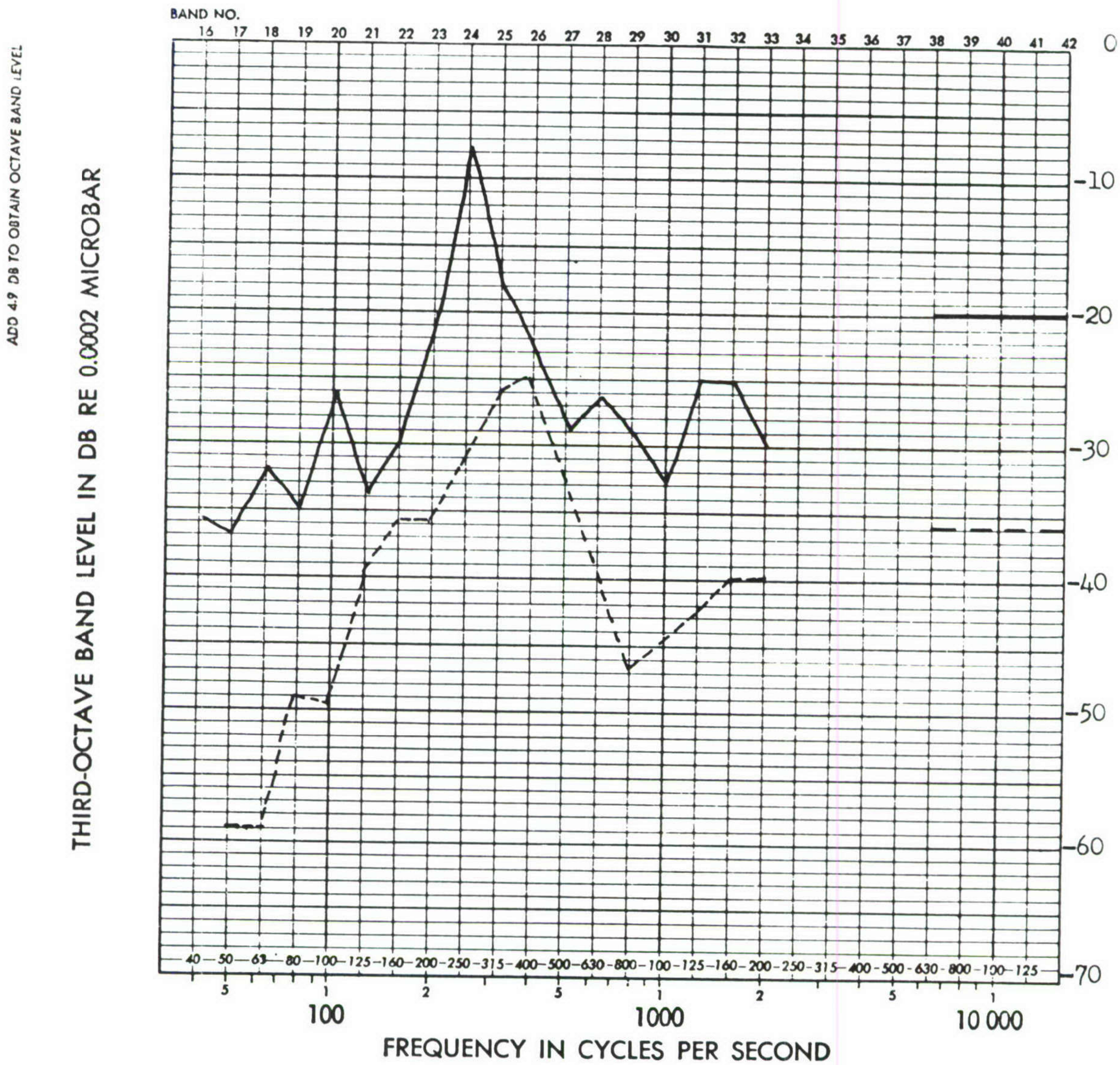

Full scale
Model

Input FS. 578
Accelerometer 4
Longitudinal response

FIGURE D97 COMPARISON OF SULL SCALE AND MODEL LONGITUDINAL RESPONSE TRANSFER FUNCTIONS (DB) FOR UPPER LEFT LONGERON AND BULKHEAD INTERSECTION AT FS. 600; EXCITATION AT FS. 578

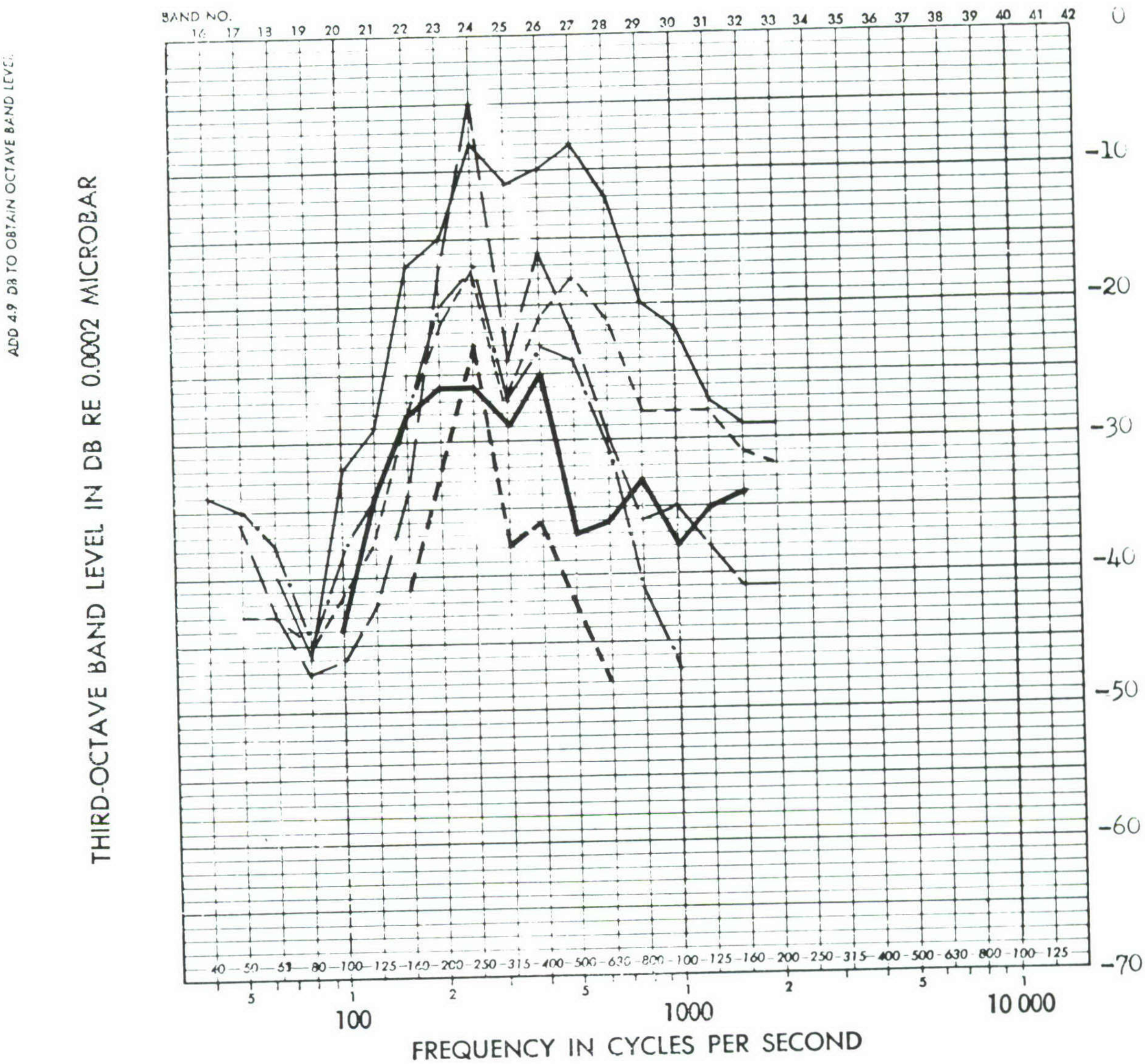

————	Model, FS. 445	Accelerometer 63
– – – – –	Model, FS. 480	Accelerometer 66
—— —— ——	Model, FS. 540	
—·—·—	Model, FS. 575	Accelerometer 72
━━━━	Full Scale, FS. 445	Accelerometer 63
━ ━ ━ ━	Full Scale, FS. 480	Accelerometer 66
	Input FS. 407	

FIGURE D98 COMPARISON OF FULL SCALE AND MODEL RADIAL RESPONSE TRANSFER FUNCTIONS (DB) FOR LOWER LEFT LONGERON: EXCITATION AT FS. 407

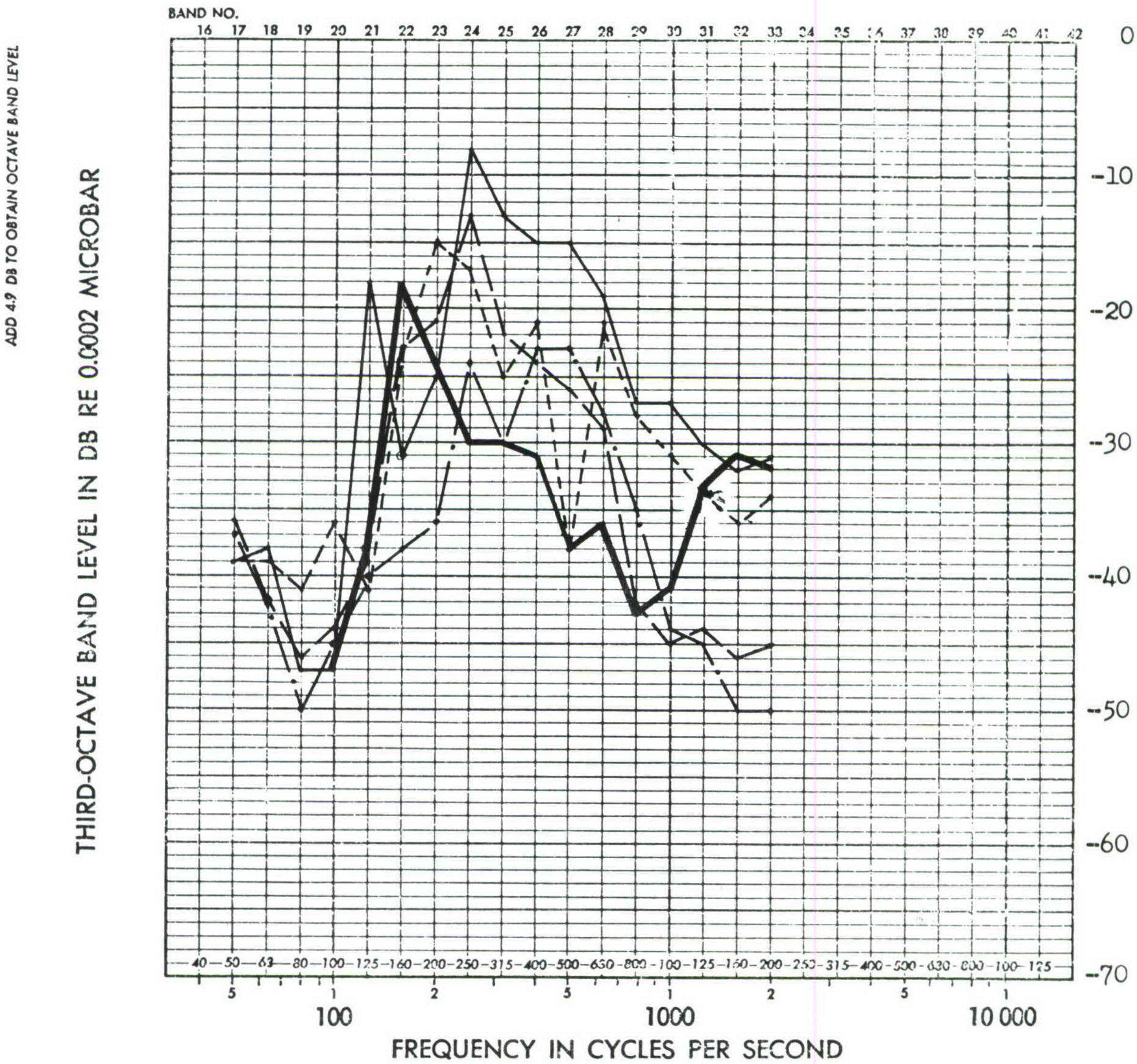

————	Model, FS. 445	Accelerometer 64
– – – – –	Model, FS. 480	Accelerometer 65
—— —— ——	Model, FS. 540	Accelerometer 69
—·—·—	Model, FS. 575	
▬▬▬▬	Full scale, FS. 445	Accelerometer 64
	Input FS. 407	

FIGURE D99 COMPARISON OF FULL SCALE AND MODEL RADIAL RESPONSE TRANSFER FUNCTIONS (DB) FOR LOWER RIGHT LONGERON; EXCITATION AT FS. 407

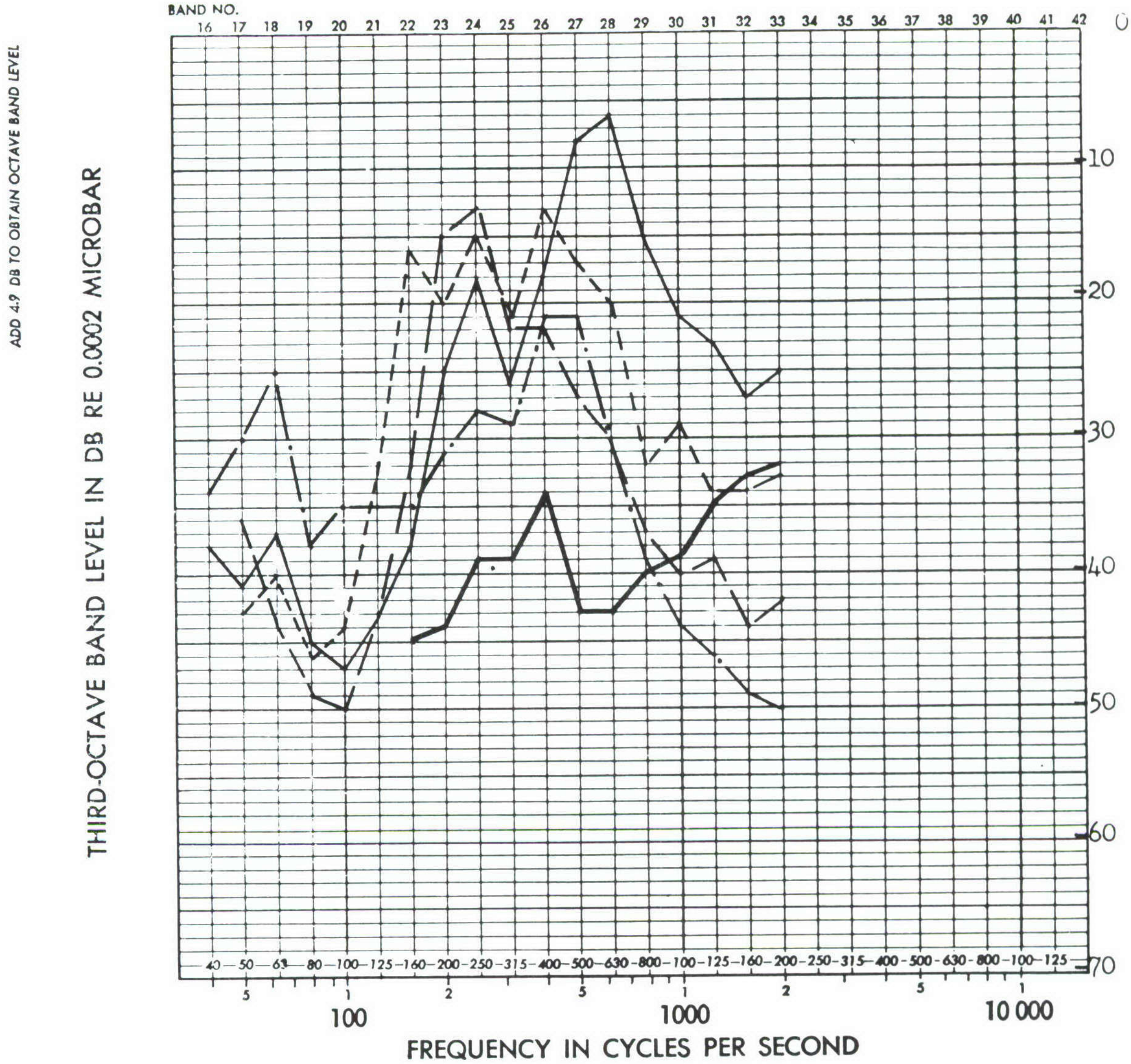

Model, FS. 445 Accelerometer 61
Model, FS. 480 Accelerometer 68
Model, FS. 540
Model, FS. 575 Accelerometer 71
Full scale, FS. 445 Accelerometer 61
Input FS. 407

FIGURE D100 COMPARISON OF FULL SCALE AND MODEL RADIAL RESPONSE TRANSFER FUNCTIONS (DB) FOR LEFT UPPER LONGERON; EXCITATION AT FS. 407

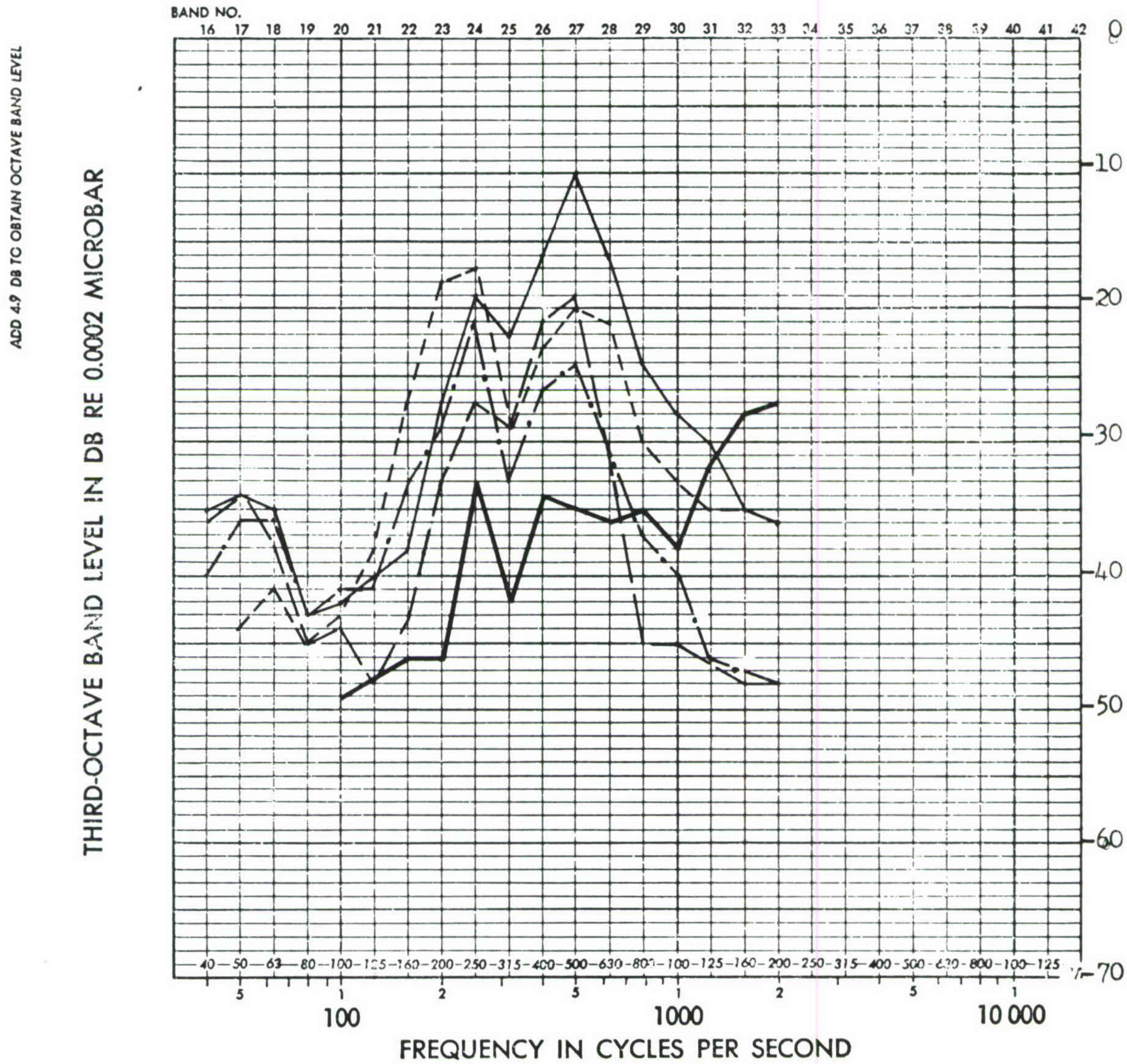

————————	Model, FS. 445	Accelerometer 59
– – – – – –	Model, FS. 480	Accelerometer 67
—— —— ——	Model, FS. 540	
——·——·—	Model, FS. 575	
━━━━━━━━	Full scale, Fs. 407 Input FS. 407	Accelerometer 59

FIGURE D101 COMPARISON OF FULL SCALE AND MODEL RADIAL RESPONSE TRANSFER FUNCTIONS (DB) FOR UPPER RIGHT LONGERON; EXCITATION AT FS. 407

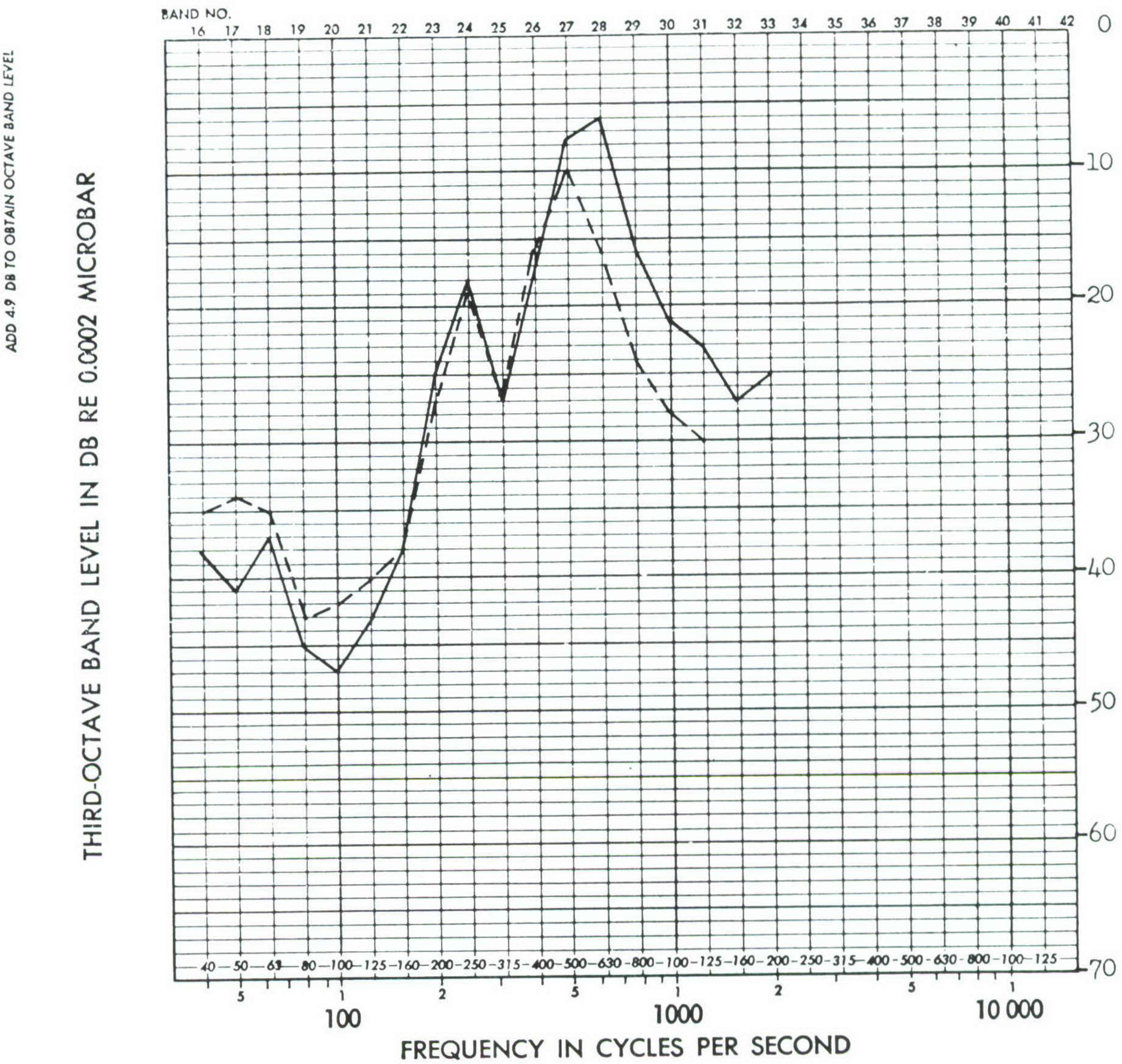

Accelerometer 61 — Input FS. 407
Accelerometer 62 — Response FS. 445
Radial response

FIGURE D102 MODEL RESPONSE TRANSFER FUNCTIONS (DB) FOR UPPER LEFT (61) AND RIGHT (62) LONGERONS AT FS. 445; EXCITATION AT FS. 407

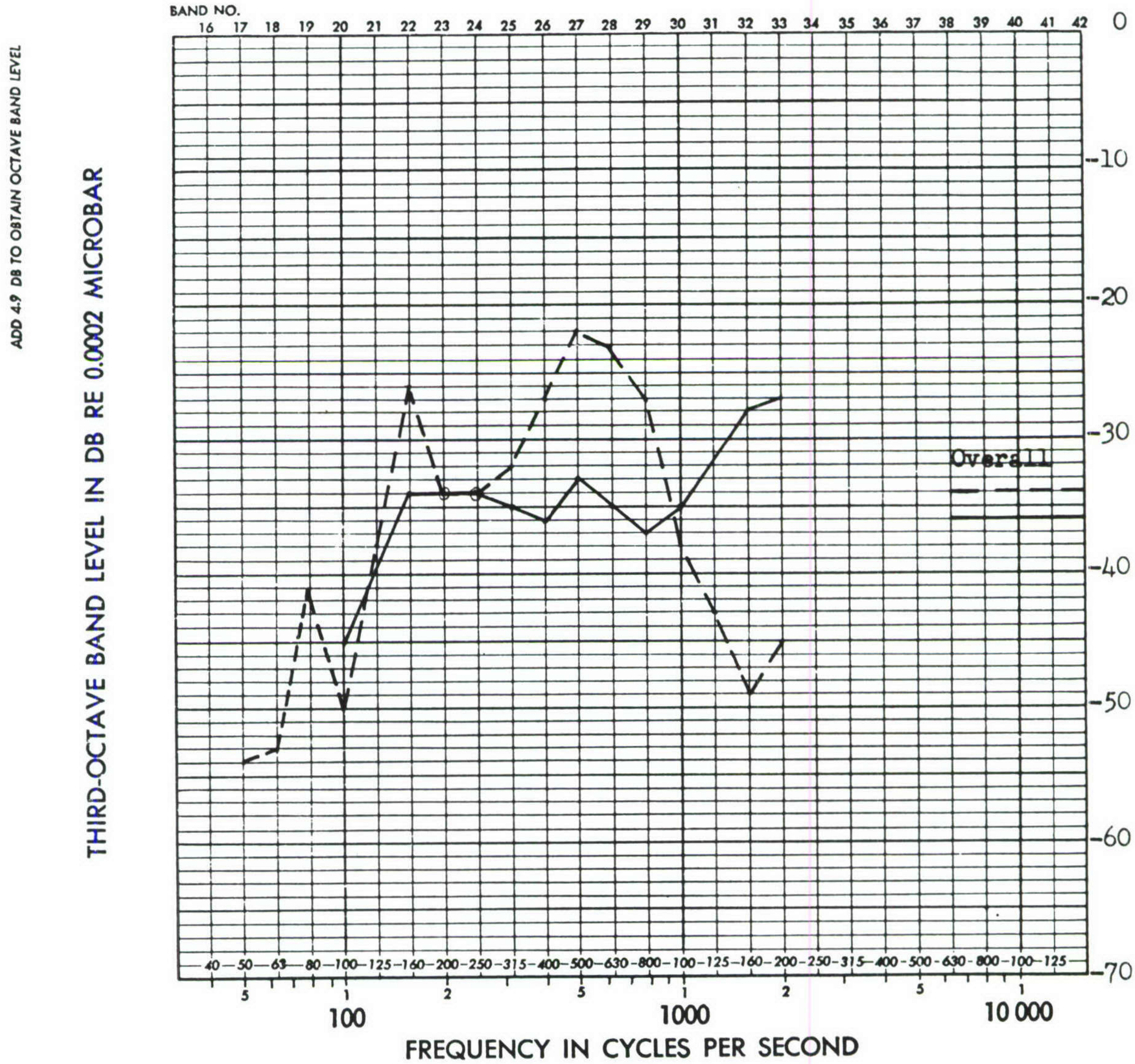

Full scale
Model

Input FS. 407
Vertical floor response
Accelerometer 11

FIGURE D103 COMPARISON OF FULL SCALE AND MODEL VERTICAL RESPONSE TRANSFER FUNCTIONS (DB) FOR FORWARD FLOOR; NEAR FLOOR, BULKHEAD, LEFT UPPER LONGERON INTERSECTION; EXCITATION AT FS. 407

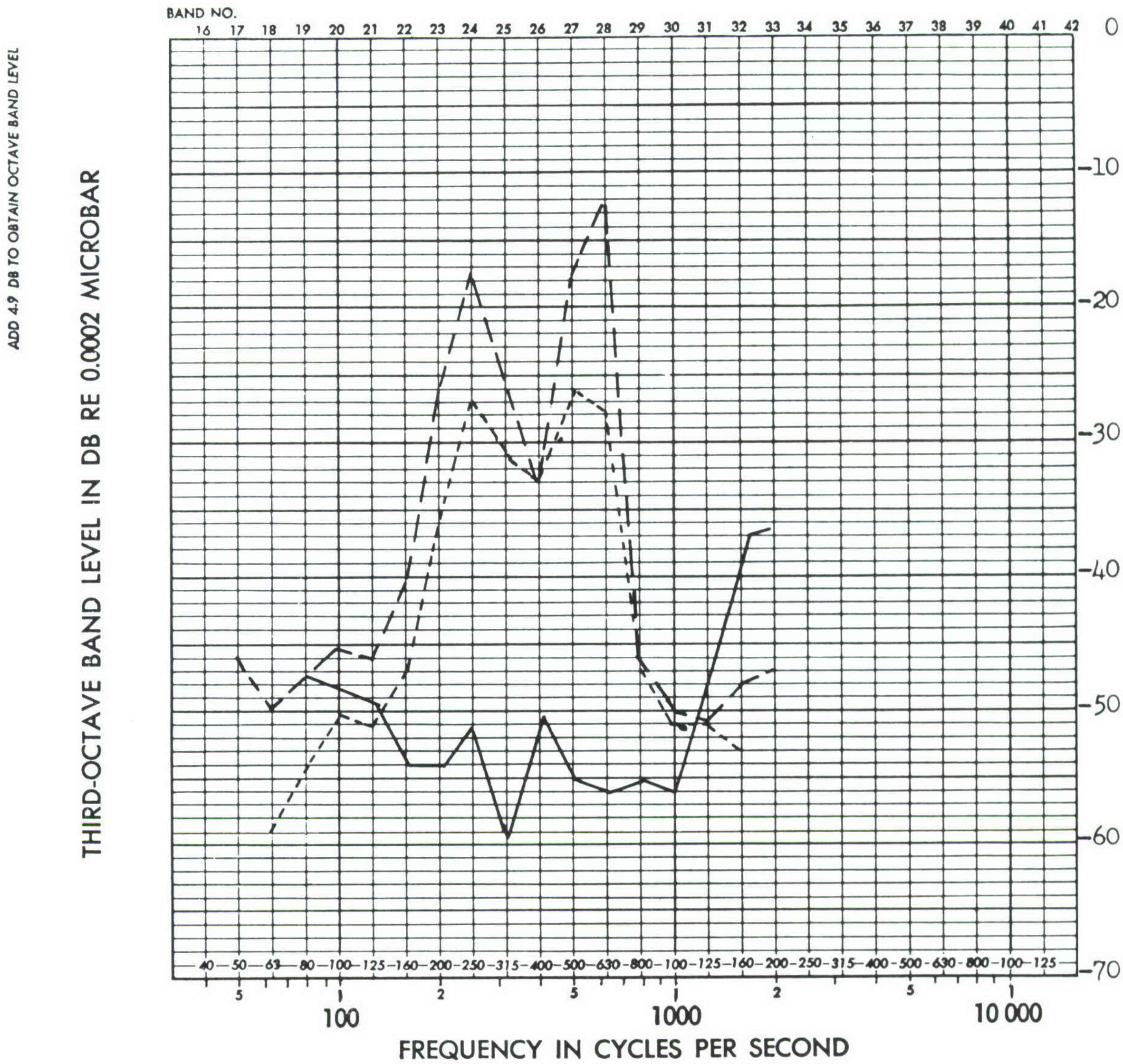

Model, Input FS. 578 (dash-long dash line)
Model, Input FS. 407 (dashed line)
Full scale, Input FS. 407 (solid line)

Lateral response
Bulkhead edge
Accelerometer 28

FIGURE D104 COMPARISON OF FULL SCALE AND MODEL LATERAL RESPONSE TRANSFER FUNCTIONS (DB) FOR BULKHEAD EDGE AT FS. 501; EXCITATION AT FS. 407

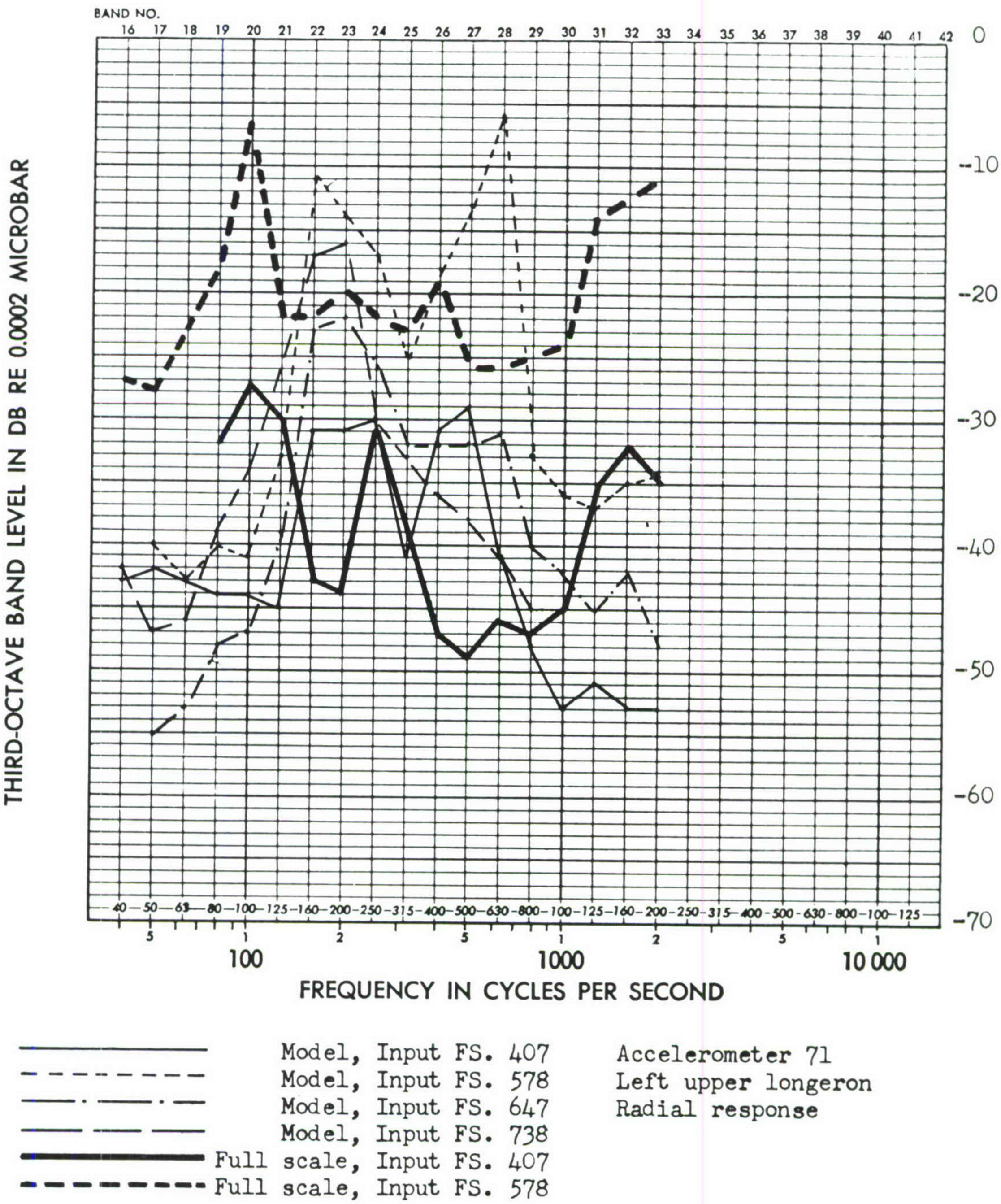

FIGURE D105 COMPARISON OF FULL SCALE AND MODEL RADIAL RESPONSE TRANSFER FUNCTIONS (DB) FOR LEFT UPPER LONGERON AT FS. 576

TABLE D1

LOCATION OF THE ACCELEROMETER 1-28 AND THEIR USE DURING THE VARIOUS TESTS

ACCELEROMETER	CLOSED BOX				OPEN BOX				HORN ONLY				ANGLE OF INCIDENCE		SIMULATED JATO	FUSELAGE STATION	ACCELEROMETER ORIENTATION	STRUCTURAL TYPE TO WHICH ATTACHED
	407	578	647	738	407	578	647	738	407	578	647	738	30°	60°				
1	●	●	●	●												384	Longitudinal	Bulkhead – Floor Intersection
2	●	●		●												384		Center Bulkhead
3	●	●	●	●												536		Center Bulkhead
4	●	●	●	●												600		Longeron – Bulkhead Intersection
5	●	●	●	●												647		Center Bulkhead
6	●															761	Longitudinal	Center Partial Bulkhead
7	●			●											●	384	Vertical	Top Center Bulkhead
8	●	●	●	●												384		Bulkhead – Floor Intersection
9	●			●												384		Bottom Center, Bulkhead
10	●	●		●												447		Bottom Center, Panel
11	●	●	●	●												463		Bulkhead – Floor Intersection
12	●			●												575		Bottom Center, Panel
13	●	●	●	●												600		Longeron – Bulkhead Intersection
14	●	●	●	●												647		Center Bulkhead
15	●	●	●	●												735		Top Center Panel
16	●	●	●	●												761		Top Center Partial Bulkhead
17	●	●														761	Vertical	Bottom Center Panel – Rib Intersection
18	●	●	●	●		●	●									384	Lateral	Bulkhead – Floor Intersection
19	●	●		●												384		Bulkhead Edge
20	●	●		●												384		Bulkhead Edge
21	●			●												407		Side Panel
22	●	●		●												426		Bulkhead Edge
23	●	●		●											●	443		Side Panel
24	●			●												447		Side Panel
25	●	●		●												485		Side Panel
26	●	●														486		Side Panel
27	●			●												501		Bulkhead Edge
28	●	●	●	●												502	Lateral	Bulkhead Edge

TABLE D2

LOCATION OF THE ACCELEROMETER 29-56 AND THEIR USE DURING THE VARIOUS TESTS

ACCELEROMETER	CLOSED BOX				OPEN BOX				HORN ONLY				ANGLE OF INCIDENCE		SIMULATED JATO	FUSELAGE STATION	ACCELEROMETER ORIENTATION	STRUCTURAL TYPE TO WHICH ATTACHED
	407	578	647	738	407	578	647	738	407	578	647	738	30°	60°				
29	•	•		•												536	Lateral	Bulkhead Edge
30	•	•	•	•												552		Ring Stiffener
31	•														•	580		Side Panel
32	•			•												582		Side Panel
33	•	•		•												600		Bulkhead Edge
34	•	•	•	•												600		Bulkhead Edge
35	•	•	•				•									600		Longeron – Bulkhead Intersection
36	•	•	•	•												600		Longeron – Bulkhead Intersection
37	•	•		•												624		Rib Stiffener Intersection
38	•			•												626		Rib Stiffener Intersection
39	•	•	•	•												647		Center Bulkhead
40	•	•	•	•												647		Curved Rib Stiffener
41	•			•												670		Side Panel
42	•			•												670		Side Panel
43	•	•		•												675		Floor Edge
44	•			•												675		Floor Edge
45	•	•		•												684		Side Panel
46	•	•		•												684		Side Panel
47	•			•												684		Rib Stiffener
48				•												684		Rib Stiffener
49	•	•														713		Side Panel
50	•			•												713		Side Panel
51				•												713		Side Panel
52	•															725		Floor Edge
53		•		•												725		Floor Edge
54	•	•	•													735		Rib Stiffener
55	•		•	•												735		Rib Stiffener
56				•												740	Lateral	Side Panel

TABLE D3

LOCATION OF THE ACCELEROMETER 57-84 AND THEIR USE DURING THE VARIOUS TESTS

ACCELEROMETER	CLOSED BOX				OPEN BOX				HORN ONLY				ANGLE OF INCIDENCE		SIMULATED JATO	FUSELAGE STATION	ACCELEROMETER ORIENTATION	STRUCTURAL TYPE TO WHICH ATTACHED
	407	578	647	738	407	578	647	738	407	578	647	738	30°	60°				
57	•	•		•												761	Lateral	Curved Rib Stiffener
58	•	•		•				•	•	•	•		•	•	•	384	Radial	Longeron -- Bulkhead Intersection
59	•			•												407		Longeron
60	•			•												410		Longeron
61	•			•												443		Longeron
62	•			•												447		Longeron
63	•	•		•												447		Longeron
64	•	•		•												447		Longeron
65	•			•												486		Longeron
66	•			•												487		Longeron
67	•			•												486		Longeron
68	•			•												487		Longeron
69	•			•												536		Longeron
70	•			•												536		Longeron -- Bulkhead Intersection
71	•	•	•	•				•	•	•	•		•	•		576		Longeron
72	•	•	•	•												576		Longeron
73	•			•				•	•	•	•		•	•	•	624		Floor Edge
74	•			•												626		Floor Edge
75	•	•														670		Curved Bottom Panel
76																670		Curved Bottom Panel
77	•															680		Curved Top Panel
78	•															680		Curved Top Panel
79	•	•	•													706		Bulkhead Edge
80	•															725		Curved Bottom Panel
81	•															725		Curved Bottom Panel
82																725		Curved Bottom Panel
83	•	•														740		Curved Top Panel
84	•	•	•					•	•	•	•		•	•	•	761	Radial	Partial Bulkhead Edge

APPENDIX E

EXPERIMENTAL SUBSTUDY DIAGRAMS

ALL ASSEMBLIES:

SYMMETRIC ABOUT ℄
RIVETED PER STD. PROC. IN F.S. DETAILS
BONDED WITH IDENTICAL METHODS MS
REMOVE ALL SHARP EDGES
PHOTOGRAPHS REQUIRED
BASE PAD OF HARD RESIN OR EQUIV. WHERE SHOWN
ALL MATERIALS 7075 T6 ALUMINUM

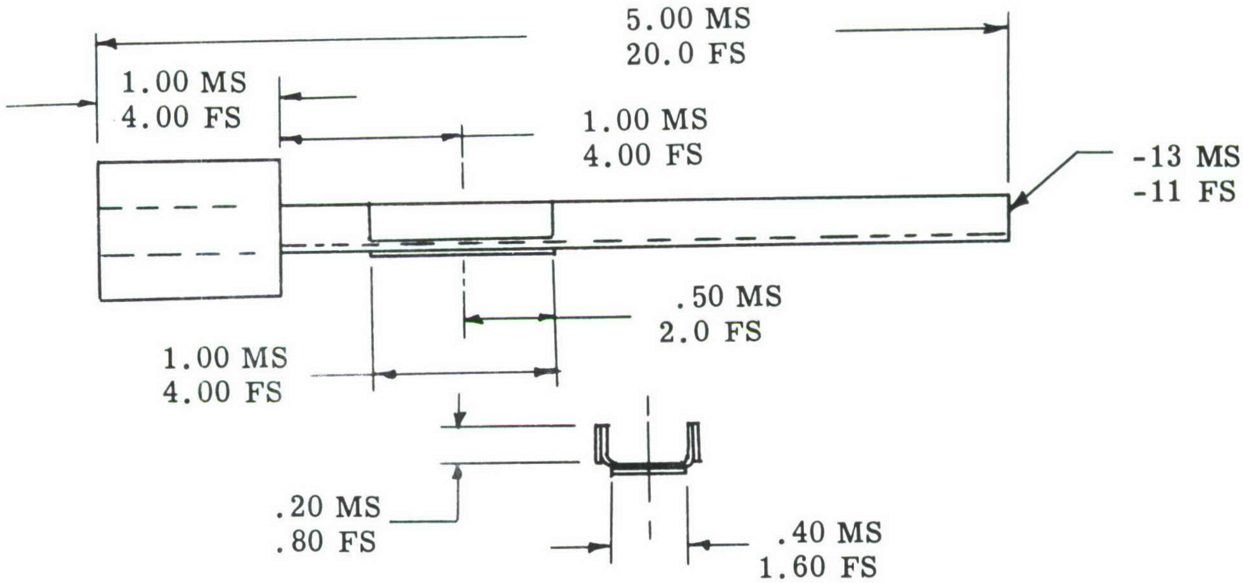

DETAIL -1 ASSEMBLY "SPLICE" 1 EA. REQ. FS & MS

FIGURE E1 DETAILS OF THE FULL SCALE STRUCTURAL COMPONENTS AND MODELS OF THESE COMPONENTS

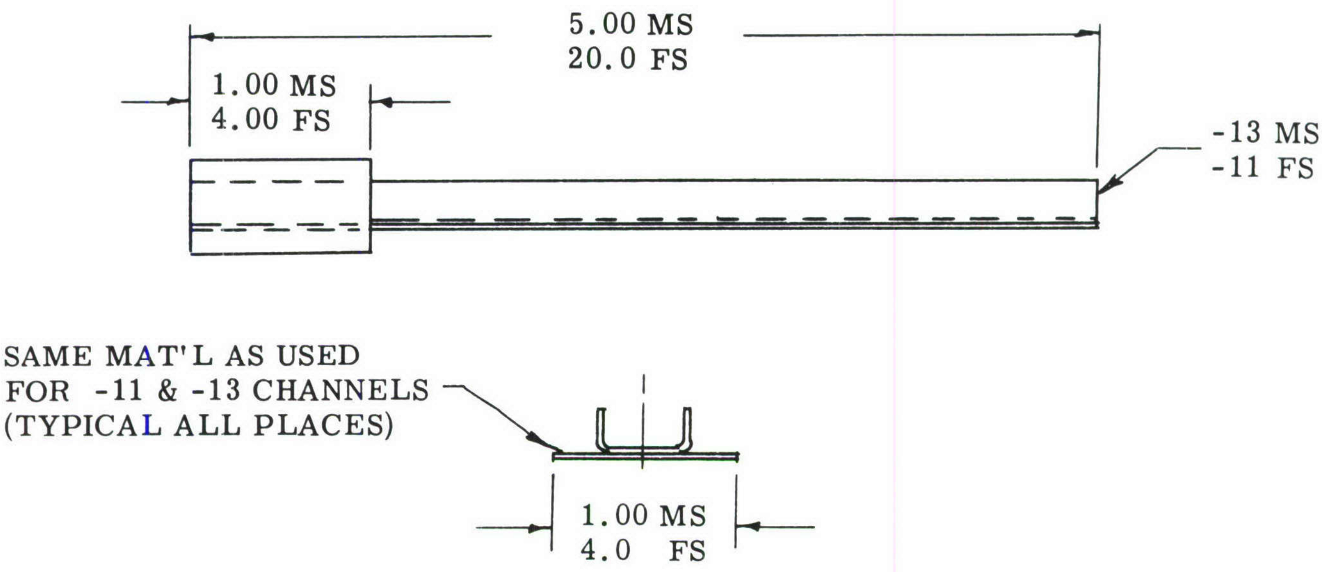

DETAIL -3 ASSEMBLY "STIFFENER" 1 EA. REQ. FS & MS

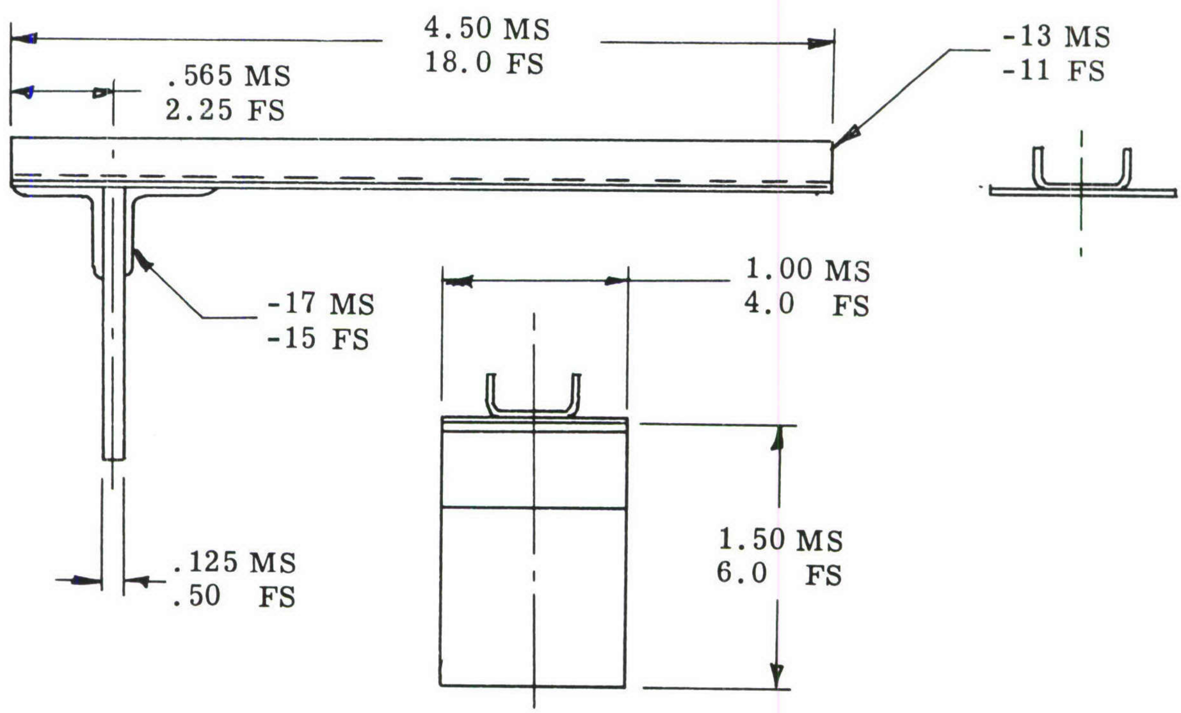

DETAIL -5 ASSEMBLY "BULKHEAD" 1 EA. REQ. FS & MS

FIGURE E1 (CONTINUED)

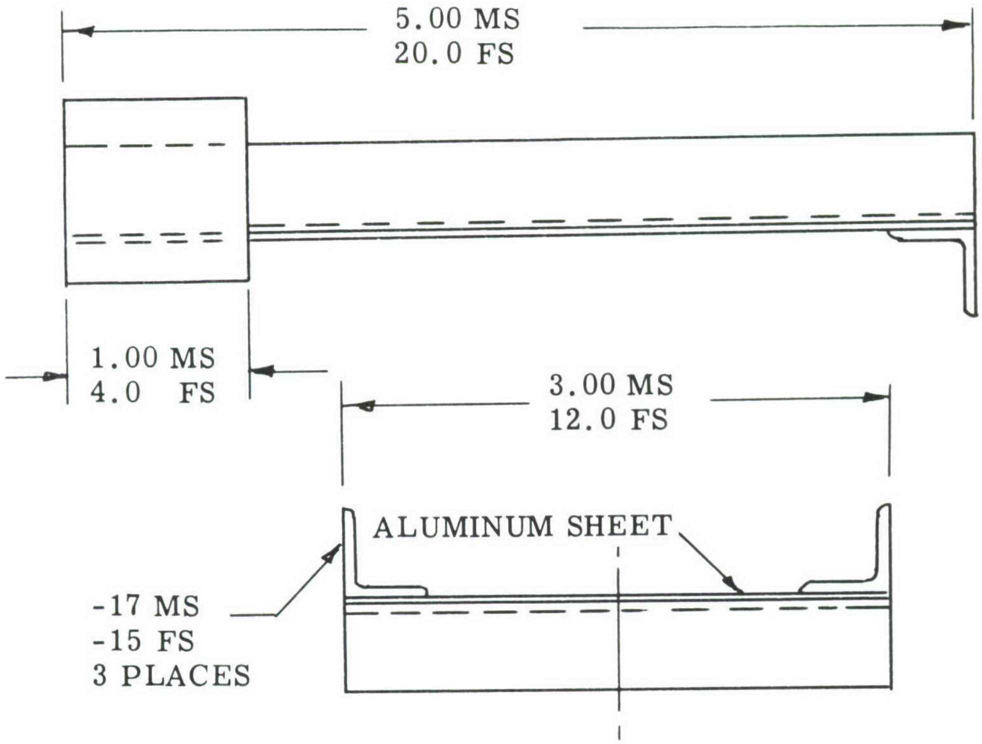

DETAIL -7 ASSEMBLY "PANEL" 1 EA. REQ. FS & MS

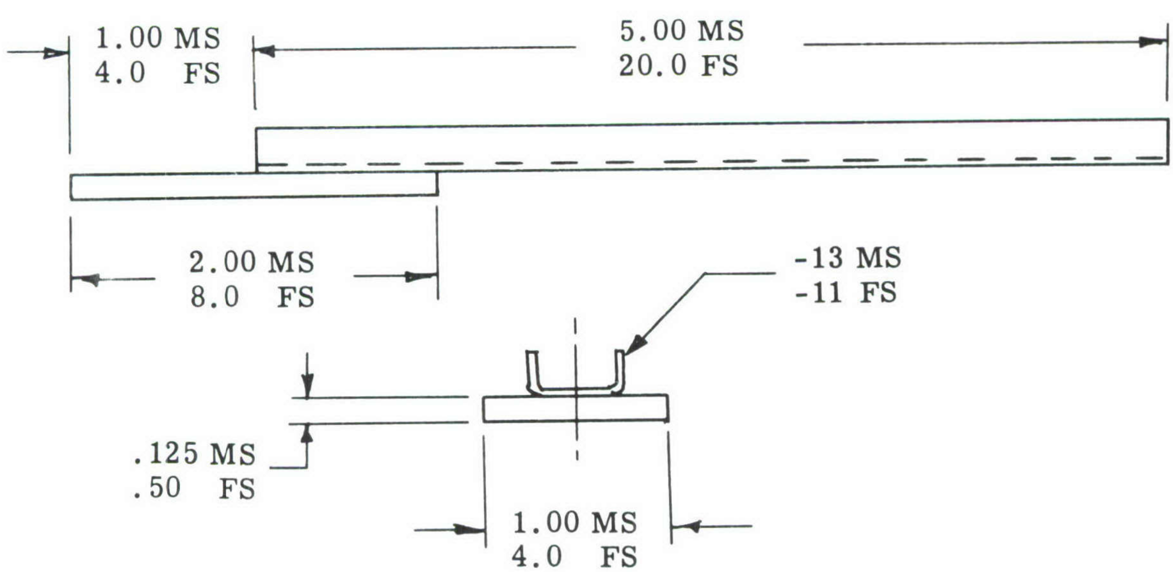

DETAIL -9 ASSEMBLY "LAP" 1 EA REQ.

FIGURE E1 (CONTINUED

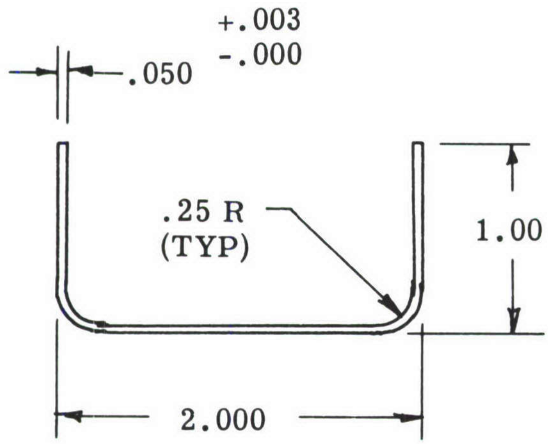

DETAIL -11
FULL SCALE CHANNEL
MATERIAL 7075-T6 SHT.

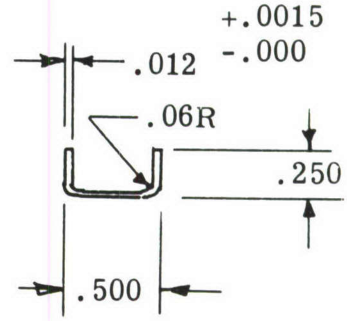

DETAIL -13
MODEL SCALE CHANNEL
MATERIAL 7075-T6 SHT.

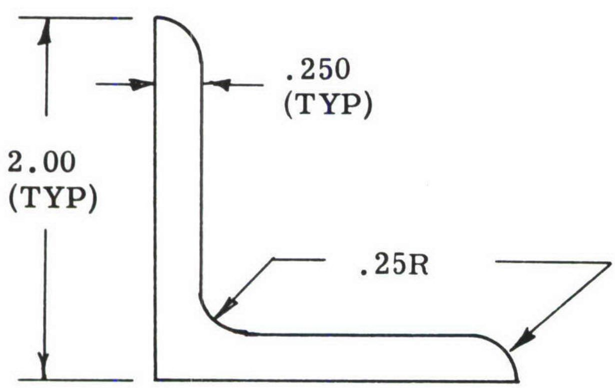

AND 10133-2004

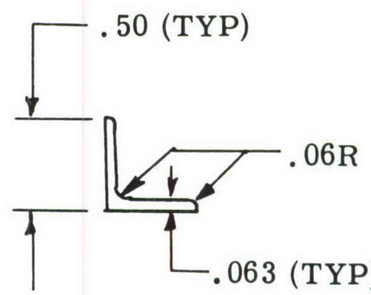

AND 10133-0401

DIMENSIONS SHOWN FOR REFERENCE ONLY

DETAIL -15
FS STANDARD ANGLE
MATERIAL 7075-T6

DETAIL -17
MS STANDARD ANGLE
MATERIAL 7075-T6

FIGURE E1 (CONTINUED)

SPECIMEN IDENTIFICATION:

A RIVETED STRUCTURE $\omega_n = 81 \sim$

B EC 1614 THIN BOND LINE $\omega_n = 125 \sim$

C HAPEX 1233 THIN BOND LINE $\omega_n = 129 \sim$

D EC 1614 .030 BOND LINE $\omega_n = 116 \sim$

E RIVETED STRUCTURE $\omega_n = 94 \sim$

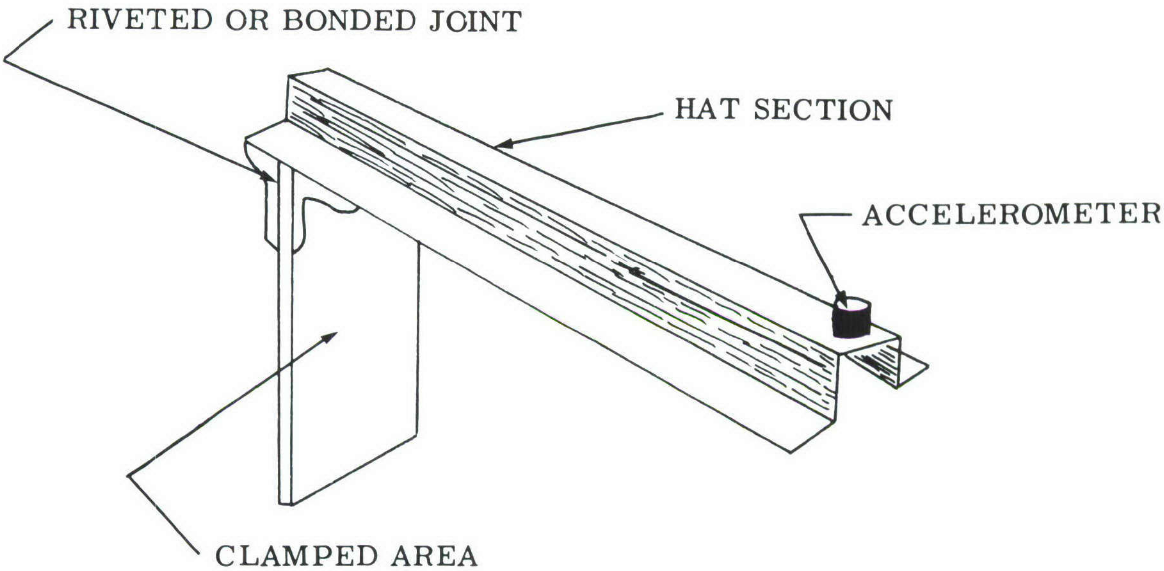

FIGURE E2 RESPONSE - HAT SECTION DAMPING

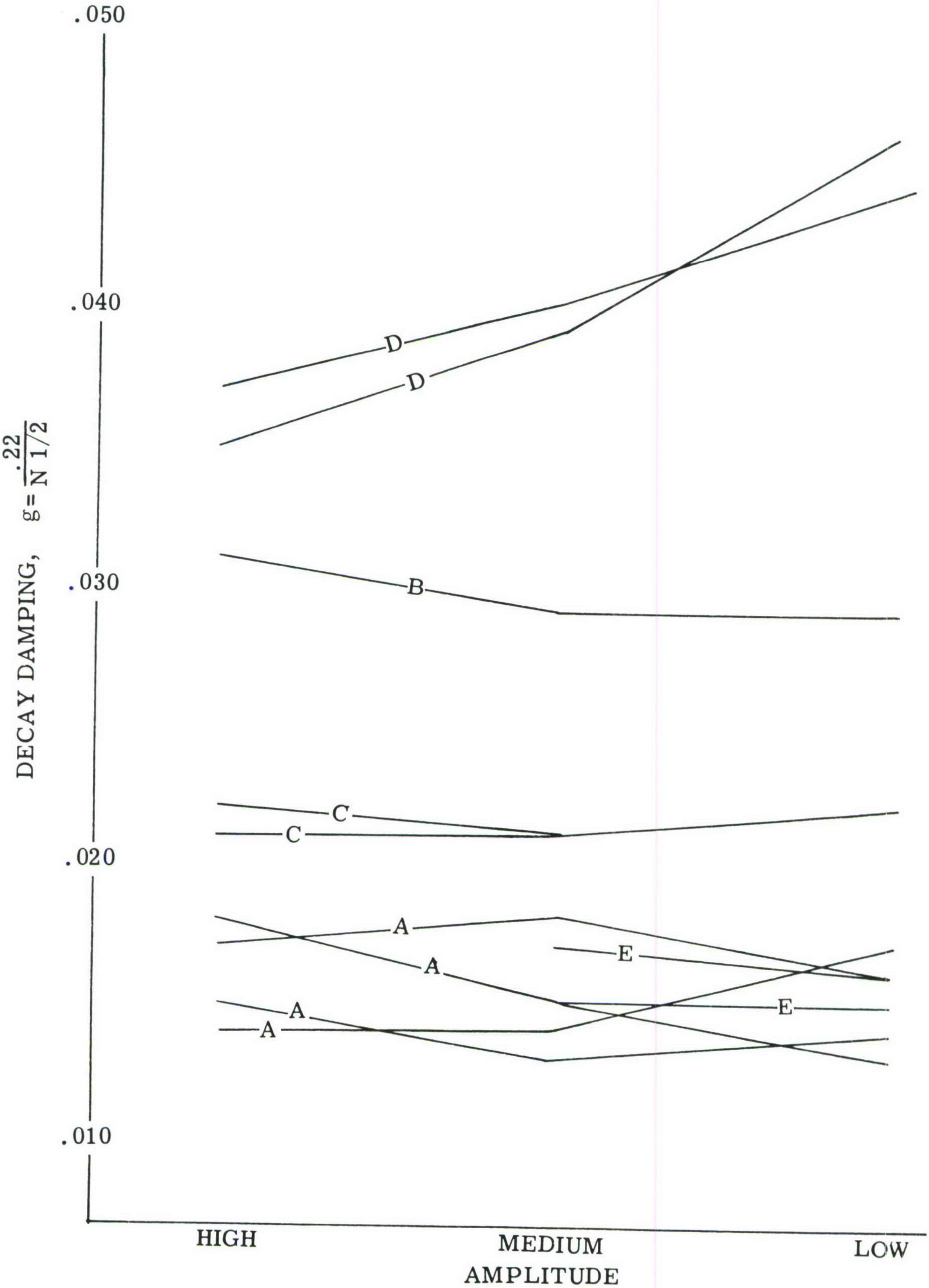

FIGURE E3 REPEATABLE IMPULSES RESPONSE - HAT SECTION DAMPING

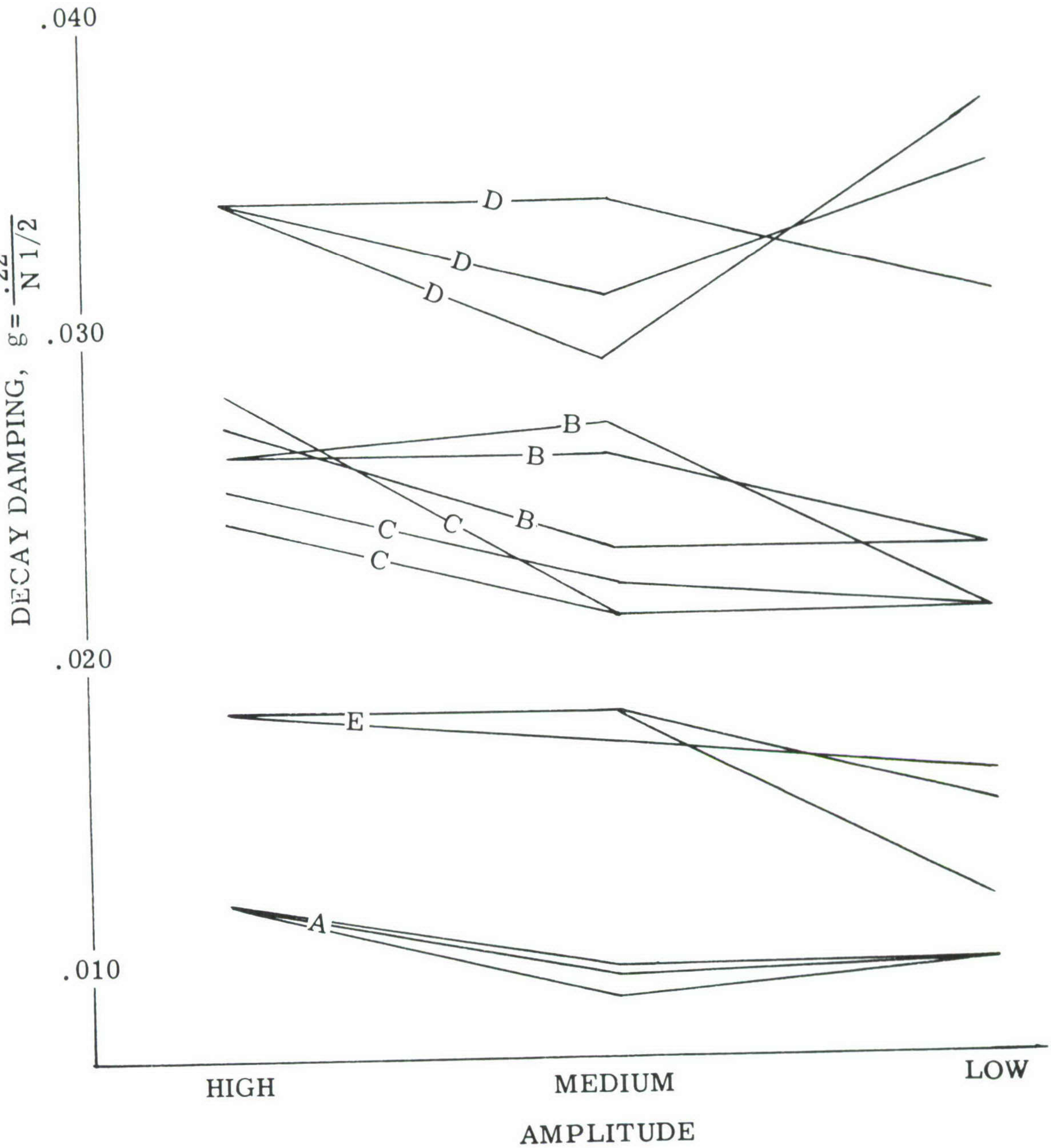

FIGURE E4 RESPONSE - HAT SECTION DAMPING

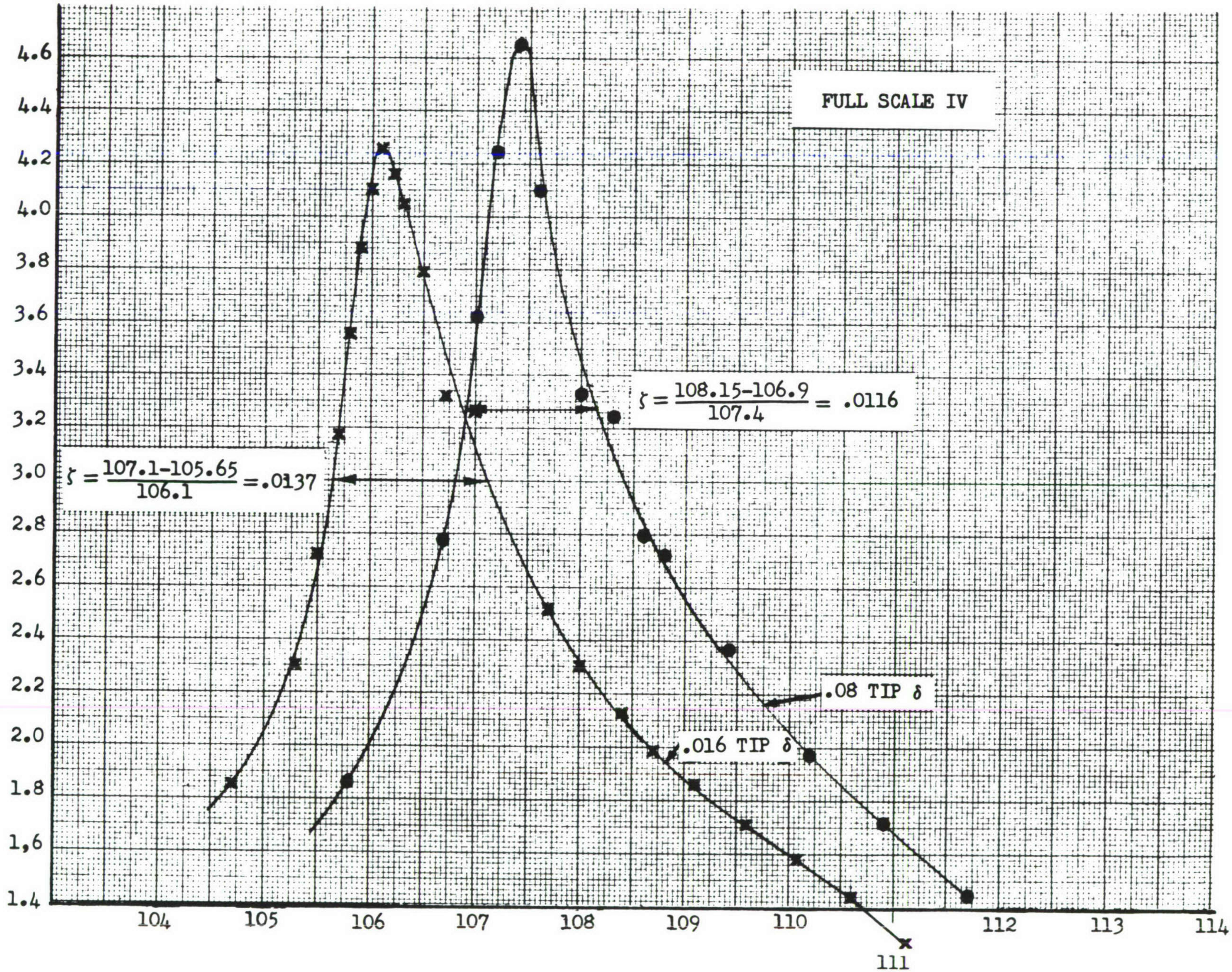

FIGURE E5 RESONANCE CURVE

SCALE	MODEL	δ	ω_n	ζ	δ	ω_n	ζ	
FULL	I	.08	99	.063	.16	101.4	.051	
FULL	II	.08	140.7	.018	.16	139.6	.025	
FULL	III	.08	93.8	.017	.16	92.7	.013	
FULL	IV	.08	107.4	.0116	.16	106.1	.0137	
FULL	V	-	-	-	-	-	-	
¼(RIVETS)	I	.02	406.3	.0052	.04	405.7	.0054	
	I'	.02	380.6	.0037	.02	399.9	.0078	TWO RESONANCES
	I"	.02	408.7	.0044	.04	408.1	.0061	
	II	.04	466.3	.0131	-	-	-	
	III	.02	298.7	.0094	.04	297.9	.0168	
	IV	.02	320	.0097	.048	319	.0078	
¼(RIVETS)	V	.01	531.2	.008	.02	528.6	.010	
¼(BONDED)	I	.02	442.2	.004	-	-	-	
	II	.02	492.5	.0108	.04	493	.0114	
	III	.02	406.1	.0079	.04	400	.007	BOND DETEREORATING
	IV	.02	403.4	.0025	.04	403.1	.0032	
¼(BONDED)	V	.01	513	.0127	.02	496	.024	2 RIVETS IN CORNERS

$\delta \triangleq$ MAX. TIP AMPLITUDE
$\omega_n \triangleq$ FREQUENCY OF MAX. TRANSMISSIBILITY
$\zeta \triangleq$ - 3DB BAND WIDTH $\div \omega_n$

FIGURE E6 SUMMARY OF RESONANCE TESTS

REFERENCES

1. Bingman, R., Resonant Fatigue Failures Associated with Noise, SAE 164B, April 1960.

2. Freudenthal, Fatigue Sensitivity and Reliability of Mechanical Systems and Aircraft Structure, WADD TR 61-53, July 1961.

3. Bouton, I., Statistical Strength Allowables for Aerospace Materials, LM-19, May 1961.

4. Lundberg, Note on the Possibility of Designing a Supersonic Transport with High Fatigue Safety, TN HE-957, Aeronautical Research Institute of Sweden.

5. Blake, Optimum Shock and Vibration Test Levels, Lockheed Missiles, a note given to 58A Dynamics Panel, ARTC, June 1962.

6. Freudenthal, Stress Interaction in Fatigue, Journal of Aerospace Sciences, July 1959.

7. Valluri, S.R., A Unified Engineering Theory of High Stress Level Fatigue, Summer Meeting Paper, IAS, 1961.

8. Wang, A., Relation of Acoustic Fatigue Failure to Valluri's Strength Remaining Concept, Northrop Report, April 1962.

9. Wang, A., Simultaneous Random Spectra and Structural Probability of Failure, Northrop Report 62-71, April 1962.

10. Bouton, I., A New Fatigue Probability of Failure Theory, LM-18, May 1961.

11. Eldred, et al, Structural Vibrations in Space Vehicles, WADD TR 61-62, March 1961.

12. Gray, C., Feasibility of Using Structural Models for Acoustic Fatigue Studies, ASD TR 61-547, October 1961.

13. Effects of Time-Temperature-Stress Histories on the Mechanical Properties of Aircraft Structural Materials, Parts I and II, WADC TR 56-585.

14. Heller, Reduction of the Endurance Limit Due to Stress Interaction in Fatigue, WADD TR 60-752, August 1960.